Volume II

SENSITIVITY and UNCERTAINTY ANALYSIS

Applications to Large-Scale Systems

Dan G. Cacuci
Mihaela Ionescu-Bujor
Ionel Michael Navon

Chapman & Hall/CRC
Taylor & Francis Group
Boca Raton London New York Singapore

Published in 2005 by
CRC Press
Taylor & Francis Group
6000 Broken Sound Parkway NW, Suite 300
Boca Raton, FL 33487-2742

Printed in the United States of America on acid-free paper
10 9 8 7 6 5 4 3 2 1

International Standard Book Number-10: 1-58488-116-X (Hardcover)
International Standard Book Number-13: 978-1-58488-116-2 (Hardcover)
Library of Congress Card Number 2003043992

Library of Congress Cataloging-in-Publication Data

Cacuci, D. G.
Sensitivity and uncertainty analysis / Dan G. Cacuci.
p. cm.
Includes bibliographical references and index.
Contents: v. 1. Theory
ISBN 1-58488-115-1 (v. 1 : alk. paper)
1. Sensitivity theory (Mathematics) 2. Uncertainty (Information theory) 3. Mathematical models—Evaluation. I. Title.

QA402.3.C255 2003
003'.5—dc21 2003043992

T&F informa
Taylor & Francis Group
is the Academic Division of T&F Informa plc.

Visit the Taylor & Francis Web site at
http://www.taylorandfrancis.com

and the CRC Press Web site at
http://www.crcpress.com

INTRODUCTION

Sensitivity and uncertainty analysis are becoming increasingly widespread in many fields of engineering and sciences, encompassing practically all of the experimental data processing activities as well as many computational modeling and process simulation activities. There are many methods, based either on deterministic or statistical concepts, for performing sensitivity and uncertainty analysis. Two of the modern deterministic methods, namely the Adjoint Sensitivity Analysis Procedure (*ASAP*) and the Global Adjoint Sensitivity Analysis Procedure (*GASAP*) were presented, in detail, in Volume I of this book. However, despite of this variety of methods, or perhaps because of it, a precise, unified terminology, across all methods, does not seem to exist yet, even though many of the same words are used by the practitioners of the various methods. For example, even the word "sensitivity" as used by analysts employing statistical methods may not necessarily mean or refer to the same quantity as would be described by the same word, "sensitivity," when used by analysts employing deterministic methods. Care must be therefore exercised, since identical words may not necessarily describe identical quantities, particularly when comparing deterministic to statistical methods. Furthermore, conflicting and contradictory claims are often made about the relative strengths and weaknesses of the various methods.

Models of complex physical systems usually involve two distinct sources of uncertainties, namely: (i) *stochastic uncertainty*, which arises because the system under investigation can behave in many different ways, and (ii) *subjective or epistemic uncertainty*, which arises from the inability to specify an exact value for a parameter that is assumed to have a constant value in the respective investigation. Epistemic (or subjective) uncertainties characterize a degree of belief regarding the location of the appropriate value of each parameter. In turn, these subjective uncertainties lead to subjective uncertainties for the response, thus reflecting a corresponding degree of belief regarding the location of the appropriate response values as the outcome of analyzing the model under consideration. A typical example of a complex system that involves both stochastic and epistemic uncertainties is a nuclear reactor power plant: in a typical risk analysis of a nuclear power plant, stochastic uncertainty arises due to the *hypothetical* accident scenarios which are considered in the respective risk analysis, while epistemic uncertainties arise because of uncertain parameters that underlie the estimation of the probabilities and consequences of the respective hypothetical accident scenarios.

Sensitivity and uncertainty analysis procedures can be either local or global in scope. The objective of *local analysis* is to analyze the behavior of the system response locally around a chosen point (for static systems) or chosen trajectory (for dynamical systems) in the combined phase space of parameters and state variables. On the other hand, the objective of *global analysis* is to determine all of the system's critical points (bifurcations, turning points, response maxima, minima, and/or saddle points) in the combined phase space formed by the

parameters and dependent (state) variables, and subsequently analyze these critical points by local sensitivity and uncertainty analysis. The methods for sensitivity and uncertainty analysis are based on either *statistical* or *deterministic* procedures. In principle, both types of procedures can be used for either local or for global sensitivity and uncertainty analysis, although, in practice, deterministic methods are used mostly for local analysis while statistical methods are used for both local and global analysis.

To assist the reader set the various methods for sensitivity and uncertainty analysis in proper perspective, Chapter I of this Volume reviews and summarizes the salient features, highlighting relative strengths and weaknesses, of the most prominent screening design methods, statistical methods (local and global), and deterministic methods (local and global), as they are currently applied in practice. The following statistical procedures are discussed: sampling-based methods (random sampling, stratified importance sampling, and Latin Hypercube sampling), first- and second-order reliability algorithms (*FORM* and *SORM*, respectively), variance-based methods (correlation ratio-based methods, the Fourier amplitude sensitivity test, and Sobol's method), and screening design methods (classical one-at-a-time experiments, global one-at-a-time design methods, systematic fractional replicate designs, and sequential bifurcation designs). It is important to note that all statistical uncertainty and sensitivity analysis methods first commence with the "uncertainty analysis" stage, and only subsequently proceed to the "sensitivity analysis" stage; this procedural path is the reverse of the procedural (and conceptual) path underlying the deterministic methods of sensitivity and uncertainty analysis, where the sensitivities are determined prior to using them for uncertainty analysis.

In practice, sensitivities cannot be computed exactly by using statistical methods; this can be done only by using *deterministic methods*. Among deterministic methods, it is noted that the direct method and the Forward Sensitivity Analysis Procedure (*FSAP*) require at least as many model-evaluations as there are parameters in the model, while the *ASAP* requires a single model-evaluation of an appropriate adjoint model, whose source term is related to the response under investigation. The *ASAP* is the most efficient method for computing local sensitivities of large-scale systems, when the number of parameters and/or parameter variations exceeds the number of responses of interest. It appears that the only genuinely global deterministic method for sensitivity analysis, published thus far, is the global adjoint sensitivity analysis procedure (*GASAP*) that was presented in Chapter VI of Volume I. The *GASAP* uses both the forward and the adjoint sensitivity system to explore, exhaustively and efficiently, the entire phase-space of system parameters and dependent variables, in order to obtain complete information about the important global features of the physical system, namely the critical points of the response and the bifurcation branches and/or turning points of the system's state variables. Notably, the adjoint sensitivity model can be developed using relatively modest additional resources, if it is developed simultaneously with the original model. However, if the adjoint sensitivity model is constructed

a posteriori, considerable skills may be required for its successful development and implementation.

Chapter II of this Volume presents applications of the *ASAP* to transient one-dimensional two-phase flow problems modeled by well-posed quasi-linear partial differential equations. The chapter commences with the presentation of a self-contained formalism for applying the *ASAP* to functional-type responses associated with two-phase flow models that comprise equations describing conservation of mass, momentum, and energy, for practical one-dimensional, two-phase flow models. This theoretical presentation is followed by a presentation of the main aspects of implementing the *ASAP* into the RELAP5/MOD3.2 code system, which is a large-scale code that simulates the thermal-hydraulic characteristics of light water nuclear reactors. The thermal-hydraulic part of the RELAP5/MOD3.2 code comprises a one-dimensional, non-equilibrium, non-homogeneous two-phase flow model, including conservation equations for boron concentration and non-condensable gases. Chapter II also highlights the fundamentally important aspect of consistency between the differential and the corresponding discretized equations used for sensitivity analysis. In particular, the following consistency correspondences must be assured: (i) the Discretized Forward Sensitivity Model must be consistent with the Differential Forward Sensitivity Model, if the *FSAP* is used; (ii) the Differential Adjoint Sensitivity Model must be consistent with the Discretized Adjoint Sensitivity Model, if the *ASAP* is used; and (iii) the Discretized (representation of the) Response Sensitivity must be consistent with the Integral (representation of the) Response Sensitivity for both the *FSAP* and the *ASAP* (in which the Integral and the Discretized Response Sensitivity are represented in terms of the corresponding adjoint functions).

From a historical perspective, in almost every field of scientific activity, the development of large-scale simulation models extended over many years, if not decades, and their respective development invariably involved large and sometimes changing teams of scientists. Furthermore, such complex models consist of many inter-coupled modules, each module simulating a particular physical sub-process. Since the *ASAP* has not been widely known in the past, most of the extant large-scale, complex simulation models were developed without having simultaneously developed and implemented the corresponding adjoint sensitivity model. Implementing *a posteriori* the *ASAP* for such large-scale code systems is not trivial, and the development and implementation of the adjoint sensitivity model can seldom be executed all at once, in one fell swoop. Actually, an "all-or-nothing" approach for developing and implementing the complete, and correspondingly complex, adjoint sensitivity model for large-scale problems is at best difficult (and, at worst, impractical), and is therefore not recommended. Instead, the recommended strategy is a module-by-module implementation of the *ASAP*. In this approach, the *ASAP* is applied to each module, in turn, to develop a corresponding adjoint sensitivity system for each component module. The final step in this "modular" implementation of the *ASAP* is to "augment" (i.e., join together) the adjoint sensitivity systems for each of the

respective modules, avoiding redundant effort and/or loss of information, until all of the component adjoint sensitivity modules are judiciously connected together, accounting for all of the requisite feedbacks and liaisons between them. In view of its high importance for practical applications, Chapter III presents the theoretical foundation for the modular implementation of the *ASAP* for complex simulations systems, by starting with a selected code module, and then augmenting the size of the adjoint sensitivity system, module by module, until completing the entire system under consideration. The presentation of the general theory (i.e., the *ASAP* for augmented systems) is followed by an illustrative application of this theory to a large-scale system involving the augmentation of the adjoint sensitivity model corresponding to the two-fluid model in RELAP5/MOD3.2 (which was the subject of Chapter II) with the adjoint sensitivity model corresponding to the heat structure models in RELAP5/MOD3.2.

Often, the response functional of a physical system is located at a critical point (i.e., a maximum, minimum, saddle point, etc.) of a function that depends on the system's state vector and parameters. In such situations, changes in the system's parameter would affect not only the magnitude of the response, but also its location in phase-space, since the perturbed response would not only differ in value from the original response, but would also occur in a different spatial location, at a different point in time, etc. The general sensitivity theory, including the *ASAP*, for such responses, defined at critical points, is presented in Chapter IV. The practical application of the general theory is illustrated by means of a simple paradigm example (a simple particle diffusion problem), and also by means of a large-scale application to a paradigm transient scenario for a nuclear reactor system. The reactor's transient behavior is simulated by using a large-scale code system that solves equations describing the following phenomena: (a) thermal-hydraulics equations describing the conservation of thermal energy, mass, and momentum for the average channel fuel pin and surrounding single-phase coolant in the reactor's core; (b) neutron point-kinetics equations describing the time-dependent behavior of the core-integrated neutron density; and (c) a loop-hydraulic equation that relates the core inlet and outlet coolant pressures.

Chapters V and VI are devoted to applications of the *ASAP* for performing efficient sensitivity analysis of paradigm large-scale models used for numerical weather prediction and climatic research. Our understanding of atmospheric processes relies on the use of mathematical models to test the consequences of various physical assumptions. An essential part of weather prediction and climatic research consists of interpreting the results of large-scale simulation models. For example, the current concern about the climatic impact of CO_2 stems from the sensitivity that climatic models exhibit to the atmospheric concentration of CO_2. A further example is the occurrence of atmospheric blocks, which strongly affect the variability in predictive skills of numerical weather prediction (NWP) models; it is therefore important to understand the model errors associated with blocking situations. As mathematical models increase in

sophistication, though, the reasons for the results they give become less clear, making the results more difficult to interpret. A quantitative procedure to help interpret the results of a mathematical model is to perform a sensitivity analysis, i.e., to investigate how the results of the model change when parameters in the model are varied. For example, the ice-albedo feedback mechanism corresponds to the observed negative sensitivity of surface air temperature to surface albedo. Furthermore, sensitivities quantify the extent that uncertainties in parameters contribute to uncertainties in results of models. For example, sub-grid processes need to be parameterized, but such parameterizations are highly simplified approximations of complex processes, so the uncertainties in the parameters involved can be large. If the corresponding sensitivities are also large, then the results of the model will have large uncertainties.

Chapter V presents paradigm applications of the *ASAP* to a radiative-convective model (RCM) for climate simulation and, respectively, to a two-layer isentropic primitive equation model for numerical weather prediction. The RCM contains the nonlinear phenomena characteristic of radiatively-coupled processes, and includes 312 variable parameters. The *ASAP* is applied to derive the adjoint sensitivity equations, to compute efficiently the response sensitivities (in terms of the adjoint functions) to all parameters, and to illustrate the use of sensitivities. Notably, the adjoint functions themselves can be interpreted as the sensitivity of a response to instantaneous perturbations of the model's dependent variables. Furthermore the adjoint functions can be used to reveal the time scales associated with the most important physical processes in the model. In particular, the adjoint functions for the RCM reveal the three time scales associated with: (i) convective adjustment; (ii) heat transfer between the atmosphere and space; and (iii) heat transfer between the ground and atmosphere. Calculating the eigenvalues and eigenvectors of the matrix of derivatives occurring in the set of adjoint equations reveals similar physical information without actually needing to solve the adjoint sensitivity model. An illustrative use of the *ASAP* for evaluating the sensitivity to feedback mechanisms, is also presented. The paradigm response considered is the increase in the average surface air temperature which occurs after the atmospheric CO_2 concentration in the model is doubled, while the paradigm feedback is the surface albedo feedback.

Chapter V continues with a paradigm application of the *ASAP* to more complex, operator-valued, responses, by considering a paradigm two-layer isentropic NWP model that simulates the nonlinear life cycles of baroclinic waves, including the occurrence of so-called "blocks." The variability in predictive skills of NWP models is strongly related to the occurrence of such blocks; this occurrence is indicated by the so-called "blocking indices." From a mathematical point of view, blocking indices are operator-valued responses. The *ASAP* is applied to perform a paradigm sensitivity analysis of a time-dependent blocking index to model parameters. This illustrative example underscores the fact that the exceptional computational efficiency of the *ASAP* yields quantitative results that could not have been obtained, in practice, by any other sensitivity analysis method, because of prohibitive computational costs.

Chapter VI sets forth the presentation of paradigm applications of the *ASAP* to large-scale models used for numerical weather prediction, by considering the following models: (i) the diagnostic equations underlying the nonlinear radiation model used in a version of the National Center for Environmental Prediction model for medium-range weather forecasting; (ii) the Florida State University Global Spectral Model; and (iii) the Relaxed Arakawa Schubert scheme in the NASA Goddard Earth Observing System-1 (GEOS-1) general circulation model, developed by the then Data Assimilation Office (now Global Modeling and Assimilation Office) at the NASA Goddard Space Flight Center. A particularly important implication of the paradigm sensitivity analysis results presented in this chapter is that accurate data for temperature, moisture and surface pressure are essential for an accurate evaluation of cumulus cloud effects, especially at the most influential vertical levels that were identified by sensitivity analysis. Of course, this is because small perturbations at such influential locations tend to exert a stronger impact on the responses than similar perturbations at other, less influential, locations. Therefore, data quality is particularly important at those levels and areas with positive feedback between cloud activities and the environment, since small errors tend to grow through positive feedback mechanisms. Such sensitivity analysis results also underscore the importance of the *ASAP* for *variational data assimilation*. For example, in variational assimilation of precipitation data, in which moist convection is the dominant process, the difference between model output rainfall and the observed rainfall is taken as input to the adjoint sensitivity model. Such information also indicates the regions where additional adaptive observations should be taken.

To keep this volume to a reasonable size, several important topics (e.g., methods of data adjustment and data assimilation in the presence of uncertainties; optimal control of fluid flow) have been deferred for presentation in subsequent volume(s). Nevertheless, by addressing computational issues and highlighting the major challenges that still remain to be resolved, the material presented in this Volume is also intended to provide a comprehensive basis for further advancements and innovations in the field sensitivity and uncertainty analysis. Two outstanding issues, whose solution would greatly advance the state of overall knowledge, would be: (i) to develop the adjoint sensitivity analysis procedure (*ASAP*) for problems describing turbulent flows, and (ii) to combine the *GASAP* with global statistical uncertainty analysis methods, striving to perform, efficiently and accurately, global sensitivity and uncertainty analyses for large-scale systems.

In closing, the authors would like to acknowledge the essential contributions made the editorial staff of Chapman & Hall / CRC. We are particularly grateful to Ms. Helena Redshaw for keeping the publication schedule on track with her friendly e-mails. Last but not least, our special thanks go to Bob Stern, Executive Editor, whose patience and unwavering support made it ultimately possible to bring this book to our readers. One of the authors (I. M. Navon) would also like to acknowledge support of NSF and NASA grants for his research.

TABLE OF CONTENTS

CHAPTER I

A COMPARATIVE REVIEW OF SENSITIVITY AND UNCERTAINTY ANALYSIS METHODS FOR LARGE-SCALE SYSTEMS

Sensitivity and uncertainty analysis are becoming increasingly widespread in many fields of engineering and sciences, as diverse as nuclear and chemical engineering, econometric modeling, electrical engineering, atmospheric and geophysical sciences, encompassing practically all of the experimental data processing activities as well as many computational modeling and process simulation activities. There are many methods, based either on deterministic or statistical concepts, for performing sensitivity and uncertainty analysis. However, despite this variety of methods, or perhaps because of it, a precise, unified terminology, across all methods, does not seem to exist yet, even though many of the same words are used by the practitioners of the various methods. For example, even the word "sensitivity" as used by analysts employing statistical methods may not necessarily mean or refer to the same quantity as would be described by the same word, "sensitivity," when used by analysts employing deterministic methods. Care must be therefore exercised, since identical words may not necessarily describe identical quantities, particularly when comparing deterministic to statistical methods. Furthermore, conflicting and contradictory claims are often made about the relative strengths and weaknesses of the various methods.

The purpose of this Chapter is to review the salient features, highlighting relative strengths and weaknesses, of the most prominent screening design methods, statistical methods (local and global), and deterministic methods (local and global), as they are currently applied in practice. In addition, by addressing computational issues and highlighting the major challenges that still remain to be resolved, the material presented in this Chapter is also intended to provide a comprehensive basis for further advancements and innovations in the field sensitivity and uncertainty analysis.

Models of complex physical systems usually involve two distinct sources of uncertainties, namely: (i) *stochastic uncertainty*, which arises because the system under investigation can behave in many different ways, and (ii) *subjective or epistemic uncertainty*, which arises from the inability to specify an exact value for a parameter that is assumed to have a constant value in the respective investigation. Epistemic (or subjective) uncertainties characterize a degree of belief regarding the location of the appropriate value of each parameter. In turn, these subjective uncertainties lead to subjective uncertainties for the response, thus reflecting a corresponding degree of belief regarding the location of the appropriate response values as the outcome of analyzing the model under

consideration. A typical example of a complex system that involves both stochastic and epistemic uncertainties is a nuclear reactor power plant: in a typical risk analysis of a nuclear power plant, stochastic uncertainty arises due to the *hypothetical* accident scenarios which are considered in the respective risk analysis, while epistemic uncertainties arise because of uncertain parameters that underlie the estimation of the probabilities and consequences of the respective hypothetical accident scenarios.

Sensitivity and uncertainty analysis procedures can be either local or global in scope. The objective of *local analysis* is to analyze the behavior of the system response locally around a chosen point (for static systems) or chosen trajectory (for dynamical systems) in the combined phase space of parameters and state variables. On the other hand, the objective of *global analysis* is to determine all of the system's critical points (bifurcations, turning points, response maxima, minima, and/or saddle points) in the combined phase space formed by the parameters and dependent (state) variables, and subsequently analyze these critical points by local sensitivity and uncertainty analysis. The methods for sensitivity and uncertainty analysis are based on either *statistical* or *deterministic* procedures. In principle, both types of procedures can be used for either local or for global sensitivity and uncertainty analysis, although, in practice, deterministic methods are used mostly for local analysis while statistical methods are used for both local and global analysis.

The most commonly used statistical methods are discussed in Section I.A, the deterministic procedures are briefly summarized in Section I.B, while the trade-offs between computational requirements and results produced by the respective methods are assessed in Section I.C, respectively. To begin with, Section I.A highlights the salient features of the most popular statistical procedures currently used for local and global sensitivity and uncertainty analysis. These statistical procedures can be classified as follows: sampling-based methods (random sampling, stratified importance sampling, and Latin Hypercube sampling), first- and second-order reliability algorithms (*FORM* and *SORM*, respectively), variance-based methods (correlation ratio-based methods, the Fourier amplitude sensitivity test, and Sobol's method), and screening design methods (classical one-at-a-time experiments, global one-at-a-time design methods, systematic fractional replicate designs, and sequential bifurcation designs). It is important to note that all statistical uncertainty and sensitivity analysis methods first commence with the "uncertainty analysis" stage, and only subsequently proceed to the "sensitivity analysis" stage; this procedural path is the reverse of the procedural (and conceptual) path underlying the deterministic methods of sensitivity and uncertainty analysis, where the sensitivities are determined prior to using them for uncertainty analysis.

In practice, sensitivities cannot be computed exactly by using statistical methods; this can be done only by using *deterministic methods*, which will be reviewed in Section I.B. To begin with, Section I.B.1 reviews briefly the deterministic methods most commonly used for computing local sensitivities,

namely the "brute-force" method based on recalculations, the direct method (including the decoupled direct method), the Green's function method, the forward sensitivity analysis procedure (*FSAP*), and the adjoint sensitivity analysis procedure (*ASAP*). The *FSAP* and *ASAP* have been presented, in detail, in Volume I of this book. In particular, it has been noted there that the direct method and the *FSAP* require at least as many model-evaluations as there are parameters in the model, while the *ASAP* requires a single model-evaluation of an appropriate adjoint model, whose source term is related to the response under investigation. The *ASAP* is the most efficient method for computing local sensitivities of large-scale systems, when the number of parameters and/or parameter variations exceeds the number of responses of interest. The adjoint model requires relatively modest additional resources to develop and implement if this is done simultaneously with the development of the original model. If, however, the adjoint model is constructed *a posteriori*, considerable skills may be required for its successful development and implementation.

Once they become available, the exact local sensitivities can be used for the following purposes: (i) understand the system by highlighting important data; (ii) eliminate unimportant data; (iii) determine effects of parameter variations on the system's behavior; (iv) design and optimize the system (e.g., maximize availability/minimize maintenance); (v) reduce over-design; (vi) prioritize the improvements to be effected in the respective system; (vii) prioritize introduction of data uncertainties; (viii) perform local uncertainty analysis by using the method of "*propagation of errors*" (also known as the "*propagation of moments*," or the "*Taylor-Series*") as presented in Section III.F of Volume I. Note that the "propagation of errors" method is used both for processing experimental data obtained from indirect measurements and also for performing uncertainty analysis of computational models. In particular, the "propagation of errors" method provides a systematic way for obtaining the uncertainties in computed results, arising not only from uncertainties in the parameters that enter the respective computational model but also from the numerical approximations themselves.

Section I.B.3 presents deterministic methods that aim towards global sensitivity analysis. The earliest attempts at extending the region of validity of local sensitivities beyond first-order were focused on computing second- and higher-order response derivatives with respect to the system's parameters. However, the number of equations that would need to be solved for obtaining the second- (and higher-) order derivatives of the response is very large, and depends on the number of parameter variations. For this reason, none of the deterministic techniques (proposed in the literature thus far) for computing second- and higher-order response derivatives with respect to the system's parameters has proven routinely practicable for large-scale problems. In particular, the computation of the second-order derivatives of the response and system's equations is already as difficult as undertaking the complete task of computing the exact value of perturbed response. Furthermore, since the Taylor-

series is a local concept, valid within some radius of convergence of the respective series around the nominal parameter values, it follows that even if the response derivatives were available to all orders, they would still merely provide local, but not global, information. Thus, they would yield little, if any, information about the important global features of the physical system, namely the critical points of the response and the bifurcation branches and/or turning points of the system's state variables. It appears that the only genuinely global deterministic method for sensitivity analysis, published thus far, is the *global adjoint sensitivity analysis procedure* (*GASAP*) developed by Cacuci (1990); this method was presented in Chapter VI of Volume I. The *GASAP* uses both the forward and the adjoint sensitivity system to explore, exhaustively and efficiently, the entire phase-space of system parameters and dependent variables, in order to obtain complete information about the important global features of the physical system, namely the critical points of the response and the bifurcation branches and/or turning points of the system's state variables.

Section I.C presents a comparative assessment of the computational effort required for implementing statistical and, respectively, deterministic methods for sensitivity and uncertainty analysis. Regarding statistical methods, the main conclusions are that such methods are conceptually easy to use but have two major inherent practical drawbacks, as follows:

(i) Since many thousands of simulations are needed to obtain reliable results, statistical methods are at best expensive (for small systems), or, at worst, impracticable (e.g., for large time-dependent systems);

(ii) Since the response sensitivities and parameter uncertainties are inherently and inseparably amalgamated in the results produced by statistical methods, improvements in parameter uncertainties cannot be directly propagated to improve response uncertainties; rather, the entire set of simulations and statistical post-processing must be repeated anew. In particular, a "fool-proof" statistical method for analyzing correctly models involving highly correlated parameters does not seem to exist currently, so that particular care must be used when interpreting regression results for such models.

On the other hand, the commonly used deterministic methods also require a substantial computational effort for computing local sensitivities; these methods also become impractical for large systems with many parameters, because of prohibitively large computational requirements. The only exception is the *ASAP*, which is by far the most efficient deterministic method for computing exactly and exhaustively the local sensitivities. However, the *ASAP* requires development of an appropriate adjoint model. If this adjoint model is developed simultaneously with the original model, then the *ASAP* requires very little additional resources to develop. If, however, the adjoint model is developed *a posteriori*, considerable skills may be required for its successful implementation and use. Finally, the *GASAP* appears to be the only deterministic method capable of genuine *global* analysis; it is both exhaustive and computationally efficient,

but its general utility for large-scale models is still untested at the time of this writing.

I. A. STATISTICAL METHODS

I.A.1. Introduction

The salient features of the most popular *sampling-based methods*, namely *random sampling*, *stratified importance sampling*, and *Latin Hypercube sampling*, are reviewed in Section I.A.2. In particular, it is there noted that Latin Hypercube sampling provides a compromise importance sampling when *a priori* knowledge of the relationships between the sampled parameters and predicted responses is not available. It is also noted that the very first step in all sampling-based uncertainty and sensitivity analysis methods is crucial to the final results produced by these methods, since this initial step defines, via "expert opinions," the distributions used to characterize the subjective uncertainty. Hence, the proper assignment of these distributions is essential for avoiding spurious results.

The salient features of the first- and second-order *reliability algorithms* (*FORM* and *SORM*, respectively) are briefly reviewed in Section I.A.3. Next, the most prominent *variance-based methods* for statistical uncertainty and sensitivity analysis, namely *the correlation ratio-based methods*, the *Fourier Amplitude Sensitivity Test* (*FAST*), and *Sobol's method*, are discussed in Section I.A.4. In particular, it is noted that the correlation ratio, the FAST, and Sobol's methods do *not* make the *a priori* assumption that the input model parameters are linearly related to the model's response; this is in contradistinction to the sampling-based methods reviewed in Section I.A.2.

The salient features of the most representative *screening design methods* are presented in Section I.A.5. Screening design methods refer to preliminary numerical experiments designed to identify the parameters that have the largest influence on a particular model response. The objective of screening is to arrive at a *short list* of important factors, based on the assumption that the number of parameters that are truly important to the model response is small by comparison to the total number of parameters underlying the model. This assumption is based on the idea that the influence of parameters in models follows Pareto's law of income distribution within nations, i.e., a complex model can be characterized by a few, very important parameters and a majority of non-influential ones.

Falling within the simplest class of screening designs are the so-called *one-at-a-time* (*OAT*) experiments, in which the impact of changing the values of each parameter is evaluated in turn. However, the results of a classical *OAT* experiment are meaningful only if the model's input-output relation can be adequately represented by a first-order polynomial in the model's parameters. If the model is affected by nonlinearities, as is often the case in practice, then

parameter changes around the "control" scenario would provide drastically different "sensitivities," depending on the chosen "control" scenario. Several alternative designs have been proposed to alleviate this severe limitation of classical *OAT* designs; among the most popular alternatives are the *systematic fractional replicate design* (*SFRD*), the *global OAT* design methods, and the *sequential bifurcation* (*SB*) design. All of these methods are computationally very intensive, which severely limits the amount of reliable information that can be extracted from a screening design. Most importantly, since the importance of parameters is not obvious *a priori* (and may often be counterintuitive) in large-scale, complex models, screening design methods may be *a priori* inadequate to identify correctly the truly important parameters.

I.A.2. Sampling-Based Methods

If the uncertainty associated with the parameters $\boldsymbol{\alpha}$ were known unambiguously, then the uncertainty in the response $\boldsymbol{R}(\boldsymbol{u},\boldsymbol{\alpha})$ could also be assessed unambiguously. In practice, however, the uncertainty in $\boldsymbol{\alpha}$ can rarely be specified unambiguously; most often, many possible values of $\boldsymbol{\alpha}$, of varying levels of plausibility, could be considered. Such uncertainties can be characterized by assigning a distribution of plausible values

$$D_1, D_2, \ldots, D_I, \tag{I.A.1}$$

to each component $\alpha_i(\boldsymbol{x})$ of $\boldsymbol{\alpha}$. Correlations and other restrictions can also be considered to affect the parameters $\alpha_i(\boldsymbol{x})$. Uncertainties characterized by distributions of the form (I.A.1) are called *epistemic or subjective uncertainties*, and characterize a degree of belief regarding the location of the appropriate value of each $\alpha_i(\boldsymbol{x})$. In turn, these subjective uncertainties for the parameters $\alpha_i(\boldsymbol{x})$ lead to subjective uncertainties for the response $\boldsymbol{R}(\boldsymbol{u},\boldsymbol{\alpha})$, which reflect a corresponding degree of belief regarding the location of the appropriate response values as the outcome of analyzing the model under consideration.

Sampling-based methods for sensitivity and uncertainty analysis are based on a sample

$$\boldsymbol{\alpha}_\kappa = [\alpha_{k1}, \alpha_{k2}, \ldots, \alpha_{kI}], \quad (k = 1,2,\ldots,n_S), \tag{I.A.2}$$

of size n_S taken from the possible values of $\boldsymbol{\alpha}$ as characterized by the distributions in Eq. (I.A.1). The response evaluations corresponding to the sample $\boldsymbol{\alpha}_\kappa$ defined in Eq. (I.A.2) can be represented in vector form as

$$\boldsymbol{R}(\boldsymbol{\alpha}_\kappa) = \left[R_1(\boldsymbol{\alpha}_\kappa), R_2(\boldsymbol{\alpha}_\kappa), \ldots, R_J(\boldsymbol{\alpha}_\kappa)\right], \quad (k = 1,2,\ldots,n_S), \tag{I.A.3}$$

where the subscript J denotes the number of components of the response $\boldsymbol{R}$. The pairs

$$\left[\boldsymbol{\alpha}_\kappa, \boldsymbol{R}(\boldsymbol{\alpha}_\kappa)\right], \quad (k = 1,2,\ldots,n_S), \tag{I.A.4}$$

represent a mapping of the uncertain "inputs" $\boldsymbol{\alpha}_\kappa$ to the corresponding uncertain "outputs" $\boldsymbol{R}(\boldsymbol{\alpha}_\kappa)$, which result from the "sampling-based uncertainty analysis." Subsequent examination and post-processing (e.g., scatter plots, regression analysis, partial correlation analysis) of the mapping represented by Eq. (I.A.4) constitute procedures for "sampling-based sensitivity analysis," in that such procedures provide means of investigating the effects of the elements of $\boldsymbol{\alpha}$ on the elements of $\boldsymbol{R}(\boldsymbol{u},\boldsymbol{\alpha})$. Thus, *a "sampling-based uncertainty and sensitivity analysis" first commences with the "uncertainty analysis" stage, and only subsequently proceeds to the "sensitivity-analysis" stage,* which is the exact reverse of the conceptual path underlying the methods of deterministic sensitivity and uncertainty analysis.

Specifically, a "sampling-based uncertainty and sensitivity analysis" involves five steps, as follows:

(i) Define the subjective distributions D_i described by Eq. (I.A.1) for characterizing the uncertain input parameters;

(ii) Use the distributions described by Eq. (I.A.1) to generate the sample $\boldsymbol{\alpha}_\kappa$ described by Eq. (I.A.2);

(iii) Use each of the elements of the sample $\boldsymbol{\alpha}_\kappa$ in order to perform model recalculations, which then generate the responses $\boldsymbol{R}(\boldsymbol{\alpha}_\kappa)$ described by Eq. (I.A.3);

(iv) Perform "uncertainty analysis" of the response $\boldsymbol{R}(\boldsymbol{u},\boldsymbol{\alpha})$, by generating displays of the uncertainty in $\boldsymbol{R}(\boldsymbol{u},\boldsymbol{\alpha})$ using the results for $\boldsymbol{R}(\boldsymbol{\alpha}_\kappa)$ obtained above, in step (iii);

(v) Perform "sensitivity analysis" of the response $\boldsymbol{R}(\boldsymbol{u},\boldsymbol{\alpha})$ to the parameters $\boldsymbol{\alpha}$, by exploring (using scatter plots, regression analysis, partial correlation analysis, etc.) the mappings represented by Eq. (I.A.4), to assess the effects of the components of $\boldsymbol{\alpha}$ on the components of $\boldsymbol{R}(\boldsymbol{u},\boldsymbol{\alpha})$.

Step 1: Of all of the above steps, the most important is the very first one, namely the definition of the distributions used to characterize subjective uncertainty. Because of its fundamental importance, the characterization of subjective uncertainty has been widely studied (see, e.g., Berger, 1985, Hora and Iman, 1989, Bonano and Apostolakis, 1991). In practice, this step invariably involves formal expert review processes. Two of the largest examples of

analyses that used formal expert review processes to assign subjective uncertainties to input parameters are the US Nuclear Regulatory Commission's reassessment of the risks from commercial nuclear reactor power stations, and the assessment of seismic risk in the Eastern USA (1990-1991). Although formal statistical procedures can be occasionally used for constructing subjective distributions, practical experience has shown that it is more useful to specify selected quantile (minimum, median, maximum, etc.) values, rather than attempt to specify a particular type of distribution (e.g., normal, beta, etc.) and its associated parameters. This is because the respective experts are more likely to be able to justify the selection of specific quantile values rather than the selection of a particular form of distribution with specific parameters. When distributions from several expert opinions are combined, it is practically very difficult to assign weights to the respective opinions; these difficulties are discussed, for example, by Clement and Winkler (1999).

Once a subjective distribution D_i has been assigned to each element $\alpha_i(\boldsymbol{x})$ of $\boldsymbol{\alpha}$, the collection of distributions (I.A.1) defines a probability space $(\mathcal{S}, \mathcal{E}, p)$, which is a formal structure where: (i) $\mathcal{S}$ denotes the sample space (containing everything that could occur in the particular universe under consideration; the elements of $\mathcal{S}$ are elementary events); (ii) $\mathcal{E}$ denotes an appropriately restricted subspace of $\mathcal{S}$, for which probabilities are defined; and (iii) p denotes a probability measure.

Step 2: The next step is to sample the probability space. The widest used sampling procedures are: random sampling, importance sampling, and Latin Hypercube sampling; the salient features of these procedures will be summarized briefly in the following. Thus, *random sampling* involves selection of the observations

$$\boldsymbol{\alpha}_\kappa = [\alpha_{k1}, \alpha_{k2}, \ldots, \alpha_{kI}], \quad (k = 1,2,\ldots,n_{RS}), \tag{I.A.5}$$

where n_{RS} represents the sample size, according to the joint probability distribution for the elements of $\boldsymbol{\alpha}$ as defined by $(\mathcal{S}, \mathcal{E}, p)$. A point from a specific region of $\mathcal{S}$ occurs as dictated by the probability of occurrence of the respective region. Moreover, each sample point is selected independently of all other sample points. Note, however, that there is no guarantee that points will be sampled from any given sub-region of $\mathcal{S}$. Furthermore, if sampled values fall closely together, the sampling of $\mathcal{S}$ is quite inefficient. To address and alleviate these shortcomings, the so-called *importance sampling* procedure has been developed by dividing $\mathcal{S}$ exhaustively into several nonoverlapping sub-regions, referred to as *strata* $\mathcal{S}_i$, $(i = 1,2,\ldots,n_S)$. Thus, n_{S_i} values for $\boldsymbol{\alpha}$ are sampled randomly from $\mathcal{S}_i$, and the resultant vectors

$$\boldsymbol{\alpha}_\kappa = [\alpha_{k1}, \alpha_{k2}, \ldots, \alpha_{kI}], \quad \left(k = 1,2,\ldots, \sum_{i=1}^{n_S} n_{S_i} \right), \tag{I.A.6}$$

form a sample obtained by importance-sampling, since the strata $\mathcal{S}_i$ are defined on the basis of how important the parameters $\boldsymbol{\alpha} \in \mathcal{S}_i$ (i.e., parameters that are contained in the strata) are to the final outcome of the analysis. Typically, only one value is sampled from each $\mathcal{S}_i$, in which case Eq. (I.A.6) reduces to Eq. (I.A.2). Importance sampling is used to ensure that specified regions in the sample space are fully covered, thereby ensuring, in particular, that parameters which have low occurrence probabilities but high consequences are included in the analysis. The idea of fully covering the range of each parameter is further extended in the *Latin Hypercube sampling* procedure (see, e.g., McKay et al., 1979). In this procedure, the range of each parameter α_i is divided into n_{LH} intervals of equal probability, and one value is randomly selected from each interval. The n_{LH} values thus obtained for the first parameter, α_1, are then randomly paired, without replacement, with the n_{LH} values obtained for α_2. In turn, these pairs are combined randomly, without replacement, with the n_{LH} values for α_3 to form n_{LH} triples. This process is continued until a set of n_{LH} I-tuples are obtained, of the form

$$\boldsymbol{\alpha}_\kappa = [\alpha_{k1}, \alpha_{k2}, \ldots, \alpha_{kI}], \quad (k = 1,2,\ldots, n_{LH}), \tag{I.A.7}$$

which is called a Latin Hypercube sample. This method is suited for uncorrelated parameters only; *if the parameters are correlated, then the respective correlation structure must be incorporated into the sample, for otherwise the ensuing uncertainty/sensitivity analysis would yield false results*. To incorporate parameter correlations into the sample, Iman and Conover (1982) proposed a restricted pairing technique for generating Latin Hypercubes based on rank-correlations (i.e., correlations between rank-transformed parameters) rather than sample correlations (i.e., correlations between the original, untransformed, parameters).

Since random sampling is easy to implement and provides unbiased estimates for the means, variances, and distribution functions, it is the preferred technique in practice, if large samples are available. However, a sufficiently "large sample," for producing meaningful results by random sampling, cannot be generated for complex models (with many parameters) and/or for estimating extremely high quantiles (e.g., the 0.99999 quantile), since the computation of the required sample becomes, computationally, prohibitively expensive and impractical. In such cases, the random sampling method of choice becomes the stratified sampling method. The main difficulty for implementing stratified

sampling lies with defining the strata and for calculating the probabilities for the respective strata, unless considerable *a priori* knowledge is already available for this purpose. For example, the fault and event trees used in risk assessment studies of nuclear power plants and other complex engineering facilities can be used as algorithms for defining stratified sampling procedures. Latin Hypercube sampling is used when very high quantiles need not be estimated, but the calculations needed for generating the "large sample" required for random sampling still remain unpractical. This is often the case in practice when assessing the effects of subjective uncertainty in medium-sized problems (e.g., ca. 30 parameters), while a 0.9 to 0.95 quantile is adequate for indicating the location of a likely outcome. For such problems, random sampling is still unfeasible computationally, but the unbiased means and distribution functions provided by the full stratification (i.e., each parameter is treated equally) of the Latin Hypercube sampling makes it the preferred alternative over the importance sampling, where the unequal strata probabilities produce results that are difficult to interpret (particularly for subsequent sensitivity analysis). In this sense, Latin Hypercube sampling provides a compromise importance sampling when *a priori* knowledge of the relationships between the sampled parameters and predicted responses is not available.

Step 3: Once the sample has been generated, its elements must be used to perform model recalculations, which then generate the responses $\boldsymbol{R}(\boldsymbol{\alpha}_\kappa)$ described by Eq. (I.A.3). These model recalculations can become the most expensive computational part of the entire uncertainty and sensitivity analysis and, if the model is complex, the model recalculations may severely limit the sample size and the other aspects of the overall analysis.

Step 4: It is customary to display the estimated expected value and the estimated variance of the response (as estimated from the sample size). However, these quantities may not be the most useful indicators about the response because information is always lost in the calculations of means and variances. In particular, the mean and variance are less useful for summarizing information about the distribution of subjective uncertainties; by comparison, quantiles associated with the respective distribution provide a more meaningful locator for the quantity under consideration. Distribution functions (e.g., cumulative and/or complementary distribution functions, density functions) provide the complete information that can be extracted from the sample under consideration.

Step 5: In the context of sampling-based methods, statistical sensitivity analysis (as opposed to deterministic sensitivity analysis) involves the exploration of the mapping represented by Eq. (I.A.4) to assess the effects of some, but not all, of the individual components of $\boldsymbol{\alpha}$ on the response $\boldsymbol{R}(\boldsymbol{\alpha})$. This exploration includes examination of scatter plots, regression and stepwise regression analysis, correlation and partial correlation analysis, rank transformation, identification of nonmonotonic patterns, and identification of

nonrandom patterns. The starting point of statistical sensitivity analysis is the generation of scatter plots, which are obtained by plotting the points

$$(\alpha_{kj}, R_k), \quad (k = 1,\ldots,n_S), \tag{I.A.8}$$

for each element α_j of $\boldsymbol{\alpha}$ for $(j = 1,\ldots,I)$. The resulting I scatter plots are then examined to find possible relations between the response $\boldsymbol{R}(\boldsymbol{\alpha})$ and the elements α_j of $\boldsymbol{\alpha}$.

A more formal analysis of the parameter-to-response mapping depicted by Eq. (I.A.4) is to perform regression analysis on a linear model between the predicted responses, $R_{predicted}$, and the input parameters α_j, of the form

$$R_{predicted} = b_0 + \sum_{j=1}^{I} b_j \alpha_j . \tag{I.A.9}$$

The calculated responses, R_k, are also formally expressed in terms of the actual parameter values, α_{kj}, used in the analysis, by means of a linear relationship of the form

$$R_k = b_0 + \sum_{j=1}^{I} b_j \alpha_{kj} + \varepsilon_k, \quad (k = 1,\ldots M), \tag{I.A.10}$$

where M denotes the actual number of calculations, and where

$$\varepsilon \equiv R_k - R_{predicted}, \tag{I.A.11}$$

denotes the error between the calculated and predicted value of the corresponding element of the response. The regression analysis then commences by assuming that the unknown regression coefficients b_j can be determined by minimizing the sums $\sum_k \left(R_k - R_{predicted}\right)^2 \equiv \sum_k \varepsilon^2$ of the squared errors. The regression coefficients b_j can be used, along with other indicators computed during the regression analysis, to assess the importance of the individual parameters α_j with respect to the uncertainty in the response components. A measure of the extent to which the regressions model can match the observed data is provided by the so-called coefficient of multiple determination, C^2, defined by the following ratio:

$$C^2 \equiv S_{reg} / S_{tot}\,, \tag{I.A.12}$$

where the quantities S_{reg} and S_{tot} are defined by means of the sums

$$S_{reg} \equiv \sum_{k=1}^{M} \left(R_{k,est} - R_{ave}\right)^2, \quad S_{tot} \equiv \sum_{k=1}^{M} \left(R_k - R_{ave}\right)^2, \tag{I.A.13}$$

and where $R_{k,est}$ denotes the estimate of R_k obtained from the regression model, while R_{ave} denotes the mean of the R_k's. A value of C^2 close to unity indicates that the regression model accounts well for most of the uncertainties in the R_k's; conversely, a value of C^2 close to zero indicates that the regression model accounts poorly for the uncertainties in the R_k's. In the important particular case when the sampling design matrix $\boldsymbol{\alpha}_\kappa$ is orthogonal, then each coefficient b_j can be determined by means of the formula

$$b_j = \left(\sum_{k=1}^{M} \alpha_{kj} R_k\right) / \left(\sum_{k=1}^{M} \alpha_{kj}^2\right), \tag{I.A.14}$$

which indicates that the addition or deletion of model parameters will not change the regression coefficients for the remaining parameters. Furthermore, when the sampling design matrix $\boldsymbol{\alpha}_\kappa$ is orthogonal, then Eq. (I.A.12) for the coefficient of multiple determinations decomposes into the additive form

$$C^2 = \sum_{k=1}^{M} C_k^2\,, \tag{I.A.15}$$

where C_k^2 denotes the value of C^2 when regressing R solely on α_k. In other words, when the sampling design matrix $\boldsymbol{\alpha}_\kappa$ is orthogonal, then C_k^2 represents the contribution of α_k to C^2.

Other useful concepts in sampling-based uncertainty/sensitivity analysis are the correlation and partial correlation coefficients. The sample correlation coefficient, $Corr(\alpha, R)$, between α and R for a sequence of observations $(\alpha_k, R_k), (k = 1,\ldots,M)$, is defined as

$$Corr(\alpha, R) \equiv \frac{\sum_{k=1}^{M} (\alpha_k - \alpha_{ave})(R_k - R_{ave})}{\left[\sum_{k=1}^{M} (\alpha_k - \alpha_{ave})^2\right]^{1/2} \left[\sum_{k=1}^{M} (R_k - R_{ave})^2\right]^{1/2}}, \qquad \text{(I.A.16)}$$

where α_{ave} and R_{ave} denote the corresponding sample average values. Thus, the correlation coefficient, $Corr(\alpha, R)$, provides a measure of the linear relationship between the elements α_j of $\boldsymbol{\alpha}$, and the response(s) $\boldsymbol{R}(\boldsymbol{\alpha})$.

The partial correlation coefficient provides a measure of the linear relation between α_j and R, when the linear effects of all of the other parameters are removed. In other words, the partial correlation coefficient provides a measure of the importance of a single parameter, α_j, under exclusion of the effects of: (i) the other parameters, (ii) the assumed distribution for α_j, and (iii) the magnitude of the impact of an input parameter on the response. The partial correlation coefficient between an individual parameter α_j and a component R of the response $\boldsymbol{R}(\boldsymbol{\alpha})$ is obtained by considering a sequence of regression models.

It is important to note that correlated variables introduce unstable regression coefficients b_j, in that the values of b_j become sensitive to the specific variables introduced into the regression model. In such situations, the regression coefficients of a regression model that includes all of the parameters are likely to give misleading indications of parameter importance. If several input parameters are suspected (or known) to be highly correlated, it is usually recommended to transform the respective parameters so as to remove the correlations or, if this is not possible, to analyze the full model by using a sequence of regression models with all but one of the parameters removed, in turn. Furthermore, if the regression model is used in an attempt to match the predictions associated with individual sample parameters rather than to match the trend displayed by the collective sample, then over-fitting of data may arise if parameters are arbitrarily forced into the regression model.

Stepwise regression analysis, which involves the use of a sequence of regression models, is often used when the model under investigation contains many parameters and a regression analysis involving all the variables simultaneously is impractical. The *first step* in a stepwise regression analysis is to use a regression model that includes the *single* specific *parameter* that has the largest correlation with the response. The *second step* is to use a regression model that involves *two parameters*, namely: (a) the single parameter from step 1, and (b) a second parameter, chosen to be that parameter, among the remaining ones, that has the largest impact on the uncertainty that has remained

unaccounted for in step 1 (i.e., the parameter that has the largest correlation with the residual uncertainty in the response R). The *third step* is to use a regression model involving *three parameters*, namely (a) the two parameters from step 2, and (b) a third parameter, chosen to be that parameter, among the remaining ones, that has the largest impact on the uncertainty that has remained unaccounted for in step 2 (i.e., the parameter that has the largest correlation with the residual uncertainty in the response R, after the impact of the most important two parameters has been accounted for). This stepwise process of constructing successively more comprehensive regression models by adding additional parameters, in the order of their importance in contributing to the uncertainty in the response, is continued until the addition of further parameters can no longer account meaningfully for the residual uncertainty in the response. Note that correlations among parameters may cause an already selected parameter to be dropped out from the next-level regression model, if the respective parameter fails to have a significant impact on the residual uncertainty in the response.

In a stepwise regression analysis, it is important to guard against over-fitting the data; this danger occurs if the individual observations rather than the overall trend are fitted. For example, it is possible to fit the data apparently "better" by using a higher-order polynomial than the order indicated by the overall trend, in which case a spurious regression model would be constructed, leading to poor subsequent predictions. To protect against over-fitting, the predicted error sum of squares (Allen, 1971) is usually used as a measure of the adequacy of the regression model, and also as a criterion for stopping the step-wise construction of the hierarchical regression models. Furthermore, F-tests or t-tests are used to determine when a variable is no longer needed and can therefore be dropped from the regression model.

Since the regression relationships discussed so far are based on linear representations of the impact of parameters on the response, these regression models will perform poorly when the relationships between the parameters and the response are nonlinear. In such cases, the *rank transformation* may be used to improve the construction of the respective regression model. The conceptual framework underlying rank transformation involves simply replacing the parameters by their respective ranks, and then performing the customary regression analysis on the ranks rather than the corresponding parameters (see, e.g., Iman and Conover, 1982, Saltelli and Sobol', 1995, Sanchez and Blower, 1997). Thus, if the number of observations is M, then the smallest value of each parameter is assigned rank 1, the next largest value is assigned rank 2, etc., until the largest value, which is assigned rank M; if several parameters have the same values, then they are assigned an averaged rank. The regression analysis is then performed by using the ranks as input/output parameters, as replacements for the actual parameter/response values. This replacement has the effect of *replacing the linearized parameter/response relationships by rank-transformed monotonic input/output relationships* in an otherwise conventional regression analysis. In practice, a regression analysis using the rank-transformed (instead of

raw) data may yield better results, but only as long as the relationships between parameters and responses are monotonically nonlinear. Otherwise, the rank-transformation does not improve significantly the quality of the results produced by regression analysis.

Departures from monotonic trends can be sometimes identified by using *F*-tests for detecting common means, χ^2-tests for detecting common medians, and the Kruskal-Wallis test for common locations (see, e.g., Conover, 1980, Kleijnen and Helton, 1999); all of these tests are performed using scatter plots. Scatter plots can also be used to identify nonrandom patterns, by using χ^2-tests for detecting statistical independence between parameters. However, if the parameters are not independent but are statistically correlated, then the magnitudes and even the signs of the regression coefficients b_j associated with the respective parameters may be erroneous, and therefore indicate incorrectly the effects of such parameters on the response.

As has been mentioned in the introductory paragraphs to this Chapter, large-scale models of complex physical systems usually involve two distinct sources of uncertainties, namely: (i) stochastic uncertainty, which arises because the system under investigation can behave in many different ways, and (ii) subjective or epistemic uncertainty, which arises from the inability to specify an exact value for a parameter that is assumed to have a constant value in the respective investigation. A typical example of such a complex system is a nuclear power reactor plant; in a typical risk analysis of a nuclear power plant, stochastic uncertainty arises due to the many hypothetical accident scenarios which are considered in the respective risk analysis, while epistemic uncertainties arise because of the many uncertain parameters that underlie the estimation of the probabilities and consequences of the respective hypothetical accident scenarios. When performing a statistical uncertainty and sensitivity analysis of a complex system such as a nuclear power plant, the effects of stochastic uncertainties are usually propagated by using importance sampling, while the effects of subjective uncertainties are propagated by using Latin Hypercube sampling. In particular, event trees, if available, are used in conjunction with importance-sampling to propagate stochastic uncertainties. This concept has been amply illustrated in two large risk assessment studies, namely: (i) the reassessment of risk associated with US commercial nuclear power plants, carried out under the auspices of the US Nuclear Regulatory Commission (1990-1991), and (ii) the Compliance Certification Application for the Waste Isolation Power Plant (1996).

I.A.3. Reliability Algorithms: FORM and SORM

In many practical problems, the primary interest of the analyst may be focused on a particular mode of failure of the system under consideration, while the detailed spectrum of probabilistic outcomes may be of secondary concern. For such problems, the so-called reliability algorithms provide much faster and more economical answers (by comparison to the sampling-based methods discussed in the previous section) regarding the particular mode of failure of the system under consideration. The typical problems that can be analyzed by using reliability algorithms must be characterized by a mathematical model (whose solution can be obtained analytically or numerically), by input parameters that can be treated as being affected by subjective (epistemic) uncertainties, and by a threshold level that specifies mathematically the concept of "failure." The reliability algorithms most often used are known as the first-order reliability methods (*FORM*) and second-order reliability methods (*SORM*), respectively. Both of these methods use optimization algorithms to seek "the most likely failure point" in the space of uncertain parameters, using the mathematical model and the response functional that defines failure. Once this most likely failure point (referred to as the "design point") has been determined, the probability of failure is approximately evaluated by fitting a first (or second-) order surface at that point. Reliability algorithms have been applied to a variety of problems, including structural safety (see, e.g., Madsen et al., 1986), offshore oil field design and operation (see, e.g., Bysveen et al., 1990), multiphase flow and transport in subsurface hydrology (see, e.g., Xiang and Mishra, 1997).

As with many optimization algorithms, the *FORM* and *SORM* algorithms are also susceptible to nonconvergence or to convergence to an erroneous design point, particularly when the failure probability approaches the extreme values of 0.0 or 1.0; therefore, the numerical optimization algorithm and convergence tolerances should be tailored, whenever possible, to the specific problem under investigation.

I.A.4. Variance-Based Methods

As has been discussed in Section I.A.2, above, the sampling-based methods use variance, among other indicators, as a measure of the importance of a parameter in contributing to the overall uncertainty in the response. The concept of variance as a measure of the importance of a parameter also underlies the conceptual foundation of three further methods for statistical uncertainty and sensitivity analysis, namely the *Fourier Amplitude Sensitivity Test* (*FAST*), *Sobol's method*, and the *correlation-ratio method* (including variants thereof). It is important to note that, in contrast to the sampling-based methods discussed in Section I.A.2, the correlation-ratio, the *FAST*, and Sobol's methods do not make

the *a priori* assumption that the input model parameters are linearly related to the model's response.

The importance of a parameter α (input) in contributing to the predictive uncertainty in a response R (output) can be assessed by considering the marginal probability distribution, $p_R(R)$, of R, which can be written in terms of the conditional probability distribution, $p_{R|\alpha}(R|\alpha)$, of R conditioned on α, as follows:

$$p_R(R) = \int p_{R|\alpha}(R|\alpha) p_\alpha(\alpha) d\alpha \,. \tag{I.A.17}$$

The above relation can be intuitively interpreted that α is important if the fixing of its value substantially reduces the conditional prediction variance relative to the marginal prediction variance. This interpretation indicates that various conditional variance ratios may be used as indicators of importance. Specifically, the methods based on correlation-ratios assume that the model simulating the system under investigation is of the form

$$R = E(R|\boldsymbol{\alpha}) + \boldsymbol{\varepsilon}\,, \tag{I.A.18}$$

where $\boldsymbol{\alpha}$ represents, as before, the set of I model parameters, and $\boldsymbol{\varepsilon}$ represents a vector of errors with the properties that $E(\boldsymbol{\varepsilon}) = 0$ and $Var[E(R|\boldsymbol{\alpha}), \boldsymbol{\varepsilon}] = known$. In numerical experiments, $\boldsymbol{\varepsilon}$ is not taken into consideration.

Recall that in standard regression analysis (discussed in Sec. I.A.2), the expectation $E(R|\boldsymbol{\alpha})$ is *a priori* assumed to have the linear form $\sum_{k=1}^{M} \alpha_k b_k$, where the quantities b_k are the regression coefficients, determined by least-square fitting. By contrast, there are no assumptions in Eq. (I.A.18) regarding the specific mathematical form of the conditional expectation $E(R|\boldsymbol{\alpha})$.

Based on the model defined by Eq. (I.A.18), the prediction variance, $Var(R)$, of R can be written in the form

$$Var(R) = Var_{\boldsymbol{\alpha}}[E(R|\boldsymbol{\alpha})] + E_{\boldsymbol{\alpha}}(Var[R|\boldsymbol{\alpha}])\,, \tag{I.A.19}$$

where

$$E(R|\boldsymbol{\alpha}) \equiv \int p_{R|\boldsymbol{\alpha}}(R) R dR, \tag{I.A.20}$$

$$Var_{\boldsymbol{\alpha}}[E(R|\boldsymbol{\alpha})] \equiv \int [E(R|\boldsymbol{\alpha}) - E(R)]^2 \, p_{\boldsymbol{\alpha}}(\boldsymbol{\alpha}) d\boldsymbol{\alpha}, \tag{I.A.21}$$

$$E_{\boldsymbol{\alpha}}(Var[R|\boldsymbol{\alpha}]) \equiv \int [R - E(R|\boldsymbol{\alpha})]^2 [p_{R|\boldsymbol{\alpha}}(R) dR] p_{\boldsymbol{\alpha}}(\boldsymbol{\alpha}) d\boldsymbol{\alpha}. \tag{I.A.22}$$

The quantity $Var_{\boldsymbol{\alpha}}\left[E\left(R \mid \boldsymbol{\alpha}\right)\right]$ is the variance of the conditional expectation (VCE) of R conditioned on $\boldsymbol{\alpha}$; this quantity measures the importance of $\boldsymbol{\alpha}$ since it indicates how the constituent parts of $Var\left(R\right)$, given by Eq. (I.A.19), relate to $\boldsymbol{\alpha}$. More specifically, $Var_{\boldsymbol{\alpha}}\left[E\left(R \mid \boldsymbol{\alpha}\right)\right]$ measures the total variation in R in the sense that, as $\boldsymbol{\alpha}$ varies, the variation in R would match the variation in $E\left(R \mid \boldsymbol{\alpha}\right)$, if the second term in Eq. (I.A.19), namely $E_{\boldsymbol{\alpha}}\left(Var\left[R \mid \boldsymbol{\alpha}\right]\right)$, were small. In fact, the term $E_{\boldsymbol{\alpha}}\left(Var\left[R \mid \boldsymbol{\alpha}\right]\right)$ is a residual term that measures the remaining variability in R due to other unobserved inputs or other unknown sources of variation when $\boldsymbol{\alpha}$ is fixed.

The additive decomposition shown in Eq. (I.A.19) can be used to define the correlation ratio, η^2, by means of the ratio

$$\eta^2 = \frac{Var_{\boldsymbol{\alpha}}\left[E\left(R \mid \boldsymbol{\alpha}\right)\right]}{Var\left(R\right)}, \tag{I.A.23}$$

which represents a measure of the magnitude of the VCE relative to the prediction variance $Var\left(R\right)$ (see, e.g., McKay, 1995). The method devised by McKay for evaluating η^2 is based on a Latin Hypercube sampling of size m with r replicates, and is computationally very expensive, requiring $rm \times \left(I+1\right)$ model evaluations, where I represents the number of parameters in $\boldsymbol{\alpha}$. A somewhat more economical method for evaluating η^2 is the resampling-based method of Saltelli et al. (1993), requiring $n\left(I+1\right)$ model evaluations, where n represents the sample size for evaluating $E\left(R \mid \alpha_i\right)$ for a specified value of α_i, and where I represents the number of parameters in $\boldsymbol{\alpha}$.

The *FAST* procedure was originally proposed by Cukier et al. (1973), and was subsequently extended by Cukier's group and other authors. This procedure uses the following Fourier transformation of the parameters α_i:

$$\alpha_i = F_i \sin\left(\omega_i z\right), \quad i = 1, \ldots, I, \tag{I.A.24}$$

where $\left\{\omega_i\right\}$ is a set of integer frequencies, while $z \in \left(-\pi, \pi\right)$ is a scalar variable. The expectation $E\left(R\right)$ and variance of the response R can be approximated, respectively, as follows

$$E\left(R\right) = \frac{1}{2\pi}\int_{-\pi}^{\pi} f\left(z\right)dz, \qquad Var\left(R\right) \cong 2\sum_{j=1}^{\infty}\left(A_j^2 + B_j^2\right), \tag{I.A.25}$$

where

$$f(z) \equiv f\left[F_1 \sin(\omega_1 z), F_2 \sin(\omega_2 z), \ldots, F_I \sin(\omega_I z)\right], \tag{I.A.26}$$

while

$$A_j \equiv \frac{1}{2\pi} \int_{-\pi}^{\pi} f(z) \cos(jz) dz \tag{I.A.27}$$

$$B_j \equiv \frac{1}{2\pi} \int_{-\pi}^{\pi} f(z) \sin(jz) dz. \tag{I.A.28}$$

The transformation given by Eq. (I.A.24) should provide, for each parameter α_i, a uniformly distributed sample in the unit I-dimensional cube. As $z \in (-\pi, \pi)$ varies for a given transformation, all parameters change simultaneously; however, their respective ranges of uncertainty is systematically and exhaustively explored (i.e., the search curve is space-filling) if and only if the set of frequencies $\{\omega_i\}$ is incommensurate (i.e., if none of the frequencies ω_i may be obtained as a linear combination, with integer coefficients, of the remaining frequencies).

The first-order sensitivity indices are computed by evaluating the coefficients A_j and B_j for the fundamental frequencies $\{\omega_i\}$ and their higher harmonics $p\omega_i$ $(p = 1,2,\ldots)$. If the frequencies $\{\omega_i\}$ are integers, the contribution to the total variance $Var(R)$ coming from the variance D_i corresponding to parameter α_i is approximately obtained as

$$D_i \cong 2 \sum_{p=1}^{M} \left(A_{p\omega_i}^2 + B_{p\omega_i}^2 \right), \tag{I.A.29}$$

where M is the maximum harmonic taken into consideration (usually $M \leq 6$). The ratio of the partial variance D_i to the total variance $Var(R)$ provides the so-called first-order sensitivity index. The minimum sample size required to compute D_i is $(2M\omega_{\max} + 1)$, where $\omega_{\max}$ is the maximum frequency in the set $\{\omega_i\}$ (see, e.g., Saltelli et al., 1999). Furthermore, the frequencies that do not belong to the set $\{p_1\omega_1, p_2\omega_2, \ldots, p_I\omega_I\}$ for $(p_i = 1,2,\ldots,\infty)$, and for any $(i = 1,2,\ldots,I)$, contain information about the residual variance $[Var(R) - D_i]$ that is not accounted for by the first-order indices. Saltelli et al. have proposed a

method that extracts information regarding this residual variance in $(I \times N_S)$ computations, where N_S is the respective sample size.

A related class of variance-based methods has its roots in a theorem by Kolmogorov that states that any multivariate function, $f(x_1, x_2, \ldots, x_n)$, defined in the unit n-dimensional cube $[0,1]^n$, can be written as a linear superposition of univariate functions, $h_j(x_i)$, of the form

$$f(\mathbf{x}) \equiv f(x_1, x_2, \ldots, x_n) = \sum_{j=1}^{2n+1} g\left[a_1 h_j(x_1) + a_2 h_j(x_2) + \cdots + a_n h_j(x_n)\right], \quad \text{(I.A.30)}$$

where the functions $h_j(x_i)$ are continuous (but highly nonsmooth). Although Kolmogorov's expansion shown in Eq. (I.A.30) is seldom used in practice for interpolation and/or approximation of multivariate functions, it has inspired the development of several (somewhat) more practical algorithms for representing multivariate functions, such as the projection pursuit algorithms (see, e.g., Stone, 1982, 1985), multilayer perceptrons (Parker, 1985), Sobol's method (1993), and ANOVA-like decompositions (see, e.g., Archer et al., 1997), which can also be used for uncertainty and sensitivity analysis.

Perhaps the most practical of the methods mentioned above is a method due to Sobol', in which the multivariate function $f(x_1, x_2, \ldots, x_n)$ is decomposed into summands of increasing dimensionality of the form

$$f(x_1, x_2, \ldots, x_n) = f_0 + \sum_{i=1}^{n} f_i(x_i) + \sum_{1 \le i < j \le n} f_{ij}(x_i, x_i) + \cdots + f_{12\ldots n}(x_1, x_2, \ldots, x_n). \quad \text{(I.A.31)}$$

The decomposition in Eq. (I.A.31) is unique, and has the following properties:
(i) the integrals of any summand over any of its own variables is zero, i.e.,

$$\int_0^1 f_{i_1 i_2 \ldots i_n}(x_{i_1}, x_{i_2}, \ldots, x_{i_n}) dx_{i_m} = 0, \quad \text{if} \quad 1 \le m \le n, \quad \text{(I.A.32)}$$

(ii) the summands are orthogonal, i.e.,

$$\int_{[0,1]^n} f_{i_1 i_2 \ldots i_n} f_{j_1 j_2 \ldots j_m} d\mathbf{x} = 0, \quad \text{if} \quad (i_1, i_2, \ldots, i_n) \ne (j_1, j_2, \ldots, j_m), \quad \text{(I.A.33)}$$

(iii) f_0 is a constant, i.e.,

$$f_0 = \int_{[0,1]^n} f(\boldsymbol{x}) d\boldsymbol{x}. \tag{I.A.34}$$

By squaring Eq. (I.A.31) and integrating the resulting expression over the unit cube $[0,1]^n$, the following relation is obtained for the total variance D of $f(\boldsymbol{x})$:

$$D \equiv \int_{[0,1]^n} f^2(\boldsymbol{x}) d\boldsymbol{x} - f_0^2 = \sum_{i=1}^{n} D_i + \sum_{1 \le i < j \le n} D_{ij} + \cdots + D_{12\ldots n}, \tag{I.A.35}$$

where the partial variances of $f(\boldsymbol{x})$ are defined as

$$D_{i_1 i_2 \ldots i_m} = \int_0^1 \cdots \int_0^1 f_{i_1 i_2 \ldots i_m}\left(x_{i_1}, x_{i_2}, \ldots, x_{i_m}\right) dx_{i_1} \ldots dx_{i_m}, \quad \text{for } 1 \le i_1 < \ldots < i_m \le n,\ m = 1, \ldots, n. \tag{I.A.36}$$

The sensitivity indices are defined as

$$S_{i_1 i_2 \ldots i_m} \equiv D_{i_1 i_2 \ldots i_m} / D, \quad \text{for } 1 \le i_1 < \ldots < i_m \le n,\ m = 1, \ldots, n. \tag{I.A.37}$$

The first-order sensitivity index, S_i, for the parameter x_i indicates the fractional contribution of x_i to the variance D of $f(\boldsymbol{x})$; the second-order sensitivity index, $S_{ij}, (i \ne j)$, measures the part of the variation in $f(\boldsymbol{x})$ due to x_i and x_j that cannot be explained by the sum of the individual effects of x_i and x_j; and so on. Note also that Eqs. (I.A.36) and (I.A.37) imply that

$$\sum_{i=1}^{n} S_i + \sum_{1 \le i < j \le n} S_{ij} + \cdots + S_{12\ldots n} = 1. \tag{I.A.38}$$

I.A.5. Design of Experiments and Screening Design Methods

Design of Experiments (*DOE*) was first introduced by Fischer (1935), and can be defined as the process of selecting those combinations of parameter values, called *design points*, which will provide the most information on the input-output relationship embodied by a model in the presence of parameter variations. However, the basic question underlying *DOE* is often a circular one: if the response function were known, then it would be easy to select the optimal design

points, but the response is actually the object of the investigation, to begin with! Often used in practice is the so-called *Factorial Design* (*FD*), which aims at measuring the additive and interactive effects of input parameters on the response. A *FD* simulates all possible combinations of assigned values, l_i, called *levels*, to each (uncertain) system parameter α_i. Thus, even though a *FD* can account for interactions among parameters, the computational cost required by a *FD* is $l_1 l_2 \ldots l_I$, where I denotes the total number of parameters in the model; such a computational effort is prohibitively high for large-scale systems. A useful alternative is the *Fractional Factorial Design* (*FFD*) introduced by Box (1987), which assumes *a priori* that higher-order interactions between parameters are unimportant.

Screening design methods refer to preliminary numerical experiments designed to identify the parameters that have the largest influence on a particular model response. The objective of screening is to arrive at a *short list* of important factors. In turn, this objective can only be achieved if the underlying numerical experiments are judiciously designed. An assumption often used as a working hypothesis in screening design is the assumption that the number of parameters that are truly important to the model response is small by comparison to the total number of parameters underlying the model. This assumption is based on the idea that the influence of parameters in models follows Pareto's law of income distribution within nations, characterized by a few, very important parameters and a majority on noninfluential ones. Since screening designs are organized to deal with models containing very many parameters, they should be computationally economical. There is an inevitable tradeoff, however, between computational costs and information extracted from a screening design. Thus, computationally economical methods often provide only qualitative, rather than quantitative information, in that they provide a parameter importance ranking rather than a quantification of how much a given parameter is more important than another.

Falling within the simplest class of screening designs are the so-called *one-at-a-time* (*OAT*) experiments, in which the impact of changing the values of each parameter is evaluated in turn (Daniel, 1973). The *standard OAT* experiment is defined as the experiment that uses *standard* or *nominal* values for each of the I parameters underlying the model. The combination of nominal values for the I parameters is called the *control experiment* (or *scenario)*. Two extreme values are then selected to represent the range of each of the I parameters. The nominal values are customarily selected at the midway between the two extremes. The magnitudes of the *residuals*, defined as the difference between the perturbed and nominal response (output) values, are then compared to assess which factors are most significant in affecting the response.

Although the strategy described above is often used in practice, it is not the only one; according to Daniel, *OAT* designs can be classified into five categories, as follows: (i) *standard OAT* designs, which vary one factor from a

standard condition; (ii) *strict OAT* designs, which vary one factor from the condition of the last preceding experimental run; (iii) *paired OAT* designs, which produce two observations and, therefore, one simple comparison at a time; (iv) *free OAT* designs, which make each new computation under new conditions; and (v) *curved OAT* designs, which produce a subset of results by varying only one parameter that is easy to vary. In general, the number of model evaluation required for an *OAT* design is of the order of $(2I+1)$ model computations. Refinements such as proposed by Kleijnen (1998) require only half (roughly) as many computations, while providing arguably more accurate estimators of the main effects.

Since classical *OAT* cannot provide information about interactions between parameters, the model's behavior can only be assessed in a small interval around the "control" scenario. In other words, the classical *OAT* experiments yield information only about the system's response *local* behavior. Therefore, the results of a classical *OAT* experiment are meaningful only if the model's input-output relation can be adequately represented by a first order polynomial in the model's parameters. If the model is affected by nonlinearities (as is often the case in practice), then parameter changes around the "control" scenario would provide drastically different "sensitivities," depending on the chosen "control" scenario.

To address this severe limitation of the classical *OAT* designs, Morris (1991) has proposed a *global OAT* design method, by covering the entire space in which the parameters may vary, independently of the specific initial "control" scenario one may commence the experiment with. A global *OAT* design assumes that the model is characterized by a large number of parameters and/or is computationally expensive (regarding computational time and computational resources) to run. The range of variation of each component of the vector $\boldsymbol{\alpha}$ of parameters is standardized to the unit interval, and each component is then considered to take on p values in the set $\{0,(p-1)^{-1},2(p-1)^{-1},\ldots,1\}$, so that the region of experimentation becomes an I-dimensional p-level grid. An *elementary effect* of the i^{th}-parameter at a point $\boldsymbol{\alpha}$ is then defined as $d_i(\boldsymbol{\alpha}) \equiv [\boldsymbol{R}(\alpha_1,\ldots,\alpha_{i-1},\alpha_i+\Delta,\alpha_{i+1},\ldots,\alpha_I)\text{-}\boldsymbol{R}(\boldsymbol{\alpha})]/\Delta$, where Δ is a predetermined multiple of $1/(1-p)$, such that $\alpha_i+\Delta$ is still within the region of experimentation. A finite distribution F_i of elementary effects for the i^{th}-parameter is obtained by sampling $\boldsymbol{\alpha}$ from within the region of experimentation. The number of elements for each F_i is $p^{k-1}[p-\Delta(p-1)]$. The distribution F_i is then characterized by its *mean* and *standard deviation*. A high mean indicates a parameter with an important overall influence on the response; a high standard deviation indicates either a parameter interacting with other parameters or a parameter whose effect is nonlinear.

In its simplest form, the total computational effort required for a random sample of r values from each distribution F_i is $n = 2rI$; each elementary effect requires the evaluation of the response $\boldsymbol{R}(\boldsymbol{\alpha})$ *twice*. For large-scale models, therefore, the *OAT* design of Morris requires a relatively high computational effort. Furthermore, a *global OAT* design can only provide a qualitative (but not quantitative) indication of the interactions of a parameter with the rest of the model; it cannot provide specific information about the identity of the interactions, and individual interactions among parameters cannot be estimated.

The alternative *systematic fractional replicate design* (*SFRD*), proposed by Cotter (1979), does not require any prior assumptions about interactions. For a model with I parameters, a *SFRD* involves the following steps: (i) one model-computation with all parameters at their low levels; (ii) I model computations with each parameter, in turn, at its upper level, while the remaining $(I-1)$ parameters remain at their low levels; (iii) I model computations with each parameter, in turn, at its low level, while the remaining $(I-1)$ parameters remain at their upper levels; (iv) one model-computation with all parameters at their upper levels. Thus, a *SFRD* requires $2(I+1)$ computations. Denoting by $(R_0, R_1, \ldots, R_I, R_{I+1}, \ldots, R_{2I}, R_{2I+1})$ the values of the responses computed in steps (i)-(iv) within a *SFRD*, the measures $M(j) \equiv |C_e(j)| + |C_o(j)|$, where the quantities $|C_e(j)|$ and $|C_o(j)|$ are defined as

$$|C_e(j)| \equiv \left[\left(R_{2I+1} - R_{I+j}\right) - \left(R_j - R_0\right)\right]/4 \text{ and}$$
$$|C_o(j)| \equiv \left[\left(R_{2I+1} - R_{I+j}\right) + \left(R_j - R_0\right)\right]/4$$

respectively, are used to estimate the order of importance of the I parameters α_i.

It is apparent from the above definitions that the measures $M(j)$ may fail when a parameter induces cancellation effects on the response; such a parameter would remain undetected by a *SFRD*. Worse yet, it is not possible to protect oneself *a priori* against such occurrences. Furthermore, a *SFRD* is not sufficiently precise, since the above definitions imply that, for one replicate, the variances are $\text{var}[C_o(j)] = \text{var}[C_e(j)] = \sigma^2/4$, whereas a fractional replicate with n-computations would allow the estimations of parameter effects (on the response) with variances σ^2/n.

In addition to screening designs that consider each parameter individually, the (originally) individual parameters can be clustered into *groups* that are subsequently treated by *group screening designs*. Perhaps the most efficient modern group screening designs techniques are the *iterated fractional factorial*

design (*IFFD*) proposed by Andres and Hajas (1993), and the *sequential bifurcation* (*SB*) technique proposed by Bettonvil (1990). In principle, the *IFFD* requires fewer model computations, n, than there are parameters, I. To identify an influential parameter, an *IFFD* investigates the groups through a fractional factorial design; the procedure is then repeated with different random groupings. Influential parameters are then sought at the intersection of influential groups. The *IFFD* samples three levels per parameter, designated low, middle, and high, while ensuring that the sampling is balanced: different combinations of values for two or three parameters appear with equal frequency. Hence, *IFFD* can be considered as a composite design consisting of multiple iterations of a basic *FFD*.

The *sequential bifurcation* (*SB*) design combines two design techniques, namely: (i) the *sequential* design, in which the parameter combinations are selected based on the results of preceding computations, and (ii) *bifurcation*, in which each group that seems to include one or more important parameters is split into two subgroups of the same size. However, the *SB* design must *a priori* assume that the analyst knows the *signs* of the effects of the individual parameter, in order to ensure that effects of parameters assigned to the same group do not cancel out. Furthermore, the sequential nature of *SB* implies a more cumbersome data handling and analysis process than other screening design methods. To assess the effects of *interactions* between parameters, the number of *SB* computations becomes the *double* of the number of computations required to estimate solely the "main effects;" *quadratic effects* cannot be currently analyzed with the *SB* design technique.

The screening designs surveyed in the foregoing are the most representative and the widest used methods aimed at identifying at the outset, in the initial phase of sensitivity and uncertainty analysis, the (hopefully not too many!) important parameters in a model. Each type of design has its own advantages and disadvantages, which can be summarized as follows: the advantages of *OAT* designs are: (i) no assumption of a monotonic input-output relation; (ii) no assumption that the model contains only "a few" important parameters; and (iii) the computational cost increases linearly with the number of parameters. The major disadvantage of *OAT* designs is the neglect of parameter interactions. Although such an assumption drastically simplifies the analysis of the model, it can rarely be accepted in practice. This simplifying assumption is absent in the *global OAT* design of Morris, which aims at determining the parameters that have (i) negligible effects, (ii) linear and additive effects, and (iii) nonlinear or interaction effects. Although the *global OAT* is easy to implement, it requires a high computational effort for large-scale models, and provides only a qualitative (but not quantitative) indication of the interactions of a parameter with the rest of the model; the *global OAT* cannot provide specific information about the identity of individual parameter interactions.

The *SFRD* does not require *a priori* assumptions about parameter interactions and/or about which few parameters are important. Although the *SFRD* is

relatively efficient computationally, it lacks precision and cannot detect parameters whose effects cancel each other out. The *IFFD* estimates the main and quadratic effects, and two-parameter interactions between the most influential parameters. Although the *IFFD* requires fewer computations than the total number of model parameters, the *IFFD* gives good results only if the model's response is actually influenced by only a few truly important parameters. The *SB* design is simple and relatively cost effective (computationally), but assumes that (i) the signs of the main effects are *a priori* known, and (ii) the model under consideration is adequately described by two-parameter interactions.

I. B. DETERMINISTIC METHODS

I.B.1. Deterministic Methods for Local Sensitivity Analysis

In large-scale, complex models, the importance of parameters is not *a priori* obvious, and may often be counterintuitive. To analyze such complex models, information about the slopes of the model's response at a given set of nominal parameter values in parameter space is of paramount importance. The exact slopes are provided by the local partial functional derivatives $\partial R/\partial \alpha_i$ of the response R with respect to the model parameters α_i; these local partial functional derivatives are called the *local sensitivities* of the model's response to parameter variations.

The simplest way of estimating local sensitivities is by *recalculations of the model's response*, using parameter values that deviate by small amounts, $\delta\alpha_i$, of the order of 1%, from their nominal values α_i^0. The sensitivities are then estimated by using a finite difference approximation to $\partial R/\partial \alpha_i$ of the form

$$\left\{\frac{\partial R}{\partial \alpha_i}\right\}_{\boldsymbol{\alpha}^0} = \frac{R\left(\alpha_1^0,\ldots,\alpha_i^0+\partial\alpha_i,\ldots,\alpha_I^0\right)-R\left(\alpha_i^0\right)}{\partial\alpha_i}, \quad (i=1,\ldots,I).$$

This procedure, occasionally called the "*brute-force method*," requires $(I+1)$ model computations; if central differences are used, the number of model computations could increase up to a total of $2I$. Although this method is conceptually simple to use and requires no additional model development, it is slow, relatively expensive computationally, and involves a trial-and-error process when selecting the parameter perturbations $\delta\alpha_i$. *Note that erroneous sensitivities will be obtained if: (i) $\delta\alpha_i$ is chosen to be too small,* in which case the computational round-off errors will overwhelm the correct values, and (ii)

the parameter dependence is nonlinear and $\delta\alpha_i$ *is chosen too large*, in which case the assumption of local linearity is violated.

Local sensitivities can be computed exactly only by using deterministic methods that involve some form of differentiation of the system under investigation. The (comparatively few) deterministic methods for calculating sensitivities exactly are as follows: the *direct method* (including its *decoupled direct method* variant), the *Green's Function method*, the *Forward Sensitivity Analysis Procedure* (*FSAP*), and the *Adjoint Sensitivity Analysis Procedure (ASAP)*. The so-called *direct method* has been applied predominantly to systems involving differential and/or algebraic equations describing chemical kinetics (including combustion kinetics) and molecular dynamics. This method involves differentiation of the system of equations underlying the model with respect to each parameter in the model. The sensitivity to each parameter is then computed by solving the respective differentiated system. The most advanced and computationally economical version of the direct method is the *decoupled direct method* (*DDM*), originally introduced by Dunker (1981, 1984), in which the Jacobian matrix needed to solve the original system at a given time-step is also used to solve the sensitivity equations at the respective time-step, before proceeding to solve both the original and sensitivity systems at the next time-step. Note that the computational effort increases linearly with the number of parameters.

Another method occasionally used for computing sensitivities for models governed by first-order derivatives in time is the *Green function method* (*GFM*). This method commences by differentiating the underlying model with respect to its initial conditions to obtain a Green's function, which is subsequently convoluted with the matrix of parameter derivatives, and is finally integrated in time to obtain the respective time-dependent sensitivities. There are several variants of the *GFM*; the integrated Magnus version (*GFM/AIM*) proposed by Kramer et al. (1981) appears to be, computationally, the most efficient *GFM*. In practice, though, the *GFM* is seldom used, since it is computationally more expensive and considerably more difficult to implement than the *DDM*.

As shown by Cacuci (1981), the most general and comprehensive way of defining *local* sensitivities for general operators (in the sense of nonlinear functional analysis) is in terms of the first *Gâteaux-differential* of the system's response, at the nominal value of the system's dependent variables and parameters. Based on the concept of Gâteaux-differentials, Cacuci has developed two procedures for calculating the local sensitivities for any type of large-scale nonlinear systems, namely: the *Forward Sensitivity Analysis Procedure* (*FSAP*) and the *Adjoint Sensitivity Analysis Procedure* (*ASAP*). As discussed in Volume I of this book, the scope of both the *FSAP* and the *ASAP* is to calculate *exactly and efficiently* the local sensitivities of the system's response to variations in the system's parameters, around their nominal values.

The *FSAP* constitutes a generalization of the *decoupled direct method* (*DDM*), since the concept of *Gâteaux*-differential (which underlies the *FSAP*) constitutes

the generalization of the concept of total-differential in the calculus sense, which underlies the *DDM*. Notably, the Gâteaux-differential exists for operators and generalized functions (e.g., distributions) that are not continuous in the ordinary calculus-sense, and therefore do not admit the "nice" derivatives required for using the *DDM*. As expected, the *FSAP* reduces to the *DDM*, whenever the continuity assumptions required by the *DDM* are satisfied. Finally, even though the *FSAP* represents a generalization of the *DDM*, the *FSAP* requires the *same* computational and programming effort to develop and implement as the *DDM*. Hence, just as the *DDM*, the *FSAP* is advantageous to employ only if the number of different responses of interest for the problem under consideration exceeds the number of system parameters and/or parameter variations to be considered. Otherwise, the use of either the *FSAP* or the *DDM* becomes impractical for large systems with many parameters, because of the very large demand on computational resources.

For large-scale systems, in which the number of system parameters and/or parameter variations to be considered exceeds the number of responses of interest, the *ASAP* is, by far, the most advantageous method to employ, even though it can only be implemented after an appropriately constructed adjoint sensitivity system is already available. The remarkable efficiency of the *ASAP* stems from the fact that the adjoint sensitivity system is linear in the adjoint function, and is independent of any parameter variations. Hence, the adjoint sensitivity equation needs to be solved only once, for each response, in order to obtain the adjoint function. In particular, if the original model is linear in the state (i.e., dependent) variables, then the adjoint sensitivity equation can be solved independently of the original model. In turn, once the adjoint function has been calculated, it is used to obtain the sensitivities to all system parameters, by simple quadratures, without needing to solve repeatedly differential and/or integral equations. Thus, for the large-scale systems, with many parameters, as usually encountered in practice, the *ASAP* is the most efficient method to use for sensitivity analysis.

The exact local sensitivities obtained by using deterministic methods can be used for the following purposes: (i) understand the system by highlighting important data; (ii) eliminate unimportant data; (iii) determine effects of parameter variations on system behavior; (iv) design and optimize the system (e.g., maximize availability/minimize maintenance); (v) reduce over-design; (vi) prioritize the improvements effected in the respective system; (vii) prioritize introduction of data uncertainties; (viii) perform local uncertainty analysis by using the "propagation of errors" method, as mentioned in Volume I of this book, and as will be described briefly in the next section.

The uses of deterministically computed sensitivities for highlighting data importance, determining effects of parameter variations, and design optimization have been illustrated in the literature on systems engineering (see, e.g., the books by: Kokotovic, 1972, Tomovic and Vucobratovic, 1972, Cruz, 1973, Frank, 1978, Fiacco, 1984, Deif, 1986, Eslami, 1994, Rosenwasser and Yusupov,

2000), chemical kinetics (see, e.g., the review article by Turanyi, 1990), core reactor physics (see, e.g., Greenspan, 1982, Gandini, 1987, Lillie et al., 1988, Ronen, 1988, and references therein), reactor thermal-hydraulics and neutron dynamics (Cacuci and Wacholder, 1982, Cacuci, Maudlin and Parks, 1983), two-phase flows with phase transition (Cacuci and Ionescu-Bujor, 2000, Ionescu-Bujor and Cacuci, 2000), geophysical fluid dynamics (see, e.g., Cacuci and Hall, 1984, Navon et al., 1992, Zhou et al., 1993, Navon, 1998), and, more recently, reliability and risk analysis (Cacuci and Ionescu-Bujor, 2002, and Ionescu-Bujor and Cacuci, 2003).

I.B.2. Deterministic Methods for Local Uncertainty Analysis

For large-scale systems, it is not possible to find an explicit, analytical solution for the probability distribution function, $PDF(R)$, of the response R. Therefore, the "*Moment Matching*" method is customarily employed to approximate $PDF(R)$, as follows: (i) given the PDF's or the (central) moments $m_j(\alpha_i)$, $(i=1,\ldots,I)$, of the system parameters α_i, calculate the first four (central) moments $m_1(R)=E(R)$, $m_2(R)$, $m_3(R)$, $m_4(R)$ of the response R; and (ii) approximate the unknown $PDF(R)$ by $P(R;\beta;\gamma)$, a two-parameter PDF that has the same four moments, $m_i(R), i=1,\ldots,4$, as calculated above. Note that $m_1(R)=E(R)$ and $m_2(R)$ determine the two parameters $(\beta;\gamma)$ of $P(R;\beta;\gamma)$, while $m_3(R)$ and $m_4(R)$ determine the shape (skewness and kurtosis) of $P(R;\beta;\gamma)$.

The current state-of-the-art methods for obtaining the moments, $m_i(R), i=1,\ldots,4$, of the $PDF(R)$ are *Statistical Methods* and the "*Propagation of Errors*" (also known as the *Propagation of Moments* or the *Taylor-Series* Method, as pesented in Volume I, Section III.F). As has been detailed in Section I.A. in this Volume, all statistical methods employ simulations to: (i) generate randomly a sample of N m-tuples $\{z_{ij}\}$, $(i=1,\ldots,m;\ j=1,\ldots,N)$, where z_{ij} denotes the j^{th} random value of the i^{th} input variable, x_i; (ii) solve the model N-times for each m-tuple z_{ij} to obtain a sample of N values of the system response R; and (iii) from this sample, estimate the moments $m_i(R), (i=1,\ldots,4)$, confidence limits, and the approximate *PDF*, $P(R;\beta;\gamma)$, of R. In principle, statistical methods are conceptually easy to use and require little additional modeling. However, as discussed in Section I.A, above, the statistical methods have two major inherent drawbacks, as follows: (i) since many thousands of simulations are needed, statistical methods are at best expensive (for small systems), or, at worst, impracticable (e.g., for large-scale time-

dependent systems); and (ii) since the response sensitivities and parameter uncertainties are amalgamated, improvements in parameter uncertainties cannot be directly propagated to improve response uncertainties; rather, the entire set of simulations must be repeated anew in order to obtain improved response uncertainties.

The deterministic alternative to statistical methods is the "*propagation of errors*" method for uncertainty analysis, which has been described in detail in Section III.F. of Volume I. From the considerations presented there, we recall that the major advantages of using the "propagation of moments" method are: (i) if all sensitivities are available, then all of the objectives of sensitivity analysis (enumerated above) can be pursued efficiently and exhaustively; and (ii) since the response sensitivities and parameter uncertainties are obtained separately from each other, improvements in parameter uncertainties can immediately be propagated to improve the uncertainty in the response, without the need for expensive model recalculations. On the other hand, the major disadvantage of the "propagation of moments" method is that the sensitivities need to be calculated *a priori*; such calculations are extremely expensive, particularly for large (and/or time-dependent) systems, unless they are performed by using the adjoint sensitivity analysis procedure (*ASAP*), for nonlinear systems. It is important to emphasize that the "propagation of moments" equations are used both for processing experimental data obtained from indirect measurements and also for performing statistical analysis of computational models. The "propagation of moments" equations provide a systematic way of obtaining the uncertainties in computed results, arising not only from uncertainties in the parameters that enter the respective computational model but also from the numerical approximations themselves.

The "propagation of moments" method has been used extensively for evaluation of experimental data obtained from indirect experiments (see, e.g., Shapiro and Gross, 1981, Smith, 1991, Cowan, 1998, Rabinovich, 2000). However, there are comparatively few works that use the "propagation of moments" method in conjunction with deterministically obtained sensitivities for performing local uncertainty analysis of large-scale systems. The most notable applications of using the "propagation of moments" together with sensitivities obtained *a priori* by means of the *ASAP* were in the fields of dosimetry (see, e.g., Lillie et al., 1988), and core reactor physics (see, e.g., Ronen, 1988, and references therein); more recently, Cacuci (2003) has provided an illustrative example of using the "propagation of moments" together with sensitivities obtained *a priori* by means of the *ASAP* for reliability and risk analysis.

I.B.3. Deterministic Methods for Extending the Use of Local Sensitivities; Global Deterministic Sensitivity Analysis

Several techniques have been proposed (see, e.g., the reviews by Greenspan, 1982, Ronen, 1988, and references therein) for calculating the higher-order response derivatives with respect to the system's parameters. However, none of these techniques has proven routinely practicable for large-scale problems. This is because the systems of equations that need to be solved for obtaining the second (and higher) order Gâteaux-differentials of the response and system's operator equations are very large and depend on the perturbation $\delta\boldsymbol{\alpha}$. Thus, even the calculation of the second-order Gâteaux-differentials of the response and system's operator equations is just as difficult as undertaking the complete task of computing the exact value of perturbed response $R\left(\alpha_1^0 + \delta\alpha_1, \ldots, \alpha_k^0 + \delta\alpha_k\right)$.

Instead of computing higher order response derivatives, Kramer et al. (1984) have proposed the so-called *feature sensitivity analysis* for nonlinear probing of a larger region in the parameter-space. This method considers that the response $\boldsymbol{R}(\boldsymbol{r}, t; \boldsymbol{\alpha})$ can be written in the equivalent form $\boldsymbol{R}(\boldsymbol{r}, t; \boldsymbol{\alpha} + \Delta\boldsymbol{\alpha}) \equiv \boldsymbol{P}[\boldsymbol{r}, t; \beta(\boldsymbol{\alpha} + \Delta\boldsymbol{\alpha})]$, where $\beta(\boldsymbol{\alpha}) \equiv (\beta_1, \beta_2, \ldots)$ is a vector whose components are the "feature" parameters, and where the form of $\boldsymbol{P}[\boldsymbol{r}, t; \beta(\boldsymbol{\alpha} + \Delta\boldsymbol{\alpha})]$ is assumed to be explicitly known. In such a case, it is possible to consider the linear expansion $\beta(\boldsymbol{\alpha} + \Delta\boldsymbol{\alpha}) \cong \beta(\alpha) + \Delta\alpha\, \partial\beta/\partial\alpha$, which can be substituted in the expression of $\boldsymbol{R}(\boldsymbol{r}, t; \boldsymbol{\alpha} + \Delta\boldsymbol{\alpha})$ to obtain a nonlinear scaling expression with respect to the parameters $\Delta\alpha$. This way, it is possible to enlarge (somewhat) the investigation of the response to a larger neighborhood of the nominal parameter values α_k^0. So far, feature sensitivity analysis method has been used only for applications presented by its authors.

It appears that the only genuinely global deterministic method for sensitivity analysis is the *Global Adjoint Sensitivity Analysis Procedure* (*GASAP*) proposed by Cacuci (1990), which was presented in Chapter VI of Volume I. Instead of attempting to extend the validity of local Taylor series, Cacuci has formulated the *GASAP* by introducing a global homotopy-based concept for exploring the entire phase-space spanned by the parameters and state-variables. As shown in Volume I, the *GASAP* yields information about the important global features of the physical system, namely the critical points of $R(\boldsymbol{\alpha})$ and the bifurcation branches and/or turning points of the system's state variables.

I. C. COMPUTATIONAL CONSIDERATIONS

Statistical uncertainty and sensitivity analysis methods aim at assessing the contributions of parameters' uncertainties in contributing to the overall uncertainty of the model response (output). The relative magnitude of this uncertainty contribution is assigned a measure of the statistical sensitivity of the response uncertainty to the respective parameter, and this measure is also used to rank the importance of the respective parameter. The simplest conceptual attempt at "sensitivity analysis" is to use screening design methods to identify a short list of parameters that have the largest influence on a particular model response. The fundamental assumption underlying all screening design methods is that the influence of parameters in models follows Pareto's law of income distribution within nations, i.e., the number of parameters that are truly important to the model response is small by comparison to the total number of parameters in the model. There is an inevitable tradeoff between the computational costs and the information extracted from a screening design. Thus, computationally economical methods provide only qualitative, rather than quantitative information, in that they provide a parameter importance ranking rather than a quantification of how much a given parameter is more important than another. Furthermore, the importance of parameters in large-scale, complex models is seldom *a priori* obvious (and may even be counterintuitive). Hence, *screening design methods should be used cautiously*, since they may be *a priori* inadequate to identify the truly important parameters.

On the other hand, "sampling-based uncertainty and sensitivity analysis" is performed in order to ascertain if model predictions fall within some region of concern ("uncertainty in model responses due to uncertainties in model parameters") and to identify the dominant parameters in contributing to the response uncertainty ("statistical sensitivity analysis"). It is particularly important to recall from Section I.A that the very first step (of the five specific steps) of "sampling-based uncertainty and sensitivity analysis," in which subjective uncertainties are assigned through expert review processes, is crucial to the results produced by the subsequent steps in the analysis. This is because *the results of sampling-based uncertainty and sensitivity analysis depend entirely on the distributions assigned to the sampled parameters; hence, the proper assignment of these distributions is essential to avoid producing spurious results.* Furthermore, the statistical "sensitivity analysis" of the response to the parameters is performed in the fifth (and last) step of these procedures (by using scatter plots, regression analysis, partial correlation analysis, etc.). Therefore, it is also important to note that *correlated variables introduce unstable regression coefficients* when performing the "statistical sensitivity analysis" part, because these coefficients become sensitive to the specific variables introduced into the regression model. In such situations, the regression coefficients of a regression model that includes *all* of the parameters are likely to give misleading indications of parameter "sensitivities." If several input parameters are suspected

(or known) to be highly correlated, it is usually recommended to transform the respective parameters so as to remove the correlations or, if this is not possible, to analyze the full model by using a sequence of regression models with all but one of the parameters removed, in turn.

From the material presented in the preceding Sections, it has also become apparent that all statistical uncertainty and sensitivity analysis procedures commence with the "uncertainty analysis" stage, and only subsequently proceed to the "sensitivity analysis" stage; this path is the exact reverse of the conceptual path underlying the methods of deterministic sensitivity and uncertainty analysis where the sensitivities are determined prior to using them for uncertainty analysis. Without any *a priori* assumption regarding the relationship between the parameters and the response, the construction of a full-space statistical uncertainty analysis requires $O\left(s^I\right)$ computations, where s denotes the number of sample values for each parameter and I denotes the number of parameters. If a local polynomial regression is used, Stone has shown that the rate of convergence is $s_N = N^{-p/(2p+I)}$, where N denotes the number of sample points, p denotes the degree of smoothness of the function representing the response in terms of the parameters, and I denotes the number of parameters. This relation indicates that the parameters-to-response mapping (function) can be approximated to a resolution of s^{-1} with $O\left(s^{I/p}\right)$ sample points. The *FAST* method appears to be the most efficient of the global statistical methods, needing $I\left(8\omega_i + 1\right)N_r$ computations for each frequency, where N_r denotes the number of replicates. For example, if the response is a function of 8 parameters, and if the sample size is 64, then Sobol's method requires 1088 model evaluations, while the *FAST* method requires 520 model evaluations; when the sample size increases to 1024, then Sobol's method requires 17 408 model evaluations, while the *FAST* method requires 8200 model evaluations. It becomes clear that even for the most efficient statistical methods (e.g., the *FAST* method) the number of required model evaluations becomes rapidly impractical for realistic, large-scale models involving many parameters. Thus, since many thousands of simulations are needed, statistical methods are at best expensive (for small systems), or, at worst, impracticable (e.g., for large time-dependent systems). Furthermore, since the response sensitivities and parameter uncertainties are inherently amalgamated, improvements in parameter uncertainties cannot be directly propagated to improve response uncertainties; rather, the entire set of simulations must be repeated anew. Currently, a general-purpose "fool-proof" statistical method for analyzing correctly mathematical models of physical processes involving highly correlated parameters does not seem to exist, so that particular care must be used when interpreting regression results for such models.

Summarizing the computational effort required by the various deterministic methods for computing local sensitivities, we recall that the "brute-force

method" is conceptually simple to use and requires no additional model development, but it is slow, relatively expensive computationally, and involves a trial-and-error process when selecting the parameter perturbations $\delta\alpha_i$, in order to avoid erroneous results for the computed sensitivities. The "brute-force method" requires $(I+1)$ model computations; if central differences are used, the number of model computations could increase up to a total of $2I$. Of the deterministic methods for obtaining the local first-order sensitivities exactly, the Green's function method is the most expensive computationally. The *DDM* requires at least as many model evaluations as there are parameters, and that the computational effort increases linearly with the number of parameters. Since it uses Gateaux-differentials, the *FSAP* represents a generalization of the *DDM*; nevertheless, the *FSAP* requires the *same* computational and programming effort to develop and implement as the *DDM*. Hence, just as the *DDM*, the *FSAP* is advantageous to employ only if the number of different responses of interest for the problem under consideration exceeds the number of system parameters and/or parameter variations to be considered. Otherwise, the use of either the *FSAP* or the *DDM* becomes impractical for large systems with many parameters, because the computational requirements become unaffordable.

By far the most efficient local sensitivity analysis method is the *ASAP*, but the *ASAP* requires development of an appropriate Adjoint Sensitivity System (or Adjoint Tangent Model). If this adjoint model is developed simultaneously with the original model, then the Adjoint Sensitivity System requires very little additional resources to develop. If, however, the Adjoint Sensitivity System is developed *a posteriori*, considerable skills may be required for its successful implementation and use. Note that the Adjoint Sensitivity System is independent of parameter variations, but depends on the response, which contributes the source-term for this system. Hence, the Adjoint Sensitivity System needs to be solved only once per response in order to obtain the adjoint function. Furthermore, the Adjoint Sensitivity System is linear in the adjoint function. In particular, for linear problems, the Adjoint Sensitivity System is independent of the original state-variables, which means that it can be solved independently of the original system. In summary, the *ASAP* is the most efficient method to use for sensitivity analysis of systems in which the number of parameters exceeds the number of responses under consideration.

It is important to emphasize that the "propagation of moments" equations are used both for processing experimental data obtained from indirect measurements and also for performing statistical analysis of computational models. The "propagation of moments" equations provide a systematic way of obtaining the uncertainties in computed results, arising not only from uncertainties in the parameters that enter the respective computational model but also from the numerical approximations themselves. The major advantages of using the "propagation of moments" method are: (i) if all sensitivities are available, then all of the objectives of sensitivity analysis (enumerated above) can be pursued

efficiently and exhaustively; and (ii) since the response sensitivities and parameter uncertainties are obtained separately from each other, improvements in parameter uncertainties can immediately be propagated to improve the uncertainty in the response, without the need for expensive model recalculations. On the other hand, the major disadvantage of the "propagation of moments" method is that the local sensitivities need to be calculated *a priori*; as we have already emphasized, such calculations are very expensive computationally, particularly for large (and/or time-dependent) systems. It hence follows that the ideal, most efficient overall methodology for performing local sensitivity and uncertainty analysis is to combine the *ASAP* (which would provide the local response sensitivities) with the "propagation of moments" method, to obtain the local response uncertainties.

Among the deterministic methods published thus far, the *GASAP* appears to be the only one capable of genuine *global* analysis; it is both exhaustive and computationally efficient, but its general utility for large-scale models is still untested at the time of this writing; in particular, it has not been tested on turbulent flows. Regarding future developments in sensitivity and uncertainty analysis, two of the outstanding issues, whose solution would greatly advance the state of overall knowledge, would be to: (i) develop the adjoint sensitivity analysis procedure (*ASAP*) for problems describing turbulent flows, and (ii) combine the *GASAP* with global statistical uncertainty analysis methods, striving to perform, efficiently and accurately, global sensitivity and uncertainty analyses for large-scale systems.

CHAPTER II

APPLICATIONS OF THE ADJOINT SENSITIVITY ANALYSIS PROCEDURE (ASAP) TO TWO-PHASE FLOW SYSTEMS

This Chapter presents applications of the adjoint sensitivity analysis procedure (*ASAP*) to transient one-dimensional two-phase flow problems modeled by well-posed quasi-linear partial differential equations (PDE's). The material in this chapter is structured in two main sections. Thus, Section II.A presents a self-contained formalism for sensitivity analysis of functional-type responses associated with two-phase flow models that comprise equations describing conservation of mass, momentum, and energy for practical one-dimensional, two-phase flow models. In particular, the characteristics of applying the *ASAP* to the so-called homogeneous equilibrium model (HEM) are analyzed in detail.

Section II.B presents the main aspects of implementing the *ASAP* for the RELAP5/MOD3.2 code, which are essentially the same as those generally described in Section II.A. The RELAP5/MOD3.2 code simulates the thermal-hydraulic characteristics of light water nuclear reactors (LWR) by using a one-dimensional, nonequilibrium, nonhomogeneous two-phase flow model, together with conservation equations for boron concentration and noncondensable gases. The RELAP5/MOD3.2 code actually solves the so-called "Numerically Convenient Set of Differential Equations" (REL/CDE), which is obtained from the basic differential equations that underlie the nonhomogeneous, nonequilibrium, one-dimensional two-fluid model. The REL/CDE are discretized by using a staggered-mesh in the spatial direction, and either a one-step ("nearly-implicit") or a two-step ("semi-implicit") discretization procedure in time. These discretization procedures yield a system of thirteen coupled nonlinear algebraic equations. Both the differential and the discretized forms of the REL/CDE are presented in Section II.B.1. Section II.B.2 highlights the application of the *ASAP* to both the REL/CDE and to the Discretized REL/CDE. Applying the *ASAP* yields the Differential Adjoint Sensitivity Model (ASM-REL/TF), which comprises nine coupled differential equations that are linear in the respective adjoint functions, and its discrete counterpart, the Discrete ASM-REL/TF, which comprises thirteen algebraic equations that are also linear in the respective discrete adjoint functions.

Section II.B.3 highlights the fundamentally important aspect of consistency between the differential and the corresponding discretized equations used for sensitivity analysis. In particular, the following consistency correspondences must be assured: (i) the Discretized Forward Sensitivity Model (FSM) must be consistent with the Differential FSM, if the *FSAP* is used; (ii) the Discretized Adjoint Sensitivity Model (ASM) must be consistent with the Differential ASM,

if the *ASAP* is used; and (iii) the Discretized (representation of the) Response Sensitivity must be consistent with the Integral (representation of the) Response Sensitivity both for the *FSAP* and for the *ASAP*, in which the Integral and the Discretized Response Sensitivity are represented in terms of the corresponding adjoint functions.

Section II.B.4 presents typical results that illustrate the verification of the numerical solution of the ASM-REL/TF corresponding to the two-fluid model with noncondensable(s) used in RELAP5/MOD3.2. This validation has been carried out by using sample problems involving: (i) liquid-phase only; (ii) gas-phase only; and (iii) two-phase mixture (of water and steam). Thus, the "Two-Loops with Pumps" sample problem supplied with RELAP5/MOD3.2 is used to verify the accuracy and stability of the numerical solution of the ASM-REL/TF when only the liquid-phase is present. By replacing the liquid (water) by gas (pure steam) but keeping the respective geometry, a modified "Two-Loops with Pumps" sample problem is obtained and used to verify the accuracy and stability of the numerical solution of the ASM-REL/TF when only the gas-phase is present. For the same verification purpose, a modified "Edwards Pipe" sample problem, in which only the gas-phase is present (thus describing the transient depressurization of a pipe filled with pure steam), is also used. Furthermore, the actual "Edwards Pipe" sample problem, also supplied with RELAP5/MOD3.2, is used to verify the accuracy and stability of the numerical solution of the ASM-REL/TF when both (i.e., liquid and gas) phases are present. The results obtained for these sample problems depict typical sensitivities of junction velocities and volume-averaged pressures to perturbations in initial conditions, and indicate that the numerical solution of the ASM-REL/TF is as robust, stable, and accurate as the original RELAP5/MOD3.2 computations. Finally, Section II.B.5 illustrates the role that sensitivities of the thermodynamic properties of water play for sensitivity analysis of thermal-hydraulic codes for light-water reactors.

II. A.ASAP FOR GENERIC TWO-PHASE FLOW PROBLEMS

This section presents a self-contained formalism for sensitivity analysis of functional-type responses associated with a well posed system of quasi-linear partial differential equations (PDE's) that describe transient one-dimensional, two-phase flow. The basic two-phase flow equations and their characteristics are presented in Sec. II.A.1. The sensitivity analysis formalism is developed in Sec. II.A.2 by applying the *ASAP* to the system of PDE's considered in Sec. II.A.1. The sensitivities are expressed in terms of adjoint functions, and the adjoint sensitivity system satisfied by these adjoint functions is explicitly constructed. The characteristics of the adjoint sensitivity system, which determine the solvability of this system, are investigated in Sec. II.A.3. This investigation shows that for a well-posed, two-phase flow problem modeled by a system of first-order *quasi-linear* PDE's of hyperbolic type, the corresponding adjoint

sensitivity system consists of a system of first-order *linear* PDE's of hyperbolic type that can always be formulated as a well-posed initial-value problem (IVP). Furthermore, the linear PDE's that constitute the adjoint sensitivity system have the same characteristics as the quasi-linear PDE's modeling the two-phase flow problem. This implies that whenever the original two-phase flow problem is solvable, the adjoint sensitivity system is also solvable, and, in principle, the same numerical methods can be used to solve both the original and the adjoint sensitivity system of PDE's.

II.A.1. Basic One-Dimensional Two-Phase Flow Equations

The basic principles of applying the *ASAP* to two-phase flow models can be illustrated by considering the governing equations that describe conservation of mass, momentum, and energy for practical one-dimensional, two-phase flow models. These conservation equations constitute a system of N (where $N \le 6$) coupled quasi-linear first-order PDE's, which can be represented in matrix form as

$$\boldsymbol{A}\frac{\partial \boldsymbol{U}}{\partial t} + \boldsymbol{B}\frac{\partial \boldsymbol{U}}{\partial x} = \boldsymbol{C}, \quad x \in \Omega, \quad t > 0 . \tag{II.A.1}$$

The quantities appearing in Eq. (II.A.1) are defined as follows: x and t denote the spatial and the time coordinates, respectively; $\Omega \subset \mathcal{R}$ is an open subset of $\mathcal{R}$, with boundary $\partial\Omega$. The components of the column vector $\boldsymbol{U} = \left[u_1(x,t),\ldots,u_N(x,t)\right]$ are the dependent (i.e., the state) variables. The $N \times N$ matrices $\boldsymbol{A}$ and $\boldsymbol{B}$ and the column vector $\boldsymbol{C}$ depend only on $(\boldsymbol{U}, x, t, \boldsymbol{\alpha})$, where $\boldsymbol{\alpha} = \left[\alpha_1,\ldots,\alpha_I\right]$ is the (column) vector of I system parameters.

Along with Eq. (II.A.1), initial conditions

$$\boldsymbol{U}(x,0) = \boldsymbol{U}_0(\boldsymbol{\alpha}) \tag{II.A.2}$$

and boundary conditions, represented here in operator form as

$$\boldsymbol{W}(\boldsymbol{U}, \boldsymbol{\alpha}, x, t) = \boldsymbol{Y}(\boldsymbol{\alpha}, x, t), \quad x \in \partial\Omega, \; t > 0, \tag{II.A.3}$$

must also be specified (for $\boldsymbol{U}$ or its derivatives) for completing the formulation of the initial value problem (IVP). For greater generality, $\boldsymbol{U}_0$ is considered here to be a function of $\boldsymbol{\alpha}$ although, in many cases, the components of $\boldsymbol{U}_0$ can simply be considered as a subset of the set of I components α_i of $\boldsymbol{\alpha}$. This IVP is well posed if Eq. (II.A.1) has real characteristics, i.e., if Eq. (II.A.1) is of

hyperbolic type. The characteristics of Eq. (II.A.1) are the N families of curves defined by the N ordinary differential equations

$$\frac{dx}{dt} = \lambda_i\left(x, t, \boldsymbol{U}, \boldsymbol{\alpha}\right), \left(i = 1, \ldots, N\right), \tag{II.A.4}$$

where the quantities λ_i are the roots (i.e., the eigenvalues) of the characteristic equation

$$\det\left(\boldsymbol{A}\lambda - \boldsymbol{B}\right) = 0. \tag{II.A.5}$$

II.A.2. The Adjoint Sensitivity Analysis Procedure (ASAP)

For the purposes of sensitivity analysis, $\boldsymbol{\alpha}$, $\boldsymbol{U}$, and $\boldsymbol{C}$ are considered to be elements of the Hilbert spaces H_α, H_U, and H_C, respectively. (For example, if all components of $\boldsymbol{\alpha}$ are real numbers, then H_α is $\mathcal{R}^I$; H_U can be taken as the space of all square integrable vector functions $\boldsymbol{U}$, etc.). Thus, Eq. (II.A.1) represents the mapping

$$\left(\boldsymbol{A}\frac{\partial \boldsymbol{U}}{\partial t} + \boldsymbol{B}\frac{\partial \boldsymbol{U}}{\partial x}\right) : S \subset H \to H_C, \tag{II.A.6}$$

where $H = H_U \times H_\alpha$, and S is an open domain in H (i.e., $S = S_U \times S_\alpha$, $S_U \subset H_U$, $S_\alpha \subset H_\alpha$). Note that an arbitrary element $\boldsymbol{e} \in H$ is of the form $\boldsymbol{e} = \left(\boldsymbol{U}, \boldsymbol{\alpha}\right)$.

The system response R associated with the problem modeled by Eq. (II.A.1) is considered to be a nonlinear functional of $\boldsymbol{e}$

$$R\left(\boldsymbol{e}\right) = \int_0^{t_f}\int_\Omega F\left(x, t, \boldsymbol{U}, \boldsymbol{\alpha}\right) dx\, dt\,, \tag{II.A.7}$$

where t_f is some final time value, and F is a nonlinear function of x, t, and $\boldsymbol{e}$.

Recall from Volume I that the most general and fundamental concept for the definition of the sensitivity of a response to variations in the system parameters is the Gâteaux- (G) differential. The G-differential $\delta N\left(\boldsymbol{e}^0; \boldsymbol{h}\right)$ of a nonlinear operator $N\left(\boldsymbol{e}\right)$ at $\boldsymbol{e}^0 = \left(\boldsymbol{U}^0, \boldsymbol{\alpha}^0\right)$ with "increment" $\boldsymbol{h}$ is defined as

$$\lim_{\varepsilon \to 0} \left[N\left(\boldsymbol{e}^0 + \varepsilon \boldsymbol{h}\right) - N\left(\boldsymbol{e}^0\right) \right] \Big/ \varepsilon \equiv \frac{d}{d\varepsilon} \left[N\left(\boldsymbol{e}^0 + \varepsilon \boldsymbol{h}\right) \right]_{\varepsilon = 0} = \delta N\left(\boldsymbol{e}^0; \boldsymbol{h}\right), \quad \text{(II.A.8)}$$

for ε a real scalar, and all (i.e., arbitrary) vectors $\boldsymbol{h} \in H$; here $\boldsymbol{h} = \left(\boldsymbol{h}_U, \boldsymbol{h}_\alpha\right)$ with $\boldsymbol{h}_U = \left(h_{u_1}, \ldots, h_{u_N}\right)$ and $\boldsymbol{h}_\alpha = \left(h_{\alpha_1}, \ldots, h_{\alpha_I}\right)$, since $H = H_U \times H_\alpha$. In view of Eq. (II.A.8), the sensitivity $\delta R\left(\boldsymbol{e}^0; \boldsymbol{h}\right)$ of $R\left(\boldsymbol{e}\right)$ at $\boldsymbol{e}^0$ is

$$\delta R\left(\boldsymbol{e}^0; \boldsymbol{h}\right) = \int_0^{t_f} \int_\Omega \left[\sum_{j=1}^{N} \left(\frac{\partial F}{\partial u_j} \right)_{\boldsymbol{e}^0} h_{u_j} \right] dx\, dt + \int_0^{t_f} \int_\Omega \left[\sum_{i=1}^{I} \left(\frac{\partial F}{\partial \alpha_i} \right)_{\boldsymbol{e}^0} h_{\alpha_i} \right] dx\, dt, \quad \text{(II.A.9)}$$

where the partial derivatives $\partial F / \partial u_j$ and $\partial F / \partial \alpha_i$ of F at the "base-case configuration point" $\boldsymbol{e}^0 = \left(\boldsymbol{U}^0, \boldsymbol{\alpha}^0\right)$ are assumed to exist. The first and the second terms on the right side of Eq. (II.A.9) are customarily called the "indirect effect term" and the "direct effect term," respectively.

It is observed from Eq. (II.A.9) that, given a vector of "changes" $\boldsymbol{h}_\alpha$ around the base-case point $\boldsymbol{\alpha}^0$, the sensitivity $\delta R\left(\boldsymbol{e}^0; \boldsymbol{h}\right)$ can be evaluated only after determining the vector $\boldsymbol{h}_U$, since $\boldsymbol{h}_U$ and $\boldsymbol{h}_\alpha$ are not independent. The relationship between $\boldsymbol{h}_U$ and $\boldsymbol{h}_\alpha$ is obtained, to first order, by taking the G-differentials of Eq. (II.A.1) and of the initial and boundary conditions represented by Eqs. (II.A.2) and (II.A.3), respectively.

The G-differential of Eq. (II.A.1) is obtained by applying the definition given in Eq. (II.A.8) to each row in Eq. (II.A.1). For example, the G-differential of the i^{th} row of Eq. (II.A.1) is

$$\frac{d}{d\varepsilon} \left\{ \sum_{j=1}^{N} \left[a_{ij}\left(\boldsymbol{U}^0 + \varepsilon \boldsymbol{h}_U, \boldsymbol{\alpha}^0 + \varepsilon \boldsymbol{h}_\alpha\right) \frac{\partial\left(u_j^0 + \varepsilon h_{u_j}\right)}{\partial t} \right.\right.$$
$$\left.\left. + b_{ij}\left(\boldsymbol{U}^0 + \varepsilon \boldsymbol{h}_U, \boldsymbol{\alpha}^0 + \varepsilon \boldsymbol{h}_\alpha\right) \frac{\partial\left(u_j^0 + \varepsilon h_{u_j}\right)}{\partial x} - c_i\left(\boldsymbol{U}^0 + \varepsilon \boldsymbol{h}_U, \boldsymbol{\alpha}^0 + \varepsilon \boldsymbol{h}_\alpha\right) \right] \right\}_{\varepsilon = 0} = 0. \quad \text{(II.A.10)}$$

Performing the above operations (i.e., differentiating with respect to ε and setting ε to zero in the resulting expression) gives

$$\sum_{j=1}^{N} L_{ij}\left(\boldsymbol{e}^0\right) h_{u_j} = S_i\left(\boldsymbol{e}^0;\boldsymbol{h}_\alpha\right),\ x \in \Omega, \tag{II.A.11}$$

where

$$\begin{aligned} L_{ij}\left(\boldsymbol{e}^0\right) &= a_{ij}\left(\boldsymbol{e}^0\right)\frac{\partial[\ ]}{\partial t} + b_{ij}\left(\boldsymbol{e}^0\right)\frac{\partial[\ ]}{\partial x} \\ &+ [\ ]\sum_{k=1}^{N}\left[\frac{\partial a_{ik}\left(\boldsymbol{e}^0\right)}{\partial u_j^0}\frac{\partial u_k^0}{\partial t} + \frac{\partial b_{ik}\left(\boldsymbol{e}^0\right)}{\partial u_j^0}\frac{\partial u_k^0}{\partial x}\right] - [\ ]\frac{\partial c_i\left(\boldsymbol{e}^0\right)}{\partial u_j}, \end{aligned} \tag{II.A.12}$$

and

$$S_i\left(\boldsymbol{e}^0;\boldsymbol{h}_\alpha\right) = \sum_{m=1}^{I}\left\{\frac{\partial c_i\left(\boldsymbol{e}^0\right)}{\partial \alpha_m^0} - \sum_{k=1}^{N}\left[\frac{\partial a_{ik}\left(\boldsymbol{e}^0\right)}{\partial \alpha_m^0}\frac{\partial u_k^0}{\partial t} + \frac{\partial b_{ik}\left(\boldsymbol{e}^0\right)}{\partial \alpha_m^0}\frac{\partial u_k^0}{\partial x}\right]\right\} h_{\alpha_m}. \tag{II.A.13}$$

In view of Eq. (II.A.11), the G-differential of Eq. (II.A.1) can be written as

$$\boldsymbol{L}\left(\boldsymbol{e}^0\right)\boldsymbol{h}_U = \boldsymbol{S}\left(\boldsymbol{e}^0;\boldsymbol{h}_\alpha\right),\ x \in \Omega, \tag{II.A.14}$$

where

$$\boldsymbol{L}\left(\boldsymbol{e}^0\right) = \left[L_{ij}\left(\boldsymbol{e}^0\right)\right]_{N\times N} \tag{II.A.15}$$

is the $N \times N$ matrix whose components are defined by Eq. (II.A.12), and

$$\boldsymbol{S}\left(\boldsymbol{e}^0;\boldsymbol{h}_\alpha\right) = \left(S_1,\ldots,S_N\right) \tag{II.A.16}$$

is the column vector whose components are defined by Eq. (II.A.13). The initial and boundary conditions associated with Eq. (II.A.14) are obtained by applying the definition given in Eq. (II.A.8) to Eqs. (II.A.2) and (II.A.3). This yields

$$\boldsymbol{h}_U\left(x,0\right) = \sum_{i=1}^{I}\left(\frac{\partial U_0}{\partial \alpha_i}\right)_{\boldsymbol{\alpha}^0} h_{\alpha_i},\ x \in \Omega, \tag{II.A.17}$$

and

$$\delta\boldsymbol{W}\left(\boldsymbol{e}^0;\boldsymbol{h}\right) = \delta\boldsymbol{Y}\left(\boldsymbol{\alpha}^0;\boldsymbol{h}_\alpha\right),\ x \in \partial\Omega,\ t > 0, \tag{II.A.18}$$

respectively. Equations (II.A.14), (II.A.17), and (II.A.18) are called the "*forward sensitivity equations* (*FSE*)," or the "*forward sensitivity model* (*FSM*)," or the "*forward variational model* (*FVM*)," or the "*tangent linear model* (*TLM*)." For a given vector of changes $\boldsymbol{h}_\alpha$, Eqs. (II.A.14), (II.A.17), and (II.A.18) could be solved to determine $\boldsymbol{h}_U$; $\boldsymbol{h}_U$ could then be used to evaluate the sensitivity $\delta R\left(\boldsymbol{e}^0;\boldsymbol{h}\right)$. However, for two-phase flow problems involving a large data base and comparatively few responses of the type given in Eq. (II.A.7), it becomes prohibitively expensive to solve Eqs. (II.A.14), (II.A.17), and (II.A.18) repeatedly, for all vectors $\boldsymbol{h}_\alpha$ of possible interest to sensitivity analysis.

The alternative procedure, which avoids the need to solve Eqs. (II.A.14), (II.A.17), and (II.A.18) repeatedly, is the *ASAP*; this procedure can be developed to evaluate the sensitivities if it is possible to eliminate the explicit appearance of $\boldsymbol{h}_U$ in Eq. (II.A.9).The elimination process relies on appropriately constructed adjoint operators. The necessary and sufficient conditions for constructing these adjoint operators have been generally discussed in Volume I. Particularizing those necessary and sufficient conditions to the present two-phase flow problem indicates that appropriate adjoint operators can be constructed if Eqs. (II.A.9), (II.A.14), (II.A.17), and (II.A.18) are linear in $\boldsymbol{h}_U$, and if the Hilbert space H_U is equipped with the inner product

$$\left(\boldsymbol{U},\boldsymbol{V}\right)=\int_0^{t_f}\int_\Omega\sum_{i=1}^{N}u_i\,v_i\,dx\,dt\ ,\ \boldsymbol{U}\in H_U\ ,\ \boldsymbol{V}\in H_U\ . \tag{II.A.19}$$

To simplify subsequent developments, the inner product in the space H_C is henceforth considered to be of the same form as shown in Eq. (II.A.19).

An examination of Eqs. (II.A.9), (II.A.14), and (II.A.17) reveals that these equations are indeed linear in $\boldsymbol{h}_U$. Equation (II.A.18) is linear in $\boldsymbol{h}_U$ if and only if $\boldsymbol{W}\left(\boldsymbol{e}\right)$ admits a Gâteaux- (G) derivative at $\boldsymbol{e}^0$. The necessary and sufficient conditions for $\boldsymbol{W}\left(\boldsymbol{e}\right)$ to admit a G-derivative at $\boldsymbol{e}^0$ are generally discussed in Volume I, and are henceforth assumed to be satisfied. In this case, Eq. (II.A.18) can be written as

$$\boldsymbol{W}_U'\left(\boldsymbol{e}^0\right)\boldsymbol{h}_U=\delta\boldsymbol{Y}\left(\boldsymbol{\alpha}^0;\boldsymbol{h}_\alpha\right)-\boldsymbol{W}_\alpha'\left(\boldsymbol{e}^0\right)\boldsymbol{h}_\alpha\ ,\ x\in\partial\Omega\ ,\ t>0\ , \tag{II.A.20}$$

where $\boldsymbol{W}_U'\left(\boldsymbol{e}^0\right)$ is the partial G-derivative at $\boldsymbol{e}^0$ of $\boldsymbol{W}\left(\boldsymbol{e}\right)$ with respect to $\boldsymbol{U}$, and $\boldsymbol{W}_\alpha'\left(\boldsymbol{e}^0\right)$ is the partial G-derivative at $\boldsymbol{e}^0$ of $\boldsymbol{W}\left(\boldsymbol{e}\right)$ with respect to $\boldsymbol{\alpha}$.

Since $\boldsymbol{L}\left(\boldsymbol{e}^0\right)$ [see Eq. (II.A.14)] is a linear operator with domain in H_U and range in H_C, the relationship

$$\left\langle \boldsymbol{\Phi}, \boldsymbol{L}\left(\boldsymbol{e}^0\right)\boldsymbol{h}_U \right\rangle = \left\langle \boldsymbol{h}_U, \boldsymbol{L}^*\left(\boldsymbol{e}^0\right)\boldsymbol{\Phi} \right\rangle + P\left(\boldsymbol{h}_U, \boldsymbol{\Phi}\right) \tag{II.A.21}$$

holds for an arbitrary vector $\boldsymbol{\Phi} = \left(\phi_1, \ldots, \phi_N\right)$, where $\boldsymbol{\Phi} \in H_C$. In Eq. (II.A.21), $\boldsymbol{L}^*\left(\boldsymbol{e}^0\right)$ is the operator formally adjoint to $\boldsymbol{L}\left(\boldsymbol{e}^0\right)$, and $P\left(\boldsymbol{h}_U, \boldsymbol{\Phi}\right)$ is the associated bilinear form. The explicit representation of $\boldsymbol{L}^*\left(\boldsymbol{e}^0\right)$ is the $N \times N$ matrix whose elements $l_{ij}\left(\boldsymbol{e}^0\right)$ are obtained by transposing the formal adjoints of $L_{ij}\left(\boldsymbol{e}^0\right)$ given in Eq. (II.A.12), i.e.,

$$\begin{aligned} l_{ij}\left(\boldsymbol{e}^0\right) = & -\frac{\partial}{\partial t}\left\{ [\,]\, a_{ji}\left(\boldsymbol{e}^0\right)\right\} - \frac{\partial}{\partial x}\left\{ [\,]\, b_{ji}\left(\boldsymbol{e}^0\right)\right\} \\ & + [\,]\left[\sum_{k=1}^{N}\left(\frac{\partial a_{jk}\left(\boldsymbol{e}^0\right)}{\partial u_i^0}\frac{\partial u_k^0}{\partial t} + \frac{\partial b_{jk}\left(\boldsymbol{e}^0\right)}{\partial u_i^0}\frac{\partial u_k^0}{\partial x}\right) - \frac{\partial c_j\left(\boldsymbol{e}^0\right)}{\partial u_i}\right], \left(i, j = 1, \ldots, N\right). \end{aligned} \tag{II.A.22}$$

An examination of Eqs. (II.A.12), (II.A.21), and (II.A.22) indicates that $P\left(\boldsymbol{h}_U, \boldsymbol{\Phi}\right)$ contains terms involving the quantity $\left(a_{ij} h_{u_j} \phi_j\right)_{t=0}^{t=t_f}$. To eliminate the appearance of the unknown values of $\boldsymbol{h}_U$ at $t = t_f$, the adjoint function $\boldsymbol{\Phi}(x,t)$ is required to satisfy the final time condition

$$\boldsymbol{\Phi}\left(x, t_f\right) = \boldsymbol{0}, \; x \in \Omega. \tag{II.A.23}$$

Appropriate adjoint boundary conditions must also be selected, following the criteria described in Volume I. These adjoint boundary conditions are represented here in operator form as

$$\boldsymbol{W}^*\left(\boldsymbol{\Phi}; \boldsymbol{e}^0\right) = \boldsymbol{Y}^*\left(\boldsymbol{\alpha}^0\right), \; x \in \partial\Omega, \; t < t_f, \tag{II.A.24}$$

and are obtained by requiring that

(i) they be independent of $\boldsymbol{h}_U$, $\boldsymbol{h}_\alpha$, and G-derivatives with respect to $\boldsymbol{\alpha}$

(ii) the substitution of Eq. (II.A.24) into the expression of $P\left(\boldsymbol{h}_U, \boldsymbol{\Phi}\right)$ must cause all terms containing unknown values of $\boldsymbol{h}_U$ to vanish.

This selection of the adjoint boundary and initial conditions reduces $P\left(\boldsymbol{h}_U, \boldsymbol{\Phi}\right)$ to a quantity designated here by $\hat{P}\left(\boldsymbol{h}_\alpha, \boldsymbol{\Phi}; \boldsymbol{e}^0\right)$, which contains terms involving

only known values of $\boldsymbol{h}_\alpha$, $\boldsymbol{\Phi}$, and $\boldsymbol{e}^0$. (In some problems, $\hat{P}$ may vanish.) Hence, Eq. (II.A.21) can be written as

$$\left\langle \boldsymbol{h}_U, \boldsymbol{L}^*\left(\boldsymbol{e}^0\right)\boldsymbol{\Phi}\right\rangle = \left\langle \boldsymbol{\Phi}, \boldsymbol{S}\left(\boldsymbol{e}^0; \boldsymbol{h}_\alpha\right)\right\rangle - \hat{P}\left(\boldsymbol{h}_\alpha, \boldsymbol{\Phi}; \boldsymbol{e}^0\right), \tag{II.A.25}$$

where Eq. (II.A.14) was used to replace $\boldsymbol{L}\left(\boldsymbol{e}^0\right)\boldsymbol{h}_U$ by $\boldsymbol{S}\left(\boldsymbol{e}^0; \boldsymbol{h}_\alpha\right)$. Equations (II.A.23), (II.A.24), and (II.A.25) hold for all (i.e., arbitrary) vectors $\boldsymbol{\Phi} \in H_C$.

A unique vector $\boldsymbol{\Phi}$ is now selected by using the Riesz representation theorem, so as to eliminate the explicit appearance of $\boldsymbol{h}_U$ in Eq. (II.A.9) and to derive an alternative expression for the sensitivity $\delta R\left(\boldsymbol{e}^0; \boldsymbol{h}\right)$. For this purpose, note that Eq. (II.A.9) is linear in $\boldsymbol{h}_U$. Hence, Eq. (II.A.19) can be used to write the first term on the right side of Eq. (II.A.9) as the inner product

$$\int_0^{t_f}\int_\Omega \left[\sum_{j=1}^{N}\left(\frac{\partial F}{\partial u_j}\right)_{\boldsymbol{e}^0} h_{u_j}\right] dx\, dt = \left(\boldsymbol{h}_U, \partial F/\partial \boldsymbol{U}\right), \tag{II.A.26}$$

where $\partial F/\partial \boldsymbol{U} = \left(\partial F/\partial u_1, \ldots, \partial F/\partial u_N\right)^T$. (The superscript T denotes "transposition.") A comparison between Eq. (II.A.26) and the left side of Eq. (II.A.25) shows that the relationship

$$\boldsymbol{L}^*\left(\boldsymbol{e}^0\right)\boldsymbol{\Phi} = \partial F/\partial \boldsymbol{U} \tag{II.A.27}$$

holds uniquely in view of the Riesz representation theorem.

Equation (II.A.27) together with the final time conditions given by Eq. (II.A.23) and the boundary conditions represented by Eq. (II.A.24) are called the "*adjoint sensitivity equations* (*ASE*)," or the "*adjoint sensitivity model* (*ASM*)," or the "*adjoint variational model* (*AVM*)," or the "*adjoint tangent model* (*ATM*)."

Equations (II.A.9), (II.A.25), (II.A.26), and (II.A.27) can now be used to obtain

$$\delta R = \int_0^{t_f}\int_\Omega \left[\sum_{i=1}^{I}\left(\frac{\partial F}{\partial \alpha_i}\right)_{\boldsymbol{e}^0} h_{\alpha_i}\right] dx\, dt + \left\langle \boldsymbol{\Phi}, \boldsymbol{S}\right\rangle - \hat{P}\left(\boldsymbol{h}_\alpha, \boldsymbol{\Phi}; \boldsymbol{e}^0\right). \tag{II.A.28}$$

Thus, the desired elimination of the unknown values of $\boldsymbol{h}_U$ from the expression of the sensitivity *VR* has been accomplished. Once the single calculation to determine $\boldsymbol{\Phi}$ has been performed [by solving Eqs. (II.A.27),

(II.A.23), and (II.A.24)], Eq. (II.A.28) provides the most efficient means to obtain the sensitivities of $R(\boldsymbol{e})$ to changes $\boldsymbol{h}_\alpha$ around $\boldsymbol{\alpha}^0$.

II.A.3. Characteristic of the Adjoint Sensitivity System

After explicitly performing the differentiation $(\partial/\partial t)\{\ \}$ and $(\partial/\partial x)\{\ \}$ in Eq. (II.A.22), Eq. (II.A.27) can be written as

$$-\boldsymbol{A}^T \frac{\partial \boldsymbol{\Phi}}{\partial t} - \boldsymbol{B}^T \frac{\partial \boldsymbol{\Phi}}{\partial x} = \boldsymbol{D}, \tag{II.A.29}$$

where $\boldsymbol{D} = (d_1, \ldots, d_N)^T$ is a (column) vector with components

$$d_i = \frac{\partial F}{\partial u_i} + \sum_{j=1}^{N} \phi_j \left[\frac{\partial a_{ji}}{\partial t} + \frac{\partial b_{ji}}{\partial x} + \frac{\partial c_j}{\partial u_i} - \sum_{k=1}^{N} \left(\frac{\partial a_{jk}}{\partial u_i} \frac{\partial u_k}{\partial t} + \frac{\partial b_{jk}}{\partial u_i} \frac{\partial u_k}{\partial x} \right) \right]. \tag{II.A.30}$$

The final time value problem represented by Eqs. (II.A.29), (II.A.23), and (II.A.24) can be transformed into an initial value problem (IVP) by introducing the new independent variable

$$\zeta = t_f - t \tag{II.A.31}$$

in Eqs. (II.A.23), (II.A.24), and (II.A.29). The resulting IVP for $\boldsymbol{\Phi}(x, \zeta)$ is

$$\boldsymbol{A}^T \frac{\partial \boldsymbol{\Phi}}{\partial \zeta} - \boldsymbol{B}^T \frac{\partial \boldsymbol{\Phi}}{\partial x} = \boldsymbol{D},\ x \in \Omega,\ \zeta > 0, \tag{II.A.32}$$

$$\boldsymbol{\Phi}(x, 0) = \boldsymbol{0},\ x \in \Omega,\ \zeta = 0, \tag{II.A.33}$$

$$\boldsymbol{W}^*(\boldsymbol{\Phi}; \boldsymbol{e}^0) = \boldsymbol{Y}^*(\boldsymbol{\alpha}^0),\ x \in \partial\Omega,\ \zeta > 0, \tag{II.A.34}$$

where $\boldsymbol{A}^T$, $\boldsymbol{B}^T$, and $\boldsymbol{D}$ depend only on x, $t_f - \zeta$, $\boldsymbol{U}^0(x, t_f - \zeta)$, and $\boldsymbol{\alpha}^0(x, t_f - \zeta)$. The characteristics of Eq. (II.A.32) are the N families of curves defined by the N ordinary differential equations

$$\frac{dx}{d\zeta} = \gamma_i,\ (i = 1, \ldots, N), \tag{II.A.35}$$

where the eigenvalues γ_i are the roots of the characteristic equation

$$\det\left(\boldsymbol{A}^T\gamma+\boldsymbol{B}^T\right)=0. \tag{II.A.36}$$

Since $\det\left(\boldsymbol{A}^T\gamma+\boldsymbol{B}^T\right)=\det\left[\left(\boldsymbol{A}\gamma+\boldsymbol{B}\right)^T\right]=\det\left(\boldsymbol{A}\gamma+\boldsymbol{B}\right)$, Eq. (II.A.36) can also be written as

$$\det\left(\boldsymbol{A}\gamma+\boldsymbol{B}\right)=0. \tag{II.A.37}$$

In view of the functional dependence of $\boldsymbol{A}$ and $\boldsymbol{B}$, it then follows from Eq. (II.A.37) that

$$\gamma_i=\gamma_i\left[x,\zeta,\boldsymbol{U}^0\left(x,t_f-\zeta\right),\boldsymbol{\alpha}^0\left(x,t_f-\zeta\right)\right], \tag{II.A.38}$$

i.e., γ_i is independent of $\boldsymbol{\Phi}\left(x,\zeta\right)$.

Comparing Eq. (II.A.37) to (II.A.5) shows that

$$\gamma_i\left[x,\zeta,\boldsymbol{U}^0\left(x,t_f-\zeta\right),\boldsymbol{\alpha}^0\left(x,t_f-\zeta\right)\right]=-\lambda_i\left[x,t_f-\zeta,\boldsymbol{U}^0\left(x,t_f-\zeta\right),\boldsymbol{\alpha}^0\left(x,t_f-\zeta\right)\right]. \tag{II.A.39}$$

Furthermore, since $dx/d\zeta=-dx/dt$, it follows from Eqs. (II.A.39) and (II.A.31) that Eqs. (II.A.35) and (II.A.4) define the same N families of curves. Thus, the characteristics of the adjoint system consisting of the *linear* PDE's given by Eq. (II.A.32) are the same as the characteristics of the original system of *quasi-linear* equations given by Eq. (II.A.1). Consequently, for a transient one-dimensional, two-phase flow problem modeled as a well-posed IVP, the adjoint sensitivity system [i.e., Eqs. (II.A.32), (II.A.33), and (II.A.34)] appropriate for performing efficient sensitivity analysis can always be solved as a well-posed IVP.

II.A.4. Illustrative Example: The Homogeneous Equilibrium Model (HEM) for Two-Phase Flow

One of the simplest, yet often used, model for simulating two-phase, single-component flow is the so-called homogeneous equilibrium model (HEM). Assuming no friction or external heat input, and considering that both phases move at the same velocity, v, the conservation equations underlying the HEM are

Conservation of mass (continuity):

$$\frac{\partial \rho_m}{\partial t} + \frac{\partial (\rho_m v)}{\partial x} = 0, \tag{II.A.40}$$

Conservation of momentum:

$$\frac{\partial (\rho_m v)}{\partial t} + \frac{\partial (\rho_m v v)}{\partial x} + \frac{\partial P}{\partial x} = 0, \tag{II.A.41}$$

Conservation of energy:

$$\frac{\partial (\rho_m S_m)}{\partial t} + \frac{\partial (\rho_m v S_m)}{\partial x} = 0. \tag{II.A.42}$$

In Eqs. (II.A.40), (II.A.41), and (II.A.42), the mixture density ρ_m is defined as

$$\rho_m \equiv \alpha_l \rho_l + \alpha_g \rho_g ; \tag{II.A.43}$$

the mean mixture entropy S_m is defined by

$$S_m \equiv \left(\alpha_l \rho_l S_l + \alpha_g \rho_g S_g\right) \Big/ \rho_m ; \tag{II.A.44}$$

and P and α denote pressure and void fractions, respectively. In Eqs. (II.A.43) and (II.A.44), the subscript l and g refer to the liquid and the vapor phases, respectively.

It is known that along the two-phase envelope, the density of the liquid and of the gas is a function of pressure only. Thus, ρ_m in Eq. (II.A.43) is a function of pressure and the void fraction α_g. Therefore,

$$\rho_m = \rho_m (P, S_m), \tag{II.A.45}$$

or, if the inverse function is assumed to exist,

$$P = P(\rho_m, S_m). \tag{II.A.46}$$

Therefore, in Eq. (II.A.41), the pressure gradient can be written as

$$\left(\frac{\partial P}{\partial x}\right)_{S_m} = \left(\frac{\partial P}{\partial \rho_m}\right)_{S_m} \frac{\partial \rho_m}{\partial x} . \tag{II.A.47}$$

Thermodynamic evaluations show that

$$\left(\frac{\partial P}{\partial \rho_m}\right)_{S_m} = \frac{\Theta\left(P'\right)^2}{\rho_m^2 C_v}, \tag{II.A.48}$$

where

$$P' = \frac{dP}{d\Theta} = \frac{1}{\Theta}\left(\frac{h_g - h_l}{V_g - V_l}\right), \tag{II.A.49}$$

where Θ denotes the mixture's temperature, C_v denotes the heat capacity of the mixture at constant volume, h_g and h_l denote the enthalpies of the gas and the liquid, respectively, while V_g and V_l denote the specific volumes of the gas and the liquid.

Equations (II.A.40) through (II.A.42) can be written in matrix-vector form as

$$\boldsymbol{A}\frac{\partial \boldsymbol{U}}{\partial t} + \boldsymbol{B}\frac{\partial \boldsymbol{U}}{\partial x} = 0, \tag{II.A.50}$$

where

$$\boldsymbol{U} \equiv \left(\rho_m, v, S_m\right)^T, \tag{II.A.51}$$

$$\boldsymbol{A} \equiv \begin{bmatrix} 1 & 0 & 0 \\ 0 & 1 & 0 \\ 0 & 0 & 1 \end{bmatrix} = \boldsymbol{I}, \tag{II.A.52}$$

$$\boldsymbol{B} \equiv \begin{bmatrix} v & \rho_m & 0 \\ \dfrac{1}{\rho_m}\left(\dfrac{\partial P}{\partial \rho_m}\right)_{S_m} & v & 0 \\ 0 & 0 & v \end{bmatrix}. \tag{II.A.53}$$

Note that the symbol T in Eq. (III.E.51) denotes "transposition," indicating that $\boldsymbol{U}$ is a column (rather than a row) vector; the symbol T will be used for this purpose throughout this Section.

The eigenvalues λ_i, $\left(i = 1,2,3\right)$, of Eq. (III.E.50) are readily obtained as:

$$\lambda_1 = v, \tag{II.A.54a}$$

$$\lambda_2 = v + c, \tag{II.A.54b}$$

$$\lambda_3 = v - c, \tag{II.A.54c}$$

where c is the equilibrium sound speed defined as

$$c = \left[\left(\frac{\partial P}{\partial \rho_m} \right)_{S_m} \right]^{1/2}. \tag{II.A.55}$$

Since the eigenvalues λ_i, $(i = 1,2,3)$, are all real and distinct, the system given by Eq. (II.A.50) is hyperbolic. The characteristics of Eq. (II.A.50) are the three families of curves defined by the three ordinary differential equations

$$\frac{dx}{dt} = \lambda_i, \ (i = 1,2,3). \tag{II.A.56}$$

A set of initial and boundary conditions must also be supplied along with Eq. (II.A.50). For illustrative purposes, it suffices to consider that

1. the initial conditions for ρ_m, v, and S_m are known, specified functions of x at $t = 0$, i.e.,

$$\rho_m(x,0) = \rho_0(x) \tag{II.A.57a}$$

$$v(x,0) = v_0(x) \tag{II.A.57b}$$

$$S_m(x,0) = S_0(x) \tag{II.A.57c}$$

2. the domain Ω is the segment $a < x < b$, with boundary $\partial\Omega$ consisting of the endpoints $x = a$ and $x = b$
3. boundary conditions are that ρ_m, v, and S_m are specified functions of t at the "inlet" $x = a$, i.e.,

$$\rho_m(a,t) = \rho_{in}(t) \tag{II.A.58a}$$

$$v(a,t) = v_{in}(t) \tag{II.A.58b}$$

$$S_m(a,t) = S_{in}(t). \tag{II.A.58c}$$

For illustrative purposes, the response is considered to have the form

$$R \equiv \int_0^{t_f} \int_a^b F(x, t, \rho_m, v, S_m, \boldsymbol{\alpha}) dx\, dt. \tag{II.A.59}$$

Examining Eqs. (II.A.48), (II.A.49), (II.A.57), (II.A.58), and (II.A.59), it follows that the vector $\boldsymbol{\alpha}$ of system parameters for this illustrative example is the (column) vector

$$\boldsymbol{\alpha} \equiv \left[\rho_0(x), v_0(x), S_0(x), \rho_{in}(t), v_{in}(t), S_{in}(t), \alpha_7, \ldots, \alpha_I\right]^T, \qquad \text{(II.A.60)}$$

where the components α_7 through α_I denote the parameters (h_g, h_l, etc.) which appear explicitly in Eqs. (II.A.48) and (II.A.49), and also denote any additional parameters that may appear in the definition of the response [i.e., in Eq. (II.A.59)].

The sensitivities of the response R to arbitrary variations ($\Delta\rho_0$, Δv_0, etc.) in the system parameters $\boldsymbol{\alpha}$, around their base-case values $\boldsymbol{\alpha}^0$, can be obtained by applying the *ASAP*, as shown in the previous sections of this Volume. Defining the vector $\boldsymbol{h}_\alpha$ of changes around $\boldsymbol{\alpha}^0$ as

$$\boldsymbol{h}_\alpha \equiv \left[\Delta\rho_0(x), \Delta v_0(x), \Delta S_0(x), \Delta\rho_{in}(t), \Delta v_{in}(t), \Delta S_{in}(t), \Delta\alpha_7, \ldots, \Delta\alpha_I\right]^T, \qquad \text{(II.A.61)}$$

defining the corresponding vector of changes in $\boldsymbol{U}$ around $\boldsymbol{U}^0$ as

$$\boldsymbol{h}_U \equiv \left(h_\rho, h_v, h_S\right)^T, \qquad \text{(II.A.62)}$$

and taking the corresponding G-derivatives of Eqs. (II.A.50), (II.A.57), and (II.A.58) leads to the following Forward Sensitivity System (or "variational tangent model"):

$$\boldsymbol{L}\left(\boldsymbol{e}^0\right)\boldsymbol{h}_U = \boldsymbol{S}\left(\boldsymbol{e}^0; \boldsymbol{h}_\alpha\right), \qquad \text{(II.A.63)}$$

where

$$\boldsymbol{L}\left(\boldsymbol{e}^0\right) \equiv \begin{bmatrix} \dfrac{\partial}{\partial t} + v^0\dfrac{\partial}{\partial x} + \dfrac{\partial v^0}{\partial x} & \dfrac{\partial \rho_m}{\partial x} + \rho_m^0\dfrac{\partial}{\partial x} & 0 \\ \dfrac{c^2}{\rho_m^0}\dfrac{\partial}{\partial x} - \dfrac{c^2}{\left(\rho_m^0\right)^2}\dfrac{\partial \rho_m^0}{\partial x} & \dfrac{\partial}{\partial t} + v^0\dfrac{\partial}{\partial x} + \dfrac{\partial v^0}{\partial x} & 0 \\ 0 & \dfrac{\partial S_m^0}{\partial x} & \dfrac{\partial}{\partial t} + v^0\dfrac{\partial}{\partial x} \end{bmatrix}, \qquad \text{(II.A.64)}$$

$$\boldsymbol{S}\left(\boldsymbol{e}^0; \boldsymbol{h}_\alpha\right) \equiv \left[0, -\frac{1}{\rho_m^0}\frac{\partial \rho_m^0}{\partial x}\sum_{i=7}^{I}\frac{\partial\left(c^2\right)}{\partial \alpha_i}, 0\right]^T, \qquad \text{(II.A.65)}$$

and where the function $\boldsymbol{h}_U$ is subject to the following initial and boundary conditions:

$$h_\rho(x,0) = \Delta\rho_0(x), \tag{II.A.66a}$$

$$h_v(x,0) = \Delta v_0(x), \tag{II.A.66b}$$

$$h_S(x,0) = \Delta S_0(x), \tag{II.A.66c}$$

and

$$h_\rho(a,t) = \Delta\rho_{in}(t), \tag{II.A.67a}$$

$$h_v(a,t) = \Delta v_{in}(t), \tag{II.A.67b}$$

$$h_S(a,t) = \Delta S_{in}(t). \tag{II.A.67c}$$

The Adjoint Sensitivity System (or "adjoint variational model") is readily obtained by applying the procedure shown in the previous section (and, generally, in Volume I); the respective derivations lead to the following system of linear partial differential equations:

$$-\boldsymbol{A}^T \frac{\partial \boldsymbol{\Phi}}{\partial t} - \boldsymbol{B}^T \frac{\partial \boldsymbol{\Phi}}{\partial x} = \boldsymbol{D}, \tag{II.A.68}$$

where

$$\boldsymbol{\Phi} \equiv \left(\phi_\rho, \phi_v, \phi_S\right)^T \tag{II.A.69}$$

denotes the adjoint function, where the (column) vector $\boldsymbol{D}$ is defined as,

$$\boldsymbol{D} \equiv \left(\frac{\partial F}{\partial \rho_m^0}, \frac{\partial F}{\partial v^0} - \phi_s \frac{\partial S_m^0}{\partial x}, \frac{\partial F}{\partial S_m^0} + \phi_s \frac{\partial v^0}{\partial x} \right)^T, \tag{II.A.70}$$

and where the adjoint function $\boldsymbol{\Phi}$ is subject to the following "final-time" conditions

$$\boldsymbol{\Phi}(x,t) = \boldsymbol{0}, \text{ at } t = t_f, \; a \le x \le b, \tag{II.A.71}$$

and following "outlet"-boundary conditions

$$\boldsymbol{\Phi}(x,t) = \boldsymbol{0}, \text{ at } x = \text{b}, \; t < t_f. \tag{II.A.72}$$

Using the transformation $\zeta = t_f - t$, the "final-time value problem" represented by Eqs. (II.A.68), (II.A.71), and (II.A.72) is transformed into the following initial-value problem (IVP) for the transformed adjoint function $\boldsymbol{\Phi}(x,\zeta)$:

$$\boldsymbol{A}^T \frac{\partial \boldsymbol{\Phi}}{\partial \zeta} - \boldsymbol{B}^T \frac{\partial \boldsymbol{\Phi}}{\partial x} = \boldsymbol{D}, \tag{II.A.73}$$

$$\boldsymbol{\Phi}(x,\zeta) = \boldsymbol{0}, \text{ at } \zeta = 0, \tag{II.A.74}$$

$$\boldsymbol{\Phi}(x,\zeta) = \boldsymbol{0}, \text{ at } x = b. \tag{II.A.75}$$

The eigenvalues γ_i, $(i = 1,2,3)$, are obtained by calculating the roots of

$$\det\left(\boldsymbol{A}^T\gamma + \boldsymbol{B}^T\right) = \begin{vmatrix} \gamma + v^0 & c^2/\rho_m^0 & 0 \\ \rho_m^0 & \gamma + v^0 & 0 \\ 0 & 0 & \gamma + v^0 \end{vmatrix} = 0,$$

which yields the expressions

$$\gamma_1 = -v^0 = -\lambda_1, \tag{II.A.76a}$$

$$\gamma_2 = -v^0 - c = -\lambda_2, \tag{II.A.76b}$$

$$\gamma_3 = -v^0 + c = -\lambda_3. \tag{II.A.76c}$$

The characteristics of Eq. (II.A.73) are the three families of curves defined by the three ordinary differential equations

$$\frac{dx}{d\zeta} = \gamma_i, \ (i = 1,2,3). \tag{II.A.77}$$

Note that Eq. (II.A.77) defines the *same* families of curves as Eq. (II.A.56), since $dx/d\zeta = -dx/dt$ and $\gamma_i = -\lambda_i$. Thus, the adjoint system is hyperbolic and has the same characteristics as the original system, i.e., Eq. (II.A.50).

The adjoint system can be solved by using the method of characteristics as outlined in the Section II.A.3. For this purpose, the eigenvectors corresponding to the eigenvalues γ_i are used to construct the matrix

$$\boldsymbol{Q} = \begin{bmatrix} 0 & 0 & 1 \\ \rho_m^0/2c & 1/2 & 0 \\ -\rho_m^0/2c & 1/2 & 0 \end{bmatrix}. \tag{II.A.78}$$

Introducing the new dependent variable $\boldsymbol{\psi} \equiv \left(\psi_\rho, \psi_v, \psi_S\right)^T$ defined as $\boldsymbol{\psi} \equiv \boldsymbol{Q}\boldsymbol{\Phi}$, and performing the operations indicated in Section II.A.3, transforms Eq. (II.A.73) into the following (equivalent) canonical form:

$$\frac{\partial \psi_\rho}{\partial \zeta} - v^0 \frac{\partial \psi_\rho}{\partial x} - \frac{\partial F}{\partial S_m^0} - \psi_\rho \frac{\partial v^0}{\partial x} = 0, \tag{II.A.79}$$

$$\begin{aligned} &\frac{\partial \psi_v}{\partial \zeta} - \left(v^0 + c\right)\frac{\partial \psi_v}{\partial x} + \frac{\rho_m^0}{2c}\left[\frac{\partial\left(c/\rho_m^0\right)}{\partial \zeta} - \left(v^0 + c\right)\frac{\partial\left(c/\rho_m^0\right)}{\partial x}\right]\psi_v \\ &- \frac{\rho_m^0}{2c}\left[\frac{\partial\left(c/\rho_m^0\right)}{\partial \zeta} - \left(v^0 + c\right)\frac{\partial\left(c/\rho_m^0\right)}{\partial x}\right]\psi_S \\ &- \frac{\rho_m^0}{2c}\frac{\partial F}{\partial \rho_m^0} - \frac{1}{2}\left(\frac{\partial F}{\partial v^0} - \psi_\rho \frac{\partial S_m^0}{\partial x}\right) = 0, \end{aligned} \tag{II.A.80}$$

$$\begin{aligned} &\frac{\partial \psi_v}{\partial \zeta} - \left(v^0 - c\right)\frac{\partial \psi_v}{\partial x} - \frac{\rho_m^0}{2c}\left[\frac{\partial\left(c/\rho_m^0\right)}{\partial \zeta} - \left(v^0 - c\right)\frac{\partial\left(c/\rho_m^0\right)}{\partial x}\right]\psi_v \\ &+ \frac{\rho_m^0}{2c}\left[\frac{\partial\left(c/\rho_m^0\right)}{\partial \zeta} - \left(v^0 - c\right)\frac{\partial\left(c/\rho_m^0\right)}{\partial x}\right]\psi_S \\ &+ \frac{\rho_m^0}{2c}\frac{\partial F}{\partial \rho_m^0} - \frac{1}{2}\left(\frac{\partial F}{\partial v^0} - \psi_\rho \frac{\partial S_m^0}{\partial x}\right) = 0. \end{aligned} \tag{II.A.81}$$

The above equations involve the derivatives of F with respect to the components ρ, v, and S of $\boldsymbol{U}$. For any given specific form of F, Eqs. (II.A.79), (II.A.80), and (II.A.81) can be integrated, as outlined in Section II.A.3, along the corresponding characteristic [see Eqs. (II.A.76) and (II.A.77)]. Once ψ_ρ, ψ_v, and ψ_S have been obtained by solving the above system of equations, the adjoint function $\boldsymbol{\Phi}$ can be readily determined by performing the matrix-vector multiplication $\boldsymbol{\Phi} = \boldsymbol{Q}^{-1}\boldsymbol{\psi}$.

In terms of the adjoint function $\boldsymbol{\Phi}$, the explicit expression for the sensitivity δR of R is obtained as

$$
\begin{aligned}
\delta R = & \int_0^{t_f}\int_a^b \sum_{i=7}^{I} \left[\Delta\alpha_i \left(\partial F/\partial\alpha_i\right)_{(U^0,\alpha^0)}\right] dx\,dt \\
& - \int_0^{t_f}\int_a^b \left[\phi_U(x,t)\frac{1}{\rho_m^0}\frac{\partial\rho_m^0}{\partial x}\sum_{i=7}^{I}\frac{\partial\left(c^2\right)}{\partial\alpha_i}\Delta\alpha_i\right] dx\,dt \\
& + \int_a^b \left[\phi_\rho(x,0)\Delta\rho_0(x) + \phi_v(x,0)\Delta v_0(x) + \phi_S(x,0)\Delta S_0(x)\right] dx \\
& + \int_0^{t_f} \left\{\phi_\rho(a,t)\left[v_{in}(t)\Delta\rho_{in}(t) + \rho_{in}(t)\Delta v_{in}(t)\right]\right. \\
& \left. + \phi_v(a,t)\left[v_{in}(t)\Delta v_{in}(t) + \Delta\rho_{in}(t)c^2/\rho_{in}(t)\right] + \phi_S(a,t)v_{in}(t)\Delta S_{in}(t)\right\} dt\ .
\end{aligned}
\tag{II.A.82}
$$

Once the adjoint function $\boldsymbol{\Phi}$ has been determined, the sensitivity *VR* can be efficiently obtained by carrying out the integrations in Eq. (II.A.82), for any specific $\boldsymbol{h}_\alpha$ (i.e., for any specific variations $\Delta\rho_0$, Δv_0, etc.).

II. B. ASAP FOR THE RELAP5/MOD3.2 TWO-FLUID MODEL (REL/TF)

This Section presents the main aspects of implementing the *ASAP* for the RELAP5/MOD3.2 code. Conceptually, these steps are the same as described in the foregoing Section II.A, when applying the *ASAP* to a well-posed system of quasi-linear partial differential equations that describe transient one-dimensional, two-phase flow. The RELAP5/MOD3.2 code simulates the thermal-hydraulic characteristics of light water nuclear reactors (LWR) by using a one-dimensional, nonequilibrium, nonhomogeneous two-phase flow model, together with conservation equations for boron concentration and noncondensable gases. The RELAP5/MOD3.2 code actually solves the so-called "Numerically Convenient Set of Differential Equations" (REL/CDE), which is obtained from the basic differential equations that underlie the nonhomogeneous, nonequilibrium, one-dimensional two-fluid model. The REL/CDE are discretized by using a staggered-mesh in the spatial direction, and either a one-step ("nearly-implicit") or a two-step ("semi-implicit") discretization procedure in time. These discretization procedures yield a system of thirteen coupled nonlinear algebraic equations. Both the differential and the discretized forms of the REL/CDE are presented in Section II.B.1. Section II.B.2 highlights the application of the *ASAP* to the REL/CDE (in Sub-section II.B.2.a), and to the Discretized REL/CDE (in Sub-section II.B.2.b), respectively. Applying the *ASAP* yields the Differential Adjoint Sensitivity Model (ASM-REL/TF), which comprises nine coupled differential equations that are linear in the respective adjoint functions, and its discrete counterpart, the Discrete ASM-REL/TF, which

comprises thirteen algebraic equations that are also linear in the respective discrete adjoint functions.

Section II.B.3 highlights the fundamentally important aspect of *consistency between the differential and the corresponding discretized equations used for sensitivity analysis*. The indispensable *a priori* assumption must be that the original system of differential equations (in this case, the REL/CDE) is discretized consistently (in RELAP5/MOD3.2); otherwise, the base-case solution could not be calculated correctly. Starting from this indispensable assumption, the following consistency correspondences must be assured: (i) the Discretized Forward Sensitivity Model (FSM) must be consistent with the Differential FSM, if the *FSAP* is used; (ii) the Discretized Adjoint Sensitivity Model (ASM) must be consistent with the Differential ASM, if the *ASAP* is used; and (iii) the Discretized (representation of the) Response Sensitivity must be consistent with the Integral (representation of the) Response Sensitivity both for the *FSAP* and for the *ASAP*, in which the Integral and the Discretized Response Sensitivity are represented in terms of the corresponding adjoint functions.

Section II.B.4 presents typical results that illustrate the verification of the numerical solution of the ASM-REL/TF corresponding to the two-fluid model with noncondensable(s) used in RELAP5/MOD3.2. This validation has been carried out by using sample problems involving: (i) liquid-phase only, (ii) gas-phase only, and (iii) two-phase mixture (of water and steam). Thus, the "Two-Loops with Pumps" sample problem supplied with RELAP5/MOD3.2 is used to verify the accuracy and stability of the numerical solution of the ASM-REL/TF when only the liquid-phase is present. By replacing the liquid (water) by gas (pure steam) but keeping the respective geometry, a modified "Two-Loops with Pumps" sample problem is obtained and used to verify the accuracy and stability of the numerical solution of the ASM-REL/TF when only the gas-phase is present. For the same verification purpose, a modified "Edwards Pipe" sample problem, in which only the gas-phase is present (thus describing the transient depressurization of a pipe filled with pure steam), is also used. Furthermore, the "Edwards Pipe" sample problem, also supplied with RELAP5/MOD3.2, is used to verify the accuracy and stability of the numerical solution of the ASM-REL/TF when both (i.e., liquid and gas) phases are present. The results obtained for these sample problems depict typical sensitivities of junction velocities and volume-averaged pressures to perturbations in initial conditions, and indicate that the numerical solution of the ASM-REL/TF is as robust, stable, and accurate as the original RELAP5/MOD3.2 calculations.

Section II.B.5 illustrates the role that sensitivities of the thermodynamic properties of water play for sensitivity analysis of thermal-hydraulic codes for light-water reactors. Using the well-known ASME Steam Tables (1993), we present typical analytical and numerical results for sensitivities of the thermodynamic properties of water to the numerical parameters that appear in the mathematical formulation of these properties. Note that the explicit, exact

expressions of all of these sensitivities have been obtained by using the symbolic computer language MAPLE V9. In particular, we highlight the very large sensitivities displayed by the specific isobaric fluid and gas heat capacities, C_{pf}, and C_{pg}, the specific fluid enthalpy, h_f, the specific gas volume, V_g, the volumetric expansion coefficient for gas, β_g, and the isothermal coefficient for gas, k_g. The dependence of β_g, and k_g, on the most sensitive parameters turns out to be nonlinear, while the dependence of C_{pf}, C_{pg}, h_f, and V_g, on the most sensitive parameters, turns out to be linear, so the respective sensitivities predict exactly the effects of variations in the respective parameters. On the other hand, the sensitivities of the specific fluid volume, V_f, the volumetric expansion coefficient for fluid, β_f, the specific gas enthalpy, h_g, and the isothermal coefficient of compressibility for fluid, k_f, to the parameters that appear in their respective mathematical formulae are quite small. Finally, we note that such deterministically calculated sensitivities can be used to rank the respective parameters according to their importance, to assess the effects of nonlinearities and, more generally, to perform comprehensive sensitivity/uncertainty analyses of thermal-hydraulic codes that use water substance as the working fluid.

II.B.1. The Relap5/Mod3.2 Two-Fluid Model

The RELAP5/MOD3.2 code simulates the thermal-hydraulic characteristics of light-water reactors (LWR) by using a nonhomogeneous, nonequilibrium, one-dimensional two-fluid model, which consists of a system of nine coupled nonlinear partial differential equations describing the conservation of mass, momentum, and energy for the liquid and gaseous phases, including noncondensable materials in the gaseous phase and boron concentration in the liquid field. These conservation equations are not solved directly in RELAP5/MOD 3.2; instead they are transformed into the so-called "Numerically Convenient Set of Differential Equations," abbreviated henceforth as REL/CDE, which comprises the following nine coupled nonlinear partial differential equations:

(i) the "noncondensable density equation"

$$\rho_g X_n \frac{\partial \alpha_g}{\partial t} + \alpha_g X_n \frac{\partial \rho_g}{\partial t} + \alpha_g \rho_g \frac{\partial X_n}{\partial t} + \frac{1}{A}\frac{\partial}{\partial x}\left(\alpha_g \rho_g X_n v_g A\right) = 0 . \qquad \text{(II.B.1)}$$

(ii) the "vapor energy equation"

$$
\begin{aligned}
&\left(\rho_g U_g + P\right)\frac{\partial \alpha_g}{\partial t} + \alpha_g U_g \frac{\partial \rho_g}{\partial t} + \alpha_g \rho_g \frac{\partial U_g}{\partial t} \\
&+ \frac{1}{A}\left[\frac{\partial}{\partial x}\left(\alpha_g \rho_g U_g v_g A\right) + P\frac{\partial}{\partial x}\left(\alpha_g v_g A\right)\right] = \\
&-\left(\frac{h_f^*}{h_g^* - h_f^*}\right) H_{ig}\left(T^s - T_g\right)\frac{P_s}{P} - \left(\frac{h_g^*}{h_g^* - h_f^*}\right) H_{if}\left(T^s - T_f\right) \\
&-\frac{P - P_s}{P} H_{gf}\left(T_g - T_f\right) + \left[\left(\frac{1+\varepsilon}{2}\right)h_g' + \left(\frac{1-\varepsilon}{2}\right)h_f'\right]\Gamma_w + Q_{wg} + DISS_g .
\end{aligned}
\tag{II.B.2}
$$

(iii) the "liquid energy equation"

$$
\begin{aligned}
&-\left(\rho_f U_f + P\right)\frac{\partial \alpha_g}{\partial t} + \alpha_f U_f \frac{\partial \rho_f}{\partial t} + \alpha_f \rho_f \frac{\partial U_f}{\partial t} \\
&+ \frac{1}{A}\left[\frac{\partial}{\partial x}\left(\alpha_f \rho_f U_f v_f A\right) + P\frac{\partial}{\partial x}\left(\alpha_f v_f A\right)\right] \\
&= \left(\frac{h_f^*}{h_g^* - h_f^*}\right) H_{ig}\left(T^s - T_g\right)\frac{P_s}{P} + \left(\frac{h_g^*}{h_g^* - h_f^*}\right) H_{if}\left(T^s - T_f\right) + \frac{P - P_s}{P} H_{gf}\left(T_g - T_f\right) \\
&-\left[\left(\frac{1+\varepsilon}{2}\right)h_g' + \left(\frac{1-\varepsilon}{2}\right)h_f'\right]\Gamma_w + Q_{wf} + DISS_f .
\end{aligned}
\tag{II.B.3}
$$

(iv) the "difference density equation"

$$
\begin{aligned}
&\alpha_g \frac{\partial \rho_g}{\partial t} - \alpha_f \frac{\partial \rho_f}{\partial t} + \left(\rho_g + \rho_f\right)\frac{\partial \alpha_g}{\partial t} + \frac{1}{A}\frac{\partial}{\partial x}\left(\alpha_g \rho_g v_g A - \alpha_f \rho_f v_f A\right) \\
&= -\frac{2\left[H_{ig}\frac{P_s}{P}\left(T^s - T_g\right) + H_{if}\left(T^s - T_f\right)\right]}{h_g^* - h_f^*} + 2\Gamma_w .
\end{aligned}
\tag{II.B.4}
$$

(v) the "sum density equation"

$$
\alpha_g \frac{\partial \rho_g}{\partial t} + \alpha_f \frac{\partial \rho_f}{\partial t} + \left(\rho_g - \rho_f\right)\frac{\partial \alpha_g}{\partial t} + \frac{1}{A}\frac{\partial}{\partial x}\left(\alpha_g \rho_g v_g A + \alpha_f \rho_f v_f A\right) = 0.
\tag{II.B.5}
$$

(vi) the "sum momentum equation"

$$\alpha_g \rho_g \frac{\partial v_g}{\partial t} + \alpha_f \rho_f \frac{\partial v_f}{\partial t} + \frac{1}{2}\alpha_g \rho_g \frac{\partial v_g^2}{\partial x} + \frac{1}{2}\alpha_f \rho_f \frac{\partial v_f^2}{\partial x} = -\frac{\partial P}{\partial x} + \rho_m B_x - \alpha_g \rho_g v_g FWG - \alpha_f \rho_f v_f FWF - \Gamma_g (v_g - v_f). \quad \text{(II.B.6)}$$

(vii) the "difference momentum equation"

$$\frac{\partial v_g}{\partial t} - \frac{\partial v_f}{\partial t} + \frac{1}{2}\frac{\partial v_g^2}{\partial x} - \frac{1}{2}\frac{\partial v_f^2}{\partial x} = -\left(\frac{1}{\rho_g} - \frac{1}{\rho_f}\right)\frac{\partial P}{\partial x} + -v_g FWG + v_f FWF + \frac{\Gamma_g\left[\rho v_I - (\alpha_f \rho_f v_g + \alpha_g \rho_g v_f)\right]}{\alpha_g \rho_g \alpha_f \rho_f} - \rho_m FI(v_g - v_f) - C\frac{\rho_m^2}{\rho_g \rho_f}\frac{\partial (v_g - v_f)}{\partial t}. \quad \text{(II.B.7)}$$

(viii) the "mass conservation equation" for each noncondensable component

$$\frac{\partial}{\partial t}(\alpha_g \rho_g X_n X_{ni}) + \frac{1}{A}\frac{\partial}{\partial x}(\alpha_g \rho_g X_n X_{ni} v_g A) = 0 \quad \text{(II.B.8)}$$

where

$$X_{ni} = \frac{M_{ni}}{\sum_{i=1}^{N} M_{ni}} = \frac{M_{ni}}{M_n},$$

and where M_{ni} represents the mass of the i^{th} noncondensable component in the gaseous phase, while M_n represents the total mass of noncondensable gas in the gaseous phase; and, finally,

(ix) the "boron conservation equation"

$$\frac{\partial \rho_b}{\partial t} + \frac{1}{A}\frac{\partial (\alpha_f \rho_f C_b v_f A)}{\partial x} = 0, \quad \text{(II.B.9)}$$

where the concentration parameter is defined as

$$C_b = \rho_b / [\rho_m (1 - X)] = \rho_b / (\alpha_f \rho_f).$$

Equations (II.B.1) through (II.B.9) can be represented mathematically as the matrix-valued operator equation

$$\boldsymbol{N}(\boldsymbol{\chi},\boldsymbol{G}) - \boldsymbol{S}(\boldsymbol{G}) = \boldsymbol{0}\,, \tag{II.B.10}$$

where $\boldsymbol{\chi} \equiv (\chi_1,\ldots,\chi_9)$ denotes a vector whose components are the nine dependent (i.e., state) variables in the REL/CDE system, as follows: the gas specific internal energy, $U_g \equiv \chi_1$, the fluid specific internal energy, $U_f \equiv \chi_2$, the pressure, $P \equiv \chi_3$, the void fraction, $\alpha_g \equiv \chi_4$, the total noncondensable mass fraction, $X_n \equiv \chi_5$, the noncondensable mass fraction for the i^{th} noncondensable species, $X_{ni} \equiv \chi_6$, the boron density, $\rho_b \equiv \chi_7$, the gas velocity, $v_g \equiv \chi_8$, and the fluid velocity, $v_f \equiv \chi_9$. The two-fluid model equations depend on a large number of parameters, such as those entering in various correlations, initial and/or boundary conditions, formulae expressing the thermodynamic properties of water (the 1993 ASME Steam Tables), and those describing the geometry of the problem under consideration, etc. These parameters are denoted in Eq. (II.B.10) by the J-component vector $\boldsymbol{G} \equiv (g_1,\ldots,g_J)$, where J denotes the total number of parameters in RELAP5/MOD3.2.

Note that Eq. (II.B.10) contains first-order derivatives in time and space; therefore, it must be supplemented with appropriate initial and boundary conditions, which are hereby denoted as

$$\boldsymbol{\chi}(x,t_o) = \boldsymbol{\chi}_{init}(x), \quad \text{for } t = t_o \text{ and all } x \tag{II.B.11}$$

$$\boldsymbol{\chi}(x_o,t) = \boldsymbol{\chi}_{bound}(t), \quad \text{for } x = x_o \text{ and all } t > 0. \tag{II.B.12}$$

At this stage, it is important to note that since Eq. (II.B.10) is nonlinear, it can, in principle, admit multiple solutions as well as discontinuous solutions (e.g., phase-changes). All of the considerations in this Section, however, are restricted to those domains in phase (x,t) and parameter-space in which the solution of Eq. (II.B.10) through Eq. (II.B.12) is unique; all physical phenomena that might lead to non-unique solutions are beyond the scope of this Section.

In RELAP5/MOD 3.2, the REL/CDE are discretized spatially using a staggered spatial mesh that defines the RELAP "volumes;" furthermore, two adjacent volumes are connected to each other by RELAP "junctions." The velocities are defined at junctions, while all other state variables are defined as volume-averaged variables. This spatial discretization procedure is illustrated in Figure II.B.1, below.

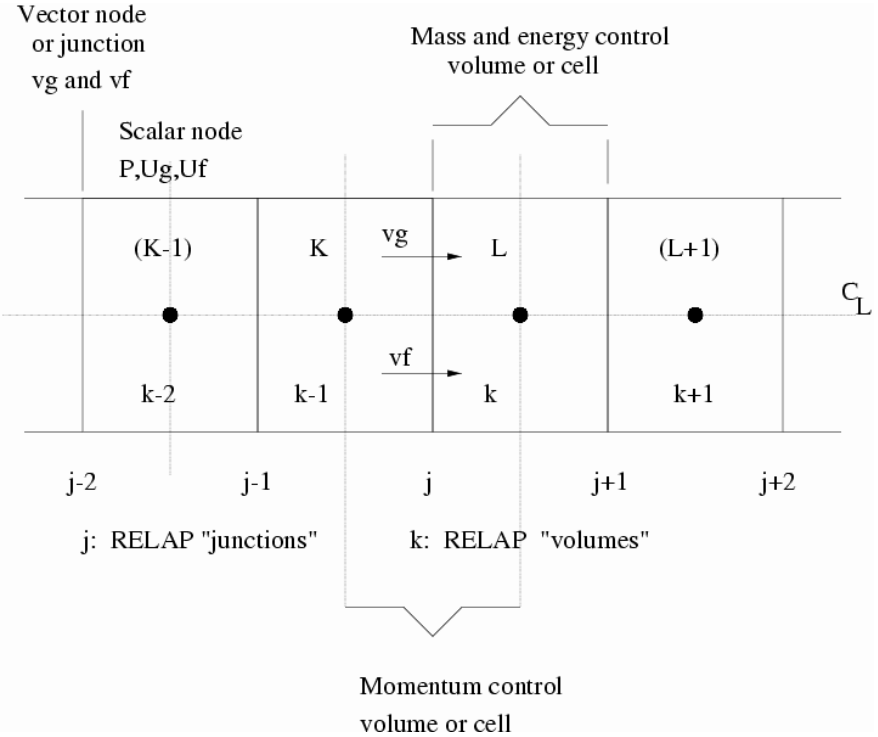

Figure II.B.1. Spatial discretization procedure (staggered mesh) for discretizing the REL/CDE.

The Discretized REL/CDE equations for each cell are obtained by (i) integrating the mass and energy equations with respect to the spatial variable x, from a junction at x_j to the next junction at x_{j+1}, and (ii) integrating the momentum equations with respect to the spatial variable x, from a cell center x_K to the adjoining cell center x_L. Two time-discretization procedures are implemented in RELAP5/MOD3.2; they are referred to as the nearly-implicit scheme, and the semi-implicit scheme, respectively. The nearly-implicit scheme is essentially a one-step integration procedure, while the semi-implicit scheme is a two-step integration procedure. Since the mathematical formalism of a one-step procedure can be formally considered to be a particular case of a two-step procedure, only the two-step procedure, i.e., the semi-implicit scheme, will be analyzed in this work.

In the semi-implicit scheme, the time advancement depends on the state of the fluid, in a control volume, for two successive time steps. The following four cases can occur in a control volume:

(a) "two-phase to two-phase," where two-phase flow conditions exist at both the old (n) time-step, and the new $(n+1)$ time step, respectively;

(b) "one-phase to one-phase," where one-phase flow conditions (either pure gas or pure liquid) exist at both the old (n) time-step, and the new $(n+1)$ time step, respectively;

(c) "two-phase to one-phase" (also referred to as "disappearance"), where two-phase flow conditions exist at the old (n) time-step, and one-phase flow conditions exist at the new $(n+1)$ time-step, respectively;

(d) "one-phase to two-phase" (also referred to as "appearance"), where one-phase flow conditions exist at the old (n) time-step, and two-phase flow conditions exist at the new $(n+1)$ time step, respectively.

After integration over x, from a junction at x_j to the next junction at x_{j+1}, the mass and energy equations yield a set of algebraic equations that can be written in matrix form as

$$\boldsymbol{A}\boldsymbol{x} = \boldsymbol{b} + \boldsymbol{g}^1 v_{g,j+1}^{n+1} + \boldsymbol{g}^2 v_{g,j}^{n+1} + \boldsymbol{f}^1 v_{f,j+1}^{n+1} + \boldsymbol{f}^2 v_{f,j}^{n+1}, \tag{II.B.13}$$

where

$$\boldsymbol{A} = \begin{bmatrix} A_{11} & A_{12} & 0 & A_{14} & A_{15} \\ A_{21} & A_{22} & A_{23} & A_{24} & A_{25} \\ A_{31} & A_{32} & A_{33} & A_{34} & A_{35} \\ A_{41} & A_{42} & A_{43} & A_{44} & A_{45} \\ A_{51} & A_{52} & A_{53} & A_{54} & A_{55} \end{bmatrix}, \qquad \boldsymbol{x} = \begin{bmatrix} \tilde{X}_{n,L}^{n+1} - X_{n,L}^{n} \\ \tilde{U}_{g,L}^{n+1} - U_{g,L}^{n} \\ \tilde{U}_{f,L}^{n+1} - U_{f,L}^{n} \\ \tilde{\alpha}_{g,L}^{n+1} - \alpha_{g,L}^{n} \\ P_L^{n+1} - P_L^{n} \end{bmatrix},$$

$$\boldsymbol{b} = \begin{bmatrix} 0 \\ b_2 \\ b_3 \\ b_4 \\ 0 \end{bmatrix}, \qquad \boldsymbol{g}^1 = \begin{bmatrix} g_1^1 \\ g_2^1 \\ 0 \\ g_4^1 \\ g_5^1 \end{bmatrix}, \qquad \boldsymbol{g}^2 = \begin{bmatrix} g_1^2 \\ g_2^2 \\ 0 \\ g_4^2 \\ g_5^2 \end{bmatrix}, \qquad \boldsymbol{f}^1 = \begin{bmatrix} 0 \\ 0 \\ f_3^1 \\ f_4^1 \\ f_5^1 \end{bmatrix}, \qquad \boldsymbol{f}^2 = \begin{bmatrix} 0 \\ 0 \\ f_3^2 \\ f_4^2 \\ f_5^2 \end{bmatrix},$$

for each time-step (n), volume k and/or junction j; the symbols with tilde indicate quantities that are evaluated at an intermediate (provisional) time-step. All of the variables appearing in the components of the matrix $\boldsymbol{A}$ and the vectors $\boldsymbol{b}, \boldsymbol{g}^1, \boldsymbol{g}^2, \boldsymbol{f}^1, \boldsymbol{f}^2$ are evaluated at old-time step, (n). The expressions of these components are listed in Appendix A.

The sum momentum equation is integrated over x, from a cell center x_K to the adjoining cell center x_L, to obtain

$$
\begin{aligned}
&\left(\alpha_g\rho_g\right)_j^n\left(v_g^{n+1}-v_g^n\right)_j\Delta x_j+\left(\alpha_f\rho_f\right)_j^n\left(v_f^{n+1}-v_f^n\right)_j\Delta x_j\\
&+\frac{1}{2}\left(\dot{\alpha}_g\dot{\rho}_g\right)_j^n\left[\left(v_g^2\right)_L^n-\left(v_g^2\right)_K^n\right]\Delta t+\frac{1}{2}\left(\dot{\alpha}_f\dot{\rho}_f\right)_j^n\left[\left(v_f^2\right)_L^n-\left(v_f^2\right)_K^n\right]\Delta t\\
&-\frac{1}{2}\left[\left(\dot{\alpha}_g\dot{\rho}_g\right)_j^n VISG_j^n-\left(\dot{\alpha}_f\dot{\rho}_f\right)_j^n VISF_j^n\right]\Delta t=-(1-\eta)\left(P_L-P_K\right)^{n+1}\Delta t\\
&+\left[\left(\rho_m\right)_j^n B_X-\left(\alpha_g\rho_g\right)_j^n FWG_j^n\left(v_g\right)_j^{n+1}-\left(\alpha_f\rho_f\right)_j^n FWF_j^n\left(v_f\right)_j^{n+1}\right.\\
&\left.-\left(\Gamma_g\right)_j^n\left(v_g-v_f\right)_j^{n+1}\right]\Delta x_j\Delta t\\
&-\left[\left(\dot{\alpha}_g\dot{\rho}_g\right)_j^n HLOSSG_j^n v_{g,j}^{n+1}-\left(\dot{\alpha}_f\dot{\rho}_f\right)_j^n HLOSSF_j^n v_{f,j}^{n+1}\right]\Delta t.
\end{aligned}
\tag{II.B.14}
$$

Similarly, the difference momentum equation is also integrated over x from a cell center x_K to the adjoining cell center x_L to obtain

$$
\begin{aligned}
&\left[1+C\rho_m^2/\left(\rho_g\rho_f\right)\right]_j^n\left[\left(v_g^{n+1}-v_g^n\right)-\left(v_f^{n+1}-v_f^n\right)\right]_j\Delta x_j\\
&+\frac{1}{2}\left[\left(\dot{\alpha}_g\dot{\rho}_g\right)/\left(\alpha_g\rho_g\right)\right]_j^n\left[\left(v_g^2\right)_L^n-\left(v_g^2\right)_K^n\right]\Delta t-\frac{1}{2}\left[\left(\dot{\alpha}_g\dot{\rho}_g\right)/\left(\alpha_g\rho_g\right)\right]_j^n VISG_j^n\Delta t\\
&-\frac{1}{2}\left[\left(\dot{\alpha}_f\dot{\rho}_f\right)/\left(\alpha_f\rho_f\right)\right]_j^n\left[\left(v_f^2\right)_L^n-\left(v_f^2\right)_K^n\right]\Delta t+\frac{1}{2}\left[\left(\dot{\alpha}_f\dot{\rho}_f\right)/\left(\alpha_f\rho_f\right)\right]_j^n VISF_j^n\Delta t\\
&=-(1-\eta)\left[\left(\rho_g-\rho_f\right)/\left(\rho_g\rho_f\right)\right]_j^n\left(P_L-P_K\right)^{n+1}\Delta t-\left\{FWG_j^n\left(v_g\right)_j^{n+1}\right.\\
&\left.-FWF_j^n\left(v_f\right)_j^{n+1}-\left(f_x\right)_j^n\left(\frac{1}{\alpha_g\rho_g}+\frac{1}{\alpha_f\rho_f}\right)^n\left[\left(f_{wg}\right)_j^n\left(v_g\right)_j^{n+1}-\left(f_{wf}\right)_j^n\left(v_f\right)_j^{n+1}\right]\right.\\
&\left.-\left[\Gamma_g^n\left(\rho_m^n v_I^{n+1}-\alpha_f^n\rho_f^n v_g^{n+1}-\alpha_g^n\rho_g^n v_f^{n+1}\right)/\left(\alpha_g\rho_g\alpha_f\rho_f\right)^n\right]_j\right.\\
&\left.+\left(\rho_m FI\right)_j^n\left(\left[1+f_x(C_1-1)\right]_j^n\left(v_g\right)_j^{n+1}-\left[1+f_x(C_0-1)\right]_j^n\left(v_f\right)_j^{n+1}\right)\right\}\Delta x_j\Delta t\\
&-\left\{\left[\left(\dot{\alpha}_g\dot{\rho}_g\right)/\left(\alpha_g\rho_g\right)\right]_j^n HLOSSG_j^n\left(v_g\right)_j^{n+1}\right.\\
&\left.-\left[\left(\dot{\alpha}_f\dot{\rho}_f\right)/\left(\alpha_f\rho_f\right)\right]_j^n HLOSSF_j^n\left(v_f\right)_j^{n+1}\right\}\Delta t.
\end{aligned}
\tag{II.B.15}
$$

Equations (II.B.13) through (II.B.15) constitute a system of 13 coupled algebraic equations that can be represented in matrix form as

$$
\boldsymbol{N}\left(\boldsymbol{\chi}_d^{n+1},\boldsymbol{G}\right)-\boldsymbol{S}\left(\boldsymbol{G}\right)=\boldsymbol{0}\ , \tag{II.B.16}
$$

where we have highlighted explicitly the functional dependence on the following quantities:

(A) $\boldsymbol{\chi}_d^{n+1} \equiv \Big[\left(U_g\right)_k^{n+1}, \left(U_f\right)_k^{n+1}, \left(P\right)_k^{n+1}, \left(\alpha_g\right)_k^{n+1}, \left(X_n\right)_k^{n+1}, \left(X_{ni}\right)_k^{n+1},$
$\left(\rho_b\right)_k^{n+1}, \left(v_g\right)_j^{n+1}, \left(v_f\right)_j^{n+1}, \left(\tilde{U}_g\right)_k^{n+1}, \left(\tilde{U}_f\right)_k^{n+1}, \left(\tilde{\alpha}_g\right)_k^{n+1}, \left(\tilde{X}_n\right)_k^{n+1} \Big]$, which represents the vector of *discretized* state variables for volume k and/or junction j. The first nine components of $\boldsymbol{\chi}_d^{n+1}$ are state variables at time-step $(n+1)$, while the last four components (with tilde) represent state variables evaluated at an intermediate (provisional) time-step, between time-steps (n) and $(n+1)$, respectively;

(B) $\boldsymbol{G} \equiv (g_1, \ldots, g_J)$, which represents a J-component column vector whose components comprise all numerical parameters in RELAP5/MOD3.2 that are subject to variations; and

(C) $\boldsymbol{S} \equiv (s_1, \ldots, s_{13})$, which represents a 13-component column vector whose components comprise all of the inhomogeneous source terms appearing in Eqs.(II.B.13) through (II.B.15).

The system of algebraic equations represented by Eq.(II.B.16) is solved to obtain (i) the pressure, the fluid, and gas velocities at the new time step $(n+1)$, and (ii) the intermediate time-step variables $\left(\tilde{U}_g\right)_k^{n+1}, \left(\tilde{U}_f\right)_k^{n+1}, \left(\tilde{\alpha}_g\right)_k^{n+1}, \left(\tilde{X}_n\right)_k^{n+1}$. For the cases (b) and (d) defined above, when one-phase conditions exist at the old time step (n), the intermediate time-step is actually skipped by setting $\left(\tilde{U}_g\right)_k^{n+1} \equiv \left(U_g\right)_k^{n+1}, \left(\tilde{U}_f\right)_k^{n+1} \equiv \left(U_f\right)_k^{n+1}, \left(\tilde{\alpha}_g\right)_k^{n+1} \equiv \left(\alpha_g\right)_k^{n+1}, \left(\tilde{X}_n\right)_k^{n+1} \equiv \left(X_n\right)_k^{n+1}$, so that the intermediate time-step variables are used directly at time-step $(n+1)$. For the cases (a) and (c) defined above, when two-phase conditions exist at the old time-step (n), the nonexpanded forms of the mass and energy equations are used to obtain $\left(U_g\right)_k^{n+1}, \left(U_f\right)_k^{n+1}, \left(\alpha_g\right)_k^{n+1}, \left(X_n\right)_k^{n+1}$. As an illustrative example, we present here the calculation of $\left(U_g\right)_L^{n+1}$, for a volume L and time-step $(n+1)$, and we present the calculation of the other three state variables in Appendix A. Thus, to calculate $\left(U_g\right)_L^{n+1}$, we first calculate the quantity $\left(\alpha_g \rho_g U_g\right)_L^{n+1}$ from the nonexpanded form of the vapor energy equation

$$
\begin{aligned}
&V_L\left[\left(\alpha_g\rho_g U_g\right)_L^{n+1}-\left(\alpha_g\rho_g U_g\right)_L^{n}\right]\\
&+\left[\dot{\alpha}_{g,j+1}\left(\dot{\rho}_{g,j+1}\dot{U}_{g,j+1}+P_L\right)v_{g,j+1}^{n+1}A_{j+1}-\dot{\alpha}_{g,j}\left(\dot{\rho}_{g,j}\dot{U}_{g,j}+P_L\right)v_{g,j}^{n+1}A_j\right]\Delta t\\
&=-V_L P_L^n\left(\tilde{\alpha}_{g,L}^{n+1}-\alpha_{g,L}^{n}\right)+\left\{-\frac{P_L^n-P_{s,L}^n}{P_L^n}H_{gf,L}^n\left(\tilde{T}_{g,L}^{n+1}-\tilde{T}_{f,L}^{n+1}\right)\right.\\
&-\left(\frac{h_f^*}{h_g^*-h_f^*}\right)_L^n\frac{P_{s,L}^n}{P_L^n}H_{ig,L}^n\left(\tilde{T}_L^{s,n+1}-\tilde{T}_{g,L}^{n+1}\right)-\left(\frac{h_g^*}{h_g^*-h_f^*}\right)_L^n H_{if,L}^n\left(\tilde{T}_L^{s,n+1}-\tilde{T}_{f,L}^{n+1}\right)\\
&\left.+\Gamma_{w,L}^n\left[\left(\frac{1-\varepsilon}{2}\right)\left(h'_{f,L}\right)^n+\left(\frac{1+\varepsilon}{2}\right)\left(h'_{g,L}\right)^n\right]+Q_{wg,L}^n+DISS_{g,L}^n\right\}V_L\Delta t.
\end{aligned}
$$

We then calculate $\left(\alpha_g\rho_g\right)_L^{n+1}$ from the nonexpanded form of the vapor density equation shown below:

$$
\begin{aligned}
&V_L\left[\left(\alpha_g\rho_g\right)_L^{n+1}-\left(\alpha_g\rho_g\right)_L^{n}\right]+\left(\dot{\alpha}_{g,j+1}\dot{\rho}_{g,j+1}v_{g,j+1}^{n+1}A_{j+1}-\dot{\alpha}_{g,j}\dot{\rho}_{g,j}v_{g,j}^{n+1}A_j\right)\Delta t\\
&=\left(-\frac{\dfrac{P_{s,L}^n}{P_L^n}H_{ig,L}^n\left(\tilde{T}_L^{s,n+1}-\tilde{T}_{g,L}^{n+1}\right)+H_{if,L}^n\left(\tilde{T}_L^{s,n+1}-\tilde{T}_{f,L}^{n+1}\right)}{\left(h_{g,L}^*\right)^n-\left(h_{f,L}^*\right)^n}+\Gamma_{w,L}^n\right)V_L\Delta t.
\end{aligned}
$$

Finally, we calculate the ratio of the results from the previous two operations to obtain $\left(U_g\right)_L^{n+1}=\left(\alpha_g\rho_g U_g\right)_L^{n+1}\Big/\left(\alpha_g\rho_g\right)_L^{n+1}$.

II.B.2. ASAP of the Two-Fluid Model in RELAP5/MOD3.2

This Section presents the application of the *ASAP* to the REL/CDE (in Sub-section II.B.2.a), and to the Discretized REL/CDE (in Sub-section II.B.2.b), respectively.

II.B.2.a ASAP for the REL/CDE

Many results, customarily referred to as "responses," $R(\boldsymbol{\chi},\boldsymbol{G})$, calculated by RELAP5/MOD3.2 can be generally represented in the integral form

$$R(\boldsymbol{\chi},\boldsymbol{G}) \equiv \int_{t_0}^{t_f} dt \int_{x_0}^{x_f} dx\, F\left[\boldsymbol{\chi}(x,t),\boldsymbol{G}(x,t)\right]. \tag{II.B.17}$$

In particular, this integral form can be used to represent either instantaneous or averaged (in space and/or time) values of the dependent variables; for example, setting $F(\boldsymbol{\chi},\boldsymbol{G}) = \delta_{ij}\delta(x-x_1)\delta(t-t_1)\cdot\boldsymbol{\chi}(x,t)$ in Eq.(II.B.17), where δ_{ij} represents the Kronecker-delta functional while $\delta(x-x_1)$ and $\delta(t-t_1)$ denote Dirac-delta functionals, yields the instantaneous value of the i^{th} dependent variable at the point (x_1,t_1) in space-time, namely $R(\boldsymbol{\chi},\boldsymbol{G}) = \chi_i(x_1,t_1)$. On the other hand, setting $F(\boldsymbol{\chi},\boldsymbol{G}) = \delta_{ij}\cdot\boldsymbol{\chi}(x,t)$ in Eq.(II.B.17), yields the space-time averaged value of the i^{th} dependent variable, namely $R(\boldsymbol{\chi},\boldsymbol{G}) = \int_{t_0}^{t_f} dt \int_{x_0}^{x_f} dx\,\chi_i(x,t)$.

Conceptually, the REL/CDE are solved using base-case (or nominal) parameter values, denoted here by $\boldsymbol{G}^o$, to obtain the base-case (or nominal) solution $\boldsymbol{\chi}^o$. In turn, the base-case (nominal) solution and parameter values are used to obtain the base-case (nominal) response value $R^o(\boldsymbol{\chi}^o,\boldsymbol{G}^o)$. The base-case (nominal) parameter values $\boldsymbol{G}^o \equiv (g_1^o,\ldots,g_J^o)$ are customarily determined from experimental data; consequently, their numerical values are not known exactly but are known only within some bounds (e.g., tolerances, variations); these bounds can be represented by the vector $\boldsymbol{\Gamma} \equiv (\gamma_1,\gamma_2,\ldots,\gamma_J) \equiv (\delta g_1,\delta g_2,\ldots,\delta g_J)$, whose components are the respective parameter variations δg_j.

When we introduce parameter variations $\boldsymbol{\Gamma} \equiv (\gamma_1,\gamma_2,\ldots,\gamma_J) \equiv (\delta g_1,\delta g_2,\ldots,\delta g_J)$ in Eqs. (II.B.10) and (II.B.17), the corresponding "perturbed" solution becomes $\boldsymbol{\chi}^o + \boldsymbol{\Phi}$, satisfying the perturbed system

$$\boldsymbol{N}(\boldsymbol{\chi}^o + \boldsymbol{\Phi},\boldsymbol{G}^o + \boldsymbol{\Gamma}) - \boldsymbol{S}(\boldsymbol{G}^o + \boldsymbol{\Gamma}) = \boldsymbol{0}\,, \tag{II.B.18}$$

while the perturbed response would become $R(\boldsymbol{\chi}^o + \boldsymbol{\Phi},\boldsymbol{G}^o + \boldsymbol{\Gamma})$, where $\boldsymbol{\Phi} \equiv (\Phi_1,\ldots,\Phi_9) \equiv (\delta U_g,\ldots,\delta v_f)$ denotes the nine-component vector of variations in the respective components of $\boldsymbol{\chi}$. We note here that, in principle, the above equation could be solved repeatedly, for each vector of variations $\boldsymbol{\Gamma} \equiv (\gamma_1,\gamma_2,\ldots,\gamma_J) \equiv (\delta g_1,\delta g_2,\ldots,\delta g_J)$ of interest, to obtain exactly the perturbed solution $(\boldsymbol{\chi}^o + \boldsymbol{\Phi})$.

Recall that the most general and fundamental concept for the definition of the *local sensitivity* of a response to parameter variations is the Gateaux (G-) differential. By definition, the G-differential $DP\left(\boldsymbol{e}^o;\boldsymbol{h}\right)$ of an operator $P\left(\boldsymbol{e}\right)$ at $\boldsymbol{e}^o$ with increment $\boldsymbol{h}$ is

$$DP\left(\boldsymbol{e}^o;\boldsymbol{h}\right)\equiv \lim_{\varepsilon\to 0}\varepsilon^{-1}\left[P\left(\boldsymbol{e}^o+\varepsilon\boldsymbol{h}\right)-P\left(\boldsymbol{e}^o\right)\right]=\frac{d}{d\varepsilon}\left\{P\left(\boldsymbol{e}^o+\varepsilon\boldsymbol{h}\right)\right\}_{\varepsilon=0}, \qquad \text{(II.B.19)}$$

for all (i.e., arbitrary) vectors $\boldsymbol{h}$, and scalar ε. The G-differential $DP\left(\boldsymbol{e}^o;\boldsymbol{h}\right)$ is related to the total variation $\left[P\left(\boldsymbol{e}^o+\boldsymbol{h}\right)-P\left(\boldsymbol{e}^o\right)\right]$ through the relationship

$$P\left(\boldsymbol{e}^o+\boldsymbol{h}\right)-P\left(\boldsymbol{e}^o\right)=DP\left(\boldsymbol{e}^o;\boldsymbol{h}\right)+W\left(\boldsymbol{h}\right),\ \text{with}\ \lim_{\varepsilon\to 0}\left[W\left(\varepsilon\boldsymbol{h}\right)/\varepsilon\right]=0. \qquad \text{(II.B.20)}$$

Applying Eq.(II.B.19) to Eq. (II.B.17), while noting that $\boldsymbol{e}=\left(\boldsymbol{\chi},\boldsymbol{G}\right)$, $\boldsymbol{e}^o=\left(\boldsymbol{\chi}^o,\boldsymbol{G}^o\right)$, and $\boldsymbol{h}=\left(\boldsymbol{\Phi},\boldsymbol{\Gamma}\right)$, yields the sensitivity $DR\left(\boldsymbol{\chi}^o,\boldsymbol{G}^o;\boldsymbol{\Phi},\boldsymbol{\Gamma}\right)$ of the response defined in Eq. (II.B.17) as

$$\begin{aligned} DR\left(\boldsymbol{\chi}^o,\boldsymbol{G}^o;\boldsymbol{\Phi},\boldsymbol{\Gamma}\right)&\equiv\frac{d}{d\varepsilon}\left\{\int_{t_o}^{t_f}dt\int_{x_o}^{x_f}dx F\left[\boldsymbol{\chi}^o+\varepsilon\boldsymbol{\Phi},\boldsymbol{G}^o+\varepsilon\boldsymbol{\Gamma}\right]\right\}_{\varepsilon=0} \\ &=\int_{t_o}^{t_f}dt\int_{x_o}^{x_f}dx\left(\partial F/\partial\boldsymbol{G}\right)^o\boldsymbol{\Gamma}\left(x,t\right)+\int_{t_o}^{t_f}dt\int_{x_o}^{x_f}dx\left(\partial F/\partial\boldsymbol{\chi}\right)^o\boldsymbol{\Phi}\left(x,t\right). \end{aligned} \qquad \text{(II.B.21)}$$

For the response $R\left(\boldsymbol{\chi},\boldsymbol{G}\right)$ defined in Eq.(II.B.17), Eq.(II.B.20) takes on the form

$$R\left(\boldsymbol{\chi}^o+\boldsymbol{\Phi},\boldsymbol{G}^o+\boldsymbol{\Gamma}\right)=R\left(\boldsymbol{\chi}^o,\boldsymbol{G}^o\right)+DR\left(\boldsymbol{\chi}^o,\boldsymbol{G}^o;\boldsymbol{\Phi},\boldsymbol{\Gamma}\right)+\mathrm{O}\left(\left\|\boldsymbol{\Phi}\right\|^2+\left\|\boldsymbol{\Gamma}\right\|^2\right), \qquad \text{(II.B.22)}$$

indicating that the exact value of the perturbed response, $R\left(\boldsymbol{\chi}^o+\boldsymbol{\Phi},\boldsymbol{G}^o+\boldsymbol{\Gamma}\right)$, namely the response-value that would be obtained by (exact) recalculations using perturbed values, is predicted by the sensitivity $DR\left(\boldsymbol{\chi}^o,\boldsymbol{G}^o;\boldsymbol{\Phi},\boldsymbol{\Gamma}\right)$ to first-order accuracy in $\left\|\boldsymbol{\Phi}\right\|$ and $\left\|\boldsymbol{\Gamma}\right\|$. As Eq. (II.B.21) indicates, the sensitivity $DR\left(\boldsymbol{\chi}^o,\boldsymbol{G}^o;\boldsymbol{\Phi},\boldsymbol{\Gamma}\right)$ can be calculated once the function $\boldsymbol{\Phi}$ is determined.

To first-order accuracy in $\left\|\boldsymbol{\Gamma}\right\|$, $\boldsymbol{\Phi}$ is the solution of the "*forward sensitivity model* (FSM)" [or the "*forward sensitivity equations* (FSE)," or the "*forward*

variational model (FVM)," or the "*tangent linear model* (TLM)"], which are obtained, as usual, by taking the G-differentials of the Differential REL/CDE. The derivation of the FSM will be illustrated now by presenting the calculations of the respective G-differentials for a typical "momentum-like"-conservation equation, a typical "density-like"-conservation equation, and a typical "energy-like"-conservation equation. For example, the G-differential of the "sum momentum equation" is obtained by calculating the expression

$$\begin{aligned}
&\frac{d}{d\varepsilon}\left\{\left[\left(\alpha_g^o+\varepsilon\delta\alpha_g\right)\rho_g\left(X_n^o+\varepsilon\delta X_n,U_g^o+\varepsilon\delta U_g,P^o+\varepsilon\delta P;g_j^o+\varepsilon\delta g_j\right)\cdot\right.\right.\\
&\frac{\partial}{\partial t}\left(v_g^o+\varepsilon\delta v_g\right)+\left(1-\alpha_g^o-\varepsilon\delta\alpha_g\right)\frac{\partial}{\partial t}\left(v_f^o+\varepsilon\delta v_f\right)\cdot\\
&\rho_f\left(U_f^o+\varepsilon\delta U_f,P^o+\varepsilon\delta P;g_j^o+\varepsilon\delta g_j\right)\\
&+\frac{1}{2}\left(\alpha_g^o+\varepsilon\delta\alpha_g\right)\cdot\rho_g\left(X_n^o+\varepsilon\delta X_n,U_g^o+\varepsilon\delta U_g,P^o+\varepsilon\delta P;g_j^o+\varepsilon\delta g_j\right)\frac{\partial}{\partial x}\left(v_g^o+\varepsilon\delta v_g\right)^2\\
&+\frac{1}{2}\left(1-\alpha_g^o-\varepsilon\delta\alpha_g\right)\rho_f\left(U_f^o+\varepsilon\delta U_f,P^o+\varepsilon\delta P;g_j^o+\varepsilon\delta g_j\right)\frac{\partial}{\partial x}\left(v_f^o+\varepsilon\delta v_f\right)^2\\
&\left.\left.+\frac{\partial}{\partial x}\left(P^o+\varepsilon\delta P\right)\right]\right\}_{\varepsilon=0}=\frac{d}{d\varepsilon}\left\{E_6\left(X_n^o+\varepsilon\delta X_n,U_g^o+\varepsilon\delta U_g,U_f^o+\varepsilon\delta U_f,\alpha_g^o+\varepsilon\delta\alpha_g,\right.\right.\\
&\left.\left.P^o+\varepsilon\delta P,v_g^o+\varepsilon\delta v_g,v_f^o+\varepsilon\delta v_f;g_j^o+\varepsilon\delta g_j\right)\right\}_{\varepsilon=0}
\end{aligned}$$

where $E_6(\boldsymbol{\chi},\boldsymbol{G})$ is defined as

$$E_6(\boldsymbol{\chi},\boldsymbol{G})\equiv\rho_m B_x-\alpha_g\rho_g FWG\,v_g-\alpha_f\rho_f FWF\,v_f-\Gamma_g\left(v_g-v_f\right),$$

and where FWG, FWF, and Γ_g are nonlinear algebraic functions of the dependent variables $\boldsymbol{\chi}$ and parameters $\boldsymbol{G}$.

Performing the differentiation operations in the above equation yields

$$\left(\alpha_g^o\left[\frac{\partial v_g^o}{\partial t}+\frac{1}{2}\frac{\partial\left(v_g^o\right)^2}{\partial x}\right]\left(\frac{\partial \rho_g}{\partial X_n}\right)_o-\left(\frac{\partial E_6}{\partial X_n}\right)_o\right)\delta X_n$$

$$+\left(\alpha_g^o\left[\frac{\partial v_g^o}{\partial t}+\frac{1}{2}\frac{\partial\left(v_g^o\right)^2}{\partial x}\right]\left(\frac{\partial \rho_g}{\partial U_g}\right)_o-\left(\frac{\partial E_6}{\partial U_g}\right)_o\right)\delta U_g$$

$$+\left(\alpha_f^o\left[\frac{\partial v_f^o}{\partial t}+\frac{1}{2}\frac{\partial\left(v_f^o\right)^2}{\partial x}\right]\cdot\left(\frac{\partial \rho_f}{\partial U_f}\right)_o-\left(\frac{\partial E_6}{\partial U_f}\right)_o\right)\delta U_f$$

$$+\left(\rho_g^o\left[\frac{\partial v_g^o}{\partial t}+\frac{1}{2}\frac{\partial\left(v_g^o\right)^2}{\partial x}\right]-\rho_f^o\left[\frac{\partial v_f^o}{\partial t}+\frac{1}{2}\frac{\partial\left(v_f^o\right)^2}{\partial x}\right]-\left(\frac{\partial E_6}{\partial \alpha_g}\right)_o\right)\delta\alpha_g$$

$$+\left(\alpha_g^o\left[\frac{\partial v_g^o}{\partial t}+\frac{1}{2}\frac{\partial\left(v_g^o\right)^2}{\partial x}\right]\left(\frac{\partial \rho_g}{\partial P}\right)_o+\alpha_f^o\left[\frac{\partial v_f^o}{\partial t}+\frac{1}{2}\frac{\partial\left(v_f^o\right)^2}{\partial x}\right]\left(\frac{\partial \rho_f}{\partial P}\right)_o-\left(\frac{\partial E_6}{\partial P}\right)_o\right)\delta P$$

$$+\frac{\partial}{\partial x}(\delta P)+\alpha_g^o\rho_g^o\left(\frac{\partial}{\partial t}\left(\delta v_g\right)+\frac{\partial}{\partial x}\left(v_g^o\cdot\delta v_g\right)\right)-\left(\frac{\partial E_6}{\partial v_g}\right)_o\delta v_g$$

$$+\alpha_f^o\rho_f^o\cdot\left(\frac{\partial}{\partial t}\left(\delta v_f\right)+\frac{\partial}{\partial x}\left(v_f^o\cdot\delta v_f\right)\right)-\left(\frac{\partial E_6}{\partial v_f}\right)_o\delta v_f$$

$$=\left(\frac{\partial E_6}{\partial A}\right)_o\delta A+\left(\frac{\partial E_6}{\partial g_j}\right)_o\delta g_j-\left(\alpha_g^o\left[\frac{\partial v_g^o}{\partial t}+\frac{1}{2}\frac{\partial\left(v_g^o\right)^2}{\partial x}\right]\left(\frac{\partial \rho_g}{\partial g_j}\right)_o\right.$$

$$\left.+\alpha_f^o\left[\frac{\partial v_f^o}{\partial t}+\frac{1}{2}\frac{\partial\left(v_f^o\right)^2}{\partial x}\right]\left(\frac{\partial \rho_f}{\partial g_j}\right)_o\right)\delta g_j.$$

As a further example, the G-differential of the "sum density equation" is calculated by performing the differentiation shown in the following equation:

$$\frac{d}{d\varepsilon}\Big\{\left(\alpha_g^o+\varepsilon\delta\alpha_g\right)\frac{\partial}{\partial t}\rho_g\left(X_n^o+\varepsilon\delta X_n,U_g^o+\varepsilon\delta U_g,P^o+\varepsilon\delta P;g_j^o+\varepsilon\delta g_j\right)$$
$$+\left(1-\alpha_g^o-\varepsilon\delta\alpha_g\right)\frac{\partial}{\partial t}\rho_f\left(U_f^o+\varepsilon\delta U_f,P^o+\varepsilon\delta P;g_j^o+\varepsilon\delta g_j\right)$$
$$+\Big(\rho_g\left(X_n^o+\varepsilon\delta X_n,U_g^o+\varepsilon\delta U_g,P^o+\varepsilon\delta P;g_j^o+\varepsilon\delta g_j\right)$$
$$-\rho_f\left(U_f^o+\varepsilon\delta U_f,P^o+\varepsilon\delta P;g_j^o+\varepsilon\delta g_j\right)\Big)\frac{\partial}{\partial t}\left(\alpha_g^o+\varepsilon\delta\alpha_g\right)$$
$$+\frac{1}{A^o+\varepsilon\delta A}\Big\{\frac{\partial}{\partial x}\Big[\left(\alpha_g^o+\varepsilon\delta\alpha_g\right)\left(v_g^o+\varepsilon\delta v_g\right)\left(A^o+\varepsilon\delta A\right)$$
$$\rho_g\left(X_n^o+\varepsilon\delta X_n,U_g^o+\varepsilon\delta U_g,P^o+\varepsilon\delta P;g_j^o+\varepsilon\delta g_j\right)+\left(1-\alpha_g^o-\varepsilon\delta\alpha_g\right)$$
$$\rho_f\left(U_f^o+\varepsilon\delta U_f,P^o+\varepsilon\delta P;g_j^o+\varepsilon\delta g_j\right)\left(v_f^o+\varepsilon\delta v_f\right)\left(A^o+\varepsilon\delta A\right)\Big]\Big\}\Big\}_{\varepsilon=0}=0.$$

Similarly, the G-differential of the "liquid energy equation" is obtained by calculating the expression

$$\frac{d}{d\varepsilon}\Big\{\left(1-\alpha_g^0-\varepsilon\delta\alpha_g\right)\left(U_f^0+\varepsilon\delta U_f\right)\frac{\partial}{\partial t}\rho_f\left(U_f^0+\varepsilon\delta U_f,P^0+\varepsilon\delta P;g_j^0+\varepsilon\delta g_j\right)$$
$$+\left(1-\alpha_g^0-\varepsilon\delta\alpha_g\right)\rho_f\left(U_f^0+\varepsilon\delta U_f,P^0+\varepsilon\delta P;g_j^0+\varepsilon\delta g_j\right)\frac{\partial}{\partial t}\left(U_f^0+\varepsilon\delta U_f\right)$$
$$-\Big[\rho_f\left(U_f^0+\varepsilon\delta U_f,P^0+\varepsilon\delta P;g_j^0+\varepsilon\delta g_j\right)\left(U_f^0+\varepsilon\delta U_f\right)+P^0+\varepsilon\delta P\Big]\frac{\partial}{\partial t}\left(\alpha_g^0+\varepsilon\delta\alpha_g\right)$$
$$+\frac{1}{A^0+\varepsilon\delta A}\Big\{\frac{\partial}{\partial x}\Big[\left(1-\alpha_g^0-\varepsilon\delta\alpha_g\right)\rho_f\left(U_f^0+\varepsilon\delta U_f,P^0+\varepsilon\delta P;g_j^0+\varepsilon\delta g_j\right)\cdot$$
$$\left(U_f^0+\varepsilon\delta U_f\right)\left(v_f^0+\varepsilon\delta v_f\right)\left(A^0+\varepsilon\delta A\right)$$
$$+\left(P^0+\varepsilon\delta P\right)\frac{\partial}{\partial x}\Big[\left(1-\alpha_g^0-\varepsilon\delta\alpha_g\right)\left(v_f^0+\varepsilon\delta v_f\right)\left(A^0+\varepsilon\delta A\right)\Big]\Big\}\Big\}_{\varepsilon=0}$$
$$=\frac{d}{d\varepsilon}\Big\{E_3\left(X_n^0+\varepsilon\delta X_n,U_g^0+\varepsilon\delta U_g,U_f^0+\varepsilon\delta U_f,\alpha_g^0+\varepsilon\delta\alpha_g,P^0+\varepsilon\delta P,\right.$$
$$\left.v_g^0+\varepsilon\delta v_g,v_f^0+\varepsilon\delta v_f;g_j^0+\varepsilon\delta g_j\right)\Big\}_{\varepsilon=0},$$

where

$$E_3(\boldsymbol{\chi},\boldsymbol{G}) \equiv \left(\frac{h_f'}{h_g'-h_f'}\right) H_{ig}\left(T^s - T_g\right) + \left(\frac{h_g'}{h_g'-h_f'}\right) H_{if}\left(T^s - T_f\right) - \left[\left(\frac{1+\varepsilon}{2}\right) h_g^s + \left(\frac{1-\varepsilon}{2}\right) h_f^s\right] \Gamma_w + Q_{wf} + DISS_f ,$$

and where H_{if}, Γ_w, Q_{wf}, and $DISS_f$ are nonlinear algebraic functions of the dependent variables $\boldsymbol{\chi}$ and parameters $\boldsymbol{G}$.

The G-differentials of the remaining equations comprising the REL/CDE are calculated similarly. Collecting all of the G-differentiated REL/CDE yields the FSM for the two-fluid model, which can be represented in the form

$$\sum_{n=1}^{9} \left\{ \frac{\partial}{\partial t}\left[S_{mn}(x,t)\Phi_n(x,t)\right] + \frac{1}{A^o(x)}\frac{\partial}{\partial x}\left[A^o(x)T_{mn}(x,t)\Phi_n(x,t)\right] + U_{mn}(x,t)\ \Phi_n(x,t) \right\}$$

$$\equiv \boldsymbol{L}\boldsymbol{\Phi} = \sum_{j=1}^{J} Q_{mj}(x,t)\Gamma_j(x,t), \quad (m = 1,\ldots 9). \tag{II.B.23}$$

where the vector-valued function $\boldsymbol{\Phi} \equiv (\Phi_1,\ldots,\Phi_9) \equiv (\delta U_g, ..., \delta v_f)$ is subject to the known initial-time condition $\boldsymbol{\Phi}(x,t_o) = \Delta\boldsymbol{\chi}(x,t_o)$, for all x, and the known boundary condition $\boldsymbol{\Phi}(x_o,t) = \Delta\boldsymbol{\chi}(x_o,t)$ at x_o for all t, respectively. The expressions for the quantities $S_{mn}(x,t)$, $T_{mn}(x,t)$, $U_{mn}(x,t)$, and $Q_{mj}(x,t)$ introduced in the above equation have been obtained by symbolic computer calculus using MAPLE V9; their explicit formulae are presented in Appendix B.

The solution of Eq. (II.B.23) could, in principle, be used in Eq.(II.B.21) to calculate the sensitivity $DR(\boldsymbol{\chi}^o,\boldsymbol{G}^o;\boldsymbol{\Phi},\boldsymbol{\Gamma})$, since the error in obtaining $\boldsymbol{\Phi} \equiv (\Phi_1,\ldots,\Phi_9)$ from Eq. (II.B.23) is of second-order in $\|\boldsymbol{\Gamma}\|$. Note, however, that Eq. (II.B.23) would need to be solved anew (i.e., repeatedly) for each Γ_i, which is impractical if there are many Γ_i. Thus, applying the Forward Sensitivity Analysis Procedure (*FSAP*) would be just as expensive, computationally, as performing repeatedly the exact recalculations by solving Eq. (II.B.18) with the RELAP5/MOD3.2 code system, and then recalculating the exact perturbed response $R(\boldsymbol{\chi}^o + \boldsymbol{\Phi}, \boldsymbol{G}^o + \boldsymbol{\Gamma})$.

Examining Eqs. (II.B.21) and (II.B.23) reveals that both are linear in $\boldsymbol{\Phi}$. Therefore, the Adjoint Sensitivity Analysis Procedure (*ASAP*) can be applied by following the general theory presented in Chapter V of Volume I, along the same lines as in Section I.A of this Chapter. To begin with, the vector

$\boldsymbol{\Phi}^*(x,t) \equiv \left(\Phi_1^*(x,t),\ldots,\Phi_9^*(x,t)\right)$ of adjoint functions is introduced by taking the inner product of $\boldsymbol{\Phi}^*$ with Eq. (II.B.23) to obtain

$$\left\langle \boldsymbol{\Phi}^*, \boldsymbol{L}\boldsymbol{\Phi} \right\rangle = \left\langle \boldsymbol{M}\boldsymbol{\Phi}^*, \boldsymbol{\Phi} \right\rangle + \left\{P\left[\boldsymbol{\Phi}, \boldsymbol{\Phi}^*\right]\right\}, \tag{II.B.24}$$

where: (i) the angular brackets denote the inner product $\langle \boldsymbol{a}, \boldsymbol{b} \rangle \equiv \int_{t_o}^{t_f} dt \int_{x_o}^{x_f} dx \boldsymbol{a}(x,t) \cdot \boldsymbol{b}(x,t)$, (ii) $\boldsymbol{M}$ is the formal adjoint of $\boldsymbol{L}$, and (iii) $\left\{P\left[\boldsymbol{\Phi}, \boldsymbol{\Phi}^*\right]\right\}$ denotes the bilinear concomitant evaluated on the surface, in space-time, of the computational domain (x,t). In practice, the right-side of Eq. (II.B.24) is obtained by first performing the vector-multiplication between $\boldsymbol{\Phi}^*$ and $\boldsymbol{L}\boldsymbol{\Phi}$, and then by integrating the resulting differential equations by parts over x and t such as to transfer all of the differentiation operations from the components of $\boldsymbol{\Phi}$ to the components of $\boldsymbol{\Phi}^*$. Following the steps shown in Section I.A, the following sequence of operations is now effected in Eq. (II.B.24): (i) set $\boldsymbol{M}\boldsymbol{\Phi}^* = (\partial F / \partial \boldsymbol{\chi})^o$; (ii) eliminate the unknown values $\boldsymbol{\Phi}(x, t_f)$ and $\boldsymbol{\Phi}(x_f, t)$ by imposing $\boldsymbol{\Phi}^*(x, t_f) = \boldsymbol{0}$ and $\boldsymbol{\Phi}^*(x_f, t) = \boldsymbol{0}$ as "final-time" and, respectively, "outlet-boundary" conditions for $\boldsymbol{\Phi}^*$; and (iii) use the known initial and boundary conditions for $\boldsymbol{\Phi}$. This sequence of operations transforms Eq. (II.B.24) to

$$\begin{aligned} \left\langle (\partial F / \partial \boldsymbol{\chi})^o, \boldsymbol{\Phi} \right\rangle = \left\langle \boldsymbol{\Phi}^*, \boldsymbol{L}\boldsymbol{\Phi} \right\rangle + \int_{x_o}^{x_f} \boldsymbol{\Phi}^*(x,t_o) \left[\boldsymbol{S}(x,t_o) \bullet \Delta\boldsymbol{\chi}(x,t_o)\right] dx \\ + \int_{t_o}^{t_f} \boldsymbol{\Phi}^*(x_o,t) \left[\boldsymbol{T}(x_o,t) \bullet \Delta\boldsymbol{\chi}(x_o,t)\right] dt \,, \end{aligned} \tag{II.B.25}$$

where the vector-valued adjoint function $\boldsymbol{\Phi}^*$ satisfies the following system of adjoint equations:

$$\begin{aligned} &\sum_{n=1}^{9} \left\{ - S_{nm} \partial \Phi_n^* / \partial t - A^o(x) T_{nm} \partial \left(\Phi_n^* / A^o\right) / \partial x + U_{nm}(x,t) \Phi_n^*(x,t) \right\} \\ &= (\partial F / \partial \chi_m)^o, \ (m = 1,\ldots, 9), \end{aligned} \tag{II.B.26}$$

and where $\boldsymbol{\Phi}^*$ is subject to the final-time conditions

$$\boldsymbol{\Phi}^*\left(x, t_f\right) = \boldsymbol{0}\ , \text{ for all } x\ , \tag{II.B.27}$$

and the outlet-boundary conditions

$$\boldsymbol{\Phi}^*\left(x_f, t\right) = \boldsymbol{0}\ , \text{ for all } t\ . \tag{II.B.28}$$

Equation (II.B.26) together with the final-time conditions given by Eq. (II.B.27) and the boundary conditions represented by Eq. (II.B.28) constitute the "*adjoint sensitivity model* (ASM)" [or the "*adjoint sensitivity equations* (ASE)," or the "*adjoint variational model* (AVM)," or the "*adjoint linear model* (ALM)"].

Comparing Eqs. (II.B.21) and (II.B.25) reveals that the sensitivity $DR\left(\boldsymbol{\chi}^o, \boldsymbol{G}^o; \boldsymbol{\Phi}, \boldsymbol{\Gamma}\right)$ can now be expressed in terms of the adjoint function $\boldsymbol{\Phi}^*$ as

$$\begin{aligned} DR\left(\boldsymbol{\chi}^o, \boldsymbol{G}^o; \boldsymbol{\Phi}, \boldsymbol{\Gamma}; \boldsymbol{\Phi}^*\right) = & \sum_{j=1}^{J} \int_{x_o}^{x_f} dx \int_{t_o}^{t_f} dt \left(\partial \mathcal{F} / \partial \gamma_j\right)^o \Gamma_j + \int_{t_o}^{t_f} dt \int_{x_o}^{x_f} dx\ \boldsymbol{\Phi}^* \bullet \left(\boldsymbol{Q}\boldsymbol{\Gamma}\right) \\ & + \int_{x_o}^{x_f} \boldsymbol{\Phi}^*\left(x, t_o\right)\left[\boldsymbol{S}\left(x, t_o\right) \bullet \Delta\boldsymbol{\chi}\left(x, t_o\right)\right] dx + \int_{t_o}^{t_f} \boldsymbol{\Phi}^*\left(x_o, t\right)\left[\boldsymbol{T}\left(x_o, t\right) \bullet \Delta\boldsymbol{\chi}\left(x_o, t\right)\right] dt. \end{aligned} \tag{II.B.29}$$

Equation (II.B.26) reveals the following important characteristics regarding the ASM:

(a) The ASM does not depend on the parameter variations Γ_j; hence, the adjoint function $\boldsymbol{\Phi}^*$ is independent of parameter variations, too.

(b) The source for (i.e., the right-side of) the ASM depends on the response R; hence, $\boldsymbol{\Phi}^*$ must be calculated anew for every R.

(c) The ASM is linear in $\boldsymbol{\Phi}^*$; hence, the numerical methods for calculating $\boldsymbol{\Phi}^*$ need not be the same as originally used for calculating the base-case solution $\boldsymbol{\chi}^o$ of the nonlinear original system described by Eq. (II.B.10); in other words, the numerical methods for solving the ASM need *not* be the same as the original numerical methods used in RELAP5/MOD3.2. In many cases, it is even easier to calculate the adjoint function (which results from the solution of a *linear* system) than the original calculation of $\boldsymbol{\chi}^o$ (which results from the solution of a *nonlinear* system).

(d) The ASM depends (in general, nonlinearly) on the base-case (nominal) solution $\boldsymbol{\chi}^o$ through the quantities $S_{mn}\left(x,t\right)$, $T_{mn}\left(x,t\right)$, and $U_{mn}\left(x,t\right)$; hence, the adjoint function $\boldsymbol{\Phi}^*$ depends, in general nonlinearly, on the base-case solution $\boldsymbol{\chi}^o$, too. Thus, the base-case solution $\boldsymbol{\chi}^o$ must be available prior to

solving the ASM. Furthermore, the programming strategy for solving the ASM must be intertwined efficiently with the programming in the original code (i. e., RELAP5/MOD3.2) in order to optimize the calculation of $\boldsymbol{\Phi}^*$ by minimizing memory requirements and CPU-time for its calculation.

From the characteristics described in items (a) through (d) above, it follows that the *ASAP* should be used whenever the number of parameter variations Γ_j exceeds the number of responses R of interest; this is generally the case in practice. The reverse case, when the number of responses R exceeds the number of parameter variations Γ_j, occurs rather seldom in practice. Should such a case occur, however, the *FSAP* might be used for sensitivity analysis, if it already exists in the respective code; otherwise, direct recalculations should be performed, since they would require no additional programming.

II.B.2.b Implementation of the ASAP for the Discretized REL/CDE

A result (response) calculated by RELAP5/MOD3.2 can be generally represented in discretized form as

$$R(\boldsymbol{\chi}_d, \boldsymbol{G}) = \sum_{n=0}^{NF} \sum_{j=1}^{NJ} \sum_{k=1}^{NV} F_{jk}^n (\boldsymbol{\chi}_d, \boldsymbol{G}), \tag{II.B.30}$$

where NF, NJ, and NV denote, respectively, the total number of time steps, the total number of junctions, and the total number of volumes in the problem under consideration.

When the parameter variations $\boldsymbol{\Gamma} \equiv (\gamma_1, \gamma_2, \ldots, \gamma_J) \equiv (\delta g_1, \delta g_2, \ldots, \delta g_J)$ are considered in Eqs. (II.B.16) and (II.B.30), the corresponding "perturbed" solution would become $\boldsymbol{\chi}_d^o + \boldsymbol{\Psi}$, satisfying the perturbed system

$$\underline{N}(\boldsymbol{\chi}_d^o + \boldsymbol{\Psi}, \boldsymbol{G}^o + \boldsymbol{\Gamma}) - \boldsymbol{S}(\boldsymbol{G}^o + \boldsymbol{\Gamma}) = \boldsymbol{0}, \tag{II.B.31}$$

while the perturbed response would become $R(\boldsymbol{\chi}_d^o + \boldsymbol{\Psi}, \boldsymbol{G}^o + \boldsymbol{\Gamma})$, where $\boldsymbol{\Psi} \equiv \left[(\delta U_g)_k^{n+1}, \ldots, (\delta \tilde{X}_n)_k^{n+1} \right]$ denotes the corresponding variations in the vector of dependent variables $\boldsymbol{\chi}_d$.

Applying the definition of the G-differential given in Eq. (II.B.19) to (II.B.30) yields the following expression for the sensitivity DR of R to variations $\boldsymbol{\Gamma}$ (in $\boldsymbol{G}$ around $\boldsymbol{G}^o$) and $\boldsymbol{\Psi}$ (in $\boldsymbol{\chi}_d$ around $\boldsymbol{\chi}_d^o$):

$$DR = \sum_{n=0}^{NF}\sum_{j=1}^{NJ}\sum_{k=1}^{NV}\left[\sum_{\nu=1}^{13}\frac{\partial F_{jk}^{n}}{\partial \chi_{d,\nu}}\Psi_{\nu} + \sum_{\alpha=1}^{J}\frac{\partial F_{jk}^{n}}{\partial G_{\alpha}}\Gamma_{\alpha}\right] \equiv DR(\boldsymbol{\Psi}) + DR(\boldsymbol{\Gamma}), \quad \text{(II.B.32)}$$

where $DR(\boldsymbol{\Gamma})$ represents the "direct effect" term while $DR(\boldsymbol{\Psi})$ represents the "indirect effect" term.

To compute the indirect effect term $DR(\boldsymbol{\Psi})$, we need to compute $\boldsymbol{\Psi}$; to first order in $\|\boldsymbol{\Gamma}\|$, $\boldsymbol{\Psi}$ is obtained by taking the G-differential of Eq.(II.B.16) to derive the Discrete FSM, and subsequently solving this system. To derive the Discrete FSM, we introduce the following notations:

(i) For variations in the volume-averaged dependent variables, over a volume k, $(k = 1,\ldots,NV)$, at time-step n, $(n = 1,\ldots,NF)$, we introduce the notations:

$$\left(X_k^1\right)^n \equiv \left(\delta U_g\right)_k^n, \left(X_k^2\right)^n \equiv \left(\delta U_f\right)_k^n, \left(X_k^3\right)^n \equiv \left(\delta P\right)_k^n, \left(X_k^4\right)^n \equiv \left(\delta \alpha_g\right)_k^n,$$

$$\left(X_k^5\right)^n \equiv \left(\delta X_n\right)_k^n, \left(X_k^6\right)^n \equiv \left(\delta X_{ni}\right)_k^n, \left(X_k^7\right)^n \equiv \left(\delta \rho_b\right)_k^n;$$

(ii) For variations in the dependent variables defined at junctions j, $(j = 1,\ldots,NJ)$, at time-step n, we introduce the notations

$$\left(Y_k^1\right)^n \equiv \left(\delta v_g\right)_j^n, \left(Y_k^2\right)^n \equiv \left(\delta v_f\right)_j^n;$$

(iii) For variations in the volume-averaged, intermediate-time-step variables, for a volume k, $(k = 1,\ldots,NV)$, at time-step n, we introduce the notations:

$$\left(Z_k^1\right)^n \equiv \left(\delta \tilde{U}_g\right)_k^n, \left(Z_k^2\right)^n \equiv \left(\delta \tilde{U}_f\right)_k^n, \left(Z_k^3\right)^n \equiv \left(\delta \tilde{\alpha}_g\right)_k^n, \left(Z_k^4\right)^n \equiv \left(\delta \tilde{X}_n\right)_k^n.$$

We also define M_1 and M_2 to denote the total number of volume-averaged dependent variables and, respectively, the total number of intermediate-time-step variables, at time step n; note that $4 \le M_1 \le 7$ and $0 \le M_2 \le 4$. Note that the quantities $\left(X_k^1\right)^n,\ldots,\left(X_k^7\right)^n$, $\left(Y_k^1\right)^n, \left(Y_k^2\right)^n$, $\left(Z_k^1\right)^n,\ldots,\left(Z_k^4\right)^n$ are actually components of $\boldsymbol{\Psi}$; they were introduced in order to simplify the notation in the derivations to follow below, aimed at eliminating the intermediate-time variables.

Applying the definition of the G-differential to Eq. (II.B.16) and using the above notations yields the following matrix representation of the Discrete FSM:

$$\sum_{\nu=1}^{M_1}\left[BV_{\mu\nu}^{n-1}X_{\nu}^{n} + CV_{\mu\nu}^{n-1}X_{\nu}^{n-1}\right] + \sum_{\nu=1}^{2}\left[DV_{\mu\nu}^{n-1}Y_{\nu}^{n} + EV_{\mu\nu}^{n-1}Y_{\nu}^{n-1}\right]$$
$$+ \sum_{\nu=1}^{M_2}\left[TV_{\mu\nu}^{n-1}Z_{\nu}^{n}\right] = FV_{\mu\nu}^{n-1},$$

$$\text{for } (\mu = 1,\ldots,M_1);\ (n = 1,\ldots,NF);$$
$$\sum_{\nu=1}^{M_1}\left[BJ_{\mu\nu}^{n-1}X_\nu^n + CJ_{\mu\nu}^{n-1}X_\nu^{n-1}\right] + \sum_{\nu=1}^{2}\left[DJ_{\mu\nu}^{n-1}Y_\nu^n + EJ_{\mu\nu}^{n-1}Y_\nu^{n-1}\right] = FJ_{\mu\nu}^{n-1},$$
$$\text{for } (\mu = 1,2);\ (n = 1,\ldots,NF);$$
$$\sum_{\nu=1}^{M_1}\left[BI_{\mu\nu}^{n-1}X_\nu^n + CI_{\mu\nu}^{n-1}X_\nu^{n-1}\right] + \sum_{\nu=1}^{2}\left[DI_{\mu\nu}^{n-1}Y_\nu^n + EI_{\mu\nu}^{n-1}Y_\nu^{n-1}\right] + \sum_{\nu=1}^{M_2}\left[TI_{\mu\nu}^{n-1}Z_\nu^n\right]$$
$$= FI_{\mu\nu}^{n-1}, \text{ for } (\mu = 1,\ldots,M_2);\ (n = 1,\ldots,NF).$$

(II.B.33)

The various matrices and vectors appearing in the above Discrete FSM are defined as follows:

$$FV_\mu^n \equiv \begin{bmatrix} (fv)_1^\mu \\ \vdots \\ (fv)_{NV}^\mu \end{bmatrix}_{(NV\times 1)};\ FJ_\mu^n \equiv \begin{bmatrix} (fj)_1^\mu \\ \vdots \\ (fj)_{NJ}^\mu \end{bmatrix}_{(NJ\times 1)};\ FI_\mu^n \equiv \begin{bmatrix} (fi)_1^\mu \\ \vdots \\ (fi)_{NV}^\mu \end{bmatrix}_{(NV\times 1)};$$

$$X_\mu^n \equiv \begin{bmatrix} X_1^\mu \\ \vdots \\ X_{NV}^\mu \end{bmatrix}_{(NV\times 1)};\ Y_\mu^n \equiv \begin{bmatrix} Y_1^\mu \\ \vdots \\ Y_{NJ}^\mu \end{bmatrix}_{(NJ\times 1)};\ Z_\mu^n \equiv \begin{bmatrix} Z_1^\mu \\ \vdots \\ Z_{NV}^\mu \end{bmatrix};$$

$$BV_{\mu\nu}^n \equiv \left[(bv)_{ij}^{\mu\nu}\right]_{(NV\times NV)};\quad CV_{\mu\nu}^n \equiv \left[(cv)_{ij}^{\mu\nu}\right]_{(NV\times NV)};$$

$$DV_{\mu\nu}^n \equiv \left[(dv)_{ij}^{\mu\nu}\right]_{(NV\times NJ)};\ EV_{\mu\nu}^n \equiv \left[(ev)_{ij}^{\mu\nu}\right]_{(NV\times NJ)};$$

$$TV_{\mu\nu}^n \equiv \left(diag\left\{\left(tv^{\mu\nu}\right)_k^n\right\}\right)_{NV\times NV};\ TI_{\mu\nu}^n \equiv \left(diag\left\{\left(ti^{\mu\nu}\right)_k^n\right\}\right)_{NV\times NV};$$

$$BJ_{\mu\nu}^n \equiv \left[(bj)_{ij}^{\mu\nu}\right]_{(NJ\times NV)};\quad CJ_{\mu\nu}^n \equiv \left[(cj)_{ij}^{\mu\nu}\right]_{(NJ\times NV)};$$

$$DJ_{\mu\nu}^n \equiv \left[(dj)_{ij}^{\mu\nu}\right]_{(NJ\times NJ)};\ EJ_{\mu\nu}^n \equiv \left[(ej)_{ij}^{\mu\nu}\right]_{(NJ\times NJ)};$$

$$BI_{\mu\nu}^n \equiv \left[(bi)_{ij}^{\mu\nu}\right]_{(NV\times NV)};\quad CI_{\mu\nu}^n \equiv \left[(ci)_{ij}^{\mu\nu}\right]_{(NV\times NV)};$$

$$DI_{\mu\nu}^n \equiv \left[(di)_{ij}^{\mu\nu}\right]_{(NV\times NJ)};\quad EI_{\mu\nu}^n \equiv \left[(ei)_{ij}^{\mu\nu}\right]_{(NV\times NJ)}.$$

The vectors on the right-side of Eqs. (II.B.33) represent the Γ-dependent terms that result from the application of the definition of the G-differential to Eq. (II.B.16). All of the components entering the definitions of the matrices appearing on the left-side of Eqs. (II.B.33) and vectors appearing on the right-side of Eqs. (II.B.33) have been obtained explicitly using the symbolic computer language MAPLE V9, and have been programmed accordingly, but will not be reproduced here because of their lengthy and cumbersome expressions.

We now define the partitioned matrices:

$$\left[\begin{array}{ccccc} BV_{11} & \cdots & BV_{1,M_1} & DV_{11} & DV_{12} \\ \vdots & & \vdots & \vdots & \vdots \\ BV_{M_1,1} & \cdots & BV_{M_1,M_1} & DV_{M_1,1} & DV_{M_1,2} \\ BJ_{11} & \cdots & BJ_{1,M_1} & DJ_{11} & DJ_{12} \\ BJ_{21} & \cdots & BJ_{2,M_1} & DJ_{21} & DJ_{22} \end{array}\right]^{(n)}_{(M_1+2)\times(M_1+2)} \equiv B_1^{(n)};$$

$$\left[\begin{array}{cccc} BI_{11} & BI_{1,M_1} & DI_{11} & DI_{12} \\ \vdots & \vdots & \vdots & \vdots \\ BI_{M_2,1} & BI_{M_2,M_1} & DI_{M_2,1} & DI_{M_2,2} \end{array}\right]^{(n)}_{M_2\times(M_1+2)} \equiv B_2^{(n)};$$

$$\left[\begin{array}{ccc} TV_{11} & \cdots & TV_{1,M_2} \\ \vdots & & \vdots \\ TV_{M_1,1} & \cdots & TV_{M_1,M_2} \\ 0 & \cdots & 0 \\ 0 & \cdots & 0 \end{array}\right]^{(n)}_{(M_1+2)\times M_2} \equiv T_1^{(n)}; \quad \left[\begin{array}{ccc} TI_{11} & \cdots & TI_{1,M_2} \\ \vdots & & \vdots \\ TI_{M_2,1} & \cdots & TI_{M_2,M_2} \end{array}\right]^{(n)}_{M_2\times M_2} \equiv T_2^{(n)};$$

$$\left[\begin{array}{ccccc} CV_{11} & \cdots & CV_{1,M_1} & EV_{11} & EV_{12} \\ \vdots & & \vdots & \vdots & \vdots \\ CV_{M_1,1} & \cdots & CV_{M_1,M_1} & EV_{M_1,1} & EV_{M_1,2} \\ CJ_{11} & \cdots & CJ_{1,M_1} & EJ_{11} & EJ_{12} \\ CJ_{21} & \cdots & CJ_{2,M_1} & EJ_{21} & EJ_{22} \end{array}\right]^{(n)}_{(M_1+2)\times(M_1+2)} \equiv C_1^{(n)};$$

$$\left[\begin{array}{cccc} CI_{11} & CI_{1,M_1} & EI_{11} & EI_{12} \\ \vdots & \vdots & \vdots & \vdots \\ CI_{M_2,1} & CI_{M_2,M_1} & EI_{M_2,1} & EI_{M_2,2} \end{array}\right]^{(n)}_{M_2\times(M_1+2)} \equiv C_2^{(n)};$$

$$\begin{bmatrix} X_1 \\ \vdots \\ X_{M_1} \\ Y_1 \\ Y_2 \end{bmatrix}^{(n)} \equiv X^n; \quad \begin{bmatrix} Z_1 \\ \vdots \\ Z_{M_2} \end{bmatrix}^{(n)} \equiv X_I^{(n)};$$

and introduce them in Eq. (II.B.33) to obtain the following system of matrix equations representing the Discrete FSM:

$$\begin{cases} B_1^{(n-1)} X^{(n)} + T_1^{(n-1)} X_I^{(n)} = F_1^{(n-1)} - C_1^{(n-1)} X^{(n-1)} \\ B_2^{(n-1)} X^{(n)} + T_2^{(n-1)} X_I^{(n)} = F_2^{(n-1)} - C_2^{(n-1)} X^{(n-1)}. \end{cases} \tag{II.B.34}$$

As shown in Appendix C, the matrix $T_2^{(n-1)}$ in Eq. (II.B.34) is always nonsingular, and therefore admits an inverse $\left[T_2^{(n-1)}\right]^{-1}$; the procedure to calculate $\left[T_2^{(n-1)}\right]^{-1}$ is also presented in Appendix C. The matrix $\left[T_2^{(n-1)}\right]^{-1}$ is used in Eq. (II.B.34) above to eliminate the vector of "intermediate-time" unknowns, $X_I^{(n)}$. The result of this elimination is the following system of matrix equations:

$$\begin{cases} G^{(n-1)} X^{(n)} + H^{(n-1)} X^{(n-1)} = K^{(n-1)}, \quad (n = 1, \ldots, NF) \\ X^{(0)} = K^{init}, \end{cases} \tag{II.B.35}$$

where K^{init} is a vector that contains the (known) perturbations in the initial conditions, and where the matrices $G^{(n-1)}$, $H^{(n-1)}$, and $K^{(n-1)}$ are defined as follows:

$$\begin{aligned} G^{(n-1)} &\equiv B_1^{(n-1)} - T_1^{(n-1)} \left[T_2^{(n-1)}\right]^{-1} B_2^{(n-1)}, \\ H^{(n-1)} &\equiv C_1^{(n-1)} - T_1^{(n-1)} \left[T_2^{(n-1)}\right]^{-1} C_2^{(n-1)}, \\ K^{(n-1)} &\equiv F_1^{(n-1)} - T_1^{(n-1)} \left[T_2^{(n-1)}\right]^{-1} F_2^{(n-1)}. \end{aligned}$$

The (Discrete) ASM corresponding to the (Discrete) FSM represented by Eq.(II.B.35) is obtained by introducing the respective adjoint, vector-valued, function via the scalar (inner) product of two vectors in a finite-dimensional Euclidean space. This inner product is formed by writing Eq.(II.B.35) as a single

(partitioned) matrix equation, and by multiplying this matrix equation on the left by a yet undefined partitioned column-vector $\Xi \equiv \left(\Xi^{(0)},\ldots,\Xi^{(NF)}\right)$, with components $\Xi^{(n)}$ of the same size and structure as $X^{(n)}$, to obtain an expression of the form $\Xi^T AX \equiv \sum_{n=0}^{NF} \Xi^{(n)} A^{(n)} X^{(n)}$, where A represents a matrix composed of the corresponding matrices $G^{(n)}$ and $H^{(n)}$. The (Discrete) ASM is then obtained by transposing the inner product $\Xi^T AX$ to obtain $X^T A^T \Xi$, and by setting this expression to be equal to the indirect effect term, as follows:

$$DR(\Psi) \equiv X^T A^T \Xi = X^T Q = \sum_{n=0}^{NF} X^{(n)} Q^{(n)} = \Xi^T AX = \Xi^T K = \sum_{n=0}^{NF} \Xi^{(n)} K^{(n)}. \tag{II.B.36}$$

The source $Q^{(n)}$ appearing in Eq.(II.B.36) is determined by the quadrature scheme chosen to calculate numerically the system response R in Eq.(II.B.30). From the identification $X^T A^T \Xi = X^T Q = \sum_{n=0}^{NF} X^{(n)} Q^{(n)}$, it follows that the (Discrete) ASM , henceforth abbreviated as ASM-REL/TF, is given by the system of matrix equations

$$\begin{cases} \left[G^{(NF-1)}\right]^T \Xi^{(NF)} = Q^{(NF)}, & n = NF \\ \left[G^{(n-1)}\right]^T \Xi^{(n)} + \left[H^{(n)}\right]^T \Xi^{(n+1)} = Q^{(n)}, & \left(n = NF-1,\ldots,1\right) \\ \Phi^{(0)} + \left[H^{(0)}\right]^T \Xi^{(1)} = Q^{(0)}, & n = 0. \end{cases} \tag{II.B.37}$$

In view of Eqs.(II.B.32) and (II.B.36), it follows that the sensitivity DR of the response R is given in terms of the adjoint function $\Xi \equiv \left(\Xi^{(0)},\ldots,\Xi^{(NF)}\right)$ by the following expression

$$DR \equiv DR(\Gamma) + DR(\Psi) = DR(\Gamma) + \sum_{n=0}^{NF} \Xi^{(n)} K^{(n)}. \tag{II.B.38}$$

Note that the (Discrete) ASM represented by Eq. (II.B.37) must be solved backwards in time, starting, in principle, from the final time-step NF. In practice, however, the calculation of the vector-valued adjoint function $\Xi \equiv \left(\Xi^{(0)},\ldots,\Xi^{(NF)}\right)$ commences backwards in time only from the time-step, n, at which the source terms $Q^{(n)}$ are nonzero. Furthermore, just as for the Differential ASM represented by Eqs. (II.B.26) through (II.B.28), Eq.(II.B.37)

reveals that: (a) the discrete adjoint function Ξ is independent of parameter variations; (b) Ξ must be calculated anew for every R; (c) the ASM is linear in Ξ, and (d) the adjoint function Ξ depends (eliminate space nonlinearly, in general) on the base-case solution χ_d^o, which must therefore be available prior to solving the ASM.

Note that the ASM-REL/TF, represented by Eq. (II.B.37), is solved by using *different* procedures than used for solving Eq. (II.B.16), i.e., for solving the discrete equations underlying RELAP5/MOD3.2. In particular, the ASM-REL/TF is solved by calling, at each time-step, the subroutine DSLUGM7, which is a generalized minimum residual (GMRES) iterative sparse-matrix solver that uses incomplete LU factorization for preconditioning nonsymmetric linear systems.

II.B.3. Consistency between the Differential/Integral and the Discretized Equations/Models for Sensitivity Analysis

This Section highlights the fundamentally important aspect of consistency between the differential and the corresponding discretized equations used for sensitivity analysis. In this context, consistency means that the discretized representation converges to the corresponding differential and/or integral representation in the limit as $\Delta x_j \to 0$ and $\Delta t \to 0$. *A priori*, it must be assumed that the original systems of differential equations (in this case, the REL/CDE) has been discretized consistently; in this case, it is assumed that Eq. (II.B.16) represents a consistent discretization of Eq. (II.B.10). This is an indispensable assumption, of course, since if it were false, then one could not calculate the base-case solution correctly. Similarly, it must also be assumed that Eq.(II.B.30) represents a consistent discretization of the response represented by Eq.(II.B.17). Starting from these essential assumptions, the following consistency correspondences must be assured:

(a) The Discretized FSM represented by Eq. (II.B.35) must be consistent with the Differential FSM represented by Eq. (II.B.23);

(b) The Discretized ASM represented by Eq. (II.B.37) must be consistent with the Differential ASM represented by Eqs. (II.B.26) - (II.B.28);

(c) The Discretized Response Sensitivity represented by Eq. (II.B.32), the Integral Response Sensitivity represented by Eq. (II.B.21), the Integral Response Sensitivity represented by Eq. (II.B.29) in terms of adjoint functions, and the Discretized Response Sensitivity represented by Eq. (II.B.38) in terms of adjoint functions must all be consistent with each other.

If item (a) above turns out to be false, i.e., if the Discretized FSM represented by Eq. (II.B.35) turns out to be *inconsistent* with the Differential FSM represented by Eq. (II.B.23), then the *a priori assumption* that the original nonlinear differential equations (in this case, the REL/CDE) have been

discretized consistently *must be carefully re-examined*. If this *a priori* assumption is still confirmed to be correct, then the Discretized FSM represented by Eq. (II.B.35) must be discarded from further consideration. Two possibilities arise at this juncture:

(a.1) If the implementation of the *FSAP* is necessary, then the Differential FSM represented by Eq. (II.B.23) must be discretized in a consistent manner, to enable its subsequent numerical solution; note that the Differential FSM represented by Eq. (II.B.23) can be discretized, in principle, independently of the original discretization procedures used to discretize the original nonlinear differential equations (in this case, the REL/CDE).

(a.2) Alternatively, if the implementation of the *FSAP* is not necessary, then we proceed to examine item (b) described above.

If item (b) above turns out to be false, i.e., if the Discretized ASM represented by Eq. (II.B.37) turns out to be *inconsistent* with the Differential ASM represented by Eqs. (II.B.26) - (II.B.28), then the Discretized ASM represented by Eq. (II.B.37) must be discarded; instead, the Differential ASM represented by Eqs. (II.B.26) - (II.B.28) must be discretized consistently, and subsequently solved numerically.

The considerations of consistency outlined so far are depicted in the flow-chart shown in Figure II.B.2.

Finally, if item (c) above turns out to be false, then the "integral" response sensitivity, represented in terms of adjoint functions, cf. Eq. (II.B.29), must be discretized in a consistent manner to enable its correct numerical computation. In closing, it is important to note that the *fundamental hypothesis* underlying all of the consistency considerations in this section is that *the differential and/or integral forms (i.e., the Differential FSM, ASM, and Integral-Response-representation)* are the forms that *contain/model physical reality*; thus, it is *the discretized forms* that *must conform to, and represent consistently, the differential/integral forms*, rather than the other way around.

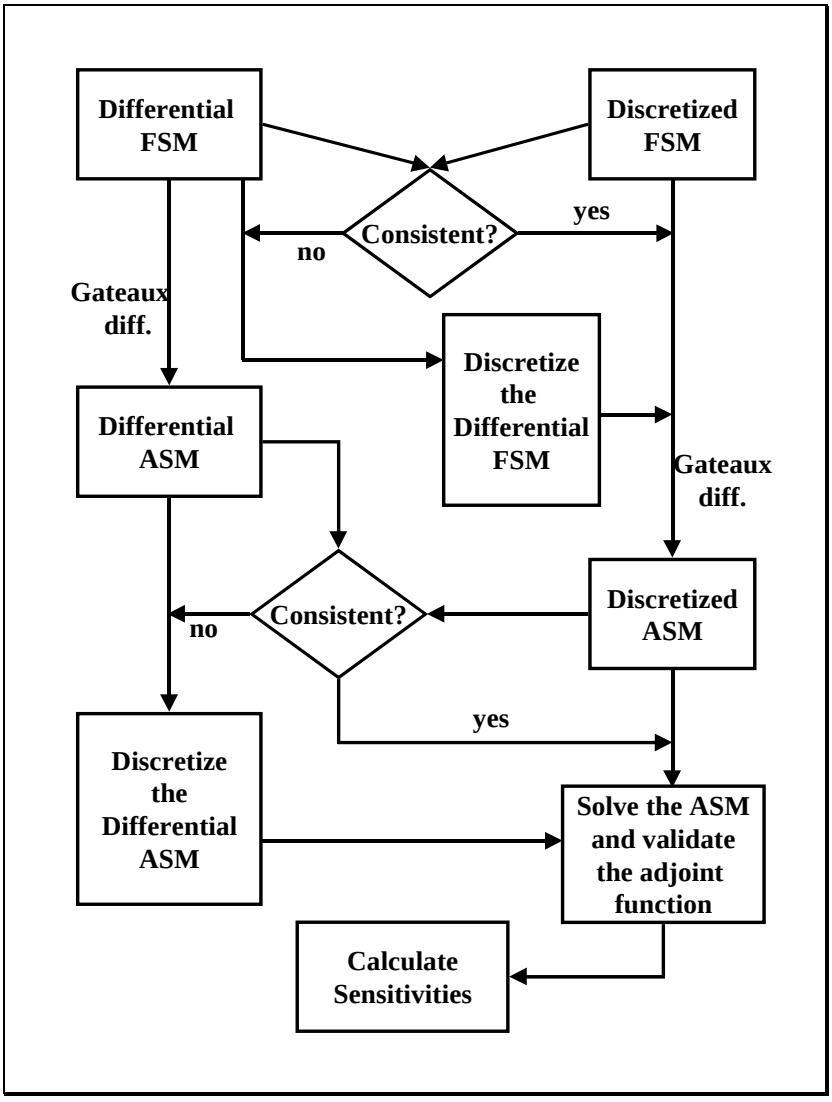

Figure II.B.2. Required consistencies between the differential and discretized formulations of FSM and ASM.

II.B.4. Validation of the Adjoint Sensitivity Model (ASM-REL/TF)

A very important use of Eq. (II.B.29) is for validating the computation of the adjoint function Φ^*. For example, by choosing the response R_i to denote the

i^{th} REL/CDE dependent variable at some discrete point (x_1, t_f) in space-time, by setting $\boldsymbol{\Gamma} = \boldsymbol{0}$, $\Delta\boldsymbol{\chi}(x_o, t) = \boldsymbol{0}$, and $\Delta\boldsymbol{\chi}(x, t_o) = [0,..., \delta(x - x_1)\Delta\chi_i(x, t_o),...0]$ in Eq. (II.B.29), i.e., by effecting solely a variation in the initial conditions of the i^{th} dependent variable in the REL/CDE, we obtain

$$DR_i\left(\boldsymbol{\chi}^o, \boldsymbol{G}^o; \boldsymbol{\Phi}, \boldsymbol{\Gamma}; \boldsymbol{\Phi}^*\right) = \Phi_i^*(x_1, t_o)\, S_{ii}(x_1, t_o)\Delta\chi_i(x_1, t_o). \qquad \text{(II.B.39)}$$

The above expression reveals that the sensitivity DR_i can be used to validate the i^{th} component of the adjoint function $\boldsymbol{\Phi}^*$, as follows: (i) on the one hand, we solve Eq. (II.B.26) to obtain the adjoint function $\boldsymbol{\Phi}^*$, and then perform the multiplications indicated on the right-side of Eq. (II.B.39) to obtain DR_i; the sensitivity DR_i would then be added to the nominal response value $R_i^o\left(\boldsymbol{\chi}^o, \boldsymbol{G}^o\right)$ to obtain the predicted perturbed response, R_{pred}, as indicated by Eq. (II.B.22); (ii) on the other hand, we recalculate the exact perturbed response, $R_{recal} \equiv R_i\left(\boldsymbol{\chi}^o + \boldsymbol{\Phi}, \boldsymbol{G}^o + \boldsymbol{\Gamma}\right)$, for the perturbation $\Delta\chi_i(x_1, t_o)$. Recall that, according to Eq. (II.B.22), the values of R_{recal} and R_{pred} agree with each other up to second order perturbations in the system parameters. Therefore, by deliberately selecting the perturbation $\Delta\chi_i(x_1, t_o)$ to be sufficiently small, to be able to neglect the effects of higher-order terms in Eq. (II.B.22), the value of R_{pred} should agree closely with the value of R_{recal} if the adjoint function Φ_i^* had been accurately computed. On the contrary, if the computation of the respective adjoint function were inaccurate, then the value of R_{pred} would differ from the value of R_{recal}, no matter how small one selected the variation $\Delta\chi_i(x_1, t_o)$.

II.B.4.a Validation of the ASM-REL/TF for Liquid-Phase Using the "Two-Loops with Pumps" RELAP5/MOD3.2 Sample Problem

Using the concepts outlined above, the accuracy and stability of the numerical solution of the ASM-REL/TF for the liquid-phase was verified by using the "*Two Loops with Pumps*" sample problem supplied with the RELAP5/MOD3.2 code. This problem models two, mostly identical, closed loops containing 19 pipe-volumes and a pump-volume. For the first loop, the pipe-volumes are numbered consecutively from 101 to 119, while the pump-volume has number 201 and connects pipe-volumes 101 and 119; similarly, the second loop consists of pipe-volume numbers 301 to 319, with pump-volume 401 connecting pipe-

volumes 301 and 319. Each loop is filled with fluid, and has friction and an orifice.

At the start of the transient, the water in the first loop is at zero (initial) velocity, but the pump is rotating in the positive direction. Thus, the pump trip is initially false, and the pump angular velocity is constant at the initial value until the pump trip becomes true. With the pump rotating at a constant angular velocity but the water at rest, the head is high and the water is accelerated. As the velocity of the water increases, wall friction and area change losses increase because these losses depend on the velocity of water. At the same time, the pump head obtained from the homologous pump data will decrease as the volumetric flow increases. A steady state is reached when the pump head and the loss effects balance. This steady state is reached after about 14.5 seconds from initiating the transient; at this time, the fluid velocity attains a value that remains constant for the next 5.5 seconds. At about 20 sec., the pump is tripped and therefore the pump speed and fluid velocities begin to decrease.

For the second loop, the initial angular rotational velocity for the (second) pump is zero; a pump motor torque curve, corresponding to an induction motor, is used. From the curve, the torque is positive at zero angular velocity; the torque increases slowly as the velocity increases, up to a value which is slightly below the synchronous speed. Then, the torque decreases sharply to zero at the synchronous speed, where the developed torque matches the frictional torque and the torque imposed by the water. As long as the net torque is positive, the water is accelerated. Once the second pump approaches synchronous speed, the transient behavior of the second loop becomes similar to that of the first loop.

The stability and accuracy of the numerical solution of the ASM-REL/TF was verified by considering various variations in the initial conditions for the pressures in the volumes and, respectively, velocities at the junctions comprising the respective loops. Note that such perturbations do not correspond to actual physical processes, but are introduced numerically, in order to verify the accuracy and stability of the numerical solution of the ASM-REL/TF. To facilitate the comparisons between the results (sensitivities) predicted by the ASM-REL/TF and the corresponding exact recalculations, the numerical values presented in the various tables below were deliberately not rounded off, but were displayed with all the decimals printed by RELAP5.

For the results reported in this section, the fluid used in the "*Two-Loops with Pumps*" sample problem described above is single-phase water. To ensure that the fluid remains in the liquid-phase throughout the transient, the initial conditions were taken as: $P_{init} = 1.56 \times 10^7 \, Pa$ and $T_{f,init} = 555K$. The solution of the ASM-REL/TF was verified by: (i) effecting various perturbations in the initial pressures, velocities, and pump head; (ii) computing the respective predicted responses; and (iii) comparing the predicted response values with exact recalculations.

The behavior of the volume-averaged pressure in volume 301 (adjacent to the pump) to various perturbations of the initial values of the pressure in the same

volume is presented in Table II.B.1. These results are typical for the pressure sensitivities to variations in the initial pressures for all of the other loop-volumes, as well. The values presented for P_{recal} are obtained by re-running the entire transient using the respective perturbed initial condition. As noted from the results in Table II.B.1, the solution of the ASM-REL/TF, which is used to compute P_{pred}, is very accurate and stable, practically coinciding with the exact recalculations for the entire duration of the transient (294 time steps).

The influence of perturbations of 0.1ft/s and 3ft/s, respectively, in the initial velocity (0.0 ft/s) in junction 301 on the subsequent time-dependent behavior of the velocity in the same junction (301) is depicted Table II.B.2. The effects of the perturbations in the initial velocity are noticeable during the early stages of the transient only, but then diminish quickly in time. Note that the results obtained using the ASM-REL/TF for the 0.1ft/s perturbation are practically indistinguishable from the exact recalculations, thus confirming the robustness, stability, and accuracy of the respective numerical solution of the ASM-REL/TF. The nonlinear effects are more prominent for the 0.9144m/s (3 ft/s) perturbation, particularly at early time values, but these effects also diminish in time and converge to the respective steady state values, as would be expected.

Table II.B.1

"*Two-Loops with Pumps*" - liquid-phase: influence of perturbations in the initial pressure in volume 301 (adjacent to the pump) on the pressure in same volume.

Perturbation	Transient Duration / No. of time steps	Nominal Value (N/m^2)	$P_{pred} - P^0$	$P_{recal} - P^0$
1% of the initial pressure	0.05 sec. / 5 t.s.	1.56259E+7	7391.4	7400
	0.2 sec. / 20 t.s.	1.56259E+7	7391.5	7400
	0.5. sec / 52 t.s.	1.56263E+7	7391.5	7300
	5. sec / 144 t.s.	1.56549E+7	7392.0	7400
	20. sec /294 t.s.	1.73607E+7	7440.8	7500
5% of the initial pressure	0.05 sec. / 5 t.s.	1.56259E+7	36957	36600
	0.2 sec. / 20 t.s.	1.56259E+7	36958	36600
	0.5. sec / 52 t.s.	1.56263E+7	36958	36600
	5. sec / 144 t.s.	1.56549E+7	36960	36600
	20. sec/ 294 t.s.	1.73607E+7	37204	36900
10% of the initial pressure	0.05 sec / 5 t.s.	1.56259E+7	73914	72400
	0.2 sec. / 20 t.s.	1.56259E+7	73915	72500
	0.5. sec / 52 t.s.	1.56263E+7	73915	72400
	5. sec / 144 t.s.	1.56549E+7	73920	72300
	20. sec/ 294 t.s.	1.73607E+7	74408	73000

Table II.B.2
"*Two-Loops with Pumps*" - liquid-phase: influence of perturbations in the initial velocity in junction 301 (adjacent to the pump) on the velocity in same junction.

Perturb. in initial velocity (j301)	Transient duration / nr. of time steps	Nominal value v_{fj}^{o} (j301) (m/s)	$v_{fj,pred} - v_{fj}^{o}$	$v_{fj,recal} - v_{fj}^{o}$
0.3048 m/s (0.1 ft/s) at t = 0	0.05 sec./5 t.s.	1.20631E-5	1.50766E-3	1.50840E-3
	0.1 sec./10 t.s.	1.13544E-4	1.60894E-3	1.60889E-3
	0.2 sec./20 t.s.	9.80435E-4	2.46784E-3	2.47489E-3
	0.5 sec./50 t.s.	1.60002E-2	1.74949E-2	1.74856E-2
	1.0 sec./100 t.s.	.12428	.12559	.12550
.9144 m/s (3 ft/s) at t = 0	0.05 sec./5 t.s.	1.20631E-5	.44879E-1	.44507E-1
	0.1 sec./10 t.s.	1.13544E-4	.44975E-1	.44186E-1
	0.2 sec./20 t.s.	9.80435E-4	.45822E-1	.44432E-1
	0.5 sec./50 t.s.	1.60002E-2	.60609E-1	.57258E-1
	1.0 sec./100 t.s.	.12428	.16369	.15583

The results presented in Tables II.B.1 and II.B.2, respectively, are typical for perturbations in all of the volume-averaged pressures and junction-velocities of the "*Two-Loops with Pumps*" problem, as we have concluded after having preformed the respective calculations (see Ionescu-Bujor and Cacuci, 2000, for additional results). As already mentioned, the perturbations introduced numerically in the volume-averaged pressures and junction velocities are irrelevant to actual physical processes, but serve only as mathematical means to verify the accuracy and stability of the numerical solution of the ASM-REL/TF. The results of these verifications indicate that the numerical methods employed for solving the ASM-REL/TF are as accurate, robust, and stable as the original numerical methods used in RELAP5/MOD3.2 for solving liquid-phase problems.

As examples of perturbations that do have physical meaning within the liquid-filled "*Two-Loops with Pumps*" problem, the ASM-REL/TF has been used to obtain sensitivities of the pressure in the loops to variations in the pump head. Typical results for such sensitivities are presented in Table II.B.3, which, in particular, shows the time-dependent (100 time-steps) sensitivities of the pressure in Vol. 101 (adjacent to the pump in Loop 1) to a small (1%) and, respectively, large (10%) variation in the pump head. These results show that the pressure variations predicted by the ASM-REL/TF for the 1%-perturbations in the pump head are very close to, albeit somewhat larger than, the exactly recalculated pressures. For the larger (10%) pump head variations, the nonlinear effects become stronger, leading to a more marked over-prediction of the exactly recalculated results by the ASM-REL/TF-calculated sensitivities.

Table II.B.3
"*Two-Loops with Pumps*" - liquid-phase: influence of pump head perturbations on pressure.

Perturbation	Transient Duration / No. of time steps	Nominal Value (N/m^2)	$P_{pred} - P^0$	$P_{recal} - P^0$
1% of the initial pump head	0.01 sec	1.57426E+7	1165.3	1100
	0.05 sec	1.57372E+7	1032.9	900
	0.1 sec	1.57238E+7	829.68	700
	0.5 sec	1.57058E+7	253.37	100
	1 sec (100 t.s.)	1.57319E+7	256.37	100
10% of the initial pump head	0.01 sec	1.57426E+7	11653	11600
	0.05 sec	1.57372E+7	10329	8700
	0.1 sec	1.57238E+7	8296.8	4300
	0.5 sec	1.57058E+7	2533.7	1200
	1 sec (100 t.s.)	1.57319E+7	2563.7	600

II.B.4.b Validation of the ASM-REL/TF for Gas-Phase Using a Modified "Two-Loops with Pumps" and the "Edward's Pipe" RELAP5/MOD3.2 Sample Problems

To validate the solution of the ASM-REL/TF for the gas-phase, the "*Two-Loops with Pumps*" problem described above in Sec. II.B.4.a has been modified by replacing the water (liquid) by steam (gas). This modification was effected by using the following initial conditions: $P_{init} = 7.0 \times 10^6 \, Pa$ and $T_{g,init} = 620K$. Otherwise, the geometry of the problem was kept unchanged.

The influence of perturbations in the initial pressure in volume 103, which is located three volumes away from pump, on the pressure in same volume is illustrated by the results presented in Table II.B.4. Just as has been noted for the liquid-phase problem analyzed in Sec. II.B.4.a, these perturbations are introduced numerically, and do not correspond to actual physical processes; they are used only as mathematical means to verify the accuracy and stability of the numerical solution of the ASM-REL/TF. The results in Table II.B.4 show that the solution of the ASM-REL/TF, which is used to obtain P_{pred}, is very accurate and stable, practically coinciding with the exact recalculations for the entire duration of the transient (292 time steps), for all the perturbations (0.1%; 1%; 10%) effected in the initial pressure.

Typical examples of the sensitivities of the volume-averaged pressures to variations in the pump-head are presented below in Table II.B.5, for volume 103, and Table II.B.6, for volume 101, respectively. Once again, the results presented in these tables are reproduced with all the digits printed by the RELAP code, in order to emphasize the respective differences; these results indicate that

the pressures predicted by using the ASM-REL/T are quite close to the exactly recomputed values.

Table II.B.4
"*Two-Loops with Pumps*" - gas-phase: influence of perturbations in the initial pressure in volume 103 (3 volumes away from pump) on the pressure in same volume.

Perturbation	Transient Duration / No. of time steps	Nominal Value (N/m^2)	$P_{pred} - P^0$	$P_{recal} - P^0$
0.1% of the initial pressure	0.1 sec. / 10 t.s.	7.00433E+6	331.48	320
	0.5 sec / 50 t.s.	7.00627E+6	331.47	320
	1 sec / 100 t.s.	7.00984E+6	331.48	330
	5. sec / 142 t.s.	7.03846E+6	331.27	330
	20. sec / 292 t.s.	7.14594E+6	330.82	320
1% of the initial pressure	0.1 sec. / 10 t.s.	7.00433E+6	3314.8	3320
	0.5 sec / 50 t.s.	7.00627E+6	3314.7	3320
	1 sec / 100 t.s.	7.00984E+6	3314.8	3330
	5. sec / 142 t.s.	7.03846E+6	3312.7	3330
	20. sec / 292 t.s.	7.14594E+6	3308.2	3320
10% of the initial pressure	0.1 sec. / 10 t.s.	7.00433E+6	33148	32590
	0.5 sec / 50 t.s.	7.00627E+6	33147	32560
	1 sec / 100 t.s.	7.00984E+6	33148	32560
	5. sec / 142 t.s.	7.03846E+6	33127	32540
	20. sec / 292 t.s.	7.14594E+6	33082	32530

Table II.B.5
"*Two-Loops with Pumps*" - gas-phase: influence of pump head perturbations on the pressure in volume 103.

Perturbation	Transient Duration / No. of time steps	Nominal Value (N/m^2)	$P_{pred} - P^0$	$P_{recal} - P^0$
1% of the initial pump head	0.1 sec (10 t.s.)	7.00433E+6	27.335	20
	0.5 sec (50 t.s.)	7.00627E+6	9.8272	9
	1 sec (100 t.s.)	7.00984E+6	9.8588	10
10% of the initial pump head	0.1 sec (10 t.s.)	7.00433E+6	273.35	160
	0.5 sec (50 t.s.)	7.00627E+6	98.272	50
	1 sec (100 t.s.)	7.00984E+6	98.588	50

To verify further the accuracy and stability of the numerical solution of the ASM-REL/TF for the gas-phase, we have modified the well-known "Edwards Pipe" problem, supplied with the RELAP5/MOD3.2 code, by filling it initially with pure steam (as opposed to water, as in the original setting of this problem). The modified "Edwards Pipe" problem thus contains steam (i.e., gas-phase) only, initially at rest in the pipe, with initial pressure and internal energy of 7 MPa and 0.27E+7 J/kg, respectively. The pipe is then depressurized by opening

an end into a large reservoir at atmospheric pressure and an internal energy of 0.25E+7 J/kg. To maintain pure gas (steam)-conditions throughout the depressurization, the transient calculation was restricted to the first 57 time steps after initiation of the transient depressurization, since condensation begins to appear beyond this point in time. The ASM-REL/TF results and the respective comparisons with exact recalculations are presented in Table II.B.7. These results indicate that the pressure response variations predicted by using the sensitivities calculated with the ASM-REL/TF agree well with the exactly recalculated variations. For the larger (10%) variations, the effect of nonlinearities becomes more evident, particularly as the condensation point is approached in time. The results shown in Table II.B.7 indicate that the numerical method used for solving the ASM-REL/TF yields accurate results, too, for the gas-phase segment of the two-fluid model.

Table II.B.6
"*Two-Loops with Pumps*" - gas-phase: influence of pump head perturbations on the pressure in volume 101 (adjacent to the pump).

Perturbation	Transient Duration / No. of time steps	Nominal Value (N/m^2)	$P_{pred} - P^0$	$P_{recal} - P^0$
1% of the initial pump head	0.1 sec (10 t.s.)	7.00487E+6	31.278	30
	0.5 sec (50 t.s.)	7.00630E+6	9.8284	10
	1 sec (100 t.s.)	7.00988E+6	9.9438	9
10% of the initial pump head	0.1 sec (10 t.s.)	7.00487E+6	312.78	180
	0.5 sec (50 t.s.)	7.00630E+6	98.284	50
	1 sec (100 t.s.)	7.00988E+6	99.438	40

Table II.B.7
"*Edwards Pipe*" - gas-phase: influence of perturbations in the initial pressure in volume 301 (near to the pipe's closed end) on the pressure in the same volume.

Perturbation	Transient duration / no. Of time steps	Nominal value (N/m^2)	$P_{pred} - P^0$	$P_{recal} - P^0$
0.1% of the initial pressure 7.0E+6 (N/m^2)	0.001 sec./19 t.s.	7.0E+6	-322.86	-320
	0.005 sec./38 t.s.	6.8909E+6	16.078	20
	0.01 sec / 57 t.s.	3.4896E+6	116.69	120
5% of the initial pressure 7.0E+6 (N/m^2)	0.001 sec./19 t.s.	7.0E+6	-16143	-14300
	0.005 sec./38 t.s.	6.8909E+6	803.90	710
	0.01 sec / 57 t.s.	3.4896E+6	5834.3	7910
10% of the initial pressure 7.0E+6 (N/m^2)	0.001 sec./19 t.s.	7.0E+6	-32286	-25060
	0.005 sec./38 t.s.	6.8909E+6	1607.8	1370
	0.01 sec / 57 t.s.	3.4896E+6	11669	13970

II.B.4.c Validation of the ASM-REL/TF for Two-Phase Using the "Edwards Pipe" RELAP5/MOD3.2 Sample Problem

In addition to having verified the numerical solution of the ASM-REL/TF by using sample problems involving single-phase fluids as described in the foregoing in Sec. II.B.4.a and Sec. II.B.4.b, the solution of the ASM-REL/TF has also been verified by using the original "*Edwards Pipe*" sample problem supplied with the RELAP5/MOD3.2 code. In this (original) setting, "*Edwards Pipe*" models the depressurization of a pipe, filled initially with single-phase water at a pressure of 7 MPa and temperature of 502 K. The transient depressurization of the single-phase water is initiated by releasing one end of the pipe. The time-dependent behavior of the liquid, namely water turning into a two-phase mixture during the pipe depressurization, simulates the basic features of a loss of coolant accident in a pressurized water reactor. It is important to mention that the calculation of the transient behavior of the pressure, temperature, and fluid- and gas-velocities that describe "*Edwards Pipe*" problem requires the complete hydrodynamics of the RELAP5/MOD3.2 two-fluid model, including several flow regimes.

Illustrative results for validating the numerical solution of the ASM-REL/TF for the first 0.1s (109 time steps) of the "*Edwards Pipe*" problem are presented in Table II.B.8. The two-phase flow regimes involved during these 109 time-steps are bubbly, slug, and mist flows, respectively; the transitions between regimes occur very rapidly. The results presented in Table II.B.8 illustrate the effects of perturbations in the initial pressure in volume 305 on the subsequent time-evolution of the pressure in the same volume. The good agreement between the results for the predicted responses obtained using the ASM-REL/TF and the exactly recalculated responses indicates that the solution of the ASM-REL/TF is calculated robustly and accurately for the respective two-phase flow regimes.

Table II.B.8
"*Edwards Pipe*" - two-phase: influence of perturbations in the initial pressure in volume 305 on the pressure in the same volume.

Perturbation	Transient duration /no. of time steps	Nominal value (N/m^2)	P_{pred}	P_{recal}
0.1% of the initial pressure 7.0E+6 (N/m^2)	0.01 sec. / 19 t.s.	2.66073E+6	2.66070E+6	2.66071E+6
	0.06. sec / 69 t.s.	2.57470E+6	2.57471E+6	2.57473E+6
	0.1 sec / 109 t.s.	2.58221E+6	2.58238E+6	2.58241E+6
10% of the initial pressure 7.0E+6 (N/m^2)	0.01 sec. / 19 t.s.	2.66073E+6	2.66218E+6	2.66222E+6
	0.06. sec / 69 t.s.	2.57470E+6	2.57609E+6	2.57613E+6
	0.1 sec / 109 t.s.	2.58221E+6	2.57538E+6	2.57548E+6

II.B.5. Sensitivities of Thermodynamic Properties of Water

The material properties of water play an essential role in all calculations with RELAP5/MOD3.2. The standard reference for the mathematical formulae of the thermodynamic properties of ordinary water substance is the well-known monograph entitled "ASME Steam Tables" (1993). In particular, this reference contains expressions for the specific fluid volume, V_f, the specific gas volume, V_g, the specific isobaric fluid heat capacity, C_{pf}, the specific isobaric gas heat capacity, C_{pg}, the volumetric expansion coefficient for fluid, β_f, the volumetric expansion coefficient for gas, β_g, the specific fluid enthalpy, h_f, the specific gas enthalpy, h_g, the isothermal coefficient of compressibility for fluid, k_f, and the isothermal coefficient for gas, k_g. The mathematical expressions for these thermodynamic properties comprise highly nonlinear functions of pressure, P, and temperature, T, and each expression involves many tens of experimentally determined numerical parameters. The influence of such parameters, as well as of P and T, on results involving water as the working fluid can be quantitatively assessed by calculating the sensitivities of the various material properties. Denoting symbolically a material property by $[\text{Mat. Prop.}]$, the *relative sensitivity* of $[\text{Mat. Prop.}]$ to a parameter β (which can, in particular, represent P, T, or any other numerical coefficient) is defined as the dimensionless number

$$\left[\left(\frac{\partial[\text{Mat. Prop.}]}{\partial\beta}\right)\left(\frac{\beta}{[\text{Mat. Prop.}]}\right)\right]^o .$$

On the other hand, the *recalculated relative change* in a material property $[\text{Mat. Prop.}]$ is defined as

$$\left[\text{Mat. Prop.}\left(\beta^o+\Delta\beta\right)-\text{Mat. Prop.}\left(\beta^o\right)\right]\frac{1}{\Delta\beta}\frac{\beta^o}{\text{Mat. Prop.}\left(\beta^o\right)},$$

where $\left[\text{Mat. Prop.}\left(\beta^o+\Delta\beta\right)\right]$ denotes the exactly recalculated (perturbed) value of the respective material property, using the perturbed parameter value $\left(\beta^o+\Delta\beta\right)$. The superscript "$o$" is used in the above expressions to denote "nominal" value. In view of Eq. (II.B.22), the difference between the relative sensitivity and the recalculated relative change provides a quantitative measure of the nonlinear dependence of the respective material property on the parameter in question. In the above definitions, the superscript zero signifies that all

quantities enclosed within the outside brackets are to be evaluated at known base-case (nominal) values. For the illustrative results presented below, in Tables II.B.9 through II.B.14, the nominal values for evaluating the sensitivities of the thermodynamic properties of fluid water have been chosen to be $T_f^o = 564.7K$, $T_g^o = 620.6K$, $P^o = 159.2bar$, which are conditions typically used in RELAP5/MOD3.2 for simulating reactor operational transients.

Illustrative results for the sensitivities of the thermodynamic properties of water to P and T are presented below, in Table II.B.9. The general trend that can be observed from these results is that the relative sensitivities are computed very accurately (as can be seen from comparisons with recalculated values for small changes), but the dependence of the material properties on T and (to a lesser extent) on P is markedly nonlinear (as can be seen from comparisons with recalculated values for larger changes). The sensitivities of the thermodynamic properties of water to the numerical parameters that enter in their respective mathematical formulae are presented in Tables II.B.10 through II.B.14, and have been grouped according to their relative importance to the fluid and gas phases, respectively. The sensitivities of the specific isobaric fluid heat capacity, C_{pf}, and the specific isobaric gas heat capacity, C_{pg}, are presented in Tables II.B.10 and II.B.11, respectively. These results show that C_{pf} is highly sensitive to variations in the first nine (of twenty nine parameters), while C_{pg} is highly sensitive to variations in the first ten (of thirty seven parameters); otherwise, the respective heat capacities are moderately or negligibly sensitive to the remaining parameters. It is important to note, though, that the dependence of C_{pf} and C_{pg} on the most sensitive parameters is linear, so the respective sensitivities predict exactly (not just to first order!) the effects of variations in the respective parameters. Nevertheless, as will be discussed in the sequel, such large sensitivities could propagate large uncertainties into the RELAP5/MOD3.2 results from the respective material properties.

Table II.B.12 presents numerical results for the sensitivities of the specific fluid enthalpy h_f to all of the 33 empirical parameters that enter in its mathematical formula. These sensitivities are again ordered according to their absolute values, from high to low, and display features that are similar to those for C_{pf} and C_{pg} in the previous two tables. Thus, the sensitivities of h_f to the first ten parameters are extremely large, the sensitivities to the next five are moderately large, while the sensitivities to the last eighteen or so are negligible regarding their respective effects on h_f. Note that h_f depends linearly on the parameters associated with the largest sensitivities; this fact is also reflected by the numerical results presented in the columns labeled $\left(h_f^{pred} - h_f^o\right)$ and $\left(h_f^{recal} - h_f^o\right)$, respectively. The respective values agree exactly, as would be

expected in case of a linear dependence. Nevertheless, such high sensitivities would lead to potentially large contributions to the overall uncertainty in h_f.

Table II.B.13 presents numerical results for the sensitivities of the specific gas volume, V_g, to all of the 34 empirical parameters that enter in its mathematical formula. These sensitivities are again ordered according to their absolute values, from high to low, and display features that are similar to those for C_{pf}, C_{pg}, and h_f in the previous tables. Thus, the sensitivities of V_g to the first seven parameters are extremely large, the sensitivities to the next nine are moderately large, while the sensitivities to the last eighteen are negligible regarding their respective effects on V_g. Just as h_f, V_g depends linearly on the parameters associated with the largest sensitivities; this fact is also reflected by the numerical results presented in the columns labeled $V_g^{pred} - V_g^o$ and $V_g^{recal} - V_g^o$, respectively. The respective values agree exactly, as would be expected in case of a linear dependence. Nevertheless, such high sensitivities would lead to potentially large contributions to the overall uncertainty in V_g.

Table II.B.9
Relative sensitivities of water material properties to temperatures and pressures typically encountered in reactor safety analysis:
$T_f^o = 564.7K, T_g^o = 620.6K, P^o = 159.2bar$.

Water Prop.	Rel. sens. with respect to T	Rel. var.	Recalc. relative change	Rel. sens. with respect to P	Rel. var.	Recalc. relative change
1. V_f	1.447	10^{-5}	1.447	-0.0358	10^{-5}	-0.0358
		10^{-4}	1.448		10^{-4}	-0.0358
		10^{-3}	1.453		10^{-3}	-0.0358
		10^{-2}	1.507		10^{-2}	-0.0357
2. V_g	12.671	10^{-5}	12.667	-3.327	10^{-5}	-3.327
		10^{-4}	12.626		10^{-4}	-3.328
		10^{-3}	12.253		10^{-3}	-3.335
		10^{-2}	10.146		10^{-2}	-3.420
3. C_{pf}	2.112	10^{-5}	2.112	-0.082	10^{-5}	-0.0816
		10^{-4}	2.114		10^{-4}	-0.0816
		10^{-3}	2.127		10^{-3}	-0.0816
		10^{-2}	2.271		10^{-2}	-0.0813
4. C_{pg}	-87.002	10^{-5}	-86.885	14.205	10^{-5}	14.208
		10^{-4}	-85.844		10^{-4}	14.232
		10^{-3}	-76.565		10^{-3}	14.479
		10^{-2}	-36.224		10^{-2}	17.440
5. β_f	6.390	10^{-5}	6.390	-0.240	10^{-5}	-0.240
		10^{-4}	6.394		10^{-4}	-0.240
		10^{-3}	6.434		10^{-3}	-0.240
		10^{-2}	6.870		10^{-2}	-0.239
6. β_g	-84.259	10^{-5}	-84.152	14.089	10^{-5}	14.091
		10^{-4}	-83.208		10^{-4}	14.114
		10^{-3}	-74.803		10^{-3}	14.345
		10^{-2}	-37.918		10^{-2}	17.115
7. h_f	3.526	10^{-5}	3.526	-0.077	10^{-5}	-0.0762
		10^{-2}	4.211		10^{-2}	-0.0752
8. h_g	3.688	10^{-4}	3.672	-0.674	10^{-4}	-0.674
		10^{-2}	2.829		10^{-2}	-0.720
9. κ_f	9.703	10^{-5}	9.703	-0.337	10^{-5}	-0.336
		10^{-2}	10.600		10^{-2}	-0.335
10. κ_g	-53.661	10^{-5}	-53.597	8.107	10^{-5}	8.108
		10^{-3}	-48.034		10^{-3}	8.250

Table II.B.10
Sensitivities of the specific isobaric fluid heat capacity, C_{pf} , to parameters in its mathematical formulation $T_f^o = 564.7K, T_g^o = 620.6K, P^o = 159.2bar$.

Param g_j	Rel. sens. $\frac{\partial C_{pf}}{\partial g_j}\frac{g_j^o}{C_{pf}^o}$	Rel. Par. Var. $\frac{\Delta g_j}{g_j^o}$	$C_{pf}^{pred} - C_{pf}^o$	$C_{pf}^{recal} - C_{pf}^o$
1.A_6	21356.05	0.1	10111.91	10111.91
	linear dep.	0.5	50559.59	50559.59
2.A_7	-20340	0.1	-9627.17	-9627.17
	linear dep.	0.5	-48135.87	-48135.87
3.A_5	-14357.93	0.1	-6795.50	-6795.50
	linear dep.	0.5	-33977.50	-33977.50
4.A_8	12085.68	0.1	5720.06	5720.06
	linear dep.	0.5	28600.31	28600.31
5.A_4	6039.87	0.1	2858.62	2858.62
	linear dep.	0.5	14293.14	14293.14
6.A_9	-4094.11	0.1	-1937.71	-1937.71
	linear dep.	0.5	-9688.57	-9688.57
7.A_3	-1458.13	0.1	-690.12	-690.12
	linear dep.	0.5	-3450.62	-3450.62
8.A_{10}	605.16	0.1	286.41	286.41
	linear dep.	0.5	1432.09	1432.09
9. A_0	156.20	0.1	73.93	73.93
	linear dep.	0.5	369.65	369.65
10.a_1	.25957	10^{-4}	$.1228*10^{-3}$	$.1228*10^{-3}$
		10^{-3}	$.1228*10^{-2}$	$.1230*10^{-2}$
		10^{-2}	$.1228*10^{-1}$	$.1251*10^{-1}$
		10^{-1}	.1228	.1502
11.a_3	-.10989	10^{-4}	$-.5201*10^{-4}$	$-.5201*10^{-4}$
		10^{-3}	$-.5201*10^{-3}$	$-.5200*10^{-3}$
		10^{-2}	$-.5201*10^{-2}$	$-.5196*10^{-2}$
		10^{-1}	$-.5201*10^{-1}$	$-.5155*10^{-1}$
12.a_4	$.786*10^{-1}$	10^{-4}	$.3720*10^{-4}$	$.3720*10^{-4}$
		10^{-3}	$.3720*10^{-3}$	$.3721*10^{-3}$
		10^{-2}	$.3720*10^{-2}$	$.3731*10^{-2}$
		10^{-1}	$.3720*10^{-1}$	$.3832*10^{-1}$
13.A_{11}	$.581*10^{-1}$	0.1	$.2750*10^{-1}$	$.2750*10^{-1}$
		0.5	.1375	.1375
14.a_5	$-.321*10^{-1}$	10^{-4}	$-.1521*10^{-4}$	$-.1521*10^{-4}$
		10^{-3}	$-.1521*10^{-3}$	$-.1521*10^{-3}$
		10^{-2}	$-.1521*10^{-2}$	$-.1519*10^{-2}$
		10^{-1}	$-.1521*10^{-1}$	$-.1497*10^{-1}$
15.a_{10}	$-.139*10^{-1}$	10^{-4}	$-.6605*10^{-5}$	$-.6604*10^{-5}$

		10^{-3}	$-.6605*10^{-4}$	$-.6593*10^{-4}$
		10^{-2}	$-.6605*10^{-3}$	$-.6486*10^{-3}$
		10^{-1}	$-.6605*10^{-2}$	$-.5561*10^{-2}$
$16.A_{20}$	$.557*10^{-2}$	0.1	$.2637*10^{-2}$	$.2637*10^{-2}$
	linear dep.	0.5	$.1318*10^{-1}$	$.1318*10^{-1}$
$17.a_6$	$.300*10^{-2}$	10^{-4}	$.1421*10^{-5}$	$.1419*10^{-5}$
		10^{-3}	$.1421*10^{-4}$	$.1400*10^{-4}$
		10^{-2}	$.1421*10^{-3}$	$.1227*10^{-3}$
		10^{-1}	$.1421*10^{-2}$	$.4146*10^{-3}$
$18.a_2$	$-.266*10^{-2}$	10^{-4}	$-.1263*10^{-5}$	$-.1263*10^{-5}$
		10^{-3}	$-.1263*10^{-4}$	$-.1263*10^{-4}$
		10^{-2}	$-.1263*10^{-3}$	$-.1263*10^{-3}$
		10^{-1}	$-.1263*10^{-2}$	$-.1262*10^{-2}$
$19.a_9$	$.829*10^{-3}$	0.1	$.3926*10^{-3}$	$.3926*10^{-3}$
	linear dep.	0.5	$.1963*10^{-2}$	$.1963*10^{-2}$
$20.A_{14}$	$-.573*10^{-3}$	0.1	$-.2712*10^{-3}$	$-.2712*10^{-3}$
	linear dep.	0.5	$-.1356*10^{-2}$	$-.1356*10^{-2}$
$21.a_{11}$	$.469*10^{-3}$	0.1	$.2222*10^{-3}$	$.2222*10^{-3}$
	linear dep.	0.5	$.1111*10^{-2}$	$.1111*10^{-2}$
$22.A_{15}$	$-.887*10^{-4}$	0.1	$-.4198*10^{-4}$	$-.4198*10^{-4}$
	linear dep.	0.5	$-.2099*10^{-3}$	$-.2099*10^{-3}$
$23.A_{17}$	$.546*10^{-5}$	0.1	$.2588*10^{-5}$	$.2588*10^{-5}$
	linear dep.	0.5	$.1294*10^{-4}$	$.1294*10^{-4}$
$24.A_{18}$	$.388*10^{-6}$	0.1	$.1839*10^{-6}$	$.1839*10^{-6}$
	linear dep.	0.5	$.9197*10^{-6}$	$.9197*10^{-6}$
$25.A_{16}$	$-.529*10^{-7}$	0.1	$-.2506*10^{-7}$	$-.2506*10^{-7}$
	linear dep.	0.5	$-.1253*10^{-6}$	$-.1253*10^{-6}$
$26.A_{19}$	$.134*10^{-7}$	0.1	$.6344*10^{-8}$	$.6344*10^{-8}$
	linear dep.	0.5	$.3172*10^{-7}$	$.3172*10^{-7}$
$27.a_8$	$-.353*10^{-8}$	10^{-4}	$-.167*10^{-11}$	$-.167*10^{-11}$
		10^{-3}	$-.167*10^{-10}$	$-.167*10^{-10}$
		10^{-2}	$-.167*10^{-9}$	$-.167*10^{-9}$
		10^{-1}	$-.167*10^{-8}$	$-.167*10^{-8}$
$28.a_7$	$.135*10^{-10}$	10^{-4}	$.642*10^{-14}$	$.642*10^{-14}$
		10^{-3}	$.642*10^{-13}$	$.642*10^{-13}$
		10^{-2}	$.642*10^{-12}$	$.642*10^{-12}$
		10^{-1}	$.642*10^{-11}$	$.642*10^{-11}$
$29.A_{22}$	$-.10*10^{-10}$	0.1	$-.509*10^{-11}$	$-.509*10^{-11}$
	linear dep.	0.5	$-.254*10^{-10}$	$-.254*10^{-10}$

Table II.B.11
Sensitivities of the specific isobaric gas heat capacity, C_{pg}, to parameters in its mathematical formulation ($T_f^o = 564.7K, T_g^o = 620.6K, P^o = 159.2bar$).

Param g_j	Rel. sens. $\frac{\partial C_{pg}}{\partial g_j}\frac{g_j^o}{C_{pg}^o}$	Rel. Par. Var. $\Delta g_j / g_j^o$	$C_{pg}^{pred} - C_{pg}^o$	$C_{pg}^{recal} - C_{pg}^o$
1.B_{93}	19063.26	0.1	23277.92	23277.92
	linear dep.	0.5	116389.6	116389.6
2.B_{94}	-18611.13	0.1	-22725.84	-22725.84
	linear dep.	0.5	-113629.2	-113629.2
3.B_{92}	-10903.58	0.1	-13314.24	-13314.24
	linear dep.	0.5	-66571.2	-66571.2
4.B_{95}	9623.61	0.1	11751.28	11751.28
	linear dep.	0.5	58756.42	58756.42
5.B_{91}	3300.47	0.1	4030.17	4030.17
	linear dep.	0.5	20150.85	20150.85
6.B_{96}	-2059.82	0.1	-2515.22	-2515.22
	linear dep.	0.5	-12576.14	-12576.14
7.B_{90}	-412.84	0.1	-504.12	-504.12
	linear dep.	0.5	-2520.61	-2520.61
8.L_1	-20.52	10^{-4}	$-.2506*10^{-1}$	$-.2573*10^{-1}$
		10^{-3}	-.2506	-.3319
		10^{-2}	-2.506	-351.46
		10^{-1}	-25.06	.5204
9.L_2	10.73	10^{-4}	$.1311*10^{-1}$	$.1293*10^{-1}$
		10^{-3}	.1311	.1146
		10^{-2}	1.311	.4654
		10^{-1}	13.11	.5204
10.L_0	10.21	10^{-4}	$.1247*10^{-1}$	$.1230*10^{-1}$
		10^{-3}	.1247	.1097
		10^{-2}	1.247	.4601
		10^{-1}	12.47	.5204
11.b	5.246	10^{-4}	$.6406*10^{-2}$	$.6410*10^{-2}$
		10^{-3}	$.6406*10^{-1}$	$.6444*10^{-1}$
		10^{-2}	.6406	.6805
		10^{-1}	6.406	15.13
12.B_{51}	1.360	0.1	1.6607	1.6607
	linear dep.	0.5	8.3039	8.3039
13.b_{81}	1.329	10^{-4}	$.1623*10^{-2}$	$.1623*10^{-2}$
		10^{-3}	$.1623*10^{-1}$	$.1628*10^{-1}$
		10^{-2}	.1623	.1672
		10^{-1}	1.623	2.248
14.B_{41}	-.9511	0.1	-1.161	-1.161
	linear dep.	0.5	-5.807	-5.807

15.B_{52}	-.7675	0.1	-.9372	-.9372
	linear dep.	0.5	-4.686	-4.686
16.B_{31}	.4262	0.1	.5204	.5204
	linear dep.	0.5	2.602	2.602
17.B_{81}	.2527	0.1	.3086	.3086
	linear dep.	0.5	1.543	1.543
18.B_{53}	.1930	0.1	.2357	.2357
	linear dep.	0.5	1.178	1.178
19.b_{82}	-.1501	10^{-4}	$-.1833*10^{-3}$	$-.1833*10^{-3}$
		10^{-1}	-.1833	-.1767
20.B_{0}	.1493	0.1	.1823	.1823
	linear dep.	0.5	.9119	.9119
21.B_{71}	.1455	0.1	.1776	.1776
	linear dep.	0.5	.8883	.8883
22.B_{21}	.1197	0.1	.1462	.1462
	linear dep.	0.5	.7314	.7314
23.B_{11}	$.615*10^{-1}$	0.1	$.7511*10^{-1}$	$.7511*10^{-1}$
	linear dep.	0.5	.3755	.3755
24.B_{12}	$.456*10^{-1}$	0.1	$.5568*10^{-1}$	$.5568*10^{-1}$
	linear dep.	0.5	.2784	.2784
25.B_{04}	$.312*10^{-1}$	0.1	$.3818*10^{-1}$	$.3818*10^{-1}$
	linear dep.	0.5	.1909	.1909
26.B_{42}	$-.283*10^{-1}$	0.1	$-.3463*10^{-1}$	$-.3463*10^{-1}$
	linear dep.	0.5	-.1731	-.1731
27.B_{32}	$.225*10^{-1}$	0.1	$.2752*10^{-1}$	$.2752*10^{-1}$
	linear dep.	0.5	.1376	.1376
28.B_{72}	$-.216*10^{-1}$	0.1	$-.2643*10^{-1}$	$-.2643*10^{-1}$
	linear dep.	0.5	-.1321	-.1321
29.B_{61}	$.137*10^{-1}$	0.1	$.1676*10^{-1}$	$.1676*10^{-1}$
	linear dep.	0.5	$.8384*10^{-1}$	$.8384*10^{-1}$
30.B_{82}	$.132*10^{-1}$	0.1	$.1612*10^{-1}$	$.1612*10^{-1}$
	linear dep.	0.5	$.8060*10^{-1}$	$.8060*10^{-1}$
31.b_{71}	$-.853*10^{-2}$	10^{-4}	$-.1041*10^{-4}$	$-.1041*10^{-4}$
		10^{-1}	$-.1041*10^{-1}$	$-.1036*10^{-1}$
32.B_{62}	$-.844*10^{-2}$	0.1	$-.1031*10^{-1}$	$-.1031*10^{-1}$
	linear dep.	0.5	$-.5158*10^{-1}$	$-.5158*10^{-1}$
33.B_{05}	$-.774*10^{-2}$	0.1	$-.9463*10^{-2}$	$-.9463*10^{-2}$
	linear dep.	0.5	$-.4731*10^{-1}$	$-.4731*10^{-1}$
34.B_{03}	$-.727*10^{-2}$	0.1	$-.8887*10^{-2}$	$-.8887*10^{-2}$
	linear dep.	0.5	$-.4443*10^{-1}$	$-.4443*10^{-1}$
35.b_{61}	$-.246*10^{-2}$	10^{-4}	$-.3015*10^{-5}$	$-.3015*10^{-5}$
		10^{-1}	$-.3015*10^{-2}$	$-.2938*10^{-2}$
36.B_{22}	$-.241*10^{-3}$	0.1	$.2954*10^{-3}$	$.2954*10^{-3}$
	linear dep.	0.5	$.1477*10^{-2}$	$.1477*10^{-2}$
37.B_{23}	$-.749*10^{-4}$	0.1	$-.9154*10^{-4}$	$-.9154*10^{-4}$
	linear dep.	0.5	$-.4577*10^{-3}$	$-.4577*10^{-3}$

Table II.B.12
Sensitivities of the specific fluid enthalpy h_f to parameters in its mathematical formulation ($T_f^o = 564.7K, T_g^o = 620.6K, P^o = 159.2bar$).

Param g_j	Rel. sens. $\frac{\partial h_f}{\partial g_j}\frac{g_j^o}{h_f^o}$	Rel. Par. Var. $\frac{\Delta g_j}{g_j^o}$	$h_f^{pred} - h_f^o$	$h_f^{recal} - h_f^o$
1. A_6	9744.20	0.1	$.105*10^7$	$.105*10^7$
	linear dep.	0.5	$.529*10^7$	$.529*10^7$
2. A_5	-8185.48	0.1	$-.888*10^6$	$-.888*10^6$
	linear dep.	0.5	$-.444*10^7$	$-.444*10^7$
3. A_7	-7730.90	0.1	$-.839*10^6$	$-.839*10^6$
	linear dep.	0.5	$-.419*10^7$	$-.419*10^7$
4. A_4	4591.12	0.1	$.498*10^6$	$.498*10^6$
	linear dep.	0.5	$.249*10^7$	$.249*10^7$
5. A_8	3937.18	0.1	$.427*10^6$	$.427*10^6$
	linear dep.	0.5	$.213*10^7$	$.213*10^7$
6. A_3	-1662.57	0.1	$-.180*10^6$	$-.180*10^6$
	linear dep.	0.5	$-.902*10^6$	$-.902*10^6$
7. A_9	-1167.03	0.1	$-.126*10^6$	$-.126*10^6$
	linear dep.	0.5	$-.633*10^6$	$-.633*10^6$
8. A_0	356.208	0.1	$.386*10^5$	$.386*10^5$
	linear dep.	0.5	$.193*10^6$	$.193*10^6$
9. A_{10}	153.33	0.1	$.166*10^5$	$.166*10^5$
	linear dep.	0.5	$.832*10^5$	$.832*10^5$
10. A_1	-35.015	0.1	-3801.97	-3801.97
	linear dep.	0.5	$-.190*10^5$	$-.190*10^5$
11. a_3	.44819	10^{-4}	$.4866*10^{-1}$	$.4866*10^{-1}$
		10^{-3}	.4866	.4866
		10^{-2}	4.866	4.864
		10^{-1}	48.66	48.50
12. a_1	$.854*10^{-1}$	10^{-4}	$.9274*10^{-2}$	$.9276*10^{-2}$
		10^{-3}	$.9274*10^{-1}$	$.9292*10^{-1}$
		10^{-2}	.9274	.9457
		10^{-1}	9.274	11.38
13.A_{11}	$-.493*10^{-1}$	0.1	-5.362	-5.362
	linear dep.	0.5	-26.81	-26.81
14. a_4	$.284*10^{-1}$	10^{-4}	$.3085*10^{-2}$	$.3085*10^{-2}$
		10^{-3}	$.3085*10^{-1}$	$.3085*10^{-1}$
		10^{-2}	.3085	.3090
		10^{-1}	3.085	3.142
15. a_{10}	$-.211*10^{-2}$	10^{-4}	$-.229*10^{-3}$	$-.229*10^{-3}$
		10^{-3}	$-.229*10^{-2}$	$-.229*10^{-2}$
		10^{-2}	$-.229*10^{-1}$	$-.225*10^{-1}$

		10^{-1}	-.2296	-.1912
16. a_2	$.861*10^{-3}$	10^{-4}	$.9355*10^{-4}$	$.9355*10^{-4}$
		10^{-3}	$.9355*10^{-3}$	$.9355*10^{-3}$
		10^{-2}	$.9355*10^{-2}$	$.9355*10^{-2}$
		10^{-1}	$.9355*10^{-1}$	$.9352*10^{-1}$
17.A_{20}	$.737*10^{-3}$	0.1	$.8009*10^{-1}$	$.8009*10^{-1}$
	linear dep.	0.5	.4004	.4004
18. a_5	$.413*10^{-3}$	10^{-4}	$.4491*10^{-4}$	$.4491*10^{-4}$
		10^{-3}	$.4491*10^{-3}$	$.4492*10^{-3}$
		10^{-2}	$.4491*10^{-2}$	$.4500*10^{-2}$
		10^{-1}	$.4491*10^{-1}$	$.4588*10^{-1}$
19. A_{12}	$-.303*10^{-3}$	0.1	$-.329*10^{-1}$	$-.329*10^{-1}$
	linear dep.	0.5	-.1649	-.1649
20. A_{14}	$-.173*10^{-3}$	0.1	$-.188*10^{-1}$	$-.188*10^{-1}$
	linear dep.	0.5	$-.940*10^{-1}$	$-.940*10^{-1}$
21. a_9	$.120*10^{-3}$	0.1	$.1303*10^{-1}$	$.1303*10^{-1}$
	linear dep.	0.5	$.6516*10^{-1}$	$.6516*10^{-1}$
22. a_6	$.424*10^{-4}$	10^{-4}	$.4610*10^{-5}$	$.4603*10^{-5}$
		10^{-3}	$.4610*10^{-4}$	$.4533*10^{-4}$
		10^{-2}	$.4610*10^{-3}$	$.3904*10^{-3}$
		10^{-1}	$.4610*10^{-2}$	$.1204*10^{-2}$
23. a_{11}	$.144*10^{-4}$	0.1	$.1567*10^{-2}$	$.1567*10^{-2}$
	linear dep.	0.5	$.7836*10^{-2}$	$.7836*10^{-2}$
24. A_{15}	$-.111*10^{-5}$	0.1	$-.121*10^{-3}$	$-.121*10^{-3}$
	linear dep.	0.5	$-.606*10^{-3}$	$-.606*10^{-3}$
25. A_{17}	$-.300*10^{-6}$	0.1	$-.326*10^{-4}$	$-.326*10^{-4}$
	linear dep.	0.5	$-.163*10^{-3}$	$-.163*10^{-3}$
26. A_{18}	$-.566*10^{-8}$	0.1	$-.615*10^{-6}$	$-.615*10^{-6}$
	linear dep.	0.5	$-.307*10^{-5}$	$-.307*10^{-5}$
27. A_{16}	$.168*10^{-8}$	0.1	$.183*10^{-6}$	$.183*10^{-6}$
	linear dep.	0.5	$.915*10^{-6}$	$.915*10^{-6}$
28. a_{12}	$.100*10^{-8}$	0.1	$.108*10^{-6}$	$.108*10^{-6}$
	linear dep.	0.5	$.544*10^{-6}$	$.544*10^{-6}$
29. A_{21}	$.100*10^{-8}$	0.1	$.108*10^{-6}$	$.108*10^{-6}$
	linear dep.	0.5	$.544*10^{-6}$	$.544*10^{-6}$
30. a_8	$.923*10^{-10}$	10^{-4}	$.100*10^{-10}$	$.100*10^{-10}$
		10^{-3}	$.100*10^{-9}$	$.100*10^{-9}$
		10^{-2}	$.100*10^{-8}$	$.100*10^{-8}$
		10^{-1}	$.100*10^{-7}$	$.100*10^{-7}$
31. A_{19}	$-.51*10^{-10}$	0.1	$-.562*10^{-8}$	$-.562*10^{-8}$
		0.5	$-.281*10^{-7}$	$-.281*10^{-7}$
32. a_7	$-.21*10^{-12}$	10^{-4}	$-.234*10^{-13}$	$-.234*10^{-13}$
		10^{-1}	$-.234*10^{-10}$	$-.234*10^{-10}$
33. A_{22}	$.606*10^{-14}$	0.1	$.658*10^{-12}$	$.658*10^{-12}$
		0.5	$.329*10^{-11}$	$.329*10^{-11}$

Table II.B.13
Sensitivities of V_g to the numerical parameters that enter its ASME mathematical formulation ($T_f^o = 564.7K, T_g^o = 620.6K, P^o = 159.2bar$).

Par. g_j	Rel. Sens. $\frac{\partial V_g}{\partial g_j}\frac{g_j^o}{V_g^o}$	Rel. Par. Var. $\frac{\Delta g_j}{g_j^o}$	$V_g^{pred} - V_g^o$	$V_g^{recal} - V_g^o$
1.B_{93}	-12239.7	0.1	-13194.8	-13194.8
	linear dep.	0.5	-65974.3	-65974.3
2.B_{94}	11250.28	0.1	12128.23	12128.23
	linear dep.	0.5	60641.1	60641.1
3.B_{92}	7454.4	0.1	8036.13	8036.13
	linear dep.	0.5	40180.65	40180.65
4.B_{95}	-5489.58	0.1	-5917.98	-5917.98
	linear dep.	0.5	-29589.91	-29589.91
5.B_{91}	-2409.25	0.1	-2597.26	-2597.26
	linear dep.	0.5	-12986.34	-12986.34
6.B_{96}	1111.1	0.1	1197.81	1197.81
	linear dep.	0.5	5989.06	5989.06
7.B_{90}	322.75	0.1	347.94	347.94
	linear dep.	0.5	1739.72	1739.72
8. I_1	1.79724	0.1	1.9374	1.9374
	linear dep.	0.5	9.6874	9.6874
9. L_1	.94649	10^{-4}	$.102*10^{-2}$	$.104*10^{-2}$
		10^{-3}	$.102*10^{-1}$	$.133*10^{-1}$
		10^{-2}	.1020	10.2894
		10^{-1}	1.020	$-.222*10^{-1}$
10.B_{51}	-.60403	0.1	-.6511	-.6511
	linear dep.	0.5	-3.255	-3.255
11.B_{41}	.55367	0.1	.59688	.59688
	linear dep.	0.5	2.9844	2.9844
12. L_2	-.50675	10^{-4}	$-.546*10^{-3}$	$-.538*10^{-3}$
		10^{-3}	$-.546*10^{-2}$	$-.479*10^{-2}$
		10^{-2}	$-.546*10^{-1}$	$-.197*10^{-1}$
13.B_{12}	-.46088	0.1	-.49685	-.49685
	linear dep.	0.5	-2.4842	-2.4842
14. L_0	-.46037	10^{-4}	$-.496*10^{-3}$	$-490*10^{-3}$
		10^{-3}	$-.496*10^{-2}$	$-.440*10^{-2}$
		10^{-2}	$-.496*10^{-1}$	$-.192*10^{-1}$
		10^{-1}	-.4963	$-.222*10^{-1}$
15. b	-.44629	10^{-4}	$-.481*10^{-3}$	$-.481*10^{-3}$
		10^{-3}	$-.481*10^{-2}$	$-.481*10^{-2}$
		10^{-2}	$-.481*10^{-1}$	$-.49*10^{-1}$
		10^{-1}	-.4811	-.6283
16.B_{52}	.44523	0.1	.47997	.47997

	linear dep.	0.5	2.3998	2.3998
17.B_{31}	-.35894	0.1	-.38696	-.38696
	linear dep.	0.5	-1.9348	-1.9348
18.B_{53}	-.15242	0.1	-.16423	-.16423
	linear dep.	0.5	-.82160	-.82160
19.B_{71}	-.11813	0.1	-.12735	-.12735
	linear dep.	0.5	-.63677	-.63677
20.B_{21}	$-.672*10^{-1}$	0.1	$-.725*10^{-1}$	$-.725*10^{-1}$
	linear dep.	0.5	-.3625	-.3625
21.B_{32}	$-.615*10^{-1}$	0.1	$-.663*10^{-1}$	$-.663*10^{-1}$
	linear dep.	0.5	-.3315	-.3315
22.B_{42}	$.526*10^{-1}$	0.1	$.567*10^{-1}$	$.567*10^{-1}$
	linear dep.	0.5	.2837	.2837
23.B_{61}	$-.508*10^{-1}$	0.1	$-.548*10^{-1}$	$-.548*10^{-1}$
	linear dep.	0.5	-.27404	-.27404
24.b_{81}	$-.506*10^{-1}$	10^{-4}	$-.545*10^{-4}$	$-.545*10^{-4}$
		10^{-3}	$-.545*10^{-3}$	$-.546*10^{-3}$
		10^{-2}	$-.545*10^{-2}$	$-.556*10^{-2}$
		10^{-1}	$-.545*10^{-1}$	$-.679*10^{-1}$
25.B_{62}	$.404*10^{-1}$	0.1	$.436*10^{-1}$	$.436*10^{-1}$
	linear dep.	0.5	.2181	.2181
26.B_{11}	$-.331*10^{-1}$	0.1	$-.356*10^{-1}$	$-.356*10^{-1}$
	linear dep.	0.5	-.17846	-.17846
27.B_{72}	$.320*10^{-1}$	0.1	$.345*10^{-1}$	$.345*10^{-1}$
	linear dep.	0.5	.17251	.17251
28.B_{81}	$-.177*10^{-1}$	0.1	$-.191*10^{-1}$	$-.191*10^{-1}$
	linear dep.	0.5	$-.959*10^{-1}$	$-.959*10^{-1}$
29.B_{23}	$.136*10^{-1}$	0.1	$.147*10^{-1}$	$.147*10^{-1}$
	linear dep.	0.5	$.737*10^{-1}$	$.737*10^{-1}$
30.B_{22}	$-.11*10^{-1}$	0.1	$-.118*10^{-1}$	$-.118*10^{-1}$
	linear dep.	0.5	$-.593*10^{-1}$	$-.593*10^{-1}$
31. b_{82}	$.691*10^{-2}$	10^{-4}	$.745*10^{-5}$	$.745*10^{-5}$
		10^{-2}	$.745*10^{-3}$	$.743*10^{-3}$
		10^{-1}	$.745*10^{-2}$	$.725*10^{-2}$
32. b_{71}	$.392*10^{-2}$	10^{-4}	$.422*10^{-5}$	$.422*10^{-5}$
		10^{-1}	$.422*10^{-2}$	$.421*10^{-2}$
33. b_{61}	$.244*10^{-2}$	10^{-4}	$.263*10^{-5}$	$.263*10^{-5}$
		10^{-3}	$.263*10^{-4}$	$.263*10^{-4}$
		10^{-2}	$.263*10^{-3}$	$.263*10^{-3}$
34.B_{82}	$-.103*10^{-2}$	0.1	$-.111*10^{-2}$	$-.111*10^{-2}$
	linear dep.	0.5	$-.558*10^{-2}$	$-.558*10^{-2}$

Table II.B.14
Sensitivities of V_f to the numerical parameters that enter its ASME mathematical formulation ($T_f^o = 564.7K, T_g^o = 620.6K, P^o = 159.2bar$).

Param.Rank	Relative Sens.	Rel. par. Var.	Recalc. relative change
1. A_{11}	1.016	0.01	1.016
		0.1	1.016
		0.5	1.016
2. a_5	.982	10^{-4}	.981
		10^{-3}	.981
		10^{-2}	.980
		10^{-1}	.978
3. a_1	.638	10^{-4}	.638
		10^{-3}	.639
		10^{-2}	.648
		10^{-1}	.765
4. a_3	-.107	10^{-4}	-.107
		10^{-3}	-.107
		10^{-2}	-.106
		10^{-1}	-.101
5. a_4	$.626*10^{-1}$	10^{-4}	$.626*10^{-1}$
		10^{-3}	$.627*10^{-1}$
		10^{-2}	$.628*10^{-1}$
		10^{-1}	$.648*10^{-1}$
6. A_{12}	$-.617*10^{-1}$	0.01	$-.617*10^{-1}$
		0.1	$-.617*10^{-1}$
		0.5	$-.617*10^{-1}$
7. A_{14}	$.410*10^{-1}$	0.01	$.410*10^{-1}$
		0.1	$.410*10^{-1}$
		0.5	$.410*10^{-1}$
8. a_{10}	$-.722*10^{-2}$	10^{-4}	$-.722*10^{-2}$
		10^{-3}	$-.720*10^{-2}$
		10^{-2}	$-.706*10^{-2}$
		10^{-1}	$-.584*10^{-2}$
9. a_6	$-.427*10^{-2}$	10^{-4}	$-.427*10^{-2}$
		10^{-3}	$-.421*10^{-2}$
		10^{-2}	$-.374*10^{-2}$
		10^{-1}	$-.139*10^{-2}$
10.A_{13}	$.313*10^{-2}$	0.01	$.313*10^{-2}$
		0.1	$.313*10^{-2}$
		0.5	$.313*10^{-2}$
11.A_{20}	$.128*10^{-2}$	0.01	$.128*10^{-2}$
		0.1	$.128*10^{-2}$
		0.5	$.128*10^{-2}$

12. a_2	$.121*10^{-2}$	10^{-4}	$.121*10^{-2}$
		10^{-3}	$.121*10^{-2}$
		10^{-2}	$.120*10^{-2}$
		10^{-1}	$.120*10^{-2}$
13. a_{11}	$-.707*10^{-3}$	0.01	$-.707*10^{-3}$
		0.1	$-.707*10^{-3}$
		0.5	$-.707*10^{-3}$
14. a_9	$.202*10^{-3}$	0.01	$.202*10^{-3}$
		0.1	$.202*10^{-3}$
		0.5	$.202*10^{-3}$
15.A_{15}	$.143*10^{-3}$	0.01	$.143*10^{-3}$
		0.1	$.143*10^{-3}$
		0.5	$.143*10^{-3}$
16.A_{21}	$-.321*10^{-4}$	0.01	$-.321*10^{-4}$
		0.1	$-.321*10^{-4}$
		0.5	$-.321*10^{-4}$
17. a_{12}	$.978*10^{-5}$	0.01	$.978*10^{-5}$
		0.1	$.978*10^{-5}$
		0.5	$.978*10^{-5}$
18.A_{17}	$-.220*10^{-5}$	0.01	$-.220*10^{-5}$
		0.1	$-.220*10^{-5}$
		0.5	$-.220*10^{-5}$
19.A_{18}	$-.331*10^{-6}$	0.01	$-.331*10^{-6}$
		0.1	$-.331*10^{-6}$
		0.5	$-.331*10^{-6}$
20.A_{19}	$-.182*10^{-7}$	0.01	$-.182*10^{-7}$
		0.1	$-.182*10^{-7}$
		0.5	$-.182*10^{-7}$
21.A_{16}	$.401*10^{-8}$	0.01	$.401*10^{-8}$
		0.1	$.401*10^{-8}$
		0.5	$.401*10^{-8}$
22. a_8	$.173*10^{-9}$	10^{-3}	$.173*10^{-9}$
		10^{-2}	$.173*10^{-9}$
		10^{-1}	$.172*10^{-9}$
23.A_{22}	$.816*10^{-12}$	10^{-2}	$.816*10^{-12}$
		10^{-1}	$.815*10^{-12}$
24. a_7	$-.617*10^{-13}$	10^{-2}	$-.617*10^{-13}$
		10^{-1}	$-.617*10^{-13}$

The sensitivities of the remaining thermodynamic properties (namely the specific fluid volume, V_f, the specific isobaric gas heat capacity, C_{pg}, the volumetric expansion coefficient for fluid, β_f, the volumetric expansion coefficient for gas, β_g, the specific gas enthalpy, h_g, the isothermal coefficient of compressibility for fluid, k_f, and the isothermal coefficient for gas, k_g), to

the coefficients that enter their respective mathematical expressions, are relatively small; their typical magnitudes are illustrated in Table II.B.14, which presents sensitivities for V_f

The sensitivities of the thermodynamic properties of water to temperature, pressure, and the experimentally-determined parameters that enter in their respective mathematical formulations play an essential role for sensitivity analyses of results calculated by thermal-hydraulic codes, such as RELAP5/MOD3.2, which use water as the working fluid. In particular, the sensitivities for the ASME 1993 Steam Tables are expected to indicate priority areas for investigating the new, IAPWS-IF97 formulations [12] for the material properties of water, since these formulations will eventually form the basis for all calculations involving water.

In closing, it is also important to discuss the essential role played by sensitivities for performing uncertainty analysis; in particular, the linear approximation of the variance of a response R is given by $\mathrm{var}\langle R\rangle = \sum_{i,j=1}^{J} S_i S_j \,\mathrm{cov}(g_i, g_j)$, where S_i is the sensitivity of R to the parameter g_i, and $\mathrm{cov}(g_i, g_j)$ is the covariance matrix for the parameters g_i and g_j. If all of the parameters are uncorrelated, then this formula reduces to $\mathrm{var}\langle R\rangle = \sum_{j=1}^{J} S_j^2 \sigma_j^2$, where σ_j^2 is the variance (uncertainty) of the distribution of the parameter g_j. These formulae highlight the interplay between the parameter sensitivities and uncertainties in contributing to the overall response uncertainty - as expressed by $\mathrm{var}\langle R\rangle$. Thus, the largest contributions to the response uncertainty, $\mathrm{var}\langle R\rangle$, come from those parameters g_j that display not only a large uncertainty σ_j^2 but also a high sensitivity S_j. If either one (e.g., the sensitivity S_j) or the other (e.g., the uncertainty σ_j^2) of these two components is small, then their respective product will obviously contribute less to $\mathrm{var}\langle R\rangle$ than if both components were simultaneously large.

APPENDIX A: THE RELAP5/MOD3.2 DISCRETIZED SET OF "NUMERICALLY CONVENIENT DIFFERENTIAL EQUATIONS"

The components of the matrix $\boldsymbol{A}$ introduced in Eq. (II.B.13) are defined as follows:

$$A_{11} = \alpha_g \left(X_n \frac{\partial \rho_g}{\partial X_n} + \rho_g \right), \quad A_{12} = \alpha_g X_n \frac{\partial \rho_g}{\partial U_g},$$

$$A_{14} = \rho_g X_n, \quad A_{15} = \alpha_g X_n \frac{\partial \rho_g}{\partial P},$$

$$A_{21} = \alpha_g U_g \frac{\partial \rho_g}{\partial X_n} + \left(\frac{h_f^*}{h_g^* - h_f^*} \right) \Delta t \frac{P_s}{P} H_{ig} \left(\frac{\partial T^s}{\partial X_n} - \frac{\partial T_g}{\partial X_n} \right)$$

$$+ \left(\frac{h_g^*}{h_g^* - h_f^*} \right) \Delta t H_{if} \frac{\partial T^s}{\partial X_n} + \Delta t \frac{P - P_s}{P} H_{gf} \frac{\partial T_g}{\partial X_n},$$

$$A_{22} = \alpha_g U_g \frac{\partial \rho_g}{\partial U_g} + \left(\frac{h_f^*}{h_g^* - h_f^*} \right) \Delta t \frac{P_s}{P} H_{ig} \left(\frac{\partial T^s}{\partial U_g} - \frac{\partial T_g}{\partial U_g} \right)$$

$$+ \left(\frac{h_g^*}{h_g^* - h_f^*} \right) \Delta t H_{if} \frac{\partial T^s}{\partial U_g} + \Delta t \frac{P - P_s}{P} H_{gf} \frac{\partial T_g}{\partial U_g},$$

$$A_{23} = -\left(\frac{h_g^*}{h_g^* - h_f^*} \right) \Delta t H_{if} \frac{\partial T_f}{\partial U_f} - \Delta t \frac{P - P_s}{P} H_{gf} \frac{\partial T_f}{\partial U_f}, \quad A_{24} = \rho_g U_g + P,$$

$$A_{25} = \alpha_g U_g \frac{\partial \rho_g}{\partial P} + \left(\frac{h_f^*}{h_g^* - h_f^*} \right) \Delta t \frac{P_s}{P} H_{ig} \left(\frac{\partial T^s}{\partial P} - \frac{\partial T_g}{\partial P} \right)$$

$$+ \left(\frac{h_g^*}{h_g^* - h_f^*} \right) \Delta t H_{if} \frac{\partial T^s}{\partial P} + \Delta t \frac{P - P_s}{P} H_{gf} \left(\frac{\partial T_g}{\partial P} - \frac{\partial T_f}{\partial P} \right),$$

$$A_{31} = -\left(\frac{h_f^*}{h_g^* - h_f^*} \right) \Delta t \frac{P_s}{P} H_{ig} \left(\frac{\partial T^s}{\partial X_n} - \frac{\partial T_g}{\partial X_n} \right) - \left(\frac{h_g^*}{h_g^* - h_f^*} \right) \Delta t H_{if} \frac{\partial T^s}{\partial X_n}$$

$$- \Delta t \frac{P - P_s}{P} H_{gf} \frac{\partial T_g}{\partial X_n},$$

$$A_{32} = -\left(\frac{h_f^*}{h_g^* - h_f^*}\right)\Delta t \frac{P_s}{P} H_{ig}\left(\frac{\partial T^s}{\partial U_g} - \frac{\partial T_g}{\partial U_g}\right) - \left(\frac{h_g^*}{h_g^* - h_f^*}\right)\Delta t H_{if} \frac{\partial T^s}{\partial U_g}$$

$$- \Delta t \frac{P - P_s}{P} H_{gf} \frac{\partial T_g}{\partial U_g},$$

$$A_{33} = \alpha_f \left(U_f \frac{\partial \rho_f}{\partial U_f} + \rho_f\right) + \left(\frac{h_g^*}{h_g^* - h_f^*}\right)\Delta t H_{if} \frac{\partial T_f}{\partial U_f} + \Delta t \frac{P - P_s}{P} H_{gf} \frac{\partial T_f}{\partial U_f},$$

$$A_{34} = -\rho_f U_f - P,$$

$$A_{35} = \alpha_f U_f \frac{\partial \rho_f}{\partial P} - \left(\frac{h_f^*}{h_g^* - h_f^*}\right)\Delta t \frac{P_s}{P} H_{ig}\left(\frac{\partial T^s}{\partial P} - \frac{\partial T_g}{\partial P}\right)$$

$$- \left(\frac{h_g^*}{h_g^* - h_f^*}\right)\Delta t H_{if} \frac{\partial T^s}{\partial P} - \Delta t \frac{P - P_s}{P} H_{gf}\left(\frac{\partial T_g}{\partial P} - \frac{\partial T_f}{\partial P}\right),$$

$$A_{41} = \alpha_g \frac{\partial \rho_g}{\partial X_n} + \left(\frac{2}{h_g^* - h_f^*}\right)\Delta t \frac{P_s}{P} H_{ig}\left(\frac{\partial T^s}{\partial X_n} - \frac{\partial T_g}{\partial X_n}\right) + \left(\frac{2}{h_g^* - h_f^*}\right)\Delta t H_{if} \frac{\partial T^s}{\partial X_n},$$

$$A_{42} = \alpha_g \frac{\partial \rho_g}{\partial U_g} + \left(\frac{2}{h_g^* - h_f^*}\right)\Delta t \frac{P_s}{P} H_{ig}\left(\frac{\partial T^s}{\partial U_g} - \frac{\partial T_g}{\partial U_g}\right) + \left(\frac{2}{h_g^* - h_f^*}\right)\Delta t H_{if} \frac{\partial T^s}{\partial U_g},$$

$$A_{43} = -\alpha_f \frac{\partial \rho_f}{\partial U_f} - \left(\frac{2}{h_g^* - h_f^*}\right)\Delta t H_{if} \frac{\partial T_f}{\partial U_f}, \quad A_{44} = \rho_g + \rho_f,$$

$$A_{45} = \alpha_g \frac{\partial \rho_g}{\partial P} - \alpha_f \frac{\partial \rho_f}{\partial P} + \left(\frac{2}{h_g^* - h_f^*}\right)\Delta t \frac{P_s}{P} H_{ig}\left(\frac{\partial T^s}{\partial P} - \frac{\partial T_g}{\partial P}\right)$$

$$+ \left(\frac{2}{h_g^* - h_f^*}\right)\Delta t H_{if} \frac{\partial T^s}{\partial P},$$

$$A_{51} = \alpha_g \frac{\partial \rho_g}{\partial X_n}, \quad A_{52} = \alpha_g \frac{\partial \rho_g}{\partial U_g}, \quad A_{53} = \alpha_f \frac{\partial \rho_f}{\partial U_f},$$

$$A_{54} = \rho_g - \rho_f, \quad A_{55} = \alpha_g \frac{\partial \rho_g}{\partial P} + \alpha_f \frac{\partial \rho_f}{\partial P}.$$

The components of the vector $\boldsymbol{b}$ introduced in Eq. (II.B.13) are defined as follows:

$$b_2 = -\left(\frac{h_f^*}{h_g^* - h_f^*}\right)\Delta t \frac{P_s}{P} H_{ig}\left(T^s - T_g\right) - \left(\frac{h_g^*}{h_g^* - h_f^*}\right)\Delta t H_{if}\left(T^s - T_f\right)$$
$$- \Delta t \frac{P - P_s}{P} H_{gf}\left(T_g - T_f\right)$$
$$+ \Delta t \Gamma_w \left[\left(\frac{1-\varepsilon}{2}\right)h_f' + \left(\frac{1+\varepsilon}{2}\right)h_g'\right] + Q_{wg}\Delta t + DISS_g \Delta t,$$

$$b_3 = \left(\frac{h_f^*}{h_g^* - h_f^*}\right)\Delta t \frac{P_s}{P} H_{ig}\left(T^s - T_g\right) + \left(\frac{h_g^*}{h_g^* - h_f^*}\right)\Delta t H_{if}\left(T^s - T_f\right)$$
$$+ \Delta t \frac{P - P_s}{P} H_{gf}\left(T_g - T_f\right)$$
$$- \Delta t \Gamma_w \left[\left(\frac{1-\varepsilon}{2}\right)h_f' + \left(\frac{1+\varepsilon}{2}\right)h_g'\right] + Q_{wf}\Delta t + DISS_f \Delta t,$$

$$b_4 = -\left(\frac{2}{h_g^* - h_f^*}\right)\Delta t \frac{P_s}{P} H_{ig}\left(T^s - T_g\right) - \left(\frac{2}{h_g^* - h_f^*}\right)\Delta t H_{if}\left(T^s - T_f\right) + 2\Delta t \Gamma_w.$$

The components of the vectors $\boldsymbol{f}^1, \boldsymbol{f}^2, \boldsymbol{g}^1, \boldsymbol{g}^2$ introduced in Eq. (II.B.13) are defined below:

$$f_3^1 = -\left[\dot{\alpha}_{f,j+1}\left(\dot{\rho}_{f,j+1}\dot{U}_{f,j+1} + P_L\right)A_{j+1}\right]\Delta t / V, \quad f_4^1 = \left(\dot{\alpha}_f \dot{\rho}_f A\right)_{j+1}\Delta t / V,$$
$$f_5^1 = -\left(\dot{\alpha}_f \dot{\rho}_f A\right)_{j+1}\Delta t / V;$$
$$f_3^2 = \left[\dot{\alpha}_{f,j}\left(\dot{\rho}_{f,j}\dot{U}_{f,j} + P_L\right)A_j\right]\Delta t / V, \quad f_4^2 = -\left(\dot{\alpha}_f \dot{\rho}_f A\right)_j \Delta t / V,$$
$$f_5^2 = \left(\dot{\alpha}_f \dot{\rho}_f A\right)_j \Delta t / V;$$

$$g_1^1 = -\left(\dot{\alpha}_g \dot{\rho}_g \dot{X}_n A\right)_{j+1}\Delta t / V, \quad g_2^1 = -\left[\dot{\alpha}_{g,j+1}\left(\dot{\rho}_{g,j+1}\dot{U}_{g,j+1} + P_L\right)A_{j+1}\right]\Delta t / V,$$
$$g_4^1 = g_5^1 = -\left(\dot{\alpha}_g \dot{\rho}_g A\right)_{j+1}\Delta t / V;$$
$$g_1^2 = \left(\dot{\alpha}_g \dot{\rho}_g \dot{X}_n A\right)_j \Delta t / V, \quad g_2^2 = \left[\dot{\alpha}_{g,j}\left(\dot{\rho}_{g,j}\dot{U}_{g,j} + P_L\right)A_j\right]\Delta t / V,$$
$$g_4^2 = g_5^2 = \left(\dot{\alpha}_g \dot{\rho}_g A\right)_j \Delta t / V.$$

The fluid specific internal energy, $\left(U_f\right)_L^{n+1}$, is calculated for a volume L at time-step $(n+1)$ by using the following sequence of three operations: (i) The nonexpanded liquid energy equation, which reads

$$
\begin{aligned}
&V_L\left[\left(\alpha_f\rho_f U_f\right)_L^{n+1}-\left(\alpha_f\rho_f U_f\right)_L^{n}\right]\\
&+\left[\dot{\alpha}_{f,j+1}\left(\dot{\rho}_{f,j+1}\dot{U}_{f,j+1}+P_L\right)v_{f,j+1}^{n+1}A_{j+1}-\dot{\alpha}_{f,j}\left(\dot{\rho}_{f,j}\dot{U}_{f,j}+P_L\right)v_{f,j}^{n+1}A_j\right]\Delta t\\
&=V_L P_L^n\left(\tilde{\alpha}_{g,L}^{n+1}-\alpha_{g,L}^n\right)+\left\{\left(\frac{h_f^*}{h_g^*-h_f^*}\right)_L^n\frac{P_{s,L}^n}{P_L^n}H_{ig,L}^n\left(\tilde{T}_L^{s,n+1}-\tilde{T}_{g,L}^{n+1}\right)\right.\\
&+\left(\frac{h_g^*}{h_g^*-h_f^*}\right)_L^n H_{if,L}^n\left(\tilde{T}_L^{s,n+1}-\tilde{T}_{f,L}^{n+1}\right)+\frac{P_L^n-P_{s,L}^n}{P_L^n}H_{gf,L}^n\left(\tilde{T}_{g,L}^{n+1}-\tilde{T}_{f,L}^{n+1}\right)\\
&\left.-\Gamma_{w,L}^n\left[\left(\frac{1-\varepsilon}{2}\right)\left(h'_{f,L}\right)^n+\left(\frac{1+\varepsilon}{2}\right)\left(h'_{g,L}\right)^n\right]+Q_{wf,L}^n+DISS_{f,L}^n\right\}V_L\Delta t,
\end{aligned}
$$

is solved to obtain $\left(\alpha_f\rho_f U_f\right)_L^{n+1}$; (ii) the nonexpanded liquid density equation, which reads

$$
\begin{aligned}
&V_L\left[\left(\alpha_f\rho_f\right)_L^{n+1}-\left(\alpha_f\rho_f\right)_L^{n}\right]+\left(\dot{\alpha}_{f,j+1}\dot{\rho}_{f,j+1}v_{f,j+1}^{n+1}A_{j+1}-\dot{\alpha}_{f,j}\dot{\rho}_{f,j}v_{f,j}^{n+1}A_j\right)\Delta t\\
&=\left(\frac{\dfrac{P_{s,L}^n}{P_L^n}H_{ig,L}^n\left(\tilde{T}_L^{s,n+1}-\tilde{T}_{g,L}^{n+1}\right)+H_{if,L}^n\left(\tilde{T}_L^{s,n+1}-\tilde{T}_{f,L}^{n+1}\right)}{\left(h'_{g,L}\right)^n-\left(h'_{f,L}\right)^n}-\Gamma_{w,L}^n\right)V_L\Delta t,
\end{aligned}
$$

is solved to obtain $\left(\alpha_f\rho_f\right)_k^{n+1}$; and (iii) the ratio of the results obtained in steps (i) and (ii), respectively, is calculated to obtain $\left(U_f\right)_L^{n+1}=\left(\alpha_f\rho_f U_f\right)_L^{n+1}\big/\left(\alpha_f\rho_f\right)_L^{n+1}$.

The total noncondensable mass fraction, $\left(X_n\right)_L^{n+1}$, for volume L at time-step $(n+1)$ is calculated by first solving the nonexpanded total noncondensable density equation

$$
\begin{aligned}
&V_L\left[\left(\alpha_g\rho_g X_n\right)_L^{n+1}-\left(\alpha_g\rho_g X_n\right)_L^{n}\right]\\
&+\left(\dot{\alpha}_{g,j+1}\dot{\rho}_{g,j+1}\dot{X}_{n,j+1}^n v_{g,j+1}^{n+1}A_{j+1}-\dot{\alpha}_{g,j}\dot{\rho}_{g,j}\dot{X}_{n,j}^n v_{g,j}^{n+1}A_j\right)\Delta t=0,
\end{aligned}
$$

to obtain $\left(\alpha_g \rho_g X_n\right)_L^{n+1}$, and then calculating directly

$$\left(X_n\right)_L^{n+1} = \left(\alpha_g \rho_g X_n\right)_L^{n+1} \Big/ \left(\alpha_g \rho_g\right)_L^{n+1}$$

by using the previously calculated value of $\left(\alpha_g \rho_g\right)_L^{n+1}$.

The gas void fraction, $\left(\alpha_g\right)_L^{n+1}$, for a volume L at time-step $(n+1)$ is calculated as follows:

$$\left(\alpha_g\right)_L^{n+1} = 1 - \alpha_{f,L}^{n+1} = 1 - \frac{\left(\alpha_f \rho_f\right)_L^{n+1}}{\hat{\rho}_{f,L}^{n+1}}, \quad \text{where}$$

$$\hat{\rho}_{f,L}^{n+1} \equiv \rho_{f,L}^{n} + \left(\frac{\partial \rho_f}{\partial P}\right)_L^n \left(P_L^{n+1} - P_L^n\right) + \left(\frac{\partial \rho_f}{\partial U_f}\right)_L^n \left(U_{f,L}^{n+1} - U_{f,L}^{n}\right).$$

The noncondensable mass fraction for the i^{th} noncondensable species, $\left(X_{ni}\right)_L^{n+1}$, for volume L at time-step $(n+1)$ is calculated by first solving the nonexpanded equation for the individual noncondensable density

$$V_L \left[\left(\alpha_g \rho_g X_n X_{ni}\right)_L^{n+1} - \left(\alpha_g \rho_g X_n X_{ni}\right)_L^{n}\right]$$
$$+ \left(\dot{\alpha}_{g,j+1} \dot{\rho}_{g,j+1} \dot{X}_{n,j+1}^{\,n} \dot{X}_{ni,j+1}^{\,n} v_{g,j+1}^{n+1} A_{j+1} - \dot{\alpha}_{g,j} \dot{\rho}_{g,j} \dot{X}_{n,j}^{\,n} \dot{X}_{ni,j}^{\,n} v_{g,j}^{n+1} A_j\right) \Delta t = 0,$$

to obtain $\left(\alpha_g \rho_g X_n X_{ni}\right)_L^{n+1}$, and then by using the previously calculated quantity $\left(\alpha_g \rho_g X_n\right)_L^{n+1}$ to obtain $\left(X_{ni}\right)_L^{n+1} = \left(\alpha_g \rho_g X_n X_{ni}\right)_L^{n+1} \Big/ \left(\alpha_g \rho_g X_n\right)_L^{n+1}$.

APPENDIX B: COEFFICIENTS IN THE EQUATIONS UNDERLYING THE FSM

By taking the G-derivative of the vapor energy equation, we obtain the following expressions for the components $S_{mn}(x,t)$, $T_{mn}(x,t)$, and $U_{mn}(x,t)$ that appear on the left-side of Eq. (II.B.23):

$$S_{11}(x,t) \equiv \alpha_g^o \rho_g^o + \alpha_g^o U_g^o \left(\frac{\partial \rho_g}{\partial U_g} \right)_o ,$$

$$T_{11}(x,t) \equiv \alpha_g^o U_g^o v_g^o \left(\frac{\partial \rho_g}{\partial U_g} \right)_o + \alpha_g^o \rho_g^o v_g^o, \quad U_{11}(x,t) \equiv -\left(\frac{\partial E_1}{\partial U_g} \right)_o ,$$

$$S_{12}(x,t) \equiv 0, \quad T_{12}(x,t) \equiv 0, \quad U_{12}(x,t) \equiv -\left(\frac{\partial E_1}{\partial U_f} \right)_o ,$$

$$S_{13}(x,t) \equiv \alpha_g^o U_g^o \left(\frac{\partial \rho_g}{\partial P} \right)_o , \qquad T_{13}(x,t) \equiv \alpha_g^o U_g^o v_g^o \left(\frac{\partial \rho_g}{\partial P} \right)_o ,$$

$$U_{13}(x,t) \equiv \frac{\partial \rho_g^o}{\partial t} + \frac{1}{A^o} \frac{\partial}{\partial x} \left(\alpha_g^o v_g^o A^o \right) - \left(\frac{\partial E_1}{\partial P} \right)_o ,$$

$$S_{14}(x,t) \equiv \rho_g^o U_g^o + P^o, \qquad T_{14}(x,t) \equiv \rho_g^o v_g^o U_g^o + P^o v_g^o ,$$

$$U_{14}(x,t) \equiv -\frac{\partial P^o}{\partial t} - \left(\frac{\partial E_1}{\partial \alpha_g} \right)_o - v_g^o \frac{\partial P^o}{\partial x} ,$$

$$S_{15}(x,t) \equiv \alpha_g^o U_g^o \left(\frac{\partial \rho_g}{\partial X_n} \right)_o , \qquad T_{15}(x,t) \equiv \alpha_g^o U_g^o v_g^o \left(\frac{\partial \rho_g}{\partial X_n} \right)_o ,$$

$$U_{15}(x,t) \equiv -\left(\frac{\partial E_1}{\partial X_n} \right)_o ,$$

$$S_{18}(x,t) \equiv 0, \quad T_{18}(x,t) \equiv \alpha_g^o \left(\rho_g^o U_g^o + P^o \right), \quad U_{18}(x,t) \equiv -\alpha_g^o \frac{\partial P^o}{\partial x} - \left(\frac{\partial E_1}{\partial v_g} \right)_o ,$$

$$S_{19}(x,t) \equiv 0, \quad T_{19}(x,t) \equiv 0, \quad U_{19}(x,t) \equiv -\left(\frac{\partial E_1}{\partial v_f} \right)_o ,$$

and where the quantity $E_1(\boldsymbol{\chi}, \boldsymbol{G})$ is defined as

$$E_1(\boldsymbol{\chi}, \boldsymbol{G}) \equiv -\left(\frac{h_f'}{h_g' - h_f'} \right) H_{ig} \left(T^s - T_g \right) - \left(\frac{h_g'}{h_g' - h_f'} \right) H_{if} \left(T^s - T_f \right)$$
$$- \frac{P - P_s}{P} H_{gf} \left(T_g - T_f \right) + \left[\left(\frac{1+\varepsilon}{2} \right) h_g^s + \left(\frac{1-\varepsilon}{2} \right) h_f^s \right] \Gamma_w + Q_{wg} + DISS_g .$$

By taking the G-derivative of the liquid energy equation, we obtain the following expressions for the components $S_{mn}(x,t)$, $T_{mn}(x,t)$, and $U_{mn}(x,t)$:

$$S_{21}(x,t) \equiv 0, \quad T_{21}(x,t) \equiv 0, \quad U_{21}(x,t) \equiv -\left(\frac{\partial E_2}{\partial U_g}\right)_o,$$

$$S_{22}(x,t) \equiv \alpha_f^o\left(\rho_f^o + U_f^o\left(\frac{\partial \rho_f}{\partial U_f}\right)_o\right), \quad T_{22}(x,t) \equiv \alpha_f^o v_f^o\left(\rho_f^o + U_f^o\left(\frac{\partial \rho_f}{\partial U_f}\right)_o\right),$$

$$U_{22}(x,t) \equiv -\left(\frac{\partial E_2}{\partial U_f}\right)_o,$$

$$S_{23}(x,t) \equiv \alpha_f^o U_f^o\left(\frac{\partial \rho_f}{\partial P}\right)_o, \quad T_{23}(x,t) \equiv \alpha_f^o v_f^o U_f^o\left(\frac{\partial \rho_f}{\partial P}\right)_o,$$

$$U_{23}(x,t) \equiv \frac{\partial \alpha_f}{\partial t} + \frac{1}{A^o}\frac{\partial}{\partial x}\left(\alpha_f^o v_f^o A^o\right) - \left(\frac{\partial E_2}{\partial P}\right)_o,$$

$$S_{24}(x,t) \equiv -\left(\rho_f^o U_f^o + P^o\right), \quad T_{24}(x,t) \equiv -v_f^o\left(\rho_f^o U_f^o + P^o\right),$$

$$U_{24}(x,t) \equiv -\left(\frac{\partial E_2}{\partial \alpha_g}\right)_o + \frac{\partial P^o}{\partial t} + v_f^o \frac{\partial P^o}{\partial x},$$

$$S_{25}(x,t) \equiv 0, \quad T_{25}(x,t) \equiv 0, \quad U_{25}(x,t) \equiv -\left(\frac{\partial E_2}{\partial X_n}\right)_o,$$

$$S_{28}(x,t) \equiv 0, \quad T_{28}(x,t) \equiv 0, \quad U_{28}(x,t) \equiv -\left(\frac{\partial E_2}{\partial v_g}\right)_o,$$

$$S_{29}(x,t) \equiv 0, \quad T_{29}(x,t) \equiv \alpha_f^o\left(\rho_f^o U_f^o + P^o\right), \quad U_{29}(x,t) \equiv -\alpha_f^o \frac{\partial P^o}{\partial x} - \left(\frac{\partial E_2}{\partial v_f}\right)_o,$$

and where the quantity $E_2(\boldsymbol{\chi}, \boldsymbol{G})$ is defined as

$$E_2(\boldsymbol{\chi}, \boldsymbol{G}) \equiv \left(\frac{h_f'}{h_g' - h_f'}\right) H_{ig}\left(T^s - T_g\right) + \left(\frac{h_g'}{h_g' - h_f'}\right) H_{if}\left(T^s - T_f\right)$$
$$+ \frac{P - P_s}{P} H_{gf}\left(T_g - T_f\right) - \left[\left(\frac{1+\varepsilon}{2}\right) h_g^s + \left(\frac{1-\varepsilon}{2}\right) h_f^s\right] \Gamma_w + Q_{wf} + DISS_f.$$

By taking the G-derivative of the sum density equation, we obtain the following expressions for the components $S_{mn}(x,t)$, $T_{mn}(x,t)$, and $U_{mn}(x,t)$:

$$S_{31}(x,t) \equiv \alpha_g^o \left(\frac{\partial \rho_g}{\partial U_g} \right)_o, \quad T_{31}(x,t) \equiv \alpha_g^o v_g^o \left(\frac{\partial \rho_g}{\partial U_g} \right)_o, \quad U_{31}(x,t) \equiv 0,$$

$$S_{32}(x,t) \equiv \alpha_f^o \left(\frac{\partial \rho_f}{\partial U_f} \right)_o, \quad T_{32}(x,t) \equiv \alpha_f^o v_f^o \left(\frac{\partial \rho_f}{\partial U_f} \right)_o, \quad U_{32}(x,t) \equiv 0,$$

$$S_{33}(x,t) \equiv \alpha_g^o \left(\frac{\partial \rho_g}{\partial P} \right)_o + \alpha_f^o \left(\frac{\partial \rho_f}{\partial P} \right)_o,$$

$$T_{33}(x,t) \equiv \alpha_g^o v_g^o \left(\frac{\partial \rho_g}{\partial P} \right)_o + \alpha_f^o v_f^o \left(\frac{\partial \rho_f}{\partial P} \right)_o, \quad U_{33}(x,t) \equiv 0,$$

$$S_{34}(x,t) \equiv \rho_g^o - \rho_f^o, \quad T_{34}(x,t) \equiv \rho_g^o v_g^o - \rho_f^o v_f^o, \quad U_{34}(x,t) \equiv 0,$$

$$S_{35}(x,t) \equiv \alpha_g^o \left(\frac{\partial \rho_g}{\partial X_n} \right)_o, \quad T_{35}(x,t) \equiv \alpha_g^o v_g^o \left(\frac{\partial \rho_g}{\partial X_n} \right)_o, \quad U_{35}(x,t) \equiv 0,$$

$$S_{38}(x,t) \equiv 0, \quad T_{38}(x,t) \equiv \alpha_g^o \rho_g^o, \quad U_{38}(x,t) \equiv 0,$$

$$S_{39}(x,t) \equiv 0, \quad T_{39}(x,t) \equiv \alpha_f^o \rho_f^o, \quad U_{39}(x,t) \equiv 0,$$

By taking the G-derivative of the difference density equation, we obtain the following expressions for the components $S_{mn}(x,t)$, $T_{mn}(x,t)$, and $U_{mn}(x,t)$:

$$S_{41}(x,t) \equiv \alpha_g^o \left(\frac{\partial \rho_g}{\partial U_g} \right)_o, \quad T_{41}(x,t) \equiv \alpha_g^o v_g^o \left(\frac{\partial \rho_g}{\partial U_g} \right)_o, \quad U_{41}(x,t) \equiv -\left(\frac{\partial E_4}{\partial U_g} \right)_o,$$

$$S_{42}(x,t) \equiv -\alpha_f^o \left(\frac{\partial \rho_f}{\partial U_f} \right)_o, \quad T_{42}(x,t) \equiv -\alpha_f^o v_f^o \left(\frac{\partial \rho_f}{\partial U_f} \right)_o, \quad U_{42}(x,t) \equiv -\left(\frac{\partial E_4}{\partial U_f} \right)_o,$$

$$S_{43}(x,t) \equiv \alpha_g^o \left(\frac{\partial \rho_g}{\partial P} \right)_o - \alpha_f^o \left(\frac{\partial \rho_f}{\partial P} \right)_o, T_{43}(x,t) \equiv \alpha_g^o v_g^o \left(\frac{\partial \rho_g}{\partial P} \right)_o - \alpha_f^o v_f^o \left(\frac{\partial \rho_f}{\partial P} \right)_o,$$

$$U_{43}(x,t) \equiv -\left(\frac{\partial E_4}{\partial P} \right)_o,$$

$$S_{44}(x,t) \equiv \rho_f^o + \rho_g^o, \quad T_{44}(x,t) \equiv \rho_g^o v_g^o + \rho_f^o v_f^o, \quad U_{44}(x,t) \equiv -\left(\frac{\partial E_4}{\partial \alpha_g} \right)_o,$$

$$S_{45}(x,t) \equiv \alpha_g^o \left(\frac{\partial \rho_g}{\partial X_n} \right)_o, \quad T_{45}(x,t) \equiv \alpha_g^o v_g^o \left(\frac{\partial \rho_g}{\partial X_n} \right)_o, \quad U_{45}(x,t) \equiv -\left(\frac{\partial E_4}{\partial X_n} \right)_o,$$

$$S_{48}(x,t) \equiv 0, \quad T_{48}(x,t) \equiv \alpha_g^o \rho_g^o, \quad U_{48}(x,t) \equiv -\left(\frac{\partial E_4}{\partial \nu_g}\right)_o,$$

$$S_{49}(x,t) \equiv 0, \quad T_{49}(x,t) \equiv -\alpha_f^o \rho_f^o, \quad U_{49}(x,t) \equiv -\left(\frac{\partial E_4}{\partial \nu_f}\right)_o,$$

and where the quantity $E_4(\boldsymbol{\chi}, \boldsymbol{G})$ is defined as

$$E_4(\boldsymbol{\chi}, \boldsymbol{G}) \equiv -\frac{2\left[H_{ig}\left(T^s - T_g\right) + H_{if}\left(T^s - T_f\right)\right]}{h_g' - h_f'} + 2\Gamma_w.$$

By taking the G-derivative of the noncondensable density equation, we obtain the following expressions for the components $S_{mn}(x,t)$, $T_{mn}(x,t)$, and $U_{mn}(x,t)$:

$$S_{51}(x,t) \equiv \alpha_g^o X_n^o \left(\frac{\partial \rho_g}{\partial U_g}\right)_o, \quad T_{51}(x,t) \equiv \alpha_g^o X_n^o \nu_g^o \left(\frac{\partial \rho_g}{\partial U_g}\right)_o, \quad U_{51}(x,t) \equiv 0,$$

$$S_{52}(x,t) \equiv 0, \quad T_{52}(x,t) \equiv 0, \quad U_{52}(x,t) \equiv 0,$$

$$S_{53}(x,t) \equiv \alpha_g^o X_n^o \left(\frac{\partial \rho_g}{\partial P}\right)_o, \quad T_{53}(x,t) \equiv \alpha_g^o \nu_g^o X_n^o \left(\frac{\partial \rho_g}{\partial P}\right)_o, \quad U_{53}(x,t) \equiv 0,$$

$$S_{54}(x,t) \equiv \rho_g^o X_n^o, \quad T_{54}(x,t) \equiv \rho_g^o X_n^o \nu_g^o, \quad U_{54}(x,t) \equiv 0,$$

$$S_{55}(x,t) \equiv \alpha_g^o \rho_g^o + \alpha_g^o X_n^o \left(\frac{\partial \rho_g}{\partial X_n}\right)_o,$$

$$T_{55}(x,t) \equiv \alpha_g^o \nu_g^o \left(\rho_g^o + X_n^o \left(\frac{\partial \rho_g}{\partial X_n}\right)_o\right), \quad U_{55}(x,t) \equiv 0,$$

$$S_{58}(x,t) \equiv 0, \quad T_{58}(x,t) \equiv \alpha_g^o \rho_g^o X_n^o, \quad U_{58}(x,t) \equiv 0,$$

$$S_{59}(x,t) \equiv 0, \quad T_{59}(x,t) \equiv 0, \quad U_{59}(x,t) \equiv 0.$$

By taking the G-derivative of the mass conservation equation for each noncondensable component, we obtain the following expressions for the components $S_{mn}(x,t)$, $T_{mn}(x,t)$, and $U_{mn}(x,t)$:

$$S_{61}(x,t) \equiv \alpha_g^o X_n^o X_{ni}^o \left(\frac{\partial \rho_g}{\partial U_g} \right)_o, \quad T_{61}(x,t) \equiv \alpha_g^o X_n^o X_{ni}^o v_g^o \left(\frac{\partial \rho_g}{\partial U_g} \right)_o, \quad U_{61}(x,t) \equiv 0,$$

$$S_{62}(x,t) \equiv 0, \quad T_{62}(x,t) \equiv 0, \quad U_{62}(x,t) \equiv 0,$$

$$S_{63}(x,t) \equiv \alpha_g^o X_n^o X_{ni}^o \left(\frac{\partial \rho_g}{\partial P} \right)_o, \quad T_{63}(x,t) \equiv \alpha_g^o v_g^o X_n^o X_{ni}^o \left(\frac{\partial \rho_g}{\partial P} \right)_o, \quad U_{63}(x,t) \equiv 0,$$

$$S_{64}(x,t) \equiv \rho_g^o X_n^o X_{ni}^o, \quad T_{64}(x,t) \equiv \rho_g^o X_n^o X_{ni}^o v_g^o, \quad U_{64}(x,t) \equiv 0,$$

$$S_{65}(x,t) \equiv \alpha_g^o X_{ni}^o \left(\rho_g^o + X_n^o \left(\frac{\partial \rho_g}{\partial X_n} \right)_o \right),$$

$$T_{65}(x,t) \equiv \alpha_g^o v_g^o X_{ni}^o \left(\rho_g^o + X_n^o \left(\frac{\partial \rho_g}{\partial X_n} \right)_o \right), \quad U_{65}(x,t) \equiv 0,$$

$$S_{66}(x,t) \equiv \alpha_g^o \rho_g^o X_n^o, \quad T_{66}(x,t) \equiv \alpha_g^o \rho_g^o v_g^o X_n^o, \quad U_{66}(x,t) \equiv 0,$$

$$S_{68}(x,t) \equiv 0, \quad T_{68}(x,t) \equiv \alpha_g^o \rho_g^o X_n^o X_{ni}^o, \quad U_{68}(x,t) \equiv 0,$$

$$S_{69}(x,t) \equiv 0, \quad T_{69}(x,t) \equiv 0, \quad U_{69}(x,t) \equiv 0.$$

By taking the G-derivative of the boron density equation, we obtain the following expressions for the components $S_{mn}(x,t)$, $T_{mn}(x,t)$, and $U_{mn}(x,t)$:

$$S_{71}(x,t) \equiv 0, \quad T_{71}(x,t) \equiv 0, \quad U_{71}(x,t) \equiv 0,$$

$$S_{72}(x,t) \equiv 0, \quad T_{72}(x,t) \equiv 0, \quad U_{72}(x,t) \equiv 0,$$

$$S_{73}(x,t) \equiv 0, \quad T_{73}(x,t) \equiv 0, \quad U_{73}(x,t) \equiv 0,$$

$$S_{74}(x,t) \equiv 0, \quad T_{74}(x,t) \equiv 0, \quad U_{74}(x,t) \equiv 0,$$

$$S_{75}(x,t) \equiv 0, \quad T_{75}(x,t) \equiv 0, \quad U_{75}(x,t) \equiv 0,$$

$$S_{76}(x,t) \equiv 0, \quad T_{76}(x,t) \equiv 0, \quad U_{76}(x,t) \equiv 0,$$

$$S_{77}(x,t) \equiv 1, \quad T_{77}(x,t) \equiv v_f^o, \quad U_{77}(x,t) \equiv 0,$$

$$S_{78}(x,t) \equiv 0, \quad T_{78}(x,t) \equiv 0, \quad U_{78}(x,t) \equiv 0,$$

$$S_{79}(x,t) \equiv 0, \quad T_{79}(x,t) \equiv \rho_b^o, \quad U_{79}(x,t) \equiv 0.$$

By taking the G-derivative of the sum momentum equation, we obtain the following expressions for the components $S_{mn}(x,t)$, $T_{mn}(x,t)$, and $U_{mn}(x,t)$:

$$S_{81}(x,t)\equiv 0,\quad T_{81}(x,t)\equiv 0,\quad U_{81}(x,t)\equiv \alpha_g^o\left(\frac{\partial v_g^o}{\partial t}+\frac{1}{2}\frac{\partial\left(v_g^o\right)^2}{\partial x}\right)\left(\frac{\partial \rho_g}{\partial U_g}\right)_o-\left(\frac{\partial E_8}{\partial U_g}\right)_o,$$

$$S_{83}(x,t)\equiv 0,\quad T_{83}(x,t)\equiv 1,$$

$$U_{83}(x,t)\equiv -\frac{1}{A^o}\frac{dA^o}{dx}+\alpha_g^o\left(\frac{\partial v_g^o}{\partial t}+\frac{1}{2}\frac{\partial\left(v_g^o\right)^2}{\partial x}\right)\left(\frac{\partial \rho_g}{\partial P}\right)_o$$

$$+\alpha_f^o\left(\frac{\partial v_f^o}{\partial t}+\frac{1}{2}\frac{\partial\left(v_f^o\right)^2}{\partial x}\right)\left(\frac{\partial \rho_f}{\partial P}\right)_o-\left(\frac{\partial E_8}{\partial P}\right)_o,$$

$$S_{84}(x,t)\equiv 0,\quad T_{84}(x,t)\equiv 0,$$

$$U_{84}(x,t)\equiv \rho_g^o\left(\frac{\partial v_g^o}{\partial t}+\frac{1}{2}\frac{\partial\left(v_g^o\right)^2}{\partial x}\right)-\rho_f^o\left(\frac{\partial v_f^o}{\partial t}+\frac{1}{2}\frac{\partial\left(v_f^o\right)^2}{\partial x}\right)-\left(\frac{\partial E_8}{\partial \alpha_g}\right)_o,$$

$$S_{85}(x,t)\equiv 0,\ T_{85}(x,t)\equiv 0,\ U_{85}(x,t)\equiv \alpha_g^o\left(\frac{\partial v_g^o}{\partial t}+\frac{1}{2}\frac{\partial\left(v_g^o\right)^2}{\partial x}\right)\left(\frac{\partial \rho_g}{\partial X_n}\right)_o-\left(\frac{\partial E_8}{\partial X_n}\right)_o,$$

$$S_{88}(x,t)\equiv \alpha_g^o\rho_g^o,\quad T_{88}(x,t)\equiv \alpha_g^o\rho_g^o v_g^o,$$

$$U_{88}(x,t)\equiv -\frac{\partial}{\partial t}\left(\alpha_g^o\rho_g^o\right)-\frac{1}{A^o}v_g^o\frac{\partial}{\partial x}\left(A^o\alpha_g^o\rho_g^o\right)-\left(\frac{\partial E_8}{\partial v_g}\right)_o,$$

$$S_{89}(x,t)\equiv \alpha_f^o\rho_f^o,\quad T_{89}(x,t)\equiv \alpha_f^o\rho_f^o v_f^o,$$

$$U_{89}(x,t)\equiv -\frac{\partial}{\partial t}\left(\alpha_f^o\rho_f^o\right)-\frac{1}{A^o}v_f^o\frac{\partial}{\partial x}\left(A^o\alpha_f^o\rho_f^o\right)-\left(\frac{\partial E_8}{\partial v_f}\right)_o,$$

where the quantity $E_8(\boldsymbol{\chi},\boldsymbol{G})$ is defined as

$$E_8(\boldsymbol{\chi},\boldsymbol{G})\equiv \rho B_x-\alpha_g\rho_g v_g FWG-\alpha_f\rho_f v_f FWF-\Gamma_g\left(v_g-v_f\right).$$

By taking the G-derivative of the difference momentum equation, we obtain the following expressions for the components $S_{mn}(x,t)$, $T_{mn}(x,t)$, and $U_{mn}(x,t)$:

$$S_{91}(x,t)\equiv 0,\ T_{91}(x,t)\equiv 0,$$

$$U_{91}(x,t)\equiv -\frac{1}{\left(\rho_g^o\right)^2}\frac{\partial P^o}{\partial x}\left(\frac{\partial \rho_g}{\partial U_g}\right)_o-\left(\frac{\partial E_9}{\partial U_g}\right)_o-\left(\frac{\partial E_{10}}{\partial U_g}\right)_o\frac{\partial\left(v_g^o-v_f^o\right)}{\partial t},$$

$$S_{92}(x,t)\equiv 0,\ T_{92}(x,t)\equiv 0,$$

$$U_{92}(x,t)\equiv \frac{1}{\left(\rho_f^o\right)^2}\frac{\partial P^o}{\partial x}\left(\frac{\partial \rho_f}{\partial U_f}\right)_o-\left(\frac{\partial E_9}{\partial U_f}\right)_o-\left(\frac{\partial E_{10}}{\partial U_f}\right)_o\frac{\partial\left(v_g^o-v_f^o\right)}{\partial t},$$

$$S_{93}(x,t)\equiv 0,\ T_{93}(x,t)\equiv \frac{1}{\rho_g^o}-\frac{1}{\rho_f^o},\ U_{93}(x,t)\equiv -\left(\frac{\partial E_9}{\partial P}\right)_o-\left(\frac{\partial E_{10}}{\partial P}\right)_o\frac{\partial\left(v_g^o-v_f^o\right)}{\partial t},$$

$$S_{94}(x,t)\equiv 0,\quad T_{94}(x,t)\equiv 0,\quad U_{94}(x,t)\equiv -\left(\frac{\partial E_9}{\partial \alpha_g}\right)_o-\left(\frac{\partial E_{10}}{\partial \alpha_g}\right)_o\frac{\partial\left(v_g^o-v_f^o\right)}{\partial t},$$

$$S_{95}(x,t)\equiv 0,\quad T_{95}(x,t)\equiv 0,$$

$$U_{95}(x,t)\equiv -\frac{1}{\left(\rho_g^o\right)^2}\frac{\partial P^o}{\partial x}\left(\frac{\partial \rho_g}{\partial X_n}\right)_o-\left(\frac{\partial E_9}{\partial X_n}\right)_o-\left(\frac{\partial E_{10}}{\partial X_n}\right)_o\frac{\partial\left(v_g^o-v_f^o\right)}{\partial t},$$

$$S_{98}(x,t)\equiv 1-E_{10}^o,\ T_{98}(x,t)\equiv v_g^o,\ U_{98}(x,t)\equiv \frac{\partial E_{10}^o}{\partial t}-\frac{1}{A^o}v_g^o\frac{\partial A^o}{\partial x}-\left(\frac{\partial E_9}{\partial v_g}\right)_o,$$

$$S_{99}(x,t)\equiv E_{10}^o-1,\quad T_{99}(x,t)\equiv -v_f^o,\quad U_{99}(x,t)\equiv \frac{1}{A^o}v_f^o\frac{\partial A^o}{\partial x}-\frac{\partial E_{10}^o}{\partial t}-\left(\frac{\partial E_9}{\partial v_f}\right)_o,$$

and where the quantities $E_9(\boldsymbol{\chi},\boldsymbol{G})$ and $E_{10}(\boldsymbol{\chi},\boldsymbol{G})$ are defined as

$$E_9(\boldsymbol{\chi},\boldsymbol{G})\equiv -v_g FWG+v_f FWF+\frac{\Gamma_g\left[\rho v_I-\left(\alpha_f\rho_f v_g+\alpha_g\rho_g v_f\right)\right]}{\alpha_g\rho_g\alpha_f\rho_f}-\rho FI\left(v_g-v_f\right),$$

and, respectively,

$$E_{10}(\boldsymbol{\chi},\boldsymbol{G})\equiv -C\frac{\rho^2}{\rho_g\rho_f}.$$

APPENDIX C: ELIMINATION OF THE INTERMEDIATE TIME-STEP VARIABLES IN THE DISCRETIZED FSM

The matrix $T_2^{(n)}$ is defined as $T_2^{(n)} \equiv \begin{bmatrix} (TI)_{11}^{(n)} & \cdots & (TI)_{1,M_2}^{(n)} \\ \vdots & & \vdots \\ (TI)_{M_2,1}^{(n)} & \cdots & (TI)_{M_2,M_2}^{(n)} \end{bmatrix}$, where M_2 is the number of intermediate time-step variables existing in the system. To simplify the notation for the derivations to follow in this Appendix, the time-step index n will be omitted, since all matrices involved in these derivations are evaluated at time-step n.

The matrix T_2 is partitioned in the form $T_2 \equiv \begin{bmatrix} T & U \\ L & V \end{bmatrix}$, where $T \equiv \begin{bmatrix} (TI)_{11} & (TI)_{12} \\ (TI)_{21} & (TI)_{22} \end{bmatrix}$, and where the matrices L, U, and V are defined below:

(a) If $M_2 = 3$, i.e., if only the quantities $\tilde{U}_g^k, \tilde{U}_f^k, \tilde{\alpha}_g^k$ appear as intermediate time-step variables in Eq. (II.B.33), then the matrices L, U, and V are defined as follows: $L \equiv \begin{bmatrix} (TI)_{31} & (TI)_{32} \end{bmatrix}$; $U \equiv \begin{bmatrix} (TI)_{13} \\ (TI)_{23} \end{bmatrix}$; $V \equiv (TI)_{33}$.

(b) If $M_2 = 4$, i.e., all intermediate time-step variables exist in Eq. (II.B.33), then the matrices L, U, and V are defined as follows:

$$L \equiv \begin{bmatrix} (TI)_{31} & (TI)_{32} \\ (TI)_{41} & (TI)_{42} \end{bmatrix}; \quad U \equiv \begin{bmatrix} (TI)_{13} & (TI)_{14} \\ (TI)_{23} & (TI)_{24} \end{bmatrix}; \quad V \equiv \begin{bmatrix} (TI)_{33} & (TI)_{34} \\ (TI)_{43} & (TI)_{44} \end{bmatrix}.$$

The inverse $[T_2]^{-1}$ of T_2 can be calculated by partitioning; this yields

$[T_2]^{-1} = \begin{bmatrix} P_{11} & P_{12} \\ P_{21} & P_{22} \end{bmatrix}$, where the matrices $P_{11}, P_{12}, P_{21}, P_{22}$ are defined as follows: $P_{22} \equiv \left[V - LT^{-1}U\right]^{-1}$, $P_{21} \equiv -P_{22}LT^{-1}$, $P_{12} \equiv -T^{-1}UP_{22}$, $P_{11} \equiv T^{-1} + T^{-1}UP_{22}LT^{-1}$.

To evaluate the matrices P_{ij}, $(i, j = 1, 2)$, it is necessary to evaluate T^{-1}. Using the same inversion-by-partitioning procedure as above for the matrix T_2, we obtain $T^{-1} \equiv \begin{bmatrix} t_{11} & t_{12} \\ t_{21} & t_{22} \end{bmatrix}$, where the matrices $t_{11}, t_{12}, t_{21}, t_{22}$ are defined as:

$$t_{22} \equiv \left[(TI)_{22} - (TI)_{21}(TI)_{11}^{-1}(TI)_{12}\right]^{-1}, \quad t_{21} \equiv -t_{22}(TI)_{21}(TI)_{11}^{-1},$$

$$t_{12} \equiv -(TI)_{11}^{-1}(TI)_{12}t_{22}, \qquad t_{11} \equiv (TI)_{11}^{-1} + (TI)_{11}^{-1}(TI)_{12}t_{22}(TI)_{21}(TI)_{11}^{-1}.$$

Since the matrices $(TI)_{\mu\nu}^{n}$ are by definition diagonal matrices, it follows that

$$t_{22} = diag\left\{\left[(ti)^{22} - (ti)^{21}(ti)^{12}/(ti)^{11}\right]^{-1}\right\}_k^n \equiv diag\{\tau_{22}\}_k^n,$$
$$t_{21} = -diag\left\{\tau_{22}(ti)^{21}/(ti)^{11}\right\}_k^n \equiv diag\{\tau_{21}\}_k^n$$
$$t_{12} = -diag\left\{\tau_{22}(ti)^{12}/(ti)^{11}\right\}_k^n \equiv diag\{\tau_{12}\}_k^n,$$
$$t_{11} = diag\left\{\left[1 + (ti)^{12}(ti)^{21}\tau_{22}/(ti)^{11}\right]/(ti)^{11}\right\}_k^n \equiv diag\{\tau_{11}\}_k^n, \text{ for } (k = 1, \ldots, NV).$$

We now calculate the matrices $P_{11}, P_{12}, P_{21}, P_{22}$ for the two cases (a) and (b) defined above:

Case (a): $M_2 = 3$:

In this case, P_{22} is obtained as follows:

$$P_{22} = \left\{(TI)_{33} - \begin{bmatrix}(TI)_{31} & (TI)_{32}\end{bmatrix}\begin{bmatrix}t_{11} & t_{12}\\ t_{21} & t_{22}\end{bmatrix}\begin{bmatrix}(TI)_{13}\\ (TI)_{23}\end{bmatrix}\right\}^{-1} = diag\{p_{22}\}_k^n,$$

where $p_{22} \equiv \left\{(ti)^{33} - (ti)^{31}\left[\tau_{11}(ti)^{13} + \tau_{12}(ti)^{23}\right] - (ti)^{32}\left[\tau_{21}(ti)^{13} + \tau_{22}(ti)^{23}\right]\right\}^{-1}$.

Furthermore, the row-matrix P_{21} is obtained in the form

$P_{21} = \begin{bmatrix}P_{21}^1 & P_{21}^2\end{bmatrix}_{(1\times 2)}$, where

$$P_{21}^1 \equiv diag\left\{-p_{22}\left[(ti)^{31}\tau_{11} + (ti)^{32}\tau_{21}\right]\right\}_k^n \equiv diag\{q_1\}_k^n$$
$$P_{21}^2 \equiv diag\left\{-p_{22}\left[(ti)^{31}\tau_{12} + (ti)^{32}\tau_{22}\right]\right\}_k^n \equiv diag\{q_2\}_k^n.$$

The column-matrix P_{12} is obtained as $P_{12} = \begin{bmatrix}P_{12}^1\\ P_{12}^2\end{bmatrix}_{(2\times 1)}$, where

$$P_{12}^1 \equiv diag\left\{-p_{22}\left[\tau_{11}(ti)^{13} + \tau_{12}(ti)^{23}\right]\right\}_k^n \equiv diag\{s_1\}_k^n,$$
$$P_{12}^2 \equiv diag\left\{-p_{22}\left[\tau_{21}(ti)^{13} + \tau_{22}(ti)^{23}\right]\right\}_k^n \equiv diag\{s_2\}_k^n.$$

Finally, the matrix P_{11}, defined as $P_{11} \equiv T^{-1}\left[I - UP_{21}\right]$, can be written in the form $P_{11} = \begin{bmatrix} R_{11} & R_{12} \\ R_{21} & R_{22} \end{bmatrix}$, where, for all $(k = 1, \ldots, NV)$, the matrices $R_{11}, R_{12}, R_{21}, R_{22}$ are defined as follows:

$$R_{11} \equiv diag\left\{\tau_{11}\left[1 - (ti)^{13} q_1\right] - \tau_{12}(ti)^{23} q_1\right\}_k^n$$
$$R_{12} \equiv diag\left\{-\tau_{11}(ti)^{13} q_2 + \tau_{12}\left[1 - (ti)^{23} q_2\right]\right\}_k^n$$
$$R_{21} \equiv diag\left\{\tau_{21}\left[1 - (ti)^{13} q_1\right] - \tau_{22}(ti)^{23} q_1\right\}_k^n$$
$$R_{22} \equiv diag\left\{-\tau_{21}(ti)^{13} q_2 + \tau_{22}\left[1 - (ti)^{23} q_2\right]\right\}_k^n .$$

Case (b): $M_2 = 4$:

In this case, the matrix P_{22} is given by the expression

$$P_{22} = \left\{\begin{bmatrix} (TI)_{33} & (TI)_{34} \\ (TI)_{43} & (TI)_{44} \end{bmatrix} - \begin{bmatrix} (TI)_{31} & (TI)_{32} \\ (TI)_{41} & (TI)_{42} \end{bmatrix}\begin{bmatrix} t_{11} & t_{12} \\ t_{21} & t_{22} \end{bmatrix}\begin{bmatrix} (TI)_{13} & (TI)_{14} \\ (TI)_{23} & (TI)_{24} \end{bmatrix}\right\}^{-1}$$
$$\equiv \begin{bmatrix} P_{22}^{11} & P_{22}^{12} \\ P_{22}^{21} & P_{22}^{22} \end{bmatrix}^{-1}$$

where the following definitions have been used:

$$P_{22}^{11} \equiv (TI)_{33} - \left\{(TI)_{31}\left[t_{11}(TI)_{13} + t_{12}(TI)_{23}\right] + (TI)_{32}\left[t_{21}(TI)_{13} + t_{22}(TI)_{23}\right]\right\}$$
$$\equiv diag\left\{p_{11}\right\}_k^n,$$
$$P_{22}^{12} \equiv (TI)_{34} - \left\{(TI)_{31}\left[t_{11}(TI)_{14} + t_{12}(TI)_{24}\right] + (TI)_{32}\left[t_{21}(TI)_{14} + t_{22}(TI)_{24}\right]\right\}$$
$$\equiv diag\left\{p_{12}\right\}_k^n,$$
$$P_{22}^{21} \equiv (TI)_{43} - \left\{(TI)_{41}\left[t_{11}(TI)_{13} + t_{12}(TI)_{23}\right] + (TI)_{42}\left[t_{21}(TI)_{13} + t_{22}(TI)_{23}\right]\right\}$$
$$\equiv diag\left\{p_{21}\right\}_k^n,$$
$$P_{22}^{22} \equiv (TI)_{44} - \left\{(TI)_{41}\left[t_{11}(TI)_{14} + t_{12}(TI)_{24}\right] + (TI)_{42}\left[t_{21}(TI)_{14} + t_{22}(TI)_{24}\right]\right\}$$
$$\equiv diag\left\{p_{22}\right\}_k^n.$$

Carrying out the above calculations leads to the following expression for P_{22}:

$P_{22} = \begin{bmatrix} W_{11} & W_{12} \\ W_{21} & W_{22} \end{bmatrix}$, where the components $W_{ij} \equiv diag\left\{w_{ij}\right\}_k^n;\ i, j = 1,2$ are calculated from the formulae

$$W_{12} \equiv -\left(P_{22}^{11}\right)^{-1} P_{22}^{12} W_{22}; \quad W_{11} \equiv \left(P_{22}^{11}\right)^{-1} - W_{12} P_{22}^{21} \left(P_{22}^{11}\right)^{-1};$$

$$W_{22} \equiv \left[P_{22}^{22} - P_{22}^{21}\left(P_{22}^{11}\right)^{-1} P_{22}^{12}\right]^{-1}; \quad W_{21} \equiv -W_{22} P_{22}^{21}\left(P_{22}^{11}\right)^{-1}.$$

Carrying out the remaining calculations for the components $W_{ij} \equiv diag\left\{w_{ij}\right\}_k^n;\ i, j = 1,2$ defined above gives:

$w_{11} = \left(1 - w_{12} p_{21}\right)/\delta;\ w_{12} = -p_{12}/\delta;\ w_{21} = -p_{21}/\delta;\ w_{22} = p_{11}/\delta,$ with $\delta \equiv p_{11} p_{22} - p_{12} p_{21}$.

Having calculated P_{22} and T^{-1}, the remaining matrices P_{21}, P_{12}, P_{11} are obtained as

$$P_{21} = -\begin{bmatrix} W_{11} & W_{12} \\ W_{21} & W_{22} \end{bmatrix}\begin{bmatrix} (TI)_{31} & (TI)_{32} \\ (TI)_{41} & (TI)_{42} \end{bmatrix}\begin{bmatrix} t_{11} & t_{12} \\ t_{21} & t_{22} \end{bmatrix} \equiv \begin{bmatrix} P_{21}^{11} & P_{21}^{12} \\ P_{21}^{21} & P_{21}^{22} \end{bmatrix},$$

where $P_{21}^{ij} \equiv diag\left\{q_{ij}\right\}_k^n; \quad (i, j = 1,2)$, with

$$q_{11} \equiv -\left\{w_{11}\left[(ti)^{31}\tau_{11} + (ti)^{32}\tau_{21}\right] + w_{12}\left[(ti)^{41}\tau_{11} + (ti)^{42}\tau_{21}\right]\right\},$$

$$q_{12} \equiv -\left\{w_{11}\left[(ti)^{31}\tau_{12} + (ti)^{32}\tau_{22}\right] + w_{12}\left[(ti)^{41}\tau_{12} + (ti)^{42}\tau_{22}\right]\right\},$$

$$q_{21} \equiv -\left\{w_{21}\left[(ti)^{31}\tau_{11} + (ti)^{32}\tau_{21}\right] + w_{22}\left[(ti)^{41}\tau_{11} + (ti)^{42}\tau_{21}\right]\right\},$$

$$q_{22} \equiv -\left\{w_{21}\left[(ti)^{31}\tau_{12} + (ti)^{32}\tau_{22}\right] + w_{22}\left[(ti)^{41}\tau_{12} + (ti)^{42}\tau_{22}\right]\right\}.$$

Similarly, we obtain

$$P_{12} = -\begin{bmatrix} t_{11} & t_{12} \\ t_{21} & t_{22} \end{bmatrix}\begin{bmatrix} (TI)_{13} & (TI)_{14} \\ (TI)_{23} & (TI)_{24} \end{bmatrix}\begin{bmatrix} W_{11} & W_{12} \\ W_{21} & W_{22} \end{bmatrix} \equiv \begin{bmatrix} P_{12}^{11} & P_{12}^{12} \\ P_{12}^{21} & P_{12}^{22} \end{bmatrix},$$

where $P_{12}^{ij} \equiv diag\left\{s_{ij}\right\}_k^n;\quad (i,j=1,2)$, with

$$
\begin{aligned}
s_{11} \equiv & -\left\{\tau_{11}\left[(ti)^{13}w_{11}+(ti)^{14}w_{21}\right]+\tau_{12}\left[(ti)^{23}w_{11}+(ti)^{24}w_{21}\right]\right\},\\
s_{12} \equiv & -\left\{\tau_{11}\left[(ti)^{13}w_{12}+(ti)^{14}w_{22}\right]+\tau_{12}\left[(ti)^{23}w_{12}+(ti)^{24}w_{22}\right]\right\},\\
s_{21} \equiv & -\left\{\tau_{21}\left[(ti)^{13}w_{11}+(ti)^{14}w_{21}\right]+\tau_{22}\left[(ti)^{23}w_{11}+(ti)^{24}w_{21}\right]\right\},\\
s_{22} \equiv & -\left\{\tau_{21}\left[(ti)^{13}w_{12}+(ti)^{14}w_{22}\right]+\tau_{22}\left[(ti)^{23}w_{12}+(ti)^{24}w_{22}\right]\right\}.
\end{aligned}
$$

Finally, we calculate $P_{11},$ to obtain

$$
\begin{aligned}
&P_{11} = T^{-1}\left[I-UP_{21}\right]\\
&=\begin{bmatrix}t_{11} & t_{12}\\ t_{21} & t_{22}\end{bmatrix}\left\{\begin{bmatrix}1 & 0\\ 0 & 1\end{bmatrix}-\begin{bmatrix}(TI)_{13} & (TI)_{14}\\ (TI)_{23} & (TI)_{24}\end{bmatrix}\begin{bmatrix}P_{21}^{11} & P_{21}^{12}\\ P_{21}^{21} & P_{21}^{22}\end{bmatrix}\right\}\equiv\begin{bmatrix}R_{11} & R_{12}\\ R_{21} & R_{22}\end{bmatrix},
\end{aligned}
$$

where the matrices $R_{11}, R_{12}, R_{21}, R_{22}$ are defined as follows:

$$R_{ij} = diag\left\{r_{ij}\right\}_k^n;\ (i,j=1,2),\ \text{with}$$

$$
\begin{aligned}
r_{11} \equiv & \ \tau_{11}\left\{1-\left[(ti)^{13}q_{11}+(ti)^{14}q_{21}\right]\right\}-\tau_{12}\left[(ti)^{23}q_{11}+(ti)^{24}q_{21}\right],\\
r_{12} \equiv & -\tau_{11}\left[(ti)^{13}q_{12}+(ti)^{14}q_{22}\right]+\tau_{12}\left\{1-\left[(ti)^{23}q_{12}+(ti)^{24}q_{22}\right]\right\},\\
r_{21} \equiv & \ \tau_{21}\left\{1-\left[(ti)^{13}q_{11}+(ti)^{14}q_{21}\right]\right\}-\tau_{22}\left[(ti)^{23}q_{11}+(ti)^{24}q_{21}\right],\\
r_{22} \equiv & -\tau_{21}\left[(ti)^{13}q_{12}+(ti)^{14}q_{22}\right]+\tau_{22}\left\{1-\left[(ti)^{23}q_{12}+(ti)^{24}q_{22}\right]\right\}.
\end{aligned}
$$

Chapter III

FORWARD AND ADJOINT SENSITIVITY ANALYSIS PROCEDURES FOR AUGMENTED SYSTEMS

Looking at the history of the development of large-scale simulation models, it becomes apparent that, in almost every field of scientific activity, such models took many years to develop, and their respective development invariably involved large and sometimes changing teams of scientists. Furthermore, such complex models consist of many inter-coupled modules, each module simulating a particular physical sub-process, serving as "bricks" within the structure of the respective large-scale simulation code system.

Since the *ASAP* has not been widely known in the past, most of the extant large-scale, complex models have been developed without also having simultaneously developed and implemented the corresponding adjoint sensitivity model. Implementing *a posteriori* the *ASAP* for large-scale simulation codes is not trivial, and the development and implementation of the adjoint sensitivity model for the entire large-scale code system can seldom be executed all at once, in one fell swoop. Actually, an "all-or-nothing" approach for developing and implementing the complete, and correspondingly complex, adjoint sensitivity model for a large-scale code is at best difficult (and, at worst, impractical), and is therefore not recommended. Instead, the recommended strategy is a module-by-module implementation of the *ASAP*. In this approach, the *ASAP* is applied step-wise, to each simulation module, in turn, to develop a corresponding adjoint sensitivity system for each module. As the final step in this "modular" implementation of the *ASAP*, the adjoint sensitivity systems for each of the respective modules are "augmented," without redundant effort and/or loss of information, until all adjoint modules are judiciously connected together, accounting for all of the requisite feedbacks and liaisons between the respective adjoint modules.

The aim of this Chapter is to provide the theoretical foundation for the modular implementation of the *ASAP* for a complex simulation system, by starting with a selected code module, and then augmenting the size of the adjoint sensitivity system, module by module, until exhaustively completing the entire system under consideration. Section III.A presents the general mathematical framework underlying the *ASAP* for augmented systems. Applying this general framework, Section III.B illustrates how the adjoint sensitivity model corresponding to the two-fluid model in RELAP5/MOD3.2 (which was the subject of Chapter II) is to be augmented with the adjoint sensitivity model corresponding to the heat structure models in RELAP5/MOD3.2, in order to obtain, efficiently, the complete adjoint sensitivity model (called ASM-REL/TFH) for the coupled fluid dynamics/heat structure packages of the large-scale simulation code

RELAP5/MOD3.2. Subsequently, the augmented adjoint sensitivity model, ASM-REL/TFH, is applied for an exhaustive sensitivity analysis of a typical experiment performed within the QUENCH experimental program at the Research Center Karlsruhe (FZK). This experimental program aims at investigating the relatively poorly understood physical and chemical processes underlying the release of hydrogen during the water re-flooding of a light water reactor core when terminating a postulated severe accident. Sensitivity analysis to the parameters entering these processes is of significant importance for both the design and the interpretation of these experiments.

III. A. THEORETICAL BASIS FOR THE ASAP FOR AUGMENTED SYSTEMS

III.A.1. Sensitivity Analysis of the Primary (Nonaugmented) System

Using a notation similar, but not identical to that used in Chapter V of Volume I, the primary (or original, nonaugmented) physical system is represented mathematically by means of K coupled nonlinear operator equations of the form

$$\boldsymbol{N}\left[\boldsymbol{u}(\boldsymbol{x}),\boldsymbol{\alpha}(\boldsymbol{x})\right]=\boldsymbol{Q}\left[\boldsymbol{\alpha}(\boldsymbol{x})\right],\quad \boldsymbol{x}\in\Omega, \tag{III.A.1}$$

where:

1. $\boldsymbol{x}=\left(x_1,\ldots,x_{J_x}\right)$ denotes the J_x-dimensional phase-space position vector for the primary system; $x\in\Omega_X\subset\mathbb{R}^{J_x}$, where Ω_x is a subset of the J_x-dimensional real vector space $\mathbb{R}^{J_x}$;
2. $\boldsymbol{u}(\boldsymbol{x})=\left[u_1(\boldsymbol{x}),\ldots,u_{K_u}(\boldsymbol{x})\right]$ denotes a K_u-dimensional (column) vector whose components are the primary system's dependent (i.e., state) variables; $\boldsymbol{u}(\boldsymbol{x})\in\mathscr{E}_u$, where $\mathscr{E}_u$ is a normed linear space over the scalar field $\mathscr{F}$ of real numbers;
3. $\boldsymbol{\alpha}(\boldsymbol{x})=\left[\alpha_1(\boldsymbol{x}),\ldots,\alpha_I(\boldsymbol{x})\right]$ denotes an I-dimensional (column) vector whose components are the primary system's parameters; $\boldsymbol{\alpha}\in\mathscr{E}_\alpha$, where $\mathscr{E}_\alpha$ is also a normed linear space;
4. $\boldsymbol{Q}\left[\boldsymbol{\alpha}(\boldsymbol{x})\right]=\left[\boldsymbol{Q}_1(\boldsymbol{\alpha}),\ldots,\boldsymbol{Q}_{K_u}(\boldsymbol{\alpha})\right]$ denotes a K_u-dimensional (column) vector whose elements represent inhomogeneous source terms that depend either linearly or nonlinearly on $\boldsymbol{\alpha}$; $\boldsymbol{Q}\in\mathscr{E}_Q$, where $\mathscr{E}_Q$ is also a normed linear space; the components of $\boldsymbol{Q}$ may be operators, rather than just functions, acting on $\boldsymbol{\alpha}(\boldsymbol{x})$ and $\boldsymbol{x}$;

5. $\boldsymbol{N} \equiv \left[N_1(\boldsymbol{u},\boldsymbol{\alpha}),\ldots,N_{K_u}(\boldsymbol{u},\boldsymbol{\alpha})\right]$ denotes a K_u-component column vector whose components are nonlinear operators (including differential, difference, integral, distributions, and/or infinite matrices) acting on $\boldsymbol{u}$ and $\boldsymbol{\alpha}$.

In view of the definitions given above, $\boldsymbol{N}$ represents the mapping $\boldsymbol{N}: \mathscr{D} \subset \mathscr{E} \to \mathscr{E}_Q$, where $\mathscr{D} = \mathscr{D}_u \times \mathscr{D}_\alpha$, $\mathscr{D}_u \subset \mathscr{E}_u$, $\mathscr{D}_\alpha \subset \mathscr{E}_\alpha$, and $\mathscr{E} = \mathscr{E}_u \times \mathscr{E}_\alpha$. Note that an arbitrary element $\boldsymbol{e} \in \mathscr{E}$ is of the form $\boldsymbol{e} = (\boldsymbol{u},\boldsymbol{\alpha})$. If differential operators appear in Eq. (III.A.1), then a corresponding set of boundary and/or initial conditions (which are essential to define $\mathscr{D}$) must also be given. The respective boundary conditions are represented in operator form as

$$\left[\boldsymbol{B}(\boldsymbol{u},\boldsymbol{\alpha}) - \boldsymbol{A}(\boldsymbol{\alpha})\right]_{\partial\Omega_x} = 0\,, \quad x \in \partial\Omega_x\,, \tag{III.A.2}$$

where $\boldsymbol{A}$ and $\boldsymbol{B}$ are nonlinear operators, and $\partial\Omega_x$ denotes the boundary of Ω_x.

The vector-valued function $\boldsymbol{u}(\boldsymbol{x})$ is considered to be the unique nontrivial solution of the physical problem described by Eqs. (III.A.1) and (III.A.2). The system response (i.e., performance parameter) $\boldsymbol{R}(\boldsymbol{u},\boldsymbol{\alpha})$ associated with the problem modeled by Eqs. (III.A.1) and (III.A.2) is a phase-space dependent mapping that acts nonlinearly on the system's state vector $\boldsymbol{u}$ and parameters $\boldsymbol{\alpha}$, and is represented in operator form as

$$\boldsymbol{R}(\boldsymbol{e}): \mathscr{D}_R \subset \mathscr{E} \to \mathscr{E}_R\,, \tag{III.A.3}$$

where $\mathscr{E}_R$ is a normed vector space.

In practice, the exact values of the parameters $\boldsymbol{\alpha}$ are not known; usually, only the nominal (mean) parameter values, $\boldsymbol{\alpha}^0$, and their covariances, $\mathrm{cov}(\alpha_i,\alpha_j)$, are available (in exceptional cases, higher moments may also be available). The nominal parameter values $\boldsymbol{\alpha}^0(\boldsymbol{x})$ are used in Eqs. (III.A.1) and (III.A.2) to obtain the nominal solution $\boldsymbol{u}^0(\boldsymbol{x})$ by solving the equations

$$\boldsymbol{N}(\boldsymbol{u}^0,\boldsymbol{\alpha}^0) = \boldsymbol{Q}(\boldsymbol{\alpha}^0), \quad \boldsymbol{x} \in \Omega_x\,, \tag{III.A.4}$$

$$\boldsymbol{B}(\boldsymbol{u}^0,\boldsymbol{\alpha}^0) = \boldsymbol{A}(\boldsymbol{\alpha}^0), \quad \boldsymbol{x} \in \partial\Omega_x\,. \tag{III.A.5}$$

Thus, Eqs. (III.A.4) and (III.A.5) represent the "base-case" (nominal) state of the primary (nonaugmented) system, and $\boldsymbol{e}^0 = (\boldsymbol{u}^0,\boldsymbol{\alpha}^0)$ represents the nominal solution of the nonaugmented system. Once the nominal solution $\boldsymbol{e}^0 = (\boldsymbol{u}^0,\boldsymbol{\alpha}^0)$

has been obtained, the nominal value $\boldsymbol{R}\left(\boldsymbol{e}^0\right)$ of the response $\boldsymbol{R}(\boldsymbol{e})$ is obtained by evaluating Eq. (III.A.3) at $\boldsymbol{e}^0 = \left(\boldsymbol{u}^0, \boldsymbol{\alpha}^0\right)$.

As was generally discussed in Volume I, the sensitivity of the response $\boldsymbol{R}$ to variations $\boldsymbol{h}$ in the system parameters is given by the Gâteaux- (G)-differential $\delta\boldsymbol{R}\left(\boldsymbol{e}^0;\boldsymbol{h}\right)$ of the response $\boldsymbol{R}(\boldsymbol{e})$ at $\boldsymbol{e}^0 = \left(\boldsymbol{u}^0, \boldsymbol{\alpha}^0\right)$ with increment $\boldsymbol{h}$, defined as

$$\delta\boldsymbol{R}\left(\boldsymbol{e}^0;\boldsymbol{h}\right) \equiv \left\{\frac{d}{dt}\left[\boldsymbol{R}\left(\boldsymbol{e}^0 + t\boldsymbol{h}\right)\right]\right\}_{t=0} = \lim_{t\to 0}\frac{\boldsymbol{R}\left(\boldsymbol{e}^0 + t\boldsymbol{h}\right) - \boldsymbol{R}\left(\boldsymbol{e}^0\right)}{t}, \qquad \text{(III.A.6)}$$

for $t \in \mathcal{T}$, and all (i.e., arbitrary) vectors $\boldsymbol{h} \in \mathcal{E}$. For the nonaugmented system considered here, it follows that $\boldsymbol{h} = \left(\boldsymbol{h}_u, \boldsymbol{h}_\alpha\right)$, since $\mathcal{E} = \mathcal{E}_u \times \mathcal{E}_\alpha$. Recall from Volume I that the G-differential $\delta\boldsymbol{R}\left(\boldsymbol{e}^0;\boldsymbol{h}\right)$ is related to the total variation $\left[\boldsymbol{R}\left(\boldsymbol{e}^0 + t\boldsymbol{h}\right) - \boldsymbol{R}\left(\boldsymbol{e}^0\right)\right]$ of $\boldsymbol{R}$ at $\boldsymbol{e}^0$ through the relation

$$\boldsymbol{R}\left(\boldsymbol{e}^0 + t\boldsymbol{h}\right) - \boldsymbol{R}\left(\boldsymbol{e}^0\right) = \delta\boldsymbol{R}\left(\boldsymbol{e}^0;\boldsymbol{h}\right) + \Delta\left(\boldsymbol{h}\right), \text{ with } \lim_{t\to 0}\left[\Delta\left(t\boldsymbol{h}\right)\right]/t = 0. \qquad \text{(III.A.7)}$$

The objective of local sensitivity analysis is to evaluate $\delta\boldsymbol{R}\left(\boldsymbol{e}^0;\boldsymbol{h}\right)$. As has been shown in Volume I, this objective can be achieved, in principle, by using either the "Forward Sensitivity Analysis Procedure" (*FSAP*), or the "Adjoint Sensitivity Analysis Procedure" (*ASAP*).

III.A.1.a The Forward Sensitivity Analysis Procedure (FSAP)

Recall that the system's state vector $\boldsymbol{u}$ and parameters $\boldsymbol{\alpha}$ are related to each other through Eqs. (III.A.1) and (III.A.2), which implies that $\boldsymbol{h}_u$ and $\boldsymbol{h}_\alpha$ are also related to each other. Therefore, the sensitivity $\delta\boldsymbol{R}\left(\boldsymbol{e}^0;\boldsymbol{h}\right)$ of $\boldsymbol{R}(\boldsymbol{e})$ at $\boldsymbol{e}^0$ can only be evaluated after determining the vector of variations $\boldsymbol{h}_u$ in terms of the vector of parameter variations $\boldsymbol{h}_\alpha$. The first-order relationship between $\boldsymbol{h}_u$ and $\boldsymbol{h}_\alpha$ is determined by taking the G-differentials of Eqs. (III.A.1) and (III.A.2), to obtain the forward sensitivity system

$$\boldsymbol{N}'_u\left(\boldsymbol{u}^0, \boldsymbol{\alpha}^0\right)\boldsymbol{h}_u = \delta\boldsymbol{Q}\left(\boldsymbol{\alpha}^0;\boldsymbol{h}_\alpha\right) - \boldsymbol{N}'_\alpha\left(\boldsymbol{u}^0, \boldsymbol{\alpha}^0\right)\boldsymbol{h}_\alpha, \quad \boldsymbol{x} \in \Omega_x, \qquad \text{(III.A.8)}$$

$$\boldsymbol{B}'_u\left(\boldsymbol{u}^0, \boldsymbol{\alpha}^0\right)\boldsymbol{h}_u = \delta\boldsymbol{A}\left(\boldsymbol{\alpha}^0;\boldsymbol{h}_\alpha\right) - \boldsymbol{B}'_\alpha\left(\boldsymbol{u}^0, \boldsymbol{\alpha}^0\right)\boldsymbol{h}_\alpha, \quad \boldsymbol{x} \in \partial\Omega_x. \qquad \text{(III.A.9)}$$

For a given vector of parameter variations $\boldsymbol{h}_\alpha$ around $\boldsymbol{\alpha}^0$, the forward sensitivity system represented by Eqs. (III.A.8) and (III.A.9) is solved to obtain

$\boldsymbol{h}_u$. Once $\boldsymbol{h}_u$ is available, it is in turn used in Eq. (III.A.6) to calculate the sensitivity $\delta\boldsymbol{R}\left(\boldsymbol{e}^0;\boldsymbol{h}\right)$ of $\boldsymbol{R}(\boldsymbol{e})$ at $\boldsymbol{e}^0$, for a given vector of parameter variations $\boldsymbol{h}_\alpha$.

Equations (III.A.8) and (III.A.9) represent the "*forward sensitivity equations* (*FSE*)," also called occasionally the "*forward sensitivity model* (*FSM*)," or the "*forward variational model* (*FVM*)," or the "*tangent linear model* (*TLM*)." The direct computation of the response sensitivity $\delta\boldsymbol{R}\left(\boldsymbol{e}^0;\boldsymbol{h}\right)$ by using the ($\boldsymbol{h}_\alpha$-dependent) solution $\boldsymbol{h}_u$ of Eqs. (III.A.8) and (III.A.9) constitutes the *Forward Sensitivity Analysis Procedure* (*FSAP*). From the standpoint of computational costs and effort, the *FSAP* is advantageous to employ only if, in the problem under consideration, the number of different responses of interest exceeds the number of system parameters and/or parameter variations to be considered. This is rarely the case in practice, however, since most problems of practical interest are characterized by many parameters (i.e., $\boldsymbol{\alpha}$ has many components) and comparatively few responses. In such situations, it is not economical to employ the *FSAP* to answer all sensitivity questions of interest, since it becomes prohibitively expensive to solve the $\boldsymbol{h}_\alpha$-dependent *FSE* repeatedly to determine $\boldsymbol{h}_u$ for all possible vectors $\boldsymbol{h}_\alpha$.

III.A.1.b The Adjoint Sensitivity Analysis Procedure (ASAP)

When the response $\boldsymbol{R}(\boldsymbol{e})$ is an operator of the form $\boldsymbol{R}:\mathscr{D}_R \to \mathscr{E}_R$, the sensitivity $\delta\boldsymbol{R}\left(\boldsymbol{e}^0;\boldsymbol{h}\right)$ is also an operator, defined on the same domain, and with the same range as $\boldsymbol{R}(\boldsymbol{e})$. To implement the *ASAP* for such responses, the spaces $\mathscr{E}_u$, $\mathscr{E}_Q$, and $\mathscr{E}_R$ are henceforth considered to be Hilbert spaces and denoted as $\mathscr{H}_u(\Omega_x)$, $\mathscr{H}_Q(\Omega_x)$, and $\mathscr{H}_R(\Omega_R)$, respectively. The elements of $\mathscr{H}_u(\Omega_x)$ and $\mathscr{H}_Q(\Omega_x)$ are, as before, vector-valued functions defined on the open set $\Omega_x \subset \mathbb{R}^{J_x}$, with smooth boundary $\partial\Omega_x$. The elements of $\mathscr{H}_R(\Omega_R)$ are vector or scalar functions defined on the open set $\Omega_R \subset \mathbb{R}^m, 1 \le m \le J_x$, with a smooth boundary denoted as $\partial\Omega_R$. Of course, if $J_x = 1$, then $\partial\Omega_x$ merely consists of two endpoints; similarly, if $m = 1$, then $\partial\Omega_R$ consists of two endpoints only. The inner products on $\mathscr{H}_u(\Omega_x)$, $\mathscr{H}_Q(\Omega_x)$, and $\mathscr{H}_R(\Omega_R)$ are denoted by $\langle\bullet,\bullet\rangle_u$, $\langle\bullet,\bullet\rangle_Q$, and $\langle\bullet,\bullet\rangle_R$, respectively. Furthermore, the *ASAP* also requires that $\delta\boldsymbol{R}\left(\boldsymbol{e}^0;\boldsymbol{h}\right)$ be linear in $\boldsymbol{h}$, which implies that $\boldsymbol{R}(\boldsymbol{e})$ must satisfy a weak Lipschitz condition at $\boldsymbol{e}^0$, and that

$$\boldsymbol{R}\left(\boldsymbol{e}^0+t\boldsymbol{h}_1+t\boldsymbol{h}_2\right)-\boldsymbol{R}\left(\boldsymbol{e}^0+t\boldsymbol{h}_1\right)-\boldsymbol{R}\left(\boldsymbol{e}^0+t\boldsymbol{h}_2\right)+\boldsymbol{R}\left(\boldsymbol{e}^0\right)=o(t);\quad \boldsymbol{h}_1,\boldsymbol{h}_2\in\mathcal{H}_u\times\mathcal{H}_\alpha;\ t\in\mathcal{T}. \tag{III.A.10}$$

If $\boldsymbol{R}(\boldsymbol{e})$ satisfies the two conditions above, then the response sensitivity $\delta\boldsymbol{R}\left(\boldsymbol{e}^0;\boldsymbol{h}\right)$ is indeed linear in $\boldsymbol{h}$, and can therefore be denoted as $D\boldsymbol{R}\left(\boldsymbol{e}^0;\boldsymbol{h}\right)$. Consequently, $\boldsymbol{R}(\boldsymbol{e})$ admits a total G-derivative at $\boldsymbol{e}^0=\left(\boldsymbol{u}^0,\boldsymbol{\alpha}^0\right)$, such that the relationship

$$D\boldsymbol{R}\left(\boldsymbol{e}^0;\boldsymbol{h}\right)=\boldsymbol{R}'_u\left(\boldsymbol{e}^0\right)\boldsymbol{h}_u+\boldsymbol{R}'_\alpha\left(\boldsymbol{e}^0\right)\boldsymbol{h}_\alpha \tag{III.A.11}$$

holds, where $\boldsymbol{R}'_u\left(\boldsymbol{e}^0\right)$ and $\boldsymbol{R}'_\alpha\left(\boldsymbol{e}^0\right)$ are the partial G-derivatives at $\boldsymbol{e}^0$ of $\boldsymbol{R}(\boldsymbol{e})$ with respect to $\boldsymbol{u}$ and $\boldsymbol{\alpha}$. Note also that $\boldsymbol{R}'_u\left(\boldsymbol{e}^0\right)$ is a linear operator, on $\boldsymbol{h}_u$, from $\mathcal{H}_u$ into $\mathcal{H}_R$, i.e., $\boldsymbol{R}'_u\left(\boldsymbol{e}^0\right)\in\mathcal{L}\left(\mathcal{H}_u(\Omega),\mathcal{H}_R(\Omega_R)\right)$. It is convenient to refer to the quantities $\boldsymbol{R}'_u\left(\boldsymbol{e}^0\right)\boldsymbol{h}_u$ and $\boldsymbol{R}'_\alpha\left(\boldsymbol{e}^0\right)\boldsymbol{h}_\alpha$ appearing in Eq. (III.A.11) as the "indirect effect term" and the "direct effect term," respectively.

The direct effect term can be evaluated efficiently at this stage. To proceed with the evaluation of the indirect effect term, we consider that the orthonormal set $\{\boldsymbol{p}_s\}_{s\in\mathcal{S}}$, where s runs through an index set $\mathcal{S}$, is an orthonormal basis of $\mathcal{H}_R(\Omega_R)$. Then, since $\boldsymbol{R}'_u\left(\boldsymbol{e}^0\right)\boldsymbol{h}_u\in\mathcal{H}_R(\Omega_R)$, it follows that $\boldsymbol{R}'_u\left(\boldsymbol{e}^0\right)\boldsymbol{h}_u$ can be represented as the Fourier series

$$\boldsymbol{R}'_u\left(\boldsymbol{e}^0\right)\boldsymbol{h}_u=\sum_{s\in\mathcal{S}}\left\langle\boldsymbol{R}'_u\left(\boldsymbol{e}^0\right)\boldsymbol{h}_u,\boldsymbol{p}_s\right\rangle_R\boldsymbol{p}_s\,. \tag{III.A.12}$$

The notation $\sum_{s\in\mathcal{S}}$ is used to signify that in the above sum only an at most countable number of elements are different from zero, and the series extended upon the nonzero elements converges unconditionally. The functionals $\left\langle\boldsymbol{R}'_u\left(\boldsymbol{e}^0\right)\boldsymbol{h}_u,\boldsymbol{p}_s\right\rangle_R$ are the Fourier coefficients of $\boldsymbol{R}'_u\left(\boldsymbol{e}^0\right)\boldsymbol{h}_u$ with respect to the basis $\{\boldsymbol{p}_s\}$. These functionals are linear in $\boldsymbol{h}_u$, since $\boldsymbol{R}(\boldsymbol{e})$ was required to satisfy the conditions stated in Eq. (III.A.10). Since $\boldsymbol{R}'_u\left(\boldsymbol{e}^0\right)\in\mathcal{L}\left(\mathcal{H}_u(\Omega_x),\mathcal{H}_R(\Omega_R)\right)$, and since Hilbert spaces are self-dual, it follows that the following relationship holds:

$$\left\langle\boldsymbol{R}'_u\left(\boldsymbol{e}^0\right)\boldsymbol{h}_u,\boldsymbol{p}_s\right\rangle_R=\left\langle\boldsymbol{\Lambda}\left(\boldsymbol{e}^0\right)\boldsymbol{p}_s,\boldsymbol{h}_u\right\rangle_u,\quad s\in\mathcal{S}\,. \tag{III.A.13}$$

In Eq. (II.A.13), the operator $\boldsymbol{\Lambda}(\boldsymbol{e}^0) \in \mathscr{L}(\mathscr{H}_R(\Omega_R), \mathscr{H}_u(\Omega_x))$ is the adjoint of $\boldsymbol{R}'_u(\boldsymbol{e}^0)$; recall that $\boldsymbol{\Lambda}(\boldsymbol{e}^0)$ is unique if $\boldsymbol{R}'_u(\boldsymbol{e}^0)$ is densely defined.

To eliminate the unknown values of $\boldsymbol{h}_u$ from the expression of each of the functionals $\langle \boldsymbol{h}_u, \boldsymbol{\Lambda}(\boldsymbol{e}^0)\boldsymbol{p}_s \rangle_u$, $s \in \mathcal{S}$, the next step of the *ASAP* is to construct the operator $\boldsymbol{L}^+(\boldsymbol{e}^0)$, which is the operator formally adjoint to $\boldsymbol{N}'_u(\boldsymbol{u}^0, \boldsymbol{\alpha}^0)$, by means of the relationship

$$\langle \boldsymbol{\psi}_s, \boldsymbol{N}'_u(\boldsymbol{u}^0, \boldsymbol{\alpha}^0)\boldsymbol{h}_u \rangle_Q = \langle \boldsymbol{L}^+(\boldsymbol{e}^0)\boldsymbol{\psi}_s, \boldsymbol{h}_u \rangle_u + \{\boldsymbol{P}(\boldsymbol{h}_u; \boldsymbol{\psi}_s)\}_{\partial\Omega_x}, \quad s \in \mathcal{S}, \quad \text{(III.A.14)}$$

which holds for every vector $\boldsymbol{\psi}_s \in \mathscr{H}_Q$, $s \in \mathcal{S}$. Recall that the operator $\boldsymbol{L}^+(\boldsymbol{e}^0)$ is defined as the $K_u \times K_u$ matrix

$$\boldsymbol{L}^+(\boldsymbol{e}^0) \equiv \left[\boldsymbol{L}^+_{ji}(\boldsymbol{e}^0)\right], \ (i, j = 1, \ldots, K_u), \quad \text{(III.A.15)}$$

obtained by transposing the formal adjoints of the operators $\left[\boldsymbol{N}'_u(\boldsymbol{u}^0, \boldsymbol{\alpha}^0)\right]_{ij}$, while $\{\boldsymbol{P}(\boldsymbol{h}_u; \boldsymbol{\psi}_s)\}_{\partial\Omega_x}$ is the associated bilinear form evaluated on $\partial\Omega_x$. The domain of $\boldsymbol{L}^+(\boldsymbol{e}^0)$ is determined by selecting appropriate adjoint boundary conditions, represented here in operator form as

$$\{\boldsymbol{B}^+(\boldsymbol{\psi}_s; \boldsymbol{e}^0) - \boldsymbol{A}^+(\boldsymbol{\alpha}^0)\}_{\partial\Omega_x} = 0, \quad s \in \mathcal{S}. \quad \text{(III.A.16)}$$

Recall from Volume I that the above boundary conditions for $\boldsymbol{L}^+(\boldsymbol{e}^0)$ are obtained by requiring that:

(a) They must be independent of $\boldsymbol{h}_u$, $\boldsymbol{h}_\alpha$, and G-derivatives with respect to $\boldsymbol{\alpha}$;

(b) The substitution of Eqs. (III.A.9) and (III.A.16) into the expression of $\{\boldsymbol{P}(\boldsymbol{h}_u; \boldsymbol{\psi}_s)\}_{\partial\Omega_x}$ must cause all terms containing unknown values of $\boldsymbol{h}_u$ to vanish.

This selection of the boundary conditions for $\boldsymbol{L}^+(\boldsymbol{e}^0)$ reduces $\{\boldsymbol{P}(\boldsymbol{h}_u; \boldsymbol{\psi}_s)\}_{\partial\Omega_x}$ to a quantity that contains boundary terms involving only known values of $\boldsymbol{h}_\alpha$, $\boldsymbol{\psi}$, and, possibly, $\boldsymbol{\alpha}^0$; this quantity will be denoted by $\hat{\boldsymbol{P}}(\boldsymbol{h}_\alpha, \boldsymbol{\psi}_s; \boldsymbol{\alpha}^0)$. In general, $\hat{\boldsymbol{P}}$ does not automatically vanish as a result of these manipulations, although it may do so in particular instances; in principle, $\hat{\boldsymbol{P}}$ could be forced to vanish by

considering extensions of $\boldsymbol{N}'_{\alpha}\left(\boldsymbol{u}^0,\boldsymbol{\alpha}^0\right)$, in the operator sense, but this is seldom needed in practice. Introducing now Eqs. (III.A.9) and (III.A.16) into Eq. (III.A.14) reduces the later to

$$\left\langle \boldsymbol{L}^{+}\left(\boldsymbol{e}^0\right)\boldsymbol{\psi}_s, \boldsymbol{h}_u \right\rangle_u = \left\langle \boldsymbol{\psi}_s, \delta\boldsymbol{Q}\left(\boldsymbol{\alpha}^0;\boldsymbol{h}_{\alpha}\right) - \boldsymbol{N}'_{\alpha}\left(\boldsymbol{u}^0,\boldsymbol{\alpha}^0\right)\boldsymbol{h}_{\alpha} \right\rangle_Q - \hat{\boldsymbol{P}}\left(\boldsymbol{h}_{\alpha},\boldsymbol{\psi}_s;\boldsymbol{\alpha}^0\right), \quad s \in \mathcal{S}\,. \tag{III.A.17}$$

The left-side of Eq. (III.A.17) and the right-side of Eq. (III.A.13) are now required to represent the same functional; this is accomplished by imposing the relation

$$\boldsymbol{L}^{+}\left(\boldsymbol{e}^0\right)\boldsymbol{\psi}_s = \boldsymbol{\Lambda}\left(\boldsymbol{e}^0\right)\boldsymbol{p}_s\,, \quad s \in \mathcal{S}\,, \tag{III.A.18}$$

which holds uniquely in view of the Riesz representation theorem. This last step completes the construction of the desired adjoint system, which consists of Eq. (III.A.18) and the adjoint boundary conditions given in Eq. (III.A.16). Furthermore, Eqs. (III.A.12-18) can now be used to obtain the following expression for the sensitivity $D\boldsymbol{R}\left(\boldsymbol{e}^0;\boldsymbol{h}\right)$ of $\boldsymbol{R}(\boldsymbol{e})$ at $\boldsymbol{e}^0$:

$$D\boldsymbol{R}\left(\boldsymbol{e}^0;\boldsymbol{h}\right) = \boldsymbol{R}'_{\alpha}\left(\boldsymbol{e}^0\right)\boldsymbol{h}_{\alpha} + \sum_{s\in\mathcal{S}}\left[\left\langle \boldsymbol{\psi}_s, \delta\boldsymbol{Q}\left(\boldsymbol{\alpha}^0;\boldsymbol{h}_{\alpha}\right) - \boldsymbol{N}'_{\alpha}\left(\boldsymbol{u}^0,\boldsymbol{\alpha}^0\right)\boldsymbol{h}_{\alpha} \right\rangle_Q - \hat{\boldsymbol{P}}\left(\boldsymbol{h}_{\alpha},\boldsymbol{\psi}_s;\boldsymbol{\alpha}^0\right)\right]\boldsymbol{p}_s\,. \tag{III.A.19}$$

As Eq. (III.A.19) indicates, the desired elimination of all unknown values of $\boldsymbol{h}_u$ from the expression of the sensitivity $D\boldsymbol{R}\left(\boldsymbol{e}^0;\boldsymbol{h}\right)$ of $\boldsymbol{R}(\boldsymbol{e})$ at $\boldsymbol{e}^0$ has thus been accomplished. Note that Eq. (III.A.19) includes the particular case of functional-type responses, in which case the summation $\sum_{s\in\mathcal{S}}$ would contain a single term $(s=1)$ only. To evaluate the sensitivity $D\boldsymbol{R}\left(\boldsymbol{e}^0;\boldsymbol{h}\right)$ by means of Eq. (III.A.19), one needs to compute as many adjoint functions $\boldsymbol{\psi}_s$ from Eqs. (III.A.18) and (III.A.16) as there are nonzero terms in the representation of $\boldsymbol{R}'_u\left(\boldsymbol{e}^0\right)\boldsymbol{h}_u$ given in Eq. (III.A.12). Although the linear combination of basis elements $\boldsymbol{p}_s$ given in Eq. (III.A.12) may, in principle, contain infinitely many terms, obviously only a finite number of the corresponding adjoint functions $\boldsymbol{\psi}_s$ can be calculated in practice. Therefore, special attention is required to select the Hilbert space $\mathcal{H}_R\left(\Omega_R\right)$, a basis $\left\{\boldsymbol{p}_s\right\}_{s\in\mathcal{S}}$ for this space, and a notion of convergence for the representation given in Eq. (III.A.12) to best suit the

problem at hand. This selection is guided by the need to represent the indirect effect term $\boldsymbol{R}'_u\left(\boldsymbol{e}^0\right)\boldsymbol{h}_u$ as accurately as possible with the smallest number of basis elements; a related consideration is the viability of deriving bounds and/or asymptotic expressions for the remainder after truncating Eq. (III.A.12) to the first few terms.

III.A.2. Sensitivity Analysis of the Augmented System

Consider now that the primary (original, nonaugmented) nonlinear system, represented by Eqs. (III.A.1) and (III.A.2), is augmented by additional equations, containing additional independent variables, additional dependent variables, and additional parameters. A general way to represent such an augmentation process is as follows:

1. The augmented system may depend on more independent variables than the original system. To reflect this possibility, the original phase-space position vector, $\boldsymbol{x} = \left(x_1, \ldots, x_{J_x}\right)$, $\boldsymbol{x} \in \Omega_x \subset \mathbb{R}^{J_x}$, is augmented by the additional phase-space position vector $\boldsymbol{y} \equiv \left[y_1, \ldots, y_{J_Y}\right]$; $\boldsymbol{y} \in \Omega_y \subset \mathbb{R}^{J_y}$, where Ω_y is a subset of the J_y-dimensional real vector space $\mathbb{R}^{J_y}$. Thus, the phase-space position vector for the (entire) augmented system will be denoted as $\boldsymbol{z} \equiv (\boldsymbol{x}, \boldsymbol{y})$; $J \equiv J_x + J_y$; $\boldsymbol{z} \in \Omega \equiv \Omega_x \bigcup \Omega_y \subset \mathbb{R}^J$.
2. The augmented system may comprise more dependent variables than the original system. To reflect this possibility, the original vector of dependent (i.e., state) variables, $\boldsymbol{u}(\boldsymbol{x}) = \left[u_1(\boldsymbol{x}), \ldots, u_{K_u}(\boldsymbol{x})\right]$, $\boldsymbol{u}(\boldsymbol{x}) \in \mathscr{E}_u$, is augmented by the vector of additional dependent variables $\boldsymbol{v}(\boldsymbol{z}) = \left[v_1(\boldsymbol{z}), \ldots, v_{K_v}(\boldsymbol{z})\right]$, $\boldsymbol{v}(\boldsymbol{z}) \in \mathscr{E}_v$ where $\mathscr{E}_v$ is a normed linear space over the scalar field $\mathscr{F}$ of real numbers, and where K_v denotes the total number of additional state (i.e., dependent) variables appearing in the augmented system.
3. The augmented system may depend on more parameters than the original system; furthermore, components of the original vector of system parameters, $\boldsymbol{\alpha}(\boldsymbol{x}) = \left[\alpha_1(\boldsymbol{x}), \ldots, \alpha_I(\boldsymbol{x})\right]$, $\boldsymbol{\alpha} \in \mathscr{E}_\alpha$, can become functions of additional parameters, $\boldsymbol{b}(\boldsymbol{z}) = \left[b_1(\boldsymbol{z}), \ldots, b_{I_b}(\boldsymbol{z})\right]$, $b \in \mathscr{E}_b$, where $\mathscr{E}_b$ is a normed linear space. In addition, feedback may be introduced in the augmented system, if some (or all) of the parameters $\boldsymbol{\alpha}$ become dependent on some (or all) of the components of $\boldsymbol{u}(\boldsymbol{x}) \in \mathscr{E}_u$ and/or the components of $\boldsymbol{v}(\boldsymbol{z}) \in \mathscr{E}_v$. Finally, a subset

$\boldsymbol{\beta}(\boldsymbol{x}) = \left[\beta_1(\boldsymbol{x}), \ldots, \beta_{I_\beta}(\boldsymbol{x})\right]$, $\boldsymbol{\beta} \in \mathcal{E}_\beta$, where $\mathcal{E}_\beta$ is also a normed linear space, of the original parameters may remain unaffected by the transition from the original to the enlarged, augmented system. In a very general manner, therefore, the transition from the original system to the enlarged, augmented system can be described mathematically by the mapping $\alpha \to \boldsymbol{a}\left[\boldsymbol{\beta}(\boldsymbol{x}), \boldsymbol{b}(\boldsymbol{z}); \boldsymbol{u}(\boldsymbol{x}), \boldsymbol{v}(\boldsymbol{z})\right]$, $\boldsymbol{a} \in \mathcal{E}_a$. Note that the normed linear space $\mathcal{E}_a$ for the augmented system will generally differ from the normed linear space $\mathcal{E}_\alpha$ to which the parameters of the original (un-augmented) system belonged.

4. In view of the extensions described above in items 1-3, the operators appearing in Eq. (III.A.1) will undergo the transformations

$$\boldsymbol{N}(\boldsymbol{u}, \boldsymbol{\alpha}) \to \boldsymbol{N}\left[\boldsymbol{u}, \boldsymbol{a}(\boldsymbol{\beta}(\boldsymbol{x}), \boldsymbol{b}(\boldsymbol{z}); \boldsymbol{u}(\boldsymbol{x}), \boldsymbol{v}(\boldsymbol{z}))\right] \equiv \left[N_1(\boldsymbol{u}, \boldsymbol{a}(\boldsymbol{\beta}, \boldsymbol{b}; \boldsymbol{u}, \boldsymbol{v})), \ldots, N_{K_u}(\boldsymbol{u}, \boldsymbol{a}(\boldsymbol{\beta}, \boldsymbol{b}; \boldsymbol{u}, \boldsymbol{v}))\right]$$

$$\boldsymbol{Q}\left[\boldsymbol{\alpha}(\boldsymbol{x})\right] \to \boldsymbol{Q}\left[\boldsymbol{a}(\boldsymbol{\beta}(\boldsymbol{x}), \boldsymbol{b}(\boldsymbol{z}); \boldsymbol{u}(\boldsymbol{x}), \boldsymbol{v}(\boldsymbol{z}))\right] \equiv \left[\boldsymbol{Q}_1\left[\boldsymbol{a}(\boldsymbol{\beta}, \boldsymbol{b}; \boldsymbol{u}, \boldsymbol{v})\right], \ldots, \boldsymbol{Q}_{K_u}\left[\boldsymbol{a}(\boldsymbol{\beta}, \boldsymbol{b}; \boldsymbol{u}, \boldsymbol{v})\right]\right].$$

Note also that, for the augmented system, $\boldsymbol{Q} \in \mathcal{E}_q$, where $\mathcal{E}_q$ is a normed linear space that differs from the original normed linear space $\mathcal{E}_Q$. Similarly, the boundary operators appearing in Eq. (III.A.2) will undergo the transformations $\boldsymbol{A}(\boldsymbol{\alpha}) \to \boldsymbol{A}\left[\boldsymbol{a}(\boldsymbol{\beta}, \boldsymbol{b}; \boldsymbol{u}, \boldsymbol{v})\right]$ and $\boldsymbol{B}(\boldsymbol{u}, \boldsymbol{\alpha}) \to \boldsymbol{B}\left[\boldsymbol{u}(\boldsymbol{x}); \boldsymbol{a}(\boldsymbol{\beta}, \boldsymbol{b}; \boldsymbol{u}, \boldsymbol{v})\right]$, respectively. Therefore, Eqs. (III.A.1) and (III.A.2) will be mapped into the following forms within the augmented system:

$$\boldsymbol{N}\left[\boldsymbol{u}, \boldsymbol{a}(\boldsymbol{\beta}, \boldsymbol{b}; \boldsymbol{u}, \boldsymbol{v})\right] = \boldsymbol{Q}\left[\boldsymbol{a}(\boldsymbol{\beta}, \boldsymbol{b}; \boldsymbol{u}, \boldsymbol{v})\right], \boldsymbol{z} \in \Omega \qquad \text{(III.A.20)}$$

and

$$\boldsymbol{B}\left[\boldsymbol{u}, \boldsymbol{a}(\boldsymbol{\beta}, \boldsymbol{b}; \boldsymbol{u}, \boldsymbol{v})\right] = \boldsymbol{A}\left[\boldsymbol{a}(\boldsymbol{\beta}, \boldsymbol{b}; \boldsymbol{u}, \boldsymbol{v})\right] \ \boldsymbol{z} \in \partial\Omega, \qquad \text{(III.A.21)}$$

respectively.

In addition to Eqs. (III.A.20) and (III.A.21), the augmented system will also contain further equations and corresponding boundary and/or initial conditions, as needed to balance the total number of state (i.e., dependent) variables $(\boldsymbol{u}, \boldsymbol{v})$ with the total number of equations, in order to have a well-posed augmented system. These additional equations can be written in operator form as

$$\boldsymbol{M}\left[\boldsymbol{u}(\boldsymbol{x}), \boldsymbol{v}(\boldsymbol{z}), \boldsymbol{b}(\boldsymbol{z})\right] = \boldsymbol{S}(\boldsymbol{b}), \boldsymbol{z} \in \Omega, \qquad \text{(III.A.22)}$$

with corresponding boundary and/or initial conditions written in operator form as

$$\boldsymbol{C}\left[\boldsymbol{u}(\boldsymbol{x}),\boldsymbol{v}(\boldsymbol{z}),\boldsymbol{b}(\boldsymbol{z})\right]=\boldsymbol{D}(\boldsymbol{b}),\ \boldsymbol{z}\in\partial\Omega\,. \tag{III.A.23}$$

Each of the vector-valued operators appearing in Eq. (III.A.22) comprise K_v-components, defined as

$$\boldsymbol{M}\left[\boldsymbol{u}(\boldsymbol{x}),\boldsymbol{v}(\boldsymbol{z}),\boldsymbol{b}(\boldsymbol{z})\right]\equiv\left[M_1(\boldsymbol{u},\boldsymbol{v},\boldsymbol{b}),\ldots,M_{K_v}(\boldsymbol{u},\boldsymbol{v},\boldsymbol{b})\right]\,, \tag{III.A.24}$$

$$\boldsymbol{S}\left[\boldsymbol{u}(\boldsymbol{x}),\boldsymbol{v}(\boldsymbol{z}),\boldsymbol{b}(\boldsymbol{z})\right]\equiv\left[S_1(\boldsymbol{u},\boldsymbol{v},\boldsymbol{b}),\ldots,S_{K_v}(\boldsymbol{u},\boldsymbol{v},\boldsymbol{b})\right]\,,\ \boldsymbol{S}\in\mathcal{E}_S\ . \tag{III.A.25}$$

In view of the definitions given above, the augmented vector of operators $(\boldsymbol{N},\boldsymbol{M})$ represents the mapping $(\boldsymbol{N},\boldsymbol{M}):\mathcal{D}_{aug}\subset\mathcal{E}_{aug}\to\mathcal{E}_q\times\mathcal{E}_S$, where $\mathcal{D}_{aug}=\mathcal{D}_u\times\mathcal{D}_v\times\mathcal{D}_a$, $\mathcal{D}_u\subset\mathcal{E}_u$, $\mathcal{D}_v\subset\mathcal{E}_v$, $\mathcal{D}_a\subset\mathcal{E}_a$, and $\mathcal{E}_{aug}=\mathcal{E}_u\times\mathcal{E}_v\times\mathcal{E}_a$. Note that a generic element $\boldsymbol{f}\in\mathcal{E}_{aug}$ is of the form $\boldsymbol{f}\equiv\left[\boldsymbol{u},\boldsymbol{v},\boldsymbol{a}(\boldsymbol{\beta},\boldsymbol{b};\boldsymbol{u},\boldsymbol{v})\right]$. The vector-valued function $\left[\boldsymbol{u}(\boldsymbol{x}),\boldsymbol{v}(\boldsymbol{z})\right]$ is considered to be the unique nontrivial solution of the physical problem described by Eqs. (III.A.20) through (III.A.23).

The system response (i.e., performance parameter) associated with the augmented system modeled by Eqs. (III.A.20) through (III.A.23) will be denoted in the sequel as $\boldsymbol{\Theta}(\boldsymbol{f})$, and is considered to be an operator that acts nonlinearly on the augmented system's state vector $\left[\boldsymbol{u}(\boldsymbol{x}),\boldsymbol{v}(\boldsymbol{z})\right]$ and parameters $\boldsymbol{a}(\boldsymbol{\beta},\boldsymbol{b};\boldsymbol{u},\boldsymbol{v})$; $\boldsymbol{\Theta}(\boldsymbol{f})$ can represented in operator form as

$$\boldsymbol{\Theta}(\boldsymbol{f}):\mathcal{D}_{Raug}\subset\mathcal{E}_{aug}\to\mathcal{E}_{Raug}\,, \tag{III.A.26}$$

where $\mathcal{E}_{Raug}$ is another normed vector space.

In practice, the exact values of the parameters $\boldsymbol{\alpha}$, $\boldsymbol{\beta}$, and $\boldsymbol{b}$ are not known; only their nominal (mean) values, $\boldsymbol{\alpha}^0$, $\boldsymbol{\beta}^0$, and $\boldsymbol{b}^0$, and their associated uncertainties are usually available. The nominal parameter values $\boldsymbol{a}^0$ are used in Eqs. (III.A.20) through (III.A.23) to obtain the nominal solution $\left[\boldsymbol{u}^0(\boldsymbol{x}),\boldsymbol{v}^0(\boldsymbol{z})\right]$, by solving the "base-case" augmented system

$$\boldsymbol{N}\left[\boldsymbol{u}^0,\boldsymbol{a}^0\left(\boldsymbol{\beta}^0,\boldsymbol{b}^0;\boldsymbol{u}^0,\boldsymbol{v}^0\right)\right]=\boldsymbol{Q}\left[\boldsymbol{a}^0\left(\boldsymbol{\beta}^0,\boldsymbol{b}^0;\boldsymbol{u}^0,\boldsymbol{v}^0\right)\right]\,,\ \boldsymbol{z}\in\Omega \tag{III.A.27}$$

$$\boldsymbol{B}\left[\boldsymbol{u}^0,\boldsymbol{a}^0\left(\boldsymbol{\beta}^0,\boldsymbol{b}^0;\boldsymbol{u}^0,\boldsymbol{v}^0\right)\right]=\boldsymbol{A}\left[\boldsymbol{a}^0\left(\boldsymbol{\beta}^0,\boldsymbol{b}^0;\boldsymbol{u}^0,\boldsymbol{v}^0\right)\right]\,,\ \boldsymbol{z}\in\partial\Omega\,, \tag{III.A.28}$$

$$\boldsymbol{M}\left[\boldsymbol{u}^0(\boldsymbol{x}),\boldsymbol{v}^0(\boldsymbol{z}),\boldsymbol{b}^0(\boldsymbol{z})\right]=\boldsymbol{S}\left(\boldsymbol{b}^0\right),\ \boldsymbol{z}\in\Omega\,, \tag{III.A.29}$$

$$\boldsymbol{C}\left[\boldsymbol{u}^0(\boldsymbol{x}),\boldsymbol{v}^0(\boldsymbol{z}),\boldsymbol{b}^0(\boldsymbol{z})\right]=\boldsymbol{D}\left(\boldsymbol{b}^0\right),\ \boldsymbol{z}\in\partial\Omega\,. \tag{III.A.30}$$

Using the base-case solution of the augmented system obtained by solving Eqs.(III.A.27) through (III.A.30) yields the base-case value, $\boldsymbol{\Theta}\left(\boldsymbol{f}^0\right)$, $\boldsymbol{f}^0\equiv\left[\boldsymbol{u}^0,\boldsymbol{v}^0,\boldsymbol{a}^0\left(\boldsymbol{\beta}^0,\boldsymbol{b}^0;\boldsymbol{u}^0,\boldsymbol{v}^0\right)\right]$, of the response for the augmented system.

The sensitivity of the response, $\boldsymbol{\Theta}(\boldsymbol{f})$, at $\boldsymbol{f}^0\equiv\left[\boldsymbol{u}^0,\boldsymbol{v}^0,\boldsymbol{a}^0\left(\boldsymbol{\beta}^0,\boldsymbol{b}^0;\boldsymbol{u}^0,\boldsymbol{v}^0\right)\right]$ to variations $\boldsymbol{h}\equiv\left[\boldsymbol{h}_u,\boldsymbol{h}_v,\boldsymbol{h}_\beta,\boldsymbol{h}_b\right]$ in the augmented system's parameters is the Gâteaux-(G)-differential, $\delta\boldsymbol{\Theta}\left(\boldsymbol{f}^0;\boldsymbol{h}\right)$, defined as

$$\delta\boldsymbol{\Theta}\left(\boldsymbol{f}^0;\boldsymbol{h}\right)\equiv\left\{\frac{d}{dt}\left[\boldsymbol{\Theta}\left(\boldsymbol{f}^0+t\boldsymbol{h}\right)\right]\right\}_{t=0}=\lim_{t\to 0}\frac{\boldsymbol{\Theta}\left(\boldsymbol{f}^0+t\boldsymbol{h}\right)-\boldsymbol{\Theta}\left(\boldsymbol{f}^0\right)}{t}, \tag{III.A.31}$$

for $t\in\mathcal{T}$, and all (i.e., arbitrary) vectors $\boldsymbol{f}\in\mathcal{E}_{aug}$.

III.A.2.a The Forward Sensitivity Analysis Procedure (FSAP)

Just as for the original system, the augmented system's state vector $\left[\boldsymbol{u}(\boldsymbol{x}),\boldsymbol{v}(\boldsymbol{z})\right]$ and parameters $\left(\boldsymbol{\beta},\boldsymbol{b}\right)$ are related to each other through Eqs. (III.A.20) - (III.A.23). Hence, it follows that the vector of variations $\left(\boldsymbol{h}_u,\boldsymbol{h}_v\right)$ around the nominal values $\left[\boldsymbol{u}^0(\boldsymbol{x}),\boldsymbol{v}^0(\boldsymbol{z})\right]$ of the state functions $\left[\boldsymbol{u}(\boldsymbol{x}),\boldsymbol{v}(\boldsymbol{z})\right]$ is also related to the vector of parameter variations $\left(\boldsymbol{h}_\beta,\boldsymbol{h}_b\right)$ around the nominal values $\left(\boldsymbol{\beta}^0,\boldsymbol{b}^0\right)$. Therefore, the sensitivity $\delta\boldsymbol{\Theta}\left(\boldsymbol{f}^0;\boldsymbol{h}\right)$ of $\boldsymbol{\Theta}(\boldsymbol{f})$ at $\boldsymbol{f}^0$ can only be evaluated after determining the variations $\left(\boldsymbol{h}_u,\boldsymbol{h}_v\right)$ in terms of the vector of parameter variations $\left(\boldsymbol{h}_\beta,\boldsymbol{h}_b\right)$. The first-order relationship between $\left(\boldsymbol{h}_u,\boldsymbol{h}_v\right)$ and $\left(\boldsymbol{h}_\beta,\boldsymbol{h}_b\right)$ is obtained by taking the G-differentials of Eqs. (III.A.20) through (III.A.23), to obtain the relations

$$\begin{pmatrix}\boldsymbol{N}'_u\left(\boldsymbol{f}^0\right)+\left[\boldsymbol{N}'_a\left(\boldsymbol{f}^0\right)-\boldsymbol{Q}'_a\left(\boldsymbol{f}^0\right)\right]\boldsymbol{a}'_u\left(\boldsymbol{f}^0\right) & \left[\boldsymbol{N}'_a\left(\boldsymbol{f}^0\right)-\boldsymbol{Q}'_a\left(\boldsymbol{f}^0\right)\right]\boldsymbol{a}'_v\left(\boldsymbol{f}^0\right)\\ \boldsymbol{M}'_u\left(\boldsymbol{f}^0\right) & \boldsymbol{M}'_v\left(\boldsymbol{f}^0\right)\end{pmatrix}\begin{pmatrix}\boldsymbol{h}_u\\ \boldsymbol{h}_v\end{pmatrix}=$$
$$\begin{pmatrix}\left[\boldsymbol{Q}'_a\left(\boldsymbol{f}^0\right)-\boldsymbol{N}'_a\left(\boldsymbol{f}^0\right)\right]\boldsymbol{a}'_\beta\left(\boldsymbol{f}^0\right) & \left[\boldsymbol{Q}'_a\left(\boldsymbol{f}^0\right)-\boldsymbol{N}'_a\left(\boldsymbol{f}^0\right)\right]\boldsymbol{a}'_b\left(\boldsymbol{f}^0\right)\\ 0 & \boldsymbol{S}'_b\left(\boldsymbol{b}^0\right)-\boldsymbol{M}'_b\left(\boldsymbol{f}^0\right)\end{pmatrix}\begin{pmatrix}\boldsymbol{h}_\beta\\ \boldsymbol{h}_b\end{pmatrix} \tag{III.A.32}$$

together with the G-differentiated boundary/initial conditions

$$\begin{aligned} &\boldsymbol{B}'_u\left(\boldsymbol{f}^0\right)\boldsymbol{h}_u + \left[\boldsymbol{B}'_a\left(\boldsymbol{f}^0\right) - \boldsymbol{A}'_a\left(\boldsymbol{f}^0\right)\right]\left[\boldsymbol{a}'_u\left(\boldsymbol{f}^0\right)\boldsymbol{h}_u + \boldsymbol{a}'_v\left(\boldsymbol{f}^0\right)\boldsymbol{h}_v\right] = \\ &\left[\boldsymbol{A}'_a\left(\boldsymbol{f}^0\right) - \boldsymbol{B}'_a\left(\boldsymbol{f}^0\right)\right]\times\left[\boldsymbol{a}'_\beta\left(\boldsymbol{f}^0\right)\boldsymbol{h}_\beta + \boldsymbol{a}'_b\left(\boldsymbol{f}^0\right)\boldsymbol{h}_b\right], \quad \boldsymbol{z}\in\partial\Omega\,, \end{aligned} \tag{III.A.33}$$

$$\boldsymbol{C}'_u\left(\boldsymbol{f}^0\right)\boldsymbol{h}_u + \boldsymbol{C}'_v\left(\boldsymbol{f}^0\right)\boldsymbol{h}_v = \delta\boldsymbol{D}\left(\boldsymbol{b}^0;\boldsymbol{h}_b\right) - \boldsymbol{C}'_b\left(\boldsymbol{f}^0\right)\boldsymbol{h}_b, \quad \boldsymbol{z}\in\partial\Omega\,. \tag{III.A.34}$$

Note that the left-side of Eq. (III.A.32) represents a block-matrix-valued linear operator, $\boldsymbol{L}_{\boldsymbol{a}}\left(\boldsymbol{f}^0\right)$, defined as

$$\begin{aligned} &\boldsymbol{L}_{\boldsymbol{a}}\left(\boldsymbol{f}^0\right) \equiv \begin{pmatrix} \boldsymbol{L}_{11}\left(\boldsymbol{f}^0\right) & \boldsymbol{L}_{12}\left(\boldsymbol{f}^0\right) \\ \boldsymbol{L}_{21}\left(\boldsymbol{f}^0\right) & \boldsymbol{L}_{22}\left(\boldsymbol{f}^0\right) \end{pmatrix} \equiv \\ &\begin{pmatrix} \boldsymbol{N}'_u\left(\boldsymbol{f}^0\right) + \left[\boldsymbol{N}'_a\left(\boldsymbol{f}^0\right) - \boldsymbol{Q}'_a\left(\boldsymbol{f}^0\right)\right]\boldsymbol{a}'_u\left(\boldsymbol{f}^0\right) & \left[\boldsymbol{N}'_a\left(\boldsymbol{f}^0\right) - \boldsymbol{Q}'_a\left(\boldsymbol{f}^0\right)\right]\boldsymbol{a}'_v\left(\boldsymbol{f}^0\right) \\ \boldsymbol{M}'_u\left(\boldsymbol{f}^0\right) & \boldsymbol{M}'_v\left(\boldsymbol{f}^0\right) \end{pmatrix}. \end{aligned} \tag{III.A.35}$$

In Eq. (III.A.35), the subscript "*a*" denotes "augmented." For a given vector of parameter variations $\left(\boldsymbol{h}_\beta, \boldsymbol{h}_b\right)$, the system of equations represented by Eqs. (III.A.32) through (III.A.34) can be solved to obtain, to first-order, the vector of variations $\left(\boldsymbol{h}_u, \boldsymbol{h}_v\right)$. In turn, the variations $\left(\boldsymbol{h}_u, \boldsymbol{h}_v\right)$ and $\left(\boldsymbol{h}_\beta, \boldsymbol{h}_b\right)$ are used in Eq. (III.A.31) to calculate the sensitivity $\delta\boldsymbol{\Theta}\left(\boldsymbol{f}^0;\boldsymbol{h}\right)$ of $\boldsymbol{\Theta}\left(\boldsymbol{f}\right)$ at $\boldsymbol{f}^0$, for given parameter variations $\left(\boldsymbol{h}_\beta, \boldsymbol{h}_b\right)$. Equations (III.A.32) through (III.A.34) represent the "*forward sensitivity equations* (*FSE*)," or the "*forward sensitivity model* (*FSM*)," or the "*forward variational model* (*FVM*)," or the "*tangent linear model* (*TLM*)." The *Forward Sensitivity Analysis Procedure* (*FSAP*) would proceed with the direct calculation of the response sensitivity $\delta\boldsymbol{\Theta}\left(\boldsymbol{f}^0;\boldsymbol{h}\right)$ by using the $\left(\boldsymbol{h}_\beta, \boldsymbol{h}_b\right)$-dependent solution of the forward sensitivity equations. From the standpoint of computational costs and effort, the *FSAP* is advantageous to employ only if, in the problem under consideration, the number of different responses of interest exceeds the number of system parameters and/or parameter variations to be considered.

III.A.2.b The Adjoint Sensitivity Analysis Procedure (ASAP)

The practical motivation underlying the development of an alternative method for sensitivity analysis is to avoid the need for repeatedly solving the *FSE* represented by Eqs. (III.A.32) through (III.A.34). This goal was achieved for the

original (un-augmented) system in Section III.A.1.b by constructing an adjoint system that was (a) uniquely defined, (b) independent of the vectors $\boldsymbol{h}_u$ and $\boldsymbol{h}_\alpha$, and (c) such that its solution can be used to eliminate all unknown values of $\boldsymbol{h}_u$ from the expression of $\delta\Theta\left(\boldsymbol{f}^0;\boldsymbol{h}\right)$. A similar path will also be followed for the augmented system. For this purpose, the spaces $\mathcal{E}_u$, $\mathcal{E}_v$, $\mathcal{E}_S$, and $\mathcal{E}_q$ will henceforth be considered to be real Hilbert spaces denoted by $\mathcal{H}_u$, $\mathcal{H}_v$, $\mathcal{H}_q$, and $\mathcal{H}_S$, respectively. The inner products on $\mathcal{H}_u \times \mathcal{H}_v$ and $\mathcal{H}_q \times \mathcal{H}_S$ will be denoted by $\langle \bullet,\bullet \rangle_{u\times v}$ and $\langle \bullet,\bullet \rangle_{q\times S}$, respectively.

To define the formal adjoint $\boldsymbol{L}_a^+\left(\boldsymbol{f}^0\right)$ of $\boldsymbol{L}_a\left(\boldsymbol{f}^0\right)$, we recall from the geometry of Hilbert spaces $\mathcal{H}_u \times \mathcal{H}_v$ and $\mathcal{H}_q \times \mathcal{H}_S$ that the following relationship holds for a (column) vector $(\boldsymbol{\psi}_u,\boldsymbol{\psi}_v)^T \in \mathcal{H}_q \times \mathcal{H}_S$, where the superscript "*T*" denotes "transposition:"

$$\left\langle \begin{pmatrix} \boldsymbol{\psi}_u \\ \boldsymbol{\psi}_v \end{pmatrix}^T, \begin{pmatrix} \boldsymbol{L}_{11}\left(\boldsymbol{f}^0\right) & \boldsymbol{L}_{12}\left(\boldsymbol{f}^0\right) \\ \boldsymbol{L}_{21}\left(\boldsymbol{f}^0\right) & \boldsymbol{L}_{22}\left(\boldsymbol{f}^0\right) \end{pmatrix} \begin{pmatrix} \boldsymbol{h}_u \\ \boldsymbol{h}_v \end{pmatrix} \right\rangle_{q\times S} = \left\langle \begin{pmatrix} \boldsymbol{h}_u \\ \boldsymbol{h}_v \end{pmatrix}^T, \boldsymbol{L}_a^+\left(\boldsymbol{f}^0\right) \begin{pmatrix} \boldsymbol{\psi}_u \\ \boldsymbol{\psi}_v \end{pmatrix} \right\rangle_{u\times v} + \left\{ P\left(\boldsymbol{f}^0;\boldsymbol{\psi}_u,\boldsymbol{\psi}_v;\boldsymbol{h}_u,\boldsymbol{h}_v\right) \right\}_{\partial\Omega} . \tag{III.A.36}$$

The quantity $\left\{ P\left(\boldsymbol{f}^0;\boldsymbol{\psi}_u,\boldsymbol{\psi}_v;\boldsymbol{h}_u,\boldsymbol{h}_v\right) \right\}_{\partial\Omega}$ in the above equation denotes the associated bilinear form (the "bilinear concomitant") evaluated on $\partial\Omega$.

Replacing Eq. (III.A.35) on the left-side of Eq. (III.A.36), and carrying out the operations indicated by the respective inner products shows that the explicit form for the formal adjoint operator $\boldsymbol{L}_a^+\left(\boldsymbol{f}^0\right)$ is the following 2×2 block-matrix:

$$\boldsymbol{L}_a^+\left(\boldsymbol{f}^0\right) \equiv \begin{pmatrix} \boldsymbol{L}_{11}^+\left(\boldsymbol{f}^0\right) & \boldsymbol{L}_{12}^+\left(\boldsymbol{f}^0\right) \\ \boldsymbol{L}_{21}^+\left(\boldsymbol{f}^0\right) & \boldsymbol{L}_{22}^+\left(\boldsymbol{f}^0\right) \end{pmatrix} \equiv \begin{pmatrix} \left[\boldsymbol{N}_u'\left(\boldsymbol{f}^0\right)\right]^+ + \left\{\left[\boldsymbol{N}_a'\left(\boldsymbol{f}^0\right) - \boldsymbol{Q}_a'\left(\boldsymbol{f}^0\right)\right]\boldsymbol{a}_u'\left(\boldsymbol{f}^0\right)\right\}^+ & \left[\boldsymbol{M}_u'\right]^+ \\ \left\{\left[\boldsymbol{N}_a'\left(\boldsymbol{f}^0\right) - \boldsymbol{Q}_a'\left(\boldsymbol{f}^0\right)\right]\boldsymbol{a}_v'\left(\boldsymbol{f}^0\right)\right\}^+ & \left[\boldsymbol{M}_v'\right]^+ \end{pmatrix}, \tag{III.A.37}$$

where the quantities $\left[\boldsymbol{N}_u'\left(\boldsymbol{f}^0\right)\right]^+$, $\left\{\left[\boldsymbol{N}_a'\left(\boldsymbol{f}^0\right) - \boldsymbol{Q}_a'\left(\boldsymbol{f}^0\right)\right]\boldsymbol{a}_u'\left(\boldsymbol{f}^0\right)\right\}^+$, $\left[\boldsymbol{M}_u'\left(\boldsymbol{f}^0\right)\right]^+$, $\left\{\left[\boldsymbol{N}_a'\left(\boldsymbol{f}^0\right) - \boldsymbol{Q}_a'\left(\boldsymbol{f}^0\right)\right]\boldsymbol{a}_v'\left(\boldsymbol{f}^0\right)\right\}^+$, $\left[\boldsymbol{M}_v'\left(\boldsymbol{f}^0\right)\right]^+$, denote the formal adjoint operators

corresponding to $\boldsymbol{N}'_u\left(\boldsymbol{f}^0\right)$, $\left[\boldsymbol{N}'_a\left(\boldsymbol{f}^0\right)-\boldsymbol{Q}'_a\left(\boldsymbol{f}^0\right)\right]\boldsymbol{a}'_u\left(\boldsymbol{f}^0\right)$, $\boldsymbol{M}'_u\left(\boldsymbol{f}^0\right)$, $\left[\boldsymbol{N}'_a\left(\boldsymbol{f}^0\right)-\boldsymbol{Q}'_a\left(\boldsymbol{f}^0\right)\right]\boldsymbol{a}'_v\left(\boldsymbol{f}^0\right)$, and $\boldsymbol{M}'_v\left(\boldsymbol{f}^0\right)$, respectively.

The boundary conditions for the adjoint operator $\boldsymbol{L}_{\boldsymbol{a}}^{+}\left(\boldsymbol{f}^0\right)$, which define its domain, must be determined next. They are represented here in operator form as

$$\left\{\boldsymbol{\Gamma}_1^{+}\left(\boldsymbol{f}^0;\boldsymbol{\psi}_u,\boldsymbol{\psi}_v\right)-\boldsymbol{\Gamma}_2^{+}\left(\boldsymbol{f}^0\right)\right\}_{\partial\Omega}=\boldsymbol{0},\quad \boldsymbol{z}\in\partial\Omega, \tag{III.A.38}$$

and are determined by requiring that:

(a) They must be independent of $\left(\boldsymbol{h}_u,\boldsymbol{h}_v\right)$ *and* $\left(\boldsymbol{h}_\beta,\boldsymbol{h}_b\right)$*, and G-derivatives with respect to* $\boldsymbol{\beta}$*, and* $\boldsymbol{b}$ *;*

(b) They must cause all terms containing unknown values of $\left(\boldsymbol{h}_u,\boldsymbol{h}_v\right)$ *to vanish when substituted together with Eqs. (III.A.33) and (III.A.34) into the expression of* $\left\{P\left(\boldsymbol{f}^0;\boldsymbol{\psi}_u,\boldsymbol{\psi}_v;\boldsymbol{h}_u,\boldsymbol{h}_v\right)\right\}_{\partial\Omega}$.

Thus, when the conditions (III.A.38) for $\boldsymbol{L}_{\boldsymbol{a}}^{+}\left(\boldsymbol{f}^0\right)$ are substituted together with Eqs. (III.A.33) and (III.A.34) into the expression of $\left\{P\left(\boldsymbol{f}^0;\boldsymbol{\psi}_u,\boldsymbol{\psi}_v;\boldsymbol{h}_u,\boldsymbol{h}_v\right)\right\}_{\partial\Omega}$, this bilinear concomitant will be reduced to a quantity that contains boundary terms involving solely known values of $\left(\boldsymbol{h}_\beta,\boldsymbol{h}_b\right)$, $\left(\boldsymbol{\psi}_u,\boldsymbol{\psi}_v\right)$, and, possibly, $\boldsymbol{f}^0$; this quantity will be denoted in the sequel by $\hat{\boldsymbol{P}}\left(\boldsymbol{f}^0;\boldsymbol{\psi}_u,\boldsymbol{\psi}_v;\boldsymbol{h}_\beta,\boldsymbol{h}_b\right)$. In general, $\hat{\boldsymbol{P}}\left(\boldsymbol{f}^0;\boldsymbol{\psi}_u,\boldsymbol{\psi}_v;\boldsymbol{h}_\beta,\boldsymbol{h}_b\right)$ does not automatically vanish as a result of these manipulations, although it may do so in particular instances. In practice, $\hat{\boldsymbol{P}}\left(\boldsymbol{f}^0;\boldsymbol{\psi}_u,\boldsymbol{\psi}_v;\boldsymbol{h}_\beta,\boldsymbol{h}_b\right)$ will ultimately appear as a readily computable quantity in the expression of the response sensitivity $\delta\boldsymbol{\Theta}\left(\boldsymbol{f}^0;\boldsymbol{h}\right)$.

Replacing now Eqs. (III.A.33) and (III.A.34) together with the adjoint boundary conditions, given in Eq. (III.A.38), for $\boldsymbol{L}_{\boldsymbol{a}}^{+}\left(\boldsymbol{f}^0\right)$, into Eq. (III.A.36) reduces the latter equation to

$$\begin{aligned}&\left\langle\begin{pmatrix}\boldsymbol{\psi}_u\\ \boldsymbol{\psi}_v\end{pmatrix}^T,\ \begin{pmatrix}\boldsymbol{L}_{11}\left(\boldsymbol{f}^0\right) & \boldsymbol{L}_{12}\left(\boldsymbol{f}^0\right)\\ \boldsymbol{L}_{21}\left(\boldsymbol{f}^0\right) & \boldsymbol{L}_{22}\left(\boldsymbol{f}^0\right)\end{pmatrix}\begin{pmatrix}\boldsymbol{h}_u\\ \boldsymbol{h}_v\end{pmatrix}\right\rangle_{q\times S}=\\ &\left\langle\begin{pmatrix}\boldsymbol{h}_u\\ \boldsymbol{h}_v\end{pmatrix}^T,\ \boldsymbol{L}_{\boldsymbol{a}}^{+}\left(\boldsymbol{f}^0\right)\begin{pmatrix}\boldsymbol{\psi}_u\\ \boldsymbol{\psi}_v\end{pmatrix}\right\rangle_{u\times v}+\hat{\boldsymbol{P}}\left(\boldsymbol{f}^0;\boldsymbol{\psi}_u,\boldsymbol{\psi}_v;\boldsymbol{h}_\beta,\boldsymbol{h}_b\right).\end{aligned} \tag{III.A.39}$$

Using now Eq. (III.A. 32) to replace the quantity $\begin{pmatrix}\boldsymbol{L}_{11}\left(\boldsymbol{f}^0\right) & \boldsymbol{L}_{12}\left(\boldsymbol{f}^0\right)\\ \boldsymbol{L}_{21}\left(\boldsymbol{f}^0\right) & \boldsymbol{L}_{22}\left(\boldsymbol{f}^0\right)\end{pmatrix}\begin{pmatrix}\boldsymbol{h}_u\\ \boldsymbol{h}_v\end{pmatrix}$ by

the quantity $\begin{pmatrix} \left[\boldsymbol{Q}'_a\left(\boldsymbol{f}^0\right) - \boldsymbol{N}'_a\left(\boldsymbol{f}^0\right)\right]\boldsymbol{a}'_\beta\left(\boldsymbol{f}^0\right) & \left[\boldsymbol{Q}'_a\left(\boldsymbol{f}^0\right) - \boldsymbol{N}'_a\left(\boldsymbol{f}^0\right)\right]\boldsymbol{a}'_b\left(\boldsymbol{f}^0\right) \\ 0 & \boldsymbol{S}'_b\left(\boldsymbol{b}^0\right) - \boldsymbol{M}'_b\left(\boldsymbol{f}^0\right) \end{pmatrix}\begin{pmatrix} \boldsymbol{h}_\beta \\ \boldsymbol{h}_b \end{pmatrix}$ in Eq. (III.A.39) transforms the latter equation into the form

$$\left\langle \begin{pmatrix} \boldsymbol{h}_u \\ \boldsymbol{h}_v \end{pmatrix}^T, \; \boldsymbol{L}_a^+\left(\boldsymbol{f}^0\right)\begin{pmatrix} \boldsymbol{\psi}_u \\ \boldsymbol{\psi}_v \end{pmatrix} \right\rangle_{u\times v} = -\hat{\boldsymbol{P}}\left(\boldsymbol{f}^0; \boldsymbol{\psi}_u, \boldsymbol{\psi}_v; \boldsymbol{h}_\beta, \boldsymbol{h}_b\right) + \left\langle \begin{pmatrix} \boldsymbol{\psi}_u \\ \boldsymbol{\psi}_v \end{pmatrix}^T, \; \begin{pmatrix} \left[\boldsymbol{Q}'_a\left(\boldsymbol{f}^0\right) - \boldsymbol{N}'_a\left(\boldsymbol{f}^0\right)\right]\boldsymbol{a}'_\beta\left(\boldsymbol{f}^0\right) & \left[\boldsymbol{Q}'_a\left(\boldsymbol{f}^0\right) - \boldsymbol{N}'_a\left(\boldsymbol{f}^0\right)\right]\boldsymbol{a}'_b\left(\boldsymbol{f}^0\right) \\ 0 & \boldsymbol{S}'_b\left(\boldsymbol{b}^0\right) - \boldsymbol{M}'_b\left(\boldsymbol{f}^0\right) \end{pmatrix}\begin{pmatrix} \boldsymbol{h}_\beta \\ \boldsymbol{h}_b \end{pmatrix} \right\rangle_{q\times S}. \tag{III.A.40}$$

To complete the *ASAP*, we need to relate the left-side of the above equation to the sensitivity $\delta\boldsymbol{\Theta}\left(\boldsymbol{f}^0; \boldsymbol{h}\right)$ defined by Eq. (III.A.31). This cannot be done yet, however, since the functional $\left\langle \begin{pmatrix} \boldsymbol{h}_u \\ \boldsymbol{h}_v \end{pmatrix}^T, \; \boldsymbol{L}_a^+\left(\boldsymbol{f}^0\right)\begin{pmatrix} \boldsymbol{\psi}_u \\ \boldsymbol{\psi}_v \end{pmatrix} \right\rangle_{u\times v}$ appearing on the left-side of Eq. (III.A.40) is linear in $\left(\boldsymbol{h}_u, \boldsymbol{h}_v\right)$, while, in general, the sensitivity $\delta\boldsymbol{\Theta}\left(\boldsymbol{f}^0; \boldsymbol{h}\right)$ defined by Eq. (III.A.31) is not necessarily linear in $\boldsymbol{h} \equiv \left[\boldsymbol{h}_u, \boldsymbol{h}_v, \boldsymbol{h}_\beta, \boldsymbol{h}_b\right]$.

Recalling the considerations detailed in the previous section (and also from Volume I), we note that the *ASAP* can only be developed if the response sensitivity $\delta\boldsymbol{\Theta}\left(\boldsymbol{f}^0; \boldsymbol{h}\right)$ is *linear* in $\boldsymbol{h} \equiv \left[\boldsymbol{h}_u, \boldsymbol{h}_v, \boldsymbol{h}_\beta, \boldsymbol{h}_b\right]$. This will be the case if $\boldsymbol{\Theta}\left(\boldsymbol{f}\right)$ satisfies a weak Lipschitz condition at $\boldsymbol{f}^0$, and also satisfies the relation

$$\boldsymbol{\Theta}\left(\boldsymbol{f}^0 + t\boldsymbol{h}_1 + t\boldsymbol{h}_2\right) - \boldsymbol{\Theta}\left(\boldsymbol{f}^0 + t\boldsymbol{h}_1\right) - \boldsymbol{\Theta}\left(\boldsymbol{f}^0 + t\boldsymbol{h}_2\right) + \boldsymbol{\Theta}\left(\boldsymbol{f}^0\right) = o(t) \tag{III.A.41}$$

for two arbitrary vectors of increments $\boldsymbol{h}_1$ and $\boldsymbol{h}_2$ that have the same form (and the same number of components) as $\boldsymbol{h}$. We shall henceforth assume that these conditions are indeed satisfied by $\boldsymbol{\Theta}\left(\boldsymbol{f}\right)$, so that the G-differential $\delta\boldsymbol{\Theta}\left(\boldsymbol{f}^0; \boldsymbol{h}\right)$ can be considered henceforth to be linear in $\boldsymbol{h}$. In this case, therefore, $\delta\boldsymbol{\Theta}\left(\boldsymbol{f}^0; \boldsymbol{h}\right)$ becomes the total G-derivative $D\boldsymbol{\Theta}\left(\boldsymbol{f}^0; \boldsymbol{h}\right)$ of $\boldsymbol{\Theta}\left(\boldsymbol{f}\right)$ at $\boldsymbol{f}^0$, and can be written as

$$\begin{aligned} D\boldsymbol{\Theta}\left(\boldsymbol{f}^0; \boldsymbol{h}\right) = {} & \boldsymbol{\Theta}'_u\left(\boldsymbol{f}^0\right)\boldsymbol{h}_u + \left[\boldsymbol{\Theta}'_v\left(\boldsymbol{f}^0\right) + \boldsymbol{\Theta}'_a\left(\boldsymbol{f}^0\right)\boldsymbol{a}'_v\left(\boldsymbol{f}^0\right)\right]\boldsymbol{h}_v + \\ & \boldsymbol{\Theta}'_a\left(\boldsymbol{f}^0\right)\left[\boldsymbol{a}'_\beta\left(\boldsymbol{f}^0\right)\boldsymbol{h}_\beta + \boldsymbol{a}'_b\left(\boldsymbol{f}^0\right)\boldsymbol{h}_b\right]. \end{aligned} \tag{III.A.42}$$

In the above expression, the quantities $\boldsymbol{\Theta}'_u(\boldsymbol{f}^0)$, $\boldsymbol{\Theta}'_v(\boldsymbol{f}^0)$, $\boldsymbol{\Theta}'_a(\boldsymbol{f}^0)$, denote the respective partial G-derivatives of $\boldsymbol{\Theta}(\boldsymbol{f})$ at $\boldsymbol{f}^0$, while $\boldsymbol{a}'_v(\boldsymbol{f}^0)$, $\boldsymbol{a}'_\beta(\boldsymbol{f}^0)$, and $\boldsymbol{a}'_b(\boldsymbol{f}^0)$ denote the respective partial G-derivatives of $\boldsymbol{a}(\boldsymbol{f})$ at $\boldsymbol{f}^0$.

As indicated by Eq. (III.A.42), the $(\boldsymbol{h}_u, \boldsymbol{h}_v)$-dependence in $D\boldsymbol{\Theta}(\boldsymbol{f}^0; \boldsymbol{h})$ is separated from the $(\boldsymbol{h}_\beta, \boldsymbol{h}_b)$-dependence. Furthermore, the 2-component column block-vector $\left[\boldsymbol{\Theta}'_u(\boldsymbol{f}^0),\ \boldsymbol{\Theta}'_v(\boldsymbol{f}^0) + \boldsymbol{\Theta}'_a(\boldsymbol{f}^0)\boldsymbol{a}'_v(\boldsymbol{f}^0)\right]^T$ (where "T" denotes "transposition") operates linearly on the vector $(\boldsymbol{h}_u, \boldsymbol{h}_v)^T$, which implies that $\left[\boldsymbol{\Theta}'_u(\boldsymbol{f}^0),\ \boldsymbol{\Theta}'_v(\boldsymbol{f}^0) + \boldsymbol{\Theta}'_a(\boldsymbol{f}^0)\boldsymbol{a}'_v(\boldsymbol{f}^0)\right]^T \in \mathscr{L}\left(\mathscr{H}_u \times \mathscr{H}_v, \mathscr{H}_{Raug}(\Omega_{Raug})\right)$. The *direct effect term* $\boldsymbol{\Theta}'_a(\boldsymbol{f}^0)\left[\boldsymbol{a}'_\beta(\boldsymbol{f}^0)\boldsymbol{h}_\beta + \boldsymbol{a}'_b(\boldsymbol{f}^0)\boldsymbol{h}_b\right]$ can be calculated directly at this stage. On the other hand, the quantity $\boldsymbol{\Theta}'_u(\boldsymbol{f}^0)\boldsymbol{h}_u + \left[\boldsymbol{\Theta}'_v(\boldsymbol{f}^0) + \boldsymbol{\Theta}'_a(\boldsymbol{f}^0)\boldsymbol{a}'_v(\boldsymbol{f}^0)\right]\boldsymbol{h}_v$ cannot be evaluated directly at this stage, since it depends on the unknown vector-valued function $(\boldsymbol{h}_u, \boldsymbol{h}_v)^T$, and is therefore called the *indirect effect term.*

To proceed with the evaluation of the indirect effect term $\left\{\boldsymbol{\Theta}'_u(\boldsymbol{f}^0)\boldsymbol{h}_u + \left[\boldsymbol{\Theta}'_v(\boldsymbol{f}^0) + \boldsymbol{\Theta}'_a(\boldsymbol{f}^0)\boldsymbol{a}'_v(\boldsymbol{f}^0)\right]\boldsymbol{h}_v\right\} \in \mathscr{H}_{Raug}(\Omega_{Raug})$, we consider that the orthonormal set $\{\boldsymbol{\theta}_s\}_{s\in\mathscr{S}}$, where s runs through an index set $\mathscr{S}$, is an orthonormal basis of $\mathscr{H}_{Raug}(\Omega_{Raug})$. Therefore, the indirect effect term $\boldsymbol{\Theta}'_u(\boldsymbol{f}^0)\boldsymbol{h}_u + \left[\boldsymbol{\Theta}'_v(\boldsymbol{f}^0) + \boldsymbol{\Theta}'_a(\boldsymbol{f}^0)\boldsymbol{a}'_v(\boldsymbol{f}^0)\right]\boldsymbol{h}_v$ can be represented as the Fourier series

$$\boldsymbol{\Theta}'_u(\boldsymbol{f}^0)\boldsymbol{h}_u + \left[\boldsymbol{\Theta}'_v(\boldsymbol{f}^0) + \boldsymbol{\Theta}'_a(\boldsymbol{f}^0)\boldsymbol{a}'_v(\boldsymbol{f}^0)\right]\boldsymbol{h}_v = \sum_{s\in\mathscr{S}} \left\langle \boldsymbol{\Theta}'_u(\boldsymbol{f}^0)\boldsymbol{h}_u + \left[\boldsymbol{\Theta}'_v(\boldsymbol{f}^0) + \boldsymbol{\Theta}'_a(\boldsymbol{f}^0)\boldsymbol{a}'_v(\boldsymbol{f}^0)\right]\boldsymbol{h}_v,\ \boldsymbol{\theta}_s \right\rangle_{Raug} \boldsymbol{\theta}_s \,. \tag{III.A.43}$$

The notation $\sum_{s\in\mathscr{S}}$ is used to signify that in the above sum only an at most countable number of elements are different from zero, and the series extended upon the nonzero elements converges unconditionally. According to customary terminology, the functionals $\left\langle \boldsymbol{\Theta}'_u(\boldsymbol{f}^0)\boldsymbol{h}_u + \left[\boldsymbol{\Theta}'_v(\boldsymbol{f}^0) + \boldsymbol{\Theta}'_a(\boldsymbol{f}^0)\boldsymbol{a}'_v(\boldsymbol{f}^0)\right]\boldsymbol{h}_v, \boldsymbol{\theta}_s \right\rangle_{Raug}$ are called the Fourier coefficients with respect to the basis $\{\boldsymbol{\theta}_s\}$. It follows from Eq. (III.A. 42) that these functionals are linear in $(\boldsymbol{h}_u, \boldsymbol{h}_v)^T$.

The next step is to express each of the functionals $\left\langle \boldsymbol{\Theta}'_u\left(\boldsymbol{f}^0\right)\boldsymbol{h}_u + \left[\boldsymbol{\Theta}'_v\left(\boldsymbol{f}^0\right) + \boldsymbol{\Theta}'_a\left(\boldsymbol{f}^0\right)\boldsymbol{a}'_v\left(\boldsymbol{f}^0\right)\right]\boldsymbol{h}_v,\ \ \boldsymbol{\theta}_s \right\rangle_{Raug}$ as an inner product of $\left(\boldsymbol{h}_u, \boldsymbol{h}_v\right)^T$ with a uniquely defined vector in $\mathcal{H}_u \times \mathcal{H}_v$, which remains to be determined. Recalling that $\left[\boldsymbol{\Theta}'_u\left(\boldsymbol{f}^0\right), \boldsymbol{\Theta}'_v\left(\boldsymbol{f}^0\right) + \boldsymbol{\Theta}'_a\left(\boldsymbol{f}^0\right)\boldsymbol{a}'_v\left(\boldsymbol{f}^0\right)\right]^T \in \mathcal{L}\left(\mathcal{H}_u \times \mathcal{H}_v, \mathcal{H}_{Raug}\left(\Omega_{Raug}\right)\right)$, it follows that we can define the linear operator $\boldsymbol{\Pi}\left(\boldsymbol{f}^0\right) \in \mathcal{L}\left(\mathcal{H}_{Raug}\left(\Omega_{Raug}\right), \mathcal{H}_u \times \mathcal{H}_v\right)$ to be the adjoint of $\left[\boldsymbol{\Theta}'_u\left(\boldsymbol{f}^0\right), \boldsymbol{\Theta}'_v\left(\boldsymbol{f}^0\right) + \boldsymbol{\Theta}'_a\left(\boldsymbol{f}^0\right)\boldsymbol{a}'_v\left(\boldsymbol{f}^0\right)\right]^T \in \mathcal{L}\left(\mathcal{H}_u \times \mathcal{H}_v, \mathcal{H}_{Raug}\left(\Omega_{Raug}\right)\right)$, by means of the relationship

$$\begin{aligned} &\left\langle \left[\boldsymbol{\Theta}'_u\left(\boldsymbol{f}^0\right) \quad \boldsymbol{\Theta}'_v\left(\boldsymbol{f}^0\right) + \boldsymbol{\Theta}'_a\left(\boldsymbol{f}^0\right)\boldsymbol{a}'_v\left(\boldsymbol{f}^0\right)\right]\begin{pmatrix}\boldsymbol{h}_u \\ \boldsymbol{h}_v\end{pmatrix},\ \ \boldsymbol{\theta}_s \right\rangle_R \\ &= \left\langle \boldsymbol{\Pi}\left(\boldsymbol{f}^0\right)\boldsymbol{\theta}_s,\ \begin{pmatrix}\boldsymbol{h}_u \\ \boldsymbol{h}_v\end{pmatrix} \right\rangle_{u\times v}, \quad s \in \mathcal{S}. \end{aligned} \tag{III.A.44}$$

The operator $\boldsymbol{\Pi}\left(\boldsymbol{e}^0\right)$ is actually a two-component operator (with components of dimensions equal to the vectors $\boldsymbol{h}_u$ and $\boldsymbol{h}_v$, respectively), and is unique if $\boldsymbol{\Theta}'_u\left(\boldsymbol{f}^0\right)\boldsymbol{h}_u + \left[\boldsymbol{\Theta}'_v\left(\boldsymbol{f}^0\right) + \boldsymbol{\Theta}'_a\left(\boldsymbol{f}^0\right)\boldsymbol{a}'_v\left(\boldsymbol{f}^0\right)\right]\boldsymbol{h}_v$ is densely defined. The right-side of Eq. (III.A.44) can now be required to represent the same functional as the left-side of Eq. (III.A.40); this requirement yields the adjoint sensitivity system

$$\boldsymbol{L}_a^+\left(\boldsymbol{f}^0\right)\begin{pmatrix}\boldsymbol{\psi}_u^s \\ \boldsymbol{\psi}_v^s\end{pmatrix} \equiv \begin{pmatrix}\boldsymbol{L}_{11}^+\left(\boldsymbol{f}^0\right) & \boldsymbol{L}_{12}^+\left(\boldsymbol{f}^0\right) \\ \boldsymbol{L}_{21}^+\left(\boldsymbol{f}^0\right) & \boldsymbol{L}_{22}^+\left(\boldsymbol{f}^0\right)\end{pmatrix}\begin{pmatrix}\boldsymbol{\psi}_u^s \\ \boldsymbol{\psi}_v^s\end{pmatrix} = \boldsymbol{\Pi}\left(\boldsymbol{f}^0\right)\boldsymbol{\theta}_s, \quad s \in \mathcal{S}, \tag{III.A.45}$$

which holds uniquely in view of the Riesz representation theorem. Note that the superscript s has been used to indicate the particular adjoint functions that are solutions of Eq. (III.A.45). This last step completes the construction of the Adjoint Sensitivity System, which consists of Eq. (III.A.45) and boundary conditions given in Eq. (III.A.38) for the adjoint function $\left(\boldsymbol{\psi}_u^s, \boldsymbol{\psi}_v^s\right)^T$. Furthermore, Eqs. (III.A.40), (III.A.42), (III.A.43), and (III.A.44) can now be used to obtain the following expression for the sensitivity $D\boldsymbol{\Theta}\left(\boldsymbol{f}^0; \boldsymbol{h}\right)$ of $\boldsymbol{\Theta}(\boldsymbol{f})$ at $\boldsymbol{f}^0$:

$$D\boldsymbol{\Theta}\left(\boldsymbol{f}^0;\boldsymbol{h}\right)=\boldsymbol{\Theta}'_a\left(\boldsymbol{f}^0\right)\left[\boldsymbol{a}'_\beta\left(\boldsymbol{f}^0\right)\boldsymbol{h}_\beta+\boldsymbol{a}'_b\left(\boldsymbol{f}^0\right)\boldsymbol{h}_b\right]+$$
$$\sum_{s\in\mathcal{S}}\theta_s\left[-\hat{\boldsymbol{P}}\left(\boldsymbol{f}^0;\boldsymbol{\psi}_u^s,\boldsymbol{\psi}_v^s;\boldsymbol{h}_\beta,\boldsymbol{h}_b\right)+\right.$$
$$\left.\left\langle\begin{pmatrix}\boldsymbol{\psi}_u^s\\ \boldsymbol{\psi}_v^s\end{pmatrix}^T,\begin{pmatrix}\left[\boldsymbol{Q}'_a\left(\boldsymbol{f}^0\right)-\boldsymbol{N}'_a\left(\boldsymbol{f}^0\right)\right]\boldsymbol{a}'_\beta\left(\boldsymbol{f}^0\right) & \left[\boldsymbol{Q}'_a\left(\boldsymbol{f}^0\right)-\boldsymbol{N}'_a\left(\boldsymbol{f}^0\right)\right]\boldsymbol{a}'_b\left(\boldsymbol{f}^0\right)\\ 0 & \boldsymbol{S}'_b\left(\boldsymbol{b}^0\right)-\boldsymbol{M}'_b\left(\boldsymbol{f}^0\right)\end{pmatrix}\begin{pmatrix}\boldsymbol{h}_\beta\\ \boldsymbol{h}_b\end{pmatrix}\right\rangle_{q\times S}\right]. \tag{III.A.46}$$

As Eq. (III.A.46) indicates, the desired elimination of all unknown values of $(\boldsymbol{h}_u,\boldsymbol{h}_v)^T$ from the expression of the sensitivity $D\boldsymbol{\Theta}\left(\boldsymbol{f}^0;\boldsymbol{h}\right)$ of $\boldsymbol{\Theta}(\boldsymbol{f})$ at $\boldsymbol{f}^0$ has thus been accomplished. To evaluate the sensitivity $D\boldsymbol{\Theta}\left(\boldsymbol{f}^0;\boldsymbol{h}\right)$ by means of Eq. (III.A.46), one needs to compute as many adjoint functions $\left(\boldsymbol{\psi}_u^s,\boldsymbol{\psi}_v^s\right)^T$, $(s=1,2,\ldots)$, using Eqs. (III.A.45) and (III.A.38) as there are nonzero terms in the representation of $\boldsymbol{\Theta}'_u\left(\boldsymbol{f}^0\right)\boldsymbol{h}_u+\left[\boldsymbol{\Theta}'_v\left(\boldsymbol{f}^0\right)+\boldsymbol{\Theta}'_a\left(\boldsymbol{f}^0\right)\boldsymbol{a}'_v\left(\boldsymbol{f}^0\right)\right]\boldsymbol{h}_v$ given in Eq. (III.A.43). Although the linear combination of basis elements $\boldsymbol{p}_s$ given in Eq. (III.A.43) may, in principle, contain infinitely many terms, only a finite number of the corresponding adjoint functions $\left(\boldsymbol{\psi}_u^s,\boldsymbol{\psi}_v^s\right)^T$ can be calculated in practice. Therefore, special attention is required to select the Hilbert space $\mathcal{H}_{R^{aug}}\left(\Omega_{R^{aug}}\right)$, the orthonormal basis $\{\theta_s\}_{s\in\mathcal{S}}$ for this space, and a notion of convergence for the representation given in Eq. (III.A.43) to best suit the problem at hand. This selection is guided by the need to represent the indirect effect term $\boldsymbol{\Theta}'_u\left(\boldsymbol{f}^0\right)\boldsymbol{h}_u+\left[\boldsymbol{\Theta}'_v\left(\boldsymbol{f}^0\right)+\boldsymbol{\Theta}'_a\left(\boldsymbol{f}^0\right)\boldsymbol{a}'_v\left(\boldsymbol{f}^0\right)\right]\boldsymbol{h}_v$ as accurately as possible with the smallest number of basis elements; a related consideration is the viability of deriving bounds and/or asymptotic expressions for the remainder after truncating Eq. (III.A.43) to the first few terms.

III.A.2.c System Responses: Functionals

In the important practical case when the space $\mathcal{E}_{R^{aug}}$ is the underlying scalar field $\mathcal{F}$ of real numbers, the response defined in Eq. (III.A.26) becomes a nonlinear functional of the form $\Theta(\boldsymbol{f}):\mathcal{D}_{R^{aug}}\subset\mathcal{E}_{aug}\to\mathcal{F}$, and the sensitivity $\delta\Theta\left(\boldsymbol{f}^0;\boldsymbol{h}\right)$ also becomes a functional that takes values in $\mathcal{F}$. Furthermore, it will be assumed that the response $\Theta(\boldsymbol{e})$ satisfies a weak Lipschitz condition at $\boldsymbol{f}^0$ and also satisfies the relation shown in Eq. (III.A.41), so that the linear (in $\boldsymbol{h}$)

G-differential $D\Theta\left(\boldsymbol{f}^0;\boldsymbol{h}\right)$ exists. In this case, the summation $\sum_{s\in\mathcal{S}}$ shown in Eq. (III.A.43) for the indirect effect term $\Theta'_u\left(\boldsymbol{f}^0\right)\boldsymbol{h}_u + \left[\Theta'_v\left(\boldsymbol{f}^0\right) + \Theta'_a\left(\boldsymbol{f}^0\right)\boldsymbol{a}'_v\left(\boldsymbol{f}^0\right)\right]\boldsymbol{h}_v$ reduces to a single term $(s=1)$; the subscript s can therefore be omitted in the sequel. Furthermore, the Riesz representation theorem ensures that there exists a unique 2-component vector $\left[\nabla_u\Theta\left(\boldsymbol{f}^0\right),\ \nabla_v\Theta\left(\boldsymbol{f}^0\right)\right]^T \in \mathcal{U}_u \times \mathcal{U}_v$, where the respective components are defined via the relationship

$$
\begin{aligned}
&\Theta'_u\left(\boldsymbol{f}^0\right)\boldsymbol{h}_u + \left[\Theta'_v\left(\boldsymbol{f}^0\right) + \Theta'_a\left(\boldsymbol{f}^0\right)\boldsymbol{a}'_v\left(\boldsymbol{f}^0\right)\right]\boldsymbol{h}_v = \\
&\left\langle \left[\nabla_u R\left(\boldsymbol{f}^0\right) \quad \nabla_u R\left(\boldsymbol{f}^0\right)\right], \begin{pmatrix}\boldsymbol{h}_u \\ \boldsymbol{h}_v\end{pmatrix} \right\rangle_{u\times v}, \quad \boldsymbol{h}_u \in \mathcal{U}_u, \boldsymbol{h}_v \in \mathcal{U}_v \\
&\nabla_u\Theta\left(\boldsymbol{f}^0\right) \equiv \left[\Theta'_u\left(\boldsymbol{f}^0\right)\right]^T \in \mathcal{U}_u, \\
&\nabla_v\Theta\left(\boldsymbol{f}^0\right) \equiv \left[\left[\Theta'_v\left(\boldsymbol{f}^0\right) + \Theta'_a\left(\boldsymbol{f}^0\right)\boldsymbol{a}'_v\left(\boldsymbol{f}^0\right)\right]\right]^T \in \mathcal{U}_v.
\end{aligned}
\tag{III.A.47}
$$

Comparison of Eq. (III.A.47) and Eq. (III.A.44) reveals that Eq. (III.A.45) becomes

$$
\boldsymbol{L}_a^+\left(\boldsymbol{f}^0\right)\begin{pmatrix}\boldsymbol{\psi}_u \\ \boldsymbol{\psi}_v\end{pmatrix} \equiv \begin{pmatrix} \boldsymbol{L}_{11}^+\left(\boldsymbol{f}^0\right) & \boldsymbol{L}_{12}^+\left(\boldsymbol{f}^0\right) \\ \boldsymbol{L}_{21}^+\left(\boldsymbol{f}^0\right) & \boldsymbol{L}_{22}^+\left(\boldsymbol{f}^0\right)\end{pmatrix}\begin{pmatrix}\boldsymbol{\psi}_u \\ \boldsymbol{\psi}_v\end{pmatrix} = \begin{pmatrix}\nabla_u R\left(\boldsymbol{f}^0\right) \\ \nabla_v R\left(\boldsymbol{f}^0\right)\end{pmatrix}. \tag{III.A.48}
$$

Furthermore, the expression for response sensitivity $D\Theta\left(\boldsymbol{f}^0;\boldsymbol{h}\right)$, cf. Eq. (III.A.46) reduces to

$$
\begin{aligned}
&D\Theta\left(\boldsymbol{f}^0;\boldsymbol{h}\right) = \Theta'_a\left(\boldsymbol{f}^0\right)\left[\boldsymbol{a}'_\beta\left(\boldsymbol{f}^0\right)\boldsymbol{h}_\beta + \boldsymbol{a}'_b\left(\boldsymbol{f}^0\right)\boldsymbol{h}_b\right] - \hat{\boldsymbol{P}}\left(\boldsymbol{f}^0;\boldsymbol{\psi}_u,\boldsymbol{\psi}_v;\boldsymbol{h}_\beta,\boldsymbol{h}_b\right) + \\
&\left\langle \begin{pmatrix}\boldsymbol{\psi}_u \\ \boldsymbol{\psi}_v\end{pmatrix}^T, \begin{pmatrix} \left[\boldsymbol{Q}'_a\left(\boldsymbol{f}^0\right) - \boldsymbol{N}'_a\left(\boldsymbol{f}^0\right)\right]\boldsymbol{a}'_\beta\left(\boldsymbol{f}^0\right) & \left[\boldsymbol{Q}'_a\left(\boldsymbol{f}^0\right) - \boldsymbol{N}'_a\left(\boldsymbol{f}^0\right)\right]\boldsymbol{a}'_b\left(\boldsymbol{f}^0\right) \\ 0 & \boldsymbol{S}'_b\left(\boldsymbol{b}^0\right) - \boldsymbol{M}'_b\left(\boldsymbol{f}^0\right)\end{pmatrix}\begin{pmatrix}\boldsymbol{h}_\beta \\ \boldsymbol{h}_b\end{pmatrix} \right\rangle_{q\times S}.
\end{aligned}
\tag{III.A.49}
$$

Thus, once the single calculation to determine the adjoint function $(\boldsymbol{\psi}_u,\boldsymbol{\psi}_v)^T$ from Eqs. (III.A.48) and (III.A.38) has been carried out, the adjoint function $(\boldsymbol{\psi}_u,\boldsymbol{\psi}_v)^T$ can be used in Eq. (III.A.49) to obtain efficiently the sensitivity $D\Theta\left(\boldsymbol{f}^0;\boldsymbol{h}\right)$ of $\Theta(\boldsymbol{f})$.

III.A.3. Discussion: Constructing the Augmented Adjoint Sensitivity Model from the Original Adjoint Sensitivity Model and Viceversa

In practice, when the *ASAP* is applied successively to the various component modules of a complex code system, the practitioner first develops an adjoint sensitivity model of the form described by Eq. (III.A.18), and then augments the adjoint operator $\boldsymbol{L}^{+}\left(\boldsymbol{e}^{0}\right)$ to construct the augmented adjoint operator $\boldsymbol{L}_{\boldsymbol{a}}^{+}\left(\boldsymbol{f}^{0}\right)$ defined in Eq. (III.A.37); for convenience, the form of $\boldsymbol{L}_{\boldsymbol{a}}^{+}\left(\boldsymbol{f}^{0}\right)$ is reproduced below:

$$\boldsymbol{L}_{\boldsymbol{a}}^{+}\left(\boldsymbol{f}^{0}\right)\equiv\begin{pmatrix}\boldsymbol{L}_{11}^{+}\left(\boldsymbol{f}^{0}\right) & \boldsymbol{L}_{12}^{+}\left(\boldsymbol{f}^{0}\right)\\ \boldsymbol{L}_{21}^{+}\left(\boldsymbol{f}^{0}\right) & \boldsymbol{L}_{22}^{+}\left(\boldsymbol{f}^{0}\right)\end{pmatrix}\equiv$$
$$\begin{pmatrix}\left[\boldsymbol{N}_{u}'\left(\boldsymbol{f}^{0}\right)\right]^{+}+\left\{\left[\boldsymbol{N}_{a}'\left(\boldsymbol{f}^{0}\right)-\boldsymbol{Q}_{a}'\left(\boldsymbol{f}^{0}\right)\right]\boldsymbol{a}_{u}'\left(\boldsymbol{f}^{0}\right)\right\}^{+} & \left[\boldsymbol{M}_{u}'\right]^{+}\\ \left\{\left[\boldsymbol{N}_{a}'\left(\boldsymbol{f}^{0}\right)-\boldsymbol{Q}_{a}'\left(\boldsymbol{f}^{0}\right)\right]\boldsymbol{a}_{v}'\left(\boldsymbol{f}^{0}\right)\right\}^{+} & \left[\boldsymbol{M}_{v}'\right]^{+}\end{pmatrix}. \qquad \text{(III.A.37)}$$

From a programmer's point of view, the adjoint operator $\boldsymbol{L}_{11}^{+}\left(\boldsymbol{f}^{0}\right)\equiv\left[\boldsymbol{N}_{u}'\left(\boldsymbol{f}^{0}\right)\right]^{+}+\left\{\left[\boldsymbol{N}_{a}'\left(\boldsymbol{f}^{0}\right)-\boldsymbol{Q}_{a}'\left(\boldsymbol{f}^{0}\right)\right]\boldsymbol{a}_{u}'\left(\boldsymbol{f}^{0}\right)\right\}^{+}$ can be formally constructed by starting from the adjoint operator $\boldsymbol{L}^{+}\left(\boldsymbol{e}^{0}\right)\equiv\left[\boldsymbol{N}_{u}'\left(\boldsymbol{u}^{0},\boldsymbol{\alpha}^{0}\right)\right]^{+}$ of the original (nonaugmented) system, and then adding the operator $\left\{\left[\boldsymbol{N}_{a}'\left(\boldsymbol{f}^{0}\right)-\boldsymbol{Q}_{a}'\left(\boldsymbol{f}^{0}\right)\right]\boldsymbol{a}_{u}'\left(\boldsymbol{f}^{0}\right)\right\}^{+}$. This is because the numerical representation of the operator $\left[\boldsymbol{N}_{u}'\left(\boldsymbol{f}^{0}\right)\right]^{+}$ is the same as that of $\left[\boldsymbol{N}_{u}'\left(\boldsymbol{u}^{0},\boldsymbol{\alpha}^{0}\right)\right]^{+}$; the fact that these two operators are then evaluated at distinct nominal parameter values clearly plays an important role in the solution evaluation, but not in the initial construction/programming of $\boldsymbol{L}_{11}^{+}\left(\boldsymbol{f}^{0}\right)$. Of course, the adjoint operators $\boldsymbol{L}_{12}^{+}\left(\boldsymbol{f}^{0}\right)$, $\boldsymbol{L}_{21}^{+}\left(\boldsymbol{f}^{0}\right)$, and $\boldsymbol{L}_{22}^{+}\left(\boldsymbol{f}^{0}\right)$ are specific to the augmented system, and must therefore be constructed/programmed *ab initio*.

Often, the adjoint sensitivity system for the augmented system can be solved by using the same numerical methods as used for solving the nonaugmented adjoint system, particularly when the numerical representation of the matrix operator $\boldsymbol{L}_{\boldsymbol{a}}^{+}\left(\boldsymbol{f}^{0}\right)$ can be inverted by partitioning. Of course, if the off-diagonal operators $\boldsymbol{L}_{12}^{+}\left(\boldsymbol{f}^{0}\right)$ and/or $\boldsymbol{L}_{21}^{+}\left(\boldsymbol{f}^{0}\right)$ vanish, then the inversion of $\boldsymbol{L}_{\boldsymbol{a}}^{+}\left(\boldsymbol{f}^{0}\right)$ becomes significantly simpler.

The inverse route, namely going from the augmented system to the nonaugmented one, is quite easy, simply by setting the operators $\boldsymbol{L}_{12}^{+}\left(\boldsymbol{f}^{0}\right)$,

$\boldsymbol{L}_{21}^{+}\left(\boldsymbol{f}^{0}\right)$, and $\boldsymbol{L}_{22}^{+}\left(\boldsymbol{f}^{0}\right)$ to zero. In this case, Eq. (III.A.46) also reduces to Eq. (III.A.19), as would be expected.

The above features can be highlighted by considering that the nonaugmented system is represented by the simple algebraic system discussed in Volume I, Section IV.C, namely a response of the form

$$R = \boldsymbol{c}^{T}\boldsymbol{u}, \tag{III.A.50}$$

where the superscript "T" denotes, as usual, "transposition," and $\boldsymbol{u}$ is the solution of the system of linear simultaneous equations

$$\boldsymbol{A}\boldsymbol{u} = \boldsymbol{b}. \tag{III.A.51}$$

In the above equations, the $n \times n$ matrix $\boldsymbol{A} = \left(a_{ij}\right), \left(i, j = 1, \ldots, n\right)$, together with the vectors $\boldsymbol{b} = \left(b_1, \ldots, b_n\right)$ and $\boldsymbol{c} = \left(c_1, \ldots, c_n\right)$, are considered to stem from experiments and/or calculations, so they are not known exactly. As is often the case in practice, only the respective nominal (i.e., mean) values $\boldsymbol{A}^{0} = \left(a_{ij}^{0}\right), \left(i, j = 1, \ldots, n\right)$, $\boldsymbol{b}^{0} = \left(b_1^{0}, \ldots, b_n^{0}\right)$, $\boldsymbol{c}^{0} = \left(c_1^{0}, \ldots, c_n^{0}\right)$, and the respective uncertainties are known. In principle, the response R can represent either the result of an indirect measurement or the result of a calculation. (As usual, all vectors are considered to be column vectors.)

The nominal solution $\boldsymbol{u}^{0}$ is obtained by solving Eq. (III.A.51) for the nominal parameter values $\boldsymbol{A}^{0}$ and $\boldsymbol{b}^{0}$:

$$\boldsymbol{A}^{0}\boldsymbol{u}^{0} = \boldsymbol{b}^{0}. \tag{III.A.52}$$

In turn, the nominal solution $\boldsymbol{u}^{0}$ is used together with the nominal parameter values $\boldsymbol{c}^{0}$ to calculate the nominal value, R^{0}, of the response by using Eq. (III.A.50), to obtain

$$R^{0} = \left(\boldsymbol{c}^{0}\right)^{T}\boldsymbol{u}^{0}. \tag{III.A.53}$$

As usual, the response sensitivities are obtained by computing the Gâteaux variation δR of the response R at the point $\left(\boldsymbol{A}^{0}, \boldsymbol{x}^{0}, \boldsymbol{b}^{0}\right)$ along the directions $\left(\delta\boldsymbol{A}, \boldsymbol{h}_u, \delta\boldsymbol{b}\right)$. Using the definition

$$\left\{\frac{d}{d\varepsilon}\left[\left(R^{0} + \varepsilon\delta R\right) - \left(\boldsymbol{c}^{0} + \varepsilon\delta\boldsymbol{c}\right)\left(\boldsymbol{u}^{0} + \varepsilon\boldsymbol{h}_u\right)\right]\right\}_{\varepsilon=0} = \boldsymbol{0}$$

yields the relation

$$\delta R = \left(\boldsymbol{c}^0\right)^T \boldsymbol{h}_u + \left(\delta \boldsymbol{c}\right)^T \boldsymbol{u}^0 . \tag{III.A.54}$$

The quantity $\left(\delta \boldsymbol{c}\right)^T \boldsymbol{u}^0$ is the "direct effect" term, which can be computed already at this stage. On the other hand, the quantity $\left(\boldsymbol{c}^0\right)^T \boldsymbol{h}_u$ is the "indirect effect" term, which can be computed only after determining the vector $\boldsymbol{h}_u$. In turn, $\boldsymbol{h}_u$ is obtained by solving the Gâteaux-differentiated Eq. (III.A.51), namely

$$\left\{\frac{d}{d\varepsilon}\left[\left(\boldsymbol{A}^0 + \varepsilon\delta\boldsymbol{A}\right)\left(\boldsymbol{u}^0 + \varepsilon\boldsymbol{h}_u\right) - \left(\boldsymbol{b}^0 + \varepsilon\delta\boldsymbol{b}\right)\right]\right\}_{\varepsilon=0} = \boldsymbol{0},$$

or, equivalently,

$$\boldsymbol{A}^0\boldsymbol{h}_u = \delta\boldsymbol{b} - \left(\delta\boldsymbol{A}\right)\boldsymbol{u}^0 . \tag{III.A.55}$$

The quantity $\boldsymbol{h}_u$ can be obtained by noting that Eq. (III.A.55) can be solved by using the same amount of effort as required to solve the base-case system, Eq. (III.A.52), since it involves inverting (directly or iteratively) the matrix $\boldsymbol{A}^0$ once only. However, if any of the elements of $\left(\delta\boldsymbol{A}\right)$ and $\delta\boldsymbol{b}$ would be modified, Eq. (III.A.55) would need to be solved anew. In practice, solving Eq. (III.A.55) repeatedly becomes impractical for large systems with many parameters, because of the large computational resources required by such repeated calculations. As has been already noted, such computationally intensive requirements limit the practical usefulness of the *FSAP*.

The alternative procedure, which avoids the need for solving Eq. (III.A.55) repeatedly, is the *Adjoint Sensitivity Analysis Procedure (ASAP).* The *ASAP* relies on constructing and using the hermitian adjoint matrix to $\boldsymbol{A}^0$, as follows:

1. Introduce an *n*-component vector $\boldsymbol{\psi} = \left(\psi_1, \ldots, \psi_n\right)$, and form the inner (scalar) product of $\boldsymbol{\psi}$ with Eq. (III.A.55) to obtain

$$\left\langle \boldsymbol{\psi},\, \boldsymbol{A}^0\boldsymbol{h}_u \right\rangle = \left\langle \boldsymbol{\psi},\, \delta\boldsymbol{b} - \left(\delta\boldsymbol{A}\right)\boldsymbol{u}^0 \right\rangle. \tag{III.A.56}$$

2. Since the hermitian adjoint of $\boldsymbol{A}^0$ is simply its transpose, $\left(\boldsymbol{A}^0\right)^+$, we transpose the left side of Eq. (III.A.54) to obtain

$$\left\langle \boldsymbol{\psi},\, \boldsymbol{A}^0 \boldsymbol{h}_u \right\rangle = \left\langle \delta \mathbf{x},\, \left(\boldsymbol{A}^0\right)^+ \boldsymbol{\psi} \right\rangle. \tag{III.A.57}$$

3. Since the vector $\boldsymbol{\psi}$ is still arbitrary at this stage, it is possible to specify it by identifying the right side of Eq. (III.A.57) with the first term on the right side of Eq. (III.A.54), to obtain

$$\left(\boldsymbol{A}^0\right)^+ \boldsymbol{\psi} = \boldsymbol{c}^0. \tag{III.A.58}$$

4. Collecting now the results of Eqs. (III.A.54-58) yields the following succession of equalities:

$$\left\langle \boldsymbol{\psi},\, \delta \boldsymbol{b} - (\delta \boldsymbol{A})\boldsymbol{u}^0 \right\rangle = \left\langle \boldsymbol{h}_u,\, \left(\boldsymbol{A}^0\right)^+ \boldsymbol{\psi} \right\rangle = \left(\boldsymbol{c}^0\right)^T \boldsymbol{h}_u = \delta R - (\delta \boldsymbol{c})^T \boldsymbol{u}^0. \tag{III.A.59}$$

5. Retaining the first and the last terms in Eq. (III.A.59) yields the expression

$$\delta R = (\delta \boldsymbol{c})^T \boldsymbol{x}^0 + \left\langle \boldsymbol{\psi},\, \delta \boldsymbol{b} - (\delta \boldsymbol{A})\boldsymbol{u}^0 \right\rangle, \tag{III.A.60}$$

where the vector $\boldsymbol{\psi}$ is the solution of Eq. (III.A.58). Since the matrix $\left(\boldsymbol{A}^0\right)^+$ is the hermitian adjoint of $\boldsymbol{A}^0$, Eq. (III.A.58) is called the *adjoint sensitivity equation,* and the vector $\boldsymbol{\psi}$ is called the *adjoint function*.

Consider now that the augmented system is

$$\boldsymbol{A}\boldsymbol{u} + \boldsymbol{B}_{12}\boldsymbol{v} = \boldsymbol{Q}_u \tag{III.A.61}$$

$$\boldsymbol{B}_{21}\boldsymbol{u} + \boldsymbol{B}_{22}\boldsymbol{v} = \boldsymbol{Q}_v \tag{III.A.62}$$

while the augmented response is

$$\Theta = \boldsymbol{c}^T \boldsymbol{u} + \boldsymbol{d}^T \boldsymbol{v}. \tag{III.A.63}$$

Note that the nominal solution $\left(\boldsymbol{u}^0, \boldsymbol{v}^0\right)$ of Eqs. (III.A.61) and (III.A.62) would clearly have different values from the nominal solution (denoted by $\boldsymbol{u}^0$) of Eq. (III.A.52). Often, the augmented system represented by Eqs. (III.A.61) and (III.A.62) can be solved by partitioning, particularly when the matrix $\boldsymbol{B}_{22}^0$ is not singular. In such cases, the solution can be computed from the matrix equation

$$\left(\boldsymbol{A}-\boldsymbol{B}_{12}\boldsymbol{B}_{22}^{-1}\boldsymbol{B}_{21}\right)\boldsymbol{u}^0=\boldsymbol{Q}_u-\boldsymbol{B}_{12}\boldsymbol{B}_{22}^{-1}\boldsymbol{Q}_v \tag{III.A.64}$$

requiring the inversion of the matrix $\left(\boldsymbol{A}-\boldsymbol{B}_{12}\boldsymbol{B}_{22}^{-1}\boldsymbol{B}_{21}\right)$, which is of the same size as the matrix $\boldsymbol{A}$ for the nonaugmented system. Often, therefore, it is possible to solve the augmented system by applying the same methods as used for solving the nonaugmented system.

The sensitivity $\delta\Theta$ of the response Θ is given by the G-differential of Eq. (III.A.63), namely

$$\delta\Theta=(\delta\boldsymbol{c})^T\boldsymbol{u}^0+(\delta\boldsymbol{d})^T\boldsymbol{v}^0+\left(\boldsymbol{c}^0\right)^T\boldsymbol{h}_u+\left(\boldsymbol{d}^0\right)^T\boldsymbol{h}_v, \tag{III.A.65}$$

where the vector $(\boldsymbol{h}_u,\boldsymbol{h}_v)$ is the solution of the forward sensitivity system (or tangent linear model)

$$\boldsymbol{A}^0\boldsymbol{h}_u+\boldsymbol{B}_{12}^0\boldsymbol{h}_v=\delta\boldsymbol{Q}_u-(\delta\boldsymbol{A})\boldsymbol{u}^0-(\delta\boldsymbol{B}_{12})\boldsymbol{v}^0 \tag{III.A.66}$$

$$\boldsymbol{B}_{21}^0\boldsymbol{h}_u+\boldsymbol{B}_{22}^0\boldsymbol{h}_v=\delta\boldsymbol{Q}_v-(\delta\boldsymbol{B}_{21})\boldsymbol{u}^0-(\delta\boldsymbol{B}_{22})\boldsymbol{v}^0. \tag{III.A.67}$$

The adjoint sensitivity system that corresponds to Eqs. (III.A.66) and (III.A.67) is derived by following the procedure outlined in Section III.A.2. This procedure leads to

$$\left(\boldsymbol{A}^0\right)^T\boldsymbol{\psi}_u+\left(\boldsymbol{B}_{21}^0\right)^T\boldsymbol{\psi}_v=\boldsymbol{c}^0 \tag{III.A.68}$$

$$\left(\boldsymbol{B}_{12}^0\right)^T\boldsymbol{\psi}_u+\left(\boldsymbol{B}_{22}^0\right)^T\boldsymbol{\psi}_v=\boldsymbol{d}^0 \tag{III.A.69}$$

where the vector $(\boldsymbol{\psi}_u,\boldsymbol{\psi}_v)$ represents the adjoint function that corresponds to $(\boldsymbol{h}_u,\boldsymbol{h}_v)$. In term of this adjoint function, the sensitivity $\delta\Theta$ of the response Θ becomes

$$\begin{aligned}\delta\Theta=&(\delta\boldsymbol{c})^T\boldsymbol{u}^0+(\delta\boldsymbol{d})^T\boldsymbol{v}^0+(\boldsymbol{\psi}_u)^T\left[\delta\boldsymbol{Q}_u-(\delta\boldsymbol{A})\boldsymbol{u}^0-(\delta\boldsymbol{B}_{12})\boldsymbol{v}^0\right]\\&+(\boldsymbol{\psi}_v)^T\left[\delta\boldsymbol{Q}_v-(\delta\boldsymbol{B}_{21})\boldsymbol{u}^0-(\delta\boldsymbol{B}_{22})\boldsymbol{v}^0\right].\end{aligned} \tag{III.A.70}$$

It is apparent from Eqs. (III.A.68) and (III.A.69) that the solution of the adjoint requires inversion of the same matrices as required for computing the nominal solution of the augmented system. Therefore, Eqs. (III.A.68) and (III.A.69) can be solved by using the same algorithms as used for solving Eqs. (III.A.61) and (III.A.62). It is important to note, though, that this simplification occurs only when the underlying systems (nonaugmented and augmented) are linear, as has been the case for the simple illustrative example presented above.

III. B. ILLUSTRATIVE EXAMPLE: ASAP FOR THE COUPLED TWO-FLUID WITH HEAT STRUCTURES MODEL IN RELAP5/MOD3.2 (REL/TF+HS)

This Section presents the application of the *ASAP* for augmented systems to the complete fluid dynamics/heat structure packages of the large-scale simulation code RELAP5/MOD3.2. Thus, based on the general theory presented in Section III.A, this Section illustrate how the adjoint sensitivity model corresponding to the two-fluid model in RELAP5/MOD3.2 (which was the subject of Chapter II) is to be augmented with the adjoint sensitivity model corresponding to the heat structure models in RELAP5/MOD3.2. Section III.B.1, below, presents the derivation of the adjoint sensitivity model for the heat structures, which is then coupled to (i.e., augmented with) the adjoint sensitivity model for the two-fluid package, ASM-REL/TF, which was derived in Section II. B. The resulting system of augmented matrix equations is denoted as the ASM-REL/TFH. Subsequently, Section III.B.2 presents illustrative sensitivity analysis results obtained by applying the augmented adjoint sensitivity model, ASM-REL/TFH, to the analysis of the QUENCH-04 experiment performed at the Research Center Karlsruhe (FZK).

III.B.1. ASM-REL/TFH: The Augmented Two-Fluid/Heat Structure Adjoint Sensitivity Model

As has been described in Section II.B, the two-fluid model in RELAP5/MOD3.2 consists of a system of nine coupled nonlinear partial differential equations describing the conservation of mass, momentum, and energy for the liquid and gaseous phases, including noncondensable materials in the gaseous phase and boron concentration in the liquid field. Corresponding to these nine equations, there are nine state (i.e., dependent) variables, as follows: the gas specific internal energy, U_g, the fluid specific internal energy, U_f, the void fraction, α_g, the pressure, P, the total noncondensable mass fraction, X_n, the noncondensable mass fraction for the i-th noncondensable species, X_{ni}, the boron density, ρ_b, the gas velocity, v_g, and the fluid velocity, v_f. The nine field equations are re-arranged into the so-called "Numerically Convenient Set of Differential Equations," which are then solved numerically by using a staggered spatial mesh and either a semi-implicit or a nearly-implicit integration procedure in time.

Heat structures in RELAP5 permit calculation of the heat transferred across solid boundaries of hydrodynamic volumes. Modeling capabilities of heat structures include fuel pins or plates with nuclear or electrical heating, heat transfer across steam generator tubes, and heat transfer from pipe and vessel

walls. In RELAP5, the heat structures are represented by one-dimensional conduction in rectangular, cylindrical, or spherical geometry. Temperature-dependent thermal conductivities and volumetric heat capacities are provided in tabular or functional form, either from built-in or user supplied data. The time-dependence of the heat source can be obtained from reactor point-kinetics, tables of power versus time, or a control variable. Boundary conditions include symmetry or insulated conditions, a correlation package, tables of surface temperature versus time, heat transfer rate versus time, and a heat transfer coefficient versus time or surface temperature. The heat transfer correlation package can be used for heat structure surfaces connected to hydrodynamic volumes, and contains correlations for convective, nucleate (and transition boiling) and film boiling heat transfer from the wall to water, and reverse transfer from the water to wall (including condensation). The coefficients that enter in these correlations, as well as the coefficients describing the initial and boundary conditions for the heat conduction equations for the respective structures (and for the two-fluid equations, too) are parameters to be investigated as part of a comprehensive sensitivity analysis.

The heat conduction equations for the heat structures together with the respective initial conditions and boundary conditions (which couple the heat transfer through the structures to the two-fluid model) are discretized by using finite difference methods. For each heat structure H_s, $[(s=1,\ldots,NH)$, NH = total number of heat structures], connected to a hydrodynamic volume L (located between hydrodynamic junctions j and $j+1$), the discretization procedure yields the following matrix equation:

$$(AS)_s^n \begin{bmatrix} T_{s1} \\ T_{s2} \\ \\ T_{sM-1} \\ T_{sM} \end{bmatrix}^{n+1} = \begin{bmatrix} hd_1^n \\ hd_2^n \\ \\ hd_{M-1}^n \\ hd_M^n \end{bmatrix}, \qquad \text{(III.B.1)}$$

where the matrix $(AS)_s^n$ is defined as

$$(AS)_s^n \equiv \begin{bmatrix} hb_1^n & hc_1^n & & & \\ ha_2^n & hb_2^n & hc_2^n & & \\ & \cdots & \cdots & \cdots & \\ & & ha_{M-1}^n & hb_{M-1}^n & hc_{M-1}^n \\ & & & ha_M^n & hb_M^n \end{bmatrix},$$

and where, for each heat structure s, the dependent variables are the surface temperatures, $T_{s,i}^n$, at the spatial mesh-point index $(i = 1, \ldots, M_s)$ (M_s denotes the maximum number of mesh points for structure s), and at the time-step index $(n = 1, \ldots, NF)$ (NF denotes the final time-step).

The components of the matrix $(AS)_s^n$ and the components of the right-side of Eq. (III.B.1) have the following functional dependencies:

(i) for the left boundary:

$$\begin{aligned} &hb_1^n\left(P_L^n, U_g^n, U_f^n, \alpha_g^n, X_n^n, v_{g,j}^n, v_{g,j+1}^n, v_{f,j}^n, v_{f,j+1}^n, T_{s,1}^n, T_{s,2}^n\right), \\ &hc_1^n\left(P_L^n, T_{s,1}^n, T_{s,2}^n\right), \\ &hd_1^n\left(P_L^n, U_g^n, U_f^n, \alpha_g^n, X_n^n, v_{g,j}^n, v_{g,j+1}^n, v_{f,j}^n, v_{f,j+1}^n, T_{s,1}^n, T_{s,2}^n\right), \end{aligned} \tag{III.B.2}$$

(ii) for each interior mesh-point $(i = 2, \ldots, M_s - 1)$:

$$\begin{aligned} &ha_i^n\left(P_L^n, T_{s,i-1}^n, T_{s,i}^n, T_{s,i+1}^n\right), \\ &hb_i^n\left(P_L^n, U_g^n, U_f^n, \alpha_g^n, X_n^n, v_{g,j}^n, v_{g,j+1}^n, v_{f,j}^n, v_{f,j+1}^n, T_{s,i-1}^n, T_{s,i}^n, T_{s,i+1}^n\right), \\ &hc_i^n\left(P_L^n, T_{s,i-1}^n, T_{s,i}^n, T_{s,i+1}^n\right), \\ &hd_i^n\left(P_L^n, U_g^n, U_f^n, \alpha_g^n, X_n^n, v_{g,j}^n, v_{g,j+1}^n, v_{f,j}^n, v_{f,j+1}^n, T_{s,i-1}^n, T_{s,i}^n, T_{s,i+1}^n\right). \end{aligned} \tag{III.B.3}$$

(iii) for the right boundary:

$$\begin{aligned} &ha_M^n\left(P_L^n, T_{s,M-1}^n, T_{s,M}^n\right), \\ &hb_M^n\left(P_L^n, U_g^n, U_f^n, \alpha_g^n, X_n^n, v_{g,j}^n, v_{g,j+1}^n, v_{f,j}^n, v_{f,j+1}^n, T_{s,M-1}^n, T_{s,M}^n\right), \\ &hd_M^n\left(P_L^n, U_g^n, U_f^n, \alpha_g^n, X_n^n, v_{g,j}^n, v_{g,j+1}^n, v_{f,j}^n, v_{f,j+1}^n, T_{s,M-1}^n, T_{s,M}^n\right). \end{aligned} \tag{III.B.4}$$

Note that the above quantities also depend on heat structure parameters (e.g., coefficients that enter in the heat transfer correlations, coefficients describing the initial and boundary conditions for the heat conduction equations, etc.), but this fact has not been shown explicitly, in order to keep the notation as simple as possible. For the mathematical derivations to follow below, the heat structure parameters will be denoted simply as p_i, $(i = 1, ..., MP_s;\ s = 1, ..., NH)$. The initial conditions for the surface temperatures for a structure s will be denoted as $T_{s,i}^0 \ (i = 1, \ldots, M_s)$.

The next step is to derive the forward sensitivity system (or linear tangent model) for the RELAP-heat structures, which is done by taking the G-derivative

of Eq. (III.B.1). Using the convenient notation $\delta T_{s,i}^{n} \equiv \tau_{s,i}^{n}$ and denoting the parameter variations by δp_i, the G-derivative of Eq. (III.B.1) can be written compactly in the form

$$u_{s,i}^{n-1}\tau_{s,i-1}^{n-1} + w_{s,i}^{n-1}\tau_{s,i}^{n-1} + x_{s,i+1}^{n-1}\tau_{s,i+1}^{n-1} + (ha)_{s,i}^{n-1}\tau_{s,i-1}^{n} + (hb)_{s,i}^{n-1}\tau_{s,i}^{n} + (hc)_{s,i}^{n-1}\tau_{s,i+1}^{n} + \sum_{\nu=1}^{MTF}\sum_{k=1}^{NV}\left(e_{s,i,k}^{\nu}\right)^{n-1}\left(X_k^{\nu}\right)^{n-1} = SH_{s,i}^{n-1}. \tag{III.B.5}$$

The following definitions have been used in the above equation:

$$u_{s,i}^{n-1} \equiv \frac{\partial\left(ha_{s,i}^{n-1}\right)}{\partial T_{s,i-1}^{n-1}}T_{s,i-1}^{n} + \frac{\partial\left(hb_{s,i}^{n-1}\right)}{\partial T_{s,i-1}^{n-1}}T_{s,i}^{n} + \frac{\partial\left(hc_{s,i}^{n-1}\right)}{\partial T_{s,i-1}^{n-1}}T_{s,i+1}^{n} - \frac{\partial\left(hd_{s,i}^{n-1}\right)}{\partial T_{s,i-1}^{n-1}},$$

$$w_{s,i}^{n-1} \equiv \frac{\partial\left(ha_{s,i}^{n-1}\right)}{\partial T_{s,i}^{n-1}}T_{s,i-1}^{n} + \frac{\partial\left(hb_{s,i}^{n-1}\right)}{\partial T_{s,i}^{n-1}}T_{s,i}^{n} + \frac{\partial\left(hc_{s,i}^{n-1}\right)}{\partial T_{s,i}^{n-1}}T_{s,i+1}^{n} - \frac{\partial\left(hd_{s,i}^{n-1}\right)}{\partial T_{s,i}^{n-1}},$$

$$x_{s,i}^{n-1} \equiv \frac{\partial\left(ha_{s,i}^{n-1}\right)}{\partial T_{s,i+1}^{n-1}}T_{s,i-1}^{n} + \frac{\partial\left(hb_{s,i}^{n-1}\right)}{\partial T_{s,i+1}^{n-1}}T_{s,i}^{n} + \frac{\partial\left(hc_{s,i}^{n-1}\right)}{\partial T_{s,i+1}^{n-1}}T_{s,i+1}^{n} - \frac{\partial\left(hd_{s,i}^{n-1}\right)}{\partial T_{s,i+1}^{n-1}},$$

$$\left(e_{s,i,k}^{\nu}\right)^{n-1} \equiv \frac{\partial\left(ha_{s,i}^{n-1}\right)}{\partial\left(TF_k^{\nu}\right)^{n-1}}T_{s,i-1}^{n} + \frac{\partial\left(hb_{s,i}^{n-1}\right)}{\partial\left(TF_k^{\nu}\right)^{n-1}}T_{s,i}^{n} + \frac{\partial\left(hc_{s,i}^{n-1}\right)}{\partial\left(TF_k^{\nu}\right)^{n-1}}T_{s,i+1}^{n} - \frac{\partial\left(hd_{s,i}^{n-1}\right)}{\partial\left(TF_k^{\nu}\right)^{n-1}},$$

$$sh_{s,i}^{n-1} \equiv \sum_{j=1}^{MP_s}\frac{\partial}{\partial p_j}\left[-\left(ha_{s,i}^{n-1}\right)T_{s,i-1}^{n} - \left(hb_{s,i}^{n-1}\right)T_{s,i}^{n} - \left(hc_{s,i}^{n-1}\right)T_{s,i+1}^{n} + \left(hd_{s,i}^{n-1}\right)\right]\delta p_j,$$

where $\left(TF_k^{\nu}\right)^{n}$ denotes the ν-th two-fluid dependent variable, at a junction or a volume k, at time n, and where $(s=1,\ldots,NH, i=1,\ldots,M_s)$. Note also that $(ha)_{s,1}^{n-1} \equiv 0$ and $(hc)_{s,M}^{n-1} \equiv 0$. The variations in initial conditions are denoted as $\delta T_{s,i}^{0}$.

Equation (III.B.5) can be written in matrix form as

$$(US)_s^{n-1}\tau_s^{n-1} + (AS)_s^{n-1}\tau_s^{n} + \sum_{\nu=1}^{MTF}\left(ES_s^{\nu}\right)^{n-1}\left(X^{\nu}\right)^{n-1} = FS_s^{n-1}, (s=1,...,NH), \tag{III.B.6}$$

by using the following definitions:

$$\begin{bmatrix} \tau_{s,1}^n \\ \vdots \\ \vdots \\ \vdots \\ \tau_{s,M_s}^n \end{bmatrix} \equiv \tau_s^n ; \begin{bmatrix} sh_{s,1}^n \\ \vdots \\ \vdots \\ \vdots \\ sh_{s,M_s}^n \end{bmatrix} \equiv SH_s^n , \quad (s = 1,...,NH);$$

$$\begin{bmatrix} w_{s,1}^n & x_{s,1}^n & & & & \\ u_{s,2}^n & w_{s,2}^n & x_{s,2}^n & & & \\ \cdots & \cdots & \cdots & \cdots & \cdots & \\ & & u_{s,M_s-1}^n & w_{s,M_s-1}^n & x_{s,M_s-1}^n & \\ & & & u_{s,M_s}^n & w_{s,M_s}^n & \end{bmatrix} \equiv (US)_s^n$$

$$\begin{bmatrix} \left(e_{s,1,1}^{\nu}\right)^n & \left(e_{s,1,2}^{\nu}\right)^n & & & \left(e_{s,1,NV}^{\nu}\right)^n \\ \left(e_{s,2,1}^{\nu}\right)^n & \left(e_{s,2,2}^{\nu}\right)^n & & & \left(e_{s,2,NV}^{\nu}\right)^n \\ \cdots & \cdots & \cdots & \cdots & \cdots \\ \left(e_{s,M_s,1}^{\nu}\right)^n & \left(e_{s,M_s,2}^{\nu}\right)^n & & & \left(e_{s,M_s,NV}^{\nu}\right)^n \end{bmatrix} \equiv \left(ES_s^{\nu}\right)^n .$$

Recalling from Section II.B the definitions

$$X^n \equiv \begin{bmatrix} \left(X^1\right)^n \\ \vdots \\ \left(X^{MTF}\right)^n \end{bmatrix} \text{ and } X_I^{(n)} \equiv \begin{bmatrix} Z_1^n \\ \vdots \\ Z_{M_2}^n \end{bmatrix},$$

and introducing in Eq. (III.B.6) the partitioned vectors and diagonal block matrices defined as

$$US^{n-1} \equiv diag\left[(US)_s^{n-1}\right], \quad AS^{n-1} \equiv diag\left[(AS)_s^{n-1}\right], \quad ES^{n-1} \equiv diag\left[(ES)_s^{n-1}\right],$$
$$(s = 1,...,NH)$$

$$\tau^n \equiv \begin{bmatrix} \tau_1^n \\ \vdots \\ \tau_{NH}^n \end{bmatrix}, \quad F_3^{n-1} \equiv \begin{bmatrix} FS_1^{n-1} \\ \vdots \\ FS_{NH}^{n-1} \end{bmatrix},$$

makes it possible to write Eq. (III.B.6) in the compact form

$$AS^{n-1}\tau^n + US^{n-1}\tau^{n-1} + ES^{n-1}X^{n-1} = F_3^{n-1}. \qquad \text{(III.B.7)}$$

Equation (III.B.7) represents the forward sensitivity system (or the linear tangent model) corresponding to the heat structure package in RELAP5/MOD3.2. Next, Eq. (III.B.7) will be augmented to (i.e., coupled with) the forward sensitivity system for the two-fluid model, which was derived in Section II.B [cf. Eq. (II.B.33) et seq.], by using the theoretical derivations generally presented in Section III.A. This leads to the following matrix form for the augmented two-fluid/heat structures forward sensitivity system:

$$\begin{bmatrix} B_1^{n-1} & T_1^{n-1} & NGQ_1^{n-1} \\ B_2^{n-1} & T_2^{n-1} & NGQ_2^{n-1} \\ 0 & 0 & AS^{n-1} \end{bmatrix} \begin{bmatrix} X^n \\ X_I^n \\ \tau^n \end{bmatrix} + \begin{bmatrix} C_1^{n-1} & 0 & OGQ_1^{n-1} \\ C_2^{n-1} & 0 & OGQ_2^{n-1} \\ ES^{n-1} & 0 & US^{n-1} \end{bmatrix} \begin{bmatrix} X^{n-1} \\ X_I^{n-1} \\ \tau^{n-1} \end{bmatrix} = \begin{bmatrix} F_1^{n-1} \\ F_2^{n-1} \\ F_3^{n-1} \end{bmatrix}, \tag{III.B.8}$$

where the block-matrices NGQ_1^{n-1}, NGQ_2^{n-1}, OGQ_1^{n-1}, and OGQ_2^{n-1} represent the additional (off-diagonal) contributions that result from taking the partial G-derivative of the two-fluid equations with respect to the surface temperatures $T_{s,i}^n$.

It is convenient to eliminate from Eq. (III.B.8) the vector $X_I^{(n)}$ of variations in the two-fluid "intermediate variables." For this purpose, Eq. (III.B.8) is written in component form as:

$$B_1^{n-1}X^n + T_1^{n-1}X_I^n + NGQ_1^{n-1}\tau^n + C_1^{n-1}X^{n-1} + OGQ_1^{n-1}\tau^{n-1} = F_1^{n-1} \tag{III.B.9a}$$

$$B_2^{n-1}X^n + T_2^{n-1}X_I^n + NGQ_2^{n-1}\tau^n + C_2^{n-1}X^{n-1} + OGQ_2^{n-1}\tau^{n-1} = F_2^{n-1} \tag{III.B.9b}$$

$$AS^{n-1}\tau^n + ES^{n-1}X^{n-1} + US^{n-1}\tau^{n-1} = F_3^{n-1}. \tag{III.B.9c}$$

As was shown in Section II.B, the matrix T_2^{n-1} is always nonsingular; therefore Eq. (III.B.9b) can be used to obtain:

$$X_I^n = \left[T_2^{n-1}\right]^{-1}\left\{F_2^{n-1} - C_2^{n-1}X^{n-1} - B_2^{n-1}X^n - NGQ_2^{n-1}\tau^n - OGQ_2^{n-1}\tau^{n-1}\right\}.$$

Inserting the above equation in Eq. (III.B.9a) gives the expression

$$B_1^{n-1}X^n + T_1^{n-1}\left[T_2^{n-1}\right]^{-1}\left\{F_2^{n-1} - C_2^{n-1}X^{n-1} - B_2^{n-1}X^n - NGQ_2^{n-1}\tau^n - OGQ_2^{n-1}\tau^{n-1}\right\}$$
$$+ NGQ_1^{n-1}\tau^n + C_1^{n-1}X^{n-1} + OGQ_1^{n-1}\tau^{n-1} = F_1^{n-1},$$

which can be re-arranged in the form

$$G^{n-1}X^{n} + NT^{n-1}\tau^{n} + H^{n-1}X^{n-1} + OT^{n-1}\tau^{n-1} = K^{n-1}. \qquad \text{(III.B.10)}$$

In Eq. (III.B.10), the matrices G^{n-1}, H^{n-1}, and K^{n-1} are the same as previously defined for the two-fluid model, namely:

$$G^{(n-1)} \equiv B_1^{(n-1)} - T_1^{(n-1)}\left[T_2^{(n-1)}\right]^{-1} B_2^{(n-1)},$$
$$H^{(n-1)} \equiv C_1^{(n-1)} - T_1^{(n-1)}\left[T_2^{(n-1)}\right]^{-1} C_2^{(n-1)},$$
$$K^{(n-1)} \equiv F_1^{(n-1)} - T_1^{(n-1)}\left[T_2^{(n-1)}\right]^{-1} F_2^{(n-1)}$$

while the matrices NT^{n-1} and OT^{n-1} are defined as

$$NT^{(n-1)} \equiv NGQ_1^{(n-1)} - T_1^{(n-1)}\left[T_2^{(n-1)}\right]^{-1} NGQ_2^{(n-1)}$$
$$OT^{(n-1)} \equiv OGQ_1^{(n-1)} - T_1^{(n-1)}\left[T_2^{(n-1)}\right]^{-1} OGQ_2^{(n-1)}.$$

Equations (III.B.9c) and (III.B.10) are now written in a single block-matrix equation of the form

$$\begin{bmatrix} H^{n-1} & OT^{n-1} \\ ES^{n-1} & US^{n-1} \end{bmatrix}\begin{bmatrix} X^{n-1} \\ \tau^{n-1} \end{bmatrix} + \begin{bmatrix} G^{n-1} & NT^{n-1} \\ 0 & AS^{n-1} \end{bmatrix}\begin{bmatrix} X^{n} \\ \tau^{n} \end{bmatrix} = \begin{bmatrix} K^{n-1} \\ F_3^{n-1} \end{bmatrix}, \qquad \text{(III.B.11)}$$
$$(n = 1, \ldots, NF).$$

Introducing in Eq. (III.B.11) the augmented matrices:

$$HA^{n-1} \equiv \begin{bmatrix} H^{n-1} & OT^{n-1} \\ ES^{n-1} & US^{n-1} \end{bmatrix}; \quad GA^{n-1} \equiv \begin{bmatrix} G^{n-1} & NT^{n-1} \\ 0 & AS^{n-1} \end{bmatrix};$$
$$XA^{n} \equiv \begin{bmatrix} X^{n} \\ \tau^{n} \end{bmatrix}; \quad KA^{n-1} \equiv \begin{bmatrix} K^{n-1} \\ F_3^{n-1} \end{bmatrix},$$

makes it possible to write this system (of block matrix equations) in the compact form

$$(GA)(XA) = KA \qquad \text{(III.B.12)}$$

where

$$GA \equiv \begin{bmatrix} I_A & 0 & 0 & & 0 \\ HA^0 & GA^0 & 0 & & 0 \\ 0 & HA^1 & GA^1 & & 0 \\ \cdots & \cdots & \cdots & \cdots & \cdots \\ & & & HA^{NF-1} & GA^{NF-1} \end{bmatrix},$$

$$XA \equiv \begin{bmatrix} XA^0 \\ XA^1 \\ XA^2 \\ \vdots \\ XA^{NF} \end{bmatrix}, \quad KA \equiv \begin{bmatrix} KA^{init} \\ KA^0 \\ KA^1 \\ \vdots \\ KA^{NF-1} \end{bmatrix}.$$

Equation (III.B.12) represents the forward sensitivity system (i.e., tangent linear model) for the augmented (coupled) two-fluid/heat structures system. Note that Eq. (III.B.12) has the same structure as Eq. (II.B.35) of Section II.B, with the following correspondences between the two-fluid and, respectively, the augmented two-fluid/heat-structures models: $G^n \to GA^n$, $H^n \to HA^n$, $X^n \to XA^n$, and $K^n \to KA^n$ (the letter "*A*" is meant to indicate "augmented").

The adjoint sensitivity system for the augmented two-fluid/heat-structures system can now be constructed along the same line as detailed in Section II.B (for the nonaugmented adjoint sensitivity system, ASM-REL/TF). Thus, defining the augmented vectors

$$\Phi A \equiv \begin{bmatrix} \Phi A^0 \\ \vdots \\ \Phi A^{NF} \end{bmatrix}, \text{ with } \Phi A^n \equiv \begin{bmatrix} \Phi^n \\ \Psi^n \end{bmatrix}, \tag{III.B.13}$$

where Φ^n and Ψ^n are the adjoint functions corresponding to X^n and τ^n, respectively (and therefore have the same number of components as the X^n and τ^n). Furthermore, the source terms for the augmented adjoint sensitivity system are defined as

$$QA \equiv \begin{bmatrix} Q^0 \\ \vdots \\ Q^{NF} \end{bmatrix}, \text{ with } QA^n \equiv \begin{bmatrix} Q^n \\ QS^n \end{bmatrix}, \tag{III.B.14}$$

where Q^n and QS^n are the source terms corresponding to the two-fluid adjoint sensitivity system and, respectively, the adjoint sensitivity system for the heat

structures. Then, following the same procedure as that leading to Eq. (II.B.38) in Section II.B, we obtain the expression of the sensitivity DR, of a generic scalar system response R, in the form

$$DR = (\Phi A)^T (KA), \tag{III.B.15}$$

where: (i) the superscript T denotes "transposition," as usual; (ii) the block column vector (KA) contains the (Gateaux-) derivatives of the augmented two-fluid/heat structure equations with respect to all of the parameters that enter in these equations; and (iii) the adjoint function $(\Phi A)^T$ is the solution of the adjoint sensitivity system for the augmented two-fluid/heat structures system. The adjoint sensitivity system for the augmented two-fluid/heat structures system will henceforth be abbreviated the ASM-REL/TFH system. In block-matrix form, the ASM-REL/TFH can be written as

$$(GA)^T (\Phi A) = QA, \tag{III.B.16}$$

where the block column vector $(QA) \equiv \left[(QA)^0, \ldots, (QA)^{NF}\right]^T$ has components $(QA)^n \equiv \left[Q^n, QS^n\right]^T$, and where Q^n and $(QS)^n$ are the adjoint sources (which depend on the response under consideration) corresponding to the two-fluid and, respectively, heat-structures systems. Written in component form, Eq. (III.B.16) becomes

$$\begin{bmatrix} I_A & (HA^0)^T & 0 & \cdots & 0 & 0 \\ 0 & (GA^0)^T & (HA^1)^T & \cdots & 0 & 0 \\ 0 & 0 & (GA^1)^T & \cdots & 0 & 0 \\ \cdots & \cdots & \cdots & \cdots & \cdots & \cdots \\ 0 & 0 & 0 & \cdots & (GA^{NF-2})^T & (HA^{NF-1})^T \\ 0 & 0 & 0 & \cdots & 0 & (GA^{NF-1})^T \end{bmatrix} \begin{bmatrix} \Phi A^0 \\ \Phi A^1 \\ \Phi A^2 \\ \cdots \\ \Phi A^{NF-1} \\ \Phi A^{NF} \end{bmatrix} = \begin{bmatrix} QA^0 \\ QA^1 \\ QA^2 \\ \cdots \\ QA^{NF-1} \\ QA^{NF} \end{bmatrix}, \tag{III.B.17}$$

where the components are themselves block-matrices of the form

$$HA^{n-1} \equiv \begin{bmatrix} H^{n-1} & OT^{n-1} \\ ES^{n-1} & US^{n-1} \end{bmatrix}; \quad GA^{n-1} \equiv \begin{bmatrix} G^{n-1} & NT^{n-1} \\ 0 & AS^{n-1} \end{bmatrix}; \quad (n = 1, \ldots, NF). \tag{III.B.18}$$

Recall, from Section II.B, that the block-matrices H^{n-1} and G^{n-1} stem from taking G-derivatives of the two-fluid equations with respect to the two-fluid dependent variables. Similarly, the block-matrices US^{n-1} and AS^{n-1} result from taking G-derivatives of the heat structure equations with respect to the heat structure dependent variables. Furthermore, the block-matrices OT^{n-1} and NT^{n-1} result from taking G-derivatives of the two-fluid equations with respect to the heat structures dependent variables. Finally, the block-matrix ES^{n-1} stems from taking G-derivatives of the heat structures equations with respect to the two-fluid dependent variables. Performing the block-matrix multiplications in Eq. (III.B.18) highlights the ASM-REL/TFH system's time-dependence, namely:

$$\begin{cases} \left[GA^{NF-1}\right]^T (\Phi A)^{NF} = (QA)^{NF}, \text{ for } n = NF; \\ \left[GA^{n-1}\right]^T (\Phi A)^{n} + \left[HA^{n}\right]^T (\Phi A)^{n+1} = (QA)^{n+1}, \text{ for } (n = NF-1,...,1); \\ (\Phi A)^{0} + \left[HA^{0}\right]^T (\Phi A)^{1} = (QA)^{1}, \text{ for } n = 0. \end{cases} \quad \text{(III.B.19)}$$

As indicated in Eq. (III.B.19), the ASM-REL/TFH equations are solved "backwards in time," commencing with the final time-step, $n = NF$, namely:

$$\begin{cases} \left(G^{NF-1}\right)^T \Phi^{NF} = Q^{NF}, \text{(two - fluid adjoint equation)}, \\ \left(AS^{NF-1}\right)^T \Psi^{NF} = QS^{NF} - \left(NT^{NF-1}\right)^T \Phi^{NF}, \text{ (adjoint equation} \\ \text{for heat structures, coupled to the eq. above).} \end{cases} \quad \text{(III.B.20)}$$

Usually, Q^{NF} and QS^{NF} are zero (due to the definition of the sensitivity DR of the response R), so that Φ^{NF} and Ψ^{NF} are usually zero.

As indicated in Eq. (III.B.19), the next set of adjoint equations to be solved backwards in time, for $n = NF-1,\ldots,1$, are

$$\begin{cases} \left(G^{n-1}\right)^T \Phi^{n} = Q^{n} - \left(H^{n}\right)^T \Phi^{n+1} - \left(ES^{n}\right)^T \Psi^{n+1}, \\ \left(AS^{n-1}\right)^T \Psi^{n} = QS^{n} - \left(NT^{n-1}\right)^T \Phi^{n} - \left(OT^{n}\right)^T \Phi^{n+1} - \left(US^{n}\right)^T \Psi^{n+1}, \end{cases} \quad \text{(III.B.21)}$$

for $(n = NF-1,...,1)$.

Note that the above equations fully couple the contributions from the two-fluid equations with those from the heat structure equations. Finally, the calculation of the ASM-REL/TFH is completed by solving the last adjoint equation in Eq. (III.B.19), for $n = 0$ namely:

$$\begin{cases} \Phi^0 = Q^0 - \left(H^0\right)^T \Phi^1 - \left(ES^0\right)^T \Psi^1, \\ \Psi^0 = QS^0 - \left(OT^1\right)^T \Phi^1 - \left(US^0\right)^T \Psi^1. \end{cases} \quad \text{for } n = 0. \qquad \text{(III.B.22)}$$

III.B.2. Summary Description of the QUENCH-04 Experiment

The most important accident management measure for terminating a postulated severe accident transient in a Light Water Reactor (LWR) is the re-flooding of the uncovered core with water. During the re-flooding process, though, the immediate consequence of the contact of water and/or steam with the core material is not the cooling of this material, as would be intuitively expected, but an enhanced oxidation of the Zircaloy fuel cladding, accompanied by an increase in temperature, hydrogen production, and fission product release. The physical and chemical processes underlying the release of hydrogen under the above circumstances are poorly known. The QUENCH Experimental Program at the Research Center Karlsruhe (FZK) aims at analyzing these processes leading to such hydrogen releases. The pre-test parameters for setting up the QUENCH experiments, and the post-test analysis and interpretation of the experimental results are partially performed with the RELAP5/MOD3.2 code system, using its two-fluid thermal-hydraulics and heat structure models. For both pre-test and post-test analyses, it is important to understand the sensitivities of measured and calculated results (such as temperature profiles, pressures, and hydrogen production) to parameters underlying the QUENCH experiment, including initial and boundary conditions, geometry, and material properties. The QUENCH experimental facility (L. Sepold et al., 2002) comprises the following component systems: a test section with fuel rod simulators; an electric power supply for heating the test bundle; a water and steam supply system; an argon-gas supply system; hydrogen measurement devices; a process control system; and a data acquisition system. The design characteristics of the test bundle are depicted in Fig. III.C.1, while a top-view of the fuel rod simulator bundle is presented in Fig. III.C.2. As Figure III.C.2 indicates, the test bundle includes four unheated corner rods and 21 fuel rod simulators, each of ca. $2.5\,m$ long. The positioning of the four corner rods helps to obtain a more uniform radial temperature profile; these rods are also used to determine the thickness of the axial oxide layer, at any given instance in time. The central fuel rod simulator is unheated, while the others rods can be heated electrically over a length of $1024\ mm$. The unheated rod is filled with solid ZrO_2 pellets, while the heated rods contain centrally located tungsten heaters surrounded by annular ZrO_2 pellets. All of the rods are clad with Zircaloy-4, identical in composition and size to that used in typical Pressurized Water Reactors (PWR), namely: $10.75\,mm$ outside diameter, and $0.725\,mm$ wall thickness. The rods are filled with a mixture of 95% argon and 5% krypton at approx. $0.22\,MPa$, just slightly above the pressure in the rest of

the test section. The krypton additive allows detection (using a mass spectrometer) of fuel rod failure during the experiment.

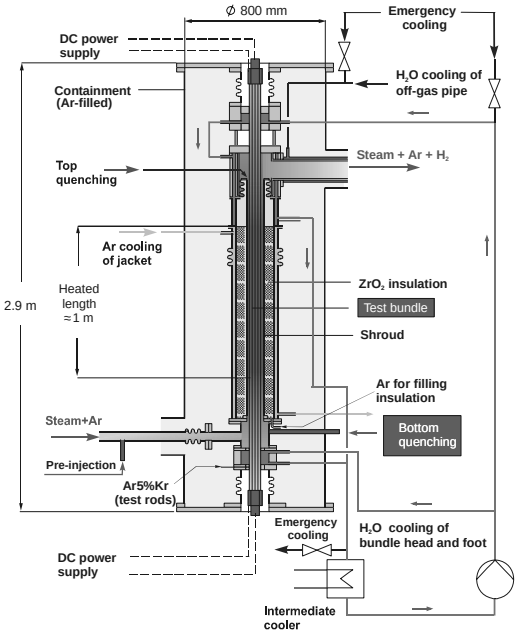

Figure III.C.1: Characteristic of the QUENCH Test Section.

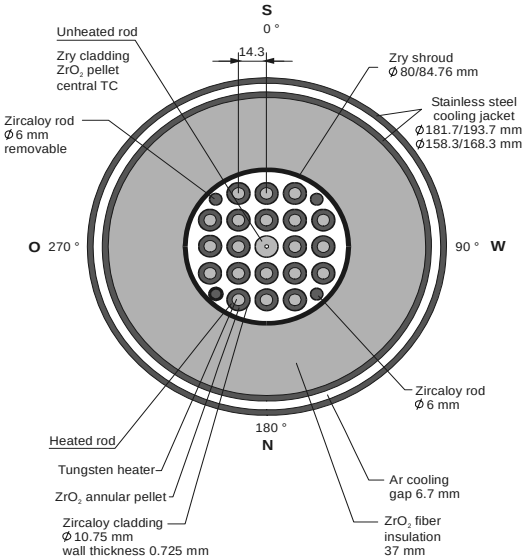

Figure III.C.2: Horizontal cross section of a QUENCH-04 Fuel Rod Simulator Bundle.

As shown in Fig.III.C.2, the test bundle is surrounded by a shroud made of Zircaloy (2.38 mm thickness), a fiber insulation of ZrO_2 (37 mm thickness), and an annular stainless steel cooling jacket. The 6.7 mm annulus of the cooling jacket is cooled by argon. To allow for higher radial heat losses, the ZrO_2 insulation extends axially only up to the 1024 mm elevation of the heated region. To reduce the magnitude of the maximum temperature in the axial direction, the top region of the cooling jacket is cooled by water.

In the QUENCH-04 experiment, the bundle was initially heated from room temperature to ca. 900 K, in an atmosphere of flowing argon (3 g/s) and steam (3 g/s). The bundle was stabilized at 900 K for about 2 hours, at an electrical power level of 4.3 kW. At the end of this stabilization period, the electrical power was increased so that the bundle was ramped at 0.31 W/s per rod, giving an average temperature increase of 0.35 K/s between 900 - 1400 K, and 1.0 K/s between 1400- 1750 K, respectively, until the power level reached 16.2 kW. Table III.C.1 presents the complete sequence of events in the QUENCH-04 experiment. The RELAP5/MOD 3.2 simulation of the QUENCH-04 experiment commenced with the initiation of the power transient and was terminated 1000 s (actual time) into the test transient in order to ensure that the physical phenomena during the respective time period did not exceed the code-system's capabilities to simulate them.

The augmented two-fluid/heat structure adjoint sensitivity model ASM-REL/TFH was validated by calculating sensitivities of various time-dependent temperatures in the test bundle to variations in various initial conditions for the Quench-04 experiment. Tables III.C.2 through III.C.4, below, present typical predictions using ASM-REL/TFH, along with comparisons with exact recalculations, for 1% variations in the initial conditions for the respective temperatures. As these tables indicate, the agreement between the ASM-REL/TFH results and the exact recalculations is very close; in turn, this close agreement indicates that the numerical solution of the coupled two-fluid/heat structure adjoint model, ASM-REL/TFH, is as robust, accurate, and stable as the nominal solution produced by the RELAP5/MOD 3.2 model.

The most important response for this experiment is the time evolution of the cladding temperature of heated fuel rod. There are 271 parameters which affect the cladding temperature; the most important 34 of these parameters (designated as α_1 through α_{34}) are listed in the Nomenclature, at the end of this Section. To illustrate the usefulness of the ASAP, Table III.C.5 presents only the largest relative sensitivities of the cladding temperature of the heated fuel rod at a height of 0.7 m (loop 1), at 1 s, 10 s, 50 s, 100 s, 200 s, 300 s, 500 s, and 800 s after the start of the transient power ramping. In addition to presenting relative sensitivities, Table III.C.5 also presents comparisons between the predicted results (computed by using the augmented adjoint sensitivity system, ASM-REL/TFH) and the exactly recomputed changes, for a perturbation of 1% in the

cladding temperature. These comparisons highlight the reliability and usefulness of the *ASAP* for computing sensitivity information, for tens of thousands of RELAP-time steps. The obtained sensitivities also illustrate the influence of nonlinear effects of parameter perturbations on the cladding temperature. Regarding their evolution in time, the relative sensitivities start out with relatively small absolute values, in the range from 10^{-3} to 10^{-4}, in the importance order $(\alpha_{19},\alpha_1,\alpha_6,\alpha_2,\alpha_{17},\alpha_{27},\alpha_{18})$; at $800\,s$ after initiation of the power ramp, the relative sensitivities attain values in the range from 10^{-1} to 10^{-2}, in the importance order $(\alpha_1,\alpha_6,\alpha_3,\alpha_4,\alpha_{13},\alpha_{12},\alpha_{19},\alpha_9,\alpha_{11})$. Additional sensitivity analysis results regarding the heated rods at the height of $0.7\,m$ are presented in Figure III.C.3, which depicts the time-evolution of the relative sensitivities of the inner ring heated rod at $0.7\,m$ to the most important parameters. Similar sensitivity analysis results are also presented in Figure III.C.4, which depicts the time-evolution of the relative sensitivities of the inner ring heated rod at a height of $1.3\,m$ to the most important parameters. Table III.C.6 presents the largest relative sensitivities of the cladding temperature of the heated fuel rod at 1.4m, where the power peak is located. Furthermore, Table III.C.7 presents the largest relative sensitivities of the inside temperature of the shroud (ZrO_2 fiber insulation) at the same location ($1.4\,m$), where the power peak is attained.

Table III.C.1
Quench-04 Sequence of Events.

Time [s]	Event
0	Start of data recording
90	Start of electric power transient
2012	Corner rod B withdrawn from the bundle (T ~ 1780 K)
2030	Begin of temperature escalation at the 750 mm level (1560 K) and at the 1050 mm level (1570 K)
2033	Begin of temperature escalation at the shroud (1050 mm, 1350 K)
2040	Begin of significant H_2 production, based on the mass spectrometer data
2065	Steam flow of 3 g/s turned off and cool-down steam turned on, cool-down steam at 42 g/s, strong temperature decrease at –250 mm
2088	16.2 kW of electric bundle power reached, start of electric power reduction from 16.2 kW to 4 kW
2103	Electric power of 4 kW reached
2302	Electric power shut off
2303	Cool-down steam flow turned off
2304	Steam flow at zero
2528	End of data recording

Table III.C.2
Comparisons of ASM-REL/TFH results with exact recalculations for the central temperature in the unheated fuel rod.

Perturbation	t (s)	No. of time steps	nominal value T_{nom} (K) at t = t_{final}	adjoint method (T_{pert}-T_{nom}) (K)	Exact Recalc. (T_{rec}-T_{nom}) (K)
1% of central temperature of the unheated rod at 0.075m	1	71	509.983	2.24750	2.252
	2	111	509.959	1.17470	1.178
	10	431	510.918	0.43609	0.436
	50	2031	516.452	0.40431	0.405
	100	4031	522.898	0.36920	0.370
	120	4831	525.339	0.35620	0.357
	150	6031	528.868	0.33772	0.338
	200	8031	534.435	0.30942	0.310
	300	12031	544.504	0.26095	0.261

Table III.C.3
Comparisons of ASM-REL/TFH results with exact recalculations for the temperatures in heated fuel rod.

Perturbation	t (s)	time steps	nominal value T_{nom} (K) at t = t_{final}	adjoint method T_{pert}-T_{nom} (K)	Exact Recalc. T_{rec}-T_{nom} (K)
1% of central temperature of the heated rod at 0.7m	1	71	740.015	5.45720	5.458
	2	111	740.075	4.10230	4.103
	10	431	742.562	0.92352	0.924
	50	2031	760.786	0.60792	0.608
	120	4831	789.881	0.53774	0.536
	150	6031	801.600	0.51035	0.508
	300	12031	864.215	0.39430	0.390
1% of cladding temperature of the heated rod at 0.7m	1	71	739.471	0.16926	0.169
	2	111	740.459	0.11829	0.118
	10	431	744.851	0.07277	0.073
	50	2031	762.938	0.06639	0.066
	300	12031	864.215	0.04309	0.043

It is beyond the purpose of this book to analyze in detail the physical meanings and implications of each of the sensitivities presented in Tables III.C.6 and Table III.C.7. Rather, the purpose of presenting these sensitivity analysis results is to illustrate the power, usefulness, and flexibility of the *ASAP*, which is actually the only practical method for exhaustive yet efficient sensitivity analysis of large-

scale systems. Sensitivity information such as provided by the *ASAP* could not have been obtained by other methods, because of prohibitive computational costs.

Table III.C.4
Comparisons of ASM-REL/TFH results with exact recalculations for the temperature in ZrO2-Insulation.

Perturbation	t (s)	time steps	nominal value T_{nom} (K) at t = t_{final}	adjoint method T_{pert}-T_{nom} (K)	Exact Recalculation T_{rec}-T_{nom} (K)
1% of temperature of ZrO_2 fiber insulation at 0.375m	1	71	575.410	0.25792	0.258
	2	111	575.353	0.14989	0.150
	10	431	574.717	0.05672	0.057
	50	2031	571.161	0.04914	0.049
	120	4831	566.360	0.03840	0.039
	300	12031	560.364	0.02024	0.021

Table III.C.5
Relative sensitivities of the cladding temperature of the heated fuel rod at 0.7m
Time $t = 1s$; nominal temperature $T_{nom} = 739.47K$.

Parameter	Relative Sensitivity	Perturbation	$T_{predicted} - T_{nom}$ (K)	$T_{recalculated} - T_{nom}$ (K)
α_{19}	1.403E-03	1% of cladding temperature of the heated rod at 0.7m	1.038E-02	1.130E-02
α_1	1.368E-03		1.013E-02	1.013E-02
α_6	1.368E-03		1.012E-02	1.013E-02
α_2	1.363E-03		1.009E-02	1.009E-02
α_{17}	-3.649E-04		-2.701E-03	-1.896E-03
α_{27}	-3.648E-04		-2.700E-03	-1.895E-03
α_{18}	-3.144E-04		-2.326E-03	-1.790E-03
α_{26}	-2.997E-04		-2.218E-03	-1.534E-03
α_{16}	-2.983E-04		-2.208E-03	-1.528E-03
α_{25}	-2.941E-04		-2.176E-03	-1.489E-03

Time $t = 10s$; nominal temperature $T_{nom} = 744.85K$:

Parameter	Relative Sensitivity	Perturbation	$T_{predicted} - T_{nom}$ (K)	$T_{recalculated} - T_{nom}$ (K)
α_1	1.098E-02	1% of cladding temperature of the heated rod at 0.7m	8.153E-02	8.156E-02
α_6	1.096E-02		8.139E-02	8.143E-02
α_2	1.049E-02		7.788E-02	7.791E-02
α_{19}	3.392E-03		2.519E-02	2.561E-02
α_{11}	-3.091E-03		-2.296E-02	-2.442E-02
α_8	-1.227E-03		-9.111E-03	-9.098E-03
α_{12}	-9.855E-04		-7.318E-03	-8.122E-03
α_3	4.910E-04		3.646E-03	3.647E-03
α_9	-4.140E-04		-3.074E-03	-3.074E-03
α_{10}	-3.108E-04		-2.308E-03	-1.626E-05

Time $t = 50s$; nominal temperature $T_{nom} = 762.94K$:

Parameter	Relative Sensitivity	Perturbation	$T_{predicted} - T_{nom}$ (K)	$T_{recalculated} - T_{nom}$ (K)
α_1	4.520E-02	1% of cladding temperature of the heated rod at 0.7m	3.439E-01	3.439E-01
α_6	4.494E-02		3.419E-01	3.420E-01
α_2	3.543E-02		2.695E-01	2.695E-01
α_{11}	-1.540E-02		-1.171E-01	-1.210E-01
α_{19}	1.233E-02		9.380E-02	9.442E-02
α_3	9.777E-03		7.438E-02	7.440E-02
α_{12}	-6.409E-03		-4.876E-02	-5.215E-02
α_8	-3.967E-03		-3.018E-02	-3.011E-02
α_9	-1.523E-03		-1.159E-02	-1.158E-02
α_{10}	-1.039E-03		-7.907E-03	-3.388E-04

Time $t = 100s$; nominal temperature $T_{nom} = 783.76K$:

Parameter	Relative Sensitivity	Perturbation	$T_{predicted} - T_{nom}$ (K)	$T_{recalculated} - T_{nom}$ (K)
α_1	8.288E-02	1% of cladding temperature of the heated rod at 0.7m	6.480E-01	6.475E-01
α_6	8.202E-02		6.413E-01	6.413E-01
α_2	4.713E-02		3.685E-01	3.680E-01
α_3	3.575E-02		2.795E-01	2.795E-01
α_{11}	-2.581E-02		-2.018E-01	-2.062E-01
α_{19}	2.370E-02		1.853E-01	1.862E-01
α_{12}	-1.415E-02		-1.106E-01	-1.176E-01
α_8	-6.444E-03		-5.038E-02	-5.023E-02
α_9	-2.847E-03		-2.226E-02	-2.224E-02
α_{10}	-1.704E-03		-1.332E-02	-1.145E-03

Time $t = 200s$; nominal temperature $T_{nom} = 823.46K$:

Parameter	Relative Sensitivity	Perturbation	$T_{predicted} - T_{nom}$ (K)	$T_{recalculated} - T_{nom}$ (K)
α_1	1.483E-01	1% of cladding temperature of the heated rod at 0.7m	1.218E+00	1.215E+00
α_6	1.455E-01		1.195E+00	1.194E+00
α_3	1.037E-01		8.522E-01	8.514E-01
α_{19}	4.651E-02		3.822E-01	3.835E-01
α_2	3.949E-02		3.245E-01	3.225E-01
α_{11}	-3.619E-02		-2.974E-01	-2.966E-01
α_{12}	-3.204E-02		-2.633E-01	-2.790E-01
α_8	-9.622E-03		-7.907E-02	-7.885E-02
α_9	-5.484E-03		-4.506E-02	-4.499E-02
α_4	5.053E-03		4.152E-02	4.155E-02

Time $t = 300s$; nominal temperature $T_{nom} = 866.03K$:

Parameter	Relative Sensitivity	Perturbation	$T_{predicted} - T_{nom}$ (K)	$T_{recalculated} - T_{nom}$ (K)
α_1	2.078E-01	1% of cladding temperature of the heated rod at 0.7m	1.795E+00	1.788E+00
α_6	2.023E-01		1.748E+00	1.746E+00
α_3	1.526E-01		1.319E+00	1.316E+00
α_{19}	6.890E-02		5.954E-01	5.973E-01
α_{12}	-5.511E-02		-4.762E-01	-5.040E-01
α_{11}	-3.746E-02		-3.237E-01	-3.090E-01
α_2	3.232E-02		2.793E-01	2.754E-01
α_4	2.279E-02		1.970E-01	1.972E-01
α_8	-1.163E-02		-1.005E-01	-1.002E-01
α_9	-8.484E-03		-7.331E-02	-7.321E-02

Time $t = 500s$; nominal temperature $T_{nom} = 958.70K$:

Parameter	Relative Sensitivity	Perturbation	$T_{predicted} - T_{nom}$ (K)	$T_{recalculated} - T_{nom}$ (K)
α_1	3.031E-01	1% of cladding temperature of the heated rod at 0.7m	2.899E+00	2.890E+00
α_6	2.888E-01		2.762E+00	2.764E+00
α_3	2.011E-01		1.924E+00	1.918E+00
α_{12}	-8.443E-02		-8.075E-01	-8.629E-01
α_4	8.084E-02		7.732E-01	7.772E-01
α_{19}	6.020E-02		5.757E-01	5.533E-01
α_{11}	-2.697E-02		-2.579E-01	-2.343E-01
α_2	2.116E-02		2.023E-01	1.956E-01
α_9	-1.495E-02		-1.430E-01	-1.436E-01
α_{13}	-1.270E-02		-1.215E-01	-1.288E-01

Time $t = 800s$; nominal temperature $T_{nom} = 1108.10K$:

Parameter	Relative Sensitivity	Perturbation	$T_{predicted} - T_{nom}$ (K)	$T_{recalculated} - T_{nom}$ (K)
α_1	3.872E-01	1% of cladding temperature of the heated rod at 0.7m	4.279E+00	4.232E+00
α_6	3.552E-01		3.926E+00	3.197E+00
α_3	1.971E-01		2.178E+00	2.136E+00
α_4	1.794E-01		1.983E+00	1.995E+00
α_{13}	-6.165E-02		-6.813E-01	-7.454E-01
α_{12}	-5.923E-02		-6.546E-01	-6.742E-01
α_{19}	2.816E-02		3.112E-01	2.818E-01
α_9	-2.101E-02		-2.321E-01	-2.321E-01
α_{11}	-1.897E-02		-2.096E-01	-1.559E-01
α_5	1.314E-02		1.453E-01	1.302E-01

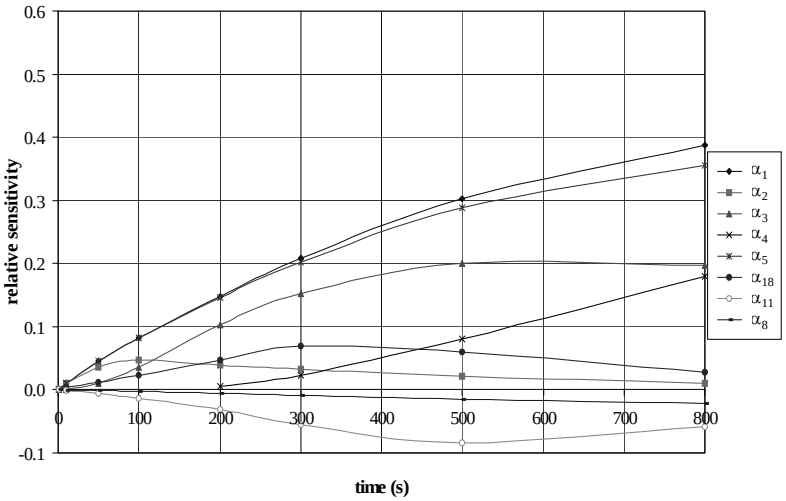

Figure III.C.3: Time-evolution of the relative sensitivities of the inner ring heated rod at 0.7m to the most important parameters.

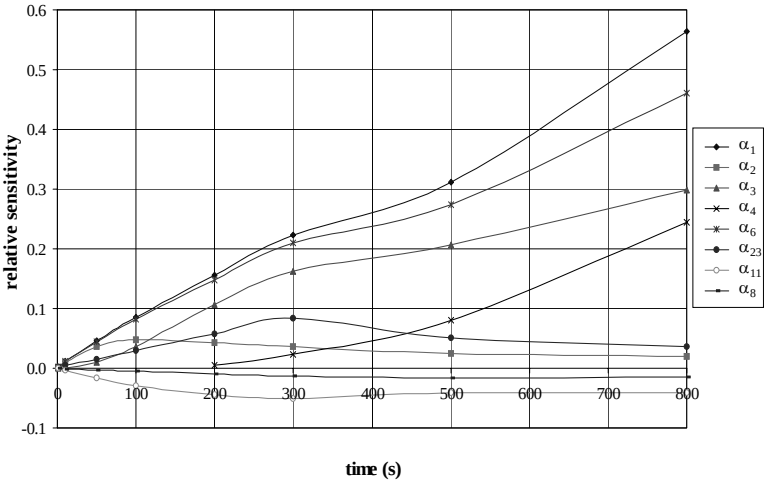

Figure III.C.4 Time-evolution of the relative sensitivities of the inner ring heated rod at 1.3m to the most important parameters.

Table III.C.6
Relative sensitivities of the cladding temperature of the heated fuel rod at 1.4m, where the power peak is located.

Param.	Rel. sens. at 10s	Param.	Rel. sens. at 100s	Param.	Rel. sens. at 500s	Param.	Rel. sens. At 800s
α_1	1.064E-02	α_1	8.217E-02	α_1	3.070E-01	α_1	5.689E-01
α_{28}	1.060E-02	α_{28}	8.002E-02	α_{28}	2.684E-01	α_{28}	4.566E-01
α_2	1.017E-02	α_2	4.703E-02	α_3	2.046E-01	α_3	3.029E-01
α_{29}	4.098E-03	α_3	3.514E-02	α_4	7.767E-02	α_4	2.445E-01
α_{12}	-3.300E-03	α_{29}	2.893E-02	α_{13}	-6.663E-02	α_{15}	-6.274E-02
α_9	-9.680E-04	α_{12}	-2.598E-02	α_{29}	6.363E-02	α_{13}	-6.094E-02
α_{13}	-5.960E-04	α_{13}	-8.662E-03	α_{12}	-3.663E-02	α_{29}	4.573E-02
α_8	-5.825E-04	α_9	-5.332E-03	α_2	2.470E-02	α_{14}	-4.046E-02
α_3	4.759E-04	α_8	-2.064E-03	α_9	-1.514E-02	α_{12}	-3.852E-02
α_{24}	-4.189E-04	α_{24}	-2.020E-03	α_{14}	-9.465E-03	α_2	2.151E-02

Table III.C.7
Relative sensitivities of the inside temperature of the shroud (ZrO_2 fiber insulation) at 1.4m.

Param.	Rel. sens. at 10s	Param.	Rel. sens. at 100s	Param.	Rel. sens. at 500s	Param.	Rel. sens. at 800s
α_8	4.659E-03	α_8	3.745E-02	α_1	8.745E-02	α_1	1.874E-01
α_9	4.035E-03	α_9	2.522E-02	α_3	6.034E-02	α_3	1.110E-01
α_{29}	3.539E-03	α_{29}	2.078E-02	α_{31}	-5.90E-02	α_{29}	-6.911E-02
α_{32}	-1.643E-03	α_{31}	-1.628E-02	α_8	5.074E-02	α_{31}	-6.609E-02
α_{31}	-1.425E-03	α_{32}	-1.393E-02	α_{32}	-2.702E-02	α_4	6.506E-02
α_{33}	-9.550E-04	α_{34}	7.298E-03	α_{30}	-2.207E-02	α_{28}	2.773E-02
α_{34}	8.546E-04	α_{30}	-5.844E-03	α_{12}	-2.008E-02	α_{12}	-2.766E-02
α_{24}	-5.146E-04	α_1	4.273E-03	α_{29}	-1.851E-02	α_7	2.718E-02
α_{23}	-4.207E-04	α_{33}	-4.194E-03	α_4	1.486E-02	α_{32}	-2.574E-02
α_{30}	-4.158E-04	α_{24}	-3.293E-03	α_9	1.356E-02	α_{30}	-2.550E-02

Nomenclature

Param.	Parameter Physical Meaning
α_1	Nominal power factor: 0.7
α_2	Nominal power from 0 to 121s: 4279W
α_3	Nominal power up to 2088.6s: 16350W
α_4	Nominal power up to 2103s: 3874W
α_5	Nominal internal source multiplier (axial peaking factor) for power of heat structure of the heated rod at 0.6m: 0.05015. This value is multiplied by the power to obtain the total power generated in this heat structure
α_6	Nominal internal source multiplier (axial peaking factor) for power of heat structure of the heated rod at 0.7m: 0.05255. This value is multiplied by the power to obtain the total power generated in this heat structure
α_7	Nominal internal source multiplier (axial peaking factor) for power of heat structure of the heated rod at 1.3m: 0.06398. This value is multiplied by the power to obtain the total power generated in this heat structure
α_8	Zircaloy, nominal volumetric heat capacity at 640K: 2168KJ/m³K
α_9	Zircaloy, nominal volumetric heat capacity at 1090K: 2456KJ/m³K
α_{10}	ZrO_2 Pellets, nominal volumetric heat capacity at 550K: 3360KJ/m³K
α_{11}	ZrO_2 Pellets, nominal volumetric heat capacity at 700K: 3510KJ/m³K
α_{12}	ZrO_2 Pellets, nominal volumetric heat capacity at 873K: 3618KJ/m³K
α_{13}	ZrO_2 Pellets, nominal volumetric heat capacity at 1083K: 3726KJ/m³K
α_{14}	ZrO_2 Pellets, nominal volumetric heat capacity at 1173K: 3774KJ/m³K

α_{15}	ZrO_2 Pellets, nominal volumetric heat capacity at 1248K: 3804KJ/m³K
α_{16}	Nominal surface area of volume: 0.00229m², volume for water of inlet pipe
α_{17}	Nominal surface area of volume: 0.006011m², volume centre at 0.075m of the pipe height
α_{18}	Nominal surface area of volume: 0.003007m², volume centre at 0.375m of the pipe height
α_{19}	Nominal surface area of volume: 0.003007m², volume centre at 0.7m of the pipe height
α_{20}	Nominal surface area of volume: 0.003007m², volume centre at 0.9m of the pipe height
α_{21}	Nominal surface area of volume: 0.003007m², volume centre at 1.0m of the pipe height
α_{22}	Nominal surface area of volume: 0.003007m², volume centre at 1.1m of the pipe height
α_{23}	Nominal surface area of volume: 0.003007m², volume centre at 1.2m of the pipe height
α_{24}	Nominal surface area of volume: 0.003007m², volume centre at 1.3m of the pipe height
α_{25}	Nominal volume length: 0.3m, volume for Argon of inlet pipe
α_{26}	Nominal volume length: 0.305m, volume for water of inlet pipe
α_{27}	Nominal volume length: 0.15m, volume centre at 0.075m of the pipe height
α_{28}	Nominal internal source multiplier (axial peaking factor) for power of heat structure of the heated rod at 1.4m: 0.06313. This value is multiplied by the power to obtain the total power generated in this heat structure
α_{29}	Nominal surface area of volume: 0.003007m², volume centre at 1.4m of the pipe height
α_{30}	Zyf b-3 isolation material: nominal thermal conductivity at 273K: 0.07W/mK
α_{31}	Zyf b-3 isolation material: nominal thermal conductivity at 550K: 0.098W/mK
α_{32}	Zyf b-3 isolation material: nominal thermal conductivity at 700K: 0.112W/mK
α_{33}	Zyf b-3 isolation material: nominal thermal conductivity at 873K: 0.133W/mK
α_{34}	Zircaloy, nominal volumetric heat capacity at 400K: 1978KJ/m³K

CHAPTER IV

FORWARD AND ADJOINT SENSITIVITY ANALYSIS PROCEDURES FOR RESPONSES DEFINED AT CRITICAL POINTS

Often, the response functional, $R(\boldsymbol{e})$, of a physical system is located at a critical point, $\boldsymbol{y}(\boldsymbol{\alpha})$, of a function that depends on the system's state vector and parameters. In such situations, the components $y_i(\boldsymbol{\alpha}), (i = 1,\ldots,M)$, of $\boldsymbol{y}(\boldsymbol{\alpha})$, must be treated as responses in addition to $R(\boldsymbol{e})$. As first shown by Cacuci (1981), the objectives of sensitivity analysis for such systems would be to determine:

(A) the G-differential $\delta R(\boldsymbol{e}^0;\boldsymbol{h})$ of $R(\boldsymbol{e})$ at the "base-case point" $\boldsymbol{e}^0 = (\boldsymbol{u}^0, \boldsymbol{\alpha}^0)$, which gives the sensitivity of $R(\boldsymbol{e})$ to changes $\boldsymbol{h} = (\boldsymbol{h}_u, \boldsymbol{h}_\alpha)$ in the systems state functions and parameters; and

(B) the vector $\delta\boldsymbol{y}(\boldsymbol{\alpha}^0;\boldsymbol{h}_\alpha) = (\delta y_1,\ldots,\delta y_M)$, whose components $\delta y_m(\boldsymbol{\alpha}^0;\boldsymbol{h}_\alpha)$ represent the G-differentials of $y_m(\boldsymbol{\alpha})$ at $\boldsymbol{\alpha}^0$, for $(m = 1,\ldots,M)$, which would thus provide the sensitivity of the critical point $\boldsymbol{y}(\boldsymbol{\alpha})$ to parameter variations $\boldsymbol{h}_\alpha$.

The material presented in this Chapter is structured in two main Sections, as follows: Section IV.A presents the general sensitivity theory (i.e., both the *FSAP* and the *ASAP*) for responses defined at critical points, together with an illustrative application to a particle diffusion problem, while Section IV.B illustrates the application of the *ASAP* for sensitivity analysis of a paradigm transient behavior of a nuclear reactor system. This transient behavior is simulated by using the MELT III.B code system, which solves equations describing the following phenomena: (a) thermal-hydraulics equations describing the conservation of thermal energy, mass, and momentum for the average channel fuel pin and surrounding single-phase coolant; (b) neutron point-kinetics equations describing the time-dependent behavior of the core-integrated neutron density; and (c) a loop-hydraulic equation that relates the core inlet and outlet pressures.

IV. A. FSAP AND ASAP FOR RESPONSES AT CRITICAL POINTS: GENERAL THEORY

Consider once again a generic physical system described mathematically by the following system of K coupled nonlinear equations written in operator form as

$$\boldsymbol{N}\left[\boldsymbol{u}(\boldsymbol{x}),\boldsymbol{\alpha}(\boldsymbol{x})\right]=\boldsymbol{Q}\left[\boldsymbol{\alpha}(\boldsymbol{x}),\right]. \tag{IV.A.1}$$

The quantities appearing in Eq. (IV.A.1) are defined as follow:

(i) $\boldsymbol{x}=(x_1,\ldots,x_J)$ is the phase-space position vector; $\boldsymbol{x}\in\Omega\subset\mathcal{R}^J$, where Ω is subset of the J-real vector space $\mathcal{R}^J$,

(ii) $\boldsymbol{u}(\boldsymbol{x})=\left[u_1(\boldsymbol{x}),\ldots,u_K(\boldsymbol{x})\right]$ is the state vector; $\boldsymbol{u}(\boldsymbol{x})\in E_u$, where E_u is a normed linear space over the scalar field Λ of real numbers,

(iii) $\boldsymbol{\alpha}(\boldsymbol{x})=\left[\alpha_1(\boldsymbol{x}),\ldots,\alpha_I(\boldsymbol{x})\right]$ is the vector of system parameters; $\boldsymbol{\alpha}\in E_\alpha$, where E_α is also a normed linear space,

(iv) $\boldsymbol{Q}\left[\boldsymbol{\alpha}(\boldsymbol{x}),\boldsymbol{x}\right]=\left[Q_1(\boldsymbol{\alpha},\boldsymbol{x}),\ldots,Q_K(\boldsymbol{\alpha},\boldsymbol{x})\right]$ is a (column) vector whose elements represent inhomogeneous source terms; $\boldsymbol{Q}\in E_Q$, where E_Q is also a normed liner space. The components of $\boldsymbol{Q}$ may be operators (rather than just functions) acting on $\boldsymbol{\alpha}(\boldsymbol{x})$ and $\boldsymbol{x}$,

(v) $\boldsymbol{N}=\left[N_1(\boldsymbol{u},\boldsymbol{\alpha}),\ldots,N_K(\boldsymbol{u},\boldsymbol{\alpha})\right]$ represents a (column) vector whose components are nonlinear operators acting in general, not only on the state vector $\boldsymbol{u}(\boldsymbol{x})$, but also on the vector of system parameters $\boldsymbol{\alpha}(\boldsymbol{x})$.

In view of the above definition, $\boldsymbol{N}$ represents the mapping $\boldsymbol{N}: S\subset E\to E_Q$, where $S=S_u\times S_\alpha$, $S_u\subset E_u$, $S_\alpha\subset E_\alpha$, and $E=E_u\times E_\alpha$. Note that an arbitrary element $\boldsymbol{e}\in E$ is of the form $\boldsymbol{e}=(\boldsymbol{u},\boldsymbol{\alpha})$. All vectors in this Section are, as usual, column vectors, unless explicitly stated otherwise. If differential operators appear in Eq. (IV.A.1), then a corresponding set of boundary conditions, which is essential to define the domain S of $\boldsymbol{N}$, must also be given. This set can be represented as

$$\left\{\boldsymbol{B}(\boldsymbol{e})-\boldsymbol{A}(\boldsymbol{\alpha})\right\}_{\partial\Omega}=\boldsymbol{0}\,, \tag{IV.A.2}$$

where $\boldsymbol{A}$ and $\boldsymbol{B}$ are operators, and $\partial\Omega$ is the boundary of Ω; the operator $\boldsymbol{A}(\boldsymbol{\alpha})$ represents all inhomogeneous boundary terms.

Consider that the system response R is a functional of $\boldsymbol{e}=(\boldsymbol{u},\boldsymbol{\alpha})$ defined at a critical point $\boldsymbol{y}(\boldsymbol{\alpha})$ of a function $F(\boldsymbol{u},\boldsymbol{x},\boldsymbol{\alpha})$. Such a response can be represented in the form

$$R(\boldsymbol{e}) = \int_{\Omega} F(\boldsymbol{u}, \boldsymbol{x}, \boldsymbol{\alpha}) \prod_{i=1}^{M} \delta[x_i - y_i(\boldsymbol{\alpha})] \prod_{j=M+1}^{J} \delta(x_j - z_j)\, dx_1 \ldots dx_J . \qquad \text{(IV.A.3)}$$

The quantities appearing in the integrand of Eq. (IV.A.3) are defined as follows:

(i) F is the nonlinear function under consideration,

(ii) $\delta(\boldsymbol{x})$ is the customary "Dirac-delta" functional,

(iii) $\boldsymbol{\alpha} \in \mathcal{R}^I$, i.e., the components α_i, $(i = 1, \ldots, I)$ are restricted throughout this section to be real numbers;

(iv) $\boldsymbol{y}(\boldsymbol{\alpha}) = [y_1(\boldsymbol{\alpha}), \ldots, y_M(\boldsymbol{\alpha})]$, $M \le J$, is a critical point of F.

This critical point can be generally defined in one of the following two ways:

If the G-differential of F vanishes at $\boldsymbol{y}(\boldsymbol{\alpha})$, then $\boldsymbol{y}(\boldsymbol{\alpha})$ is a critical point defined implicitly as the solution of the system of equations

$$\{\partial F / \partial x_i\}_{\boldsymbol{y}(\boldsymbol{\alpha})} = 0; \; (i = 1, \ldots, J). \qquad \text{(IV.A.4)}$$

In this case, $\boldsymbol{y}(\boldsymbol{\alpha})$ has J components (i.e., $M = J$), and $\prod_{j=M+1}^{J} \delta(x_j - z_j) \equiv 1$ in the integrand of Eq. (IV.A.3). Note that, in general, $\boldsymbol{y}(\boldsymbol{\alpha})$ is a function of $\boldsymbol{\alpha}$.

Occasionally, it may happen that $\partial F / \partial x_j$ takes on nonzero constant values (i.e., values that do not depend on $\boldsymbol{x}$) for some of the variables x_j, $(j = M+1, \ldots, J)$. Then, as a function of these variable x_j, F attains its extreme values at the points $x_j = z_j$, $z_j \in \partial\Omega$. Evaluating F at z_j, $(j = M+1, \ldots, J)$, yields a function G which depends on the remaining phase-space variables x_i, $(i = 1, \ldots, M)$; G may then have a critical point at $\boldsymbol{y}(\boldsymbol{\alpha}) = [y_1(\boldsymbol{\alpha}), \ldots, y_M(\boldsymbol{\alpha})]$ defined implicitly as the solution of

$$\{\partial G / \partial x_i\}_{\boldsymbol{y}(\boldsymbol{\alpha})} = 0, \; (i = 1, \ldots, M). \qquad \text{(IV.A.5)}$$

With the above specifications, the definition of $R(\boldsymbol{e})$ given in Eq. (IV.A.3) is sufficiently general to include treatment of extrema (local, relative, or absolute), saddle, and inflexion points of the function F of interest. Note that, in practice, the base-case solution path, and therefore the specific nature and location of the critical point under consideration, are completely known prior to initiating the sensitivity studies.

It is thus apparent that in the formulation of a complete sensitivity theory, the components $y_i(\boldsymbol{\alpha})$, $(i = 1, \ldots, M)$, of $\boldsymbol{y}(\boldsymbol{\alpha})$, must be treated as responses in

addition to $R(\boldsymbol{e})$. Hence, the objective of this sensitivity theory is twofold, namely:

(A) To determine the G-differential $\delta R(\boldsymbol{e}^0;\boldsymbol{h})$ of $R(\boldsymbol{e})$ at the "base-case point" $\boldsymbol{e}^0 = (\boldsymbol{u}^0, \boldsymbol{\alpha}^0)$, which gives the sensitivity of $R(\boldsymbol{e})$ to changes $\boldsymbol{h} = (\boldsymbol{h}_u, \boldsymbol{h}_\alpha)$ in the systems state functions and parameters; and

(B) To determine the (column) vector $\delta \boldsymbol{y}(\boldsymbol{\alpha}^0;\boldsymbol{h}_\alpha) = (\delta y_1, \ldots, \delta y_M)$ whose components $\delta y_m(\boldsymbol{\alpha}^0;\boldsymbol{h}_\alpha)$ are the G-differentials of $y_m(\boldsymbol{\alpha})$ at $\boldsymbol{\alpha}^0$, for $(m = 1, \ldots, M)$. The vector $\delta \boldsymbol{y}(\boldsymbol{\alpha}^0;\boldsymbol{h}_\alpha)$ gives the sensitivity of the critical point $\boldsymbol{y}(\boldsymbol{\alpha})$ to changes $\boldsymbol{h}_\alpha$.

To achieve the objective mentioned above, the two alternative formalisms, the Forward Sensitivity Analysis Procedure (*FSAP*) and the Adjoint Sensitivity Analysis Procedure (*ASAP*), are developed along the same general lines as discussed in detail in Volume I.

IV.A.1. The Forward Sensitivity Analysis Procedure (FSAP)

Applying the definition of the G-differential to Eq. (IV.A.3) shows that

$$\delta R(\boldsymbol{e}^0;\boldsymbol{h}) = \int_\Omega \left[F'_u(\boldsymbol{e}^0)\boldsymbol{h}_u + F'_\alpha(\boldsymbol{e}^0)\boldsymbol{h}_\alpha\right] \prod_{i=1}^{M} \delta\left[x_i - y_i(\boldsymbol{\alpha}^0)\right] \prod_{j=M+1}^{J} \delta(x_i - z_j)d\boldsymbol{x}$$
$$+ \sum_{m=1}^{M}\left[-\boldsymbol{h}_\alpha \bullet \left(\frac{dy_m}{d\boldsymbol{\alpha}}\right)_{\boldsymbol{\alpha}^0}\right] \int_\Omega F\delta'(x_m - y_m) \prod_{i=1, i\neq m}^{M} \delta(x_i - y_i) \prod_{j=M+1}^{J} \delta(x_j - z_j)d\boldsymbol{x}\,. \tag{IV.A.6}$$

The last term on the right side of Eq. (IV.A.6) vanishes, since

$$\int_\Omega F\delta'(x_m - y_m) \prod_{i=1, i\neq m}^{M} \delta(x_i - y_i) \prod_{j=M+1}^{J} \delta(x_j - z_j)d\boldsymbol{x} =$$
$$-\int_\Omega (\partial F/\partial x_m) \prod_{i=1}^{M} \delta(x_i - y_i) \prod_{j=M+1}^{J} \delta(x_j - z_j)\, d\boldsymbol{x} = 0, \ (m = 1, \ldots, M), \tag{IV.A.7}$$

in view of the well-known definition of the δ' functional and in view of either Eq. (IV.A.4) if $M = J$, or of Eq. (IV.A.5) if $M < J$. Therefore, the expression of $\delta R(\boldsymbol{e}^0;\boldsymbol{h})$ simplifies to

$$\delta R\left(\boldsymbol{e}^0;\boldsymbol{h}\right)=\int_{\Omega}\left[F_u'\left(\boldsymbol{e}^0\right)\boldsymbol{h}_u+F_\alpha'\left(\boldsymbol{e}^0\right)\boldsymbol{h}_\alpha\right]\prod_{i=1}^{M}\delta\left[x_i-y_i\left(\boldsymbol{\alpha}^0\right)\right]\prod_{j=M+1}^{J}\delta\left(x_i-z_j\right)d\boldsymbol{x}. \quad \text{(IV.A.8)}$$

Thus, the sensitivity $\delta R\left(\boldsymbol{e}^0;\boldsymbol{h}\right)$ of $R(\boldsymbol{e})$ to specified changes $\boldsymbol{h}_\alpha$ can in principle be evaluated once the vector $\boldsymbol{h}_u$ is determined from the *FSAP*, i.e.,

$$\begin{cases}\delta\boldsymbol{N}\left(\boldsymbol{u}^0,\boldsymbol{\alpha}^0;\boldsymbol{h}_u,\boldsymbol{h}_\alpha\right)-\delta\boldsymbol{Q}\left(\boldsymbol{\alpha}^0;\boldsymbol{h}_\alpha\right)=\boldsymbol{0},\\ \left\{\delta\boldsymbol{B}\left(\boldsymbol{u}^0,\boldsymbol{\alpha}^0;\boldsymbol{h}_u,\boldsymbol{h}_\alpha\right)-\delta\boldsymbol{A}\left(\boldsymbol{\alpha}^0;\boldsymbol{h}_\alpha\right)\right\}_{\partial\Omega}=\boldsymbol{0}.\end{cases} \quad \text{(IV.A.9)}$$

As already mentioned, the sensitivity of the location in phase space of the critical point is given by the G-differential $\delta\boldsymbol{y}\left(\boldsymbol{\alpha}^0;\boldsymbol{h}_\alpha\right)$ of $\boldsymbol{y}(\boldsymbol{\alpha})$ at $\boldsymbol{\alpha}^0$. In view of either Eq. (IV.A.4) or Eq. (IV.A.5), each of the components $y_1(\boldsymbol{\alpha}),\ldots,y_M(\boldsymbol{\alpha})$ of $\boldsymbol{y}(\boldsymbol{\alpha})$ is a real-valued function of the real variables $(\alpha_1,\ldots,\alpha_I)$, and may be viewed as a functional defined on a subset of $\mathcal{X}^I$. Therefore, each G-differential $\delta y_m\left(\boldsymbol{\alpha}^0;\boldsymbol{h}_\alpha\right)$ of $y_m(\boldsymbol{\alpha})$ at $\boldsymbol{\alpha}^0$ is given by

$$\delta y_m\left(\boldsymbol{\alpha}^0;\boldsymbol{h}_\alpha\right)=\left\{\frac{dy_m}{d\boldsymbol{\alpha}}\right\}_{\boldsymbol{\alpha}^0}\bullet\boldsymbol{h}_\alpha=\sum_{i=1}^{I}\left\{\frac{\partial y_m}{\partial\alpha_i}\right\}_{\boldsymbol{\alpha}^0}h_{\alpha_i};\ (m=1,\ldots,M), \quad \text{(IV.A.10)}$$

provided that $\partial y_m/\partial\alpha_i$, $(i=1,\ldots,I)$ exist at $\boldsymbol{\alpha}^0$ for all $(m=1,\ldots,M)$.

The explicit expression of $\delta\boldsymbol{y}\left(\boldsymbol{\alpha}^0;\boldsymbol{h}_\alpha\right)$ is obtained as follows. First, it is observed that both Eq. (IV.A.4) and Eq. (IV.A.5) can be represented as

$$\int_{\Omega}\left(\partial F/\partial x_m\right)\prod_{i=1}^{M}\delta\left[x_i-y_i(\boldsymbol{\alpha})\right]\prod_{j=M+1}^{J}\delta\left(x_j-z_j\right)d\boldsymbol{x}=0;\ (m=1,\ldots,M). \quad \text{(IV.A.11)}$$

Taking the G-differential of Eq. (IV.A.11) at $\boldsymbol{e}^0$ yields the following system of equations involving the components δy_m:

$$\int_{\Omega} \left\{\partial\left(F_u' \boldsymbol{h}_u + F_\alpha' \boldsymbol{h}_\alpha\right)/\partial x_m\right\}_{\boldsymbol{e}^0} \prod_{i=1}^{M} \delta\left[x_i - y_i\left(\boldsymbol{\alpha}^0\right)\right] \prod_{j=M+1}^{J} \delta\left(x_i - z_j\right) d\boldsymbol{x}$$
$$- \sum_{s=1}^{M} \delta y_s\left(\boldsymbol{\alpha}^0; \boldsymbol{h}_\alpha\right) \int_{\Omega} \left\{\partial F/\partial x_m\right\}_{\boldsymbol{e}^0} \delta'\left[x_s - y_s\left(\boldsymbol{\alpha}^0\right)\right] \prod_{i=1, i\neq s}^{M} \delta\left[x_i - y_i\left(\boldsymbol{\alpha}^0\right)\right] \prod_{j=M+1}^{J} \delta\left(x_i - z_j\right) d\boldsymbol{x}$$
$$= 0; \left(m = 1, \ldots, M\right). \tag{IV.A.12}$$

The above system is algebraic and linear in the components $\delta y_s\left(\boldsymbol{\alpha}^0; \boldsymbol{h}_\alpha\right)$; therefore, it can be represented in matrix form as

$$\boldsymbol{\Phi}\left(\delta \boldsymbol{y}\right) = \boldsymbol{\Gamma} \tag{IV.A.13}$$

by defining $\boldsymbol{\Phi} = \left[\phi_{ms}\right]$ to be the $M \times M$ matrix with elements

$$\phi_{ms} \equiv \int_{\Omega} \left\{\partial^2 F/\partial x_m \partial x_s\right\}_{\boldsymbol{e}^0} \prod_{i=1}^{M} \delta\left[x_i - y_i\left(\boldsymbol{\alpha}^0\right)\right] \prod_{j=M+1}^{J} \delta\left(x_j - z_j\right) d\boldsymbol{x}, \left(m, s = 1, \ldots, M\right), \tag{IV.A.14}$$

and by defining $\boldsymbol{\Gamma}$ to be the M-component (column) vector

$$\boldsymbol{\Gamma} \equiv \left(f_1 + g_1, \ldots, f_M + g_M\right)^T, \tag{IV.A.15}$$

where

$$f_m \equiv -\int_{\Omega} \left\{\partial\left(F_\alpha' \boldsymbol{h}_\alpha\right)/\partial x_m\right\}_{\boldsymbol{e}^0} \prod_{i=1}^{M} \delta\left[x_i - y_i\left(\boldsymbol{\alpha}^0\right)\right] \prod_{j=M+1}^{J} \delta\left(x_i - z_j\right) d\boldsymbol{x}; \left(m = 1, \ldots, M\right), \tag{IV.A.16}$$

and

$$g_m \equiv -\int_{\Omega} \left\{\partial\left(F_u' \boldsymbol{h}_u\right)/\partial x_m\right\}_{\boldsymbol{e}^0} \prod_{i=1}^{M} \delta\left[x_i - y_i\left(\boldsymbol{\alpha}^0\right)\right] \prod_{j=M+1}^{J} \delta\left(x_i - z_j\right) d\boldsymbol{x}; \left(m = 1, \ldots, M\right). \tag{IV.A.17}$$

Notice that the definition of the δ' functional has been used to recast the second integral in Eq. (IV.A.12) into the equivalent expression given in Eq. (IV.A.14).

As this stage, the quantities ϕ_{ms} and f_m can be evaluated by directly using Eqs. (IV.A.14) and (IV.A.16). It is of interest to observe here that if $M = J$,

then $\boldsymbol{\Phi}$ is the Hessian of F evaluated at the critical point $\boldsymbol{y}\left(\boldsymbol{\alpha}^0\right)$; alternatively, if $M < J$, then $\boldsymbol{\Phi}$ is the Hessian of the function G [considered in Eq. (IV.A.5)] evaluated at the respective critical point. The quantities g_m defined in Eq. (IV.A.17) can also be evaluated, since $\boldsymbol{h}_u$ will have already been determined to compute the sensitivity $\delta R\left(\boldsymbol{e}^0;\boldsymbol{h}\right)$ given in Eq. (IV.A.8). Upon completing the computation of the elements of $\boldsymbol{\Phi}$ and $\boldsymbol{\Gamma}$, Eq. (IV.A.13) can be solved by employing methods of linear algebra to obtain

$$\delta\boldsymbol{y}\left(\boldsymbol{\alpha}^0;\boldsymbol{h}_\alpha\right)=\boldsymbol{\Phi}^{-1}\boldsymbol{\Gamma}\,. \tag{IV.A.18}$$

As underscored by the derivations presented so far, the availability of the solution $\boldsymbol{h}_u$ of the "forward sensitivity equations" given in Eq. (IV.A.9) is essential to evaluate both $\delta R\left(\boldsymbol{e}^0;\boldsymbol{h}\right)$ and $\delta\boldsymbol{y}\left(\boldsymbol{\alpha}^0;\boldsymbol{h}_\alpha\right)$. This is a distinctive characteristic of the "forward sensitivity formalism," which, from an economical standpoint, makes this formalism ill-suited for sensitivity analysis of problems with large data bases (i.e., when $\boldsymbol{\alpha}$ has many components).

IV.A.2. The Adjoint Sensitivity Analysis Procedure (ASAP)

Since most of the problems encountered in practice are characterized by large data bases, the development of this formalism is motivated by the need for a tool to perform sensitivity analyses of such problems economically. To this end, the development of this formalism is centered on eliminating the explicit appearance of the unknown values of the vector $\boldsymbol{h}_u$ from Eqs. (IV.A.8) and (IV.A.18), and hence on circumventing the need to repeatedly solve Eq. (IV.A.9). However, as detailed in Volume I, $\boldsymbol{h}_u$ can be eliminated if and only if (iff) the following three conditions, labeled below as C.1 through C.3, are satisfied:

(C.1) The partial G-derivatives at $\boldsymbol{e}^0$ of $R\left(\boldsymbol{e}\right)$ with respect to $\boldsymbol{u}$ and $\boldsymbol{\alpha}$ exist,

(C.2) The partial G-derivatives at $\boldsymbol{e}^0$ of the operators $\boldsymbol{N}$ and $\boldsymbol{B}$ with respect to $\boldsymbol{u}$ and $\boldsymbol{\alpha}$ exist,

(C.3) The spaces E_u and E_Q are real Hilbert spaces, denoted by H_u and H_Q, respectively. For $\boldsymbol{u}_1,\boldsymbol{u}_2 \in H_u$, the inner product in H_u will be denoted by $\left[\boldsymbol{u}_1,\boldsymbol{u}_2\right]$, and is given by the integral $\int_\Omega \boldsymbol{u}_1 \bullet \boldsymbol{u}_2\, d\boldsymbol{x}$. The inner product in H_Q will be denoted by $\left\langle\,,\right\rangle$.

An examination of Eq. (IV.A.8) shows that $\delta R\left(\boldsymbol{e}^0;\boldsymbol{h}\right)$ is linear in $\boldsymbol{h}$. Hence, the condition (C.1) mentioned above is satisfied, and the H_u-dependent component

of $\delta R\left(\boldsymbol{e}^0;\boldsymbol{h}\right)$, i.e., the "indirect effect term," can be written in inner product form as

$$\int_{\Omega} F_u'\left(\boldsymbol{e}^0\right)\boldsymbol{h}_u \prod_{i=1}^{M}\delta\left[x_i - y_i\left(\boldsymbol{\alpha}^0\right)\right]\prod_{j=M+1}^{J}\delta\left(x_i - z_j\right)d\boldsymbol{x} = \left[\nabla_u R\left(\boldsymbol{e}^0\right),\boldsymbol{h}_u\right], \tag{IV.A.19}$$

where

$$\nabla_u R\left(\boldsymbol{e}^0\right) = \prod_{i=1}^{M}\delta\left[x_i - y_i\left(\boldsymbol{\alpha}^0\right)\right]\prod_{j=M+1}^{J}\delta\left(x_i - z_j\right)\times\left(\frac{\partial F\left(\boldsymbol{e}^0\right)}{\partial u_1},\ldots,\frac{\partial F\left(\boldsymbol{e}^0\right)}{\partial u_K}\right)^T. \tag{IV.A.20}$$

The adjoint system is constructed by following the procedure set forth in Volume I; for brevity, the details will be omitted here. Thus, condition (C.2) makes it possible to write the system of equations given in Eq. (IV.A.9) as

$$\boldsymbol{N}_u'\left(\boldsymbol{e}^0\right)\boldsymbol{h}_u = \delta\boldsymbol{Q}\left(\boldsymbol{\alpha}^0;\boldsymbol{h}_\alpha\right) - \boldsymbol{N}_\alpha'\left(\boldsymbol{e}^0\right)\boldsymbol{h}_\alpha \tag{IV.A.21}$$

and

$$\left\{\boldsymbol{B}_u'\left(\boldsymbol{e}^0\right)\boldsymbol{h}_u\right\}_{\partial\Omega} = \left\{\delta\boldsymbol{A}\left(\boldsymbol{\alpha}^0;\boldsymbol{h}_\alpha\right) - \boldsymbol{B}_\alpha'\left(\boldsymbol{e}^0\right)\boldsymbol{h}_\alpha\right\}_{\partial\Omega}. \tag{IV.A.22}$$

Next, in view of Eq. (IV.A.21) and condition (C.3), the following relationship holds for a vector $\boldsymbol{v}\in H_Q$:

$$\left\langle\boldsymbol{v},\boldsymbol{N}_u'\left(\boldsymbol{e}^0\right)\boldsymbol{h}_u\right\rangle = \left[\boldsymbol{L}^*\left(\boldsymbol{e}^0\right)\boldsymbol{v},\boldsymbol{h}_u\right] + \left\{P\left[\boldsymbol{h}_u;\boldsymbol{v}\right]\right\}_{\partial\Omega}, \tag{IV.A.23}$$

where $\boldsymbol{L}^*\left(\boldsymbol{e}^0\right)$ is the operator formally adjoint to $\boldsymbol{N}_u'\left(\boldsymbol{e}^0\right)$, and $\left\{P\left[\boldsymbol{h}_u;\boldsymbol{v}\right]\right\}_{\partial\Omega}$ is the associated bilinear form evaluated on $\partial\Omega$. The domain of $\boldsymbol{L}^*\left(\boldsymbol{e}^0\right)$ is determined by selecting appropriate adjoint boundary conditions, represented here in operator form as

$$\left\{\boldsymbol{B}^*\left(\boldsymbol{v};\boldsymbol{e}^0\right) - \boldsymbol{A}^*\left(\boldsymbol{e}^0\right)\right\}_{\partial\Omega} = \boldsymbol{0}. \tag{IV.A.24}$$

As discussed in Volume I, these boundary conditions are obtained by requiring that

(i) They be independent of $\boldsymbol{h}_u$, $\boldsymbol{h}_\alpha$, and G-derivatives with respect to $\boldsymbol{\alpha}$, and

(ii) The substitution of Eqs. (IV.A.22) and (IV.A.24) into the expression of $\{P[\boldsymbol{h}_u;\boldsymbol{v}]\}_{\partial\Omega}$ must cause all terms containing unknown values of $\boldsymbol{h}_u$ to vanish.

This selection of the adjoint boundary conditions reduces $\{P[\boldsymbol{h}_u;\boldsymbol{v}]\}_{\partial\Omega}$ to a quantity designated here by $\hat{P}(\boldsymbol{h}_\alpha,\boldsymbol{v};\boldsymbol{e}^0)$, where $\hat{P}$ contains boundary terms involving only known values of $\boldsymbol{h}_\alpha$, $\boldsymbol{v}$, and (possibly) $\boldsymbol{e}^0$. In general, $\hat{P}$ does not automatically vanish as a result of these manipulations, although it may do so in particular instances. Hence, Eq. (IV.A.23) can be written as

$$\left[L^*(\boldsymbol{e}^0)\boldsymbol{v},\boldsymbol{h}_u\right]=\left\langle \boldsymbol{v},\delta\boldsymbol{Q}(\boldsymbol{\alpha}^0;\boldsymbol{h}_\alpha)-N'_\alpha(\boldsymbol{e}^0)\boldsymbol{h}_\alpha\right\rangle-\hat{P}(\boldsymbol{h}_\alpha,\boldsymbol{v};\boldsymbol{e}^0), \qquad \text{(IV.A.25)}$$

where Eq. (IV.A.21) was used to replace $\boldsymbol{N}'_u(\boldsymbol{e}^0)\boldsymbol{h}_u$. Comparing the left-hand side of Eq. (IV.A.25) with the right-hand side of Eq. (IV.A.19) shows that

$$\boldsymbol{L}^*(\boldsymbol{e}^0)\boldsymbol{v}=\nabla_u R(\boldsymbol{e}^0). \qquad \text{(IV.A.26)}$$

Note that the uniqueness of the above relationship is ensured by the Riesz representation theorem. This completes the construction of the adjoint system. Furthermore, Eqs. (IV.A.19), (IV.A.25), and (IV.A.26) can be used to express Eq. (IV.A.8) as

$$\begin{aligned}\delta R(\boldsymbol{e}^0;\boldsymbol{h})=&\int_\Omega F'_\alpha(\boldsymbol{e}^0)\boldsymbol{h}_\alpha\prod_{i=1}^{M}\delta\left[x_i-y_i(\boldsymbol{\alpha}^0)\right]\prod_{j=M+1}^{J}\delta(x_i-z_j)d\boldsymbol{x}\\&+\left\langle\delta\boldsymbol{Q}(\boldsymbol{\alpha}^0;\boldsymbol{h}_\alpha)-\boldsymbol{N}'_\alpha(\boldsymbol{e}^0)\boldsymbol{h}_\alpha,\boldsymbol{v}\right\rangle-\hat{P}(\boldsymbol{h}_\alpha,\boldsymbol{v};\boldsymbol{e}^0).\end{aligned} \qquad \text{(IV.A.27)}$$

The desired elimination of the unknown values of $\boldsymbol{h}_u$ from the expression giving the sensitivity $\delta R(\boldsymbol{e}^0;\boldsymbol{h})$ has thus been accomplished.

Unknown values of $\boldsymbol{h}_u$ can be eliminated from the expression of $\delta\boldsymbol{y}(\boldsymbol{\alpha}^0;\boldsymbol{h}_\alpha)$ given in Eq. (IV.A.18) only if they can be eliminated from appearing in Eq. (IV.A.17). Examination of Eq. (IV.A.17) reveals that each quantity g_m is a functional that can be expressed in the equivalent form

$$g_m=\int_\Omega F'_u(\boldsymbol{e}^0)\boldsymbol{h}_u\delta'(x_m-y_m)\prod_{i=1,i\neq m}^{M}\delta[x_i-y_i]\prod_{j=M+1}^{J}\delta(x_i-z_j)d\boldsymbol{x} \qquad \text{(IV.A.28)}$$

by employing the definition of the δ' functional. In turn, the above expression can be written as the inner product

$$g_m = \left[\gamma_m\left(\boldsymbol{e}^0\right), \boldsymbol{h}_u\right], \tag{IV.A.29}$$

where

$$\gamma_m\left(\boldsymbol{e}^0\right) \equiv \delta'\left[x_m - y_m\left(\boldsymbol{\alpha}^0\right)\right] \prod_{i=1, i\neq m}^{M} \delta\left[x_i - y_i\right] \prod_{j=M+1}^{J} \delta\left(x_i - z_j\right) \left(\frac{\partial F\left(\boldsymbol{e}^0\right)}{\partial u_1}, \ldots, \frac{\partial F\left(\boldsymbol{e}^0\right)}{\partial u_K}\right)^T . \tag{IV.A.30}$$

The desired elimination of the unknown values of $\boldsymbol{h}_u$ from Eq. (IV.A.29) can now be accomplished by letting each of the functions $\gamma_m\left(\boldsymbol{e}^0\right)$ play, in turn, the role previously played by $\nabla_u R\left(\boldsymbol{e}^0\right)$ [cf. Eq. (IV.A.19)], and by following the same procedure as that leading to Eq. (IV.A.27). The end result is

$$g_m = \left\langle \delta\boldsymbol{Q}\left(\boldsymbol{\alpha}^0; \boldsymbol{h}_\alpha\right) - \boldsymbol{N}'_\alpha\left(\boldsymbol{e}^0\right)\boldsymbol{h}_\alpha, \boldsymbol{w}_m \right\rangle - \hat{P}\left(\boldsymbol{h}_\alpha, \boldsymbol{w}_m; \boldsymbol{e}^0\right), \tag{IV.A.31}$$

where each function $\boldsymbol{w}_m$ is the solution of the adjoint system

$$\begin{cases} \boldsymbol{L}^*\left(\boldsymbol{e}^0\right)\boldsymbol{w}_m = \gamma_m\left(\boldsymbol{e}^0\right) \\ \left\{\boldsymbol{B}^*\left(\boldsymbol{w}_m; \boldsymbol{e}^0\right) - \boldsymbol{A}^*\left(\boldsymbol{e}^0\right)\right\}_{\partial\Omega} = \boldsymbol{0} \end{cases} \tag{IV.A.32}$$

for $\left(m = 1, \ldots, M\right)$.

It is important to note that $\boldsymbol{L}^*\left(\boldsymbol{e}^0\right)$, $\boldsymbol{B}^*\left(\boldsymbol{w}_m; \boldsymbol{e}^0\right)$, and $\boldsymbol{A}^*\left(\boldsymbol{e}^0\right)$ appearing in Eq. (IV.A.32) are the same operators as those appearing in Eqs. (IV.A.26) and (IV.A.24). Only the source term $\gamma_m\left(\boldsymbol{e}^0\right)$ in Eq. (IV.A.32) differs from the corresponding source term $\nabla_u R\left(\boldsymbol{e}^0\right)$ in Eq. (IV.A.26). Therefore, the computer code employed to solve the adjoint system given in Eqs. (IV.A.26) and (IV.A.24) can be used, with relatively trivial modifications, to compute the functions $\boldsymbol{w}_m$ from Eq. (IV.A.32). Comparing now the right sides of Eqs. (IV.A.25) and (IV.A.31) reveals that the quantity $\hat{P}\left(\boldsymbol{h}_\alpha, \boldsymbol{v}; \boldsymbol{e}^0\right)$ is formally identical to the quantity $\hat{P}\left(\boldsymbol{h}_\alpha, \boldsymbol{w}_m; \boldsymbol{e}^0\right)$ and that the vector $\delta\boldsymbol{Q}\left(\boldsymbol{\alpha}^0; \boldsymbol{h}_\alpha\right) - \boldsymbol{N}'_\alpha\left(\boldsymbol{e}^0\right)\boldsymbol{h}_\alpha$ appears in both of the inner products denoted by $\langle , \rangle$. This indicates that the computer program employed to evaluate the second and third terms on the right side of Eq. (IV.A.27) can also be used to evaluate the functionals g_m, $\left(m = 1, \ldots, M\right)$, given by Eq. (IV.A.31). Of course, the values of

$\boldsymbol{v}$ required to compute $\delta R\left(\boldsymbol{e}^0;\boldsymbol{h}\right)$ are to be replaced by the respective values of $\boldsymbol{w}_m$, when computing the g_m's.

In most practical problems, the total number of parameters I greatly exceeds the number of phase-space variables J, and hence M, since $M \le J$. Therefore, if the *ASAP* can be developed as described in this section, then a large amount of computing costs can be saved by employing this formalism rather than the *FSAP*. In the case, only $M+2$ "large" computations (one for the "base-case computation," one for computing the adjoint function $\boldsymbol{v}$, and M computations for obtaining for the adjoint functions $\boldsymbol{w}_1,\ldots,\boldsymbol{w}_M$) are needed to obtain the sensitivities $\delta R\left(\boldsymbol{e}^0;\boldsymbol{h}\right)$ and $\delta \boldsymbol{y}\left(\boldsymbol{\alpha}^0;\boldsymbol{h}_\alpha\right)$ to changes in *all* of the parameters. By contrast at least $(I+1)$ computations (one for the "base-case," and I to obtain the vector $\boldsymbol{h}_u$) would be required if the "forward sensitivity formalism" were employed.

IV.A.3. Discussion

Note that, as shown in Eqs. (IV.A.6)-(IV.A.8), the contributions to $\delta R\left(\boldsymbol{e}^0;\boldsymbol{h}\right)$ arising from the $\boldsymbol{\alpha}$ dependence of $\boldsymbol{y}(\boldsymbol{\alpha})$ vanish only because $\boldsymbol{y}(\boldsymbol{\alpha})$ is a critical point of F. An important consequence of this fact can be demonstrated by *considering the point* $\boldsymbol{y}$ *not to be a function of* $\boldsymbol{\alpha}$. The response would then take on the form

$$R_1(\boldsymbol{e}) = \int_\Omega F(\boldsymbol{u},\boldsymbol{x},\boldsymbol{\alpha}) \prod_{i=1}^{M} \delta(x_i - y_i) \prod_{j=M+1}^{J} \delta(x_j - z_j) d\boldsymbol{x} \ . \qquad \text{(IV.A.33)}$$

In the above equation, the subscript "1" indicates that the mathematical characteristics of $R_1(\boldsymbol{e})$ differ from those of $R(\boldsymbol{e})$, although both responses take on identical values at $\boldsymbol{e} = \boldsymbol{e}^0$, i.e.,

$$R_1\left(\boldsymbol{e}^0\right) = R\left(\boldsymbol{e}^0\right). \qquad \text{(IV.A.34)}$$

Calculating the G-differential $\delta R_1\left(\boldsymbol{e}^0;\boldsymbol{h}\right)$ of $R_1(\boldsymbol{e})$ at $\boldsymbol{e}^0$ gives

$$\delta R_1\left(\boldsymbol{e}^0;\boldsymbol{h}\right) = \int_\Omega \left[F_u'\left(\boldsymbol{e}^0\right)\boldsymbol{h}_u + F_\alpha'\left(\boldsymbol{e}^0\right)\boldsymbol{h}_\alpha\right] \prod_{i=1}^{M} \delta(x_i - y_i) \prod_{j=M+1}^{J} \delta(x_j - z_j) d\boldsymbol{x} \ . \qquad \text{(IV.A.35)}$$

Comparison of Eqs. (IV.A.35) and (IV.A.8) shows that

$$\delta R_1\left(\boldsymbol{e}^0;\boldsymbol{h}\right)=\delta R\left(\boldsymbol{e}^0;\boldsymbol{h}\right). \tag{IV.A.36}$$

Consider now the total variations of $R(\boldsymbol{e})$ and $R_1(\boldsymbol{e})$ at $\boldsymbol{e}=\boldsymbol{e}^0$, i.e.,

$$R\left(\boldsymbol{e}^0+\boldsymbol{h}\right)-R\left(\boldsymbol{e}^0\right)=\delta R\left(\boldsymbol{e}^0;\boldsymbol{h}\right)+\Delta(\boldsymbol{h}),\ \text{where}\ \lim_{t\to 0}\left[\Delta(t\boldsymbol{h})/t\right]=0, \tag{IV.A.37}$$

and

$$R_1\left(\boldsymbol{e}^0+\boldsymbol{h}\right)-R_1\left(\boldsymbol{e}^0\right)=\delta R_1\left(\boldsymbol{e}^0;\boldsymbol{h}\right)+\Delta_1(\boldsymbol{h}),\ \text{where}\ \lim_{t\to 0}\left[\Delta_1(t\boldsymbol{h})/t\right]=0. \tag{IV.A.38}$$

Subtracting Eq. (IV.A.38) from Eq. (IV.A.37) and taking into account Eqs. (IV.A.34) and (IV.A.36) yields the relationship

$$R\left(\boldsymbol{e}^0+\boldsymbol{h}\right)-R_1\left(\boldsymbol{e}^0+\boldsymbol{h}\right)=\varepsilon(\boldsymbol{h}),\ \text{where}\ \lim_{t\to 0}\left[\varepsilon(t\boldsymbol{h})/t\right]=0. \tag{IV.A.39}$$

The result given in Eq. (IV.A.39) can be strengthened if R is Fréchet differentiable [i.e., if $\delta R\left(\boldsymbol{e}^0;\boldsymbol{h}\right)$ is continuous and linear in $\boldsymbol{h}$ at $\boldsymbol{e}^0$, and is continuous in $\boldsymbol{e}$ at $\boldsymbol{e}^0$. In such a case, R_1 is also Fréchet differentiable; hence, the relations $\lim_{t\to 0}\left[\Delta(t\boldsymbol{h})/t\right]=0$ in Eq. (IV.A.37) and $\lim_{t\to 0}\left[\Delta_1(t\boldsymbol{h})/t\right]=0$ in Eq. (IV.A.38) hold uniformly with respect to $\boldsymbol{h}$ on the set $\left\{\boldsymbol{h}:\|\boldsymbol{h}\|=1\right\}$. Consequently, $\lim_{t\to 0}\left[\varepsilon(t\boldsymbol{h})/t\right]=0$ in Eq. (IV.A.39) holds uniformly with also respect to $\boldsymbol{h}$ on $\left\{\boldsymbol{h}:\|\boldsymbol{h}\|=1\right\}$, and can be written in the equivalent form $\lim_{h\to 0}\left[\|\varepsilon(\boldsymbol{h})\|/\|\boldsymbol{h}\|\right]=0$. Thus, the stronger result

$$\left\|R\left(\boldsymbol{e}^0+\boldsymbol{h}\right)-R_1\left(\boldsymbol{e}^0+\boldsymbol{h}\right)\right\|=O\left(\|\boldsymbol{h}\|^2\right) \tag{IV.A.40}$$

holds if R is Fréchet differentiable at $\boldsymbol{e}=\boldsymbol{e}^0$.

A simple illustration of the distinctions between $R(\boldsymbol{e})$ and $R_1(\boldsymbol{e})$ is shown in Figure IV.A.1. There, the critical point $y_1(\boldsymbol{\alpha})$ of $F(\boldsymbol{u},\boldsymbol{x},\boldsymbol{\alpha})$ is a maximum occurring in the (one-dimensional) direction x_1. Changes $\boldsymbol{h}=(\boldsymbol{h}_u,\boldsymbol{h}_\alpha)$ would cause the new maximum of F to take on the value $R\left(\boldsymbol{e}^0+\boldsymbol{h}\right)$ at $y_1\left(\boldsymbol{\alpha}^0+\boldsymbol{h}_\alpha\right)$. The sensitivity $\delta R\left(\boldsymbol{e}^0;\boldsymbol{h}\right)$ of $R(\boldsymbol{e})$ at $\boldsymbol{e}^0$ is given by Eq. (IV.A.8) [or Eq.

(IV.A.27)], while the sensitivity $\delta y_1\left(\boldsymbol{\alpha}^0;\boldsymbol{h}_\alpha\right)$ of $y_1(\boldsymbol{\alpha})$ at $\boldsymbol{\alpha}^0$ is given by Eq. (IV.A.18). However, if y_1 is considered *not* to be a function of $\boldsymbol{\alpha}$, then $R_1\left(\boldsymbol{e}^0+\boldsymbol{h}\right)$ would be the altered value of the functional $R_1(\boldsymbol{e})$. Nevertheless, the sensitivity $\delta R_1\left(\boldsymbol{e}^0;\boldsymbol{h}\right)$ of $R_1(\boldsymbol{e})$ at $\boldsymbol{e}^0$ is the same as the sensitivity $\delta R\left(\boldsymbol{e}^0;\boldsymbol{h}\right)$ of $R(\boldsymbol{e})$ at $\boldsymbol{e}^0$, as shown in Eq. (IV.A.36). This results solely from the fact that $y_1(\boldsymbol{\alpha})$ is a critical point of $F(\boldsymbol{u},\boldsymbol{x},\boldsymbol{\alpha})$.

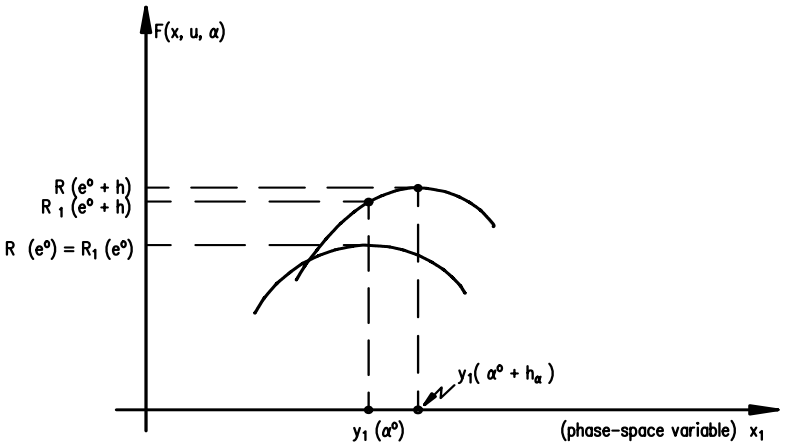

Figure IV.A.1. Illustration of the distinction between $R(\boldsymbol{e})$ and $R_1(\boldsymbol{e})$.

IV.A.4. Illustrative Example: A Particle Diffusion Problem

The sensitivity analysis theory for responses defined at critical points, presented in the foregoing Sections, will now be illustrated by considering a simple diffusion problem of neutral particles (e.g., neutrons) within a slab of material of extrapolated thickness $a\left[cm\right]$, placed in vacuum, which contains distributed particle sources of strength $Q\left[particles\cdot cm^{-3}\cdot s^{-1}\right]$, and is also driven externally by a flux of particles of strength $\varphi_{in}\left[particles\cdot cm^{-2}\cdot s^{-1}\right]$ which impinges on one side (e.g., on the left side) of the slab. Consider, also for simplicity, that the material within the slab only scatters the particles, but does not absorb them. The linear particle diffusion equation that simulates mathematically this problem is

$$L(\boldsymbol{\alpha})\varphi \equiv D\frac{d^2\varphi}{dx^2} = -Q\,, \quad x\in(0,a)\,, \tag{IV.A.41}$$

where $\varphi(x)$ is the (everywhere positive) particle flux, D is the diffusion coefficient in units of $[cm]$, and Q is the corresponding distributed source term within the slab. The boundary conditions considered for $\varphi(x)$, namely

$$\varphi(0) = \varphi_{in}, \quad \varphi(a) = 0, \tag{IV.A.42}$$

simulate an incoming flux φ_{in} at the boundary $x = 0$, and a vanishing flux at the extrapolated distance $x = a$. Thus, the vacuum at the right-side of the slab plays the role of a perfect absorber, in that particles which have left the slab can never return. The response R considered for the diffusion problem modeled by Eqs. (IV.A.41) and (IV.A.42) is the reading of a particle detector placed at the position y within the slab where the flux attains its maximum value, $\varphi_{\max}$. Such a response (i.e., the reading of the particle reaction rate at y) would be simulated mathematically by the following particular form of Eq. (IV.A.3):

$$R(\boldsymbol{e}) = \int_0^a \Sigma_d \varphi(x) \delta[x - y(\boldsymbol{\alpha})]\, dx, \tag{IV.A.43}$$

where Σ_d represents the detector's equivalent reaction cross section, in units of $\left[cm^{-1}\right]$. The location $y(\boldsymbol{\alpha})$ where the flux attains its maximum value is defined implicitly as the solution of the equation

$$\int_0^a \frac{d\varphi(x)}{dx} \delta[x - y(\boldsymbol{\alpha})]\, dx = 0. \tag{IV.A.44}$$

The parameters for this problem are the positive constants Σ_d, D, Q, and φ_{in}, which will be considered to be the components of the vector $\boldsymbol{\alpha}$ of system parameters, defined as

$$\boldsymbol{\alpha} \equiv (\Sigma_d, D, Q, \varphi_{in}). \tag{IV.A.45}$$

The vector $\boldsymbol{e}(x)$ appearing in the functional dependence of R in Eq. (IV.A.43) denotes the concatenation of $\varphi(x)$ with $\boldsymbol{\alpha}$, i. e., $\boldsymbol{e} \equiv (\varphi, \boldsymbol{\alpha})$. The parameters $\boldsymbol{\alpha}$ are considered to be experimentally determined quantities, with known nominal values $\boldsymbol{\alpha}^0 = (\Sigma_d^0, D^0, Q^0, \varphi_{in}^0)$ and known variances $[\mathrm{var}(\Sigma_d), \mathrm{var}(D), \mathrm{var}(Q), \mathrm{var}(\varphi_{in})]$, but being otherwise uncorrelated to one

another. These parameter variances will give rise to variances in the value of the response R (i.e., variance in the maximum flux measured by the detector) and the location $y(\boldsymbol{\alpha})$ of R within the slab. The goal of this illustrative example is to determine the variances of R and $y(\boldsymbol{\alpha})$ by using the "Sandwich Rule" of the "Propagation of Moments" method presented in Section III.F of Volume I.

The nominal value $\varphi^0(x)$ of the flux is determined by solving Eqs. (IV.A.41) and (IV.A.42) for the nominal parameter values $\boldsymbol{\alpha}^0 = \left(\Sigma_d^0, D^0, Q^0, \varphi_{in}^0\right)$. For this simple example, the expression of $\varphi^0(x)$ can be readily obtained in closed form as

$$\varphi^0(x) = \frac{Q^0}{2D^0}\left(ax - x^2\right) + \left(1 - \frac{x}{a}\right)\varphi_{in}^0 . \tag{IV.A.46}$$

Note that even though Eq. (IV.A.41) is *linear* in φ, the solution $\varphi(x)$ depends *nonlinearly* on $\boldsymbol{\alpha}$, as evidenced by Eq. (IV.A.46). Using Eq. (IV.A.46), the nominal value, $\varphi_{\max}^0$, of the maximum of $\varphi^0(x)$, and $y\left(\boldsymbol{\alpha}^0\right)$, respectively, are readily obtained as

$$\varphi_{\max}^0 = \frac{Q^0 a^2}{8D^0} + \frac{D^0\left(\varphi_{in}^0\right)^2}{2a^2 Q^0} + \frac{\varphi_{in}^0}{2}. \tag{IV.A.47}$$

and

$$y\left(\boldsymbol{\alpha}^0\right) = \frac{a}{2} - \frac{\varphi_{in}^0 D^0}{aQ^0}. \tag{IV.A.48}$$

From Eqs. (IV.A. 43) and (IV.A.47), it follows that the nominal value, $R\left(\boldsymbol{e}^0\right)$, of the response $R(\boldsymbol{e})$ is obtained as

$$R\left(\boldsymbol{e}^0\right) = \Sigma_d^0 \varphi_{\max}^0 . \tag{IV.A.49}$$

Of course, for the complex large-scale problems analyzed in practice, it is not possible to obtain exact, closed form expressions for $\varphi^0(x)$, $\varphi_{\max}^0$, $R\left(\boldsymbol{e}^0\right)$, and $y\left(\boldsymbol{\alpha}^0\right)$.

For uncorrelated parameters, the "Sandwich Rule" formula presented in Section III.F of Volume I can be readily applied to this illustrative problem, to obtain the following expression for the variance, $\mathrm{var}(R)$, of R:

$$\mathrm{var}(R)=\left(\frac{\delta R}{\delta \Sigma_d}\right)^2 \mathrm{var}(\Sigma_d)+\left(\frac{\delta R}{\delta D}\right)^2 \mathrm{var}(D)+\left(\frac{\delta R}{\delta Q}\right)^2 \mathrm{var}(Q)+\left(\frac{\delta R}{\delta \varphi_{in}}\right)^2 \mathrm{var}(\varphi_{in}), \tag{IV.A.50}$$

where the symbol $(\delta R/\delta \alpha_i)$ denotes the partial sensitivity (i.e., the partial G-derivative) of $R(\boldsymbol{e})$ to a generic parameter α_i. In turn, the sensitivities of the response $R(\boldsymbol{e})$ are obtained by applying Eq. (IV.A.6) to Eq. (IV.A.43), to compute the G-differential $\delta R(\boldsymbol{e}^0;\boldsymbol{h})$ of $R(\boldsymbol{e})$ at $\boldsymbol{e}^0$, for variations

$$\boldsymbol{h} \equiv (h_\varphi, \boldsymbol{h}_\alpha);\ \boldsymbol{h}_\alpha \equiv (\delta\Sigma_d, \delta D, \delta Q, \delta\varphi_{in}). \tag{IV.A.51}$$

This gives the following expression for $\delta R(\boldsymbol{e}^0;\boldsymbol{h})$:

$$\begin{aligned}\delta R(\boldsymbol{e}^0;\boldsymbol{h}) = &\int_0^a \delta\Sigma_d \varphi(x)\delta\left[x-y(\boldsymbol{\alpha}^0)\right]dx + \\ &\int_0^a h_\varphi(x)\delta\left[x-y(\boldsymbol{\alpha}^0)\right]dx - \\ &\left(\boldsymbol{h}_\alpha \bullet \left(\frac{dy}{d\boldsymbol{\alpha}}\right)_{\boldsymbol{\alpha}^0}\right)\int_0^a \varphi(x)\delta'\left[x-y(\boldsymbol{\alpha}^0)\right]dx.\end{aligned} \tag{IV.A.52}$$

The last term on the right-side of Eq. (IV.A.52) vanishes in view of Eq. (IV.A.44), namely

$$\int_0^a \varphi\delta'(x-y)dx = -\int_0^a (\partial\varphi/\partial x)\delta(x-y)dx = 0.$$

Therefore, Eq. (IV.A.52) reduces to

$$\delta R(\boldsymbol{e}^0;\boldsymbol{h}) = R'_\alpha(\boldsymbol{e}^0)\boldsymbol{h}_\alpha + R'_\varphi(\boldsymbol{e}^0)h_\varphi\,, \tag{IV.A.53}$$

where the "direct-effect" term $R'_\alpha \boldsymbol{h}_\alpha$ is defined as

$$R'_\alpha(\boldsymbol{e}^0)\boldsymbol{h}_\alpha \equiv \int_0^a \delta\Sigma_d \varphi(x)\delta\left[x-y(\boldsymbol{\alpha}^0)\right]dx = \delta\Sigma_d \varphi^0_{\max} \tag{IV.A.54}$$

while the "indirect-effect" term $R'_\varphi h_\varphi$ is defined as

$$R'_\varphi\left(\boldsymbol{e}^0\right)h_\varphi \equiv \int_0^a \Sigma_d^0 h_\varphi(x)\delta\left[x - y\left(\boldsymbol{\alpha}^0\right)\right]dx\,. \tag{IV.A.55}$$

The "direct-effect" term $R'_\alpha \boldsymbol{h}_\alpha$ can be evaluated at this stage by replacing Eq. (IV.A.47) into Eq. (IV.A.54), to obtain

$$R'_\alpha\left(\boldsymbol{e}^0\right)\boldsymbol{h}_\alpha = \delta\Sigma_d\left[\frac{Q^0 a^2}{8D^0} + \frac{D^0\left(\varphi_{in}^0\right)^2}{2a^2Q^0} + \frac{\varphi_{in}^0}{2}\right]. \tag{IV.A.56}$$

The "indirect-effect" term $R'_\varphi h_\varphi$, though, cannot be evaluated at this stage, since $h_\varphi(x)$ is not yet available. The first-order (in $\|\boldsymbol{h}_\alpha\|$) approximation to the exact value of $h_\varphi(x)$ is obtained by calculating the G-differentials of Eqs. (IV.A.41) and (IV.A.42) and solving the resulting "forward sensitivity equations" (FSE)

$$L\left(\boldsymbol{\alpha}^0\right)h_\varphi + \left[L'_\alpha\left(\boldsymbol{\alpha}^0\right)\varphi^0\right]\boldsymbol{h}_\alpha = O\left(\|\boldsymbol{h}_\alpha\|^2\right), \tag{IV.A.57}$$

together with the boundary conditions

$$h_\varphi(0) = \delta\varphi_{in}\,, \quad h_\varphi(a) = 0. \tag{IV.A.58}$$

In Eq. (IV.A.57), the operator $L\left(\boldsymbol{\alpha}^0\right)$ is defined as

$$L\left(\boldsymbol{\alpha}^0\right) \equiv D^0\frac{d^2}{dx^2}, \tag{IV.A.59}$$

while the quantity

$$\left[L'_\alpha\left(\boldsymbol{\alpha}^0\right)\varphi^0\right]\boldsymbol{h}_\alpha \equiv \delta D\frac{d^2\varphi^0}{dx^2} + \delta Q\,, \tag{IV.A.60}$$

which is the partial G-differential of $L\varphi$ at $\boldsymbol{\alpha}^0$ with respect to $\boldsymbol{\alpha}$, contains all of the first-order parameter variations $\boldsymbol{h}_\alpha$. Solving the FSE yields the solution

$$h_{\varphi}(x)=\frac{1}{2D^0}\left(\delta Q-\frac{Q^0\delta D}{D^0}\right)\left(ax-x^2\right)+\left(1-\frac{x}{a}\right)\delta\varphi_{in}. \tag{IV.A.61}$$

Replacing Eq. (IV.A.61) in Eq. (IV.A.55) gives the following expression for the "indirect-effect:"

$$R'_{\varphi}\left(\boldsymbol{e}^0\right)h_{\varphi}=\Sigma_d^0\left[\frac{1}{2D^0}\left(\delta Q-\frac{Q^0\delta D}{D^0}\right)\left(\frac{a^2}{4}-\left(\frac{D^0\varphi_{in}^0}{aQ^0}\right)^2\right)+\delta\varphi_{in}\left(\frac{1}{2}+\frac{D^0\varphi_{in}^0}{a^2Q^0}\right)\right]. \tag{IV.A.62}$$

From Eq. (IV.A.56), it follows that the partial sensitivity (i.e., the partial G-derivative) of R with respect to Σ_d has the expression

$$\frac{\delta R}{\delta\Sigma_d}=\varphi_{\max}^0=\frac{Q^0a^2}{8D^0}+\frac{D^0\left(\varphi_{in}^0\right)^2}{2a^2Q^0}+\frac{\varphi_{in}^0}{2}. \tag{IV.A.63}$$

Similarly, from Eq. (IV.A.62), it follows that the partial sensitivities (i.e., the partial G-derivatives) of R with respect to $D, Q,$ and φ_{in} are:

$$\frac{\delta R}{\delta D}=-\frac{\Sigma_d^0Q^0}{2\left(D^0\right)^2}\left[\frac{a^2}{4}-\left(\frac{D^0\varphi_{in}^0}{aQ^0}\right)^2\right]. \tag{IV.A.64}$$

$$\frac{\delta R}{\delta Q}=\frac{\Sigma_d^0}{2D^0}\left[\frac{a^2}{4}-\left(\frac{D^0\varphi_{in}^0}{aQ^0}\right)^2\right]. \tag{IV.A.65}$$

$$\frac{\delta R}{\delta\varphi_{in}}=\Sigma_d^0\left(\frac{1}{2}+\frac{D^0\varphi_{in}^0}{a^2Q^0}\right). \tag{IV.A.66}$$

Since the sensitivities of the response $R(\boldsymbol{e})$ have thus been determined, Eqs. (IV.A.63) through (IV.A.66) can be replaced in Eq. (IV.A.50) to compute the variance $\mathrm{var}(R)$.

The "Sandwich Rule" presented in Section III.F of Volume I can also be applied to obtain the variance, $\mathrm{var}(y)$, of the critical point $y(\boldsymbol{\alpha})$, where the flux attains its maximum (and where the particle detector is located in this illustrative problem). The corresponding expression for $\mathrm{var}(y)$ is:

$$\mathrm{var}(y)=\left(\frac{\delta y}{\delta D}\right)^2\mathrm{var}(D)+\left(\frac{\delta y}{\delta Q}\right)^2\mathrm{var}(Q)+\left(\frac{\delta y}{\delta \varphi_{in}}\right)^2\mathrm{var}(\varphi_{in}), \quad \text{(IV.A.67)}$$

where the symbol $(\delta y/\delta\alpha_i)$ denotes the partial sensitivity (i.e., the partial G-derivative) of $y(\boldsymbol{\alpha})$ to a generic parameter α_i. In turn, the sensitivity $\delta y(\boldsymbol{\alpha}^0;\boldsymbol{h}_\alpha)$ of the critical (i.e., maximum) point $y(\boldsymbol{\alpha})$ at $\boldsymbol{\alpha}^0$ is obtained by applying Eq. (IV.A.18) to our illustrative example. Thus, Eq. (IV.A.14) takes on the following specific form for our problem:

$$\phi_{11}\equiv\int_0^a\left\{\partial^2\varphi/\partial x^2\right\}_{\boldsymbol{e}^0}\delta\left[x-y(\boldsymbol{\alpha}^0)\right]dx=-\frac{Q^0}{D^0}. \quad \text{(IV.A.68)}$$

Evaluating Eq. (IV.A.17) for our problem gives

$$g_1\equiv-\int_0^a\left\{\partial h_\varphi/\partial x\right\}_{\boldsymbol{e}^0}\delta\left[x-y(\boldsymbol{\alpha}^0)\right]dx=-\frac{\varphi_{in}^0}{a}\left(\frac{\delta Q}{Q^0}-\frac{\delta D}{D^0}-\frac{\delta\varphi_{in}}{\varphi_{in}^0}\right). \quad \text{(IV.A.69)}$$

Replacing Eqs. (IV.A.68) and (IV.A.69) into the particular form taken on by Eq. (IV.A.18) for this illustrative example leads to

$$\delta y(\boldsymbol{\alpha}^0;\boldsymbol{h}_\alpha)=\frac{D^0\varphi_{in}^0}{aQ^0}\left(\frac{\delta Q}{Q^0}-\frac{\delta D}{D^0}-\frac{\delta\varphi_{in}}{\varphi_{in}^0}\right). \quad \text{(IV.A.70)}$$

The above expression indicates that the partial sensitivities (i.e., the partial G-derivatives) of $y(\boldsymbol{\alpha})$ with respect to $D, Q,$ and φ_{in} are as follows:

$$\frac{\delta y}{\delta D}=-\frac{\varphi_{in}^0}{aQ^0}, \quad \text{(IV.A.71)}$$

$$\frac{\delta y}{\delta Q}=\frac{D^0\varphi_{in}^0}{a\left(Q^0\right)^2}, \quad \text{(IV.A.72)}$$

$$\frac{\delta y}{\delta\varphi_{in}}=-\frac{D^0}{aQ^0}. \quad \text{(IV.A.73)}$$

The variance $\mathrm{var}(y)$, of the critical point of $y(\boldsymbol{\alpha})$, can now be computed by replacing Eqs. (IV.A.71) through (IV.A.73) in Eq. (IV.A.67)

In practice, though, it would not be possible to solve analytically the FSE [namely, Eqs. (IV.A.57) and (IV.A.58)], as has been done for this simple illustrative example, in order to obtain the sensitivities of R shown in Eqs. (IV.A.63) through (IV.A.67). Instead, the solution $h_\varphi(x)$ would need to be computed by solving the FSE numerically. Therefore, the FSE would need to be solved anew for each parameter variation $\boldsymbol{h}_\alpha$. Furthermore, the first-derivative of $h_\varphi(x)$ with respect to the independent-variables (x, for this illustrative example) would be needed, for each parameter variation $\boldsymbol{h}_\alpha$, in order to compute the partial sensitivities of $y(\boldsymbol{\alpha})$. It is thus apparent that, for large-scale problems, the *FSAP* would become very expensive computationally.

The need to solve repeatedly the FSE can be circumvented by using the Adjoint Sensitivity Analysis Procedure *(ASAP)*. The first prerequisite for applying the *ASAP* is that the "indirect-effect" term $R'_\varphi(\boldsymbol{e}^0)h_\varphi$ be expressible as a *linear functional of* h_φ. An examination of Eq. (IV.A.55) readily reveals that $R'_\varphi(\boldsymbol{e}^0)h_\varphi$ is indeed a linear functional of h_φ. Therefore, $R'_\varphi(\boldsymbol{e}^0)h_\varphi$ can be represented as an inner product in an appropriately defined Hilbert space $\mathcal{H}_u$; for our illustrative example, $\mathcal{H}_u$ is chosen to be the real Hilbert space $\mathcal{H}_u \equiv \mathcal{L}_2(\Omega)$, with $\Omega \equiv (0,a)$, equipped with the inner product

$$\begin{aligned} &\langle f(x),\, g(x)\rangle \equiv \int_0^a f(x)g(x)dx\,, \\ &\text{for } f, g \in \mathcal{H}_u \equiv \mathcal{L}_2(\Omega), \quad \Omega \equiv (0,a). \end{aligned} \tag{IV.A.74}$$

In $\mathcal{H}_u \equiv \mathcal{L}_2(\Omega)$, the linear functional $R'_\varphi(\boldsymbol{e}^0)h_\varphi$ defined in Eq. (IV.A.55) can be represented as the inner product

$$R'_\varphi(\boldsymbol{e}^0)h_\varphi = \left\langle \Sigma_d^0\, \delta\left[x - y(\boldsymbol{\alpha}^0)\right],\, h_\varphi \right\rangle. \tag{IV.A.75}$$

The next step underlying the *ASAP* is the construction of the operator $L^+(\boldsymbol{\alpha}^0)$ that is *formally adjoint* to $L(\boldsymbol{\alpha}^0)$. Using Eq. (I.B.20) of Volume I readily yields

$$L^+(\boldsymbol{\alpha}^0) \equiv D^0 \frac{d^2}{dx^2}. \tag{IV.A.76}$$

Note that $L^+(\boldsymbol{\alpha}^0)$ and $L(\boldsymbol{\alpha}^0)$ are *formally self-adjoint*. The qualifier "formally" must still be kept at this stage, since the boundary conditions for $L^+(\boldsymbol{\alpha}^0)$ have

not been determined yet. The boundary conditions for $L^+\left(\boldsymbol{\alpha}^0\right)$ are derived by applying Eq. (IV.A.23) to the operators $L\left(\boldsymbol{\alpha}^0\right)h_\varphi$ and $L^+\left(\boldsymbol{\alpha}^0\right)\psi$, to obtain

$$\int_0^a \psi(x)\left[D^0\,\frac{d^2h_\varphi(x)}{dx^2}\right]dx = \int_0^a\left[D^0\,\frac{d^2\psi(x)}{dx^2}\right]h_\varphi(x)\,dx + \left\{P\left[h_\varphi,\psi\right]\right\}_{x=0}^{x=a}. \tag{IV.A.77}$$

Note that the function $\psi(x)$ is still arbitrary at this stage, except for the requirement that $\psi \in \mathscr{H}_Q = \mathscr{L}_2(\Omega)$; note also that the Hilbert spaces $\mathscr{H}_u$ and $\mathscr{H}_Q$ have now both become the same space, i.e., $\mathscr{H}_u = \mathscr{H}_Q = \mathscr{L}_2(\Omega)$.

Integrating the left-side of Eq. (IV.A.77) by parts twice and canceling terms yields the following expression for the bilinear boundary form:

$$\left\{P\left[h_\varphi,\psi\right]\right\}_{x=0}^{x=a} = D^0\left[\psi\,\frac{dh_\varphi}{dx} - h_\varphi\,\frac{d\psi}{dx}\right]_{x=0}^{x=a}. \tag{IV.A.78}$$

The boundary conditions for $L^+\left(\boldsymbol{\alpha}^0\right)$ can now be selected by applying to Eq. (IV.A.78) the general principles (i) and (ii) outlined immediately following Eq. (IV.A.24). From Eq. (IV.A.58), h_φ is known at $x=0$ and $x=a$; however, the quantities $\left\{dh_\varphi/dx\right\}_{x=0}^{x=a}$ are not known. These unknown quantities can be eliminated from Eq. (IV.A.78) by choosing

$$\psi(0)=0, \quad \psi(a)=0, \tag{IV.A.79}$$

as boundary conditions for the adjoint function $\psi(x)$. Implementing Eqs. (IV.A.79) and (IV.A.58) into Eq. (IV.A.78) yields

$$\left\{P\left[h_\varphi,\psi\right]\right\}_{x=0}^{x=a} = D^0\delta\varphi_{in}\left[\frac{d\psi}{dx}\right]_{x=0} \equiv \hat{P}\left(\boldsymbol{h}_\alpha,\psi;\boldsymbol{\alpha}^0\right). \tag{IV.A.80}$$

Note that the quantity $\hat{P}\left(\boldsymbol{h}_\alpha,\psi;\boldsymbol{\alpha}^0\right)$ appearing in Eq. (IV.A.25) *does not vanish; furthermore, the boundary conditions in Eq. (IV.A.79) for the adjoint operator* $L^+\left(\boldsymbol{\alpha}^0\right)$ *differ from the boundary conditions in Eq. (IV.A.58) for* $L\left(\boldsymbol{\alpha}^0\right)$. *Hence even though the operators* $L^+\left(\boldsymbol{\alpha}^0\right)$ *and* $L\left(\boldsymbol{\alpha}^0\right)$ *are formally self-adjoint, they are* ***not*** *self-adjoint for this illustrative example.*

The last step in the construction of the adjoint system is the identification of the source term, which is done by applying Eq. (IV.A.26) to Eqs. (IV.A.75). This identification readily shows that

$$\nabla_{\varphi} R\left(\boldsymbol{e}^{0}\right) = \Sigma_{d}^{0}\ \delta\left[x - y\left(\boldsymbol{\alpha}^{0}\right)\right], \tag{IV.A.81}$$

so that the complete adjoint system becomes

$$L^{+}\left(\boldsymbol{\alpha}^{0}\right)\psi \equiv D^{0}\frac{d^{2}\psi}{dx^{2}} = \Sigma_{d}^{0}\ \delta\left[x - y\left(\boldsymbol{\alpha}^{0}\right)\right], \tag{IV.A.82}$$

where the adjoint function $\psi(x)$ is subject to the boundary conditions given in Eq. (IV.A.79).

Using Eqs. (IV.A.82), (IV.A.81), (IV.A.80), and (IV.A.77) in Eq. (IV.A.75) gives the following expression for the "indirect-effect" term $R'_{\varphi}\left(\boldsymbol{e}^{0}\right)h_{\varphi}$:

$$R'_{\varphi}\left(\boldsymbol{e}^{0}\right)h_{\varphi} = -\int_{0}^{a}\psi(x)\left[\delta D\frac{d^{2}\varphi^{0}(x)}{dx^{2}} + \delta Q\right]dx - D^{0}\left(\delta\varphi_{in}\right)\left\{\frac{d\psi(x)}{dx}\right\}_{x=0}, \tag{IV.A.83}$$

where $\psi(x)$ is the solution of the adjoint sensitivity system defined by Eqs. (IV.A.82) and (IV.A.79).

As expected, Eqs. (IV.A.82) and (IV.A.79), which underlie the adjoint sensitivity system, are independent of parameter variations $\boldsymbol{h}_{\alpha}$; thus, the adjoint sensitivity system needs to be solved only once to obtain the adjoint function $\psi(x)$. Very important for our illustrative example is also the fact (characteristic of linear systems) that the adjoint system is independent of the original solution $\varphi^{0}(x)$, and can therefore be solved directly, without any knowledge of the (original) flux $\varphi(x)$. Of course, the adjoint sensitivity system depends on the response, which provides the source term as shown in Eq. (IV.A.82).

Solving the adjoint sensitivity system, namely Eqs. (IV.A.82) and (IV.A.79), for our illustrative example yields the following expression for the adjoint function $\psi(x)$:

$$\psi(x) = \frac{\Sigma_{d}^{0}}{D^{0}}\left\{\left[x - y\left(\boldsymbol{\alpha}^{0}\right)\right]H\left[x - y\left(\boldsymbol{\alpha}^{0}\right)\right] - \left[a - y\left(\boldsymbol{\alpha}^{0}\right)\right]\frac{x}{a}\right\}, \tag{IV.A.84}$$

where $H\left[x - y\left(\boldsymbol{\alpha}^{0}\right)\right]$ is the Heaviside-step functional defined as

$$H(x)=\begin{cases}0, & \text{for } x<0\\ 1, & \text{for } x\geq 0\end{cases}.$$

Noting from Eq. (IV.A.41) that

$$\frac{d^2\varphi^0(x)}{dx^2}=-\frac{Q^0}{D^0},$$

using the above result together with Eq. (IV.A.84) in Eq. (IV.A.83), and carrying out the respective integrations over x yields, as expected, the same expression for the "indirect-effect" term $R'_\varphi\left(\boldsymbol{e}^0\right)h_\varphi$ as obtained (by having used the *FSAP*) in Eq. (IV.A.62), namely in:

$$R'_\varphi\left(\boldsymbol{e}^0\right)h_\varphi=\Sigma_d^0\left[\frac{1}{2D^0}\left(\delta Q-\frac{Q^0\delta D}{D^0}\right)\left(\frac{a^2}{4}-\left(\frac{D^0\varphi_{in}^0}{aQ^0}\right)^2\right)+\delta\varphi_{in}\left(\frac{1}{2}+\frac{D^0\varphi_{in}^0}{a^2Q^0}\right)\right].$$

Using the *ASAP*, the sensitivities of the critical point $y(\boldsymbol{\alpha})$ can be computed by specializing Eqs. (IV.A.30) through (IV.A.32) to our illustrative example. Thus, applying Eq. (IV.A.30) to our example shows that

$$\gamma_1\left(\boldsymbol{e}^0\right)\equiv\delta'\left[x-y\left(\boldsymbol{\alpha}^0\right)\right]. \qquad \text{(IV.A.85)}$$

Furthermore, Eq. (IV.A.31) reduces to

$$g_1=-\int_0^a w_1(x)\left[\delta D\frac{d^2\varphi^0(x)}{dx^2}+\delta Q\right]dx-D^0(\delta\varphi_{in})\left\{\frac{dw_1(x)}{dx}\right\}_{x=0}, \qquad \text{(IV.A.86)}$$

where the function w_1 is the solution of the following particular form taken on by the adjoint system shown in Eq. (IV.A.32) for our illustrative example:

$$\begin{cases}L^+\left(\boldsymbol{\alpha}^0\right)w_1(x)\equiv D^0\dfrac{d^2w_1(x)}{dx^2}=\delta'\left[x-y\left(\boldsymbol{\alpha}^0\right)\right],\\ w_1(0)=0, \quad w_1(a)=0.\end{cases} \qquad \text{(IV.A.87)}$$

It is important to note that the same operator, namely $L^+\left(\boldsymbol{\alpha}^0\right)$, appears in both Eq. (IV.A.82) and in Eq. (IV.A.87). Furthermore, the functions $\psi(x)$ and w_1 satisfy formally identical boundary conditions, as can be noted by comparing Eq.

(IV.A.79) to Eq. (IV.A.87), respectively. Only the source term, $\gamma_1\left(\boldsymbol{e}^0\right)$, in Eq. (IV.A.87) differs from the corresponding source term $\nabla_u R\left(\boldsymbol{e}^0\right)$ in Eq. (IV.A.82). Therefore, the computer code employed to solve the adjoint system given in Eqs. (IV.A.82) to compute the adjoint function $\psi(x)$ can be used, with relatively trivial modifications, to compute the function w_1 by solving Eq. (IV.A.87). Comparing now the right-sides of Eqs. (IV.A.83) and (IV.A.86) reveals that they are formally identical, except that the function $\psi(x)$, which appears in Eq. (IV.A.83), is formally replaced by the function w_1 in Eq. (IV.A.86). This indicates that the computer program employed to evaluate the "indirect effect term" $R'_\varphi\left(\boldsymbol{e}^0\right)h_\varphi$ can also be used, with only formal modifications, to evaluate the functional g_1, in Eq. (IV.A.86).

To finalize this illustrative example, we note that the explicit form of w_1 can be readily obtained by solving Eq. (IV.A.87), as

$$w_1(x)=\frac{1}{D^0}\left\{H\left[x-y\left(\boldsymbol{\alpha}^0\right)\right]-\frac{x}{a}\right\}, \tag{IV.A.88}$$

where $H\left[x-y\left(\boldsymbol{\alpha}^0\right)\right]$ is the previously defined Heaviside-step functional. Replacing Eq. (IV.A.88) in Eq. (IV.A.86) and carrying out the respective integrations over x yields

$$g_1=-\frac{1}{2D^0}\left(\delta Q-\frac{Q^0\delta D}{D^0}\right)\left[a-2y\left(\boldsymbol{\alpha}^0\right)\right]+\frac{\delta\varphi_{in}}{a}=-\frac{\varphi_{in}^0}{a}\left(\frac{\delta Q}{Q^0}-\frac{\delta D}{D^0}-\frac{\delta\varphi_{in}}{\varphi_{in}^0}\right), \tag{IV.A.89}$$

which is the same expression as was obtained in Eq.(IV.A.69) by having used the *FSAP*. The foregoing derivations have clearly underscored the important advantages offered by the *ASAP*, which should be applied, whenever possible, for computing sensitivities efficiently.

IV. B. ILLUSTRATIVE EXAMPLE: ASAP FOR THE MAXIMUM CLAD TEMPERATURE PREDICTED BY A REACTOR SAFETY CODE

As has also been illustrated by the example presented in Chapter II, the transient behavior of a nuclear reactor system is typically simulated by solving coupled time- and spatially-dependent differential equations that model the

neutron-, mass-, momentum-, and energy-balances within the system. In particular, the RELAP5/MOD3.2 code, which has been analyzed from the point of view of the *ASAP* in Section II.B, simulates the thermal-hydraulic characteristics of light water nuclear reactors (LWR) by using a one-dimensional, nonequilibrium, nonhomogeneous two-phase flow model, together with conservation equations for boron concentration and non-condensable gases. A similar code system, called MELT IIIB, can be used for simulating the transient behavior of sodium-cooled fast reactors. Since sodium remains in its liquid-phase during the normal transient operation of a fast reactor, the equations solved within the MELT IIIB code system are somewhat simpler than those solved within the RELAP5/MOD3.2 code system. Specifically, the MELT code solves equations simulating the following phenomena: (a) thermal-hydraulics equations describing the conservation of thermal energy, mass, and momentum for the average channel fuel pin and surrounding single-phase coolant, for each channel type j $(j=1,\ldots,NC)$, where NC denotes the maximum number of channels in the reactor core; (b) neutron point-kinetics equations describing the time-dependent behavior of the core-integrated neutron density; and (c) a loop-hydraulic equation that relates the core inlet and outlet pressures, P_{inlet} and P_{exit}, respectively. The explicit forms for these equations are as follows:

(a) Suppressing, for notational convenience, the channel index j, the thermal-hydraulics equations comprise the following conservation equations:

(i) thermal energy conservation equations for the average channel fuel pin, surrounding coolant, and structure, respectively:

$$\rho C_p \frac{\partial T}{\partial t} - \frac{1}{r}\frac{\partial}{\partial r}\left(rk\frac{\partial T}{\partial r}\right) - \psi n = \psi n_\gamma, \quad r \in (0, R_f) \cup (R_g, R); z \in (0, L); t \in (0, t_f), \tag{IV.B.1}$$

$$A_c \rho_c C_{pc} \frac{DT_c}{Dt} - \frac{\partial}{\partial z}\left(A_c k_c \frac{\partial T_c}{\partial z}\right) - \psi n - 2\pi h\{R[T(R,z,t) - T_c(z,t)] + R_s(T_s - T_c)\} = \psi n_\gamma, \quad z \in (0, L), t \in (0, t_f), \tag{IV.B.2}$$

$$A_s \rho_s C_{ps} \frac{DT_s}{Dt} - 2\pi h R_s (T_c - T_s) = 0, \quad z \in (0, L), t \in (0, t_f). \tag{IV.B.3}$$

(ii) mass conservation equations for each coolant channel:

$$A_c \frac{\partial \rho_c}{\partial t} + \frac{\partial (A_c \rho_c u)}{\partial z} = 0, \quad z \in (0, L), t \in (0, t_f). \tag{IV.B.4}$$

(iii) momentum conservation equations for each coolant channel:

$$-\frac{\partial P}{\partial z}-\rho_c\frac{Du}{Dt}-\frac{f\rho_c u^2}{2D}-\rho_c g-\sum_m \delta(z-z_m)\frac{1}{2}\rho_c u^2 K_L=0, \quad z\in(0,L), t\in(0,t_f). \tag{IV.B.5}$$

(b) The point kinetics equations for the reactor core are

$$\frac{dn}{dt}-\frac{\bar{\rho}-\beta}{\Lambda}n-\sum_{i=1}^{NG}\lambda_i C_i=0, \tag{IV.B.6}$$

and

$$\frac{dC_i}{dt}+\lambda_i C_i-\frac{\beta_i n}{\Lambda}=0, \tag{IV.B.7}$$

for $t\in(0,t_f)$, and $(i=1,\ldots,NG)$, where the NG denotes the total number of precursor groups considered in the simulation.

(c) The loop-hydraulic equation relating P_{inlet} to P_{exit} is

$$P_{inlet}-\left(P_{exit}-f_L W^2+\Delta H+\Delta P\right)=0, \tag{IV.B.8}$$

where

$$W=\sum_{j=1}^{NC}\left[N_j(\rho_c A_c u)_j\right]_{z=0}. \tag{IV.B.9}$$

Note that coupling among the various channels occurs solely through Eq. (IV.B.8) and is specifically due to the mass flow rate W defined in Eq. (IV.B.9). In contrast to the thermal-hydraulic equations, the point-kinetics equations and the primary-loop hydraulics equations apply to the total reactor domain; thus, these equations are time dependent but are channel independent.

The initial and boundary conditions for Eqs. (IV.B.1) through (IV.B.7) are as follows:

$$T(t=0)=\tilde{T}, \tag{IV.B.10}$$

$$\left(\frac{\partial T}{\partial r}\right)_{r=0}=0, \tag{IV.B.11}$$

$$\left(rk\frac{\partial T}{\partial r}\right)_{R_f} - \left(rk\frac{\partial T}{\partial r}\right)_{R_g} = 0, \tag{IV.B.12}$$

$$\left(k\frac{\partial T}{\partial r} + h_g T\right)_{R_f} - \left(h_g T\right)_{R_g} = 0, \tag{IV.B.13}$$

$$\left(k\frac{\partial T}{\partial r} + hT\right)_{R} - hT_c = 0, \tag{IV.B.14}$$

$$T_c\left(t=0\right) = \tilde{T}_c, \tag{IV.B.15}$$

$$T_c\left(z=0\right) = T_{in}, \tag{IV.B.16}$$

$$\left(A_c k_c \frac{\partial T_c}{\partial z}\right)_{z=L} = 0, \tag{IV.B.17}$$

$$T_s\left(t=0\right) = \tilde{T}_s, \tag{IV.B.18}$$

$$u\left(t=0\right) = \tilde{u}, \tag{IV.B.19}$$

$$P\left(z=L\right) = P_{exit}, \tag{IV.B.20}$$

$$P\left(z=0\right) = P_{inlet}, \tag{IV.B.21}$$

$$n\left(t=0\right) = \tilde{n}, \tag{IV.B.22}$$

$$C_i\left(t=0\right) = \tilde{C}_i = \frac{\beta_i \tilde{n}}{\Lambda \lambda_i}. \tag{IV.B.23}$$

The physical meaning of the symbols appearing in the above equations is provided in the "***Nomenclature***", at the end of this Section.

The total reactor domain, henceforth denoted by Ω, consists of the union of all the (pin) domains Ω_j, i.e.,

$$\Omega = \bigcup_{j=1}^{NC} \Omega_j \ . \tag{IV.B.24}$$

The domain Ω_j is the set $\Omega_j = \left\{r, z, t \,/\, r \in \left(0, R_f\right) \cup \left(R_g, R\right); \; z \in \left(0, L\right); t \in \left(0, t_f\right)\right\}$, and its boundary $\partial\Omega_j$ consists of the set of points $\partial\Omega_j = \left\{r = 0, R_f, R_g, R; \; z = 0, L; \; t = 0, t_f\right\}$. Thus, $\boldsymbol{x} \in \Omega_j$ for the thermal-hydraulic equations, since these equations describe the physical behavior of the average channel fuel pin, surrounding coolant, and structure for each channel of type j. Similarly, $\boldsymbol{x} \in \partial\Omega_j$ for the boundary and initial conditions associated with these thermal-hydraulic equations. Note that there are N_j pins in each channel j.

Thus, integrals over Ω are related to integrals over Ω_j through the relationship

$$\int_{\Omega}[\ ]d\Omega = \sum_{j=1}^{NC} N_j \int_{\Omega_j}[\ ]2\pi r\, dr\, dz\, dt\,. \tag{IV.B.25}$$

The system of coupled nonlinear partial differential equations represented by Eqs. (IV.B.1) through (IV.B.9) can be written in operator form as

$$\boldsymbol{N}\left[\boldsymbol{U}(\boldsymbol{x}),\boldsymbol{\alpha}\right] = \boldsymbol{Q}(\boldsymbol{\alpha}),\ \ \boldsymbol{x}\in\Omega_j\,, \tag{IV.B.26}$$

where $\boldsymbol{x} = (r,z,t)$ is the phase-space position vector whose components are the radial, axial, and time-independent variables, respectively, and $\boldsymbol{U} = (\boldsymbol{T},\boldsymbol{T}_c,\boldsymbol{T}_s,\boldsymbol{P},\boldsymbol{u},n,C_1,\ldots,C_{NG})$ is the state vector whose components are the dependent variables. Note that the vectors $\boldsymbol{T},\boldsymbol{T}_c,\boldsymbol{T}_s,\boldsymbol{P}$, and $\boldsymbol{u}$ are channel-dependent; therefore, each of these vectors has NC components; for example, $\boldsymbol{T} = (T_1,\ldots,T_j,\ldots,T_{NC})$, where T_j refers to the temperature in the j^{th} channel. Thus, $\boldsymbol{U}$ is an M-dimensional (column) vector, where $M = NG + 5\times NC + 1$. In Eq. (IV.B.26), the vector $\boldsymbol{\alpha}$ denotes, as usual, the system parameters, which, in this case, comprise various coefficients, scale factors, boundary and initial conditions; the total number of such parameters will be denoted by I.

The boundary and initial conditions shown in Eqs. (IV.B.10) through (IV.B.23) can also be written in operator form as

$$\boldsymbol{B}\left[U,\boldsymbol{\alpha}\right] = \boldsymbol{A}(\boldsymbol{\alpha}),\ \ \boldsymbol{x}\in\partial\Omega_j\,. \tag{IV.B.27}$$

The responses that will be analyzed in the sequel are the maximum power and the maximum temperature attained in the reactor. These responses are of fundamental importance both for the reactor's performance and for reactor safety. The equations satisfied by $n(t)$ and $\boldsymbol{T}(\boldsymbol{x})$ reveal that both of these (dependent) variables are continuous; in particular, their first derivatives with respect to the independent variables exist at the locations where $n(t)$ and $\boldsymbol{T}(\boldsymbol{x})$ attain their respective maxima. From the viewpoint of sensitivity analysis, the maximum power response, denoted henceforth as $R_n(\boldsymbol{e})$, and the maximum fuel temperature response, denoted as $R_T(\boldsymbol{e})$, are functionals of $\boldsymbol{e} = (\boldsymbol{U},\boldsymbol{\alpha})$, where $\boldsymbol{e}$ denotes the concatenation of the state vector $\boldsymbol{U}$ and the vector $\boldsymbol{\alpha}$ of system parameters.

The maximum power response can be represented as

$$R_n(\boldsymbol{e}) = K \int_{\Omega} n(t)\delta\left[t - t_n(\boldsymbol{\alpha})\right] d\Omega\,, \tag{IV.B.28}$$

where the constant

$$K \equiv 1 \Big/ \left[\sum_j N_j \pi\, L\left(R_f^2 + R^2 - R_g^2\right) \right] \tag{IV.B.29}$$

serves as a normalization factor, and where $t_n(\boldsymbol{\alpha})$ represents the phase-space location of the maximum; $t_n(\boldsymbol{\alpha})$ is defined implicitly as the solution of

$$\left\{dn(t)/dt\right\} = 0\,, \quad \text{at } t = t_n(\boldsymbol{\alpha})\,. \tag{IV.B.30}$$

Note that $t_n(\boldsymbol{\alpha})$ is a function of $\boldsymbol{\alpha}$, so variations in the system parameters will induce variations in the phase-space location of the maximum power.

The maximum fuel temperature response for any channel J can be represented as

$$R_T(\boldsymbol{e}) = \int_{\Omega} (1/N_J)\, \boldsymbol{g}_J\, \boldsymbol{T}(\boldsymbol{x})\delta\left[\boldsymbol{x} - \boldsymbol{x}_T(\boldsymbol{\alpha})\right] d\Omega\,. \tag{IV.B.31}$$

In Eq. (IV.B.31), $\boldsymbol{g}_J$ represents an NC – components vector

$$\boldsymbol{g}_J = (0,\ldots,0,1,0,\ldots,0)\,, \tag{IV.B.32}$$

whose only nonzero component is the unit-value taken on by its J^{th} component. Also, in Eq. (IV.B.31), the vector

$$\boldsymbol{x}_T(\boldsymbol{\alpha}) = \left[r_T(\boldsymbol{\alpha}), z_T(\boldsymbol{\alpha}), t_T(\boldsymbol{\alpha})\right] \tag{IV.B.33}$$

represents the location in the phase-space where the maximum fuel temperature in channel J occurs, while the functional

$$\delta\left[\boldsymbol{x} - \boldsymbol{x}_T(\boldsymbol{\alpha})\right] = \delta\left[r - r_T(\boldsymbol{\alpha})\right]\delta\left[z - z_T(\boldsymbol{\alpha})\right]\delta\left[t - t_T(\boldsymbol{\alpha})\right] \tag{IV.B.34}$$

represents the customary three-dimensional Dirac-delta functional. Note that $\boldsymbol{x}_T(\boldsymbol{\alpha})$ is defined implicitly as the solution of the system of equations

$$\left(\partial T_J / \partial r\right)_{\boldsymbol{x}_T(\boldsymbol{\alpha})} = 0\,, \tag{IV.B.35a}$$

$$\left(\partial T_J / \partial z\right)_{\boldsymbol{x}_T(\boldsymbol{\alpha})} = 0, \tag{IV.B.35b}$$

$$\left(\partial T_J / \partial t\right)_{\boldsymbol{x}_T(\boldsymbol{\alpha})} = 0, \tag{IV.B.35c}$$

which express the conditions necessary for $T_j(\boldsymbol{x})$ to have a maximum at $\boldsymbol{x}_T(\boldsymbol{\alpha})$. Due to the boundary condition $\left(\partial T_j / \partial r\right)_{r=0} = 0$, the fuel temperature will attain its maximum in the radial direction at the center of the fuel rod. Thus, the components $z_T(\boldsymbol{\alpha})$ and $t_T(\boldsymbol{\alpha})$ of $\boldsymbol{x}_T(\boldsymbol{\alpha})$ are functions of (the system parameters) $\boldsymbol{\alpha}$, but the radial location of the maximum is always

$$r_T \equiv 0 \tag{IV.B.36}$$

regardless of $\boldsymbol{\alpha}$.

As discussed in Section IV.A, sensitivity analysis of responses defined at critical points has a twofold objective, namely: (i) to determine the sensitivities of R_n and R_T (i.e., the sensitivities of the numerical values of the maximum power and maximum fuel temperature responses, respectively) to changes in the system parameters $\boldsymbol{\alpha}$; and (ii) to determine the sensitivities of the critical points t_n and $\boldsymbol{x}_T$ (i.e., the sensitivities of the phase-space locations where the respective maxima occur) to changes in the system parameters $\boldsymbol{\alpha}$.

Recall that the most general concept for the definition of the sensitivity of a response $R(\boldsymbol{e})$ to variations in the system parameters is the Gateaux (G-) differential $\delta R\left(\boldsymbol{e}^0; \boldsymbol{h}\right)$ of $R(\boldsymbol{e})$ at $\boldsymbol{e}^0$, defined as

$$\delta R\left(\boldsymbol{e}^0; \boldsymbol{h}\right) \equiv \frac{d}{d\varepsilon}\left\{\left[R\left(\boldsymbol{e}^0 + \varepsilon \boldsymbol{h}\right)\right]\right\}_{\varepsilon=0}, \tag{IV.B.37}$$

where ε is a real scalar, and $\boldsymbol{h} = \left(\boldsymbol{h}_U, \boldsymbol{h}_\alpha\right)$ represents a fixed, but otherwise arbitrary, vector of "changes" around the base-case configuration $\boldsymbol{e}^0 = \left(\boldsymbol{U}^0, \boldsymbol{\alpha}^0\right)$. The vectors $\boldsymbol{h}_U$ and $\boldsymbol{h}_\alpha$ have the same number of components as $\boldsymbol{U}$ and $\boldsymbol{\alpha}$, respectively; for example, $\boldsymbol{h}_U = \left(\boldsymbol{h}_T, \boldsymbol{h}_{T_c}, \boldsymbol{h}_{T_s}, \boldsymbol{h}_P, \boldsymbol{h}_u, h_n, h_{C_1}, \ldots, h_{C_{NG}}\right)$. Recall also that if the G-differential $\delta R\left(\boldsymbol{e}^0; \boldsymbol{h}\right)$ is linear in $\boldsymbol{h}$, then it is customarily denoted by $DR\left(\boldsymbol{e}^0; \boldsymbol{h}\right)$. The necessary and sufficient conditions for a G-differential of an operator that acts nonlinearly on $\boldsymbol{e} = \left(\boldsymbol{U}, \boldsymbol{\alpha}\right)$ to be linear in $\boldsymbol{h}$ have been generally discussed in Volume I. As will be shown in the sequel by the actual computation of the various G-derivatives, all of the operators that act on $\boldsymbol{e} = \left(\boldsymbol{U}, \boldsymbol{\alpha}\right)$ in this problem admit G differentials that are linear in $\boldsymbol{h}$.

The G differential of $R_n(\boldsymbol{e})$ at $\boldsymbol{e}^0$, which gives the sensitivity of R_n to changes $\boldsymbol{h}$, is obtained by applying the definition given in Eq. (IV.B.37) to Eq. (IV.B.28), to obtain

$$\begin{aligned} DR_n(\boldsymbol{e}^0;\boldsymbol{h}) &\equiv K\int_\Omega \left(\frac{d}{d\varepsilon}\left\{\left(n^0+\varepsilon\, h_n\right)\delta\left[t-t_n\left(\boldsymbol{\alpha}+\varepsilon\boldsymbol{h}_\alpha\right)\right]\right\}\right)_{\varepsilon=0} d\Omega \\ &= K\int_\Omega h_n\,\delta\left[t-t_n\left(\boldsymbol{\alpha}^0\right)\right]d\Omega - K\sum_{i=1}^{I}\left(\partial t_n/\partial\alpha_i\right)_{\boldsymbol{\alpha}^0} h_{\alpha_i}\int_\Omega n^0\delta'\left[t-t_n\left(\boldsymbol{\alpha}^0\right)\right]d\Omega. \end{aligned} \tag{IV.B.38}$$

Using the definition of the δ' functional, i.e.,

$$\int f(x)\delta'(x-x_0)dx = -\int (df/dx)\delta(x-x_0)dx\,, \tag{IV.B.39}$$

and recalling Eq. (IV.B.30), the last term appearing on the right side of Eq. (IV.B.38) can be shown to vanish, since

$$\int_\Omega n^0(t)\delta'(t-t_n)d\Omega = -\left[dn(t)/dt\right]_{t_n} = 0\,. \tag{IV.B.40}$$

Thus, Eq. (IV.B.38) simplifies to

$$DR_n(\boldsymbol{e}^0;\boldsymbol{h}) = K\int_\Omega h_n(t)\delta\left[t-t_n\left(\boldsymbol{\alpha}^0\right)\right]d\Omega\,. \tag{IV.B.41}$$

The sensitivity $DR_T(\boldsymbol{e}^0;\boldsymbol{h})$ of $R_T(\boldsymbol{e})$ at $\boldsymbol{e}^0$ is determined by using Eq. (IV.B.31) and by following the same procedure as that leading to Eq. (IV.B.41). The result is

$$DR_T = \int_\Omega \left(1/N_J\right)\boldsymbol{g}_J\cdot\boldsymbol{h}_T(\boldsymbol{x})\delta\left[\boldsymbol{x}-\boldsymbol{x}_T\left(\boldsymbol{\alpha}^0\right)\right]d\Omega\,. \tag{IV.B.42}$$

The sensitivities of the critical points $t_n(\boldsymbol{\alpha})$ and $\boldsymbol{x}_T(\boldsymbol{\alpha})$ to changes $\boldsymbol{h}_\alpha$ are given by the respective G-differentials of $t_n(\boldsymbol{\alpha})$ and $\boldsymbol{x}_T(\boldsymbol{\alpha})$ at $\boldsymbol{\alpha}^o$. In view of Eqs. (IV.B.30), (IV.B.33), and (IV.B.35), each of the quantities t_n, z_T, and t_T is a real-valued function of the real variables $(\alpha_1,\ldots,\alpha_I)$ and can therefore be regarded as a functional defined on a subset of $\mathcal{X}^I$. Applying now the definition given in Eq. (IV.B.37) to the functionals $t_n(\boldsymbol{\alpha})$, $z_T(\boldsymbol{\alpha})$, and $t_T(\boldsymbol{\alpha})$ yields

$$Dt_n\left(\boldsymbol{\alpha}^0;\boldsymbol{h}_\alpha\right)=\sum_{i=1}^{I}h_{\alpha_i}\left(\partial t_n/\partial\alpha_i\right)_{\boldsymbol{\alpha}^0}\,, \tag{IV.B.43}$$

$$Dz_T\left(\boldsymbol{\alpha}^0;\boldsymbol{h}_\alpha\right)=\sum_{i=1}^{I}h_{\alpha_i}\left(\partial z_T/\partial\alpha_i\right)_{\boldsymbol{\alpha}^0}\,, \tag{IV.B.44}$$

$$Dt_T\left(\boldsymbol{\alpha}^0;\boldsymbol{h}_\alpha\right)=\sum_{i=1}^{I}h_{\alpha_i}\left(\partial t_T/\partial\alpha_i\right)_{\boldsymbol{\alpha}^0}\,. \tag{IV.B.45}$$

In view of Eqs., (IV.B.33), (IV.B.36), (IV.B.44), and (IV.B.45), the sensitivity of the critical point $\boldsymbol{x}_T(\boldsymbol{\alpha})$ to changes $\boldsymbol{h}_\alpha$ around $\boldsymbol{\alpha}^0$ is given by the three-component column vector

$$D\boldsymbol{x}_T\left(\boldsymbol{\alpha}^0;\boldsymbol{h}_\alpha\right)=\left(0,Dz_T,Dt_T\right). \tag{IV.B.46}$$

To determine Dt_n, Eq. (IV.B.30) is recast in the equivalent form

$$\int_\Omega\left(dn/dt\right)\delta\left[t-t_n(\boldsymbol{\alpha})\right]d\Omega=0. \tag{IV.B.47}$$

Taking the G differential of Eq. (IV.B.47) gives

$$\int_\Omega\left(dh_n/dt\right)\delta\left[t-t_n(\boldsymbol{\alpha})\right]d\Omega-Dt_n\left(\boldsymbol{\alpha}^0;\boldsymbol{h}_\alpha\right)\int_\Omega\left(dn/dt\right)\delta'\left[t-t_n(\boldsymbol{\alpha})\right]d\Omega=0.$$

Solving the above equation for Dt_n gives

$$Dt_n=\left(dh_n/dt\right)_{t_n\left(\boldsymbol{\alpha}^0\right)}\Big/\left(d^2n/dt^2\right)_{t_n\left(\boldsymbol{\alpha}^0\right)}. \tag{IV.B.48}$$

The explicit expressions for Dz_T and Dt_T are obtained by following the same procedure as that leading to Eq. (IV.B.48). Thus, Eqs. (IV.A.35b) and (IV.A.35c) are recast in the forms

$$\int_\Omega\left[\partial\left(\boldsymbol{g}_J\cdot\boldsymbol{T}\right)/\partial z\right]\delta\left[\boldsymbol{x}-\boldsymbol{x}_T(\boldsymbol{\alpha})\right]d\Omega=0$$

and

$$\int_{\Omega}\left[\partial\left(\boldsymbol{g}_J\cdot\boldsymbol{T}\right)/\partial t\right]\delta\left[\boldsymbol{x}-\boldsymbol{x}_T\left(\boldsymbol{\alpha}\right)\right]d\Omega=0\,.$$

Taking the G-differentials of the above equations and simultaneously solving the resulting equations for Dz_T and Dt_T leads to

$$\begin{pmatrix}Dz_T\\ Dt_T\end{pmatrix}=\boldsymbol{M}^{-1}\boldsymbol{F}\,, \tag{IV.B.49}$$

where

$$\boldsymbol{F}\equiv\begin{bmatrix}-\left(\partial h_T/\partial z\right)_{\boldsymbol{x}_T\left(\boldsymbol{\alpha}^0\right)}\\ -\left(\partial h_T/\partial t\right)_{\boldsymbol{x}_T\left(\boldsymbol{\alpha}^0\right)}\end{bmatrix} \tag{IV.B.50}$$

and

$$\boldsymbol{M}\equiv\begin{bmatrix}\left(\partial^2 T_J/\partial z^2\right)_{\boldsymbol{x}_T\left(\boldsymbol{\alpha}^0\right)} & \left(\partial^2 T_J/\partial z\partial t\right)_{\boldsymbol{x}_T\left(\boldsymbol{\alpha}^0\right)}\\ \left(\partial^2 T_J/\partial t\partial z\right)_{\boldsymbol{x}_T\left(\boldsymbol{\alpha}^0\right)} & \left(\partial^2 T_J/\partial t^2\right)_{\boldsymbol{x}_T\left(\boldsymbol{\alpha}^0\right)}\end{bmatrix}. \tag{IV.B.51}$$

Computing the G-differentials at $\boldsymbol{e}^o$ of Eqs. (IV.B.26) and (IV.B.27) yields

$$\boldsymbol{N}'_U\left(\boldsymbol{e}^0\right)\boldsymbol{h}_U=\left[\boldsymbol{Q}'_\alpha\left(\boldsymbol{\alpha}^0\right)-\boldsymbol{N}'_\alpha\left(\boldsymbol{e}^0\right)\right]\boldsymbol{h}_\alpha\,,\qquad \boldsymbol{x}\in\Omega_j\,, \tag{IV.B.52}$$

and

$$\boldsymbol{B}'_U\left(\boldsymbol{e}^0\right)\boldsymbol{h}_U=\left[\boldsymbol{A}'_\alpha\left(\boldsymbol{\alpha}^0\right)-\boldsymbol{B}'_\alpha\left(\boldsymbol{e}^0\right)\right]\boldsymbol{h}_\alpha\,,\qquad \boldsymbol{x}\in\partial\Omega_j\,. \tag{IV.B.53}$$

The explicit representation of $\boldsymbol{N}'_U\left(\boldsymbol{e}^0\right)$ is the $M\times M$ matrix whose elements are the partial G-derivatives at $\boldsymbol{e}^0$ of the components of $\boldsymbol{N}$ with respect to the components U_j of $\boldsymbol{U}$, namely

$$\boldsymbol{N}'_U\left(\boldsymbol{e}^0\right)\equiv\left[L_{ij}\left(\boldsymbol{e}^0\right)\right];\ L_{ij}\left(\boldsymbol{e}^0\right)\equiv\left(N'_i\right)_{U_j}\left(\boldsymbol{e}^0\right);\ \left(i,j=1,\ldots,M\right). \tag{IV.B.54}$$

The representation of $\boldsymbol{N}'_\alpha\left(\boldsymbol{e}^0\right)$ is the $M\times I$ matrix whose elements are the partial G-derivatives at $\boldsymbol{e}^0$ of the components of $\boldsymbol{N}\left(\boldsymbol{e}\right)$ with respect to the

components of $\boldsymbol{\alpha}$. The elements of the matrices representing $\boldsymbol{B}'_U\left(\boldsymbol{e}^0\right)$, $\boldsymbol{Q}'_\alpha\left(\boldsymbol{\alpha}^0\right)$, and $\boldsymbol{A}'_\alpha\left(\boldsymbol{\alpha}^0\right)$ are obtained in a similar manner. Note that $\boldsymbol{N}'_U\left(\boldsymbol{e}^0\right)\boldsymbol{h}_U$ and $\boldsymbol{B}'_U\left(\boldsymbol{e}^0\right)\boldsymbol{h}_U$ are linear in $\boldsymbol{h}_U$ and are independent of $\boldsymbol{h}_\alpha$; on the other hand, $\boldsymbol{N}'_\alpha\left(\boldsymbol{e}^0\right)\boldsymbol{h}_\alpha$ and $\boldsymbol{B}'_\alpha\left(\boldsymbol{e}^0\right)\boldsymbol{h}_\alpha$ are linear in $\boldsymbol{h}_\alpha$, and are independent of $\boldsymbol{h}_U$.

For a given vector of changes $\boldsymbol{h}_\alpha$, Eqs. (IV.B.52) and (IV.B.53) could be solved to determine $\boldsymbol{h}_U$; $\boldsymbol{h}_U$ could then be used to evaluate the sensitivities DR_n, DR_T, $D\boldsymbol{x}_T$, and Dt_n. However, due to the large number of system parameters, it would be prohibitively expensive to repeatedly solve Eqs. (IV.B.52) and (IV.B.53) for all vectors $\boldsymbol{h}_\alpha$ of possible interest to the sensitivity analysis of the problem at hand. The alternative procedure, which avoids the need to solve Eqs. (IV.B.52) and (IV.B.53) repeatedly, relies on the implementation of the *ASAP*, in order to evaluate the above-mentioned sensitivities by using appropriately constructed adjoint operators.

As Eqs. (IV.B.41), (IV.B.42), (IV.B.48), and (IV.B.49) respectively indicate, each of the functionals DR_n, DR_T, Dt_n, Dz_T, and Dt_T is linear in $\boldsymbol{h}_U$. Considering now that $\boldsymbol{h}_U \in H$, where H denotes an appropriately defined Hilbert space equipped with the inner product

$$\left\langle \boldsymbol{V}, \boldsymbol{W} \right\rangle = \sum_{j=1}^{M} \int_\Omega v_j \, w_j \, d\Omega, \quad \boldsymbol{V} \in H, \; \boldsymbol{W} \in H, \tag{IV.B.55}$$

it follows that the Riesz representation theorem ensures that each of the functionals DR_n, DR_T, Dt_n, Dz_T, and Dt_T can be written as the inner product of $\boldsymbol{h}_U$ with a uniquely defined vector in H. Thus, the functional DR_n given by Eq. (IV.B.41) can be represented as

$$DR_n = \left\langle \boldsymbol{h}_U, \boldsymbol{S}_n^* \right\rangle, \tag{IV.B.56}$$

where the M-component vector $\boldsymbol{S}_n^*$ is defined as

$$\boldsymbol{S}_n^* \equiv K\delta\left[t - t_n\left(\boldsymbol{\alpha}^0\right)\right] \; (\boldsymbol{0},\boldsymbol{0},\boldsymbol{0},\boldsymbol{0},\boldsymbol{0},1,0,\ldots,0)^T. \tag{IV.B.57}$$

Similarly, the functional DR_T given by Eq. (IV.B.42) can be represented as

$$DR_T = \left\langle \boldsymbol{h}_U, \boldsymbol{S}_T^* \right\rangle, \tag{IV.B.58}$$

where the M -component vector $\boldsymbol{S}_T^*$ is defined as

$$\boldsymbol{S}_T^* \equiv (1/N_J)\delta\left[\boldsymbol{x} - \boldsymbol{x}_T\left(\boldsymbol{\alpha}^0\right)\right]\ (\boldsymbol{g}_J, \boldsymbol{0}, \boldsymbol{0}, \boldsymbol{0}, \boldsymbol{0}, 0, \ldots, 0)^T\ . \quad \text{(IV.B.59)}$$

With the help of the δ' functional, Eq. (IV.B.48) can be written in the inner product form as

$$Dt_n = \left\langle \boldsymbol{h}_U, \boldsymbol{G}^* \right\rangle \Big/ \left(d^2 n / dt^2\right)_{t_n\left(\boldsymbol{\alpha}^0\right)}, \quad \text{(IV.B.60)}$$

where

$$\boldsymbol{G}^* \equiv K\delta'\left[t - t_n\left(\boldsymbol{\alpha}^0\right)\right]\ (\boldsymbol{0}, \boldsymbol{0}, \boldsymbol{0}, \boldsymbol{0}, \boldsymbol{0}, 1, 0, \ldots, 0)^T\ . \quad \text{(IV.B.61)}$$

Similarly, Eq. (IV.B.49) can be expressed as

$$\begin{pmatrix} Dz_T \\ Dt_T \end{pmatrix} = \boldsymbol{M}^{-1} \begin{pmatrix} \left\langle \boldsymbol{h}_U, \boldsymbol{F}_1^* \right\rangle \\ \left\langle \boldsymbol{h}_U, \boldsymbol{F}_2^* \right\rangle \end{pmatrix}, \quad \text{(IV.B.62)}$$

where

$$\boldsymbol{F}_1^* \equiv (1/N_J)\delta'\left[z - z_T\left(\boldsymbol{\alpha}^0\right)\right]\delta\left[t - t_T\left(\boldsymbol{\alpha}^0\right)\right]\delta(r)(\boldsymbol{g}_J, \boldsymbol{0}, \ldots, 0)^T, \quad \text{(IV.B.63)}$$

and

$$\boldsymbol{F}_2^* \equiv (1/N_J)\delta'\left[t - t_T\left(\boldsymbol{\alpha}^0\right)\right]\delta\left[z - z_T\left(\boldsymbol{\alpha}^0\right)\right]\delta(r)(\boldsymbol{g}_J, \boldsymbol{0}, \ldots, 0)^T\ . \quad \text{(IV.B.64)}$$

To proceed with the construction of the appropriate adjoint system, recall that both Eqs. (IV.B.52) and (IV.B.53) are linear in $\boldsymbol{h}_U$. Consequently, the following relationship holds for an arbitrary vector $\boldsymbol{V} \in H$:

$$\left\langle \boldsymbol{V}, \boldsymbol{N}_U'\left(\boldsymbol{e}^0\right)\boldsymbol{h}_U \right\rangle = \left\langle \boldsymbol{h}_U, \boldsymbol{L}^*\left(\boldsymbol{e}^0\right)\boldsymbol{V} \right\rangle + \left[P(\boldsymbol{h}_U; \boldsymbol{V})\right]_{\partial\Omega}\ . \quad \text{(IV.B.65)}$$

In Eq. (IV.B.65), $\boldsymbol{L}^*\left(\boldsymbol{e}^0\right)$ is the operator formally adjoint to $\boldsymbol{N}_U'\left(\boldsymbol{e}^0\right)$, and $\left[P(\boldsymbol{h}_U; \boldsymbol{V})\right]_{\partial\Omega}$ represents the associated bilinear form that consists of terms evaluated on the boundary $\partial\Omega$ of Ω. Note that the use of the inner product defined by Eq. (IV.B.55) in conjunction with Eq. (IV.B.65) requires the use of

appropriate normalization constants for those components of $\boldsymbol{N}_U'\left(\boldsymbol{e}^0\right)\boldsymbol{h}_U$ which are functions of only some, rather than all, of the independent variables (r,z,t). Specifically, the formal adjoint operator $\boldsymbol{L}^*\left(\boldsymbol{e}^0\right)$ is the $M\times M$ matrix

$$\boldsymbol{L}^*\left(\boldsymbol{e}^0\right)=\left(l_{ij}\right);\ l_{ij}=L_{ji}^*,\ (i,j=1,\ldots,M), \tag{IV.B.66}$$

obtained by transposing the formal adjoints of the operators $L_{ij}\left(\boldsymbol{e}^0\right)$ given by Eq. (IV.B.54). The explicit representation of the adjoint sensitivity system is given below:

$$-\rho\left(T^0\right)C_p\left(T^0\right)\frac{\partial H^*}{\partial t}-k\left(T^0\right)\frac{1}{r}\frac{\partial}{\partial r}\left(r\frac{\partial H^*}{\partial r}\right)-\frac{n^0}{\Lambda}\left(\frac{\partial\overline{\rho}}{\partial T}\right)^0 n^*=S_1; \tag{IV.B.67}$$
$$r\in\left(0,R_f\right)\cup\left(R_g,R\right);\ z\in(0,L);\ t\in\left(0,t_f\right),$$

$$\begin{aligned}&-A_c\rho_cC_{pc}\frac{\partial H_c^*}{\partial t}-\rho_cC_{pc}\frac{\partial}{\partial z}\left(A_cuH_c^*\right)-A_ck_c\frac{\partial^2H_c^*}{\partial z^2}\\&+2\pi Rh\left(H_c^*-H^*\right)+2\pi R_sh\left(H_c^*-H_s^*\right)\\&-\left(\frac{\partial P}{\partial z}\frac{1}{\rho_c}\frac{\partial\rho_c}{\partial T_c}-\frac{\rho_cu^2}{2D}\frac{\partial f}{\partial T_c}\right)p^*-A_c\frac{\partial\rho_c}{\partial T_c}\frac{Dm^*}{Dt}-\frac{n}{\Lambda}\frac{\partial\overline{\rho}}{\partial T_c}n^*=S_2;\end{aligned} \tag{IV.B.68}$$
$$z\in(0,L),t\in\left(0,t_f\right),$$

$$-A_s\rho_sC_{ps}\frac{\partial H_s^*}{\partial t}+2\pi R_sh\left(H_s^*-H_c^*\right)=S_3; \tag{IV.B.69}$$
$$z\in(0,L),t\in\left(0,t_f\right),$$

$$\begin{aligned}&-\rho_cA_c\frac{\partial m*}{\partial z}-\frac{\partial}{\partial t}\left(\rho_cp^*\right)-\frac{\partial}{\partial z}\left(u\rho_cp^*\right)\\&+\rho_c\left[\frac{fu}{D}+\frac{u^2}{2D}\frac{\partial f}{\partial u}+\sum_m\delta\left(t-z_m\right)uK_L\right]p^*\\&+A_c\rho_cC_{pc}\frac{\partial T_c}{\partial z}H_c^*=S_4;\end{aligned} \tag{IV.B.70}$$
$$z\in(0,L),t\in\left(0,t_f\right),$$

$$-\frac{\partial p*}{\partial z}=S_5;\ z\in(0,L),t\in\left(0,t_f\right), \tag{IV.B.71}$$

$$
\begin{aligned}
&-\frac{dn^*}{dt}-\frac{\overline{\rho}-\beta}{\Lambda}n^*-\sum_{j=1}^{NC}N_j\left\{\int_r\int_z\psi H^*2\pi r dr dz+\int_z\psi H_c^* dz\right.\\
&-\sum_{i=1}^{NC}\frac{\beta_i}{\Lambda}C_i^*-\delta(t-t_0)\left(\frac{1}{dn/dt}\right)_{t=t_0}\\
&\left.\times\left[\frac{1}{\Lambda}\int_{t_0+\Delta t}^{t_f}nn^*\frac{\partial\overline{\rho}}{\partial\tau}dt+\int_{t_0+\Delta t_p}^{t_f}\frac{\partial(\Delta P)}{\partial\tau_p}\sum_{j=1}^{NC}N_j p_j^* dt\right]\right\}=S_6;\\
&t\in(0,t_f),
\end{aligned}
\tag{IV.B.72}
$$

$$
-\frac{dC_i^*}{dt}+\lambda_i\left(C_i^*-n^*\right)=S_{6+i};\ (i=1,\ldots,NG),\ t\in(0,t_f),
\tag{IV.B.73}
$$

and, for the j^{th} channel, the "adjoint loop-balance" relationship

$$
\left(up^*+A_c m^*\right)_j-2f_L WA_c\sum_{i=1}^{NC}N_i p_i^*=0\ \text{ at }\ z=0.
\tag{IV.B.74}
$$

The source terms of the form S_i, which appear on the right-sides of Eqs. (IV.B.67) through (IV.B.73), will be determined in the sequel, below, by the specific response under consideration. Furthermore, the superscript "0" is used in Eq. (IV.B.67) to denote explicitly that the components of $\boldsymbol{L}^*\left(\boldsymbol{e}^0\right)$ depend on the nominal value $\boldsymbol{e}^0$ of $\boldsymbol{e}=(\boldsymbol{U},\boldsymbol{\alpha})$. Although the explicit display of this dependence has been omitted in subsequent equations, in order to keep the notation simple, it should be understood that all $\boldsymbol{e}^0$-dependent values in the expression of $\boldsymbol{L}^*\left(\boldsymbol{e}^0\right)$ are known from the base-case solution. Also, note that the term involving $\delta(t-t_0)$ in Eq. (IV.B.72) is due to the particular problem (i.e., a protected transient with scram on high-power) analyzed in this illustrative example.

Of course, there is a one-to-one correspondence between Eqs. (IV.B.67) through (IV.B.73) and Eqs. (IV.B.1) through (IV.B.7), respectively. Thus, just like in the case of Eqs. (IV.B.1) through (IV.B.5), Eqs. (IV.B.67) through (IV.B.71) are actually vector equations (in that they refer to *NC* distinct channels) although, as written here, this fact was not explicitly indicated. Note also that coupling between channels in the adjoint sensitivity system occurs solely via Eq. (IV.B.74); this fact is explicitly indicated in Eq. (IV.B.74) by the use of the index j. Thus, Eq. (IV.B.74) is the counterpart of Eq. (IV.B.8).

The adjoint sensitivity system represented by Eqs. (IV.B.67) through (IV.B.74) can be written in matrix form as

$$\boldsymbol{L}^*\left(\boldsymbol{e}^0\right)\boldsymbol{V} = \boldsymbol{S}, \tag{IV.B.75}$$

where

$$\boldsymbol{V} = \left(\boldsymbol{H}^*, \boldsymbol{H}_c^*, \boldsymbol{H}_s^*, \boldsymbol{p}^*, \boldsymbol{m}^*, n^*, C_1^*, \ldots, C_{NG}^*\right) \tag{IV.B.76}$$

is, at this stage, an arbitrary vector with components and structure as shown above, while the vector

$$\boldsymbol{S} = \left(\boldsymbol{S}_1, \boldsymbol{S}_2, \boldsymbol{S}_3, \boldsymbol{S}_4, \boldsymbol{S}_5, S_6, \ldots, S_{13}\right) \tag{IV.B.77}$$

has the same structure as $\boldsymbol{V}$.

The domain of $\boldsymbol{L}^*\left(\boldsymbol{e}^0\right)$ is determined by selecting adjoint boundary conditions such as to satisfy the following requirements: (i) be independent of $\boldsymbol{h}_U$, $\boldsymbol{h}_\alpha$, and G-derivatives with respect to $\boldsymbol{\alpha}$, and (ii) substitution of Eq. (IV.B.53) together with the selected adjoint boundary conditions into the expression of $\left[P\left(\boldsymbol{h}_U;\boldsymbol{V}\right)\right]_{\partial\Omega}$ must cause all terms containing unknown values of $\boldsymbol{h}_U$ to vanish. Implementing these requirements leads to the following explicit expressions for the resulting adjoint boundary conditions and final-time conditions for Eqs. (IV.B.67) through (IV.B.73):

$$\boldsymbol{V} = \boldsymbol{0} \text{ at } t = t_f, \tag{IV.B.78}$$

$$H_c^* = 0 \text{ at } z = 0, \tag{IV.B.79}$$

$$u\rho_c C_{pc} H_c^* + k_c \frac{\partial H_c^*}{\partial z} + u\frac{\partial \rho_c}{\partial T_c} m^* = 0 \text{ at } z = L, \tag{IV.B.80}$$

$$A_c m^* + p^* u = 0 \text{ at } z = L, \tag{IV.B.81}$$

$$\left(k\frac{\partial H^*}{\partial r} + h_g H^*\right)_{r=R_f} - \left(h_g H^*\right)_{r=R_g} = 0, \tag{IV.B.82}$$

$$\left(rk\frac{\partial H^*}{\partial r} + hH^*\right)_{r=R} - hH_c^* = 0, \tag{IV.B.83}$$

$$\left(\frac{\partial H^*}{\partial r}\right)_{r=0} = 0. \tag{IV.B.84}$$

The above adjoint boundary conditions can be represented in operator form as

$$\boldsymbol{B}^*\left(\boldsymbol{V};\boldsymbol{e}^0\right) = \boldsymbol{A}^*\left(\boldsymbol{e}^0\right), \ \boldsymbol{x} \in \partial\Omega_j. \tag{IV.B.85}$$

Substituting Eqs. (IV.B.85) and (IV.B.53) into Eq. (IV.B.65) reduces the later to the form

$$\left\langle \boldsymbol{h}_U, \boldsymbol{L}^*\left(\boldsymbol{e}^0\right)\boldsymbol{V}\right\rangle = \left\langle \boldsymbol{V}, \left[\boldsymbol{Q}'_\alpha\left(\boldsymbol{\alpha}^0\right) - \boldsymbol{N}'_\alpha\left(\boldsymbol{e}^0\right)\right]\boldsymbol{h}_\alpha\right\rangle - \hat{P}\left(\boldsymbol{h}_\alpha, \boldsymbol{V}; \boldsymbol{e}^0\right), \quad \text{(IV.B.86)}$$

where Eq. (IV.B.52) has been used to replace the quantity $\boldsymbol{N}'_U\left(\boldsymbol{e}^0\right)\boldsymbol{h}_U$, and where $\hat{P}\left(\boldsymbol{h}_\alpha, \boldsymbol{V}; \boldsymbol{e}^0\right)$ contains boundary terms involving only known values of $\boldsymbol{h}_\alpha$, $\boldsymbol{V}$, and $\boldsymbol{e}^0$.

Equations (IV.B.75), (IV.B.85), and (IV.B.86) hold for all (i.e., arbitrary) vectors $\boldsymbol{V} \in H$. Five such vectors will now be determined, in a unique manner, to eliminate the vector $\boldsymbol{h}_U$ from Eqs. (IV.B.56), (IV.B.58), (IV.B.60), and (IV.B.62), respectively, in order to obtain, correspondingly, alternative expressions for the sensitivities DR_n, DR_T, Dt_n, and $D\boldsymbol{x}_T$.

The alternative expression for DR_n is obtained by using Eq. (IV.B.56) and by considering Eqs. (IV.B.85) and (IV.B.86) as written specifically for the vector $\boldsymbol{V}_n^* \in H$, namely

$$\left\langle \boldsymbol{h}_U, \boldsymbol{L}^*\left(\boldsymbol{e}^0\right)\boldsymbol{V}_n^*\right\rangle = \left\langle \boldsymbol{V}_n^*, \left[\boldsymbol{Q}'_\alpha\left(\boldsymbol{\alpha}^0\right) - \boldsymbol{N}'_\alpha\left(\boldsymbol{e}^0\right)\right]\boldsymbol{h}_\alpha\right\rangle - \hat{P}\left(\boldsymbol{h}_\alpha, \boldsymbol{V}_n^*; \boldsymbol{e}^0\right), \quad \text{(IV.B.87)}$$

and

$$\boldsymbol{B}^*\left(\boldsymbol{V}_n^*; \boldsymbol{e}^0\right) = \boldsymbol{A}^*\left(\boldsymbol{e}^0\right), \ \boldsymbol{x} \in \partial\Omega_j . \quad \text{(IV.B.88)}$$

Comparing the left side of Eq. (IV.B.87) with the right side of Eq. (IV.B.56) shows that

$$\boldsymbol{L}^*\left(\boldsymbol{e}^0\right)\boldsymbol{V}_n^* = \boldsymbol{S}_n^*, \ \boldsymbol{x} \in \Omega_j . \quad \text{(IV.B.89)}$$

Equations (IV.B.56), (IV.B.87), and (IV.B.89) can now be used to express DR_n as

$$DR_n = \left\langle \boldsymbol{V}_n^*, \left[\boldsymbol{Q}'_\alpha\left(\boldsymbol{\alpha}^0\right) - \boldsymbol{N}'_\alpha\left(\boldsymbol{e}^0\right)\right]\boldsymbol{h}_\alpha\right\rangle - \hat{P}\left(\boldsymbol{h}_\alpha, \boldsymbol{V}_n^*; \boldsymbol{e}^0\right). \quad \text{(IV.B.90)}$$

With the derivation of Eq. (IV.B.90), the unknown values $\boldsymbol{h}_U$ that appeared in the original expression of DR_n [namely, in Eq. (IV.B.56)] have been eliminated. Consequently, the adjoint system given by Eqs. (IV.B.88) and (IV.B.89)] needs

to be solved once only, and the adjoint vector $\boldsymbol{V}_n^*$ thus determined is used in Eq. (IV.B.90) to compute efficiently the sensitivity DR_n of $R_n(\boldsymbol{e})$ to changes $\boldsymbol{h}_\alpha$ around $\boldsymbol{\alpha}^o$.

To derive an alternative expression for DR_T, the same procedure as outlined in the foregoing paragraph is applied to Eqs. (IV.B.58), (IV.B.85), and (IV.B.86) to obtain

$$DR_T = \left\langle \boldsymbol{V}_T^*, \left[\boldsymbol{Q}'_\alpha\left(\boldsymbol{\alpha}^0\right) - \boldsymbol{N}'_\alpha\left(\boldsymbol{e}^0\right)\right]\boldsymbol{h}_\alpha \right\rangle - \hat{P}\left(\boldsymbol{h}_\alpha, \boldsymbol{V}_T^*; \boldsymbol{e}^0\right), \tag{IV.B.91}$$

where the adjoint function $\boldsymbol{V}_T^*$ satisfies the adjoint system

$$\boldsymbol{L}^*\left(\boldsymbol{e}^o\right)\boldsymbol{V}_T^* = \boldsymbol{S}_T^*, \ \boldsymbol{x} \in \Omega_j, \tag{IV.B.92}$$

including the final-time and adjoint boundary conditions

$$\boldsymbol{B}^*\left(\boldsymbol{V}_T^*; \boldsymbol{e}^0\right) = \boldsymbol{A}^*\left(\boldsymbol{e}^0\right), \ \boldsymbol{x} \in \partial\Omega_j. \tag{IV.B.93}$$

Repeating the above procedure, an alternative expression is obtained for Dt_n by using Eq. (IV.B.60), and by considering Eqs. (IV.B.85) and (IV.B.86) as written specifically for the vector $\boldsymbol{Y}^* \in H$. The ensuing result is

$$Dt_n = \left\{\left\langle \boldsymbol{Y}^*, \left[\boldsymbol{Q}'_\alpha\left(\boldsymbol{\alpha}^0\right) - \boldsymbol{N}'_\alpha\left(\boldsymbol{e}^0\right)\right]\boldsymbol{h}_\alpha \right\rangle - \hat{P}\left(\boldsymbol{h}_\alpha, \boldsymbol{Y}^*; \boldsymbol{e}^0\right)\right\} \Big/ \left(d^2 n / dt^2\right)_{t_n\left(\boldsymbol{\alpha}^0\right)}, \tag{IV.B.94}$$

where the adjoint function $\boldsymbol{Y}^*$ satisfies the adjoint system

$$\boldsymbol{L}^*\left(\boldsymbol{e}^0\right)\boldsymbol{Y}^* = \boldsymbol{G}^*, \ \boldsymbol{x} \in \Omega_j, \tag{IV.B.95}$$

subject to

$$\boldsymbol{B}^*\left(\boldsymbol{Y}^*; \boldsymbol{e}^0\right) = \boldsymbol{A}^*\left(\boldsymbol{e}^0\right), \ \boldsymbol{x} \in \partial\Omega_j. \tag{IV.B.96}$$

The above procedure is repeated once again to derive an alternative expression for the left side of Eq. (IV.B.62). The final result is

$$\begin{pmatrix} Dz_T \\ Dt_T \end{pmatrix} = M^{-1}\begin{pmatrix} \left\langle \boldsymbol{W}_1^*, \left[\boldsymbol{Q}'_\alpha\left(\boldsymbol{\alpha}^0\right) - \boldsymbol{N}'_\alpha\left(\boldsymbol{e}^0\right)\right]\boldsymbol{h}_\alpha \right\rangle - \hat{P}\left(\boldsymbol{h}_\alpha, \boldsymbol{W}_1^*; \boldsymbol{e}^0\right) \\ \left\langle \boldsymbol{W}_2^*, \left[\boldsymbol{Q}'_\alpha\left(\boldsymbol{\alpha}^0\right) - \boldsymbol{N}'_\alpha\left(\boldsymbol{e}^0\right)\right]\boldsymbol{h}_\alpha \right\rangle - \hat{P}\left(\boldsymbol{h}_\alpha, \boldsymbol{W}_2^*; \boldsymbol{e}^0\right) \end{pmatrix}, \tag{IV.B.97}$$

where the adjoint function $\boldsymbol{W}_1^* \in H$ satisfies the adjoint system

$$\boldsymbol{L}^*\left(\boldsymbol{e}^0\right)\boldsymbol{W}_1^* = \boldsymbol{F}_1^*, \ \boldsymbol{x} \in \Omega_j, \tag{IV.B.98}$$

subject to

$$\boldsymbol{B}^*\left(\boldsymbol{W}_1^*; \boldsymbol{e}^0\right) = \boldsymbol{A}^*\left(\boldsymbol{e}^0\right), \ \boldsymbol{x} \in \partial\Omega_j, \tag{IV.B.99}$$

while the adjoint function $\boldsymbol{W}_2^* \in H$ satisfies the adjoint system

$$\boldsymbol{L}^*\left(\boldsymbol{e}^0\right)\boldsymbol{W}_2^* = \boldsymbol{F}_2^*, \ \boldsymbol{x} \in \Omega_j, \tag{IV.B.100}$$

subject to

$$\boldsymbol{B}^*\left(\boldsymbol{W}_2^*; \boldsymbol{e}^0\right) = \boldsymbol{A}^*\left(\boldsymbol{e}^0\right), \ \boldsymbol{x} \in \partial\Omega_j. \tag{IV.B.101}$$

Note from Eq. (IV.B.97) that each sensitivity Dz_T and Dt_T depends on both $\boldsymbol{W}_1^*$ and $\boldsymbol{W}_2^*$. Thus, two adjoint calculations are needed to evaluate the sensitivity $D\boldsymbol{x}_T$ [via Eq. (IV.B.62)] of the critical point $\boldsymbol{x}$ (where the fuel temperature attains a maximum) for *all* changes $\boldsymbol{h}_\alpha$ around $\boldsymbol{\alpha}^0$.

Note that the same operator, namely $\boldsymbol{L}^*\left(\boldsymbol{e}^0\right)$, appears on the left sides of Eqs. (IV.B.89), (IV.B.92), (IV.B.95), (IV.B.98), and (IV.B.100); only the source terms appearing on the right sides of these equations differ from one another. Furthermore, as evidenced by a comparison of Eqs. (IV.B.88), (IV.B.93), (IV.B.96), (IV.B.99), and (IV.B.101), the adjoint functions $\boldsymbol{V}_n^*$, $\boldsymbol{V}_T^*$, $\boldsymbol{Y}^*$, $\boldsymbol{W}_1^*$, and $\boldsymbol{W}_2^*$ satisfy formally identical boundary conditions. Therefore, apart from the relatively trivial modifications required to accommodate the distinct source terms $\boldsymbol{S}_n^*$, $\boldsymbol{S}_T^*$, $\boldsymbol{G}^*$, $\boldsymbol{F}_1^*$, and $\boldsymbol{F}_2^*$, the same computer code can be used to solve all the respective adjoint systems to determine the functions $\boldsymbol{V}_n^*$, $\boldsymbol{V}_T^*$, $\boldsymbol{Y}^*$, $\boldsymbol{W}_1^*$, and $\boldsymbol{W}_2^*$. An examination of the right sides of Eqs. (IV.B.90), (IV.B.91), (IV.B.94), and (IV.B.97) reveals that the function $\left[\boldsymbol{Q}'_\alpha\left(\boldsymbol{\alpha}^0\right) - \boldsymbol{N}'_\alpha\left(\boldsymbol{e}^0\right)\right]\boldsymbol{h}_\alpha$ appears in all of the respective inner products denoted by $\langle , \rangle$; furthermore, the residual bilinear concomitants $\hat{P}$ appearing in those inner products are formally identical. Therefore, the computer code used to evaluate the sensitivity DR_n can

also be used to evaluate the sensitivities DR_T, Dt_n, and $D\boldsymbol{x}_t$. Of course, the values of $\boldsymbol{V}_n^*$ required to compute DR_n are to be replaced by the respective values of $\boldsymbol{V}_T^*$, $\boldsymbol{Y}^*$, $\boldsymbol{W}_1^*$, and $\boldsymbol{W}_2^*$.

The components of the adjoint functions $\boldsymbol{V}_n^*$, $\boldsymbol{V}_T^*$, $\boldsymbol{Y}^*$, $\boldsymbol{W}_1^*$, and $\boldsymbol{W}_2^*$ can be interpreted as "***importance functions***," by recalling that each of these adjoint functions can be represented generically as the M-component vector

$$\boldsymbol{V} = \left(\boldsymbol{H}^*, \boldsymbol{H}_c^*, \boldsymbol{H}_s^*, \boldsymbol{p}^*, \boldsymbol{m}^*, n^*, C_1^*, \ldots, C_{NG}^*\right). \qquad \text{(IV.B. 76)}$$

Thus, when evaluating the response sensitivities DR_n and DR_T, $\boldsymbol{V}$ represents $\boldsymbol{V}_n^*$ and $\boldsymbol{V}_T^*$, respectively. In this case, a dimensional analysis of Eqs. (IV.B.90) and (IV.B.91), respectively, shows that the dimensions $\left[V_j\right]$ of each component $V_j \left(j = 1, \ldots, M\right)$ of $\boldsymbol{V}$ are

$$\left[V_j\right] = \frac{\left[\text{response}\right]}{\left[\begin{matrix}\text{terms in the } j\text{'th} \\ \text{forward equation}\end{matrix}\right]\left[\begin{matrix}\text{region of} \\ \text{integration}\end{matrix}\right]\left[\begin{matrix}\text{normalization} \\ \text{constant}\end{matrix}\right]}. \qquad \text{(IV.B.102a)}$$

Similarly, $\boldsymbol{V}$ represents $\boldsymbol{Y}^*$, $\boldsymbol{W}_1^*$, and $\boldsymbol{W}_2^*$ when evaluating the critical point sensitivities Dt_n, Dz_T, and Dt_T, respectively. In this case, a dimensional analysis of Eqs. (IV.B.94) and (IV.B.97) shows that

$$\left[V_j\right] = \frac{\left[\text{response}\right]/\left[\text{component of critical point}\right]}{\left[\begin{matrix}\text{terms in the } j\text{'th} \\ \text{forward equation}\end{matrix}\right]\left[\begin{matrix}\text{region of} \\ \text{integration}\end{matrix}\right]\left[\begin{matrix}\text{normalization} \\ \text{constant}\end{matrix}\right]}. \qquad \text{(IV.B.102b)}$$

The considerations leading to Eqs. (IV.B.102a) and (IV.B.102b) hold generally for any maximum-type response. According to Eq. (IV.B.102a), each component of the adjoint function used to compute response sensitivities can be viewed as a measure of the importance of the physical quantity described by the corresponding forward equation in contributing to the response. Furthermore, according to Eq. (IV.B.102b), each component of the adjoint function used to compute critical point sensitivities can be viewed as a measure of the importance of the physical quantity described by the corresponding forward equation in contributing to the response movement in phase space. As a specific example, consider the coolant temperature equation for channel j [see Eq. (IV.B.4)] and the corresponding component H_{cj}^* of $\boldsymbol{V}$. The dimensions of the terms in this

equation are $\left[\mathrm{J}\cdot\mathrm{cm}^{-1}\cdot\mathrm{s}^{-1}\right]$. The respective region of integration is volume and time, with dimensions $\left[\mathrm{cm}^3\cdot\mathrm{s}\right]$. The dimension of the appropriate normalization constant, i.e., $1/\pi\left(R_f^2 - R^2 + R_g^2\right)$, is $\left[\mathrm{cm}^{-2}\right]$. Thus, Eq. (IV.B.102a) gives

$$\left[H_{cj}^*\right] = \frac{\left[\text{response}\right]}{\left[\mathrm{J}\cdot\mathrm{cm}^{-1}\cdot\mathrm{s}^{-1}\right]\left[\mathrm{cm}^3\cdot\mathrm{s}\right]\left[\mathrm{cm}^{-2}\right]} = \frac{\left[\text{response}\right]}{\left[\mathrm{J}\right]}.$$

For the responses R_n and R_T, the dimensions of H_{cj}^* are $\left[\mathrm{MW/J}\right]$ and $\left[\mathrm{K/J}\right]$, respectively. For the critical point t_n, Eq. (IV.B.102b) indicates that H_{cj}^* has units of $\left[\mathrm{MW}\cdot\mathrm{s}^{-1}/\mathrm{J}\right]$, while the units of H_{cj}^* corresponding to the components z_T and t_T of the critical point $\boldsymbol{x}_T$ are $\left[\mathrm{K}\cdot\mathrm{cm}^{-1}/\mathrm{J}\right]$ and $\left[\mathrm{K}\cdot\mathrm{s}^{-1}/\mathrm{J}\right]$, respectively. This dimensional analysis shows that H_{cj}^* is a measure of enthalpy importance in the coolant region of the j^{th} channel. Similar analyses indicate that, for each channel, the components of $\boldsymbol{H}^*$, $\boldsymbol{H}_s^*$, $\boldsymbol{m}^*$, and $\boldsymbol{p}^*$ are measures of enthalpy importance in the fuel pin region, enthalpy importance in the structure region, coolant mass importance, and momentum flux importance, respectively. Furthermore, n^* and $C_1^*,\ldots,C_{NG}^*$ are measures of power importance and precursor amplitude importances, respectively. Therefore, the adjoint variables $\boldsymbol{H}^*$, $\boldsymbol{m}^*$, etc., can justifiably be called "adjoint enthalpy," "adjoint mass," etc.

As already discussed in the closing paragraphs of Section IV.A, it is instructive to examine the differences between the sensitivities of the "maximum response" considered in the foregoing, and a response which simply happens to be located at the position in phase-space where the maximum of the respective dependent variable occurs in the base-case calculation, but the position itself is considered to remain invariable, regardless of variations $h_{\alpha i}$ in the system parameters α_i. Specifically, consider the responses

$$P_T(\boldsymbol{e}) = \int_\Omega \left(1/N_J\right)\boldsymbol{g}_J\cdot\boldsymbol{T}(\boldsymbol{x})\delta(\boldsymbol{x}-\boldsymbol{y}_T)\,d\Omega, \qquad \text{(IV.B.104)}$$

and

$$P_n(\boldsymbol{e}) = K\int_\Omega n(t)\delta(t-\tau_n)\,d\Omega, \qquad \text{(IV.B.105)}$$

respectively, where $\boldsymbol{y}_T$ and τ_n represent the same physical locations as $\boldsymbol{x}_T(\boldsymbol{\alpha})$ and $t_n(\boldsymbol{\alpha})$, respectively, but where the points $\boldsymbol{y}_T$ and τ_n are considered to be independent of $\boldsymbol{\alpha}$. Based on the concluding paragraphs of Section IV.A, the following relationships are valid at $\boldsymbol{e}^0$ for the pair of responses $P_T(\boldsymbol{e})$ and $R_T(\boldsymbol{e})$:

$$R_T(\boldsymbol{e}^0) = P_T(\boldsymbol{e}^0), \tag{IV.B.106a}$$

$$DR_T(\boldsymbol{e}^0;\boldsymbol{h}) = DP_T(\boldsymbol{e}^0;\boldsymbol{h}), \tag{IV.B.106b}$$

$$\left\| R_T(\boldsymbol{e}^0+\boldsymbol{h}) - P_T(\boldsymbol{e}^0+\boldsymbol{h}) \right\| = O\left(\left\|\boldsymbol{h}_\alpha\right\|^2\right). \tag{IV.B.106c}$$

Equation (IV.B.106a) indicates that the nominal values of $P_T(\boldsymbol{e})$ and $R_T(\boldsymbol{e})$ are identical. Equation (IV.B.106b) indicates that, for a given vector $\boldsymbol{h}_\alpha$, the sensitivities of these two responses are also identical. As generally discussed in Section IV.A, the equality expressed by Eq. (IV.B.106b) holds only because $\boldsymbol{x}_T(\boldsymbol{\alpha}^0)$ is a critical point of $T(\boldsymbol{x})$. The fact that $R_T(\boldsymbol{e})$ and $P_T(\boldsymbol{e})$ are nevertheless two distinct responses is clearly demonstrated by the relationship given by Eq. (IV.B.106c). This relationship shows that, if the system parameters $\boldsymbol{\alpha}$ are changed by $\boldsymbol{h}_\alpha$ from their base-case value $\boldsymbol{\alpha}^0$, and if the values of these two responses are recalculated for the new configuration $(\boldsymbol{e}^0+\boldsymbol{h})$, then the difference between the recalculated values $R_T(\boldsymbol{e}^0+\boldsymbol{h})$ and $P_T(\boldsymbol{e}^0+\boldsymbol{h})$ is of second order in $\|\boldsymbol{h}_\alpha\|$.

Similar relationships and, consequently, similar conclusions hold for the pair of responses $R_n(\boldsymbol{e})$ and $P_n(\boldsymbol{e})$, i.e.,

$$R_n(\boldsymbol{e}^0) = P_n(\boldsymbol{e}^0), \tag{IV.B.107a}$$

$$DR_n(\boldsymbol{e}^0;\boldsymbol{h}) = DP_n(\boldsymbol{e}^0;\boldsymbol{h}), \tag{IV.B.107b}$$

$$\left\| R_n(\boldsymbol{e}^0+\boldsymbol{h}) - P_n(\boldsymbol{e}^0+\boldsymbol{h}) \right\| = O\left(\left\|\boldsymbol{h}_\alpha\right\|^2\right). \tag{IV.B.107c}$$

As will be seen from the numerical results to be presented in Section IV.B.2, below, the second-order terms in Eq. (IV.B.106c) are practically negligible, while those in Eq. (IV.B.107c) are not.

Typical quantitative sensitivity analysis results obtained by applying the *ASAP* to the simulation of a subprompt-critical transient in the Fast Flux Test Facility (FFTF) will be presented in the sequel. The geometry of the FFTF is modeled using the MELT code, with a two-channel representation of the reactor flow

path. Channel two (for which $J = 2$) is designated as the hot channel and consists of 227 pins. Channel one represents the remainder of the FFTF core and consists of 15624 pins. Only one flow loop is considered. The dimensions of the outer radii for the fuel, gap, and cladding are $R_f = 0.249\,\text{cm}$, $R_g = 0.254\,\text{cm}$, and $R = 0.292\,\text{cm}$. The channel height is $L = 800\,\text{cm}$; the bottom of the core is located axially at $z = 105.16\,\text{cm}$, and the core length is $91.44\,\text{cm}$.

The simulated sub-prompt-critical transient power excursion involves a $0.23\,\text{dollar/s}$ ramp reactivity insertion with scram that trips the control rods and primary pumps on high-power level. The power profile for this transient is given in Figure IV.B.1. Although the high-power level for trip is attained at $t_0 = 0.518\,\text{s}$, a time delay of $\Delta t = 0.19\,\text{s}$ postpones the actual control rod insertion and pump shutdown until $0.708\,\text{s}$ after initiation of the transient conditions. Just after this point in time, the power $n(t)$ attains its maximum value of $467.7\,\text{MW}$. Note that the scram component $\bar{\rho}_{scram}(t)$ of the's sy total reactivity $\bar{\rho}(t)$ is usi a reactivity ramp ρ_0 that is switched on $t_0 + \Delta t$, i.e.,

$$\bar{\rho}_{scram}(t) = \bar{\rho}_0(t - t_0 - \Delta t)H_+(t - t_0 - \Delta t), \qquad \text{(IV.B.108)}$$

where

$$H_+(t) = \begin{cases} 0, & t < 0 \\ 1, & t \geq 0 \end{cases}$$

is the Heaviside unit-step functional. The large magnitude of ρ_0 and the discontinuous time derivatives of $\bar{\rho}_{scram}$ are thei causes for the highly nonlinear behavior of the power $n(t)$ and of the asymmetric shape of its maximum, which can be readily noted in Figure IV.B.1.

An examination of the temperature distribution $T(t, z, t)$ for this transient shows that the fuel temperature in the hot channel attains a maximum value of $2734.1\,\text{K}$. Spatially, this maximum is located at $r_T = 0$ at $z_T = 155\,\text{cm}$, i.e., at the center of the fuel rod and just above the core mid-plane. The time variation of the temperature at this spatial location is plotted in Figure IV.B.2, which shows that the maximum occurs in time at $t_T = 0.870\,\text{s}$. Note that this maximum fuel temperature occurs later in time than the maximum power (compare Figs. IV.B.2 and IV.B.3) due to the time delay in the power-to-thermal energy integration.

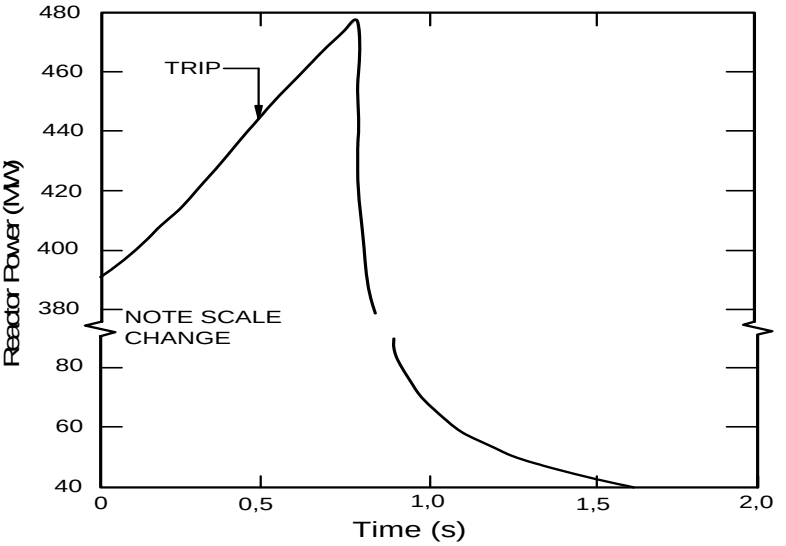

Figure IV.B.1. Power profile for the coupled neutron kinetics/thermal-hydraulics transient with reactor scram on high-power level.

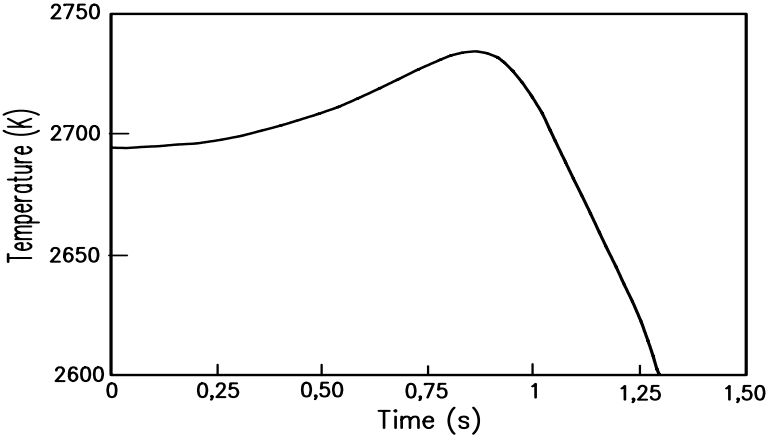

Figure IV.B.2. Time variation of the temperature at the spatial location ($r_T = 0$, $z_T = 155\,\text{cm}$).

The sensitivities of the numerical value of the maximum fuel temperature response $R_T(\boldsymbol{e})$ are calculated using Eq. (IV.B.91), where the adjoint function $\boldsymbol{V}_T^*$ is the solution of the adjoint system represented by Eqs. (IV.B.92) and (IV.B.93). Numerical values for the quantities appearing in the source term $\boldsymbol{S}_T^*$

are $\boldsymbol{x}_T\left(\boldsymbol{\alpha}^0\right)=(0, 155, 0.870)$, $N_J = 227$, and $\boldsymbol{g}_J = (0,1)$. Recall that the same adjoint function, $\boldsymbol{V}_T^*$, would be used to compute the sensitivities of either $R_T(\boldsymbol{e})$ or $P_T(\boldsymbol{e})$.

Illustrative sensitivity results for those parameters that have the largest impact on the numerical value of the maximum fuel temperature response, R_T, are presented in Table IV.B.1. Note that, for every value of the index i, these results correspond to a vector of parameter variations $\boldsymbol{h}_\alpha$ whose components are all zero except for the i-component h_{α_i}. The parameters are ranked in order of decreasing absolute magnitude of relative sensitivity. Based on these relative sensitivities, it can be concluded that the numerical value of the maximum fuel temperature is practically insensitive to variations in any of the system parameters except for variations in $\tilde{T}$, n_0, and k_{fuel}.

The results presented in Table IV.B.1 also serve to illustrate the use of sensitivities for predicting the effects of parameter variations on the response, highlighting both similarities and fundamental distinctions between the responses $R_T(\boldsymbol{e})$ and, respectively, $P_T(\boldsymbol{e})$. The basis for using sensitivities to predict the effects of parameter variations $\boldsymbol{h}_\alpha$ on these responses is the general relationship expressed by Eqs. (IV.A.37) and (IV.A.38), which take on the following particular forms, respectively:

$$R_T\left(\boldsymbol{e}^0 + \boldsymbol{h}\right) - R_T\left(\boldsymbol{e}^0\right) = DR_T + O\left(\left\|\boldsymbol{h}_\alpha\right\|^2\right), \tag{IV.B.109}$$

and

$$P_T\left(\boldsymbol{e}^0 + \boldsymbol{h}\right) - P_T\left(\boldsymbol{e}^0\right) = DP_T + O\left(\left\|\boldsymbol{h}_\alpha\right\|^2\right). \tag{IV.B.110}$$

The $O\left(\left\|\boldsymbol{h}_\alpha\right\|^2\right)$ terms in Eqs. (IV.B.109) and (IV.B.110) result from the facts that: (a) DR_T and DP_T are both linear in $\boldsymbol{h}$; and (b) the vectors $\boldsymbol{h}_U$ and $\boldsymbol{h}_\alpha$ are linearly related via Eqs. (IV.B.52) and (IV.B.53). As Eq. (IV.B.109) indicates, the sensitivity DR_T predicts changes (i.e., deviations from the base-case value) that occur in the numerical value of the response R_T when the base-case parameter values $\boldsymbol{\alpha}^0$ are varied by $\boldsymbol{h}_\alpha$. These predictions, though, do not take into account effects of second- and higher order terms in $\boldsymbol{h}_\alpha$. For each specific fractional variation h_{α_i}/α_i^0, the fifth column of Table IV.B.1 correspondingly lists the (sensitivity-based) predicted changes in the numerical value of the response R_T.

On the other hand, the results presented under the heading "$R_T\left(\boldsymbol{e}^0+\boldsymbol{h}\right)-R_T\left(\boldsymbol{e}^0\right)$" are the exact differences, obtained by direct recalculations, between the base-case numerical value of the response, $R_T\left(\boldsymbol{e}^0\right)$, and the numerical value of the new maximum, $R_T\left(\boldsymbol{e}^0+\boldsymbol{h}\right)$, which is attained at $\boldsymbol{x}_T\left(\boldsymbol{\alpha}^0+\boldsymbol{h}_\alpha\right)$. Thus, for each specific h_{α_i}/α_i^0, these results represent the corresponding numerical value taken on by the left-side of Eq. (IV.B.109). Note that for each α_i, the results presented in the fifth and sixth columns of Table IV.B.1 are in close agreement. This close agreement indicates that the nonlinear terms in h_{α_i} [see Eq. (IV.B.109)] have relatively little practical impact on the numerical value of the maximum fuel temperature response, and highlights the usefulness of sensitivities for predicting the actual numerical value of the "perturbed" response $R_T\left(\boldsymbol{e}^0+\boldsymbol{h}\right)$.

The results presented in Table IV.B.1 also serve to highlight similarities and distinctions between $R_T\left(\boldsymbol{e}\right)$ and $P_T\left(\boldsymbol{e}\right)$. Using those results, the relative sensitivities $\left[DP_T\left(\boldsymbol{e}^0;\boldsymbol{h}\right)/P_T\left(\boldsymbol{e}^0\right)\right]\left(\alpha_i^0/h_{\alpha i}\right)$ of P_T can be readily calculated and, in view of Eqs. (IV.B.106a) and (IV.B.106b), they are identical to the corresponding relative sensitivities of R_T presented here in Table IV.B.1. For a given h_{α_i}, the predicted changes in the numerical value of the respective responses R_T and P_T are also identical; this is because of Eqs. (IV.B.106b), (IV.B.109), and (IV.B.110).

The results presented in the last column of Table IV.B.1 represent the value of the quantity $\left[P_T\left(\boldsymbol{e}^0+\boldsymbol{h}\right)-P_T\left(\boldsymbol{e}^0\right)\right]$. A comparison between the fifth and the last columns of Table IV.B.1 shows that, for each α_i, the respective results are in close agreement. In view of Eq. (IV.B.110), this close agreement indicates that the second- and higher order terms in h_{α_i} have relatively little impact on $P_T\left(\boldsymbol{e}\right)$. Recall that the same conclusion was reached when the effects of such terms on the numerical value of $R_T\left(\boldsymbol{e}\right)$ were examined.

A comparison between the results presented in the last two columns in Table IV.B.1 evidences the fact that the quantities $\left[R_T\left(\boldsymbol{e}^0+\boldsymbol{h}\right)-R_T\left(\boldsymbol{e}^0\right)\right]$ and $\left[P_T\left(\boldsymbol{e}^0+\boldsymbol{h}\right)-P_T\left(\boldsymbol{e}^0\right)\right]$ are not identical. According to Eqs. (IV.B.106a), (IV.B.106b), and (IV.B.106c), the differences between these two quantities arise from second- and higher order terms in h_{α_i}. Although small, the numerical differences between these two quantities are nonetheless sufficiently noticeable to highlight the existence of conceptual and, consequently, mathematical

distinctions between the maximum fuel temperature response $R_T(\boldsymbol{e})$ and the response $P_T(\boldsymbol{e})$.

Sensitivity analysis results for the critical point $\boldsymbol{x}_T(\boldsymbol{\alpha})$, at which the fuel temperature attains its maximum in phase space, are discussed next. As shown in Eq. (IV.B.97), the sensitivity $D\boldsymbol{x}_T(\boldsymbol{\alpha}^0;\boldsymbol{h}_\alpha)$ has two nonzero components, namely Dz_T and Dt_T. The adjoint functions $\boldsymbol{W}_1^*$ and, respectively, $\boldsymbol{W}_2^*$, which must be determined prior to using Eq. (IV.B.97), are obtained by solving the adjoint systems represented by Eqs. (IV.B.98) and (IV.B.99) and, respectively, Eqs. (IV.B.100) and (IV.B.101). The source terms $\boldsymbol{F}_1^*$ and $\boldsymbol{F}_2^*$ are computed by using $N_J = 227$, $z_T(\boldsymbol{\alpha}^0) = 155\,\text{cm}$, $t_T(\boldsymbol{\alpha}^0) = 0.870\,\text{s}$, and $g_J = (0,1)$.

Table IV.B.1
Sensitivities for the Maximum Fuel Temperature Response $R_T(\boldsymbol{e})$.

i	α_i	Relative sensitivity $\frac{DR_T(\boldsymbol{e}^0;\boldsymbol{h})}{R_T(\boldsymbol{e}^0)}\frac{\alpha_i^0}{h_{\alpha_i}}$	$\frac{h_{\alpha_i}}{\alpha_i^0}$ (%)	Predicted change in response value (K) $DR_T(\boldsymbol{e}^0;\boldsymbol{h})$	Recalculated change in response value (K)	
					$R_T(\boldsymbol{e}^0+\boldsymbol{h}) - R_T(\boldsymbol{e}^0)$	$P_T(\boldsymbol{e}^0+\boldsymbol{h}) - P_T(\boldsymbol{e}^0)$
1	$\tilde{T}$	0.746	0.5	10.20	10.0	9.7
2	n_0	0.155	0.3	1.27	1.3	1.2
3	k_{fuel}	-0.128	5.0	-17.5	-17.0	-18.3
4	ρC_p	-0.015	1.0	-0.41	-0.4	-0.4
5	T_{in}	0.013	1.0	0.35	0.2	0.2
6	h_g	-0.012	5.0	-1.58	-1.5	-1.6
7	Δt	0.008	10.0	2.23	2.3	2.0
8	β	0.007	1.0	0.20	0.2	0.2
9	$\tilde{n}$	-0.007	0.4	-0.08	-0.1	-0.1
10	$\bar{\rho}_{prog}$	-0.006	5.0	-0.82	-0.4	-1.0
11	C_{pc}	-0.005	10.0	-1.29	-0.8	-1.3

For illustrative purposes, the profiles of the adjoint momentum in channels one and two, adjoint power, and adjoint precursors are depicted in Figures IV.B.3 through IV.B.5, below. These profiles reveal that each of the respective adjoint functions undergo rapid and sizable variations around $0.518\,\text{s}$. At this point in time, a scram source, represented by a Dirac-delta functional in time, is triggered in the adjoint equation satisfied by the adjoint power $n^*(t)$. The effect of this

scram source is clearly seen in Figure IV.B.4, as a large positive spike. This spike then quickly propagates, causing the large and rapid shape changes in the other components of W_2^*.

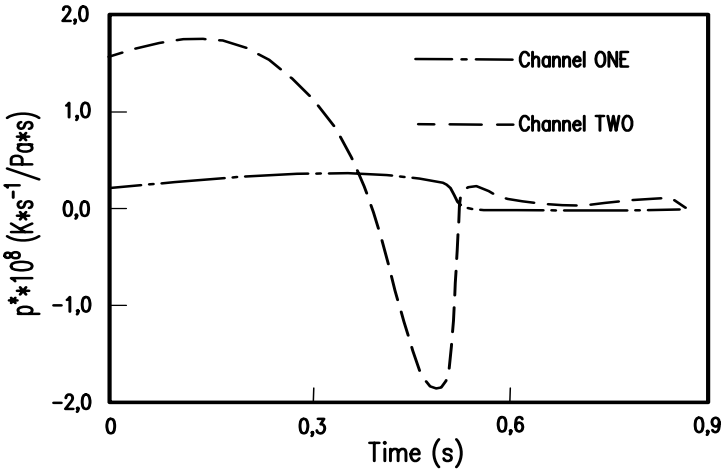

Figure IV.B.3. Profiles of the adjoint function W_2^* [see Eqs. (IV.B.100) and (IV.B.101)]: adjoint momentum in channels one and two.

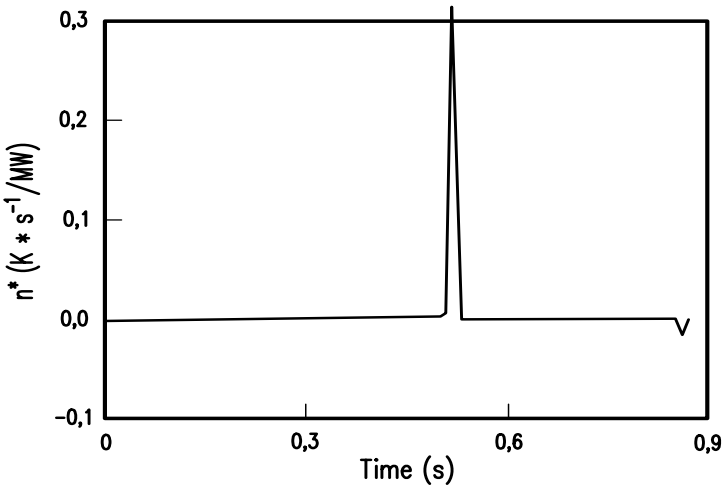

Figure IV.B.4. Profiles of the adjoint function W_2^* [see Eqs. (IV.B.100) and (IV.B.101)]: adjoint power.

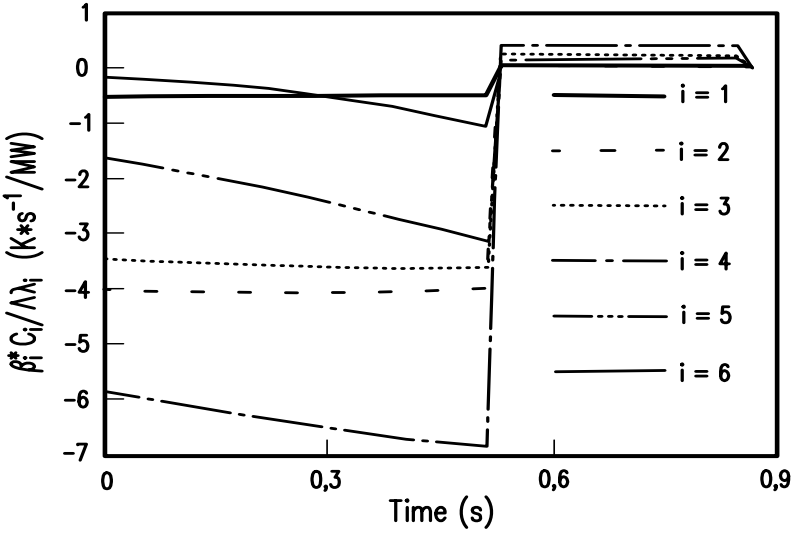

Figure IV.B.5. Profiles of the adjoint function W_2^* [see Eqs. (IV.B.100) and (IV.B.101)]: adjoint precursors.

When the numerical calculations based on Eq. (IV.B.97) were performed, it was found that all of the sensitivities Dz_T and most of the sensitivities Dt_T are negligibly small. Several of the sensitivities Dt_T, though, were found to be quite large. This implies that variations in the system parameters will affect almost exclusively the time component $t_T(\boldsymbol{\alpha})$ of $x_T(\boldsymbol{\alpha})$; they will have negligible effects on the axial component $z_T(\boldsymbol{\alpha})$, and, as already discussed, they have no effects on the radial component r_T.

Table IV.B.2 presents sensitivity results for those parameters that have the largest impact on $t_T(\boldsymbol{\alpha})$. Just as in Table IV.B.1, these results correspond to a vector of changes $\boldsymbol{h}_\alpha$ whose components are zero except for the i^{th} component, h_{α_i}. The parameters are ranked in order of decreasing absolute magnitude of relative sensitivity, a process equivalent to ranking the importance of their effects on $t_T(\boldsymbol{\alpha})$.

The relative sensitivity results presented in Tables IV.B.1 and IV.B.2 indicate that, in both tables, the largest relative sensitivities involve the parameters $\tilde{T}$ and n_0. Thus, if varied, $\tilde{T}$ and n_0 would have the largest impact on the numerical value of the maximum fuel temperature response, and would also cause the largest time shifts in the phase-space location of the resulting (i.e., new) maximum. Since all the relative sensitivities in Tables IV.B.1 and IV.B.2

to $\tilde{T}$ and n_0 are positive, it follows that when a positive variation in $\tilde{T}$ and/or n_0 is affected, the resulting maximum fuel temperature is both larger and occurs later in time than the original (nominal) maximum fuel temperature.

Table IV.B.2.
Sensitivities for the Time Component $t_T(\boldsymbol{\alpha})$ of $x_T(\boldsymbol{\alpha})$.

i	α_i	Relative sensitivity	h_{α_i}/α_i^0 (%)	Predicted change (s)	Recalculated change (s)
1	$\tilde{T}$	4.828	0.5	0.021	0.02
2	n_0	4.598	0.3	0.012	0.01
3	$\tilde{n}$	-3.448	0.4	-0.012	-0.01
4	T_{in}	1.149	1.0	0.01	0.01
5	β	0.575	1.0	0.005	0.01
6	$\overline{\rho}_{prog}$	-0.575	5.0	-0.025	-0.03
7	k_{fuel}	-0.552	5.0	-0.024	-0.02
8	h_g	-0.322	5.0	-0.014	-0.01
9	C_{pc}	-0.276	10.0	-0.024	-0.02
10	Δt	0.230	10.0	0.02	0.02
11	ρC_p	-0.115	1.0	-0.001	0.00

Comparing the second and the third columns in Table IV.B.1 to the respective columns in Table IV.B.2, it becomes apparent that, except for $\tilde{T}$ and n_0, the parameter ranking in Table IV.B.1 differs from the ranking in Table IV.B.2, although the same ranking procedure was used for both tables. The implications of this fact can be illustrated by considering the system parameters k_{fuel} and T_{in}. In Table IV.B.1, k_{fuel} is ranked ahead of T_{in}, but this ranking is reversed in Table IV.B.2. Consequently, a fractional variation in k_{fuel} causes a larger change in the numerical value of the maximum fuel temperature, but causes a smaller time shift of the maximum than does the same fractional variation in T_{in}.

Comparison of the relative sensitivities in Tables IV.B.1 and IV.B.2 also shows that, in general, the parameters affect the time location of the maximum fuel temperature significantly more than they affect the numerical value of this maximum. This conclusion is clearly illustrated by examining the two sensitivities to the initial value $\tilde{n}$ of the reactor power amplitude. It becomes readily apparent that a variation in $\tilde{n}$ is of no practical importance to the

numerical value of the maximum fuel temperature, but is of significant importance to $t_T(\boldsymbol{\alpha})$.

The sensitivities presented in Table IV.B.2 were used to predict the time shift [namely, the difference between the time location $t(\boldsymbol{\alpha}^0 + \boldsymbol{h}_\alpha)$ at which the perturbed maximum $R_T(\boldsymbol{e}^0 + \boldsymbol{h})$ occurs, and the time location $t(\boldsymbol{\alpha}^0) = 0.870\,\text{s}$ at which $R_T(\boldsymbol{e}^0)$ occurs] which is caused by each of the fractional parameter variations shown in the fourth column. The results for these predicted time shifts are presented in the fifth column. These predicted changes are in good agreement with the actual changes presented in the last column of Table IV.B.2. These actual changes were obtained by direct recalculation of the fuel temperature, using the respective fractional parameter variations. It is informative to mention that, in all "forward" calculations, results are only printed at 0.01 s time intervals, although the actual time step used in such calculations is not fixed to 0.01 s, but varies as computed internally by the MELT-code.

The sensitivities of the numerical value of the maximum normalized power level response $R_n(\boldsymbol{e})$ are calculated using Eq. (IV.B.90), where the adjoint function $\boldsymbol{V}_n^*$ is the solution of the adjoint system represented by Eqs. (IV.B.88) and (IV.B.89). The sensitivities of the critical point $t_n(\boldsymbol{\alpha})$, at which the power level attains its maximum, are calculated using Eq. (IV.B.94), where the adjoint function $\boldsymbol{Y}^*$ is the solution of the adjoint system represented by Eqs. (IV.B.95) and (IV.B.96). In the base-case computation, the power level $n(t)$ attains its maximum value of 467.7 MW at $t(\boldsymbol{\alpha}^0) = 0.71\,\text{s}$. This time value is used in both Eq. (IV.B.57) and (IV.B.61) to calculate the source terms $\boldsymbol{S}_n^*$ and $\boldsymbol{G}^*$.

The power transient induced by reactor scram is characterized by the important fact that $t(\boldsymbol{\alpha}^0) \cong t_0 + \Delta t = 0.708\,\text{s}$; this implies that the time at which the power level attains its maximum in the base-case calculation practically coincides with the time of control rod insertion. The sensitivities DR_n contain the effects of the scram mechanism, since $t_n(\boldsymbol{\alpha}^0) > t_0 + \Delta t$. Therefore, these sensitivities can be used to predict the effects of only those variations h_{α_i} that cause the time of control rod insertion to occur earlier (i.e., to be less than) than $t_n(\boldsymbol{\alpha}^0)$, since otherwise the perturbed case would not contain the scram mechanism in the time domain of the adjoint calculation. Thus, prior to using the sensitivities DR_n to predict the effects of variations h_{α_i} on the numerical value of the maximum power response, it is essential to know whether the respective variations h_{α_i} cause the perturbed maximum (and, hence, the scram) to occur before or after control rod insertion.

At this stage, it is also possible to conclude that the maximum temperature predictions obtained using the sensitivities DR_T would also be invalid if the variations h_{α_i} moved the time scram beyond $t_T\left(\boldsymbol{\alpha}^0\right)= 0.87\,\text{s}$. However, it would require extremely large variations h_{α_i} to move the time of scram from $t_0 + \Delta t = 0.708\,\text{s}$ to beyond $t_n\left(\boldsymbol{\alpha}^0\right)= 0.87\,\text{s}$.

Since the maximum power response, R_n, is located extremely close to the discontinuity caused by the scram insertion, it is apparent that the information provided by the sensitivities DR_n can be fully exploited only after having established the signs of the "time shifts" induced in the maximum power response by variations h_{α_i}. Valuable information regarding the signs of these time shifts is provided by the sensitivities Dt_n. Since Dt_n can be calculated independently of DR_n, the expected signs of the time shifts can be established prior to performing a sensitivity analysis of the numerical value of the maximum.

Table IV.B.3 presents sensitivity results for those parameters that have the largest impact on $t_n(\boldsymbol{\alpha})$. These results were obtained by taking all components of $\boldsymbol{h}_\alpha$ to be zero, except for the i^{th} component h_{α_i}. The parameters are ranked in order of decreasing absolute magnitude of relative sensitivity. For the critical point $t_n(\boldsymbol{\alpha})$, we note that

$$t_n\left(\boldsymbol{\alpha}^0 + \boldsymbol{h}_\alpha\right) - t_n\left(\boldsymbol{\alpha}^0\right) = Dt_n + O\left(\left\|\boldsymbol{h}_\alpha\right\|^2\right), \qquad \text{(IV.B.111)}$$

where $t_n\left(\boldsymbol{\alpha}^0 + \boldsymbol{h}_\alpha\right)$ is the time location at which the perturbed maximum $R_n\left(\boldsymbol{e}^0 + \boldsymbol{h}\right)$ occurs. Equation (IV.B.111) is the basis for using the sensitivities Dt_n to predict the time shifts $\left[t_n\left(\boldsymbol{\alpha}^0 + \boldsymbol{h}_\alpha\right) - t_n\left(\boldsymbol{\alpha}^0\right)\right]$ caused by each of the fractional variations $h_{\alpha_i} / \alpha_i^0$ shown in Table IV.B.3. The results for the predicted time shifts are presented in the fifth column, and they were found to agree well with the actual time shifts (presented in the last column) obtained by direct recalculations. For the parameters with large sensitivities, relatively small fractional variations were used in the direct recalculations to minimize the nonlinear effects.

Table IV.B.4 presents sensitivity analysis results for those parameters that have the largest impact on the numerical value of the maximum power response R_n. The parameters are again ranked in order of decreasing absolute magnitude of relative sensitivity. Note that this ranking procedure produces identical parameter sequences in both Tables IV.B.3 and IV.B.4, which is in contrast to the situation depicted by Tables IV.B.1 and IV.B.2. Nevertheless, Tables IV.B.3

and IV.B.4 show that, in general, the parameters affect the time location of the maximum power response significantly more than they affect the numerical value of this maximum; this situation is similar to that depicted by Tables IV.B.1 and IV.B.2 regarding the response R_T .

Table IV.B.3
Sensitivities for the Time Location $t_n(\boldsymbol{\alpha})$ of the Maximum Power Response.

i	α_i	Relative sensitivity	h_{α_i}/α_i^0 (%)	Predicted change (s)	Recalculated change (s)
1	n_0	11.299	-0.1	-0.008	-0.01
2	T	8.475	-0.5	-0.030	-0.03
3	$\tilde{n}$	-5.650	0.5	-0.020	-0.02
4	T_{in}	1.554	-1.0	-0.011	-0.01
5	β	0.989	-1.0	-0.007	-0.01
6	$\bar{\rho}_{prog}$	-0.847	5.0	-0.030	-0.03
7	Δt	0.565	-10.0	-0.02	-0.02
8	k_{fuel}	-0.508	5.0	-0.018	-0.02
9	C_{pc}	-0.424	5.0	-0.015	-0.02
10	h_g	-0.424	5.0	-0.015	-0.02
11	ΔP	-0.212	10.0	-0.015	-0.02
12	f	0.141	-10.0	-0.010	-0.01

As previously discussed, the sensitivities presented in Table IV.B.4 can be used to predict the effects of only those values of h_{α_i} that cause the perturbed maximum $R_n(\boldsymbol{e}^0 + \boldsymbol{h})$ (and, hence, the scram) to occur earlier in time than the nominal maximum $R_n(\boldsymbol{e}^0)$. For this reason, the sign of each parameter variation h_{α_i}/α_i^0 was chosen to be the opposite of the sign of the relative sensitivity $(Dt_n/t_n)(\alpha_i^0/h_{\alpha_i})$ shown in Table IV.B.3. Note that the expected negative time shifts did indeed occur, as confirmed by the direct recalculation results shown in the last column of Table IV.B.3.

Table IV.B.4 also highlights the similarities and distinctions between the response $R_n(\boldsymbol{e})$ and $P_n(\boldsymbol{e})$. In view of Eqs. (IV.B.107a) and (IV.B.107b), the relative sensitivities for P_n are identical to the corresponding relative sensitivities of R_n. For a given h_{α_i}, the predicted changes in the numerical

value of the respective responses are also identical; this is because of Eq. (IV.B.107b) and because the relationships

$$R_n\left(\boldsymbol{e}^0+\boldsymbol{h}\right)-R_n\left(\boldsymbol{e}^0\right)=DR_n+O\left(\left\|h_\alpha\right\|^2\right), \tag{IV.B.112}$$

and

$$P_n\left(\boldsymbol{e}^0+\boldsymbol{h}\right)-P_n\left(\boldsymbol{e}^0\right)=DP_n+O\left(\left\|h_\alpha\right\|^2\right), \tag{IV.B.113}$$

hold for the same reasons as those underlying the validity of Eqs. (IV.B.109) and (IV.B.110).

Numerical results for the quantity $\left[P_n\left(\boldsymbol{e}^0+\boldsymbol{h}\right)-P_n\left(\boldsymbol{e}^0\right)\right]$ are presented in the last column of Table IV.B.4. These results are in good agreement with the sensitivity-based predicted changes, which indicates that the $O\left(\left\|\boldsymbol{h}_\alpha\right\|^2\right)$ terms in Eq. (IV.B.113) are relatively small. The results presented in the sixth column of Table IV.B.4 are the actual differences between the base-case numerical value of the response R_n, and the numerical value of the new maximum, $R_n\left(\boldsymbol{e}^0+\boldsymbol{h}\right)$, which is attained at $t_n\left(\boldsymbol{\alpha}^0+\boldsymbol{h}_\alpha\right)$. It is observed that these results disagree with the sensitivity-based predictions presented in the adjacent column. This (IV.B.90) disagreement indicates that the $O\left(\left\|\boldsymbol{h}_\alpha\right\|^2\right)$ terms in Eq. (IV.B.112) are larger than the first-order effects DR_n.

The complexities of the problem analyzed prohibit a complete analytical analysis of the causes underlying the fact that the $O\left(\left\|\boldsymbol{h}_\alpha\right\|^2\right)$ terms in Eq. (IV.B.112) are much larger than the $O\left(\left\|\boldsymbol{h}_\alpha\right\|^2\right)$ terms in Eq. (IV.B.113). Nonetheless, this fact can be largely attributed to the form of $\overline{\rho}_{scram}$ represented by Eq. (IV.B.108), and to the fact that the maximum power level occurs practically at the same time as the time of reactivity insertion. Consequently, the derivatives of the reactivity $\rho(t)$ are continuous at the fixed point τ_n (= 0.71 s), but are discontinuous at the point of reactivity insertion. Since the maximum power occurs practically at the same time as the scram, these discontinuities occur, for all practical purposes, at $t_n\left(\boldsymbol{\alpha}^0+\boldsymbol{h}_\alpha\right)$ regardless of whether $\boldsymbol{h}_\alpha$ is identically zero or not. Also, note that a discontinuity in the first- and higher-order derivatives of $\rho(t)$ induces a discontinuity in the second- and higher-order derivatives of $n(t)$. It follows that the second- and higher-order derivatives of $n(t)$ are discontinuous at points that practically coincide with $t_n\left(\boldsymbol{\alpha}^0+\boldsymbol{h}_\alpha\right)$, but these derivatives are generally continuous at τ_n. These distinctive characteristics

of the second- and higher order derivatives of $n(t)$ are not discerned by the first-order sensitivity analysis methods, but are probably the main cause underlying the large differences between the magnitudes of the $O\left(\left\|\boldsymbol{h}_\alpha\right\|^2\right)$ terms appearing in Eqs. (IV.B.112) and (IV.B.113), respectively. By highlighting the conceptual distinctions between the responses R_n and P_n, the foregoing analysis also underscored the need for a careful understanding of the use of sensitivities to predict response changes.

Table IV.B.4
Sensitivities for the Maximum Power Response $R_n(\boldsymbol{e})$.

i	α_i	Relative sensitivity	$\frac{h_{\alpha_i}}{\alpha_i^0}$ (%)	Predicted change in response value (MW)	Recalculated change in response value (MW)	
					$R_n\left(\boldsymbol{e}^0+\boldsymbol{h}\right)-R_n\left(\boldsymbol{e}^0\right)$	$P_n\left(\boldsymbol{e}^0+\boldsymbol{h}\right)-P_n\left(\boldsymbol{e}^0\right)$
1	n_0	3.784	-0.1	-1.77	-0.1	-1.7
2	T	2.805	-0.5	-6.56	0.0	-8.3
3	$\tilde{n}$	-1.920	0.5	-4.50	0.3	-5.4
4	T_{in}	0.541	-1.0	-2.53	0.8	-2.8
5	β	0.425	-1.0	-1.99	0.7	-1.5
6	$\overline{\rho}_{prog}$	-0.278	1.0	-1.30	-0.9	-1.4
7	Δt	0.171	-10.0	-8.00	-2.5	-9.7
8	k_{fuel}	-0.153	5.0	-3.58	0.6	-3.4
9	C_{pc}	-0.139	5.0	-3.25	0.3	-3.5
10	h_g	-0.133	5.0	-3.11	0.5	-3.7
11	ΔP	-0.068	10.0	-3.18	0.4	-3.3
12	f	0.049	-10.0	-2.30	1.1	-2.6

Nomenclature

A_c / A_s = cross area of coolant/structure, m^2
C_i = precursor amplitude for group i, MW
C_i^* = adjoint precursor amplitude for group i, (response dimension)/MW
C_p / C_{pc} / C_{ps} = heat capacity of fuel pin/coolant/structure, J/kg K
D = equivalent diameter for coolant channel, m
D/Dt = one-dimensional substantial (i.e., total) derivative operator
f = channel friction factor
f_L = loop friction multiplier, Pa/(kg/s)^2
g = gravitational constant = 9.807 m/s^2
ΔH = cold leg pressure head, Pa
H^* / H_c^* / H_s^* = adjoint enthalpy of fuel pin/coolant/structure, (response dimension)/J
h_g / h = heat transfer coefficient for gap/coolant, W/m^2 K
K_L = pressure head loss coefficient for an abrupt area change
k / k_c = thermal conductivity in fuel pin/coolant, W/m K
L = length of coolant channel, m
m^* = adjoint mass, (response dimension)/kg
N_j = number of pins in channel j
NC = number of coolant channels
NG = number of precursor groups
n = neutronic power amplitude, MW
n^* = adjoint power, (response dimension)/MW
n_γ = gamma-ray heating power amplitude, MW
n_o = trip power level for reaction scram, MW
ΔP = pressure drop across pump, Pa
P = coolant channel pressure, Pa
P_{inlet} = inlet plenum pressure, Pa
P_{exit} = exit plenum pressure, Pa
P^* = adjoint momentum flux, (response dimension)/[(kg m/s)/m^2]
R_f / R_g / R = outer radius of fuel/gap/cladding, m
R_s = inner radius of structure, m
r = fuel pin radius variable, m
T / T_c / T_s = temperature in fuel pin/coolant/structure, K
T_{in} = inlet coolant temperature, K

t = time variable, s

t_f = final time value (also used to initiate adjoint calculations), s

t_o = trip time of reactor scram, s

Δt = time delay between scram trip and scram reactivity insertion, s

Δt_p = time delay between scram trip and pump coastdown, s

u = channel coolant velocity, m/s

W = reactor mass flow rate, kg/s

z = axial direction variable, m

Greek symbols

β_i = delayed neutron fraction for i precursor group

$\beta = \sum_{i=1}^{NG} \beta_i$

Λ = prompt neutron generation time, s

λ_i = precursor decay constant for group i, s^{-1}

$\rho / \rho_c / \rho_s$ = density in fuel pin/coolant/structure, kg/m^3

$\overline{\rho}$ = total reactivity

$\overline{\rho}_{prog}$ = programmed input reactivity

$\overline{\rho}_{scram}$ = programmed scram reactivity

$\overline{\rho}_{Dopp}$ = Doppler and other feedback reactivity

ψ = normalized power shaping function, which includes the coolant regions, $W/(m^3\ MW)$

Subscripts

m = coolant channel abrupt area change m

Superscripts

~ = steady-state quantity

* = adjoint quantity

0 = base-case (nominal) value

CHAPTER V

USING THE ASAP TO GAIN NEW INSIGHTS INTO PARADIGM ATMOSPHERIC SCIENCES PROBLEMS

Our understanding of atmospheric processes relies considerably on the use of mathematical models to test the consequences of a collection of physical assumptions. An essential part of weather prediction and climatic research consists of interpreting the results of large-scale simulation models. For example, the current concern about the climatic impact of CO_2 stems from the sensitivity that climatic models exhibit to the atmospheric concentration of CO_2. A further example is the occurrence of atmospheric blocks, which strongly affect the variability in predictive skills of numerical weather prediction (NWP) models; it is therefore important to understand the model errors associated with blocking situations. As mathematical models increase in sophistication, though, the reasons for the results they give become less clear, making the results more difficult to interpret. A quantitative procedure to help interpret the results of a mathematical model is to perform a sensitivity analysis, i.e., to investigate how the results of the model change when parameters in the model are varied. Valuable information for this purpose comes from analyzing sensitivities of the results to parameters involved in modeling physical processes. For example, the ice-albedo feedback mechanism corresponds to the observed negative sensitivity of surface air temperature to surface albedo. Furthermore, sensitivities quantify the extent that uncertainties in parameters contribute to uncertainties in results of models. For example, sub-grid processes need to be parameterized. These parameterizations are highly simplified approximations of complex processes, so the uncertainties in the parameters involved can be large. If the corresponding sensitivities are also large, then the results of the model will have large uncertainties.

This Chapter presents paradigm applications of the Adjoint Sensitivity Analysis Procedure (*ASAP*) to a radiative-convective model (RCM) for climate simulation and to a two-layer isentropic primitive equation model for numerical weather prediction (NWP). The material presented in this Chapter is organized as follows: Section V.A presents a brief mathematical description of the RCM. This model includes 312 parameters and contains the nonlinear phenomena characteristic of radiatively-coupled processes. Section V.B presents the application of the Adjoint Sensitivity Analysis Procedure (*ASAP*) to derive the adjoint equations satisfied by the adjoint functions, to compute efficiently the response sensitivities in terms of these adjoint functions, and to illustrate the use of sensitivities. Section V.C shows that the adjoint functions themselves can be interpreted as the sensitivity of a response to instantaneous perturbations of the model's dependent variables. Furthermore these adjoint

functions can be used to reveal the time scales associated with the most important physical processes in the model. In particular, the adjoint functions for the RCM reveal the three time scales associated with: (i) convective adjustment; (ii) heat transfer between the atmosphere and space; and (iii) heat transfer between the ground and atmosphere. Calculating the eigenvalues and eigenvectors of the matrix of derivatives occurring in the set of adjoint equations reveals similar physical information without actually solving for the adjoint functions. Section V.D illustrates the use of the *ASAP* for evaluating the sensitivity to feedback mechanisms. The paradigm response considered is the increase in the average surface air temperature which occurs after the atmospheric CO_2 concentration in the model is doubled, while the paradigm feedback is the surface albedo feedback, which is introduced by making the surface albedo a function of the surface air temperature averaged over the preceding 24 hours.

Section V.E describes a paradigm two-layer isentropic NWP model which simulates the nonlinear life cycles of baroclinic waves, including the occurrence of blocks. The variability in predictive skills of numerical weather prediction (NWP) models is strongly related to the occurrence of blocks; it is therefore important to understand the sensitivities of blocking indexes to model parameters. Section V.F illustrates the application of the *ASAP* for performing sensitivity analysis of a time-dependent blocking index, underscoring the fact that the exceptional computational efficiency of the *ASAP* yields quantitative results that could not have been obtained, in practice, by any other sensitivity analysis method because of prohibitively computational costs.

V. A.A PARADIGM RADIATIVE-CONVECTIVE MODEL (RCM) OF THE ATMOSPHERE

The RCM to be considered in this Section is based on the Oregon State University two-level atmospheric general circulation model (Schlesinger and Gates, 1980); it simulates the equilibrium vertical temperatures for a single atmospheric column and its underlying surface, subject to prescribed insolation, atmospheric composition, and surface albedo. The RCM includes models for the transfer of solar and terrestrial radiation, the heat exchange between the earth's surface and atmosphere, the vertical redistribution of heat within the atmosphere, the atmospheric water vapor content, and clouds. For the solar radiation, this model includes the effects of water vapor and ozone absorption, molecular scattering, and the scattering and absorption by clouds. For the terrestrial radiation, the RCM includes emission and absorption by water vapor, carbon dioxide, and clouds. The exchange of heat between the earth's surface and atmosphere is treated as a Newtonian heating with a prescribed heat transfer coefficient multiplied by the temperature difference between the earth's surface and surface air. The vertical redistribution of heat

within the atmosphere is modeled following Manabe and Wetherald (1967) such that the lapse rate does not exceed a prescribed critical value of $6.5°\text{C}\cdot\text{km}^{-1}$. For the results to be presented in this Section, the atmospheric water vapor content is determined from the saturation vapor pressure of water as a function of temperature, and from a prescribed vertical profile of relative humidity taken as that of Manabe and Wetherald (1967). Consequently, the water vapor content depends on the temperature, but clouds do not exist for the results presented in Section V.B.

In the RCM, the atmosphere is modeled by two layers of equal mass between the earth's surface with pressure $p_4\ (=1000\,\text{mb})$, and the level 0 surface, with pressure $p_0\ (=200\,\text{mb})$. The pressure thickness of each layer is given by $\Delta p = (p_4 - p_0)/2$. The mass-averaged temperatures of the layers are determined prognostically at their mid-levels by solving the equations

$$\begin{aligned} C_1 \frac{\partial T_1}{\partial t} &= R_0 - R_2 + Q_2 \\ C_3 \frac{\partial T_3}{\partial t} &= R_2 - R_4 + Q_4 - Q_2\,, \end{aligned} \tag{V.A.1}$$

where $C_k = c_{pk}\Delta p/g$, and where: c_{pk} denotes the equivalent specific heat for moist air at constant pressure; g denotes the acceleration of gravity; t denotes the time; R_l denotes the net downward flux of solar plus terrestrial radiation at level $(l = 0,2,4)$; Q_4 denotes the upward heat flux from the earth's surface to the atmosphere; and Q_2 denotes the upward heat flux from the lower to the upper layer required to prevent the lapse rate $\Gamma = -(\partial T/\partial z)$ from exceeding a prescribed critical value $\Gamma_c = 6.5°\text{C km}^{-1}$.

The state of radiative-convective equilibrium is computed as an asymptotic state by integrating Eqs (V.A.1) in time from some prescribed initial state at $t = a$. For each time step Δt, the temperatures are first updated to include the effects of radiative heating, namely:

$$T_k^{(n+1)*} = T_k^{(n)} + \frac{\Delta t}{C_k}\left[R_{k-1}^{(n)} - R_{k+1}^{(n)}\right],\ (k = 1,3), \tag{V.A.2}$$

where the superscripts are the time-step index, and $t^{(n)} = a + n\Delta t$. Next, the temperature of the lower layer is updated to include the heating from the earth's surface:

$$T_3^{(n+1)**} = T_3^{(n+1)*} + \frac{\Delta t}{C_3} Q_4^{(n)}, \tag{V.A.3}$$

where $Q_4^{(n)}$ is obtained as a Newtonian heating

$$Q_4^{(n)} = C_s \left[T_s^{(n)} - T_4^{(n)} \right] \tag{V.A.4}$$

with a prescribed heat transfer coefficient $C_s \left(= 1.0 \text{ ly} \cdot \text{day}^{-1} \text{K}^{-1} \right)$. The surface air temperature $T_4^{(n)}$ is obtained by linear extrapolation of the temperature profile with respect to pressure, i.e.,

$$T_4^{(n)} = \frac{3}{2} T_3^{(n)} - \frac{1}{2} T_1^{(n)}. \tag{V.A.5}$$

The temperature of the earth's surface $T_s^{(n)}$ satisfies (at equilibrium) the surface energy budget

$$\sigma \left[T_s^{(n)} \right]^4 + Q_4^{(n)} = DR_4^{(n)}, \tag{V.A.6}$$

where $\sigma \left[T_s^{(n)} \right]^4$ is the upward flux of terrestrial radiation (with σ denoting the Stefan-Boltzmann constant) which, along with $Q_4^{(n)}$, is required to balance the absorbed solar plus downward terrestrial radiation at the earth's surface $DR_4^{(n)}$. Because of the dependence of $Q_4^{(n)}$ on $T_s^{(n)}$, Eq. (V.A.6) is an implicit equation which must be solved by iteration. To avoid such iterations, at each time step during the integration toward equilibrium, Eq. (V.A.6) is approximated by the explicit form

$$\sigma \left[T_s^{(n)} \right]^4 = DR_4^{(n-1)} - Q_4^{(n-1)}; \tag{V.A.7}$$

this computational expedient is based on the consideration that Eq. (V.A.7) is identical to Eq. (V.A.6) at equilibrium.

Finally, the temperature of each layer is affected by the interlayer heat flux Q_2 which is required to prevent a supercritical lapse rate $\Gamma > \Gamma_c$, which leads to

$$T_1^{(n+1)} = T_1^{(n+1)*} + \frac{\Delta t}{C_1} Q_2$$
$$T_3^{(n+1)} = T_3^{(n+1)**} - \frac{\Delta t}{C_1} Q_2 . \qquad \text{(V.A.8)}$$

Using the hydrostatic equation it can be shown that the temperature $(T_1)_c$, at the isobaric level 1 for the critical lapse rate Γ_c, is related to a given T_3 by the relation

$$(T_1)_c = T_3 \left(\frac{P_1}{P_3} \right)^{\Gamma_c R/g}, \qquad \text{(V.A.9)}$$

where R is the gas constant. Thus Q_2 is zero, except when $T_1^{(n+1)*}$ is less than the value of $(T_1)_c$, given by (V.A.9) with T_3 set to $T_3^{(n+1)**}$. In the latter case, Q_2 is determined by (V.A.8) and the condition for the critical lapse rate is

$$\frac{T_1^{(n+1)}}{T_3^{(n+1)}} = \left(\frac{P_1}{P_3} \right)^{\Gamma_c R/g} . \qquad \text{(V.A.10)}$$

In the RCM, the insolation at the top of the atmosphere $(p = 0\,\text{mb})$ is

$$S_0 = \bar{S}_0 \left(\frac{\bar{r}_e}{r_e} \right)^2 F_d \, \overline{\cos\zeta}, \qquad \text{(V.A.11)}$$

where $\bar{S}_0$ (=2793.6 ly day^{-1}) is the solar constant at one astronomical unit, $\bar{r}_e$; r_e is the earth-sun distance ($\bar{r}_e = r_e$); $\overline{\cos\zeta}$ (=0.5) is an averaged cosine of the solar zenith angle ζ; and F_d (=0.5) is an averaged fraction of a day that the sun is above the horizon. The insolation is absorbed by a prescribed amount of ozone Ω (=367 Dobson units) above the p_0 surface, by water vapor below the p_0 surface, and by the earth's surface with a prescribed albedo α_s (=0.1). The terrestrial radiation is emitted and absorbed by water vapor and a prescribed CO_2 concentration μ_{CO_2} (=320 ppmv). The water vapor mixing ratios q_k are determined from

$$q_k = q_k^* \, RH_k \,, \quad (k = 1,3), \qquad \text{(V.A.12)}$$

where RH_k is the relative humidity and

$$q_k^* = 0.622 \frac{e^*(T_k)}{p_k - e^*(T_k)} \tag{V.A.13}$$

is the saturation mixing ratio. The saturation vapor pressure e^* is obtained from the relation given by the polynomial fit of Lowe and Ficke (1974), i.e.,

$$e^*(T) = \sum_{i=1}^{7} A_{j,i} T_c^{i-1}, \tag{V.A.14}$$

where

$$T_c = T - 273.155\,K \text{ and } j = \begin{cases} 1 \text{ if } T_c \geq -50°C \\ 2 \text{ if } T_c < -50°C \end{cases}. \tag{V.A.15}$$

The relative humidities are prescribed from the profile of Manabe and Wetherald (1967),

$$RH_k = 0.77 \left(\frac{\frac{p_k}{p_4} - 0.02}{1 - 0.02} \right), \quad (k = 1,3). \tag{V.A.16}$$

By prescribing the relative humidities rather than the mixing ratios, the water vapor content becomes a variable which depends on temperature. Although the radiative transfer model treats both convective (cumuloform) and large-scale (stratiform) clouds in both the solar and terrestrial radiative calculations, the clouds are prescribed not to exist for the results presented in Sec. V.B, below. However, in the subsequent investigation presented in Sec. V.C, the stratiform clouds are made time dependent through an existence criterion that RH_k exceed some prescribed critical RH, and by prescribing q_k rather than RH_k.

The difference equations (V.A.2), (V.A.3), and (V.A.8) for T_1 and T_3, and the explicit equation (V.A.7) for T_s, can all be written in the form

$$T_k^{(n+1)} = T_k^{(n)} + F_k \left[T_1^{(n)}, T_3^{(n)}, T_s^{(n)}, \alpha \right] \Delta t, \quad (k = 1,3,s), \tag{V.A.17}$$

where the F_k are functions of T_1, T_3, T_s, and the vector $\boldsymbol{\alpha} = (\alpha_1, \ldots, \alpha_p)$ contains the system parameters. Eq. (V.A.17) represents the numerical method of solving the set of coupled first-order equations

$$\frac{du_i}{dt} = f_i(u_1, u_2, u_3, \alpha_1, \ldots, \alpha_p), \quad (i = 1,2,3). \tag{V.A.18}$$

The variables $u_1 \equiv T_1$ and $u_2 \equiv T_3$ represent the temperatures of the two layers of the model atmosphere, while $u_3 \equiv T_s$ represents the temperature of the earth's surface. The functions f_i, $(i = 1,2,3)$ represent all processes that affect these temperatures. In practice, each f_i is a nonlinear function of u_1, u_2, and u_3. The real scalars $\alpha_1, \ldots, \alpha_P$ represent parameters of the model such as specific heats, transmission functions, albedos, and initial conditions. For this study, the total number of model parameters is 312 (i.e., P =312). The state of radiative-convective equilibrium is computed as an asymptotic state of an initial-value problem, by time integration of the model's set of three nonlinear, coupled differential equations represented by Eq. (V.A.18).

V. B. APPLYING THE ASAP FOR EFFICIENT AND EXHAUSTIVE SENSITIVITY ANALYSIS OF THE RCM

To apply the Adjoint Sensitivity Analysis Procedure (*ASAP*), Eq. (V.A.18) is written in operator form as

$$N_i(\boldsymbol{u}, \boldsymbol{\alpha}) = 0, \quad (i = 1,2,3), \tag{V.B.1}$$

where the operator $N_i(\boldsymbol{u}, \boldsymbol{\alpha})$ is defined by

$$N_i(\boldsymbol{u}, \boldsymbol{\alpha}) = \frac{du_i}{dt} - f_i(\boldsymbol{u}, \boldsymbol{\alpha}). \tag{V.B.2}$$

In Eqs. (V.B.1) and (V.B.2) the components of the column vector

$$\boldsymbol{u}(t) = [u_1(t), u_2(t), u_3(t)] \tag{V.B.3}$$

are the dependent variables, and the components of the column vector

$$\boldsymbol{\alpha} = (\alpha_1, \ldots, \alpha_P) \tag{V.B.4}$$

are the real scalars representing the parameters in the model.

The initial conditions at time $t = a$ associated with the set of differential equations represented by Eq. (V.B.1) are

$$B_i(\boldsymbol{u}, \boldsymbol{\alpha}) = 0, \quad (i = 1,2,3), \tag{V.B.5}$$

where

$$B_i(\boldsymbol{u}, \boldsymbol{\alpha}) = u_i(a) - \alpha_i . \tag{V.B.6}$$

Thus, as indicated by Eqs. (V.B.5) and (V.B.6), the initial conditions are considered as the first three components of the vector of model parameters $\boldsymbol{\alpha}$.

For sensitivity analysis, the results of interest calculated with the model are customarily referred to as responses. To begin with, we consider that the response, to be denoted as $R(\boldsymbol{u}, \boldsymbol{\alpha})$, is a functional of $\boldsymbol{u}$ and $\boldsymbol{\alpha}$ of the form

$$R(\boldsymbol{u}, \boldsymbol{\alpha}) = \int_a^b r(\boldsymbol{u}, \boldsymbol{\alpha}, t)\, dt . \tag{V.B.7}$$

In this equation, b represents the final time value considered in the model, and $r(\boldsymbol{u}, \boldsymbol{\alpha}, t)$ is a function of $\boldsymbol{u}$, $\boldsymbol{\alpha}$, and t. The form of R given in (V.B.7) is sufficiently general to represent a wide variety of specific responses. For example, if the response is the surface air temperature at some time c (where $a \le c \le b$), then r is given by

$$r(\boldsymbol{u}, \boldsymbol{\alpha}, t) = \boldsymbol{d} \cdot \boldsymbol{u}\delta(t - c), \tag{V.B.8}$$

where $\boldsymbol{d} = (-0.5,\ 1.5,\ 0)$. Note that the traditional definition of the response for an RCM corresponds to $c \to \infty$. In practice, c is a sufficiently large but finite time value at which equilibrium in the RCM is judged to have been reached.

The sensitivity $\delta R(\boldsymbol{u}^0, \boldsymbol{\alpha}^0; \boldsymbol{h}, \boldsymbol{g})$ of the response $R(\boldsymbol{u}, \boldsymbol{\alpha})$ is obtained by taking the G-differential of Eq. (V.B.8); this yields

$$\delta R\left(\boldsymbol{u}^0,\boldsymbol{\alpha}^0;\boldsymbol{h},\boldsymbol{g}\right)=\left\{\frac{d}{d\varepsilon}\int_a^b r\left(\boldsymbol{u}^0+\varepsilon\boldsymbol{h},\boldsymbol{\alpha}^0+\varepsilon\boldsymbol{g},t\right)dt\right\}_{\varepsilon=0}$$
$$=\int_a^b \boldsymbol{r}_u'\cdot\boldsymbol{h}\,dt+\int_a^b \boldsymbol{r}_\alpha'\cdot\boldsymbol{g}\,dt, \tag{V.B.9}$$

where $\boldsymbol{r}_u'$ is the column vector

$$\boldsymbol{r}_u'=\left\{\left(\frac{\partial r}{\partial u_1},\frac{\partial r}{\partial u_2},\frac{\partial r}{\partial u_3}\right)\right\}_{\left(\boldsymbol{u}^0,\boldsymbol{\alpha}^0\right)} \tag{V.B.10}$$

and $\boldsymbol{r}_\alpha'$ is the column vector

$$\boldsymbol{r}_\alpha'=\left\{\left(\frac{\partial r}{\partial \alpha_1},\ldots,\frac{\partial r}{\partial \alpha_P}\right)\right\}_{\left(\boldsymbol{u}^0,\boldsymbol{\alpha}^0\right)}. \tag{V.B.11}$$

Here $\boldsymbol{u}^0(t)$ represents the nominal solution of Eqs. (V.B.1) and (V.B.5), obtained by using the nominal parameter values $\boldsymbol{\alpha}^0$. Note that Eq. (V.B.10) is linear in both $\boldsymbol{h}$ and $\boldsymbol{g}$.

When performing sensitivity analysis, the vector $\boldsymbol{g}$ of variations around the base case parameter values $\boldsymbol{\alpha}^0$ is chosen at the outset. The sensitivity $\delta R\left(\boldsymbol{u}^0,\boldsymbol{\alpha}^0;\boldsymbol{h},\boldsymbol{g}\right)$, though, can be evaluated only after determining the corresponding vector $\boldsymbol{h}(t)$ of variations around the base-case solution $\boldsymbol{u}^0(t)$. The first-order relationship between $\boldsymbol{h}$ and $\boldsymbol{g}$ is obtained by taking G-differentials of Eqs. (V.B.1) and (V.B.5), which yields

$$\frac{dh_i}{dt}-\sum_{j=1}^{3}h_j\left\{\frac{\partial f_j(\boldsymbol{u},\boldsymbol{\alpha})}{\partial u_j}\right\}_{\left(\boldsymbol{u}^0,\boldsymbol{\alpha}^0\right)}=\sum_{k=1}^{P}g_k\left\{\frac{\partial f_j(\boldsymbol{u},\boldsymbol{\alpha})}{\partial \alpha_k}\right\}_{\left(\boldsymbol{u}^0,\boldsymbol{\alpha}^0\right)},\ (i=1,2,3), \tag{V.B.12}$$

$$h_i(a)=g_i,\ (i=1,2,3). \tag{V.B.13}$$

Equations (V.B.12) and (V.B.13) constitute the "forward sensitivity equations" (or "tangent linear model"). In principle, given an arbitrary vector of parameter variations $\boldsymbol{g}$, Eqs. (V.B.12) and (V.B.13) can be solved to obtain $\boldsymbol{h}(t)$. This value of $\boldsymbol{h}(t)$ can then be used in Eq. (V.B.9) to evaluate the sensitivity δR. In practice, though, since there are P linearly independent

choices of $\boldsymbol{g}$, a complete sensitivity analysis using this procedure would involve solving Eqs. (V.B.12) and (V.B.13) anew P times.

The alternative procedure for evaluating the sensitivity δR, which circumvents the need to solve Eqs. (V.B.12) and (V.B.13) repeatedly, is the *ASAP*. To apply the *ASAP*, we write Eq. (V.B.13) in matrix form as

$$\boldsymbol{L}\boldsymbol{h} = \boldsymbol{Q}\boldsymbol{g}, \tag{V.B.14}$$

where the components L_{ij} of the 3×3 matrix $\boldsymbol{L}$ are

$$L_{ij} = \delta_{ij}\frac{d}{dt} - \frac{\partial f_i}{\partial u_j}, \ (i, j = 1,2,3) \tag{V.B.15}$$

and the components Q_{ik} of the $3\times P$ matrix $\boldsymbol{Q}$ are

$$Q_{ik} = \frac{\partial f_i}{\partial \alpha_k}, \ (i = 1,2,3, \ k = 1,\ldots,P). \tag{V.B.16}$$

The quantity δ_{ij} appearing in Eq. (V.B.15) denotes the customary Kronecker-delta.

The operator $\boldsymbol{L}^*$ that is adjoint to $\boldsymbol{L}$ is introduced through the relationship

$$\int_a^b \boldsymbol{h}\cdot\left(\boldsymbol{L}^*\boldsymbol{v}\right)dt = \int_a^b \boldsymbol{v}\cdot\left(\boldsymbol{L}\boldsymbol{h}\right)dt - \left[\boldsymbol{h}\cdot\boldsymbol{v}\right]_a^b, \tag{V.B.17}$$

where $\boldsymbol{v} = \left[v_1(t), v_2(t), v_3(t)\right]$ is a column vector that at this stage is arbitrary. In view of (V.B.17) and (V.B.15), the elements L_{ij}^* of the 3×3 matrix $\boldsymbol{L}^*$ are given by

$$L_{ij}^* = -\delta_{ij}\frac{d}{dt} - \frac{\partial f_j}{\partial u_i}, \ (i, j = 1,2,3). \tag{V.B.18}$$

The vector $\boldsymbol{v}$ is now chosen by identifying the term on the left side of (V.B.17) with the first term on the right side of (V.B.9). Note that this identification is only possible if the response is defined by a functional.

This identification gives the relationship

$$\boldsymbol{L}^*\boldsymbol{v} = \boldsymbol{r}_u'. \tag{V.B.19}$$

The value of $\boldsymbol{h}(a)$ is known from Eq. (V.B.13); the unknown value of $\boldsymbol{h}(b)$ can be eliminated from Eq. (V.B.17) by choosing

$$\boldsymbol{v}(b) = \boldsymbol{0}. \tag{V.B.20}$$

Eqs. (V.B.19) and (V.B.20) uniquely determine the adjoint function $\boldsymbol{v}$. Note that these equations are independent of $\boldsymbol{h}$ and $\boldsymbol{g}$.

In view of Eqs. (V.B.19), (V.B.20), (V.B.13), and (V.B.14), Eq. (V.B.19) is recast into the form

$$\int_a^b \boldsymbol{h} \cdot \boldsymbol{r}_u' \, dt = \int_a^b \boldsymbol{v} \cdot (\boldsymbol{Q}\boldsymbol{g}) dt + \sum_{j=1}^{3} g_j v_j(a). \tag{V.B.21}$$

Comparison of Eqs. (V.B.22) and (V.B.10) shows that the sensitivity δR is given by

$$\delta R = \int_a^b \boldsymbol{r}_\alpha' \cdot \boldsymbol{g} \, dt + \int_a^b \boldsymbol{v} \cdot (\boldsymbol{Q}\boldsymbol{g}) dt + \sum_{j=1}^{3} g_j v_j(a). \tag{V.B.22}$$

Note that this expression is independent of $\boldsymbol{h}$. Once the single calculation to determine the adjoint function $\boldsymbol{v}$ has been performed, Eq. (V.B.22) can be used to efficiently evaluate the sensitivity δR of R for any vector of variations $\boldsymbol{g}$ around the base case parameter values $\boldsymbol{\alpha}^0$.

If a variation occurs solely in the n^{th} parameter, then the vector of parameter variations $\boldsymbol{g}$ is denoted by $\boldsymbol{g}^n$, where

$$\boldsymbol{g}^n = (0, \ldots, g_n, \ldots, 0). \tag{V.B.23}$$

In this case, the corresponding sensitivity δR is denoted by δR^n, where

$$\delta R^n = \delta R(\boldsymbol{u}^0, \boldsymbol{\alpha}^0; \boldsymbol{h}, \boldsymbol{g}^n). \tag{V.B.24}$$

The value of δR^n can be used to predict the change in the response when the value of the n^{th} parameter is changed by an amount g_n.

The relative sensitivity of R to α_n^0, denoted by s_n, is defined as the dimensionless quantity

$$s_n = \frac{\delta R^n}{R} \Big/ \frac{g_n}{\alpha_n^0}. \tag{V.B.25}$$

In view of Eq. (V.B.25), the relative sensitivity s_n is a measure of the ratio between the fractional change in R and the corresponding fractional change in α_n^0. In practice, relative sensitivities are used to rank the importance of parameters.

Sensitivities can also be used to calculate the uncertainty in R due to uncertainties in the parameters. If $\boldsymbol{\alpha}^0$ represents the nominal values of the parameters, and $\boldsymbol{g}$ represents the error in the parameters, then the corresponding error in R is given, to first order in $\boldsymbol{g}$, by $\delta R\left(\boldsymbol{u}^0, \boldsymbol{\alpha}^0; \boldsymbol{h}, \boldsymbol{g}\right)$. Consequently, the standard deviation $\sigma(R)$ of R is given by

$$\sigma(R) = \left(\left\langle \delta R^2 \right\rangle\right)^{1/2}, \tag{V.B.26}$$

where the angular braces denote the expected value. Neglecting second- and higher-order effects, the relative standard deviation of R can be expressed in the customary form

$$\frac{\sigma(R)}{R} = \left[\boldsymbol{s}^T \boldsymbol{C} \boldsymbol{s}\right]^{1/2}. \tag{V.B.27}$$

In this equation the elements of $\boldsymbol{s}$ are the relative sensitivities defined in (V.B.25), and $\boldsymbol{C}$ is the relative covariance matrix with elements given by

$$C_{nm} = \frac{\left\langle g_n g_m \right\rangle}{\left(\alpha_n^0 \alpha_m^0\right)}, \quad (n, m = 1, \ldots, P). \tag{V.B.28}$$

Note that the square root of the n^{th} diagonal element of $\boldsymbol{C}$ is the relative standard deviation of the n^{th} parameter. This procedure for evaluating $\sigma(R)/R$ is customarily called uncertainty analysis.

For illustrative purposes, the explicit form of the adjoint system and the expression for δR are given below for the particular case when $r\left(\boldsymbol{u}, \boldsymbol{\alpha}, t\right)$ is specified by Eq. (V.B.8). Since $\boldsymbol{r}_u' = \boldsymbol{d}\delta(t - c)$, the adjoint system [namely, Eqs. (V.B.19) and (V.B.20)] becomes

$$-\frac{dv_i}{dt}-\sum_{j=1}^{3}v_j\left\{\frac{\partial f_j}{\partial u_i}\right\}_{(\boldsymbol{u}^0,\boldsymbol{\alpha}^0)}=d_i\delta(t-c),$$
$$v_i(b)=0,\quad (i=1,2,3). \tag{V.B.29}$$

Since $\boldsymbol{r}'_\alpha=\boldsymbol{0}$ and $Q_{ik}=\partial f_i/\partial\alpha_k$, the expression for δR [i.e., Eq. (V.B.22)] becomes

$$\delta R=\int_a^b\sum_{i=1}^{3}\sum_{j=1}^{P}v_i g_j\left\{\frac{\partial f_i}{\partial\alpha_j}\right\}_{(\boldsymbol{u}^0,\boldsymbol{\alpha}^0)}dt+\sum_{j=1}^{3}g_j v_j(a). \tag{V.B.30}$$

Since radiative-convective processes do not depend explicitly on initial conditions, f_1, f_2, and f_3 are independent of α_1, α_2, and α_3. In this case, Eq. (V.B.30) yields the following expressions for the sensitivities δR^n:

$$\delta R^n=g_n v_n(a),\quad (n=1,2,3), \tag{V.B.31}$$
$$\delta R^n=\int_a^b\sum_{i=1}^{3}v_i g_n\left\{\frac{\partial f_i}{\partial\alpha_n}\right\}_{(\boldsymbol{u}^0,\boldsymbol{\alpha}^0)}dt,\quad (n=4,\ldots,P). \tag{V.B.32}$$

In view of Eq. (V.B.31), the value of the adjoint function v_n at $t=a$ is the ratio of the variation in the response to the variation in the initial value of the dependent variable u_n at $t=a$.

For a response that is a linear combination of two other responses, i.e.,

$$R=\gamma R_1+\beta R_2, \tag{V.B.33}$$

application of G-differentials gives

$$\delta R=\gamma\delta R_1+\beta\delta R_2. \tag{V.B.34}$$

This equation can be used to obtain the sensitivities for a CO_2 -doubling experiment by taking R to represent the response with the normal concentration of CO_2 and R_2 to represent the response with double this concentration, and by setting γ to -1 and β to 1 in Eqs. (V.B.33) and (V.B.34).

The adjoint system represented by Eq. (V.B.31) is solved numerically by using the modified Euler's method. The true solution $\boldsymbol{v}(t)$ is approximated at

$(M+1)$ evenly spaced values of time, $t = a, t^1, \ldots, t^{M-1}, b$. The time interval is given by

$$\Delta t = (b-a)/M, \tag{V.B.35}$$

and the discrete times are given by

$$t^m = a + m\Delta t, \quad (m = 0, \ldots, M). \tag{V.B.36}$$

Integrating Eq. (V.B.29) from t^{m-1} to t^m gives

$$-\left[v_i(t^m) - v_i(t^{m-1})\right] - \int_{t^{m-1}}^{t^m} \sum_{j=1}^{3} v_j(t) \left\{\frac{\partial f_j}{\partial u_i}\right\}_{(\mathbf{u}^0, \boldsymbol{\alpha}^0, t)} = \begin{cases} d_i, & t^m > c > t^{m-1} \\ 0, & \text{otherwise.} \end{cases} \tag{V.B.37}$$

If the approximate value of $v_i(t^m)$ is denoted by v_i^m, then the modified Euler's method gives the following relationship between v_i^m and v_i^{m-1}:

$$-\left(v_i^m - v_i^{m-1}\right) - \Delta t \sum_{j=1}^{3} \bar{v}_j \left\{\frac{\partial f_j}{\partial u_i}\right\}_{(\mathbf{u}^0, \boldsymbol{\alpha}^0, t^{m-1/2})} = \begin{cases} d_i, & t^m > c > t^{m-1} \\ 0, & \text{otherwise,} \end{cases} \tag{V.B.38}$$

where $\bar{v}_j$ is given by

$$-\left(v_j^m - \bar{v}_j\right) - (\Delta t/2) \sum_{k=1}^{3} v_k \left\{\frac{\partial f_k}{\partial u_j}\right\}_{(\mathbf{u}^0, \boldsymbol{\alpha}^0, t^m)} = \begin{cases} d_j, & t^m > c > t^{m-1/2} \\ 0, & \text{otherwise.} \end{cases} \tag{V.B.39}$$

The above equations are solved sequentially for v_i, $(i = 1,2,3)$ and $m = (M, \ldots, 0)$, starting from the final time condition

$$v_i^M = 0, \quad (i = 1,2,3). \tag{V.B.40}$$

Note that the adjoint equations are solved by incrementing backward in time. Also note that Eqs. (V.B.40) and (V.B.41) require information about the nominal solution through the values of $\{\partial f_j / \partial u_i\}_{(\mathbf{u}^0, \boldsymbol{\alpha}^0, t)}$. In practice, these values are obtained during the base-case calculation using relationships of the type

$$\frac{\partial f_j}{\partial u_i} = \frac{f_j\left(\ldots, u_i^0 + \varepsilon, \ldots, \boldsymbol{\alpha}^0\right) - f_j\left(\mathbf{u}^0, \boldsymbol{\alpha}^0\right)}{\varepsilon} \qquad \text{(V.B.41)}$$

for small ε; in this work the value of ε was chosen to be $f_i \Delta t$.

The sensitivities themselves are calculated using Eqs. (V.B.31) and (V.B.32). Eq. (V.B.32) is approximated using the trapezoidal rule to give

$$\delta R^n = \Delta t \sum_{m=0}^{M} w_m \sum_{i=1}^{3} v_i^m g_n \left\{ \frac{\partial f_i}{\partial \alpha_n} \right\}_{\left(\mathbf{u}^0, \boldsymbol{\alpha}^0, t^m\right)}, \qquad \text{(V.B.42)}$$

where

$$w_m = \begin{cases} \dfrac{1}{2}, & (m = 0, M), \\ 1, & \text{otherwise.} \end{cases}$$

The values of $\partial f_j / \partial \alpha_n$ are obtained in the same way as are $\partial f_j / \partial u_i$, but with $\varepsilon = 0.001 \alpha_n^0$. Despite sharp changes in the adjoint functions arising from convective adjustment switching on and off during a diurnal cycle, the first-order modified Euler's method for solving the adjoint equations gives agreement with direct recalculations to three significant figures, as will be illustrated by the results presented in the next section.

The accuracy of the numerical calculations of the adjoint functions can be assessed by considering the sensitivities to the initial conditions using Eq. (V.B.31). Illustrative results depicting the behavior of the sensitivities of the surface air temperature to the initial conditions are presented in Table V.B.1; the surface air temperature and the corresponding sensitivities are evaluated at 3, 300, and 800 days after $t = a$. The results presented in the columns labeled "Actual change" represent the changes in the surface air temperature after actually varying each initial condition in turn by 0.1%, and rerunning the model. (The small variations of 0.1% were chosen in order to reduce the effect of higher order terms.) The results in the columns labeled "Predicted change" are the values of the sensitivities δR^n calculated by using Eq. (V.B.31). These results are related directly to the value of the adjoint functions at $t = a$. The close agreement between the actual and predicted changes shown in Table V.B.1 gives confidence in the adequacy of the numerical method used to solve the adjoint system.

The other purpose served by the results presented in Table V.B.1 is to show that as time increases, the absolute values of the sensitivities decrease. This

confirms the fact that if the calculation is extended over sufficiently long times, the results become independent of initial conditions.

Presented in Table V.B.2 are the sensitivities of the equilibrium surface air temperature to the solar constant, the surface albedo, the relative humidity at the surface, and the atmospheric CO_2 concentration. As shown in this table, the relative sensitivity of the surface air temperature to the solar constant is 0.381. Note that if the Stefan-Boltzmann law were valid for the surface air temperature, then the relative sensitivity would be exactly 0.25. The value of 0.381 obtained for this model indicates the existence of a feedback mechanism that enhances temperature changes. Such a mechanism is the effect of constant relative humidity: an increase in temperature will increase the moisture content of the atmosphere, and hence increase the "greenhouse" effect. To verify this, the sensitivity was calculated with fixed absolute humidity, and the value was found to be 0.234. Note that the agreement between predicted changes, using the sensitivity given by Eq. (V.B.32), and the actual changes is excellent for both 0.1% and 10% variations in the solar constant. This indicates that the surface temperature varies linearly with the solar constant, at least for variations in this range.

Table V.B.1
Sensitivity of surface air temperature to initial conditions.

Time after $t = a$ days		3		300		800	
Surface air temperature (response)		292.63 K		283.32 K		283.28 K	
		Change in response (K)		Change in response (K)		Change in response (K)	
Param	$\frac{g_n}{\alpha_n^0}$	Predicted change	Actual change	Predicted change	Actual change	Predicted change	Actual change
$u_1(a)$	0.1%	9.42E-2	8.37E-2	3.29E-4	3.39E-4	2.45E-8	2.45E-8
$u_2(a)$	0.1%	2.00E-1	2.24E-1	7.10E-4	9.24E-4	5.28E-8	6.70E-8
$u_3(a)$	0.1%	4.53E-3	4.61E-3	1.63E-5	1.58E-5	1.21E-9	1.15E-9

Table V.B.2 also shows that, as expected, the sensitivity to the surface albedo is negative; in more complicated models this causes the ice-albedo feedback mechanism. The sensitivity to the relative humidity at the surface is positive confirming the greenhouse effect caused by water vapor. The sensitivity to the CO_2 concentration was used to predict the result of a CO_2 doubling experiment (i.e., a change of 100%). The discrepancy between the predicted change of 3.43 K and the actual change of 2.42 K arises from neglecting the higher order terms.

Table V.B.2
Sensitivity of equilibrium surface air temperature to physically significant parameters.

Equilibrium surface temperature = 283.28 K (response)				
Parameter	Relative sensitivity	Fractional variation in parameter	Predicted change in response	Actual change in response
Solar constant	0.381	0.1 % 10%	0.108 10.8	0.108 10.8
Surface albedo	-0.0299	0.1 % 10%	-0-00847 -0.847	-0.00850 -0.853
Relative humidity at surface	0.0285	0.1 % 10%	0.00807 0.807	0.00811 0.795
Atmospheric CO_2 concentration	0.0121	0.1 % 10%	0.00343 3.43	0.00343 2.42

The equilibrium surface temperature is most sensitive to the coefficient $A_{1.3}$ in Eq. (V.A.14) used to calculate the saturation vapor pressure of water. The results given in Table V.B.3 illustrate the nonlinear dependence of the equilibrium surface air temperature on this parameter. For small variations in this parameter (i.e., 0.1%), the predicted change [again calculated using Eq. (V.B.32)] agrees well with the actual change in the response. By contrast, for larger variations (i.e., 1.0%), the nonlinear behavior becomes clear; for positive parameter variations the change is over-predicted, while for negative parameter variations the change is under-predicted. Once again, the differences between predicted and actual change arise from neglecting higher order terms.

Table V.B.3
Sensitivity of equilibrium surface air temperature to the coefficient $A_{1.3}$ in Eq. (V.A 14) used to calculate the saturation vapor pressure of water.

Relative sensitivity	Fractional variation in parameter	Predicted change in response (K)	Actual change in response (K)
1.19	-1%	-3.37	-6.73
	-0.1%	-0.337	-0.390
	0.1%	0.337	0.328
	1%	3.37	2.10

It is instructive to note the relative computing times needed to compute sensitivities using the *ASAP*, taking the CPU-time needed for the RCM to reach equilibrium as the "unit measure" (i.e., 1 "unit measure" ≡ "the total CPU required for the RCM to reach equilibrium"). The CPU-time needed to compute the adjoint functions amounted to 0.6 "unit measures," while the CPU-time needed to compute the derivatives $\partial f_i / \partial \alpha_j$,

$(i = 1,2,3;\ j = 1,\ldots,312)$, and subsequently the 312 sensitivities using the *ASAP* amounted to 0.8 "unit measures." The additional computing time needed to obtain the same information by rerunning, with each of the parameters changed in turn, would have been at least 312 "unit measures." A complete list of the sensitivities to all 312 parameters in the RCM is presented in the article by Hall, Cacuci, and Schlesinger (1982).

Note that Eqs. (V.B.1) and (V.B.6) describe both radiative convective and general circulation models. For general circulation models, the vector of dependent variables $\boldsymbol{u}$ represents a spatially discrete form of the synoptic state, and $\boldsymbol{f}$ includes terms that represent spatial derivatives of $\boldsymbol{u}$. Although the number I of dependent variables is of practical importance, it does not affect the interpretation of the adjoint functions.

V. C.PHYSICAL INTERPRETATION OF SOLUTIONS, EIGENVALUES, AND EIGENVECTORS OF THE ADJOINT SENSITIVITY SYSTEM FOR ATMOSPHERIC MODELS

As detailed in Section V.B, the adjoint functions for an atmospheric model are the solution to a system of equations derived from the "forward sensitivity equations" (also known as "tangent variational model," or "tangent linear model"). Each component of the solution to the adjoint equations is an adjoint function that uniquely corresponds to one of the model's dependent variables. This Section will show that the adjoint functions themselves can be interpreted as the sensitivity of a response to instantaneous perturbations of the model's dependent variables. Furthermore these adjoint functions can be used to reveal the time scales associated with the most important physical processes in the model. This interpretation is illustrated by using the same radiative convective model (RCM) as introduced in Section V.A, but the interpretation holds equally well for general circulation models of the atmosphere. In particular, the adjoint functions for the RCM reveal the three time scales, associated with: (i) convective adjustment; (ii) heat transfer between the atmosphere and space; and (iii) heat transfer between the ground and atmosphere. Calculating the eigenvalues and eigenvectors of the matrix of derivatives occurring in the set of adjoint equations reveals similar physical information without actually solving for the adjoint functions.

As detailed by Hall and Cacuci (1983), the three time-scales mentioned above are evidenced by activating options in the RCM such as to cause the clouds and the connective adjustment to switch on and off during a diurnal cycle. By activating the respective options, the specific humidities in both atmospheric layers are fixed so that the relative humidity becomes a function of temperature. The lower level relative humidity determines the fractional cloud cover. Diurnal insolation, corresponding to a perpetual equinox at 30° latitude, causes both connective adjustment of lapse rate and cloud cover to

switch on and off periodically. The ground has a thermal capacity equivalent to a 0.1 m depth of water.

Table V.C.1
Values of variables during the last integration day of the radiative convective model.

Day: hour	Upper level atm. temp. (K)	Lower level atm. temp. (K)	Surface air temp. (K)	Ground temp. (K)	Conv. Adjust.	Fractional cloud cover
199:0000	226.69	275.17	299.41	301.82	Yes	0
199:0100	226.66	275.14	299.38	300.16	Yes	0
199:0200	226.64	275.10	299.34	298.65	No	0
199:0300	226.61	275.05	299.28	297.26	No	0
199:0400	226.58	275.00	299.21	295.98	No	0
199:0500	226.56	274.94	299.12	294.80	No	0
199:0600	226.53	274.86	299.03	293.71	No	0
199:0700	226.52	274.80	298.94	294.18	No	0
199:0800	226.51	274.74	298.86	296.23	No	0.00023
199:0900	226.51	274.74	298.86	299.59	No	0.00122
199:1000	226.51	274.70	298.80	303.84	No	0.00184
199:1100	226.52	274.72	298.83	308.47	No	0.00199
199:1200	226.52	274.77	298.90	312.96	No	0.00161
199:1300	226.53	274.85	299.01	316.80	No	0.00068
199:1400	226.53	274.95	299.16	319.54	No	0
199:1500	226.57	275.03	299.26	320.87	Yes	0
199:1600	226.63	275.10	299.33	320.62	Yes	0
199:1700	226.67	275.15	299.39	318.74	Yes	0
199:1800	226.70	275.19	299.43	315.59	Yes	0
199:1900	226.72	275.21	299.46	312.72	Yes	0
199:2000	226.73	275.22	299.47	310.12	Yes	0
199:2100	226.73	275.22	299.46	307.75	Yes	0
199:2200	226.72	275.21	299.46	305.60	Yes	0
199:2300	226.71	275.20	299.44	303.62	Yes	0
200:0000	226.69	275.17	299.41	301.82	Yes	0

The time integration of the nominal solution starts at time a from arbitrary initial values of the dependent variables (i.e., temperatures) u_i. These initial values are the first I components of the vector $\boldsymbol{\alpha}$ of parameters. The integration proceeds until the final time b. For the results presented in this paper, the total time span of the model (i.e., $b-a$) is 200 days. Table V.C.1 shows the values of some of the model variables during the last integration day. Convective adjustment occurs from 1500 to 2000, and clouds exist from 0800 to 1300 (all times are local standard). The temperature of the air at the earth's surface (the surface air temperature) is obtained by linearly

extrapolating the temperatures of the two atmospheric layers (i.e., $-0.5u_1 + 1.5u_2$). The seasonal and regional conditions simulated by this model could be interpreted to correspond to late March at the same latitude as Florida.

V.C.1. Physical Interpretation of the Adjoint Functions

To highlight the physical interpretation of the adjoint functions, it is sufficient to consider responses of the form

$$R(\boldsymbol{u},\boldsymbol{\alpha}) = \int_a^b \boldsymbol{d}\cdot\boldsymbol{u}(t)r(t)dt, \tag{V.C.1}$$

where $\boldsymbol{d}$ is a constant vector, and $r(t)$ is a function of time. In general, the vector $\boldsymbol{d}$ represents the spatial and physical properties that characterize the result, and the function $r(t)$ defines either an averaging time period or an instantaneous time for the result. For example, with the radiative convective model, if $\boldsymbol{d}$ is the vector $(-0.5, 1.5, 0)$, then $\boldsymbol{d}\cdot\boldsymbol{u}$ is the surface air temperature. If, in addition, $r(t)$ is the Heaviside function $[(1/\tau)H(t-b+\tau)]$, then the result defined by Eq. (V.C.1) is the average surface air temperature from time $b-\tau$ to time b. On the other hand, if $r(t)$ is the Dirac delta function $\delta(t-c)$, then the response defined by Eq. (V.C.1) is the instantaneous surface air temperature at time c. Henceforth, this response will be denoted by R_c.

Recall from Eq. (V.B.30) that the sensitivity δR of R for any vector of variations $\boldsymbol{g}$ around the base case parameter values $\boldsymbol{\alpha}^0$ is given by

$$\delta R = \int_a^b \sum_{i=1}^{I} v_i \sum_{p=1}^{P} g_p \left\{\frac{\partial f_i}{\partial \alpha_p}\right\}_{(\boldsymbol{u}^0,\boldsymbol{\alpha}^0)} dt + \sum_{j=1}^{I} v_j(a)\, g_j . \tag{V.C.2}$$

In this above equation number, I represents the total number of dependent variables, while v_i, $(i = 1,\ldots,I)$ denote the adjoint functions that satisfy the adjoint sensitivity system

$$\begin{aligned} &-\frac{dv_i}{dt} - \sum_{j=1}^{I} v_j \left\{\frac{\partial f_j}{\partial u_i}\right\}_{(\boldsymbol{u}^0,\boldsymbol{\alpha}^0)} = d_i r(t),\ t \in (a,b), \\ &v_i(b) = 0. \end{aligned} \tag{V.C.3}$$

As indicated by Eq. (V.C.3), the adjoint functions $\boldsymbol{v}$ are independent of the parameter variations $\boldsymbol{g}$, but depend on the source term $d_i r(t)$, derived from the response functional defined by Eq. (V.C.1). Thus, there is a different set of adjoint functions for each response. For example, $\boldsymbol{v}^c$ will denote the adjoint functions associated with the response R_c.

Note from Eq. (V.C.2) that, if a variation occurs *only* in the initial value of the i^{th} dependent variable [i.e., $\boldsymbol{g} = (0,\ldots,0,g_j,0,\ldots,0)$, $(j \le I)$], then Eq. (V.C.2) becomes $\delta R = v_j(a) g_j$. This implies that the value of the adjoint function v_j at the initial time is the sensitivity of the result to the initial value of the corresponding dependent variable u_j. The considerations to be presented in this Section will show the more general result that the value of the adjoint function v_j at an arbitrary time s is the sensitivity of the result to an impulsive perturbation at time s of the corresponding dependent variable u_j.

If the system is perturbed impulsively so that the solution $\boldsymbol{u}$ of Eq. (V.B.2) jumps by an amount $\boldsymbol{\gamma}$ at time s, then this perturbed solution satisfies the equations

$$\begin{aligned} &\frac{du_i}{dt} = f_i(\boldsymbol{u},\boldsymbol{\alpha}) + \delta(t-s)\gamma_i \\ &u_i(a) = \alpha_i, \ (i = 1,\ldots,I). \end{aligned} \qquad \text{(V.C.4)}$$

In order that Eqs. (V.B.2) and (V.C.4) describe the same nominal model, the elements of $\boldsymbol{\gamma}$ must be parameters having vanishing nominal values (i.e., $\boldsymbol{\gamma}^0 = 0$). Then Eqs. (V.B.2) and (V.C.4) will have the same nominal solution $\boldsymbol{u}^0$, and will lead to the same adjoint solution $\boldsymbol{v}$, although a variation of $\boldsymbol{y}$ about $\boldsymbol{\gamma}^0 = 0$ represents an impulsive perturbation to the nominal solution $\boldsymbol{u}^0$ at time s. Figure V.C.1 illustrates schematically the effect of such a perturbation: of course, at times $t > s$, the perturbed solution will differ from $\boldsymbol{u}^0$.

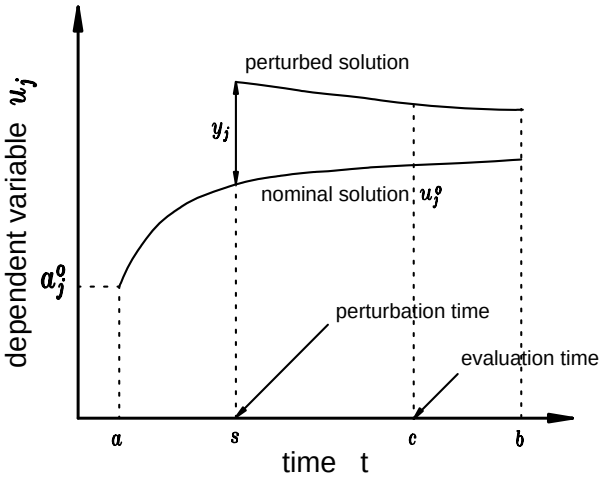

Figure V.C.1. Illustration of the effect of an impulsive perturbation y_j at time s on the nominal solution.

Deriving the adjoint equations for Eq. (V.C.4) uses the same procedure as deriving the adjoint equations for Eq. (V.B.2), except that $\boldsymbol{f} + \delta(t-s)\boldsymbol{\gamma}$ replaces $\boldsymbol{f}$, $(\boldsymbol{\alpha}, \boldsymbol{\gamma})$ replaces $\boldsymbol{\alpha}$, and $(\boldsymbol{g}, \boldsymbol{y})$ replaces $\boldsymbol{g}$. Introducing these replacements in Eq. (V.C.3) shows explicitly that the same adjoint equations arise respectively from Eqs. (V.B.2) and (V.C.4). Introducing the same replacements in Eq. (V.C.2), though, introduces additional terms into Eq. (V.C.2), which now becomes

$$\delta R = \sum_{j=1}^{I} v_j(a) g_j + \int_a^b \sum_{i=1}^{I} v_i \left\{ \left[\sum_{p=1}^{P} g_p \left(\frac{\partial}{\partial \alpha_p} \right) + \sum_{j=1}^{I} y_i \left(\frac{\partial}{\partial \gamma_i} \right) \right] \left[f_i + \delta(t-s)\gamma_i \right] \right\}_{(\boldsymbol{u}^0, \boldsymbol{\alpha}^0, \boldsymbol{\gamma}^0)} dt .$$

Note that $(\partial/\partial \alpha_p)\gamma_i = 0$, $(\partial/\partial \gamma_j) f_i = 0$, and $(\partial/\partial \gamma_j)\gamma_i = \delta_{ij}$ (where δ_{ij} is the Kronecker delta), so the above expression reduces to

$$\delta R = \int_a^b \sum_{i=1}^{I} v_i \sum_{p=1}^{P} g_p \left(\frac{\partial f_i}{\partial \alpha_p} \right) dt + \sum_{j=1}^{I} v_j(s) y_j + \sum_{j=1}^{I} v_j(a) g_j .$$

Choosing $(\boldsymbol{g},\boldsymbol{y})=(0,0,\ldots,0,y_j,0,\ldots,0)$ (i.e., all parameters variations are zero except for the perturbation y_j at time $t=s$) gives

$$\delta R = v_j(s)\,y_j\,. \tag{V.C.5}$$

This equation shows that the adjoint function v_j at time s is the sensitivity of the result R to an impulsive perturbation y_j of the solution u_j^0 at time s.

V.C.2. Interpretation of Eigenvalues and Eigenvectors Associated with the Adjoint Equations

Recall that, for the response R_c, the corresponding adjoint sensitivity system represented by Eq. (V.C.3) takes on the matrix form

$$\begin{aligned}&\dot{\boldsymbol{v}}+\boldsymbol{A}(t)\boldsymbol{v}=-\boldsymbol{d}\,\delta(t-c)\\&\boldsymbol{v}(b)=0,\end{aligned}$$

where the dot denotes differentiation with respect to t, and where

$$A_{ij}(t)\equiv\left\{\frac{\partial f_j}{\partial u_i}\right\}_{(\boldsymbol{u}^0,\boldsymbol{\alpha}^0)},\quad (i,j=1,\ldots,I).$$

The matrix $\boldsymbol{X}(t)$ is now defined to consist of the normalized column eigenvectors, of $\boldsymbol{A}(t)$, i.e., $\boldsymbol{X}=(\boldsymbol{x}^1,\ldots,\boldsymbol{x}^I)$ where $\boldsymbol{A}\boldsymbol{x}^k=\lambda_k\boldsymbol{x}^k$ and $\boldsymbol{x}^k\cdot\boldsymbol{x}^k=1$, $(k=1,\ldots I)$. Provided the eigenvectors of $\boldsymbol{A}$ are linearly independent, the use of the linear transformation $\boldsymbol{v}(t)=\boldsymbol{X}(t)\boldsymbol{w}(t)$ in the above equations leads to

$$\begin{aligned}&\dot{\boldsymbol{w}}+\boldsymbol{X}^{-1}\dot{\boldsymbol{X}}\boldsymbol{w}+\boldsymbol{D}\boldsymbol{w}=-\boldsymbol{X}^{-1}\boldsymbol{d}\,\delta(t-c)\\&\boldsymbol{w}(b)=0,\end{aligned} \tag{V.C.6}$$

where the diagonal matrix $\boldsymbol{D}$ of eigenvalues is given in terms of the Kronecker delta by

$$D_{ij}(t)=\delta_{ij}\lambda_j(t).$$

The physical significance of the eigenvectors of $\boldsymbol{A}$ can be analyzed by choosing the vector $\boldsymbol{d}$ to be the k^{th} eigenvector of $\boldsymbol{A}$ evaluated at $t = c$, i.e., $\boldsymbol{d} = \boldsymbol{x}^k(c)$. Substituting this value in (V.C.6) gives the equations

$$\begin{aligned} &\dot{w}_i + \lambda_i w_i = -\delta_{ik}\delta(t-c) - \sum_{j=1}^{I}\left(\boldsymbol{X}^{-1}\dot{\boldsymbol{X}}\right)_{ij} w_j \\ &w_i(b) = 0, \quad (i = 1,\ldots,I). \end{aligned} \tag{V.C.7}$$

Treating the right side of Eq. (V.C.7) as an inhomogeneous source term, and solving this equation by using the integrating factor method gives

$$\begin{aligned} w_i(t) = &-\int_b^t \exp\left[\int_t^{t'} \lambda_i(t'')dt''\right]\sum_{j=1}^{I} w_j(t')\left\{\left(\boldsymbol{X}^{-1}\dot{\boldsymbol{X}}\right)_{ij}\right\}_{(t')} dt' \\ &+ \delta_{ik}\exp\left[\int_t^c \lambda_i(t'')dt''\right], \quad (t < c). \end{aligned} \tag{V.C.8}$$

The above equation can be solved iteratively. The initial iterate w_i^0 is chosen to be

$$w_i^0(t) = H(c-t)\delta_{ik}\exp\left[\int_t^c \lambda_i(t'')dt''\right], \tag{V.C.9}$$

where H is the Heaviside function. The fractional difference between the next iterate $\boldsymbol{w}^1$ and the initial iterate $\boldsymbol{w}^0$ can be obtained by substituting Eq. (V.C.9) in the right side of Eq. (V.C.8) and evaluating the resulting expression using the mean value theorem. This gives

$$\frac{w_k^1(t) - w_k^0(t)}{w_k^0(t)} = (c-t)\left\{\left(\boldsymbol{X}^{-1}\dot{\boldsymbol{X}}\right)_{kk}\right\}_{(\tau_1)}, \tag{V.C.10}$$

$$\begin{aligned} \frac{w_i^1(t) - w_i^0(t)}{w_k^0(t)} &= \frac{\left\{\left(\boldsymbol{X}^{-1}\dot{\boldsymbol{X}}\right)_{ik}\right\}_{(\tau_4)}}{\lambda_i(\tau_2) - \lambda_k(\tau_3)} \\ &\times\left(\exp\left\{\left[\lambda_i(\tau_2) - \lambda_k(\tau_5)\right](c-t)\right\} - \exp\left\{\left[\lambda_k(\tau_3) - \lambda_k(\tau_5)\right](c-t)\right\}\right), \ (i \neq k), \end{aligned} \tag{V.C.11}$$

where the quantities τ_n, $(n = 1,2,\ldots,5)$, take values somewhere in the range $t \le \tau_n \le c$. Provided the magnitudes of the right-sides of both Eqs. (V.C.10)

and (V.C.11) are much less than unity, the first iterate $\boldsymbol{w}^0$ given by Eq. (V.C.9) is an adequate solution to Eq. (V.C.8). Further use of the linear transformation $\boldsymbol{v}(t) = \boldsymbol{X}(t)\boldsymbol{w}(t)$ on Eq. (V.C.9) then implies that the adjoint solution $\boldsymbol{v}(t)$ associated with the response

$$R_k = \boldsymbol{x}^k(c)\boldsymbol{u}(c) \tag{V.C.12}$$

is

$$\boldsymbol{v}^k(t) = \boldsymbol{x}^k(t)\boldsymbol{H}(c-t)\exp\left[\overline{\lambda}_k(c-t)\right], \tag{V.C.13}$$

where

$$\overline{\lambda}_k = \int_t^c \frac{\lambda_i(t'')}{c-t}\,dt''. \tag{V.C.14}$$

Equations (V.C.12), (V.C.13), and (V.C.14) indicate that each eigenvector $\boldsymbol{x}^k$ of $\boldsymbol{A}(c)$ can be used to construct a response as shown in Eq. (V.C.12) whose sensitivity to previous states takes on the form of the adjoint function shown in Eq. (V.C.13), which is governed solely by the eigenvalue λ_k. Furthermore, the mean value of this eigenvalue, cf. Eq. (V.C.14), determines the exponential rate at which this sensitivity changes.

The practical usefulness of the preceding mathematical discussion is now illustrated by using the radiative convective model with the value of c taken as midnight on the 200th day after the start of time integration of the model, i.e., $c = a + 200:0000$. At this value of c, convective adjustment is occurring and the unphysical transients in the model have decayed. In view of Eq. (V.C.12), the matrix $\boldsymbol{X}(t)$ of eigenvectors of $\boldsymbol{A}(t)$ needs to be evaluated at time c. The matrix $\boldsymbol{A}(c)$ is

$$\boldsymbol{A}(c) = \begin{pmatrix} -0.587 & 0.501 & -0.0291 \\ 0.480 & -0.418 & 0.0923 \\ 0.00308 & 0.00374 & -0.0855 \end{pmatrix} \text{h}^{-1},$$

giving the matrix of normalized column eigenvectors,

$$\boldsymbol{X}(c)=\begin{pmatrix} 0.772 & 0.648 & -0.405 \\ -0.636 & 0.759 & -0.353 \\ 4.84\times10^{-13} & 0.0576 & 0.844 \end{pmatrix}. \qquad \text{(V.C.15)}$$

Recall that Eq. (V.C.13) is valid provided the magnitude of the right side of both Eqs. (V.C.10) and (V.C.11) is much less than unity. Investigation of these magnitudes requires evaluation of the matrices $\boldsymbol{D}(\tau)$ and $\left\{\boldsymbol{X}^{-1}\dot{\boldsymbol{X}}\right\}_{(\tau)}$ at times τ anywhere in the range $t \le \tau \le c$. At $\tau = c$, these matrices are

$$\boldsymbol{D}(\tau)=\begin{pmatrix} -1.000 & 0 & 0 \\ 0 & -1.53\times10^{-3} & 0 \\ 0 & 0 & -8.86\times10^{-2} \end{pmatrix}\text{h}^{-1}, \qquad \text{(V.C.16)}$$

$$\left\{\left(\boldsymbol{X}^{-1}\dot{\boldsymbol{X}}\right)\right\}_{(\tau)}=\begin{pmatrix} 2.28\times10^{-14} & -3.88\times10^{-6} & 9.03\times10^{-5} \\ -1.72\times10^{-12} & 8.29\times10^{-5} & -5.7\times10^{-3} \\ -8.38\times10^{-14} & 1.71\times10^{-4} & -2.72\times10^{-3} \end{pmatrix}\text{h}^{-1}. \qquad \text{(V.C.17)}$$

Evaluation of the matrices $\boldsymbol{D}$ and $\boldsymbol{X}^{-1}\dot{\boldsymbol{X}}$ at several additional values of t shows that in the range $c_{-10} \le \tau \le c$, where $c_{-10} = c - 10\text{h} = a + 199:1400$, the eigenvalues appearing in $\boldsymbol{D}(\tau)$ vary by only a few percent and the elements of $\left\{\boldsymbol{X}^{-1}\dot{\boldsymbol{X}}\right\}_{(\tau)}$ remain at the same order of magnitude. But since the right side of both Eqs. (V.C.10) and (V.C.11) involves τ_n in the range $t \le \tau_n \le c$, use of Eqs. (V.C.16) and (V.C.17) imposes on t the lower bound $t \ge c_{-10}$.

For $k = 1$, the quantities appearing on the right sides of Eqs. (V.C.10) and (V.C.11) are computed by using Eqs. (V.C.16) and (V.C.17), to obtain:

$$\left|\left\{\left(\boldsymbol{X}^{-1}\dot{\boldsymbol{X}}\right)_{11}\right\}_{(\tau_1)}\right| \sim 10^{-14}\,\text{h}^{-1},$$
$$\left|\lambda_i(\tau_2)-\lambda_1(\tau_3)\right| \sim 1\text{h}^{-1}, \quad (i=2,3),$$
$$\left|\left\{\left(\boldsymbol{X}^{-1}\dot{\boldsymbol{X}}\right)_{i1}\right\}_{(\tau_4)}\right| < 10^{-12}\text{h}^{-1}, \ (i=2,3),$$
$$\exp\{[\lambda_i(\tau_2)-\lambda_1(\tau_5)](c-t)\} \sim \exp\left\{\left(1\text{h}^{-1}\right)(c-t)\right\}, \ (i=2,3)$$
$$\exp\{[\lambda_1(\tau_3)-\lambda_1(\tau_5)](c-t)\} \sim 1,$$

for $c_{-10} \le \tau \le c$, $(n = 1,2,\ldots,5)$. Therefore, for $c_{-10} \le t \le c$, the right side of Eq. (V.C.10) has a magnitude less than 10^{-13}, and the right side of Eq.

(V.C.11) has a magnitude less than 10^{-8}. Thus Eq. (V.C.13) is valid for $k=1$, and for $t=s$ the sensitivity of the response $R_1 = \boldsymbol{x}^1(c)\cdot\boldsymbol{u}(c)$ where $\boldsymbol{x}^1(c) = \left(0.772, -0.636, 4.84\times10^{-13}\right)$ decays as $\exp\left[(c-s)\overline{\lambda}_1\right]$ with $1/\overline{\lambda}_1 = -1.000\,\text{h}$.

The physical significance of $R_1 = \boldsymbol{x}^1\cdot\boldsymbol{u}$ can be deduced by examination of the above components of $\boldsymbol{x}^1$. The last component of $\boldsymbol{x}^1$ is effectively zero, indicating that R_1 is independent of the ground temperature. The first and second components of $\boldsymbol{x}^1$ are approximately of equal magnitudes but opposite signs. This indicates that R_1 is related to the difference between the two atmospheric temperatures, i.e., R_1 is related to the lapse rate. In this model, the critical lapse rate for convective adjustment occurs when $u_1 = 0.824u_2$. Note that R_1 can be written $R_1 = 0.772(u_1 - 0.824u_2)$; therefore R_1 measures the departure of the lapse rate from its critical value for convective adjustment. Thus, it can be concluded that convective adjustment of lapse rate takes place on a time scale of $1/\overline{\lambda}_1 = 1.000\,\text{h}$. Since the time step in this model is one hour, this conclusion agrees with the observation that convective adjustment occurs every time step in this RCM.

A similar line of reasoning to that above can be used to deduce the physical significance of $\boldsymbol{x}^k$ and λ_k when $k=2$ and $k=3$. Evaluation of Eqs. (V.C.10) and (V.C.11) shows that Eq. (V.C.13) is valid for both $k=2$ and $k=3$. The components of $\boldsymbol{x}^2 = (0.648,\ 0.759,\ 0.0576)$ are approximately in the ratio $c_a : c_a : c_g$ (recall that $c_a \approx 4.1\times10^6\,\text{J K}^{-1}\text{m}^{-2}$ is the heat capacity of each atmospheric layer, and $c_g \approx 4.2\times10^5\,\text{J K}^{-1}\text{m}^{-2}$ is the heat capacity of the ground). Therefore $R_2 = \boldsymbol{x}^2\cdot\boldsymbol{u}$ is a measure of the total heat energy of both the ground and the atmosphere. Since Eq. (V.C.13) is valid, it can be concluded that changes in the total heat energy of the ground and atmosphere take place on a time scale of $1/\overline{\lambda}_2 = 27\,\text{days}$. Since in this RCM most of the heat resides in the atmosphere, this conclusion agrees with the previous conclusion that perturbations to atmospheric temperature decay on a time scale of 28 days.

The components of $\boldsymbol{x}^3 = (-0.405,\ -0.353,\ 0.844)$ are in the ratio $-0.48 : -0.42 : 1.00$. Thus, the response $R_3 = \boldsymbol{x}^3\cdot\boldsymbol{u}$ indicates the difference between the ground temperature and an average atmospheric temperature. Again, since Eq. (V.C.13) is valid, it can be concluded that changes in this difference (between the ground temperature and an average atmospheric temperature) take place on a time scale of $1/\overline{\lambda}_3 = 11\,\text{h}$. This conclusion agrees

with the previous conclusion that a perturbation of the ground temperature diminishes because of heat transfer to the atmosphere on a time scale of 11h .

V.C.3. Numerical efficiency

The dependent variables $\boldsymbol{u}$ have been obtained numerically using a first-order finite difference approximation for Eq. (V.B.2), of the form

$$\boldsymbol{u}^{m+1} = \boldsymbol{u}^m + \Delta t \boldsymbol{f}\left(\boldsymbol{u}^m, \boldsymbol{\alpha}^0\right),$$

where $\boldsymbol{u}^m$ is the approximate value of $\boldsymbol{u}$ at time $t^m = a + m\Delta t$, and the time step Δt is 1h . The numerical adjoint solution has been obtained similarly, leading to the equation

$$\boldsymbol{v}^{m-1} = \boldsymbol{v}^m - \Delta t \boldsymbol{A}\left(t^m\right)\boldsymbol{v}^m - \int_{t^{m-1}}^{t^m} \boldsymbol{d}\boldsymbol{r}(t)\,dt,$$

where the Jacobian matrix $\boldsymbol{A}$ of derivatives was obtained using

$$A_{ij}\left(t^m\right) = \left\{\frac{\partial f_j}{\partial u_i}\right\}_{\left(\boldsymbol{u}^0, \boldsymbol{\alpha}^0\right)} \approx \left\{\frac{f_j\left(u_1^0, \ldots, u_i + \varepsilon, \ldots, u_I^0, \boldsymbol{\alpha}^0\right) - f_j\left(\boldsymbol{u}^0, \boldsymbol{\alpha}^0\right)}{\varepsilon}\right\}_{\left(t^m\right)},$$

with $\varepsilon = 0.01 f_i\left(\boldsymbol{u}^0, \boldsymbol{\alpha}^0\right)\Delta t$.

In the radiative convective model, most of the computation consists of evaluating the function $f\left(\boldsymbol{u}, \boldsymbol{\alpha}\right)$ at each time step. Since there is a 1h time step, the numerical solution requires 96 evaluations of $\boldsymbol{f}$ during days 196-200. The perturbation to u_j^m occurs at the m^{th} time step, and recalculation of the solution occurs for all time steps after the m^{th} . For three different values of j and 96 different values of m, these recalculations require $3 \times 96 \times (96+1)/2 = 13968$ evaluations of $\boldsymbol{f}$. To obtain the adjoint function $\boldsymbol{v}$ requires values of $\partial \boldsymbol{f} / \partial u_j$, at each time step. Calculating these derivatives for three different values of j using a finite difference expression requires $3 \times 96 = 288$ evaluations of $\boldsymbol{f}$.

V. D.EFFICIENT ESTIMATION OF FEEDBACK EFFECTS FOR CLIMATE MODELS

For certain types of feedback, it is physically meaningful to vary the strength of the feedback continuously, compare the actual effect with the sensitivity, and verify that as the strength of the feedback tends to zero, the actual effect tends to the respective sensitivity. For any feedback, even for one that may lose physical meaning if varied continuously, a comparison between the actual effect of feedback and the corresponding sensitivity shows the effect of neglecting second- and higher-order terms in the strength of the feedback, and provides guidance for judging when the sensitivity to feedback provides a realistic estimate of the actual effects of feedback.

Following the original work by Cacuci and Hall (1984), this Section illustrates the application of the *ASAP* to evaluate the sensitivity of temperature changes to feedback processes in the RCM. Specifically, the response, $R\left(\boldsymbol{u}^0, \boldsymbol{\alpha}^0\right)$, considered in the sequel is the increase in the average surface air temperature which occurs after the atmospheric CO_2 concentration in the model is doubled; the nominal solution $\boldsymbol{u}^0$ is that described in Section V.C. The averaging period τ for the average surface air temperature is the last day of the model integration. Hence, the response can be written as

$$R = R_2 - R_1, \tag{V.D.1}$$

where R_1 and R_2 denote, respectively, the average surface air temperatures with the normal and twice the normal atmospheric CO_2 concentrations. Mathematically, R_1 and R_2 can be expressed in the form

$$R_i \equiv \frac{1}{T}\int_a^b \left[\boldsymbol{d}\cdot\boldsymbol{u}_i H\left(t-b+\tau\right)\right]dt, \quad \left(i=1,2\right), \tag{V.D.2}$$

where $\boldsymbol{d} = \left(-0.5, 1.5, 0\right)$, $\boldsymbol{u}_1$ represents the RCM-solution with the normal atmospheric CO_2 concentration, $\boldsymbol{u}_2$ represents the RCM-solution with twice the normal atmospheric CO_2 concentration, and H denotes the Heaviside step function.

The sensitivity of R to a feedback $\boldsymbol{A}$ is obtained by applying the *ASAP* presented in Chapter V of Volume I. This gives

$$\delta R_{\boldsymbol{A}} = \int_a^b dt \sum_{i=1}^{3}\left[v_i \sum_{p=1}^{P} A_p\left(\boldsymbol{u}^0\right)\left\{\frac{\partial f_i}{\partial \alpha_p}\right\}_{\left(\boldsymbol{u}^0,\boldsymbol{\alpha}^0\right)}\right], \tag{V.D.3}$$

where the adjoint functions $v_i(t)$ satisfy, for $(i = 1,2,3)$, the adjoint sensitivity system

$$-\frac{dv_i}{dt} - \sum_{j=1}^{3} v_j \left\{ \frac{\partial f_j}{\partial u_i} \right\}_{(\boldsymbol{u}^0, \boldsymbol{\alpha}^0)} = H(t - b + \tau)\frac{d_i}{\tau} \qquad \text{(V.D.4)}$$

$$v_i(b) = 0.$$

Note that in this model the result R does not depend explicitly on $\boldsymbol{\alpha}$, and the initial conditions α_1, α_2, and α_3 are not involved in the feedback $\boldsymbol{A}$.

A surface albedo feedback can be introduced by making the surface albedo α_s (i.e., the s^{th} component of $\boldsymbol{\alpha}$) a function of the surface air temperature averaged over the preceding 24 hours. For this albedo feedback, the only nonzero components of the feedback operator $\boldsymbol{A}$ is A_s; this component has the form

$$A_s(u) = F\left[\overline{T}_4(t)\right], \qquad \text{(V.D.5)}$$

where

$$\overline{T}_4(t) = \int_{t-\tau}^{t} \frac{\boldsymbol{d} \cdot \boldsymbol{u}(t')dt'}{\tau}, \qquad \text{(V.D.6)}$$

and F is a function of $\overline{T}_4$. Here, $\boldsymbol{d} \cdot \boldsymbol{u}$ is the surface air temperature and $\tau = 24$ hours, so $\overline{T}_4$ is the average surface air temperature during the day before time t. The function F is depicted i Fig.V.D.1, below, and defined as follows:

$$|F| \le 0.025.$$

For $|F| < 0.025$, F causes the surface albedo to depend linearly on $\overline{T}_4$, so α_s changes from its nominal value of $\alpha_s^0 = 0.1$ at a rate $\beta\,\mathrm{K}^{-1}$. $F(299.17\,\mathrm{K}) = 0$, so when $\overline{T}_4 = 299.17\,\mathrm{K}$, the value of the average surface air temperature without feedback, the surface albedo takes on its nominal value.

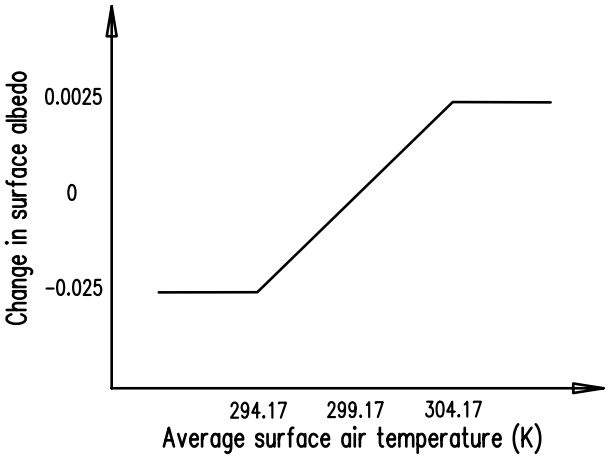

Figure V.D.1. Change in surface albedo as a function of the average surface air temperature for feedback parameter $ß = 0.005K^{-1}$.

Table V.D.1 shows the effect of the surface albedo feedback on the results of a CO_2 doubling experiment using the RCM. As expected, negative values of β correspond to positive feedback, which enhances the CO_2 warming. For the weaker feedbacks (i.e., $\beta = \pm 0.0005$), the actual effect agrees with the sensitivity to within 4%, indicating that the numerical implementation of the adjoint method is correct. For the stronger positive feedback (i.e., $\beta = -0.005$), the sensitivity is about 30% smaller than the actual effect, while for the stronger negative feedback (i.e., $\beta = 0.005$), the sensitivity is about 30% larger than the actual effect. Thus, even for the severe effects of the stronger feedback, the sensitivities calculated using adjoint functions give useful estimates of the actual effects of the feedbacks.

Table V.D.1
Effects of surface albedo feedback on a CO_2-doubling experiment using the RCM. (CO_2 warming without feedback was 1.664 K.)

	Feedback parameter β			
	0.005	0.0005	-0.0005	-0.005
CO_2 warming with feedback (K)	1.27	1.614	1.717	2.389
Actual effect of feedback (K)	-0.39	-0.050	0.053	0.72
Sensitivity to feedback (K)	-0.51	-0.051	0.051	0.51

A more complicated but also well-recognized feedback is that caused by water vapor. This feedback can be introduced in the RCM by allowing the water vapor mixing ratios α_{m1} and α_{m2} of the two atmospheric layers to be determined by a prescribed relative humidity profile. The water vapor mixing ratios thus become functions of temperature. For this feedback, the only nonzero components of the feedback operator $\boldsymbol{A}$ are A_{m1} and A_{m2}. These components are

$$A_{mk} = RH_k q_k^*[u_k(t)] - \alpha_{mk}^0 ,$$

where, for the k^{th} atmospheric layer, RH_k is the prescribed relative humidity, q_k^* is the saturation mixing ratio, and u_k is the temperature.

Table V.D.2
Effects of water vapor feedback on a CO_2-doubling experiment using the radiative-convective model.

CO_2 warming without feedback (K)	1.66
CO_2 warming with feedback (K)	2.77
Actual effect of feedback (K)	1.11
Sensitivity to feedback (K)	0.67

Table V.D.2 shows the effect of this water vapor feedback on the results of a CO_2-doubling experiment using the RCM. The actual effect of introducing water vapor feedback is to increase the CO_2 warming by $1.11\,\mathrm{K}$. For this feedback, the sensitivity calculated using adjoint functions is $0.67\,\mathrm{K}$. Thus, although the sensitivity is about 40% less than the actual effect, it still provides a useful estimate of the effect of the water vapor feedback.

V. E. AN ISENTROPIC TWO-LAYER MODEL FOR NUMERICAL WEATHER PREDICTION

The variability in predictive skills of numerical weather prediction (NWP) models is strongly related to the occurrence of blocks (Kimoto et al., 1992; Tracton et al., 1989). It is therefore important to understand the model errors associated with blocking situations. This Section describes a paradigm two-layer isentropic NWP model, which will be employed subsequently to illustrate the application of the *ASAP* to compute sensitivities of a blocking index to model parameters. The material presented in this Section is based on the article entitled "An Adjoint Sensitivity Study of Blocking in a Two-Layer Isentropic Model," by X. Zou, A. Barcilon, I. M. Navon, J. Whitaker, and D. G. Cacuci (1993).

The isentropic primitive equations can be written as

$$\frac{\partial(\zeta + f)}{\partial t} + \nabla \cdot \boldsymbol{J} = 0 \text{, (vorticity equation)} \tag{V.E.1}$$

$$\frac{\partial D}{\partial t} - \boldsymbol{k} \cdot \nabla \times \boldsymbol{J} + \nabla^2 \left(M + \frac{\boldsymbol{V} \cdot \boldsymbol{V}}{2} \right) = 0 \text{, (divergence equation)} \tag{V.E.2}$$

$$\frac{\partial \sigma}{\partial t} + \nabla \cdot (\boldsymbol{V}\sigma) + \frac{\partial(\dot{\theta}\sigma)}{\partial \theta} = 0 \text{, (continuity equation)} \tag{V.E.3}$$

$$\frac{\partial M}{\partial \theta} = \pi \text{, (hydrostatic equation)} \tag{V.E.4}$$

where: (i) the quantity $\zeta + f$ gives the absolute vorticity, or potential vorticity (PV) per unit volume; (ii) the quantity $\boldsymbol{J} = \left[u(\zeta + f) + \dot{\theta}\partial v/\partial\theta - F_j\right]\mathbf{i} + \left[v(\zeta + f) - \dot{\theta}\partial u/\partial\theta + F_i\right]\mathbf{j}$ represents the flux of PV per unit volume due to advective, diabatic, and frictional effects; (iii) $\pi = C_p (p/p_0)^k$ represents the Exner function; (iv) $M = \pi\theta + gz$ represents the Montgomery potential; (v) $\sigma = -g^{-1}\partial p/\partial\theta$ represents the isentropic mass density; and (vi) $\boldsymbol{F} = F_i\mathbf{i} + F_j\mathbf{j}$ represents the local friction force per unit mass.

In view of Eq. (V.E.1), "PV substance," that is, the amount of PV per unit volume, can not be created or destroyed in an isentropic layer, except where that layer intersects a boundary. The "PV substance" is thus concentrated within the respective layer by advective, diabatic, and friction forces (Haynes and McIntyre, 1987).

The nonlinear relationship between σ and M in Eq. (V.E.3) can be eliminated approximately by noting that

$$\sigma = \rho_a \frac{\partial z_a}{\partial \theta}, \tag{V.E.5}$$

where

$$\rho_a = \frac{p_0}{R\theta_0}\left(\frac{\pi}{C_p}\right)^{C_v/R}, \quad z_a = \frac{\theta_0}{g}(C_p - \pi) \tag{V.E.6}$$

are the density and height in an isentropic atmosphere with potential temperature θ_0, and by introducing the Boussinesq approximation $\rho_a = \rho_0 = p_0/R\theta_0$, which reduces Eq. (V.E.5) to

$$\sigma = -\frac{p_0}{R\theta_0}\frac{\partial \pi}{\partial \theta}. \tag{V.E.7}$$

Replacing Eq. (V.E.5) into (V.E.3) reduces the latter to the form

$$\frac{\partial}{\partial t}\left(\frac{\partial \pi}{\partial \theta}\right) + \nabla \cdot \left(\boldsymbol{V}\frac{\partial \pi}{\partial \theta}\right) + \frac{\partial}{\partial \theta}\left(\dot{\theta}\frac{\partial \pi}{\partial \theta}\right) = 0. \tag{V.E.8}$$

The fluid system to be studied consists of two layers of constant potential temperature on a rotating sphere. The subscripts 1 and 2 are used to denote the lower and upper layers, respectively, while the subscripts $1/2$, $3/2$, and $5/2$ indicate the surface, layer interface, and upper boundary, respectively. The boundary conditions are taken as

$$\dot{\theta}_{5/2} = \dot{\theta}_{1/2} = 0. \tag{V.E.9}$$

The condition given in Eq. (V.E.9) implies that mass is not exchanged through the upper and lower boundaries. In addition, the upper boundary is assumed to be a free surface, which implies that $\pi_{5/2} = \text{constant}$. Therefore, the continuity equation represented by Eq. (V.E.8) in the upper layer becomes an equation for the layer interface pressure $\pi_{3/2}$.

Using the hydrostatic equation, $\partial \pi / \partial z = -g/\theta$, it can be shown that $\partial M / \partial z = \pi \, \partial \theta / \partial z$. Therefore, M can change only in the vertical direction when θ changes, and is, therefore, independent of height within each layer. The horizontal momentum equations then require that u and v (hence ζ and D) be independent of height within each layer, if they are initially so. The dynamics of each layer is then similar to that of a shallow-water model.

From the definition of M at the surface, it follows that

$$M_1 \approx \pi_{1/2}\theta_1 + gz_s, \tag{V.E.10}$$

where z_s represents the topographic height. Integrating the hydrostatic equation across the layer interface leads to

$$M_2 = M_1 + \pi_{3/2}\Delta\theta = \theta_1\left(\Delta\pi_1 + \Delta\pi_2 + \pi_{5/2}\right) + gz_s + \Delta\theta\left(\Delta\pi_2 + \pi_{5/2}\right). \tag{V.E.11}$$

Equations (V.E.1), (V.E.2), and (V.E.8) are discretized by using Eqs. (V.E.10) and (V.E.11) together with the discretization procedure of Hsu and Arakawa (1990) for the vertical advection terms appearing in $\boldsymbol{J}$, to obtain

$$\frac{\partial \zeta_k}{\partial t} + \nabla \cdot \left[\left(A_k , B_k \right) \right] = 0 , \tag{V.E.12}$$

$$\frac{\partial D_k}{\partial t} + \nabla \cdot \left[\left(- B_k , A_k \right) \right] + \nabla^2 \left[M_k + \frac{1}{2} \left(u_k^2 + v_k^2 \right) \right] = 0 , \tag{V.E.13}$$

$$\frac{\partial \Delta \pi_k}{\partial t} + \nabla \cdot \left[\left(u_k \Delta \pi_k , v_k \Delta \pi_k \right) \right] = \frac{(-1)^k \dot{\theta}_{3/2}}{\Delta \theta} \left(\Delta \pi_2 + \Delta \pi_1 \right), \ (k = 1,2), \tag{V.E.14}$$

where

$$A_k = u_k \left(\zeta + f \right) + \frac{\dot{\theta}_{3/2} \left(\Delta \pi_1 + \Delta \pi_2 \right)}{2 \Delta \theta \Delta \pi_k} \left(v_2 - v_1 \right) - \left(\alpha \nabla^{\nu} - \frac{\delta_{k1}}{\tau_{drag}} \right) v_k , \tag{V.E.15a}$$

$$B_k = v_k \left(\zeta + f \right) - \frac{\dot{\theta}_{3/2} \left(\Delta \pi_1 + \Delta \pi_2 \right)}{2 \Delta \theta \Delta \pi_k} \left(u_2 - u_1 \right) + \left(\alpha \nabla^{\nu} - \frac{\delta_{k1}}{\tau_{drag}} \right) u_k , \tag{V.E.15b}$$

$$\Delta \pi_k = \pi_{k-1/2} - \pi_{k+1/2} , \tag{V.E.15c}$$

$$\Delta \theta = \theta_2 - \theta_1 . \tag{V.E.15d}$$

In the above equations, the frictional force $\boldsymbol{F}$ was parameterized by using hyperdiffusion in both layers (to control the enstrophy cascade), and a linear mechanical damping applied in the lower layer only (to simulate surface drag).

The diabatic heating $\dot{\theta}_{3/2}$ is parameterized as a Newtonian relaxation toward an equilibrium interface Exner function π_e. Therefore, for $k = 2$, Eq. (V.E.14) becomes

$$\frac{\partial \Delta \pi_{3/2}}{\partial t} + \nabla \cdot \left[\left(u_2 \Delta \pi_2 , v_2 \Delta \pi_2 \right) \right] = \frac{\dot{\theta}_{3/2}}{\Delta \theta} \left(\Delta \pi_2 + \Delta \pi_1 \right) \equiv \frac{\pi_e - \pi_{3/2}}{\tau_{diab}} . \tag{V.E.16}$$

Thus, the diabatic heating at the interface is

$$\dot{\theta}_{3/2} = \frac{\left(\pi_e - \pi_{3/2} \right) \Delta \theta}{\tau_{diab} \left(\Delta \pi_2 + \Delta \pi_1 \right)}, \tag{V.E.17}$$

implying that mass can be transferred between the layers.

The prognostic equations (V.E.12)-(V.E.14), together with the diagnostic relations (V.E.10), (V.E.11), (V.E.15), and (V.E.17), are integrated numerically in spherical geometry using a spectral transform technique similar to that described by Browning et al. (1989). The specific basis functions used are spherical harmonics with triangular truncation, truncated at wavenumber 31, together with a semi-implicit time integration procedure using a time step of 45 minutes. This semi-implicit scheme requires that the layer thickness $\Delta\pi$ be split into a horizontally uniform reference state $\Delta\overline{\pi}$ and a horizontally varying part $\Delta\pi'$, as follows:

$$\Delta\pi = \Delta\overline{\pi} + \Delta\pi', \tag{V.E.18}$$

where

$$\overline{\Delta}\pi_1 = C_p - \pi_{mid},$$
$$\overline{\Delta}\pi_2 = \pi_{mid} - \pi_{5/2},$$
$$\pi_{mid} = \frac{1}{2}\left(C_p + \pi_{top}\right).$$

The divergence equation (V.E.13) and the continuity equation (V.E.14) can then be written in the form

$$\frac{\partial D_k}{\partial t} + \nabla\cdot\left[\left(-B_k, A_k\right)\right] + \nabla^2\left[gz_s + \frac{1}{2}\left(u_k^2 + v_k^2\right)\right] + \nabla^2 M_k' = 0, \tag{V.E.19}$$

$$\frac{\partial \Delta\pi_k'}{\partial t} + \nabla\cdot\left[\left(u_k\Delta\pi_k', v_k\Delta\pi_k'\right)\right] + \Delta\overline{\pi}_k D_k = (-1)^k\,\frac{\pi_e - \pi_{mid} - \Delta\pi_2'}{\pi_{diab}}, \tag{V.E.20}$$

$(k = 1,2).$

All dependent variables are expanded in spherical harmonics, i. e.,

$$F_k(\phi,\lambda,t) = \sum_{l=-J}^{J}\sum_{n=|l|}^{J} F_{l,n,k}(t)\,Y_n^l, \tag{V.E.21}$$

where the expansion is truncated at $J = 31$, and where the spherical harmonics Y_n^l are defined as

$$Y_n^l(\phi,\lambda) = P_n^l(\sin\phi)\,e^{il\lambda}, \tag{V.E.22}$$

with P_n^l denoting the customary associated Legendre polynomials.

Using the expansion shown in Eq. (V.E.21) yields the following spectral form of the model equations (V.E.12), (V.E.19), and (V.E.20):

$$\frac{d\zeta_{l,n,k}}{dt} = A_{l,n,k} + \delta_1(n)\zeta_{l,n,k}\,, \tag{V.E.23}$$

$$\frac{dD_{l,n,k}}{dt} = B_{l,n,k} + \delta_1(n)D_{l,n,k} + \delta_2(n)M'_{l,n,k}\,, \tag{V.E.24}$$

$$\frac{d\Delta\pi'_{l,n,k}}{dt} = C_{l,n,k} - D_{l,n,k}\Delta\overline{\pi}_k\,. \tag{V.E.25}$$

In Eqs. (V.E.23) through (V.E.25), the quantities $A_{l,n,k}$ represent the spectral coefficient of all terms except the diffusion term in Eq. (V.E.12); the quantities $B_{l,n,k}$ represent the spectral coefficient of all terms except the diffusion and $\nabla^2 M'$ terms in Eq. (V.E.19); the quantities $C_{l,n,k}$ represent the spectral coefficient of all terms except the $\Delta\overline{\pi}_k D_{l,n,k}$ term in Eq. (V.E.20); and the quantities $\delta_1(n)$ and $\delta_2(n)$ are defined as follows

$$\delta_1(n) = -\alpha\left[\frac{n(n+1)}{a^2}\right]^{\nu/2}, \tag{V.E.26a}$$

$$\delta_2(n) = -\frac{n(n+1)}{a^2}. \tag{V.E.26b}$$

The last terms on the left-sides of Eqs. (V.E.24) and (V.E.25) are responsible for gravity-wave propagation and are therefore treated implicitly using the Crank-Nicholson time-differencing scheme; the other terms are treated explicitly using the leapfrog scheme. The vorticity equation (V.E.23) is integrated explicitly using the leapfrog scheme. A weak time filter is applied to all three prognostic equations to damp the computational mode.

The following specific parameter values are used in this model: $\phi_1 = 280\,K$, $\phi_2 = 320\,K$, $p_0 = 1000\,mb$, $z_{top} = 10^4\,m$, $\pi_{5/2} = C_p - gz_{top}/\theta_1$, $\nu = 12$, $\tau_{drag} = 5\,days$, $\tau_{diab} = 15\,days$; furthermore, α is chosen so that the smallest resolvable scale is damped within an e-folding time scale of 3h. The topographic height is given by $z_s = 4h_0\left(\mu^2 - \mu^4\right)\sin 2\lambda$, while the equilibrium interface Exner function is expressed as

$$\pi_e = \pi_{mid} - \frac{1}{2}\pi_\beta\left(C_p - \pi_{mid}\right)\cos 2\phi\left(\sin^2 2\phi + 2\right),$$

where $\mu = \sin\phi$, $h_0 = 2000\,m$, $\pi_{mid} = \left(C_p + \pi_{5/2}\right)/2$, and $\pi_\beta = 0.75$.

Following Zou et al. (1993), a time- and space-dependent blocking index, $R(\lambda,t)$, is defined as

$$R(\lambda,t) \equiv \left(\psi_{\phi_l}(\lambda,t) - \psi_{\phi_h}(\lambda,t)\right) H_-\left(\psi_{\phi_l}(\lambda,t) - \psi_{\phi_h}(\lambda,t)\right), \qquad \text{(V.E.27)}$$

where

$$H_-(x) \equiv \begin{cases} 1, \text{ if } x > 0 \\ 0, \text{ if } x \le 0 \end{cases}, \qquad \text{(V.E.28)}$$

denotes the unsymmetrical Heaviside function, ψ_{ϕ_l} denotes the upper-level stream function at the latitude ϕ_l, and ψ_{ϕ_h} denotes the upper-level stream function at the latitude ϕ_h. For the illustrative sensitivity analysis results presented in the following Sections, ϕ_l and ϕ_h were empirically selected as the Gaussian latitudes 39° and 65°N, respectively.

Between day 250 and day 350 during the simulation interval, three model blocks form: the first one, denoted as "block 272," formed about day 272; the second block, denoted as "block 283," formed about day 283; while the third block, denoted as "block 322," formed about day 322, respectively. The formation of blocks is particularly difficult to predict, and several theories have attempted to offer mechanisms for this process; no single theory is universally accepted yet. The illustrative sensitivity analysis results presented in the sequel are not aimed at resolving differences between blocking theories, but aim at indicating the powerful insights provided by the *ASAP* even for such difficult simulation problems.

The index defined by Eq. (V.E.27) is a function of both time and space. A simplified blocking index can be defined by selecting a fixed longitude λ, for a given block, and redefine the blocking index response as a function of time only as

$$R(t) = \left(\psi_{\phi_l}(t) - \psi_{\phi_h}(t)\right) H_-\left(\psi_{\phi_l}(t) - \psi_{\phi_h}(t)\right). \qquad \text{(V.E.29)}$$

Specifically, the following constant longitude are selected for the blocks under consideration: longitude $\lambda_l = 23°\text{W}$ for "block 272," $\lambda_l = 150°\text{W}$ for "block 283," and $\lambda_l = 360°\text{W}$ for "block 322." In the experiments to be described, a time window $t_0 \le t \le t_a$ which encompasses the respective "block" must be selected, with t_0 being selected from a few to several days before blocking,

and t_a chosen past the duration time of blocking, such that the response vanishes there, i.e., $R(t_a)=0$. Since the predictive capabilities of first-order sensitivities deteriorate when nonlinearities become significant, it is very important to select an appropriate time window for the sensitivity study of a specific problem in order to avoid, as much as possible, the loss of predictability due to nonlinearities.

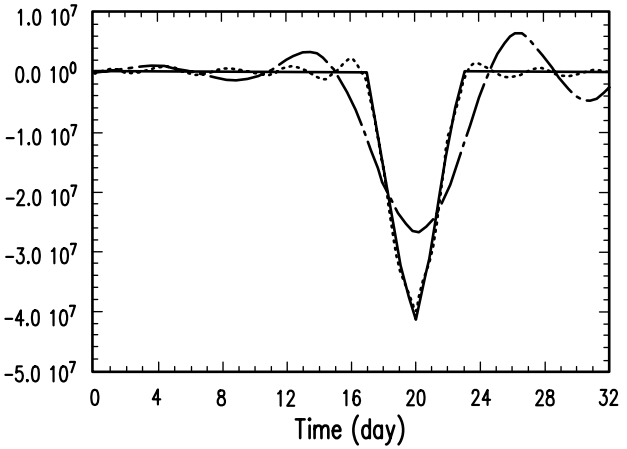

Figure V.E.1. Variation of the blocking index in time (solid line) and its approximation of the finite Fourier sine expansion truncated at $M=8$ (dash-dotted line) and $M=16$ (dotted line).

As a representative measure of the blocking index, we first select a time window extending from $t_0=267$ days to $t_a=298$ days for "block 283" and calculate the response once a day, shown as a solid line in Fig. V.E.1. The finite Fourier sine expansion

$$R(t)=\frac{2}{t_a-t_0}\sum_{m=1}^{M}a_m\sin\frac{\pi m(t-t_0)}{t_a-t_0} \qquad \text{(V.E.30)}$$

is also shown in Fig. V.E.1 as a dash-dotted line, for $M=8$, and as a dotted line, for $M=16$. The $M=16$ representation matches the response extremely well in the region where the computed response differs from zero, that is, between day t_0+18 and t_0+22. When the response is zero, the approximation given by Eq. (V.E.30) suffers from Gibbs oscillations, and therefore, one should be careful in interpreting pre-blocking results that are tainted by this shortcoming. Therefore, the subsequent developments in this Section are all based on the truncated basis function

$w_m(t) = \sin[\pi m(t-t_0)/(t_a - t_0)]$ and $(m = 1,\ldots,16)$, with $M = 16$. Using the relation $x\delta(x) = 0$, and noting that the response does not depend on the model parameters, it follows that the direct effect $R'_\alpha \boldsymbol{h}_\alpha$ is zero and the indirect effect is

$$R'_x\left(\boldsymbol{x}^0(t), \boldsymbol{\alpha}^0\right)\boldsymbol{h}_x = \left[h_{\phi_l}(t) - h_{\phi_h}(t)\right]H_-\left[\psi_{\phi_l}(t) - \psi_{\phi_h}(t)\right]. \qquad \text{(V.E.31)}$$

V. F. APPLYING THE ASAP FOR EFFICIENT SENSITIVITY ANALYSIS OF BLOCKING INDEXES IN THE TWO-LAYER ISENTROPIC MODEL

Equations (V.E.23) through (V.E.25) can be written in operator form as

$$\frac{d\boldsymbol{x}}{dt} = \boldsymbol{F}(t; \boldsymbol{x}, \boldsymbol{\alpha}), \qquad \text{(V.F.1)}$$

subject to known initial conditions

$$\boldsymbol{x}(t)_{t=t_0} = \boldsymbol{x}(t_0). \qquad \text{(V.F.2)}$$

The quantities appearing in Eq. (V.F.1) are defined as follows: (i) $\boldsymbol{\alpha} \equiv (\alpha_1,\ldots,\alpha_N)$ represents the N-dimensional vector of model parameters; (ii) $\boldsymbol{x} \equiv (x_1,\ldots,x_P)$ denotes the P-dimensional state vector; and (iii) the operator $\boldsymbol{F}$ represents all processes that change the model state $\boldsymbol{x}$. The dimension P of the model variable $\boldsymbol{x}$ is taken to be $P = 6 \times \text{NMDIM}$, where $\text{NMDIM} \equiv [J(J-1)+2]/2$ denotes all of the spectral coefficients of vorticity, ζ, divergence, D, and perturbation layer thickness, $\Delta\pi'$, while J denotes the total zonal wave numbers. When $\boldsymbol{x}$ represents the model variables on a Gaussian grid, with NLONS and NLATSH denoting the total number of grid points along longitude and latitude, then P takes on the value $P = 6 \times \text{NLONS} \times \text{NLATSH}$.

The time integration of the model starts at time $t = 0$ from arbitrary initial values of the dependent variables, and the first ca. 100 days are discarded. The integration then proceeds until a final time, t_a, is reached. For the results presented in this Section, the total time span of the model is 1100 days. For sensitivity analysis, a 32-day time window $[t_0, t_a]$ was used when a blocking event occurred.

The first step towards constructing the adjoint sensitivity system for applying the *ASAP* is to derive the forward sensitivity system (or tangent linear model)

corresponding to Eqs. (V.F.1) and (V.F.2). This is accomplished by computing the G-differential of Eqs. (V.F.1) and (V.F.2) around the nominal solution $\left(\boldsymbol{x}^0, \boldsymbol{\alpha}^0\right)$, for arbitrary variations $\left(\boldsymbol{h}_x, \boldsymbol{h}_\alpha\right)$, to obtain

$$\boldsymbol{L}\left[\boldsymbol{x}^0(t), \boldsymbol{\alpha}^0\right] \boldsymbol{h}_x(t) = \boldsymbol{Q}\left[\boldsymbol{x}^0(t), \boldsymbol{\alpha}^0\right] \boldsymbol{h}_\alpha , \tag{V.F.3}$$

where the function $\boldsymbol{h}_x(t)$ is subject to the known initial conditions

$$\boldsymbol{h}_x(t_0) \equiv \delta \boldsymbol{x}(t_0). \tag{V.F.4}$$

The operators $\boldsymbol{L}$ and $\boldsymbol{Q}$ in Eq. (V.F.3) are matrix-valued operators defined, respectively, as

$$\boldsymbol{L}\left[\boldsymbol{x}^0(t), \boldsymbol{\alpha}^0\right] \equiv \boldsymbol{I} \frac{d}{dt} - \frac{\partial \boldsymbol{F}}{\partial \boldsymbol{x}}, \tag{V.F.5}$$

$$\boldsymbol{Q}\left[\boldsymbol{x}^0(t), \boldsymbol{\alpha}^0\right] \equiv \frac{\partial \boldsymbol{F}}{\partial \boldsymbol{\alpha}}, \tag{V.F.6}$$

where $\boldsymbol{I}$ is the P-dimensional unit matrix.

The operator $\boldsymbol{L}^*$, adjoint to $\boldsymbol{L}$, is defined through the relationship

$$\int_{t_0}^{t_a} \boldsymbol{h}_{\boldsymbol{x}} \cdot \left(\boldsymbol{L}^* \boldsymbol{q}\right) dt = \int_{t_0}^{t_a} \boldsymbol{q} \cdot \left(\boldsymbol{L} \boldsymbol{h}_x\right) dt - \left(\boldsymbol{h}_{\boldsymbol{x}} \cdot \boldsymbol{q}\right)_{t_0}^{t_a}, \tag{V.F.7}$$

where $\boldsymbol{q}$ is at this stage an arbitrary column vector of dimension P. Carrying out the integration shown in Eq. (V.F.7) yields

$$\boldsymbol{L}^*\left[\boldsymbol{x}^0(t), \boldsymbol{\alpha}^0\right] \equiv -\boldsymbol{I} \frac{d}{dt} - \left(\frac{\partial \boldsymbol{F}}{\partial \boldsymbol{x}}\right)^T, \tag{V.F.8}$$

where the superscript "T" denotes "transposition."

The accuracy of the numerical procedures for discretizing the operators $\boldsymbol{L}$, $\boldsymbol{L}^*$, and $\boldsymbol{Q}$, for solving the adjoint sensitivity system, and for computing sensitivities can be verified by considering the simple functional response (not related to blocking) $R\left(\boldsymbol{x}(t_0), \boldsymbol{\alpha}\right)$ defined below:

$$R\left(\boldsymbol{x}(t_0), \boldsymbol{\alpha}\right) = \sum_{i,j,r} \psi^2\left(\lambda_i, \phi_j, k; t_r\right), \ \left(k = 2, \text{upper layer}\right), \tag{V.F.9}$$

where the summation is extended over longitude, latitude, and time, once a day for 32 days, starting at $t_0 = 267$ days.

The sensitivity of the response to variations $\boldsymbol{h}_x(t_0)$ in the model's state variables, and to parameter variations $\boldsymbol{h}_\alpha$, can be obtained in three different ways, as follows:

(a) Computing the sensitivity δR^{adj}, formulated in terms of the adjoint functions $\boldsymbol{q}(t_r)$, namely

$$\delta R^{adj} = \sum_r \boldsymbol{q}(t_r)\boldsymbol{Q}\left(\boldsymbol{x}^0(t_r), \boldsymbol{\alpha}^0\right)\boldsymbol{h}_\alpha + \boldsymbol{h}_x(t_0)\boldsymbol{q}(t_0), \tag{V.F.10}$$

where the adjoint function $\boldsymbol{q}(t_r)$ is the solution of the adjoint sensitivity system

$$\boldsymbol{L}^*\boldsymbol{q} = \boldsymbol{r}'_{\boldsymbol{x}}, \tag{V.F.11}$$

$$\boldsymbol{q}(t_a) = 0, \tag{V.F.12}$$

and where the components of the inhomogeneous source-term $\boldsymbol{r}'_{\boldsymbol{x}}$ are nonzero only for the forcing terms of the form $r'_x = 2\psi^0(t_r)$, which are present at times t_r, $r = t_a, \ldots, t_0$, where $t_a = 298$ days and $t_0 = 267$ days.

(b) Computing the sensitivity δR^{dir} by applying the *FSAP*, i.e., by using the corresponding solution $\boldsymbol{h}_\psi(t_r)$, obtained by integrating, forward in time, the "forward sensitivity system" (or "linear tangent model"), to compute:

$$\delta R^{dir} = \sum_r 2\psi^0(t_r)\boldsymbol{h}_\psi(t_r). \tag{V.F.13}$$

(c) Computing the total variation of the response

$$\begin{aligned} dR &= R\left(\boldsymbol{x} + \boldsymbol{h}_x, \boldsymbol{\alpha} + \boldsymbol{h}_\alpha\right) - R\left(\boldsymbol{x}, \boldsymbol{\alpha}\right) \\ &= \sum_r \psi^2\left(\boldsymbol{x}^0 + \boldsymbol{h}_x, \boldsymbol{\alpha}^0 + \boldsymbol{h}_\alpha; t_r\right) - \psi^2\left(\boldsymbol{x}^0, \boldsymbol{\alpha}^0; t_r\right). \end{aligned} \tag{V.F.14}$$

It is expected that Eqs. (V.F.10) and (V.F.13) would yield identical results, to within numerical accuracy. However, Eq. (V.F.14) is expected to produce results which would be close to those produced by either Eq. (V.F.10) or Eq. (V.F.13) only for changes $\|\boldsymbol{h}_x\|$ and $\|\boldsymbol{h}_\alpha\|$ that are sufficiently small for rendering the higher-order effects negligible.

Table V.F.1
Sensitivity of R, defined by Eq. (V.F.9), to the increments $\varepsilon\psi(t_0)$ in the field of the stream-function $\psi(t_0)$.

	Predicted change		
	Adjoint method[a]	Direct method[b]	Actual change[c]
10E-3	4.683E16	4.683E16	4.721E16
10E-4	4.683E15	4.683E15	4.709E15
10E-5	4.683E14	4.683E14	4.686E14
10E-6	4.683E13	4.683E13	4.683E13

[a]Predicted change (*ASAP*) $= \left[\boldsymbol{q}(0), \boldsymbol{h}_x(0)\right]$. [b]Predicted change (*FSAP*) $= \left[R'_x, \boldsymbol{h}_x\right]$. [c]Actual change $= R\left(\boldsymbol{x}^0 + \boldsymbol{h}_x, \boldsymbol{\alpha}^0\right) - R\left(\boldsymbol{x}^0, \boldsymbol{\alpha}^0\right)$.

Table V.F.1, above, presents illustrative results for δR^{adj}, δR^{dir}, and dR for $\boldsymbol{h}_x = \left(\varepsilon\psi^0(t_0), 0, 0\right)^T$ and $\boldsymbol{h}_\alpha = 0$, where ε ranges from 10^{-2} to 10^{-6}. The results presented in the columns labeled "actual change" represent the actual changes in the blocking index obtained by rerunning the two-layer isentropic model after ψ has been increased by $\varepsilon\psi$. The column labeled "predicted change (direct method)" presents the sensitivities values δR^{dir}, while the columns labeled "predicted change (adjoint method)" displays the results δR^{adj}. The *ASAP* results (given by δR^{adj}) are practically identical to the results produced by the *FSAP* (δR^{dir}), and also agree with direct computations, for small values of ε. For larger values of ε ($>10^{-3}$), the nonlinear effects become apparent.

An additional investigation of the effects of nonlinearities on the behavior of the response R defined by Eq. (V.F.9) is presented in Figures V.F.1a and V.F.1b, below. Thus, Fig.V.F.1a depicts the time-behavior, for $\varepsilon = 10^{-2}$, of the quantities $2\psi^0(t_r)\boldsymbol{h}_\psi(t_r)$ and $\left\{\psi^2\left(\boldsymbol{x}^0 + \boldsymbol{h}_x, \boldsymbol{\alpha}^0; t_r\right) - \psi^2\left(\boldsymbol{x}^0, \boldsymbol{\alpha}^0; t_r\right)\right\}$, respectively. The two curves are very close for the first 9 days of integration and begin to diverge afterward, indicating that the cumulative effects of the nonlinear terms, for this value of ε, are no longer negligible. This result implies that the tangent linear model approximation is valid for 9 days of integration for a perturbation of size $\varepsilon = 10^{-2}$. However, when $\varepsilon = 10^{-6}$, the agreement between these same curves (Fig. V.F.1b) is excellent, confirming the results shown in Table V.F.1, and thereby indicating the extent to which the forward sensitivity system (i.e., tangent linear model) yields reliable predictions.

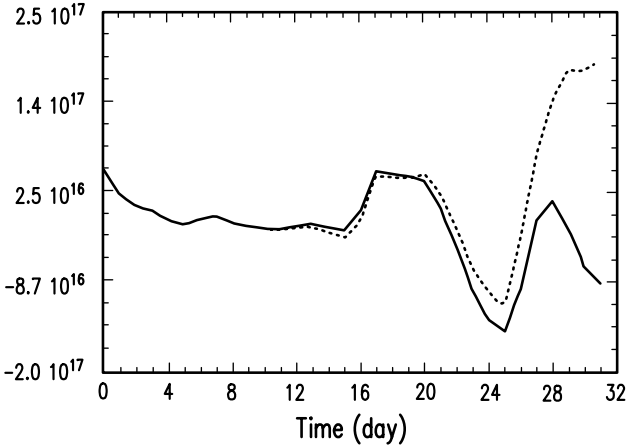

Figure V.F.1a. Variation of $dR(t)$ (dotted line for $\varepsilon = 10^{-2}$ and solid line for $\varepsilon = 10^{-6}$) and $\delta R^{dir}(t)$ (solid line for $\varepsilon = 10^{-2}$ and circles for $\varepsilon = 10^{-6}$) with time in the time window of $[t_0, t_\alpha]$, for a variation of $\varepsilon\psi(t_0)$ in the field of ψ, at time t_0, for $\varepsilon = 10^{-2}$.

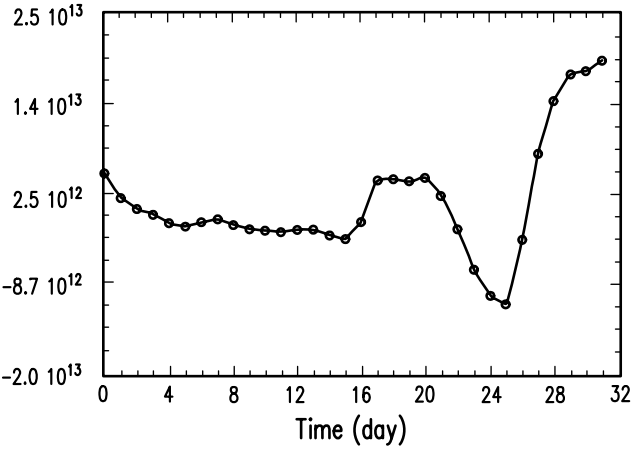

Figure V.F.1b. Variation of $dR(t)$ (dotted line for $\varepsilon = 10^{-2}$ and solid line for $\varepsilon = 10^{-6}$) and $\delta R^{dir}(t)$ (solid line for $\varepsilon = 10^{-2}$ and circles for $\varepsilon = 10^{-6}$) with time in the time window of $[t_0, t_\alpha]$, for variation of $\varepsilon\psi(t_0)$ in the field of ψ, at time t_0, for $\varepsilon = 10^{-6}$.

Having verified the adequacy of the numerical solution of the adjoint sensitivity model, we now apply the *ASAP* to the time-dependent blocking index $R(t)$ defined in (V.E.29) and reproduced, for convenience, below:

$$R(t) = \left(\psi_{\phi_l}(t) - \psi_{\phi_h}(t)\right) H_-\left(\psi_{\phi_l}(t) - \psi_{\phi_h}(t)\right). \qquad \text{(V.E.29)}$$

The above blocking index can be considered either as being dependent upon the vector $\boldsymbol{X}(t)$ in *physical* space or as being dependent upon the vector of time-dependent *spectral* coefficients $\boldsymbol{x}$. Both points of view will be treated in the sub-sections below.

V.F.1. Blocking Index in Physical Space

The blocking index, $R(t)$, defined by Eq. (V.E.29), and the indirect effect, $R'_X \boldsymbol{h}_X$, given by Eq. (V.E.31), can be expressed as functions of the model variables on a Gaussian grid space, in matrix form, as

$$R(t) = \boldsymbol{a}^T \boldsymbol{X} H_-\left(-\boldsymbol{a}^T \boldsymbol{X}\right), \qquad \text{(V.F.15)}$$

$$R'_X \boldsymbol{h}_X = \boldsymbol{a}^T \boldsymbol{h}_X H_-\left(-\boldsymbol{a}^T \boldsymbol{X}^0\right), \qquad \text{(V.F.16)}$$

where the components of the vector $\boldsymbol{a}$ are defined as

$$a_l = \begin{cases} 1, & \text{if } l = (j_1 - 1)I + i_1; \\ -1, & \text{if } l = (j_2 - 1)I + i_1; \\ 0, & \text{otherwise}, \end{cases} \qquad \text{(V.F.17)}$$

and where j_1, j_2, and i_1 correspond to ϕ_l, ϕ_h, and λ_l, respectively, while $I = \text{NLONS}$ denotes the total number of grid points in the longitudinal direction. It follows that the partial G-derivative of the response with respect to the model variables $\boldsymbol{X}$ is given by

$$R'_X = \left(\ldots, H_-\left(-\boldsymbol{a}^T \boldsymbol{X}^0\right) \boldsymbol{a}^T \frac{\partial \boldsymbol{X}}{\partial X_i}, \ldots \right). \qquad \text{(V.F.18)}$$

Expressing the indirect effect term (which gives, at the same time, the sensitivity of the blocking index) in terms of the basis function $\{\sin[\pi m(t - t_0)/(t_a - t_0)], (m = 1, \ldots, M)\}$ leads to

$$R'_X \boldsymbol{h}_X = \delta R\left(\boldsymbol{X}^0(t), \boldsymbol{\alpha}^0; \boldsymbol{h}_X(t), \boldsymbol{h}_\alpha\right) = \frac{2}{t_a - t_0} \sum_{m=1}^{M} a_m \sin \frac{\pi m(t - t_0)}{t_a - t_0}, \quad \text{(V.F.19)}$$

where the coefficients a_m are defined as

$$\begin{aligned} a_m &\equiv \int_{t_0}^{t_a} R'_X \boldsymbol{h}_X \sin \frac{\pi m(t - t_0)}{t_a - t_0} dt \equiv \left\langle R'_X \boldsymbol{h}_X, \sin \frac{\pi m(t - t_0)}{t_a - t_0} \right\rangle \\ &= \left[\boldsymbol{h}_X, (R'_X)^T \sin \frac{\pi m(t - t_0)}{t_a - t_0} \right]. \end{aligned} \quad \text{(V.F.20)}$$

It follows from the last term of the above sequence of equalities that the source term for the adjoint sensitivity system is provided by the quantity $(R'_X)^T \sin \pi m(t - t_0)/(t_a - t_0)$. Hence, the adjoint sensitivity system becomes

$$\boldsymbol{G}^* \boldsymbol{L}^* \boldsymbol{S}^* q_m(t) = (R'_X)^T \sin \frac{\pi m(t - t_0)}{t_a - t_0}, \quad \text{(V.F.21)}$$

where $\boldsymbol{G}$ is a transform from the Gaussian grid space of $(\psi, D, \Delta\pi')$ to the spectral space of $(\zeta, D, \Delta\pi')$, while $\boldsymbol{S} = \boldsymbol{G}^{-1}$. Replacing the left-side of Eq. (V.F.21) into the last term of Eq. (V.F.20), and using the definition of adjoint operators yields

$$a_m = \left[\boldsymbol{h}_X, \boldsymbol{G}^* \boldsymbol{L}^* \boldsymbol{S}^* q_m(t)\right] = \left[q_m(t), \boldsymbol{SLG} \boldsymbol{h}_X(t)\right] + \left[\boldsymbol{h}_X(t_0), q_m(t_0)\right]. \quad \text{(V.F.22)}$$

The appearance of $\boldsymbol{h}_X$ can be eliminated from the above expression by using the forward sensitivity system,

$$\boldsymbol{SLG} \boldsymbol{h}_X = \boldsymbol{SQ} \boldsymbol{h}_\alpha, \quad \text{(V.F.23)}$$

in the inner product on the rightmost side of Eq. (V.F.22). Hence, the coefficients a_m can be expressed in terms of the adjoint functions as

$$a_m = \left[q_m, \boldsymbol{SQ} \boldsymbol{h}_\alpha\right] + \left[\boldsymbol{h}_X(t_0), q_m(t_0)\right]. \quad \text{(V.F.24)}$$

Substituting the above expression into Eq. (V.F.19) yields the following expression for the sensitivity $\delta R\left(\boldsymbol{X}^0(t), \boldsymbol{\alpha}^0; \boldsymbol{h}_X(t), \boldsymbol{h}_\alpha\right)$ of the blocking index $R(t)$:

$$\delta R\left(\boldsymbol{X}^0(t), \boldsymbol{\alpha}^0; \boldsymbol{h}_X(t), \boldsymbol{h}_\alpha\right)$$
$$= \frac{2}{t_a - t_0} \sum_{m=1}^{M} \left\{ \left[q_m, \boldsymbol{SQh}_\alpha \right] + \left[\boldsymbol{h}_X(t_0), q_m(t_0) \right] \right\} \sin \frac{\pi m (t - t_0)}{t_a - t_0}. \quad \text{(V.F.25)}$$

The nominal solution of the nonlinear two-layer isentropic model is used in Eqs. (V.F.15) and (V.F.18) to obtain the nominal value of the blocking index response, $R(t)$, and, respectively, the partial G-derivative $(R'_X)^T$. Then, the adjoint sensitivity model is integrated backwards in time sixteen times, with sixteen different right-sides $(R'_X)^T \sin\left[\pi m (t - t_0)/(t_a - t_0)\right]$ for $(m = 1, \ldots, M = 16)$, to obtain the values of the respective adjoint functions $q_m(t)$. The values of $q_m(t)$, $(m = 1, \ldots, M)$ thus obtained are replaced in Eq. (V.F.25) to obtain the sensitivities of the blocking index to all model parameters, as well as model-states at any point in time. Note that the inner product in Eq. (V.F.25) is of the form

$$\left[\boldsymbol{g}^{(1)}(t), \boldsymbol{g}^{(2)}(t) \right] = \sum_{i=1}^{P} \left\langle g_i^1(t), g_i^2(t) \right\rangle$$
$$= \sum_{i=1}^{P} \Delta t \left(\frac{1}{2} g_i^1(t_0) g_i^2(t_0) + \sum_{j=1}^{N-2} g_i^1(t_j) g_i^2(t_j) + \frac{1}{2} g_i^1(t_{N-1}) g_i^2(t_{N-1}) \right), \quad \text{(V.F.26)}$$

where $\boldsymbol{g}^{(1)}$ and $\boldsymbol{g}^{(2)}$ represent two arbitrary vectors in physical space. The time-integration was performed by using an extended trapezoidal rule, with $t_j = t_0 + j\left[(t_a - t_0)/(N-1)\right]$, $(j = 0, \ldots, N-1)$, where $N - 1 = 31$ denotes the total number of subintervals in the integration period $[t_0, t_a]$. Furthermore, since the summation in Eq. (V.F.25) is actually of the form

$$\delta R\big|_{t=t_j} = \frac{2}{t_a - t_0} \sum_{m=1}^{M} a_m \sin \frac{\pi m j}{N-1}, \ (j = 0, \ldots, N-1), \quad \text{(V.F.27)}$$

the value of the sensitivity $\delta R\big|_{t=t_j}$ of the blocking index is computed using a Fast Fourier Sine Transform.

V.F.2. Blocking Index in Spectral Space

Expressing the response $R(t)$ and the indirect effect $R'_x \boldsymbol{h}_x$ as functions of the model variables in spectral space enables sensitivity analysis of the blocking index response to variations in amplitudes of the various wavenumber. Then (V.F.15) and (V.F.16) are written, respectively, as

$$R(t) = \boldsymbol{a}^T \boldsymbol{S}\boldsymbol{x} H_-\left(-\boldsymbol{a}^T \boldsymbol{S}\boldsymbol{x}\right), \tag{V.F.28}$$

$$R'_x \boldsymbol{h}_x = \boldsymbol{a}^T \boldsymbol{S}\boldsymbol{h}_x H_-\left(-\boldsymbol{a}^T \boldsymbol{S}\boldsymbol{x}^0\right), \tag{V.F.29}$$

where the vector $\boldsymbol{a}$ has been defined in Eq. (V.F.17). The partial G-derivative of the response with respect to the spectral model variables $\boldsymbol{x}$ is

$$R'_x = \left(\ldots, H_-\left(-\boldsymbol{a}^T \boldsymbol{S}\boldsymbol{x}^0\right)\boldsymbol{a}^T \boldsymbol{S}\frac{\partial \boldsymbol{x}}{\partial x_i}, \ldots\right). \tag{V.F.30}$$

Applying the *ASAP* as outlined in Chapter V of Volume I along the same lines as in the previous subsection, the sensitivity of the blocking index representation in spectral space is obtained as

$$\begin{aligned}&\delta R\left(\boldsymbol{x}^0(t), \boldsymbol{\alpha}^0; \boldsymbol{h}_x(t), \boldsymbol{h}_\alpha\right) \\ &= \sum_m \left\{\left[\boldsymbol{q}^n, \boldsymbol{Q}\left(\boldsymbol{x}^0(t), \boldsymbol{\alpha}^0\right)\boldsymbol{h}_\alpha\right] + \left[\boldsymbol{h}_x(0), \boldsymbol{q}_m^n(0)\right]\right\} \sin\frac{\pi m(t-t_0)}{t_a - t_0},\end{aligned} \tag{V.F.31}$$

where the adjoint function $\boldsymbol{q}_m(t)$ is the solution of the adjoint sensitivity system

$$\boldsymbol{L}^*\left(\boldsymbol{x}^0(t), \boldsymbol{\alpha}^0\right)\boldsymbol{q}_m(t) = \left(R'_X\right)^T \sin\frac{\pi m(t-t_0)}{t_a - t_0}, \tag{V.F.32}$$

$$\boldsymbol{q}_m(t_a) = 0. \tag{V.F.33}$$

V.F.3. Illustrative Sensitivity Analysis Results

Table V.F.2 presents relative sensitivities of the blocking index for block 272 to different wavenumbers in the upper layer; these results were computed using Eq. (V.F.31). The quantities (m, n) represent the zonal wavenumber and the number of nodes in the meridional direction. A Cartesian meridional wavenumber, l, could be approximately obtained by writing $l \approx (m-n)/2$. The sets of waves that contribute most to block intensification could thus be

characterized as being planetary $(m=0; n=7; l\approx 2)$, synoptic $(m=6; n=11; l\approx 2)$, or zonal $(m=0; n=11; l\approx 5-6)$. The results shown in Table V.F.2 highlight the importance of zonal flow, planetary waves, as well as synoptic-scale features; positive relative sensitivities imply block intensification, and the scales $(m,n)=(2,7;0,11;6,11)$ bring the dominant contribution. The waves producing negative values of relative sensitivity contribute most to block demise; the respective scales are $(m,n)=(0,3;0,7;4,7;5,6)$, indicating again that zonal flow is important. The largest sensitivities in the wave band $m=0-6$ occur mainly for meridional wavenumbers $n=0-9$. The sensitivities within wavenumbers $m=7-12$ are an order of magnitude smaller than those occurring within wavenumbers $m=0-6$.

Recall that when a variation occurs solely in the n^{th} parameter, the corresponding vector of parameter variation $\boldsymbol{h}_\alpha^n$ takes on the form

$$\boldsymbol{h}_\alpha^n=\left(0,\ldots,h_\alpha^n,\ldots,0\right)^T. \tag{V.F.34}$$

Denoting the corresponding response sensitivity by δR^n, we recall that the relative sensitivity s_n is defined as the dimensionless quantity

$$s_n=\frac{\delta R^n}{R}\left(\frac{h_\alpha^n}{\alpha_n^0}\right)^{-1}. \tag{V.F.35}$$

Note that because $R\le 0$ and $h_\alpha^n/\alpha_n^0>0$, s_n and δR^n have opposite signs; thus, $s_n>0$ implies block intensification.

Figure V.F.2 shows the relative sensitivity of the blocking index at longitude $\lambda_1=23°\text{W}$ during the time window $[\text{day } 267, \text{day } 298]$. Only the relative sensitivities for the five days when the blocking index differs from zero are plotted. Note that although the variation of the blocking index response is quite symmetric (see Figure V.E.1), the time evolution of the relative sensitivities is antisymmetric. As can be seen from Figure V.F.2, the largest sensitivity is to the mountain height h_0; the second most important parameter affecting the blocking index is the quantity π_β (which represents a measure of the slope of the layer interface and, therefore, a measure of the upper-level zonal jet in the radiative drive). The third most important parameter is τ_{drag}, which denotes the surface drag that controls the baroclinic life cycle via the barotropic governor mechanism of James and Gray (1986) and James (1987). Mechanical drag is an order of magnitude more important than the Newtonian damping,

τ_{diab} , which is the fourth most important parameter in the two-layer isentropic model.

Table V.F.2
Values of relative sensitivities of the blocking index at longitude 150°W and day 271 to 1% perturbations of ψ in spectral space at the upper layer, at time $t_0 = 267$ (day).

	$m=0$	$m=1$	$m=2$	$m=3$	$m=4$	$m=5$	$m=6$	$m=7$
$n=0$								
$n=1$	-3.0E-2							
$n=2$		-4.6E-4						
$n=3$	-2.7E-1		-2.3E-2					
$n=4$		-4.4E-2		2.7E-2				
$n=5$	8.6E-3		-4.9E-2		-5.0E-2			
$n=6$		-5.0E-2		-3.4E-2		-1.7E-3		
$n=7$	-1.2E-1		8.8E-2		-1.2E-1		1.3E-2	
$n=8$		-4.1E-3		6.4E-2		-8.7E-2		8.8E-3
$n=9$	-2.5E-2		3.5E-2		-5.0E-2		-2.2E-2	
$n=10$		-4.0E-3		-1.3E-2		-4.8E-2		-1.2E-2
$n=11$	9.5E-2		-7.7E-3		-2.0E-2		8.4E-2	
$n=12$		3.1E-2		-9.8E-2		-1.0E-2		-8.4E-3
$n=13$	-4.6E-4		-8.1E-4		-6.4E-3		-1.9E-2	
$n=14$		2.0E-3		-7.8E-3		2.9E-3		-4.2E-4

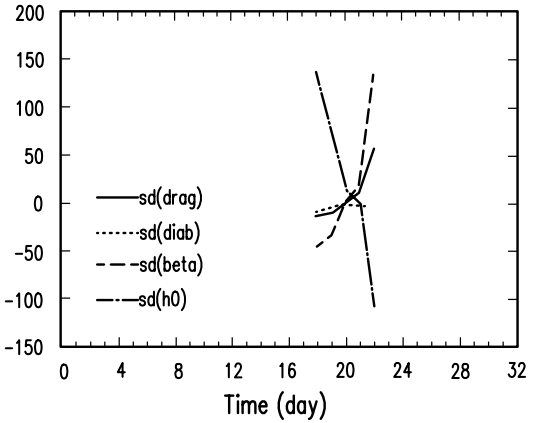

Figure V.F.2. The relative sensitivities of the blocking index to model parameters τ_{drag} (solid line), τ_{diab} (dotted line), $\pi_{ß}$ (dashed line), and h_0 (dash-dotted line).

V.F.4. Computational Costs

A few adjoint calculations, each involving a similar amount of computation as would be required for solving once the tangent linear of the original model, sufficed to obtain sensitivities of a blocking index to all the relevant model parameters and model states (the total dimension is 3076 in spectral space and 13 828 in grid space). The sensitivity of the blocking index to mountain height was found to be the largest. The sensitivity analysis in grid space and spectral space has shown that the significant sensitivities for blocking occur in some preferred regions and spectral wave bands.

It is instructive to analyze the computational cost of applying the *ASAP* for performing sensitivity analysis of a time-dependent blocking index. The CPU time required to compute the nominal solution by a 32-day time-integration of the two-layer isentropic model, namely Eq. (V.F.1), was 46 seconds. Hence, the CPU time for calculating an exact change in the response would be 92 seconds (namely: twice the time needed for a base-case computation). On the other hand the CPU time needed for the 32-day time-integration of the adjoint sensitivity model described by Eq. (V.F.21), for a given right-side, was 86 seconds. Consequently, the CPU times for calculating the sixteen adjoint functions $q_m, (m = 1, \ldots, M = 16)$, which are needed to obtain the sensitivities of the blocking index using the *ASAP*, was 1455 seconds. Once the values of the adjoint variables $q_m, (m = 1, \ldots, M = 16)$ are available, the subsequent sensitivity analysis is computationally very efficient. The computation of the response sensitivity to any change in any of the model's state variables parameter requires only 1 second, while the CPU for computing the sensitivity of the response to any parameter variation requires only 33 s [which is the CPU time required to compute the quadrature in Eq. (V.F.25)]. This underscores the fact that the *ASAP* is most economical for sensitivity analysis of large-scale models, as is the case for the two-layer isentropic model under consideration (the total model dimension is 3076 in spectral space and 13 828 in grid space).

Using the *ASAP*, the CPU for computing the sensitivities of the blocking index to vorticity sources placed in different locations is quite modest. Once the values of the adjoint variables $q_m, (m = 1, \ldots, M = 16)$ have been computed for this blocking index, the *ASAP* computation to any perturbations of the model dynamic fields takes only a few seconds of CPU time. In particular, the CPU time required to compute the sensitivities to perturbation at different grid points of the model variables [namely: $2 \times \mathrm{NLONS} \times \mathrm{NLATSH} = 4608$ computations using Eq. (V.F.25) or $2 \times \mathrm{NMDIM} = 1024$ computations using Eq. (V.F.31)] required only tens of seconds; such sensitivity analyses would be practically unfeasible by using the *FSAP* or brute-force recalculations.

CHAPTER VI

ADJOINT SENSITIVITY ANALYSIS PROCEDURE FOR OPERATIONAL METEOROLOGICAL APPLICATIONS

Adjoint sensitivity analyses in meteorological applications have been gaining in popularity since the pioneering work of Hall and Cacuci (1983) and Hall, Cacuci and Schlesinger (1982), which applied the basic sensitivity analysis theory for nonlinear systems (*ASAP*) provided by Cacuci (1981; see also Volume I). This chapter presents three additional illustrative examples of applying the *ASAP* to representative large-scale models used in operational numerical weather prediction. Thus, Section VI.A presents the illustrative sensitivity analysis results, first obtained by Li and Navon (1998), by applying the *ASAP* to the diagnostic equations underlying the nonlinear radiation model used in the National Center for Environmental Prediction (NCEP) model for medium-range weather forecasting. Section VI.B presents illustrative results of a sensitivity analysis of the localized model forecast error to the initial conditions, for a test case occurring during the Indian summer monsoon. These results were obtained by Zhu and Navon (1998) by applying the *ASAP* to the FSU Global Spectral Model (GSM), developed by Krishnamurti and Dignon (1988). Finally Section VI.C presents illustrative sensitivity analysis results obtained by Yang, Navon, Todling (1997) and Yang et al. (1999), who have applied the *ASAP* to develop the adjoint sensitivity model (Yang, Navon and Todling, 1997) corresponding to the moisture part of the physics module (namely, the Relaxed Arakawa Schubert (RAS) scheme) in the NASA Goddard Earth Observing System-1 (GEOS-1) general circulation model (GCM) developed by the Data Assimilation Office (DAO) at the National Aeronautics and Space Administration (NASA) Goddard Space Flight Center (GSFC). The response-functions considered in Section VI.C measure the strength of the convective cloud precipitation, and the cloud induced heating and drying, in both an instantaneous and a time-integrated sense.

VI. A. ADJOINT SENSITIVITY ANALYSIS PROCEDURE (ASAP) FOR THE EARTH'S RADIATION BUDGET IN THE NCEP MEDIUM-RANGE FORECASTING MODEL

This Section presents illustrative sensitivities of the Earth's radiation budget (ERB) to cloud cover water vapor, atmospheric temperature, and Earth's surface temperature, by applying the *ASAP* to the nonlinear radiation model used by the National Center for Environmental Prediction (NCEP) in their medium range weather forecasting system. Section VI.A.1 briefly describes the relevant

parameterizations in the NCEP radiation model, and presents the salient features (including verifications) of the corresponding adjoint sensitivity model. Section VI.B presents paradigm sensitivity analysis results for the clear sky and cloudy sky shortwave and long-wave radiation, as well as for the ERB.

VI.A.1. Derivation and Verification of the Adjoint Sensitivity Model Corresponding to the NCEP Nonlinear Radiation Model

The radiation codes considered in this Section were operationally used in the NCEP medium-range weather forecasting model [Kanamitsu et al., 1991]. The effects of the major radiatively active atmospheric constituents, including water vapor (H_2O), carbon dioxide (CO_2), ozone (F_{toa}), and clouds, are taken into account in the modeling of both shortwave (SW) and longwave (LW) processes. The model forecasts layer radiative heating rates, upward SW (F_{stoa}) and LW (F_{ltoa}) fluxes at top of the atmosphere, as well as downward LW and net SW fluxes at the earth's surface. The radiation is calculated with 28 vertical layers and the horizontal resolution of 2.8125 degrees.

The cloud parameterization is a diagnostic scheme based on Slingo (1987). The main difference between this parameterization and Slingo's scheme and its performance were detailed in Campana (1990, 1994). The SW radiation parameterization scheme is based on Lacis and Hansen (1974). A mean cosine of the solar zenith angle, $\bar{\mu}$, is employed to calculate the SW fluxes at each model grid point, and it is computed for each model latitude as in the following equation (Manabe and Strickler, 1964)

$$\bar{\mu} = \frac{\int_{daylight} \mu(t)dt}{\int_{daylight} dt} \quad , \qquad \text{(VI.A.1)}$$

where $\mu(t)$ is the cosine of the solar zenith angle at time t . The mean cosine of the solar zenith angle is a function of latitude. The longwave radiation model was developed by Fels and Schwarzkopf, and its details can be found in Fels and Schwarzkopf (1975), and Schwarzkopf and Fels (1985, 1991).

To apply the *ASAP*, the following five variables were selected in the NCEP radiation model to be perturbed: the atmospheric moisture q , temperature T , pressure p , surface temperature T_s , and cloud fractions C_i , $(i = 1,2,3)$, where $i = 1$ corresponds to high clouds, $i = 2$ corresponds to middle clouds, and $i = 3$ corresponds to low clouds. The amounts of O_3 and CO_2 were not perturbed in

the NCEP model, since these two variables were given climatological values with seasonal variations.

As described by Navon et al. (1992) and Zou (1997), the forward sensitivity model (i.e., linear tangent model), obtained by G-differentiation of the NCEP radiation model, can be written in the form

$$\delta F_{toa} = \sum_{i=1}^{3} \frac{\partial F_{toa}}{\partial C_i}\delta C_i + \frac{\partial F_{toa}}{\partial q}\delta q + \frac{\partial F_{toa}}{\partial T}\delta T + \frac{\partial F_{toa}}{\partial T_s}\delta T_s + \frac{\partial F_{toa}}{\partial p}\delta p\,, \qquad \text{(VI.A.2)}$$

where F_{toa} stands for either F_{stoa} or F_{ltoa}. Applying the *ASAP* to Eq. (VI.A.2) yields the following adjoint sensitivity model:

$$\delta F^*_{toa} = \sum_{i=1}^{3} \frac{\partial F^T_{toa}}{\partial C_i}\delta C^*_i + \frac{\partial F^T_{toa}}{\partial q}\delta q^* + \frac{\partial F^T_{toa}}{\partial T}\delta T^* + \frac{\partial F^T_{toa}}{\partial T_s}\delta T^*_s + \frac{\partial F^T_{toa}}{\partial p}\delta p^*\,, \quad \text{(VI.A.3)}$$

where the variables with the superscript * denote the corresponding adjoint variables.

For the sensitivity analyses to be presented in the sequel, the responses considered are of the form

$$R_s(C_i, q, T, T_s, p) = \sum_k \left(S^{\downarrow}_k - F_{stoa}\right)_k\,, \qquad \text{(VI.A.4)}$$

$$R_l(C_i, q, T, T_s, p) = \sum_k (F_{ltoa})_k\,, \qquad \text{(VI.A.5)}$$

where $S^{\downarrow}_k$ represents the downward day-averaged solar fluxes at the top of the atmosphere, R_l represents the total *outgoing long wave radiation* (OLR), R_s represents the total *absorbed shortwave radiation* (ASR) by the Atmospheric Environment Service (AES), Environment Canada's model ground surface temperature data, while k denotes all horizontal model grid points. The sensitivities of the above responses to the five variables mentioned in the foregoing are obtained from Eqs.(VI.A.2) through (VI.A.5) by using the chain rule and noting that $\partial R_s/\partial(F_{stoa})_k = -1$ and $\partial R_l/\partial(F_{ltoa})_k = 1$. The resulting expressions for these sensitivities can be written in the form

$$\left(\frac{\partial R_s}{\partial C_i}, \frac{\partial R_s}{\partial q}, \frac{\partial R_s}{\partial T}, \frac{\partial R_s}{\partial T_s}, \frac{\partial R_s}{\partial p}\right) =$$

$$-\left[\sum_{i=1}^{3} \left(\frac{\partial F_{stoa}}{\partial C_i}\right)^T I_{C_i} + \left(\frac{\partial F_{stoa}}{\partial q}\right)^T I_q + \left(\frac{\partial F_{stoa}}{\partial T}\right)^T I_T + \left(\frac{\partial F_{stoa}}{\partial T_s}\right)^T I_{T_s} + \left(\frac{\partial F_{stoa}}{\partial p}\right)^T I_p\,, \right. \qquad \text{(VI.A.6)}$$

and, respectively,

$$\left(\frac{\partial R_l}{\partial C_i}, \frac{\partial R_l}{\partial q}, \frac{\partial R_l}{\partial T}, \frac{\partial R_l}{\partial T_s}, \frac{\partial R_l}{\partial p}\right) =$$
$$-\left[\sum_{i=1}^{3} \left(\frac{\partial F_{\mathrm{ltoa}}}{\partial \mathrm{C_i}}\right)^T I_{\mathrm{C_i}} + \left(\frac{\partial F_{\mathrm{ltoa}}}{\partial q}\right)^T I_{\mathrm{q}} + \left(\frac{\partial F_{\mathrm{ltoa}}}{\partial T}\right)^T I_{\mathrm{T}} + \left(\frac{\partial F_{\mathrm{ltoa}}}{\partial T_s}\right)^T I_{T_s} + \left(\frac{\partial F_{\mathrm{ltoa}}}{\partial p}\right)^T I_{\mathrm{p}}\right], \tag{VI.A.7}$$

where $I(C_i, q, T, T_s, p)$ are column vectors of the form $(1,1,1,k,1)^T$.

The correctness of the adjoint sensitivity model can be verified in several ways. One way is to use the relationship

$$z^*\left(\delta F_{toa}\right) = z^T\left(\delta F_{toa}^*\right), \tag{VI.A.8}$$

which holds (to computer accuracy) for any $z=(\delta C_i, \delta q, \delta T, \delta T_s, \delta p)^T$ and $z^*=(\delta C_i{}^*, \delta q^*, \delta T^*, \delta T_s{}^*, \delta p^*)^T$, where δF_{toa} and δF_{toa}^* are computed from Eqs. (VI.A.2) and (VI.A.3), respectively. The nonlinear effects of parameter variations on the responses can be assessed by comparing the values of δF_{toa} obtained from Eq. (VI.A.2) with the quantity ΔF_{toa}, defined as

$$\Delta F_{\mathrm{toa}} = F_{toa}(C_i + \delta C_i, q + \delta q, T + \delta T, T_s + \delta T_s, p + \delta p) - F_{toa}(C_i, q, T, T_s, p) \tag{VI.A.9}$$

which is computed by recalculations using perturbed parameter values. In addition, the nonlinear effects of parameter variations can also be assessed by using the so-called gradient test (see, e.g., Navon et al., 1992; Li et al., 1993), in which one computes the quantity t, defined as

$$t \equiv \frac{R\left(C_i + \delta C_i, q + \delta q, T + \delta T, T_s + \delta T_s, p + \delta p\right) - R\left(C_i, q, T, T_s, p\right)}{\nabla R\left(C_i, q, T, T_s, p\right)} \tag{VI.A.10}$$

where $\nabla R(C_i, q, T, T_{s,} p)$ is evaluated from (VI.A.6) and (VI.A.7). The quantity t measures both the accuracy of the forward sensitivity model and the effect of nonlinearities. In particular, if t tends to 1 (at computer accuracy) as z tends to zero, it can be concluded that the forward sensitivity model, given by Eq. (VI.A.2), is consistent with the nonlinear model, and the adjoint sensitivity model has also been implemented correctly.

Table VI.A.1 presents illustrative results for computed correlations between δF_{toa} and ΔF_{toa}, as well as results for the gradient test t. The nominal state of the NCEP model, taken at 00GMT on 29 June 1989, was perturbed by removing part of the largest spatial scale components for wind components, temperature, pressure and the surface temperature. The sizes of the respective perturbations are controlled by multiplying perturbations by a given constant a (where a ranges between 10^{-1} and 10^{-9}, as shown in Table VI.A.1). Perturbed moisture and cloud fractions are obtained by simply multiplying the corresponding nominal states by $3a$ (rather than a), since $3a$ is needed to account for large variabilities of moisture and cloud cover. The sizes of perturbations tend to zero when $a \to 0$. Table VI.A.1 indicates that $t \to 1$ as the computer accuracy is reached for $a = 10^{-7}$; this result verifies the consistency between the linear and nonlinear models and the correctness of the adjoint.

Table VI.A.1
Gradient test and correlation coefficients between the nonlinear and linear solutions (the size of atmospheric and surface perturbations is proportional to a)

	Gradient test t		Correlation coefficients	
a	shortwave	longwave	shortwave F_{stoa}	longwave F_{ltoa}
10^{-1}	0.998111620665	0.537319071595	0.999803252808	0.891854024493
10^{-2}	1.000121232373	0.987566689942	0.999984396298	0.987636759208
10^{-3}	1.000083505989	0.996395394981	0.999995154225	0.999135310713
10^{-4}	1.000000034075	0.999999408383	0.999999999999	0.999999999998
10^{-8}	0.999994658625	0.999999991261	0.999999999994	0.999999999999
10^{-9}	0.999996809749	0.999995380071	0.999999999474	0.999999999971

The results shown in Table VI.A.1 also indicate that the nonlinear effects are weak for a considerable range of perturbation sizes. For example, when $a = 0.1$, the perturbations are, respectively: $4\,K$ for temperature, $5\,m/s$ for wind speed, $10\,hPa$ for pressure, $4\ g/kg$ for moisture mixed ratios, and 0.2 for cloud fraction. The linearization approximation inherent to Eq. (VI.A.2) is valid with a

high degree of accuracy for SW radiation, while the accuracy is lower, but still within a tolerable range, for LW radiation, as indicated by a correlation coefficient as high as 0.89. This suggests that the linearization is valid even for values of a as large as 0.1. Similar computations, with similar results and conclusions, have also been carried out for different nominal states, representative of different months and seasons.

Note that the above conclusions are true only when the discontinuities (in both functions and the first order derivatives) in the original radiation models are properly handled, since discontinuities associated with table look-ups and cloud calculations may invalidate the linearization; the validity is restored when these discontinuities are replaced with cubic spline interpolations or Fourier sine/ cosine expansions.

VI.A.2. Illustrative Sensitivity Analysis Results

Two nominal states of the NCEP model were used for the sensitivity analysis results to be presented in this section, namely: 00GMT, June 19-29 and December 19-29, 1989, which are representative of the northern summer and winter seasons, respectively. Computations were performed for both clear and cloudy skies. In cloud radiative forcing computations, clear and cloudy skies were defined with a slight difference (Cess and Potter, 1987, Zhang et al., 1994). The definition of clear sky has been taken as used in so-called "method II" (Cess and Potter, 1987), where the clear sky atmosphere retains the states unchanged while the clouds are set zero.

In addition to the response functions defined in Eqs. (VI.A.4) and (VI.A.5), another response function is defined as

$$R_{net} = R_s - R_l \,. \qquad \text{(VI.A.11)}$$

Note that R_{net} is representative of the total net ERB. The following sub-sections present illustrative time-averaged (daily) sensitivities of atmospheric moisture, temperature, clouds, and surface temperature.

VI.A.2.a Clear Sky Shortwave Radiation Sensitivities

Shortwave (SW) radiation can be absorbed by water vapor (Lacis and Hansen, 1974). An increase in water vapor will cause an increase in ASR. Figure VI.A.1 presents the zonally averaged sensitivity of moisture. A remarkable feature is that ASR is most sensitive to water vapor mixing ratios at high latitudes in the summertime hemisphere, while the tropics region is insensitive to these ratios. These latitude dependent features are linked to the surface albedo. Water vapor

may have a larger absorption ratio and cause larger atmospheric heating rates at the tropics due to stronger incident solar radiation. Since the tropical surface is characterized by oceans with large darkness (near black bodies), the incident radiation is almost fully absorbed by the atmosphere and surface system irrespective of the absorption by water vapor. Thus the absorption by water vapor has little effect on ASR. In contrast, the surface at high latitudes is characterized by snow or ice cover with large brightness, the absorption by water vapor being nearly equal to the net increase in ASR.

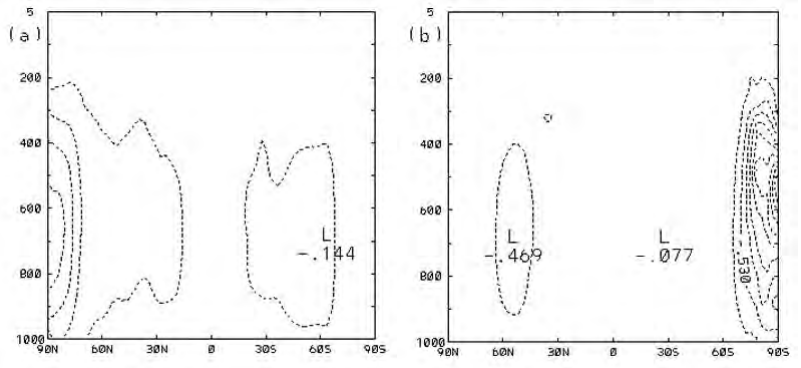

Figure VI.A.1. Zonally averaged sensitivities of the ASR by the atmosphere and earth's surface to water vapor mixing ratios ($g.kg^{-1}$) for 19-29 June 1989 (a) and 19-29 December 1989 (b). The contour interval is 0.2 $Wm^{-2}g^{-1}kg$ in (a) and 0.3 in (b). Note that panel (a) is for 19-29 June 1989 and panel (b) is for 19-29 December 1989 in all of the following figures.

The sensitivity structure at 600 *hPa* (Fig. VI.A.2), which corresponds to the maximum absorption height, illustrates the predominant linkage to the surface albedo, i.e., a larger sensitivity is found over the summer polar areas and lands with larger albedo. Note also that the sensitivity structures are rather symmetric about the equator between the northern and southern summertime, though the sensitivity at high latitudes in the southern summer hemisphere is stronger than that in the northern summer hemisphere.

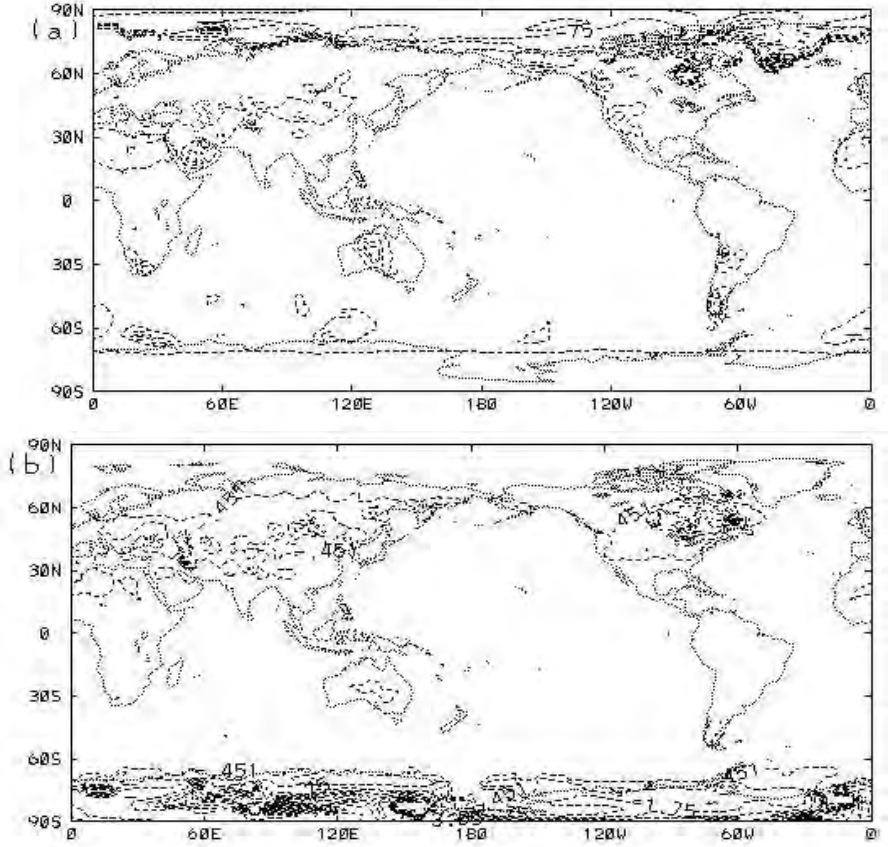

Figure VI.A.2. Same information as in Fig. VI.A.1, but for sensitivities of the ASR to water vapor mixing ratios at 560 hPa . The contour interval is 0.2 $Wm^{-2}g^{-1}kg$ in (a) and 0.4 $Wm^{-2}g^{-1}kg$ in (b). The stippled region is under the surface.

VI.A.2.b Clear Sky Longwave Radiation Sensitivities

The vertical structure of the atmospheric temperature strongly affects OLR variations since OLR depends strongly on the AES temperature, and on the amount and spatial distribution of water vapor.

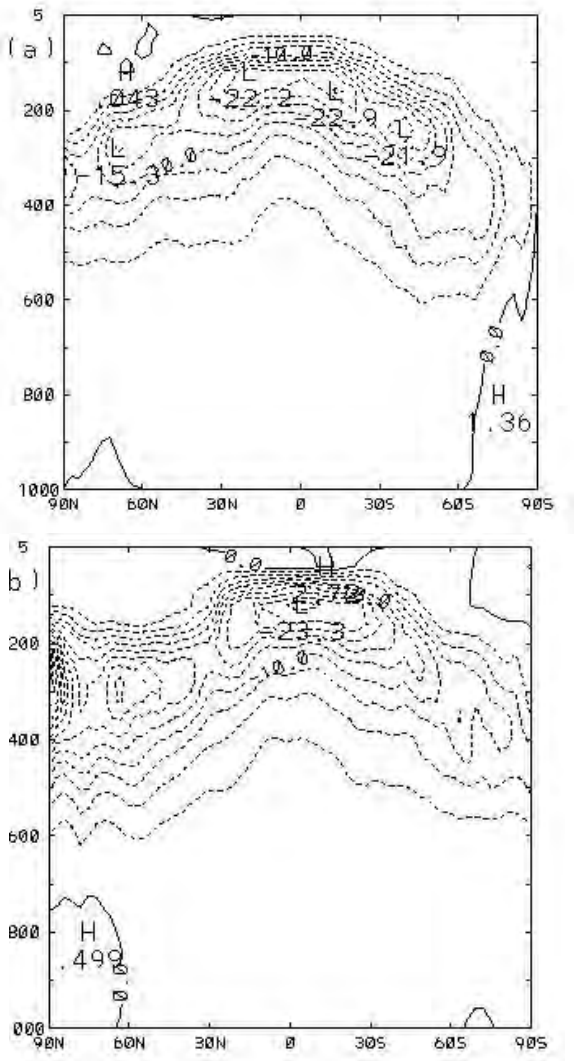

Figure VI.A.3. The zonally averaged sensitivities of the OLR at the top of the atmosphere to water vapor mixing ratios. The contour interval is 2.5 $Wm^{-2}g^{-1}kg$. Dashed lines denote negative values.

Figure VI.A.3, above, illustrates the zonally averaged sensitivity structure of the moisture for OLR. A striking feature is the larger sensitivity found near the tropopause, with a maximum of 22 $Wm^{-2}g^{-1}kg$. The middle and lower troposphere have a magnitude of less than 2.5 $Wm^{-2}g^{-1}kg$. On the whole, OLR is one order of magnitude more sensitive to the mixing ratio in the upper

troposphere than in the middle and lower troposphere. The high sensitivity of OLR to the water vapor in the upper troposphere has been noted in observational studies. Kiehl and Briegleb (1992) clearly indicated that the differences in upper tropospheric moisture were the major cause for the OLR difference during a two year observation period in most regions over the tropical oceans. This result may help understanding the super greenhouse effect over tropical oceans, which will be discussed in the following section.

The meridional features depicted in Fig. VI.A.3 indicate that, in the middle and lower troposphere, sensitivities have a small positive value at the high latitudes, while the positive value is slightly larger in the winter hemisphere than in the summer hemisphere. Near the tropopause, sensitivities are relatively large between the subtropics of the summer hemisphere and the middle latitude of the winter hemisphere. The existence of two weak sensitivity regions at the latitudes of around 30° N in the northern winter and 45° N in the northern summer are of interest since these two regions are linked to activities of polar fronts (Palmén and Newton, 1967).

Qualitatively, the above results may be understood by considering the radiation transfer equation. We may write the perturbed radiation transfer equation in the form (Stephens, 1984):

$$F'_{ltoa} = -\int_0^{\infty}\int_0^{\infty} \tau'_v(z,h)\frac{dB_v(h)}{dh}\,dh\,dv \qquad \text{(VI.A.12)}$$

where v is wavenumber, B_v represents the Planck function, F'_{ltoa} represents the perturbed OLR flux associated with water vapor perturbations, and $\tau'_v(z,h)$ represents the perturbed transmission function between levels h and z; note that B_v is a function of the temperature T, which implies that $dB_v(h)/dh$ depends on temperature lapse rates. A large temperature lapse rate leads to a large magnitude of perturbed OLR. The inversion enhances OLR, which is the leading cause to positive values of sensitivities at high latitudes.

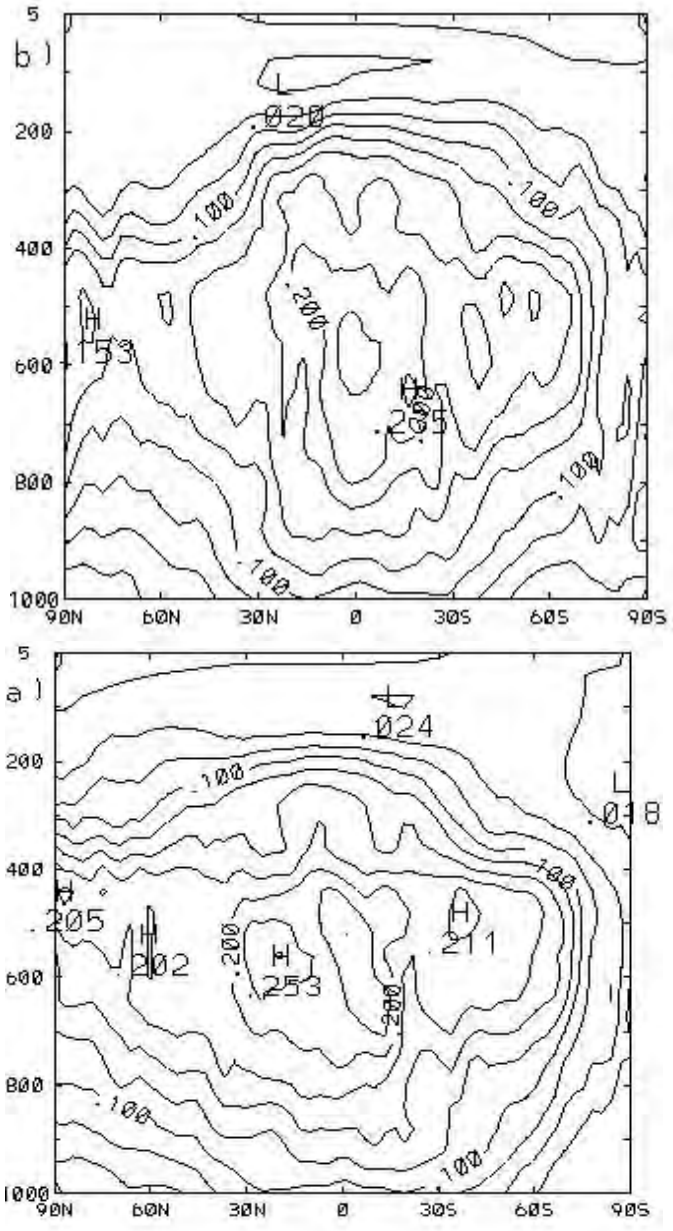

Figure VI.A.4. Same as Fig. VI.A.3, but for atmospheric temperature. The contour interval is 0.025 $Wm^{-2}g^{-1}kg$.

The sensitivity of atmospheric temperature depicted above in Fig. VI.A.4 displays a strong spatial variation. In the vertical direction, the largest sensitivities are located between 600 and 500 hPa, and the globally averaged sensitivity at 600 hPa is approximately 0.2 $Wm^{-2}g^{-1}kg$. The sensitivities rapidly decrease above and below the largest sensitivity regions. The sensitivity between 600 and 500 hPa is one order of magnitude larger than that near the tropopause, and three times stronger than that near the surface. The latitudinal variation shows that the sensitivities are largest over tropical areas, and decrease toward the poles. Unlike water vapor, the sensitivity structure of the atmospheric temperature does not present a significant difference between the northern summer and southern summer. It is worth noting that a $1\,K$ temperature perturbation in the middle troposphere produces an OLR increase equivalent to that produced by a 0.1 g/kg water vapor perturbation in the middle and lower troposphere or by a perturbation of about $0.15\,K$ in the surface temperatures (see also the following discussion). Thus, temperature perturbations in the middle troposphere have a significant effect on OLR variabilities.

Figure VI.A.5, below, shows the sensitivity structures of the surface temperature. A positive surface temperature perturbation leads to an increase in the emission of LW radiation, and thus an increase in OLR when feedbacks are not taken into account. Note that an increase in sea surface temperatures may lead to a decrease in OLR when the feedback of water vapor is involved, as discussed by Inamdar and Ramanathan (1994). The globally averaged sensitivity is $1.4\,Wm^{-2}g^{-1}kg$. As expected, the tropical areas display the smallest sensitivities due to the strong greenhouse trapping by an abundant water vapor. On the average, the tropical sensitivities are about half as large as those in the middle and high latitude. The sensitivities tend to increase from the tropics to the polar regions. The northeastern regions of the Pacific and Atlantic oceans, which are associated with the upward motion in the front of the semi-permanent troughs over the central oceans, are relatively insensitive (Palmén and Newton, 1967).

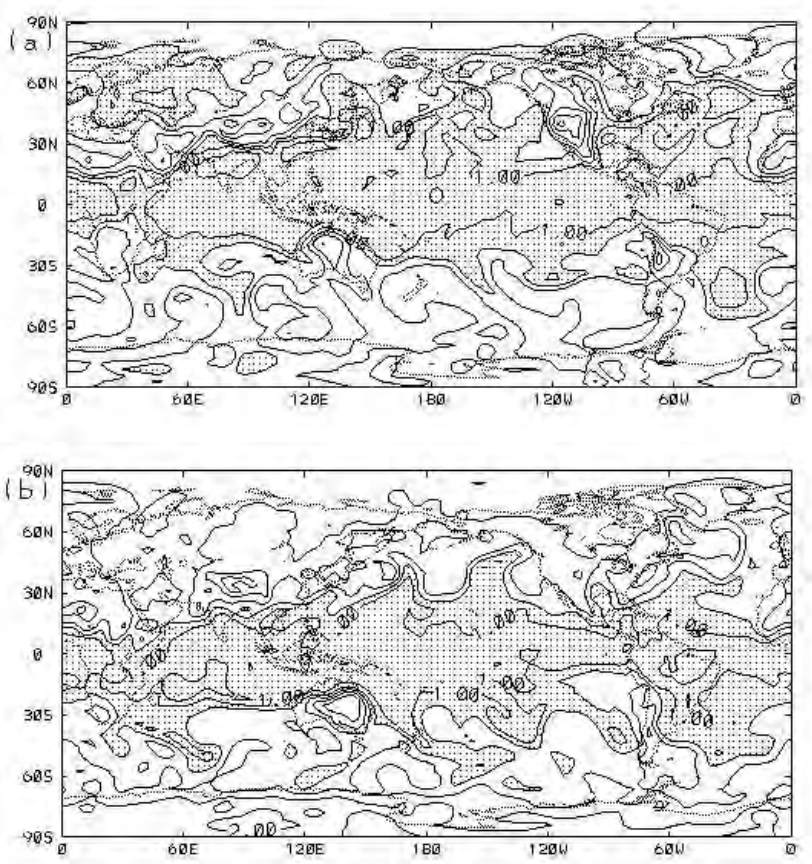

Figure VI.A.5. Sensitivities of the OLR to the earth's surface temperature. The contour interval is $0.25\,Wm^{-2}g^{-1}kg$. Stippled regions denote sensitivities smaller than $1.2\,Wm^{-2}g^{-1}kg$.

To describe the greenhouse trapping, we analyzed the sensitivity of the surface LW emission. The gradient, $\nabla_{se}R_l$, of the OLR response with respect to the surface emission is not a direct output of the adjoint sensitivity model, but can be obtained from $\nabla_{T_s}R_l$, using the relationship

$$\nabla_{se}R_1 = \frac{\nabla_{T_s}R_l}{4\ \sigma T_s^3},\quad \nabla_{se}R_l = \frac{\nabla_{T_s}R_l}{4\sigma T_s^3} \tag{VI.A.13}$$

where $\nabla_{T_s}R_l$ is the gradient of the OLR with respect to the surface temperatures

T_s, and σ denotes the Stefan-Boltzmann constant. Note that $\nabla_{se} R_l$ varies between 0 and 1, and actually represents the fractional perturbed OLR. An increased perturbation emission at the surface is completely trapped by the column atmosphere when the gradient is 0, and escapes completely through the top of the atmosphere when the gradient is 1.

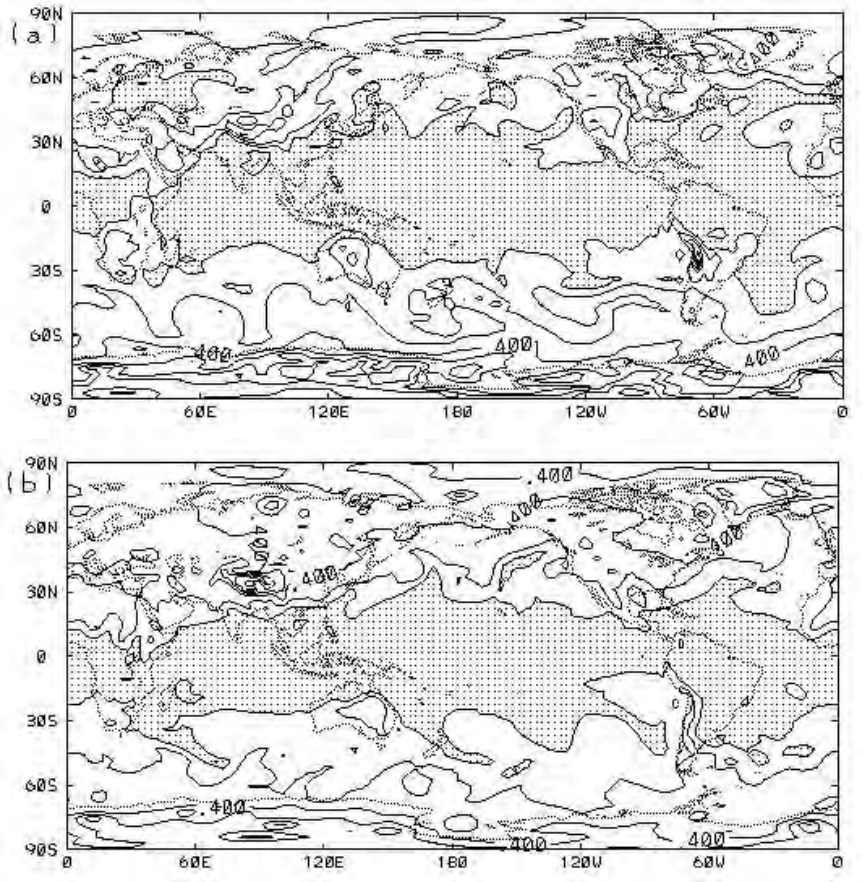

Figure VI.A.6. Sensitivities of the OLR to the earth's surface perturbation emission. These sensitivities are the ratios between an increase in the earth's surface emission and the corresponding increase in OLR. The contour interval is 0.05. Stippled regions denote ratios larger than 0.2, or indicate that atmospheric columns trap more than 80% of a perturbation increase in the earth's surface emission.

Figure VI.A.6, above, illustrates the structure of $\nabla_{se} R_l$. Note that less than 20% of an increased perturbation emission at the surface escapes through the top of the atmosphere over the tropical areas. In other words, the column tropical atmosphere traps more than 80% of a perturbation increase in the emission at the surface. The magnitude of $\nabla_{se} R_l$ at mid-latitudes is in general larger than 30%, increasing to over 40% at high latitudes. Previous studies (e.g., Raval and Ramanathan, 1989) have shown that the moistening effect of deep convection activity strongly enhances the atmospheric greenhouse effect. The computations presented in the foregoing have also confirmed that the regions with a greenhouse trapping larger than 80% significantly correlate with deep convection activities. Additional analysis (not discussed here) has shown that this conclusion also holds for the region within the inner Eurasian continent in northern summer. It is also of interest to note that the deep upward motion in the front of the semi-permanent troughs over the middle Pacific and Atlantic oceans in the wintertime may play a role similar to deep convective activities, and the greenhouse trapping is about 70-80% over these areas.

VI.A.2.c Cloudy Sky Shortwave Radiation Sensitivities

An accurate modeling of the interaction between radiation and clouds is very difficult. In atmospheric general circulations models, for example, the representation of this interaction has improved considerably in recent years, but substantial deficiencies are still present, as indicated by model comparisons (Cess et al., 1996). This interaction comprises two feedback processes, since clouds affect radiation by absorption and reflection, while radiation, in turn, affects clouds through changing the structure of the atmosphere by heating and cooling. The former feedback is generally considered easy to model; nevertheless, its modeling is still unsatisfactory (Baer et al., 1996; Ellingson et al., 1991).

The sensitivity analysis results presented in this sub-section illustrate the effects of variations in cloud fraction on the ASR and OLR. Thus, Figure VI.A.7, below, presents the zonally averaged sensitivity structure of clouds for SW radiation. The cloud reflection effect on SW radiation is illustrated by the negative sensitivity. The sensitivity has a tendency to increase proportionally with the incident solar radiation, but there are important features that result from atmospheric variations. The ASR is most sensitive to low clouds; this result may stem primarily from the larger reflectivity assigned to the lower clouds. On the contrary, the high latitudes in both the wintertime and summertime hemispheres are extremely insensitive to low clouds. This lack of sensitivity is due to the high albedo of the surface in these regions; an increase in cloud fraction has little additional reflective effect on ASR over snow and ice at high latitudes.

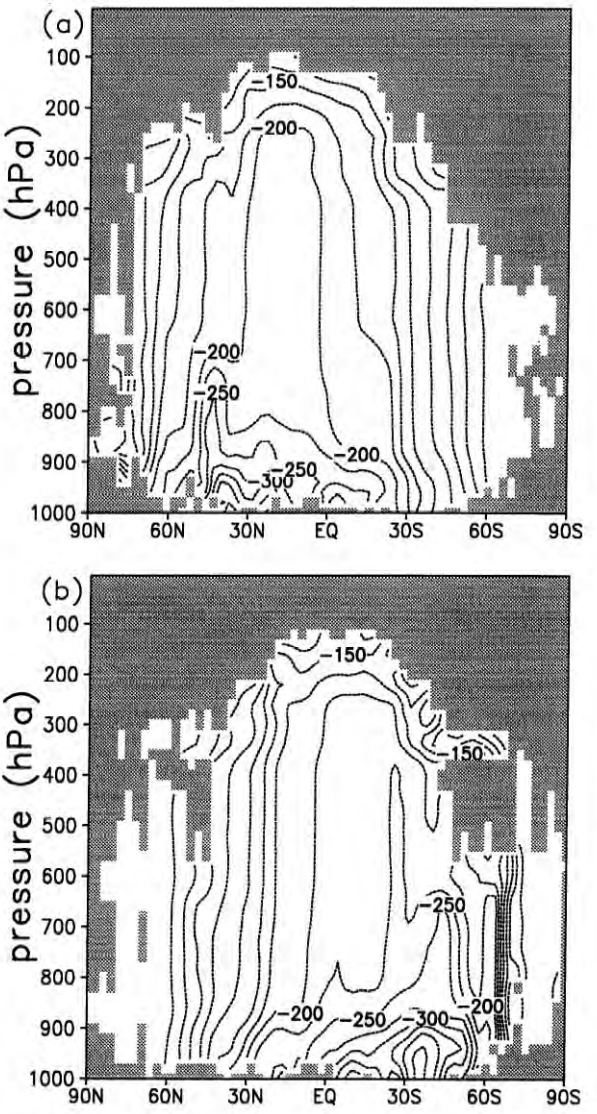

Figure VI.A.7. Zonally averaged sensitivities of the ASR. The contour interval is $50\,Wm^{-2}$ per cloud fraction, i.e., equivalent to an increase of $5\,Wm^{-2}$ in the ASR due to a 0.1 cloud fraction increase. Regions without presence of clouds in the basic states are stippled, where sensitivities are not calculated.

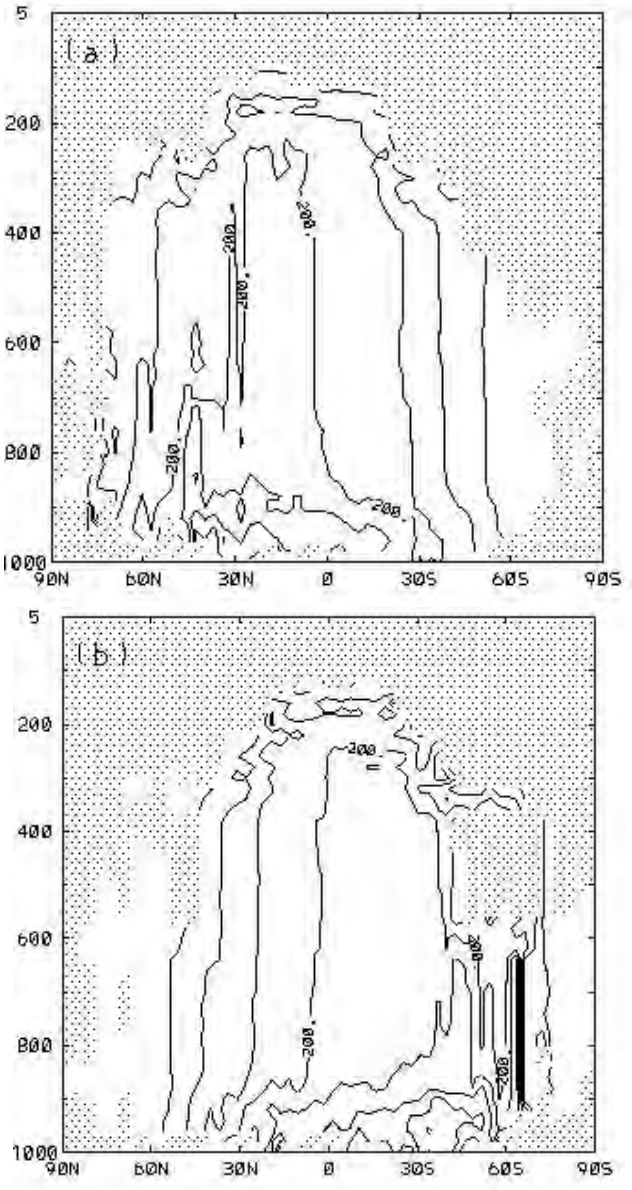

Figure VI.A.8. Zonally averaged sensitivities of the ASR to three types of clouds (high, middle, and low). Thick solid curves are for high clouds, dotted curves for middle clouds, and thin solid curves for low clouds, respectively. The unit is Wm^{-2} per cloud fraction.

Figure VI.A.8, above, depicts the latitudinal variations of sensitivity of the three types of clouds (high, middle, and low) defined in the NCEP model. In the wintertime hemispheres, the sensitivity to the three types of clouds consistently increases from zero, at high latitudes, to about $20\,Wm^{-2}$, for a 0.1 cloud fraction increase at the equator; the lower cloud has slightly larger sensitivity. While the high clouds are most sensitive at latitudes consistent with the location of the largest incident solar radiation, the lower clouds tend to have the largest sensitivity at mid-latitudes in the summertime hemisphere. Consequently, the difference between the high and lower clouds reaches its maximum in the summer middle latitudes; at these latitudes, the lower cloud sensitivity is on the average about $30\,Wm^{-2}$ per 0.1 cloud fraction. This sensitivity is twice as large as that of the high clouds, which is about $15\,Wm^{-2}$ per 0.1 cloud fraction.

VI.A.2.d Cloudy Sky Long-wave Radiation Sensitivities

Figure VI.A.9 shows the zonally averaged sensitivity structure of clouds for LW radiation. The effects of clouds on OLR are similar to the effects of water vapor, and are intimately related to temperature lapse rates. The largest sensitivity is located near the tropopause and at the tropics with a shift of about 10^0 to the summertime hemispheres. Associated with the inversion at the polar latitude, the sensitivity has a small positive value. The rates of vertical decrease in the sensitivities are largest between 900 and 700 hPa. Such features indicate that the OLR is more sensitive to the high and middle clouds than to lower clouds. Figure VI.A.10 further illustrates this feature by depicting the sensitivity variation of the three types of the clouds with latitude. The sensitivity to high and low clouds displays a consistent meridional variation, whereas the lower cloud presents a significantly smaller sensitivity, except for high latitudes. At the tropics, the sensitivities of the middle and high clouds are, on the average, approximately 11 Wm^{-2} per 0.1 cloud fraction, a value which is twice as large as that of the lower cloud. At high latitudes, the sensitivity of all the three types of clouds becomes smaller, even attaining smaller positive values at polar latitudes. Such a feature was also observed by Yamanouchi and Charlock (1995).

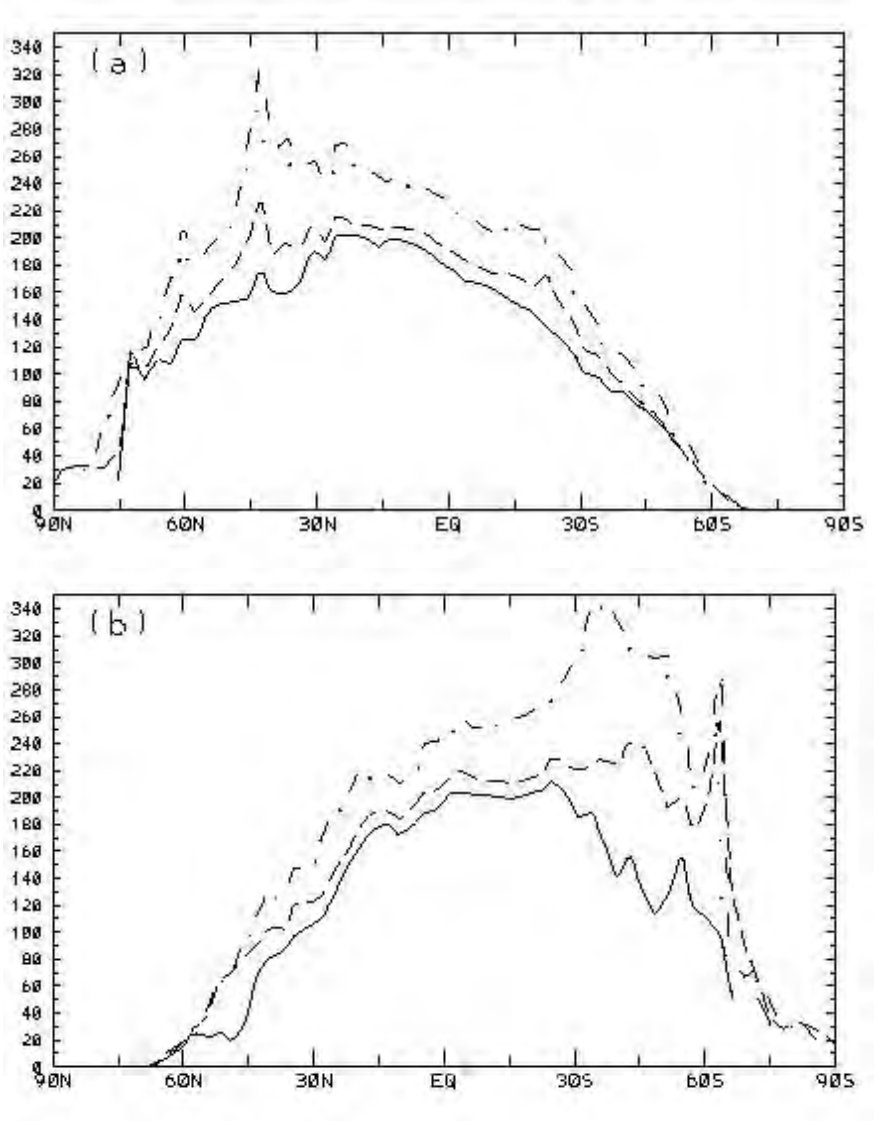

Figure VI.A.9. Same as in Fig. VI.A.7, but for the OLR and with a contour interval of 25 Wm^{-2}.

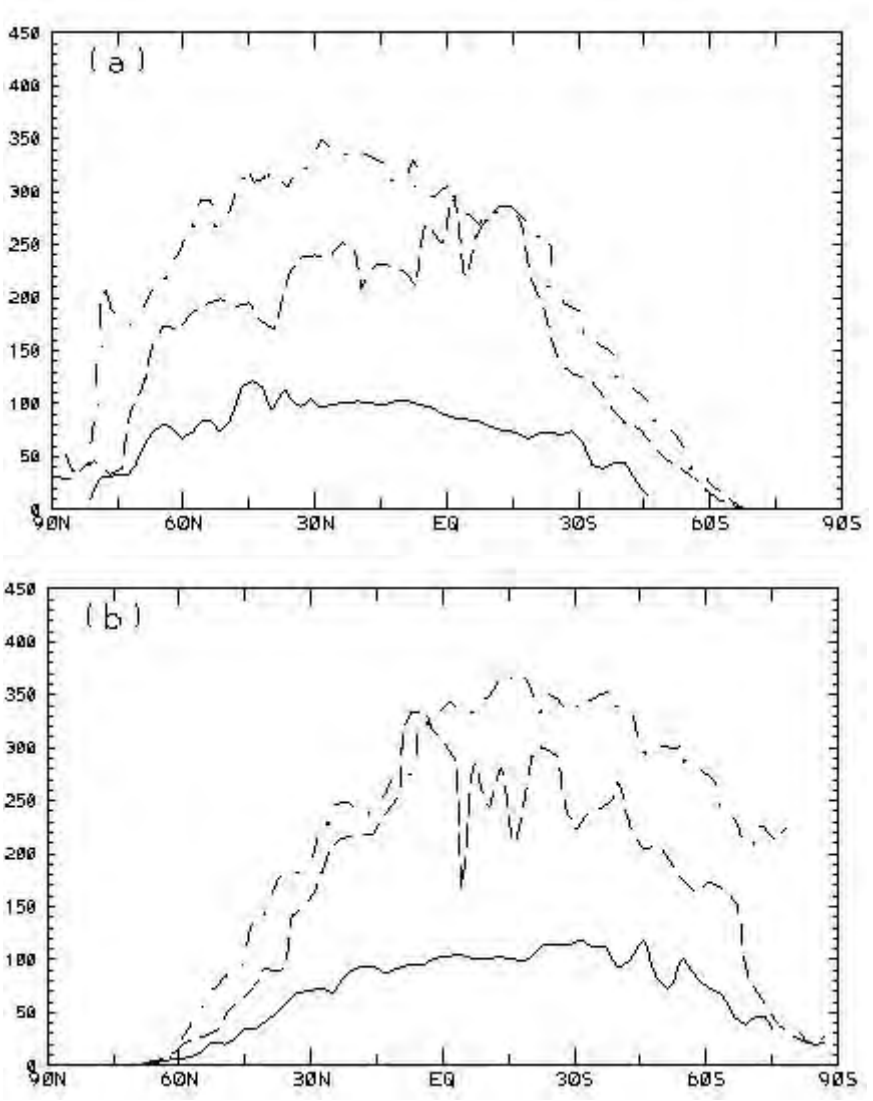

Figure VI.A.10. Same as in Fig. VI.A.8, but for the OLR.

VI.A.2.e Cloudy Sky Net Earth's Radiation Budget Sensitivity

The sensitivity of clouds to the net ERB is closely related to the cloud radiative forcing. Figure VI.A.11 illustrates the zonally averaged sensitivity structure. There are two striking features: a cancellation occurring between the LW greenhouse effect and the SW reflection for middle and high clouds at lower latitudes, and a strong negative sensitivity of the lower cloud at the summer mid-latitudes. These two features become apparent by comparing the sensitivity structures of SW and LW radiation depicted in Figures VI.A.7 and VI.A.9, respectively. The middle and high clouds at lower latitudes strongly trap the LW radiation, and simultaneously strongly reflect the SW radiation. Thus, a large cancellation occurs in the middle and high cloud areas at lower latitudes. The low clouds cause a smaller LW trapping, but a larger SW reflection. Such an opposite tendency creates a larger positive sensitivity to low clouds. Note also the importance of low clouds at the summer mid-latitudes, i.e., where the net ERB displays the strongest sensitivities to low clouds. This latitudinal dependence is consistent with observed results which indicate that the net cloud cooling effect on the earth is larger over the middle and high latitude oceans (e.g., Ramanathan et al., 1989). Such features are also depicted in Fig. VI.A.12, which presents sensitivity variations of the three types of the clouds with latitude. The lower clouds, especially at mid-latitudes, may play a role in the earth's radiation budget variations.

The main results illustrated by the sensitivity analysis of the radiation model in the NCEP medium-range weather forecasting system can be summarized as follows:

(a) For a clear sky, the absorbed shortwave radiation (ASR) is much more sensitive to the water vapor in the middle troposphere at high latitudes in the summertime hemisphere than at the tropical and subtropical areas. The outgoing long wave radiation (OLR) is one order of magnitude more sensitive to water vapor mixing ratios in the upper troposphere than to that in the middle and lower troposphere. In the tropics, more than 80% of a perturbation increase in the earth's surface emission is trapped by the clear sky column atmosphere, while only about 60% to 70% is trapped at middle and high latitudes. Rapidly decreasing latitude bands of trapping are found within the subtropics, and the semi-permanent troughs over the central oceans display a significant effect.

(b) For a cloudy sky, the ASR is more sensitive to low clouds than to middle and high clouds. The most sensitive lower clouds tend to be located at mid-latitudes rather than in the tropical regions. The OLR, as expected, is most sensitive to high clouds, and displays similar sensitivity to middle clouds.

(c) The net ERB is most sensitive to lower clouds at mid-latitudes in the summer hemisphere.

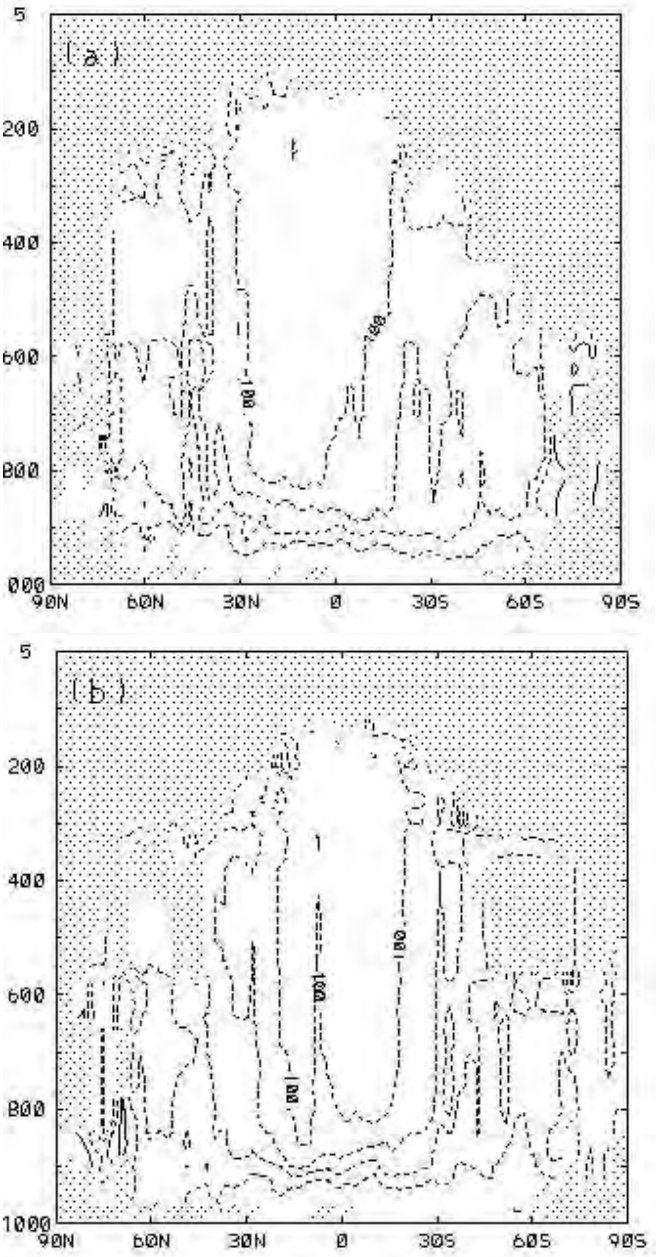

Figure VI.A.11. Same as Fig. VI.A.8, but for the zonally averaged sensitivities of the net earth's radiation budget to clouds. The negative values indicate a net decrease in the net earth's radiation with cloud increase.

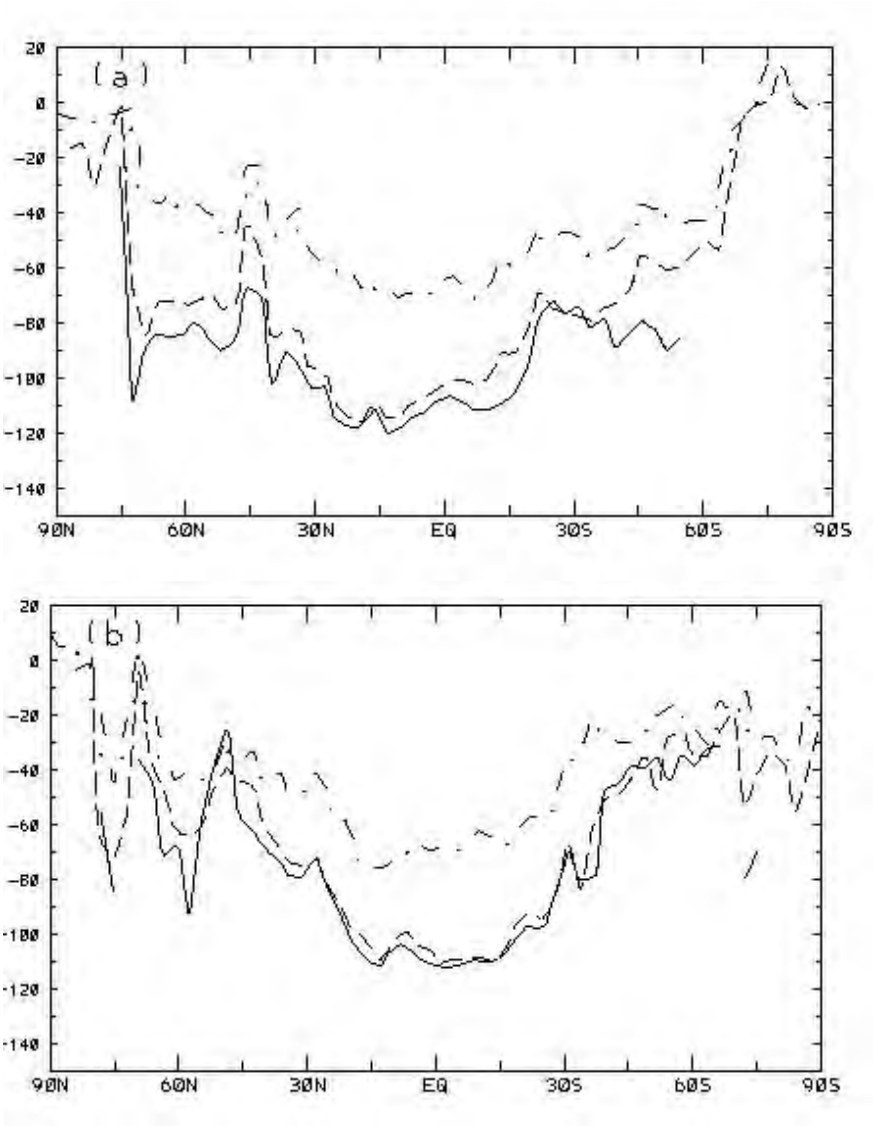

Figure VI.A.12. Same as in Fig. VI.A.9, but for the sensitivity of the net earth's radiation budget to three types of clouds (high, middle, and low).

VI. B. FSU-GSM FORECAST ERROR SENSITIVITY TO INITIAL CONDITIONS: APPLICATION TO INDIAN SUMMER MONSOON

The modern use of adjoint operators in sensitivity studies was initiated by the early work of Cacuci (1981a, b), who introduced a general sensitivity theory for nonlinear systems, generally referred to as the Adjoint Sensitivity Analysis Procedure (*ASAP*). Hall, Cacuci, and Schlesinger (1982) applied the *ASAP* to perform an exhaustive sensitivity analysis of a climate radiative-convective model of the atmosphere. An in-depth review of the entire range of applications of sensitivity theory has been presented by Cacuci (1988).

Since the numerical weather prediction model forecasts are generally sensitive to the small but inevitable errors in the initial conditions, the errors might amplify rapidly in model computations, leading to large forecast errors. An important application of the adjoint sensitivity model is to identify the geographical regions that are responsible for originating large forecast errors. Errico and Vukicevic (1992) indicated that the adjoint fields quantify the previous conditions that most affect a specified forecast aspect. Rabier et al. (1992) used the adjoint sensitivity model of a global primitive equation model to investigate the following question: to which aspects of the initial conditions is cyclogenesis most sensitive to, in a simple idealized situation? Morss et al. (1998) examined adaptive observation strategies using a multilevel quasi-geostrophic channel model and a realistic data assimilation scheme. Pu et al. (1998) applied the quasi-inverse linear and adjoint methods to targeted observations during FASTEX. Both of these works indicated that the adjoint method was useful in determining the optimal locations for introducing adaptive observations.

This Section presents a sensitivity analysis, using the *ASAP*, of the 1-day forecast error over a localized region of interest with respect to the initial conditions for the nominal-conditions extant on June 8, 1988, when the Indian summer monsoon entered its active stage. Thus, Section VI.B.1 presents the salient features of simulating the nominal conditions on Florida State University (FSU) Global Spectral Model (GSM). Section VI.B.2 presents the gradients of the 1-day forecast error with respect to the initial conditions of the model state variables (these gradients are called sensitivity patterns). These sensitivity patterns are then used as a diagnostic tool to identify regions, characterized by large uncertainties, which are responsible for originating large forecast errors. This way, the sensitivity patterns (to initial conditions) indeed indicate the locations where the placement of adaptive observations is most needed. The subsequent reduction of the forecast errors can then be accomplished by adding observations in the areas of large uncertainty (Lorenz and Emanuel, 1998), as identified by the sensitivities to initial conditions obtained via the *ASAP*.

VI.B.1. Modeling the Nominal Conditions on June 8, 1988 with the FSU GSM

The model used in this study is a version of the Florida State University (FSU) Global Spectral Model (GSM) developed by Krishnamurti et al. (1988); this version employs 12 levels in the vertical resolution, and a triangular truncation limiting the horizontal resolution to a total wavenumber of 42. The full physical processes were active in both the forecast model and the adjoint sensitivity model (Zhu et al., 1997), including planetary boundary layer processes, vertical diffusion, dry adjustment, large-scale condensation and evaporation, deep cumulus condensation, horizontal diffusion, and radiation processes.

In the FSU GSM, the components of the model's state vector, X, are vorticity, divergence, virtual temperature, logarithm of the surface pressure, and the dewpoint depression. The time evolution of the model's state vector X simulates the time evolution of the atmosphere, and is governed by the equation

$$\frac{dX}{dt} = F(X) \tag{VI.B.1}$$

where the nonlinear operator $F(X)$ represents all of the physical processes active during the time period under consideration. The discretized tangent linear model (i.e., discretized forward sensitivity model) corresponding to Eq. (VI.B.1) can be written in the form of the evolution equation

$$\delta X(t_1) = P(t_1, t_0)\delta X(t_0), \tag{VI.B.2}$$

where $\delta X(t)$ denotes the vector of perturbation variable, and t_0 and t_1 denote the initial time and verification time, respectively. The adjoint of the tangent linear model (i.e., the adjoint sensitivity model) can be written in the form of a "backward evolution equation," as

$$\delta X^*(t_0) = P(t_1, t_0)^T \delta X^*(t_1), \tag{VI.B.3}$$

where $\delta X^*(t)$ denotes the vector of adjoint variable, and $P(t_1, t_0)^T$ is the adjoint of the operator $P(t_1, t_0)$. As shown in Rabier (1992), the gradient of a forecast aspect (i.e., response), $J[X(t)]$, evaluated at $t = t_1$, with respect to $X(t_0)$ can be computed by means of

$$\nabla_{X(t_0)} J = P^T(t_0, t_1)\nabla_{X(t_1)} J \tag{VI.B.4}$$

where the operator $\nabla_{X(t_0)} J(X)$ denotes the gradient of $J[X(t)]$ in the direction $X(t)$, evaluated at $t = t_0$. The gradients of the 1-day forecast error with respect to the initial conditions are called *sensitivity patterns*.

A small perturbation or a small analysis error, $\delta X(t)$, in the initial conditions $X(t_0)$ will cause a forecast error $\delta J[X(t)]$ in the forecast $J[X(t)]$: this aspect, forecast error can be computed by means of the relation $\delta J = <\nabla_{X(t_0)} J, \delta X(t_0)>$. Hence, in geographical areas with a large (small) value of the gradient $\nabla_{X(t_0)} J(X)$, a change in the initial conditions will cause a large (small) impact upon the forecast error $\delta J[X(t)]$ in the $\delta X(t_0)$ direction.

To compute the sensitivity patterns (i.e., sensitivity of 1-day forecast error), integrated from 12UTC on June 7, 1988, over the Indian Monsoon region, with respect to the initial conditions from ECMWF analysis data, the forecast aspect was defined as the square norm of the differences between the model 1-day forecasts and the verifying analysis over the Indian Monsoon region. The Indian Monsoon region of interest is defined to be the area between $60\,E$ and $100E$ in longitude, equator, and $30\,N$ in latitude. A projection operator (masking operator) was applied to obtain the localized model forecast error over this limited region of interest. On June 8, 1988, the Indian summer monsoon entered its active stage. A cross-equatorial flow set in, both the Arabian Sea and the Bay of Bengal branches were established, with depressions over the east central Arabian Sea and over the northern Bay of Bengal. Figures VI.B.1 and VI.B.2 display the geopotential height fields at 500 *hPa* at 12UTC on June 7 and June 8, 1988 and the model 1-day forecast, respectively. Note that the depression over the northern Bay of Bengal did not fully develop in the model 1-day forecast. The difference field of the geopotential height field at 500 *hPa* between the model 1-day forecast and the verifying analysis is displayed in Fig. VI.B.3. These differences are found to be rather large over the northern Bay of Bengal around 17.5N.

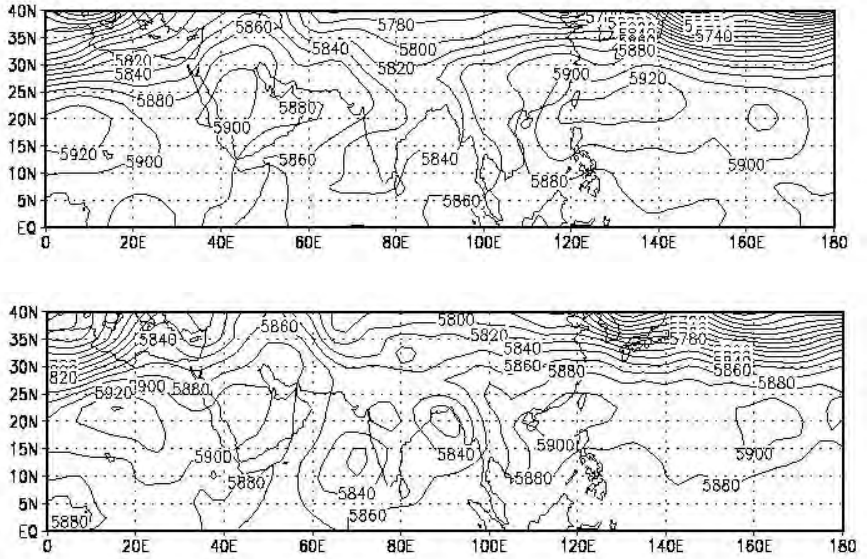

Figure VI.B.1. The geopotential height field at 500 *hPa* for 12 UTC June 7. (upper panel) and June 8 (bottom panel), 1988.

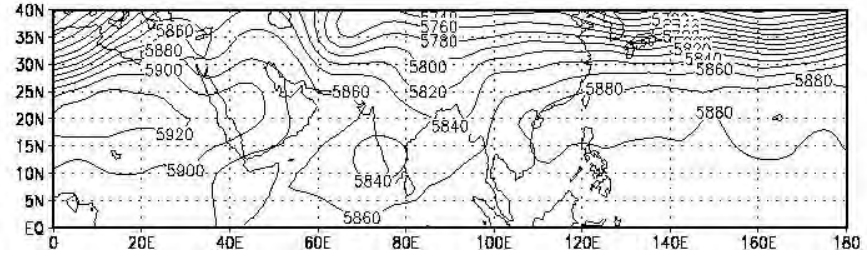

Figure VI.B.2. The geopotential height field at 500 *hPa* of the model 1-day forecast.

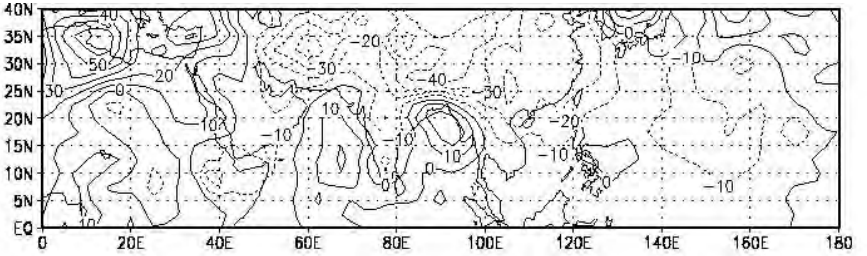

Figure VI.B.3. The difference field of the geopotential height field at 500 *hPa* between the model 1-day forecast and the verifying analysis.

VI.B.2. Illustrative Sensitivity Analysis Results

Recall that the objective is to identify the geographical areas to which the forecast aspect is most sensitive. The gradients $\nabla_{X(t_0)}J(X)$, i.e., the sensitivity patterns, are evaluated with respect to the model state variables by integrating the adjoint sensitivity model backwards in time along the nominal solution derived from the forward nonlinear FSU GSM, which started from the ECMWF analysis, valid 24 hours before the verification time (as described in the previous sub-section).

It is known that the analysis of moisture field is usually unreliable over the tropics due to the lack of sufficient observations, i.e., there is a large uncertainty in this analysis. Figure VI.B.4 depicts the squared sum of sensitivities with respect to the initial analysis of dewpoint depression for each model vertical level. The striking feature is that the forecast error is very sensitive to the initial analyses of dewpoint depression at the lowest three model vertical levels, while the sensitivities to the upper model levels are small.

Additional, more detailed, sensitivity patterns with respect to the dewpoint depression at model vertical levels 12, 11, and 10, are presented in Figures VI.B.5 - Fig. VI.B.7, respectively. A large positive maximum center located at the upstream of the region with large forecast errors over the northern Bay can be observed for both of the lowest two model levels, but a large negative maximum center appears to be more pronounced at the third lowest level. The analyses of dewpoint depression at time t_0 were diagnosed to be too dry over the northern Bay of Bengal at the lowest two model vertical levels.

The results depicted in these figures also show that the model 1-day forecast error is most sensitive to the analysis errors in the dewpoint depression around $90\,E$, $20\,N$. Therefore, additional observations around this point are expected to improve the model 1-day forecast. In particular, Figure VI.B.8 shows the vertical cross-section at $20\,N$ for the sensitivity with respect to the dewpoint depression at time t_0. This pattern is tilted in the vertical to the west, which indicates that further growth of the depression is sensitive to baroclinic perturbations at the initial time.

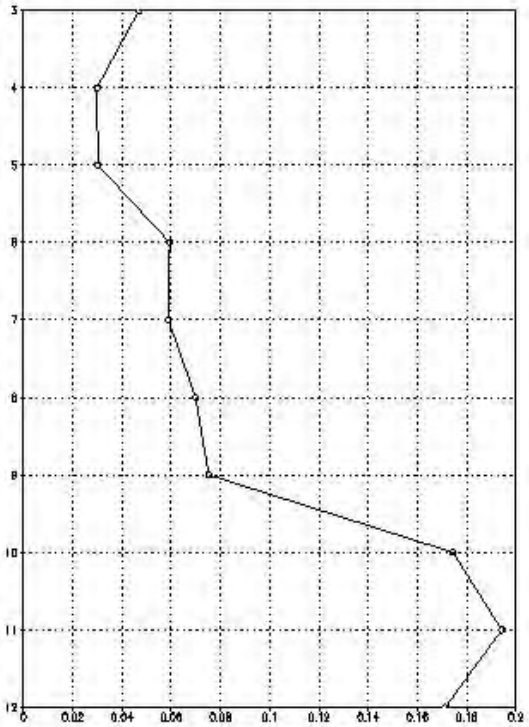

Figure VI.B.4. Evolution of the squared sum of sensitivities with respect to the initial analysis of dewpoint depression for each model vertical level.

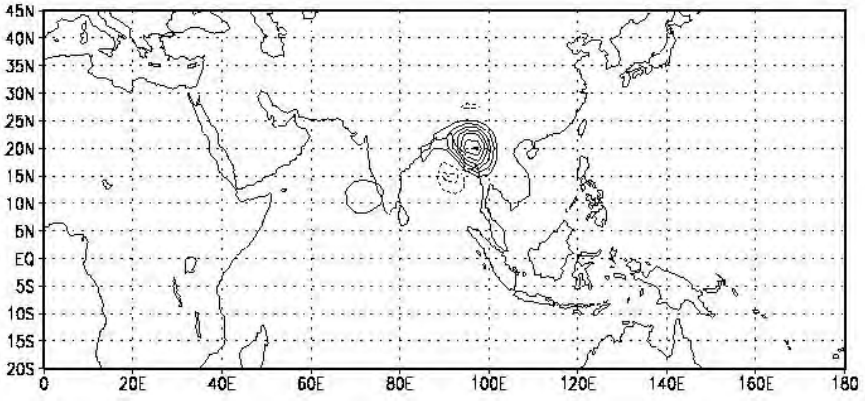

Figure VI.B.5. Sensitivities with respect to the dewpoint depression at the lowest model level. Isolines interval is 1 K^{-1}.

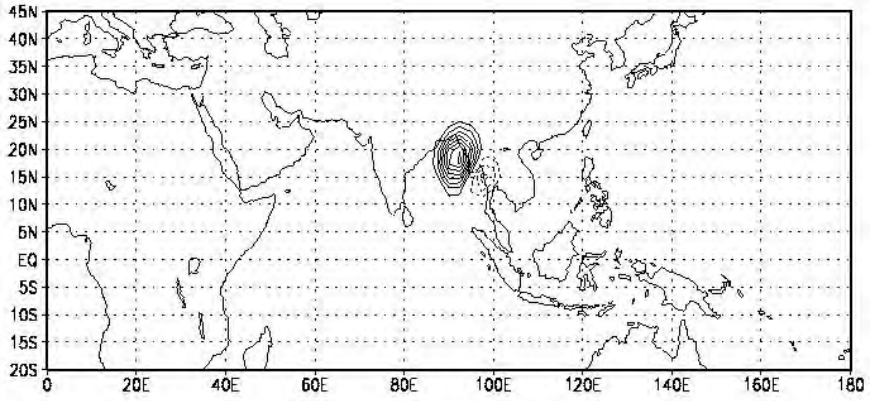

Figure VI.B.6. Sensitivities with respect to the initial analysis of dewpoint depression at the second lowest model level. Isolines interval is $1\,K^{-1}$.

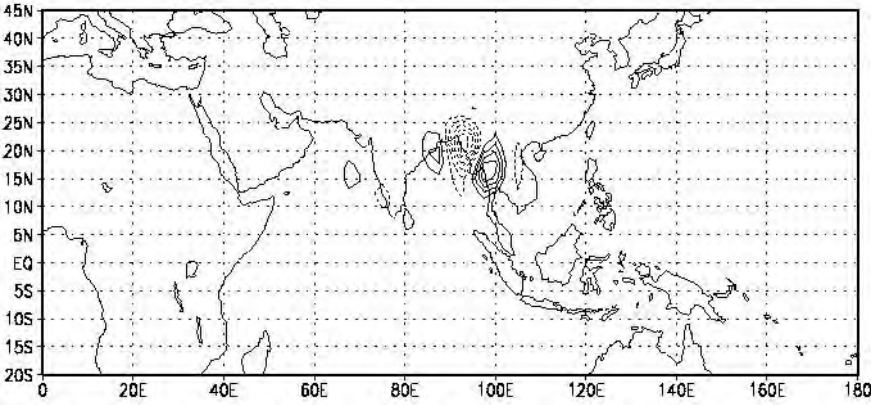

Figure VI.B.7. Sensitivities with respect to the initial analysis of dewpoint depression at the third lowest model level. Isolines interval is $1\,K^{-1}$.

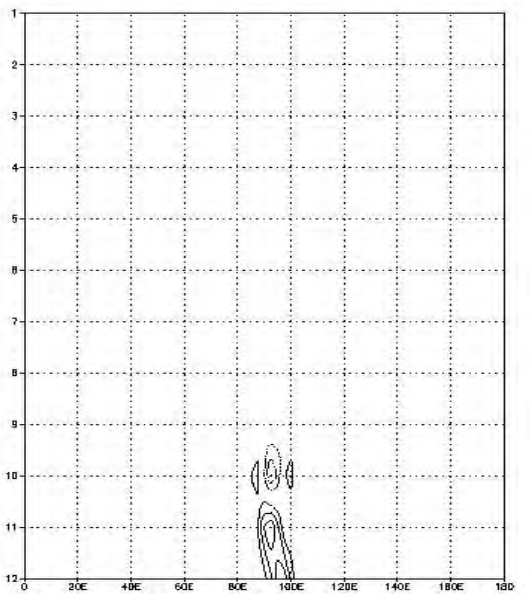

Figure VI.B.8. Vertical cross-section at 20 N for the sensitivity with respect to the dewpoint depression at time t_0. Isolines interval is 2 K^{-1}.

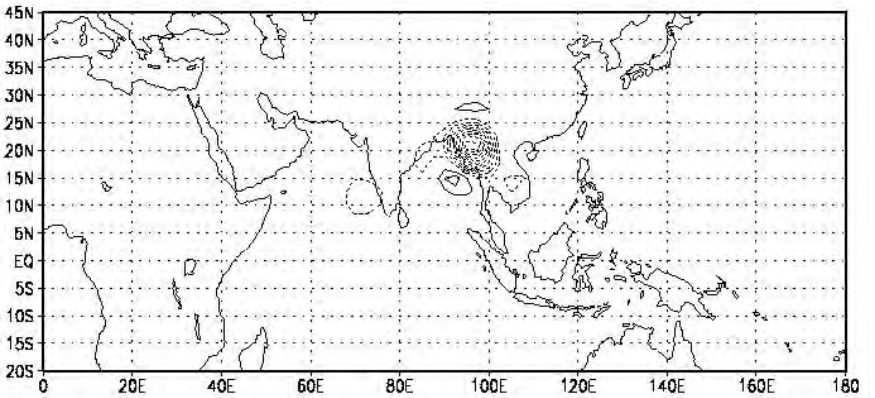

Figure VI.B.9. Sensitivity pattern with respect to the initial analysis of virtual temperature at model vertical level 12. Isolines interval is 1 K^{-1}.

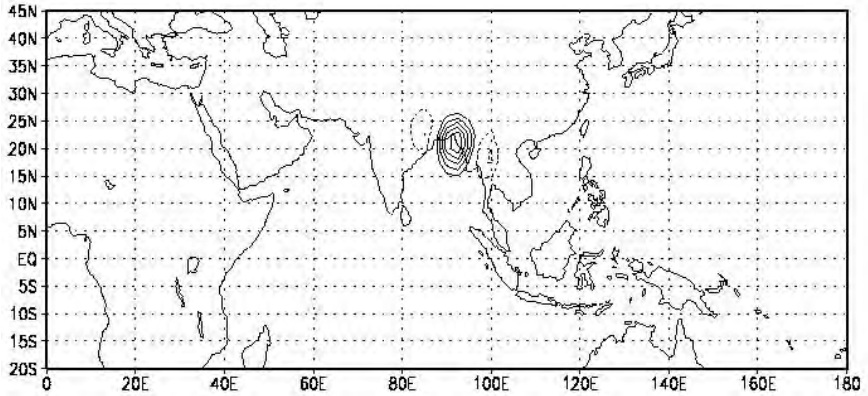

Figure VI.B.10. Sensitivity pattern with respect to the initial analysis of virtual temperature at model vertical level 10. Isolines interval is 2 K^{-1}.

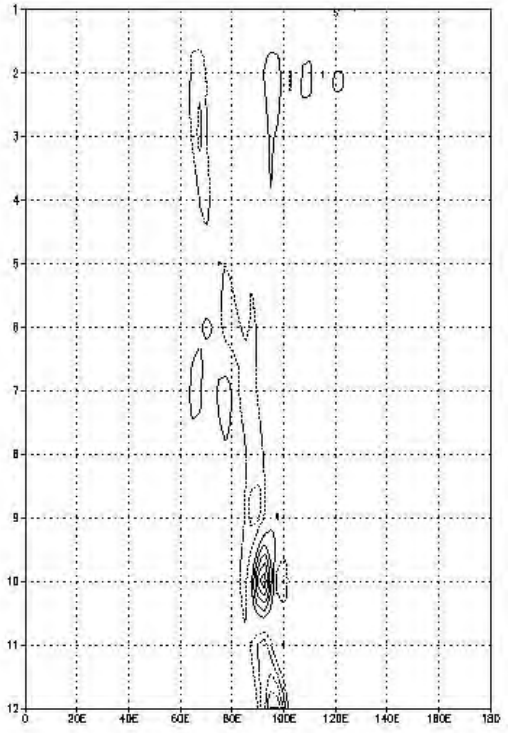

Figure VI.B.11. Vertical cross-section at 20 N for the sensitivity pattern with respect to the virtual temperature at time t_0. Isoline interval is 2 K^{-1}.

As illustrated in Figures VI.B.9 and VI.B.10, the sensitivity patterns with respect to the initial analysis of virtual temperature at model vertical levels 12 and 10 also indicate the locations of the geographical regions where the analysis problems lie in. The analyses of virtual temperature over the northern Bay of Bengal were diagnosed to be too low at model vertical level 12 and too high at model vertical level 10. The vertical cross-section at 20 N is displayed in Fig. VI.B.11.

The evolution of the squared sum of sensitivities with respect to the initial analysis of vorticity for each model vertical level (shown in Figure VI.B.4) indicates that the model 1-day forecast error is sensitive to the uncertainties in the analysis at model vertical levels 11 and 7, which are located (approximately) above the surface and at 700 hPa, respectively. The sensitivity pattern with respect to the initial analyses of vorticity at model vertical levels 11 and 7 are displayed in Fig. VI.B.12 and Fig. VI.B.13, respectively. Two important areas with opposite signs are observed for both sensitivity patterns.

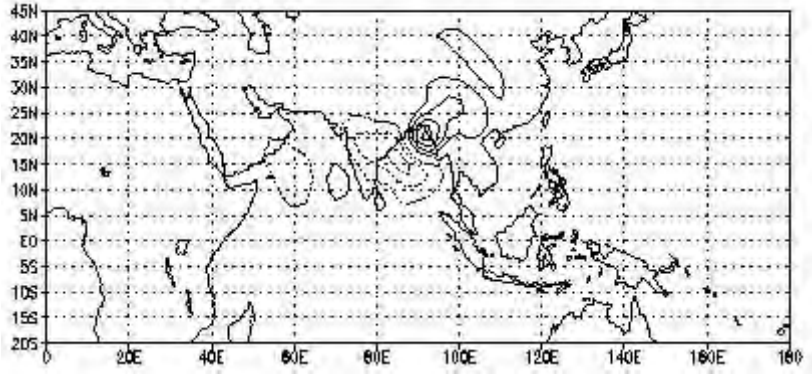

Figure VI.B.12. Sensitivity pattern with respect to the initial analysis of vorticity at model vertical level 11. Isoline interval is 200000 s.

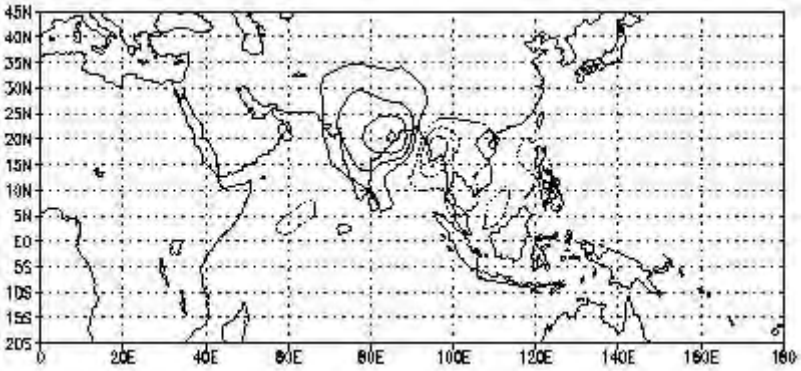

Figure VI.B.13. Sensitivity pattern with respect to the initial analysis of vorticity at model vertical level 7. Isoline interval is 200000 s.

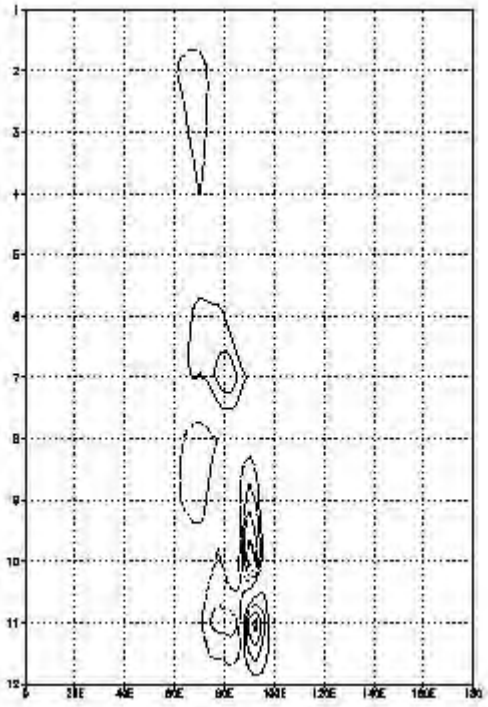

Figure VI.B.14. Vertical cross-section at 20 N for the sensitivity pattern with respect to vorticity at time t_0. Isoline interval is 200000 s.

As depicted in Fig. VI.B.14, above, the vertical cross-section at $20\,N$ for the sensitivity pattern with respect to vorticity at time t_0 exhibits two large centers with opposite signs, both of which were located in the lower troposphere around $90\,E$, $20\,N$. This indicates that the forecast error is very sensitive to the vorticity analysis uncertainties in the lower atmosphere. One maximum center, which is located at model vertical level 7, was also observed in the vertical cross-section at $10\,N$ for the sensitivity pattern with respect to the initial analysis of vorticity (see Fig. VI.B.15); a westward-tilting of the vertical structure was not observed. The analysis uncertainties at model vertical level 7 are mainly distributed over the eastern Arabian Sea, while the analysis uncertainties at model vertical level 11 are mainly located around $90\,E$, $20\,N$.

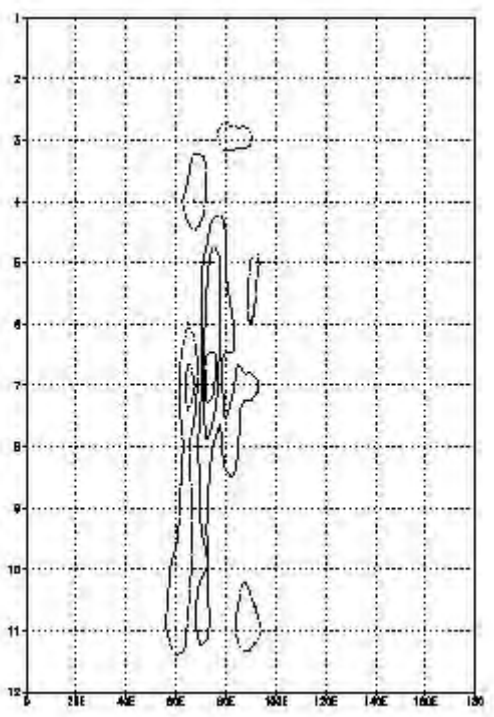

Figure VI.B.15. Vertical cross-section at $10\,N$ for the sensitivity pattern with respect to vorticity at time t_0. Isoline interval is $200000\,s$.

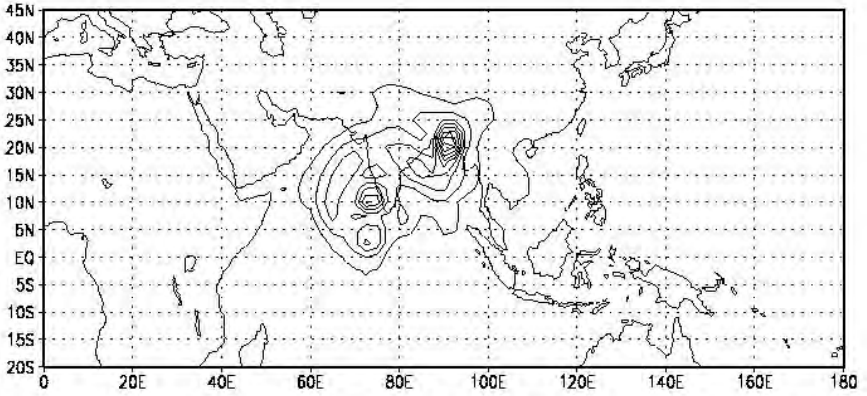

Figure VI.B.16. Sensitivity signal for vorticity at time t_0.

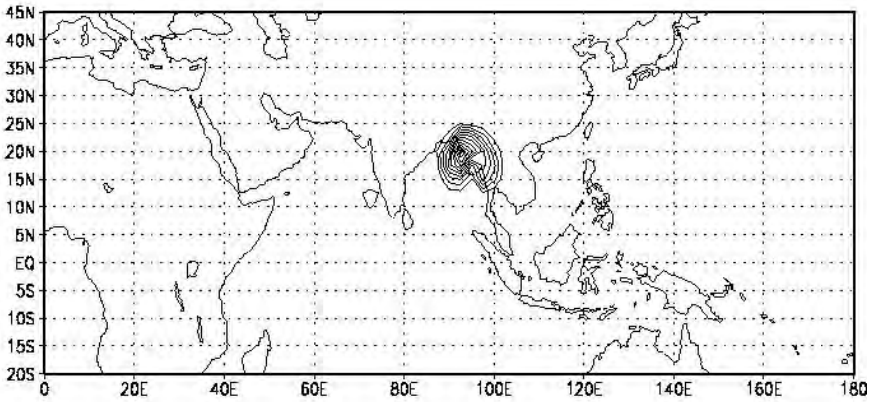

Figure VI.B.17. Sensitivity signal for dewpoint depression at time t_0.

To pinpoint the overall locations of the analysis uncertainties, the sensitivity signal, represented by the sum of squares of the sensitivity patterns throughout the whole range of vertical levels, has also been computed. Figures VI.B.16 and VI.B.17 depict the sensitivity signals for vorticity and dewpoint depression, respectively. It is apparent that the model 1-day forecast error is most sensitive to the analysis errors located at around $90\,E$, $20\,N$ over the northern Bay of Bengal.

VI. C. SENSITIVITY TO LARGE-SCALE ENVIRONMENTAL FIELDS OF THE RELAXED ARAKAWA-SCHUBERT PARAMETERIZATION IN THE NASA GEOS-1 GCM

The heating and moistening induced by convection clouds play an important role in the energy balance and water budget in the global atmosphere. Therefore, the representation of the effects of convective clouds is recognized as a key process in numerical weather prediction for time scales ranging from short-term forecasting to seasonal prediction and climate simulation. Moreover an accurate parameterization of sub-grid moisture processes in a general circulation model (GCM) is essential for assimilating observational data such as precipitation, cloudiness, and outgoing radiation, which are closely related to moisture and convection.

The Goddard Earth Observing System-1 (GEOS-1) GCM was developed by the Data Assimilation Office (DAO) at NASA/GSFC/Goddard Laboratory for Atmospheres (GLA), in collaboration with the Climate and Radiation Branch (Takacs et al., 1994). This GCM has been used to produce multiple 10-year climate simulations, and is currently used to produce a multi-year global atmospheric data set for climate research.

There are four physics packages in the GEOS-1 GCM, namely: the RAS parameterization and large-scale convection package; the short-wave radiation and long-wave radiation packages; and the turbulence parameterization package. Among them, the moisture simulation process plays an essential role towards improving the quality of the products of the Data Assimilation System (DAS). The Relaxed Arakawa-Schubert (RAS) parameterization scheme (Moorthi and Suarez, 1992) is the central part of the moisture simulation processes.

The RAS parameterizes sub-grid cumulus convection in terms of the large-scale fields. It computes the cloud-induced variations in the potential temperature θ and moisture q, and also computes convective precipitation according to large-scale conditions in θ and q. To improve the model forecast and the quality of data assimilation products, a thorough understanding of the interactions between large-scale fields and convective clouds in the model, and an evaluation of the performance of the parameterization scheme in terms of its sensitivity to the large-scale environmental fields are indispensable.

This Section presents an application of the *ASAP* to evaluate, qualitatively and quantitatively, the impact of grid-scale perturbations on the RAS-output. The following issues are addressed:

- Examining the spatial variation of the sensitivity and identifying the vertical levels where the perturbations have the largest impact on RAS output;
- Evaluating the relative importance of the perturbations in the temperature, moisture, and wind fields of the surrounding air in changing the outputs of RAS scheme;

- Discussing the feedback between the convective clouds and the large-scale fields.

In Section VI.C.2, we describe the theory and algorithm of adjoint sensitivity. Section VI.C.3 consists of a brief description of the RAS scheme in the GEOS-1 GCM. Section VI.C.4 presents an analysis of the results of the sensitivity analyses. Summary, conclusions, and the implications of this work for further research are provided in Section VI.C.5.

VI.C.1. Sensitivity Analysis of the GEOS-1 GCM Using the ASAP

To sketch the application of the *ASAP* for computing the sensitivities of the output vector, $y(t)$, of RAS model to the vector $x(t)$ of the large-scale environmental fields which are inputs of RAS model, it is convenient to represent the nonlinear time-dependent RAS operator in the generic form

$$y = A(x,t) \tag{VI.C.1}$$

where t denotes time. Three general types of response functionals of y, denoted as $R_1(y)$, $R_2(y)$, and $R_3(y)$, will be considered in this section. Thus, $R_1(y)$ is defined as

$$R_1(y) \equiv \langle y, y \rangle_S \equiv y^T S y \tag{VI.C.2}$$

where $\langle y, y \rangle_S$ denotes the inner product between two vectors weighted by a real symmetric matrix S which is specified according to the field of interest, and where the superscript T denotes transposition. Next, $R_2(y)$ is defined as

$$R_2(y) \equiv \langle W, y \rangle_E \equiv W^T y \tag{VI.C.3}$$

where W is a specified weighting vector and $\langle W, y \rangle_E$ denotes the usual Euclidean inner product. Finally, $R_3(y)$ is defined as

$$R_3(y) \equiv \int_{t_0}^{t_N} \langle y, y \rangle_S \, dt \equiv \int_{t_0}^{t_N} y^T S y dt \, . \tag{VI.C.4}$$

The responses $R_1(y)$, $R_2(y)$ are instantaneous responses, in that they are determined at the same time level as that of the input variables, while $R_3(y)$ represents a time-integrated response.

The G-differential of $\delta R_1(y)$ of $R_1(y)$ can de readily determined from Eqs. (VI.C.1) and (VI.C.2) to obtain

$$\begin{aligned}\delta R_1(y) &= 2\langle y, \delta y\rangle_S = 2\left\langle y, \frac{\partial A(x,t)}{\partial x}\delta x\right\rangle_S = 2y^T S\left[\frac{\partial A(x,t)}{\partial x}\delta x\right] \\ &= 2\left\{\left[\frac{\partial A(x,t)}{\partial x}\right]^T S^T\right\}\delta x = 2\left\langle\left[\frac{\partial A(x,t)}{\partial x}\right]^T S^T y, \delta x\right\rangle_S\end{aligned} \tag{VI.C.5}$$

where $\dfrac{\partial A(x,t)}{\partial x}$ is the Jacobian representing the discretized tangent-linear model (i.e., the discretized forward sensitivity model) of the RAS scheme, while $\left[\dfrac{\partial A(x,t)}{\partial x}\right]^T$ is actually the adjoint of the Jacobian.

From Eq. (VI.C.5), it follows that the gradient $\nabla_x R_1(y)$ of $R_1(y)$ with respect to x is

$$\nabla_x R_1(y) = 2\left[\frac{\partial A(x,t)}{\partial x}\right]^T S^T y\,. \tag{VI.C.6}$$

In practice, $\nabla_x R_1(y)$ is computed by first running the original RAS with prescribed large-scale conditions at a certain time t to obtain the output $y = A(x,t)$, then apply the operator S, and finally using the result as the input to the adjoint of RAS. The output of the adjoint of the RAS model yields the gradient vector $\nabla_x R_1(y)$.

For the response $R_2(y)$, a similar reasoning as above leads to:

$$\nabla_x R_2(y) = \left[\frac{\partial A(x,t)}{\partial x}\right]^T W\,, \tag{VI.C.7}$$

implying that the input to the adjoint of RAS is, in this case, the weighting vector W.

The G-differential of $\delta R_3(y)$ of $R_3(y)$ can be readily determined from Eqs. (VI.C.1) and (VI.C.4) to obtain

$$\delta R_3(y) \equiv 2\int_{t_0}^{t_N} \left\langle \left[\frac{\partial A(x,t)}{\partial x}\right]^T S^T y, \delta x \right\rangle dt \,. \qquad \text{(VI.C.8)}$$

To evaluate the gradient $\nabla_{x_0} R_3(y)$ of $R_3(y)$ with respect to the initial perturbations $\delta x_0 = \delta x \,\big|_{t=t_0}$, we recall that a small perturbation $\delta x(t)$ can be related to δx_0 through the resolvent operator $L(t,t_0)$ of the tangent-linear model (i.e., forward sensitivity model) of the GCM by means of the evolution equation

$$\delta x = L(t,t_0)\delta x_0 \,. \qquad \text{(VI.C.9)}$$

Defining the operator $L^*(t,t_0)$ to be the adjoint of $L(t,t_0)$, and using Eq. (VI.C.9) in Eq. (VI.C.8) transforms the latter to

$$\delta R_3(y) = \left\langle 2\int_{t_0}^{t_N} L^*(t,t_0)\left[\frac{\partial A(x,t)}{\partial x}\right]^T S^T y dt, \delta x \right\rangle. \qquad \text{(VI.C.10)}$$

It follows from Eq.(VI.C.10) that the gradient $\nabla_{x_0} R_3(y)$ of $R_3(y)$ with respect to the initial perturbations $\delta x_0 = \delta x \,\big|_{t=t_0}$ is given by

$$\nabla_{x_0} R_3(y) = 2\int_{t_0}^{t_N} L^*(t,t_0)\left[\frac{\partial A(x,t)}{\partial x}\right]^T S^T y dt \,. \qquad \text{(VI.C.11)}$$

As has been already discussed in Section IV.B, in areas with a large gradient $\nabla_{x_0} R_3(y)$, a perturbation δx_0 would cause a larger impact on $R_3(y)$ than the same perturbation would cause in areas where $\nabla_{x_0} R_3(y)$ is small. Thus the 3-D distribution of $\nabla_{x_0} R_3(y)$ provides the sensitivity pattern of $R_3(y)$ to x_0. Furthermore, $\nabla_{x_0} R_3(y)$ yields an optimal initial perturbation pattern in the sense that for all the initial perturbations with a given value of the norm $\|x_0\|$, the initial distribution that has the same spatial distribution as $\nabla_{x_0} R_3(y)$ (i.e., the one which is parallel to $\nabla_{x_0} R_3(y)$ in phase space) would cause the largest changes in $R_3(y)$. The same argument applies to $\nabla_x R_1(y)$ and $\nabla_x R_2(y)$. Note that the terms gradient and sensitivity will be used interchangeably in this section.

In practice, the algorithm for computing the gradient vector $\nabla_{x_0} R_3(y)$, via Eq. (VI.C.10), is as follows:

1) Integrate the GCM from time $t = t_0$ to $t = t_N$, saving in Eq. (VI.C.11) both the environmental fields and the RAS output $y(t)$, at all times t_n, for $n = 0,1,2,\ldots,N$;
2) At each time t_n, use the stored trajectory of RAS [i.e., $y = A(x,t)$] and the adjoint RAS to compute Eq. (VI.C.6), to obtain $\nabla_{x_0} R_3(y)$ with respect to instantaneous perturbations of the large-scale fields at each time t_n;
3) Finally, integrate backward in time the adjoint of the GCM from $t = t_N$ to $t = t_0$, using the result of step 2 at $t = t_0$ as the "initial condition." Since the operator $L^*(t,t_0)$ is linear, the result of step 2 is added to the corresponding environmental fields of the adjoint GCM at each time step t_n. The final result thus obtained at the "final" time step $t = t_0$ in the backward integration yields the gradient vector $\nabla_{x_0} R_3(y)$.

Note also that while Eq. (VI.C.6) provides the sensitivity of the response $R_1(y)$ with respect to instantaneous perturbation in the surrounding air, the integration of the adjoint of the GCM yields the time evolution of this sensitivity.

The above considerations clearly highlight the advantages of using the *ASAP* for such applications, since a single integration of the adjoint sensitivity model yields the gradient of one response function to all the model variables, at all model grid points. If the forward sensitivity analysis method were used, then obtaining the same information would require integrating the original model $N \times M$ times, where N denotes the number of variables and M denotes the number of model grid points (on the order of 10^5). Such a large number of computations cannot be performed even with the most powerful computers available today.

VI.C.2. The RAS Parameterization Scheme in GEOS-1 GCM

There are four physics packages in the GEOS-1 GCM, namely the RAS parameterization and large-scale convection schemes, the short-wave radiation and long-wave radiation schemes, and the turbulence parameterization scheme. Among these physical processes, the moist process, in which the RAS scheme is the central part, plays an essential role towards improving the quality of the products of the Data Assimilation System (DAS). The adjoint sensitivity model of the adiabatic GCM and the RAS scheme were developed by and documented in Yang and Navon (1996), and Yang et al. (1997). For the results to be reported

in this Section, only the RAS scheme is considered in the GCM and its adjoint sensitivity model.

The effect of convective clouds on large-scale environment will be illustrated now by presenting paradigm numerical experiments performed with the RAS scheme, using a $5^0 \times 4^0$ horizontal resolution on 20 vertical σ levels. The initial time was arbitrarily chosen at 00GMT, Jan. 1st, 1985. The initial data was extracted from the DAO archived data set, which is assimilated and analyzed with the data assimilation system of DAO. This set has the same resolution as the RAS model, and includes five independent variables, namely the potential temperature, the zonal and meridional winds, the surface pressure, and the specific humidity. The model time integration was set to 6 hours.

The convective cloud precipitation from RAS at the initial time is depicted in Fig. VI.C.1.a. It indicates that strong convective activities occur over the low latitude oceans, especially over the eastern Indian and the western Pacific Oceans as well as the Atlantic Ocean.

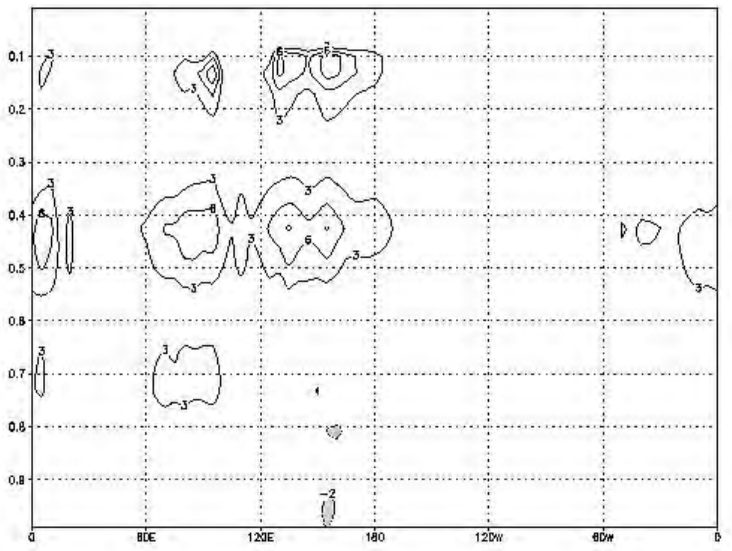

Figure VI.C.1.a. Convective cloud precipitation (interval 1.5 mm/day) output from the RAS scheme at the initial time, at 00GMT, Jan. 1st, 1985.

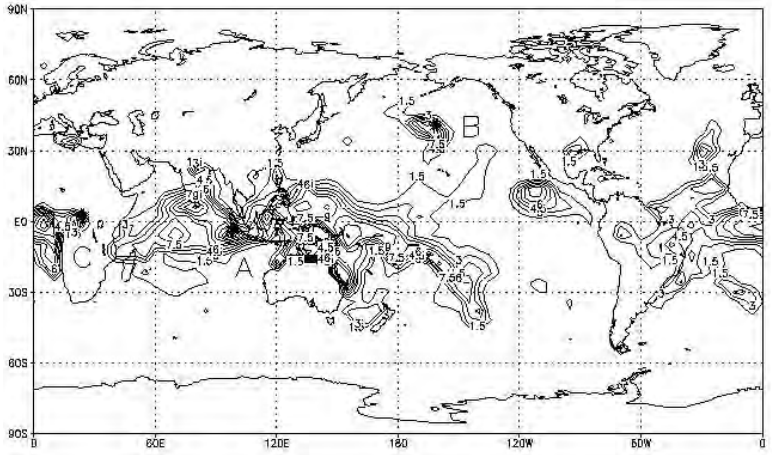

Figure VI.C.1.b. Output from the RAS scheme at 00GMT, Jan. 1st, 1985: cloud-induced change $\Delta\theta$ in the potential temperature (interval 2.0×10^{-4} K/s), averaged between 100^0 S and 100^0 N. The ordinates indicate σ levels.

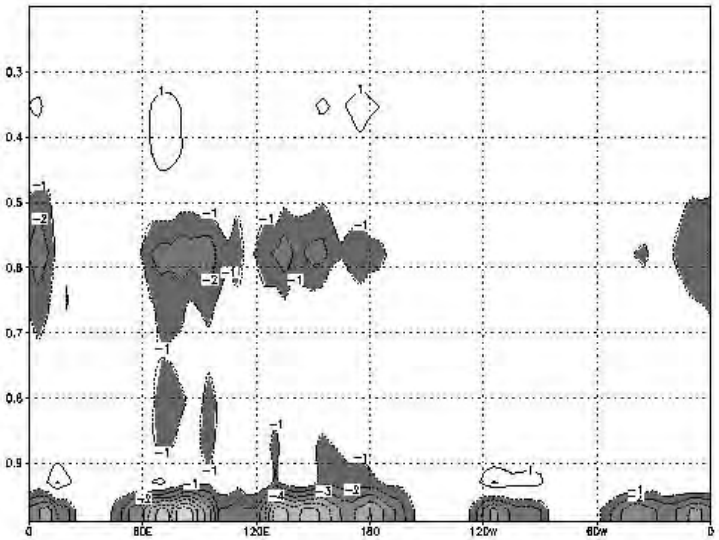

Figure VI.C.1.c. Output from the RAS scheme at 00GMT, Jan. 1st, 1985: cloud-induced moisture change Δq (interval 1.0×10^{-4} $(g/kg)/s$). Shading indicates negative values. The ordinates indicate σ levels.

Figure VI.C.1.b depicts the longitude-height distribution of the rate of convection-induced potential temperature change $\Delta\theta$, averaged between 100^0 S and 100^0 N. Note that the heating rate is represented by $\Delta\theta$, rather than by ΔT, for the results presented in this Section. (To be converted into an actual temperature change $\Delta\theta$, $\Delta\theta$ should be multiplied by a factor $(p/p_0)^{\kappa}$, where p denotes p is the pressure and p_0 is a reference pressure, $\kappa = R/C_p$, R is the gas constant, and C_p is the specific heat at constant pressure. Therefore the heating at the higher levels is scaled down more than at the lower levels.) The ordinate represents the vertical σ level. The results in this figure indicate that convective clouds act as a heat source to the environmental air at all levels. The strongest heating occurs at the mid-troposphere between σ = 0.4and σ = 0.5 (between 400 and 500 hPa). Longitudinally, the Indian and Western Pacific Oceans are the areas with the strongest convective heating. The levels between σ = 0.1 and 0.2 (approximately 100 to 200 hPa) also exhibit very strong heating rates. This feature is probably due to the fact that here the heating rate $\Delta\theta$ is calculated by the change of $\Delta\theta$ in unit etim

Figure VI.C.1.c depicts the rate of cloud-induced moisture change Δq. Only the layers below σ = 0.3 are shown. The convective cloud generally dries out the layers below 500 hPa, especially the subcloud layers and around 600 hPa, but only weakly moistens the upper layers. At mid-troposphere, the layer with the strongest convective drying is lower than that with the strongest heating.

The convective clouds impact upon the large-scale fields through $\Delta\theta$ and Δq. On the other hand, variations in grid scale vertical profile in the environing air, in turn, influence the convective activities. In the following sections we will investigate the sensitivity of the RAS outputs to large scale environmental fields, i.e., the effects of small perturbations in the surrounding air on the RAS outputs.

The range of the validity of the model predictions that can be made using a first-order functional Taylor-series expansion of the model response can be assessed by computing the functional:

$$F(\beta) = \frac{R(X + \beta h_x) - R(x)}{\langle \nabla_x R, \beta h_x \rangle_E} \qquad \text{(VI.C.12)}$$

where h_x is a prescribed distribution of perturbation and β is a scaling factor which controls the magnitude of the perturbation. A unit value of $F(\beta)$ indicates that a first-order functional Taylor-series expansion of the model response can be reliably used to predict effects of perturbations. An illustrative example of the use of $F(\beta)$ is presented in Table VI.C.1, below, where h_x was obtained by taking the difference between the result of a 6 hour integration of the original GCM and the initial condition. The results in this table indicate that

a first-order functional Taylor-series expansion can be used to make reliable predictions within several orders of magnitude of β.

Table VI.C.1
Range of validity of first-order predictions.

β	F(β)
1.0×10^{0}	1.075056131
1.0×10^{-1}	1.001115046
1.0×10^{-3}	1.000012075
1.0×10^{-5}	1.000000098
1.0×10^{-7}	0.9999898195
1.0×10^{-9}	1.000668568
1.0×10^{-11}	0.9696400849

VI.C.3. Sensitivity Analysis Results

(1) Instantaneous sensitivity

This subsection present the illustrative results for instantaneous sensitivities (meaning that the response functionals are for a single time-level) for convective precipitation to the temperature field, θ and, respectively, moisture field q. The response functional for convective precipitation is defined as:

$$R_p = \sum_{\Omega} P_r \qquad \text{(VI.C.13)}$$

where P_r denotes the convective cloud precipitation rate, and Ω denotes the low-latitude belt from $300^0\,S$ to $30^0\,N$, where most of the precipitation occurs. Figure VI.C.2.a, below, shows the longitude-vertical distribution of the sensitivity of precipitation to θ potential temperature field, averaged between $10^0\,S$ and $10^0\,N$. A large positive sensitivity is observed below the cloud-base level, together with a negative sensitivity from 850 to 450 hPa, which means that if the surrounding air in the boundary layer becomes warmer while the mid-troposphere becomes colder, there will be stronger convective activities and stronger cloud precipitation. For instance, if $1\,K$ positive θ perturbation occurs at the point with the largest gradient in the sub-cloud layer, it will induce an

increase of approximately 9 mm/day in the overall precipitation rate. On the other hand, if this θ perturbation occurs at the point with the largest negative gradient around 500 hPa, it will result in a decrease of approximately 14 mm/day in the total convective rain. This is due to the fact that warming at lower level destabilizes the surrounding air and cooling at upper level strengthens the cloud buoyancy force (which is measured by the difference between the moisture static energy in the cloud plume and the environment), thus favoring convective cloud development. From 500 to 400 hPa, the gradient changes its sign from negative to positive, which indicates that precipitation is very sensitive to the vertical profile of temperature perturbations in mid-troposphere. For instance, if some heat source produces a positive θ potential temperature perturbation at around 500 hPa, it tends to suppress convective activities as a whole, whereas if this perturbation occurs at a slightly higher level, say around 400 hPa, it will induce stronger convection and stronger precipitation.

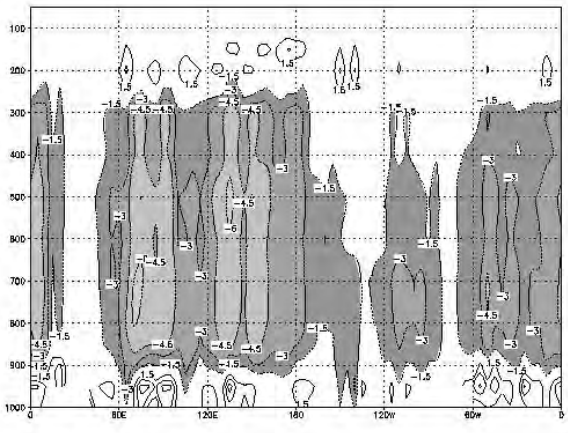

Figure VI.C.2.a. Longitude-vertical distribution of the sensitivity of RAS precipitation to perturbations in θ [interval 1.5, one unit corresponds to 2.0 $(mm/day)/K$]. Shading indicates negative values. The ordinates are in hPa.

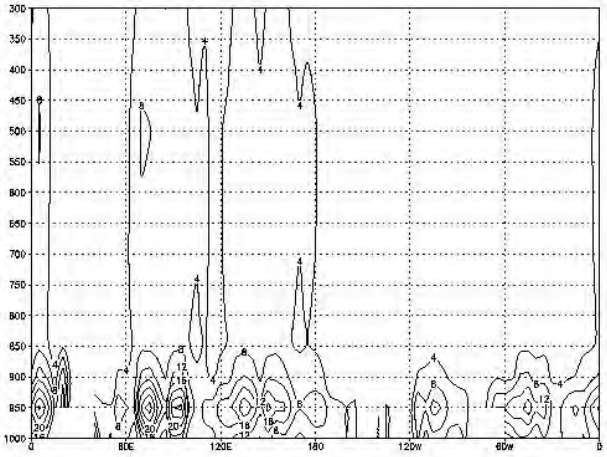

Figure VI.C.2.b. Longitude-vertical distribution of the sensitivity of RAS precipitation to perturbations in moisture field q [interval 1.0, one unit corresponds to 0.144 $\left[(mm/day)/(g/kg)\right]$]. Shading indicates negative values. The ordinates are in hPa.

The variation with height of the sensitivity of precipitation to moisture is displayed in Fig. VI.C.2b, above. Only the levels below 850 hPa show significant positive sensitivity with the largest near 950 hPa, the cloud-base level. This means that more moisture near the cloud base level favors convective activities and induces stronger convective precipitation. Specifically, if a 1 (g/kg) perturbation in q occurs at the largest gradient point at 950 hPa, it tends to induce about 2.3 mm/day increase in total cloud precipitation. At upper levels around 450 hPa, there is a weak negative gradient, indicating opposite effects to these obtained at the lowest levels.

Based on the results depicted in Figures VI.C.2, four representative grid points, with high convective activities and high sensitivity, are now selected for further analysis. Three of the four selected points are: (i) Point A: at ($100^0 E$, $6^0 S$) over the eastern Indian Ocean; (ii) Point B: at ($165^0 W$, $42^0 N$) over the mid-latitude Pacific Ocean; and (iii) Point C: at ($25^0 E$, $2^0 S$) over the tropical African continent.

The response functionals corresponding to these points are defined as

$$R_\theta = \Delta\theta(i, j, k)/\Delta t \qquad \text{(VI.C.14)}$$

and

$$R_q = \Delta q(i, j, k) / \Delta t \qquad \text{(VI.C.15)}$$

where (i, j, k) indicates a particular grid point (i, j) at a particular vertical level k, and Δt denotes the RAS time step. Since the RAS scheme is implemented column-wise, the output at a particular point at certain level can be sensitive to all the other vertical levels at this point, but not to the surrounding grid points. Thus, the gradients of R_θ and R_q with respect to the environmental variables θ and q constitute the four component blocks of the Jacobian matrix

$$\begin{vmatrix} \nabla_\theta(R_\theta) & \nabla_q(R_\theta) \\ \nabla_\theta(R_q) & \nabla_q(R_q) \end{vmatrix}. \qquad \text{(VI.C.16)}$$

Figures VI.C.3.a through VI.C.3.d, below, display the four components of the above Jacobian at point A ($100^0 E$, $6^0 S$). The ordinate is the σ level corresponding to k in R_θ, is directed upwards from the surface, and is referred to as the *response level*. The abscissa consists of the σ levels of the surrounding air where perturbations occur, which are referred to as the *influential levels*. For example, the large negative value at point (0.5, 0.45) in Fig. VI.C.3.a provides the gradient of R_θ at the point ($100^0 E$, $6^0 S$) at level σ = 0.45 (near 450 *hPa*) with respect to perturbations in θ at level σ = 0.5 (around 500 *hPa*).

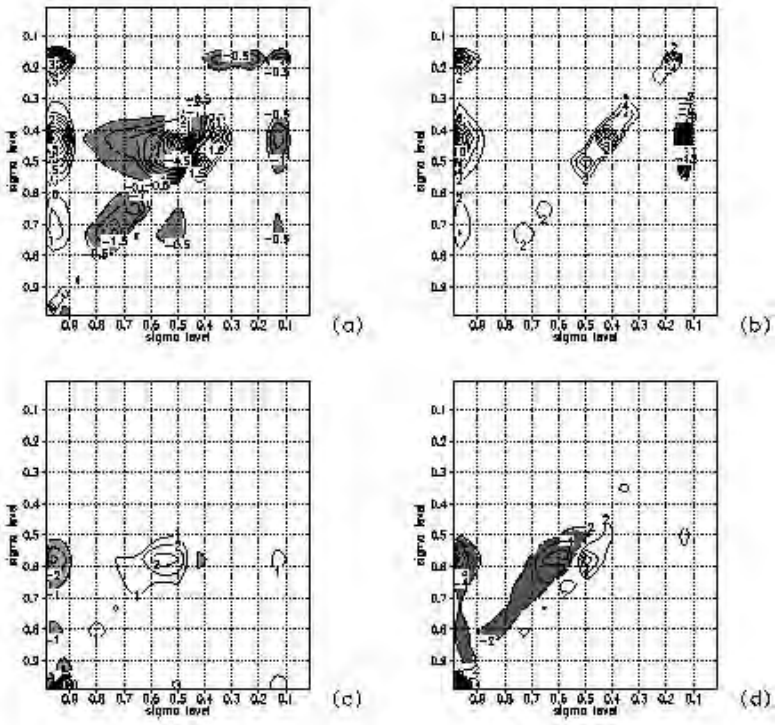

Figure VI.C.3. The four blocks of Jacobian at point ($100^0 E$, $6^0 S$). a: $\nabla_\theta(R_\theta)$, interval 0.5, one unit corresponds to 0.86 $(K/day)/day$; b: $\nabla_q(R_\theta)$, interval 2.0, one unit corresponds to 0.62 $(K/day)/(g/kg)$; c: $\nabla_\theta(R_q)$ interval 1.0, one unit corresponds to 1.2×10^{-3} $(g/kg/day)/K$; d: $\nabla_q(R_q)$, interval 2.0, one unit corresponds to 0.86×10^{-3} $(g/kg/day)/(g/kg)$. Shading indicates negative values.

Figures VI.C.3.a and VI.C.3.b indicate that for R_θ, the level around 450 hPa displays the largest sensitivity, with positive gradient to both θ and q, in the sub-cloud layers, where a $1\,K$ increase in θ leads to about $4\,K/day$ increase in cloud heating at 450 hPa level, whereas an additional $1\ g/kg$ in the moisture content leads to about 8.7 K/day increase in heating at 450 hPa level, in terms of θ change. This impact is very significant. Figure VI.C.3.a also shows a significant negative gradient with respect to θ near 500 hPa, where a $1\,K$ decrease in θ leads to a 5.6 K/day increase in cloud heating rate at around 450

hPa. This implies a negative feedback between the θ perturbation in the environing air and the cloud-induced heating at around 450 hPa. However, at height 400 hPa, a positive θ perturbation tends to enhance convective heating and the θ perturbation will grow, thus indicating a positive feedback.

The opposite impacts of perturbations occurring at 500 and 400 hPa on the convective heating can be explained by the fact that environmental heating is mainly accomplished by compensating downdrafts outside the clouds induced by the updrafts inside (Redelsperger and Guichard, 1996). Lower environmental air temperature in the mid-troposphere increases the difference of static energy between the cloud and the environment, thus increasing the buoyant force. This induces stronger updraft inside the cloud and downdraft outside it and stronger heating of the air column. On the other hand, if the layer around 400 hPa becomes colder, the heating at the 450 hPa level through subsidence will be less effective. This explains the two opposite centers observed below and above 450 hPa in Fig. VI.C.3.a. The implication is that in order to parameterize accurately the cloud effects, an accurate vertical profile of the surrounding air is an essential prerequisite.

For R_q, the most influential layer is the sub-cloud layer (depicted in Figs. VI.C.3.c and VI.C.3.d). The mid-level perturbation also can exert significant influence, but only on the adjacent layers. The layer around 500 to 600 hPa is significantly influenced by the θ- and q-perturbations in the surrounding air at the same level, as well as at sub-cloud levels. A raise of $1\,K$ in temperature and $1\,g/kg$ in moisture content at sub-cloud layer tends to enhance convection, leading to a stronger convective drying of about $7\times10^{-3}\ g/kg/day$ and, respectively, $5\times10^{-3}\ g/kg/day$ in the mid-troposphere (note from Fig. VI.C.1.c that Δq is negative at most of the vertical levels). On the other hand, occurrence of positive θ- and negative q-perturbations at mid-troposphere around 600 hPa tends to suppress convective drying at the same level. Note the opposite effect of the q-perturbations at σ = 0.5 (500 hPa) and σ = 0.6 (600 hPa) levels on the convective drying at 600 hPa. At around 600 hPa, the negative gradient implies that the feedback between the moisture perturbation and cloud drying effect is negative. The behavior of point A is typical of model grid-point locations over low-latitude oceans with strong deep convective clouds.

Now we turn our attention to point B ($165^0 W$, $42^0 N$). Fig. VI.C.4 shows the four components of the Jacobian at this point. Comparing Figs. VI.C.4a and VI.C.4b with Figs. VI.C.3a and VI.C.3b, one can see that for R_θ, the most sensitive response level is lowered to σ = 0.5 (around 500 hPa). This layer shows significant sensitivity to θ perturbations at the same level as well as at the levels below it. For R_q, Fig. VI.C.4c and d shows that the most sensitive

response level is even confined to below σ = 0.8 level. Negative θ and positive q perturbations between σ = 0.8 and σ = 0.9 (800 to 900 hPa) induce stronger convective drying. Also, the positive θ perturbation around σ = 0.6 level can lead to a suppression of convective drying at the layers lower than 850 hPa. This may be attributed to the reduced buoyancy force by higher environmental temperature.

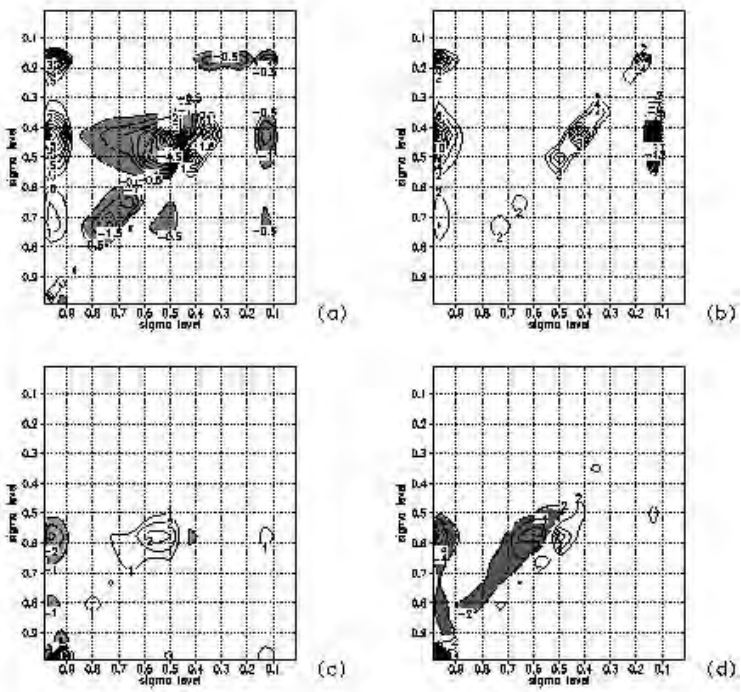

Figure VI.C.4. Same as Fig. VI.C.3 but for point ($165^0 W$, $42^0 N$); a: $\nabla_\theta(R_\theta)$, interval 0.5, one unit corresponds to 0.86 $(K/day)/K$; b: $\nabla_q(R_\theta)$, interval 1.5, one unit corresponds to 0.62 $(K/day)/(g/kg)$; c: $\nabla_\theta(R_q)$, interval 0.2, one unit corresponds to 1.2×10^{-3} $(g/kg/day)/K$; d: $\nabla_q(R_q)$, interval 2.0, one unit corresponds to 0.86×10^{-3} $(g/kg/day)/(g/kg)$. Shading indicates negative values.

The diagonal structure of the Jacobian, which is most evident in Fig. VI.C.4.d, indicates the local effect of the perturbations on convective drying. The R_q at layers above 500 hPa shows little sensitivity to the θ- and q-perturbations at any level, probably since at high latitudes the convective clouds can not

penetrate to very high levels, due to the fact that the moisture content in the air column is lower than that at low latitudes.

Figure VI.C.5 displays the Jacobian at grid point C ($25^0\,E$, $2^0\,S$). For R_θ, the major difference between the points C and A is the fact that the sensitivity of mid-troposphere R_θ to both θ- and q-perturbations is now about an order of magnitude weaker (notice the difference in the contour intervals). Here the impact on convective heating from perturbations at mid- to upper troposphere is relatively more important than that from sub-cloud layers.

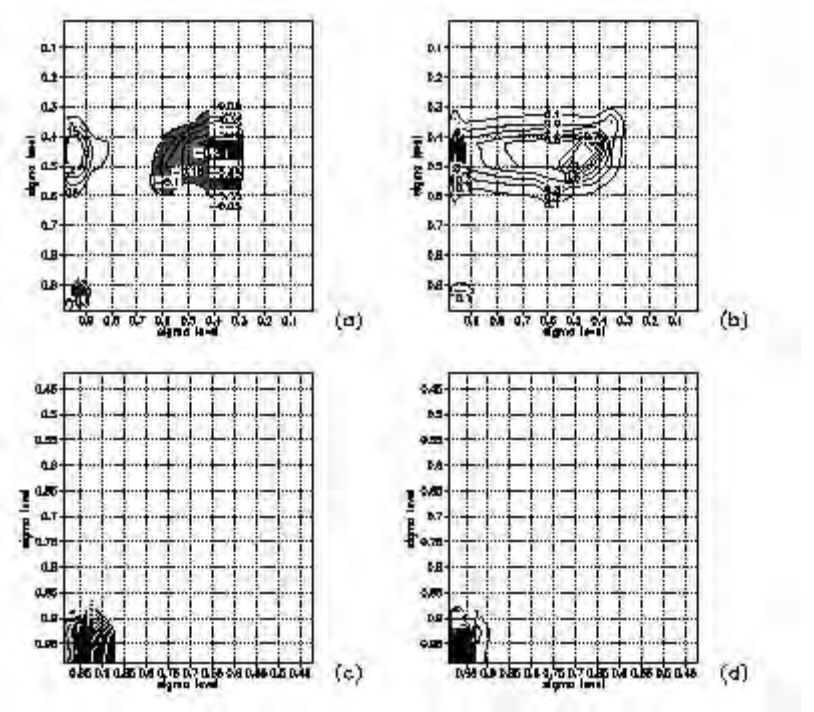

Figure VI.C.5. Same as Fig. VI.C.3 but for point ($25^0\,E$, $2^0\,S$); a: $\nabla_\theta(R_\theta)$, interval 0.05, one unit corresponds to 0.86 $(K/day)/K$; b: $\nabla_q(R_\theta)$, interval 0.1, one unit corresponds to 0.62 $(K/day)/(g/kg)$; c: $\nabla_\theta(R_q)$, interval 1.0, one unit corresponds to 1.2×10^{-3} $(g/kg/day)/K$; d: $\nabla_q(R_q)$, interval 1.0, one unit corresponds to 0.86×10^{-3} $(g/kg/day)/(g/kg)$. Shading indicates negative values.

For R_q, Figures VI.C.5.c and VI.C.5.d show a marked difference compared to locations A and B. Now both the significantly sensitive layer and the influential

layer are confined to below 900 hPa (notice the difference of the scale on the ordinate and abscissa between Figs. VI.C.5.c, VI.C.5.d, and the corresponding figures for points A and B). This is probably due to the presence of less moisture content in the air column and lower cloud top over land area than over low-latitude oceans. However, Figures VI.C.5.c and VI.C.5.d still display detailed sensitivity structures with respect to the temperature and moisture perturbations, i.e., positive θ- and q-perturbations at the lowest model level and negative perturbations higher above (between 900 to 950 hPa) tend to destabilize the sub-cloud layers and strengthen convective drying. In fact at locations A and B such sensitivity structures at the lowest model levels are also observed. At the lowest model layers those points depict strong negative feedback between q and the convective drying, whereas in the slightly higher layers, the feedback is positive.

The foregoing analysis of perturbations at the three types of grid point locations (A, B, and C) indicates that the conditions in the sub-cloud layers can most significantly influence the convective activities at each of these locations. For cloud effects at mid-troposphere, the influence from sub-cloud layer disturbances may surpass that arising from perturbations in the immediate surrounding air at the same level, especially for R_θ at grid points over the oceans. Regarding the response functions, the mid-troposphere is the one most easily influenced. When forced by the same perturbation, the variations in cloud heating and drying effects are larger at these levels than at other levels. Over land and high latitude oceans, the moisture perturbation exhibits more localized effects, which are mostly confined to the lowest model levels, whereas over the low latitude oceans with high sea surface temperature (SST) and stronger deep clouds, the impact of the boundary layer can be more readily transferred to higher levels.

Most of the layers display negative feedback between R_θ and the θ-perturbation and between R_q and q-perturbation. This suggests that perturbations in the environing air are suppressed by cloud activities. Therefore the cloud effect acts, by and large, as a stabilizing factor for large-scale perturbations, except for the vertical levels with positive feedback, which can cause rapid growth of the initial perturbations in the environing air.

The gradient of a time-integrated response is expected to yield a more stable and reliable sensitivity pattern than that of the instantaneous sensitivity. Moreover, it can provide us with the time evolution of the sensitivity. To investigate the strength of the impact of convective clouds on the large-scale fields, the matrix S in Eq. (VI.C.4) is now chosen to define the response functionals

$$R_{qq} \equiv \int_{t_0}^{t_N} \sum_G \left(\frac{\partial q}{\partial t} \right)^2 dt, \quad \textit{and} \quad R_{\theta\theta} \equiv \int_{t_0}^{t_N} \sum_G \left(\frac{\partial \theta}{\partial t} \right)^2 dt, \text{ (VI.C.17)}$$

where $\sum_G$ represents summation over the globe. In Eq. (VI.C.17), the time-integrations were carried out for 6 hours, from 00 to 06GMT, on Jan. 1st, 1985. To avoid repetitious language in the presentation of the results to follow, the sensitivity of the time-integrated response with respect to the perturbation of that variable at initial time will simply be called the "sensitivity" or "gradient" to the respective variable.

Figures VI.C.6.a and VI.C.6.b display the longitude-height distribution of $R_{\theta\theta}$ and R_{qq} to θ- and q-perturbations, respectively, averaged in the latitudinal band between $10^0 S$ and $10^0 N$. Comparing these two figures to Figure VI.C.2.a reveals a major difference, namely that now all the levels above 700 hPa display negative gradients instead of a sharp change from negative to positive from 500 hPa to 400 hPa. The most influential levels are around 950 hPa, and between 500 to 600 hPa, in that the perturbations occurring at these levels lead to larger variations in $R_{\theta\theta}$ than similar perturbations at other levels. Specifically, a 1 K increase at sub-cloud layer, or a 1 K decrease around 500 hPa in θ leads to about $5\times10^{-6}\ K^2/s$ increase, or a $2\times10^{-6}\ K^2/s$ increase in $R_{\theta\theta}$, respectively. Figures VI.C.6.a and VI.C.6.b also indicate that, longitudinally, the perturbations over the eastern Indian Ocean and the western Pacific Ocean exert the strongest influence on the convective heating and drying. Over the western Indian Ocean and the eastern Pacific Ocean, however, only the temperature perturbations under 800 hPa level can have a significant impact.

In summary, the cloud impacts on the large-scale fields are most sensitive to the initial perturbations in θ-field at two levels: one is the sub-cloud layer, and the other is the mid-troposphere layer between 500 hPa and 600 hPa. The perturbations at these layers have opposite effects on the convective parameterization, namely positive perturbations in the lower layers and negative perturbations in the upper layers, which lead to enhanced convective activities and to stronger impact on the environmental fields.

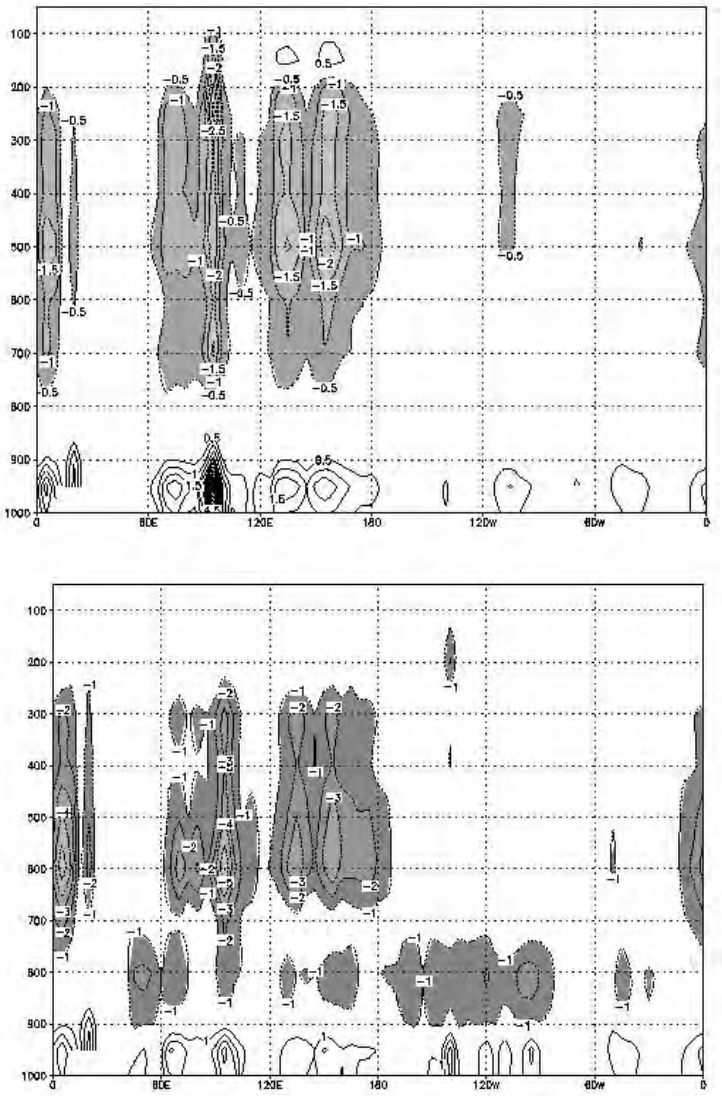

Figure VI.C.6. Variations with longitude and height of the sensitivity to θ perturbations of the response (a) $R_{\theta\theta}$ [interval 0.5; one unit corresponds to 7.2 $\times 10^{-7}$ $\left(K^2/s\right)/K$], and (b) R_{qq} [interval 1.0; one unit corresponds to 1.4 $\times$ 10^{-8} $\left(g/kg\right)^2/s/K$]. Shading indicates negative values. The ordinates are in hPa .

Figures VI.C.7.a and VI.C.7.b show the vertical distribution of the sensitivity to moisture perturbations of $R_{\theta\theta}$ and R_{qq}, respectively, again averaged between 100S and 100N. Note the differences from Fig. VI.C.2.b, which depicted the sensitivity of precipitation to the q-perturbation. As depicted in Fig. VI.C.7.a, $R_{\theta\theta}$ displays a positive sensitivity to all the vertical levels, especially to the layers around 950 hPa and, respectively, 400 hPa, where a 1 g/kg increase in moisture content can result in a $1\times10^{-5}\ K^2/s$ and, respectively, $1.5\times10^{-6}\ K^2/s$ increases in $R_{\theta\theta}$ (which means an increase in convective heating).

Figure VI.C.7.b depicts the (more complex) behavior of the R_{qq} sensitivity to moisture. Only the levels below 300 hPa are displayed, since there is very little moisture above this level. The most significant positive gradient is observed around 950 hPa and 600 hPa. From 600 hPa to 500 hPa, the gradient changes from large positive to negative. At around the 600 hPa layer, an addition of 1 g/kg in the moisture field leads to an increase of approximately $2\times10^{-7}\ (g/kg)^2/s$ in R_{qq}. On the contrary, adding 1 g/kg moisture at around 500 hPa tends to suppress convection (cf. Fig. VI.C.2.b) and reduce the convective drying effect, as manifested by the ca. $1.5\times10^{-7}\ (g/kg)^2/s$ decrease in R_{qq}.

This intricate structure is also manifest in Fig. VI.C.3.d but with reversed sign since in that figure, the response function is the Δq itself, which is negative, whereas in Fig. VI.C.7.b the response is the square sum of Δq which is always positive.

As Fig. VI.C.2.b shows, the q-perturbation around 600 hPa does not significantly influence the strength of convection, which is represented there by convective precipitation, but Figure VI.C.7.b indicates that it can very significantly influence the convective drying. A possible explanation is that the convective drying in the environing air, like the convective heating, is mainly due to the compensating subsidence outside the clouds (Redelsperger and Guichard, 1996). This effect is most significant at around 600 hPa (see Fig. VI.C.1.c). Presence of additional moisture in the environing air at this level will cause more water vapor to be transported to lower layers by downdrafts, thus leading to a larger depletion of moisture and larger negative Δq, even though the strength of convection does not increase significantly. If, on the other hand, there is additional moisture at higher levels, it tends to suppress convective activity (cf. Fig. VI.C.2.b) so that the cloud-induced drying is reduced accordingly.

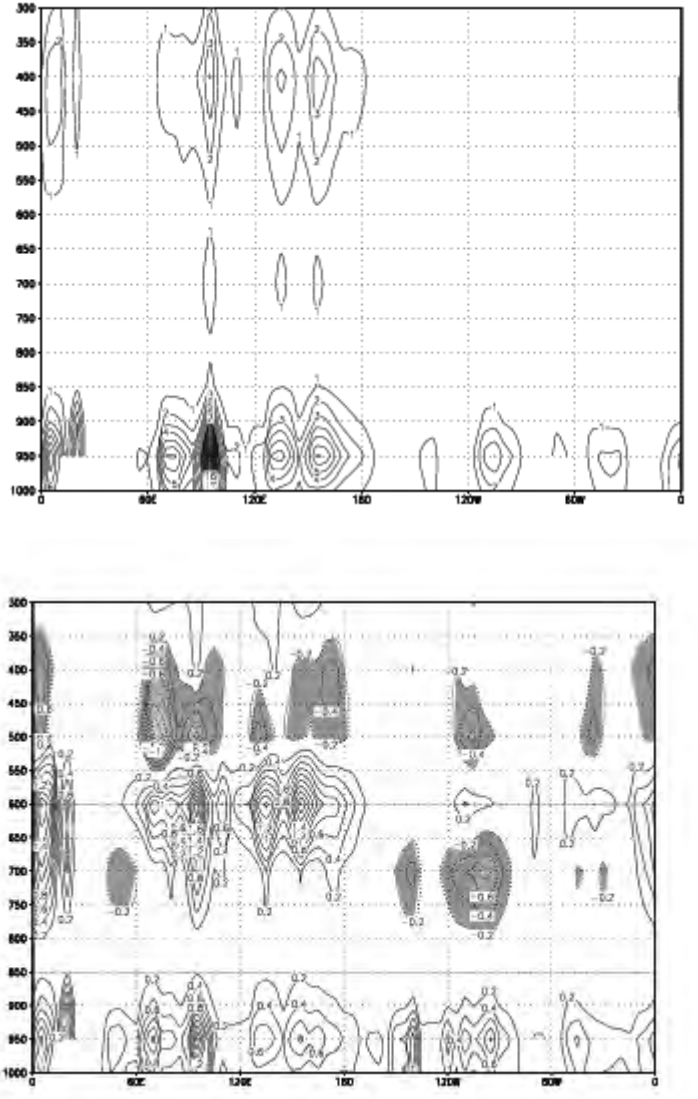

Figure VI.C.7. Height-longitude distribution of sensitivity to moisture perturbations of: (a) $R_{\theta\theta}$ [interval 1.0, one unit corresponds to $5.18\times10^{-7}\ \left(K^2/s\right)/\left(g/kg\right)$], and (b) R_{qq} [interval 0.2, one unit corresponds to $1.0\times10^{-7}\ \left(g/kg\right)^2/s/\left(g/kg\right)$]. Shading indicates negative values. The ordinates are in hPa.

The wind field does not exert an immediate impact on RAS scheme, so there is no instantaneous sensitivity to wind field. However the wind field redistributes the θ- and q-perturbations through advection and convergence/divergence. In this way, it provides an indirect influence on the output of the RAS scheme. The integration of the adjoint model can provide the gradient of $R_{\theta\theta}$ and R_{qq}, from RAS, with respect to the wind field. A concise view of the sensitivity to the perturbations in the wind vector can be obtained by displaying, in vector form, the gradient of $R_{\theta\theta}$ with respect to the u- and v-components of the wind. Figures VI.C.8.a and VI.C.8.b show the horizontal distribution of the sensitivity of $R_{\theta\theta}$ to the wind vector at 200 hPa (upper level) and 700 hPa (lower level). The gradients of $R_{\theta\theta}$ at these layers have opposite signs, again indicating a baroclinic character. The most significant influence is due to the divergent component; the vorticity component is very weak except at some isolated areas at high latitudes. The lower (upper) level gradient vector is largely convergent (divergent). The sensitivity of R_{qq} to wind is very similar to that of $R_{\theta\theta}$, and is therefore not shown here. As already discussed previously, wind perturbations with the same structure and distribution (i.e., convergence at lower levels and divergence at upper levels over the convectively active regions at initial time) will lead to stronger cloud impacts on the environment in the ensuing several hours. The most sensitive region extends geographically from the eastern Indian Ocean to the western Pacific Ocean at low latitudes.

To complete the sensitivity analysis results, Table VI.C.2 illustrates the relative importance of the impacts of the perturbations in potential temperature, moisture, and wind fields on the response functions. The perturbations shown in this table are effected at the most sensitive grid-point for that variable (i.e., the point with the largest gradient). As Table VI.C.2 illustrates, the precipitation, θ, is the most influential factor; its impact is 2 to 3 times larger than that arising from q-perturbations. For convective heating and drying, q-perturbations become the most influential factors, although θ-perturbations are almost as important. The variations caused by wind perturbations are at least one order of magnitude smaller than those due to the θ and q-perturbations, respectively.

Table VI.C.2
1st order variations in response functionals.

			δR_p (mm/day)	$R_{\theta\theta}$ ($^oK^2$/s)	R_{qq} ($g^2/kg^2/s$)
$\delta\theta$	1×10^{-2}	^{0}K	1.4×10^{-1}	1.4×10^{-7}	2.2×10^{-9}
δq	1×10^{-2}	g/kg	5.0×10^{-2}	2.9×10^{-7}	5.0×10^{-9}
δW	1×10^{-2}	m/s		1.5×10^{-10}	1.0×10^{-10}

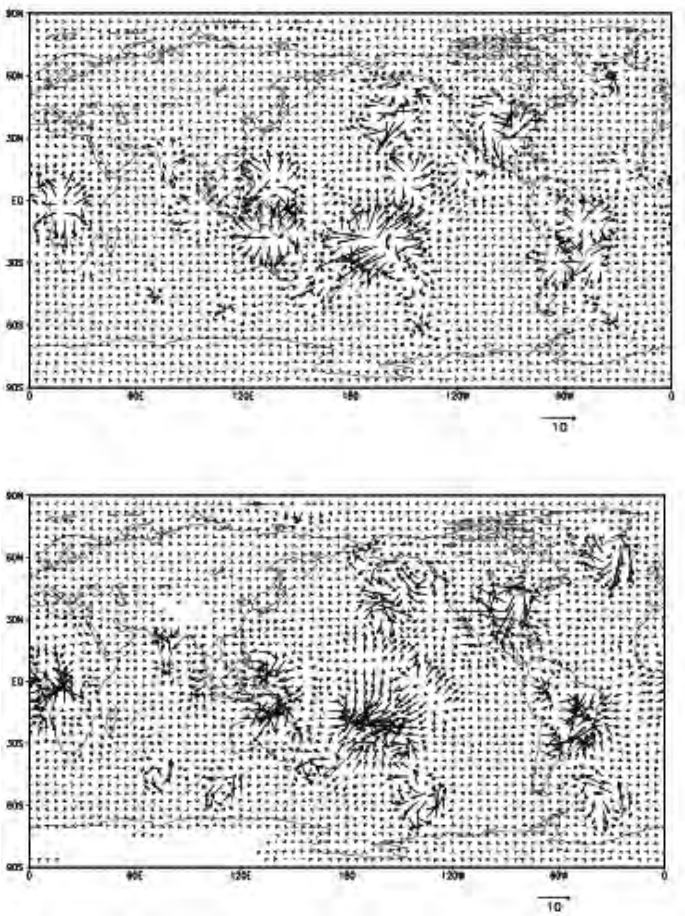

Figure VI.C.8. Sensitivity of $R_{\theta\theta}$ to perturbations in wind vector at (a) 200 hPa and (b) 700 hPa; one unit corresponds to $5.2\times10^{-10}\ \left(K^2/s\right)/(m/s)$.

In summary, the sensitivity analysis results presented in this sub-section showed that the θ-perturbation has a significant impact on all the response functionals analyzed, especially on the convective precipitation. The perturbations at sub-cloud layers and at mid-troposphere, from $500\,hPa$ to $600\,hPa$, were found to be the most influential. The effects at the lower layers and upper layers are opposite to each other, i.e., higher (lower) temperature perturbations at lower (upper) levels tend to produce positive variations to the response functions, indicating stronger convectivities and stronger cloud impact on the environing air. The impact from moisture fields is most significant on the cloud heating and drying effects; the strongest influence comes from the sub-cloud layers, where additional moisture is conducive to stronger convective activities. The cloud-induced drying (moistening) is also significantly influenced by the moisture perturbations at mid-troposphere, with completely opposite effects from the $500\,hPa$ compared to the $600\,hPa$ disturbances, indicating a strong sensitivity of the response to grid-scale vertical profiles at mid-troposphere.

The regions where the perturbations are most effective in inducing variations in these response functions extended geographically from the eastern Indian Ocean to the western Pacific Ocean at low latitudes, where the convective activities are intense and frequent in a climatological sense. The implications of these sensitivity analysis results are that accurate data for temperature, moisture, and surface pressure are essential for an accurate evaluation of cumulus cloud effects, especially at the most influential vertical levels which were identified by this sensitivity analysis, since small perturbations at these locations tend to exert a stronger influence on the RAS outputs than the same perturbations at other locations. Therefore, the illustrative results presented in this sub-section indicate that data quality is particularly important at those levels and areas with positive feedback between cloud activities and the environment, since small errors tend to grow through this feedback.

Finally, we note that the *ASAP* is also important for *variational data assimilation*. For example, in variational assimilation of precipitation data, in which moist convection is the dominant process, the difference between model output rainfall and the observed rainfall (or the derivative of the cost function) is taken as input to the adjoint RAS scheme, and the output is the gradient of this cost function with respect to the large-scale variables. We may expect that the most influential levels identified by the sensitivity analysis presented in this sub-section are the ones most responsible for the reduction of the misfit, or the forecast error, which is represented by the cost function. In other words, these levels are the ones which would experience the largest impact from observational data. Such information also indicates the regions where additional adaptive observations should be taken. A thorough discussion of these and related topics (such as optimal control of fluid flow) is planned for a future volume.

REFERENCES

1. Allen, D.M., The prediction sum of squares as a criterion for selecting predictor variables, Technical Report No. 23, Department of Statistics, University of Kentucky, Lexington, 1971.
2. Andres, T.H. and Hajas, W.C., Using iterated fractional factorial design to screen parameters in sensitivity analysis of a probabilistic risk assessment model; Proceedings of the Joint International Conference on Mathematical Methods and Supercomputing in Nuclear Applications, Vol.2, 328, 19-23 April 1993, Karlsruhe, Germany, 1993.
3. Archer, G., Saltelli, A. and Sobol', I.M., Sensitivity measures, ANOVA like techniques and the use of bootstrap, *J. Statist. Comput. Simul*., 58, 99, 1997.
4. ASME Steam Tables, *Thermodynamic and Transport Properties of Steam*. 6th Edition, The American Society of Mechanical Engineers, New York, 1993.
5. Baer, F. et al., Intercomparison of heating rates generated by global climate model longwave radiation codes, *J. Geophys. Res.*, 101, 26589, 1996.
6. Berger, J., *Statistical Decision Theory and Bayesian Analysis*, 2nd ed., Springer Verlag, New York, 1985.
7. Bettonvil, B., *Detection of Important Factors by Sequential Bifurcation*, Tilburg University Press, Tilburg, 1990.
8. Bonano, E.J. and Apostolakis, G.E., Theoretical foundations and practical issues for using expert judgments in uncertainty analysis of high-level radioactive waste disposal, *Radioactive Waste Manag. and Nucl. Fuel Cycle*, 16, 137, 1991.
9. Box, G.E.P. and Draper, N.R., *Empirical Model-Building and Response Surfaces*, Wiley, New York, 1987.
10. Box, G.E.P., Hunter, W.G., and Hunter, J.S., *Statistics for Experimenters*, Chap.15, John Wiley & Sons, New York, 1978.
11. Browning, G.L., Hack, J.J., and Swarztrauber, P.N., A comparison of 3 numerical methods for solving differential equations on the sphere, *Mon. Wea. Rev*., 117, 1058, 1989.
12. Bysveen, S. et al., Experience from application of probabilistic methods in Offshore field activities, in Proceedings of the Ninth International Conference on Off-shore Mechanics and Arctic Engineering, Saga Petroleum AS, Norway, 1990.
13. Cacuci, D.G., Sensitivity theory for nonlinear systems. I. Nonlinear functional analysis approach, *J. Math. Phys.*, 22, 2794, 1981.
14. Cacuci, D.G., Sensitivity theory for nonlinear systems. II. Extensions to additonal classes of responses, *J. Math. Phys.*, 22, 2803, 1981.
15. Cacuci, D.G., The forward and the adjoint methods of sensitivity analysis, in *Uncertainty Analysis*, Ronen, Y., Ed., CRC Press, Boca Raton, FL, 71, 1988.

16. Cacuci, D.G., Global optimization and sensitivity analysis, *Nucl. Sci. Eng*., 104, 78, 1990.
17. Cacuci, D.G., *Sensitivity and Uncertainty Analysis: I. Theory*, Vol. 1, Chapman & Hall/CRC Press, Boca Raton, 2003.
18. Cacuci, D.G. and Hall, M.C.G., Efficient estimation of feedback effects with application to climate models, *J. Atmos. Sci*., 41, 2063, 1984.
19. Cacuci, D.G. and Ionescu-Bujor, M., Adjoint sensitivity analysis of the RELAP5/MOD3.2 two-fluid thermal-hydraulic code system: I. Theory, *Nucl. Sci. Eng.*, 136, 59, 2000.
20. Cacuci, D.G. and Ionescu-Bujor, M., Adjoint sensitivity and uncertainty analysis for reliability/availability models, with application to the International Fusion Materials Irradiation Facility, A&QT-R 2002 (THETA 13), International Conference on Automation, Quality and Testing, Robotics, May 23-25, 2002, Cluj-Napoca, Romania, 2002.
21. Cacuci, D.G., Maudlin, P.J., and Parks, C.V., Adjoint sensitivity analysis of extremum-type responses in reactor safety, *Nucl. Sci. Eng*., 83, 112, 1983.
22. Cacuci, D.G. and Wacholder, E., Adjoint sensitivity analysis for transient two-phase flow, *Nucl. Sci. Eng.*, 82, 461, 1982.
23. Campana, K.A., Radiation and cloud parameterization at the National Meteorological Center, *ECMWF Workshop on Clouds, Radiation, and the Hydrological Cycle*, 1990.
24. Campana, K.A., Use of cloud analyses to validate and improve model-diagnostic clouds at NMC, *ECMWF Workshop on Modelling, Validation and Assimilation of Clouds*, 1994.
25. Cess R.D., et al., Cloud feedback in atmospheric general circulation models: An update, *J. Geophys. Res.*, 101, 12791, 1996.
26. Cess R.D. and Potter, G.L., Exploratory studies of the cloud radiative forcing with a general circulation model, *Tellus* 39(A), 460, 1987.
27. Clement, R.T. and Winkler, R.L., Combining probability distributions from experts in risk analysis, *Risk Anal*., 19, 187, 1999.
28. Conover, W.J., *Practical Nonparametric Statistics*, 2nd ed., John Wiley & Sons, New York, 1980.
29. Cotter, S.C., A screening design for factorial experiments with interactions, *Biometrika*, 66, 317, 1979.
30. Cowan, G., *Statistical Data Analysis*, Clarendon Press, Oxford, 1998.
31. Cruz, J.B., *System Sensitivity Analysis*, Dowden, Hutchinson and Ross, Stroudsburg, PA, 1973.
32. Cukier, R.I. et al., Study of the sensitivity of coupled reaction systems to uncertainties in rate coefficients. I : Theory, *J. Chem. Phys*., 59, 3873, 1973.
33. Daniel, C., One-at-a-time-plans, *J. Am. Statist. Assoc*., 68, 353, 1973.
34. D'Auria, F. and Giannotti, W., Development of a code with the capability of internal assessment of uncertainty, *Nuclear Technology*, 131, 159, 2000.
35. Deif, A.S., *Sensitivity Analysis in Linear Systems*, Springer-Verlag, New York, 1986.

36. Dunker, A.M., Efficient calculation of sensitivity coefficients for complex atmospheric models, *Atmos. Environ.*, 15, 1155, 1981.
37. Dunker, A.M., The decoupled direct method for calculating sensitivity coefficients in chemical kinetics, *J. Chem. Phys.*, 81, 2385, 1984.
38. Ellingson, R.G. and Fouquart, Y., The intercomparison of radiation codes used in climate models: An overview, *J. Geophys. Res.*,, 95, 8925, 1991.
39. Errico, R.M. and Vukicevic, T., A sensitivity analysis using an adjoint of the PSU-NCAR Mesoscale Model, *Mon. Wea. Rev.*, 120, 1644-1660, 1992.
40. Eslami, M., *Theory of Sensitivity in Dynamic Systems*, Springer-Verlag, Heidelberg, 1994.
41. Fels, B.S. and Schwarzkopf, M.D., The simplified exchange approximation. A new method for radiative transfer calculation, *J. Atmos. Sci.*, 32, 1475, 1975.
42. Fiacco, A.V., Ed., *Sensitivity, Stability, and Parametric Analysis* (A publication of the Mathematical Programming Society), North-Holland, Amsterdam, 1984.
43. Fischer, R.A., *The Design of Experiments*, Oliver & Boyd, Edinburgh, 1935.
44. Frank, P.M., *Introduction to System Sensitivity Theory*, Academic Press, New York, 1978.
45. Gandini, A., Generalized Perturbation Theory (GPT) methods: A heuristic approach, in *Advances in Nuclear Science and Technology*, 19, Plenum Press, New York, 1987.
46. Greenspan, E., New developments in sensitivity theory, in *Advances in Nuclear Science and Technology*, 14, Plenum Press, New York, 1982.
47. Hall, M.C.G., Cacuci, D.G., and Schlesinger, AE., Sensitivity analysis of a radiative convective model by the adjoint method, *J. Atmos. Sci.*, 39, 2038-2050, 1982.
48. Hall, M.C.G. and Cacuci, D.G., Physical interpretation of the adjoint functions for sensitivity analysis of atmospheric models, *J. Atmos. Sci.*, 40, 2537, 1983.
49. Haynes, P.H. and McIntyre, M.E., On the evolution of vorticity and potential vorticity in the presence of diabatic heating and frictional or other forces, *J. Atmos. Sci.*, 44, 828, 1987.
50. Hora, S.C. and Iman, R.L., Expert opinion in risk analysis: The NUREG-1150 methodology, *Nucl. Sci. Eng.*, 102, 323, 1989.
51. Hsu, Y. J. and Arakawa, A., Numerical modeling of the atmosphere with an isentropic vertical coordinate, *Mon. Wea. Rev.*, 118, 1933, 1990.
52. Iman, R.L. and Conover, W.J., A distribution-free approach to inducing rank correlation among input variables, *Commun. Statist. Simul. Comput.* B, 11, 311, 1982.
53. Inamdar, A.K. and Ramanathan, V., Physics of greenhouse and convection in warm oceans, *J. Clim.*, 7, 715, 1994.

54. Ionescu-Bujor, M. and Cacuci, D.G., Adjoint sensitivity analysis of the RELAP5/MOD3.2 two-fluid thermal-hydraulic code system: II. Applications, *Nucl. Sci. Eng*., 136, 85, 2000.
55. Ionescu-Bujor, M., and Cacuci, D.G., Illustrative application of the adjoint sensitivity analysis procedure to reliability models of electromechanical devices, SIELMEN 2003, The 4th International Conference on Electromechanical and Energetic Systems, September 26-27, 2003, Chisinau, Republic of Moldavia, 2003.
56. James, I.N., Suppression of baroclinic instability in horizontally sheared flows, *J. Atmos. Sci.*, 44, 3710, 1987.
57. James, I.N. and Gray, L.J., Concerning the effect of surface drag on the circulation of a baroclinic planetary atmosphere, *Quart. J. Roy. Meteor. Soc.*, 112, 1231, 1986.
58. Kanamitsu, M. et al., Recent changes implemented into the global forecast system at NMC, *Wea. Forecasting*, 124, 1145-1160, 1991.
59. Kiehl, J.T. and Briegleb, B.P., Comparison of the observed and calculated clear sky greenhouse effect: Implications for climate studies, *J. Geophys. Res.*, 97, 100037, 1992.
60. Kimoto, M., Mukougawa, H., and Yoden, S., Medium-range forecast skill variation and blocking transition: A case study, *Mon. Wea. Rev.*, 120, 1616, 1992.
61. Kleijnen, J.P.C., Experimental design for sensitivity analysis, optimization and validation of simulation models. In: *Handbook of Simulation – Principles, Methodology, Advances, Applications, and Practice*, Banks, J. (ed), Wiley, New York, 1998.
62. Kleijnen, J.P.C. and Helton, J.C., Statistical analyses of scatterplots to identify important factors in large-scale simulations. 1. Review and comparison of techniques, *Reliab. Eng., Syst. Safety*, 65, 147, 1999.
63. Kleijnen, J.P.C. and Helton, J.C., Statistical analyses of scatterplots to identify important factors in large-scale simulations. 2. Robustness of techniques, *Reliab. Eng., Syst. Safety*, 65, 187, 1999.
64. Kleijnen, J.P.C. and Helton, J.C., Statistical analyses of scatterplots to identify important factors in large-scale simulations, SAND98-2202, Sandia National Laboratories, Albuquerque, NM, 1999.
65. Kokotovic, P.V. et al., Singular perturbations: Order reduction in control system design, *JACC*., 1972.
66. Kramer, M.A. et. al., An improved computational method for sensitivity analysis: Green's function method with AIM, *Appl. Math. Modeling*, 5, 432, 1981.
67. Kramer, M.A. et. al., Parameter scaling of mathematical models, *Appl. Math. Modeling*, 8, 341, 1984.
68. Krishnamurti, T.N. and Dignon, N., The FSU global spectral model. *Dept. of Meteorology, Florida State University*, 1988.

69. Lacis, A.A. and Hansen, J.E., A parameterization for the absorption of solar radiation in the Earth's atmosphere, *J. Atmos. Sci.*, 31, 118, 1974.
70. Li, Y. et al., Variational data assimilation with a semi-implicit global shallow water equation model and its adjoint, *Mon. Wea. Rev.*, 121, 1759, 1993.
71. Li, Z. and Navon, I.M., Sensitivity analysis of outgoing radiation at the top of the atmosphere in the NCEP/MRF model, *Journal of Geophysical Research-Atmospheres*, 103, 3801, 1998.
72. Lillie, R.A. et al., Sensitivity/Uncertainty analysis for free-in-air tissue kerma at Hiroshima and Nagasaki due to initial radiation, *Nucl. Sci. Eng.*, 100, 105, 1988.
73. Lorenz, E.N. and Emanuel, K.A., Optimal sites for supplementary weather observations: Simulation with a small model**,** *Journal of the Atmospheric Sciences*, 55, No. 3, 399, 1998.
74. Lowe, P.R. and Ficke, J.M., The computation of saturation vapor pressure, Tech. Pap. No. 4-74, Environmental Research Prediction Facility, Naval Postgraduate School, Monterey, 27, [NTIS AD-7783161], 1974.
75. Madsen, H.O. et al., *Methods of Structural Safety*, Prentice Hall, Englewood Cliffs, NJ, 1986.
76. Manabe, S. and Strickler, R.F., Thermal equilibrium of an atmosphere with a convective adjustment, *J. Atmos. Sci.*, 21, 361, 1964.
77. Manabe, S. and Wetherald, R.T., Thermal equilibrium of the atmosphere with a given distribution of relative humidity, *J. Atmos. Sci.*, 24, 241, 1967.
78. McKay, M.D. et al., A comparison of three methods of selecting values of input variables in the analysis of output from a computer code, *Technometrics*, 21, 239, 1979.
79. McKay, M.D., Evaluating prediction uncertainty, Technical Report NUREG/CR-6311, US Nuclear Regulatory Commission and Los Alamos National Laboratories, 1995.
80. Moorthi, S. and Suarez, M.J., Relaxed Arakawa-Schubert: A parameterization of moist convection for general circulation models, *Mon. Wea. Rev.*, 120, 978, 1992.
81. Morris, M.D., Factorial sampling plans for preliminary computational experiments, *Technometrics*, 33, 161, 1991.
82. Morss R. E., Emanuel, K.A., and Snyder, C., Adaptive observations in a quasi-geostrophic model. *12th Conference on Numerical Weather Prediction*, 11-16 January 1998, Phoenix, Arizona, 10-11, 1998.
83. Navon, I.M. et al., Variational data assimilation with an adiabatic version of the NMC spectral model, *Mont. Wea. Rev.*, 120, 1433, 1992.
84. Navon, I.M., Practical and theoretical aspects of adjoint parameter estimation and identifiability in meteorology and oceanography, *Dynamics of Atmospheres and Oceans*, 27, (1-4), 55, 1998.
85. Palmén, E. and Newton, C.W., *Atmospheric Circulation Systems*, New York Academic, 1967.

86. Parker, D., Learning logic, Working paper 47, Center for Computational Research in Economics and Management Science, MIT, 1985.
87. Pu, Z.X., Kalnay, E., and Toth, Z., Application of the quasi-inverse linear and adjoint NCEP global models to targeted observations during FASTEX. *12th Conference on Numerical Weather Prediction*, 11-16 January 1998, Phoenix, Arizona, 8-9, 1998.
88. Rabier, F., Courtier, P., and Talagrand, O., An application of adjoint models to sensitivity analysis, *Beitr. Phys. Atmosph.*, 65, 177, 1992.
89. Rabinovich, S.G., *Measurement Errors and Uncertainties: Theory and Practice*, 2nd ed., Springer-Verlag, New York, 2000.
90. Ramanathan, V. et al., Cloud-radiative forcing and climate: Results from the Earth Radiation Budget Experiment, *Science*, 243, 57, 1989.
91. Raval, A. and Ramanathan, V., Observational determination of the greenhouse effect, *Nature*, 342, 758, 1989.
92. Redelsperger, J. L. and Guichard, F., Detailed analysis of cloud systems observed during TOGA-COARE: Simulations forced & unforced by the large scale motions. *New insights and approaches to convective parameterization. Proc. ECMWF Workshop*, Reading, United Kingdom, ECMWF, 58, 1996.
93. Ronen, Y., Uncertainty analysis based on sensitivity analysis, in *Uncertainty Analysis*, Ronen, Y., Ed., CRC Press, Boca Raton, FL, 1988.
94. Rosenwasser, E. and Yusupov, R., *Sensitivity of Automatic Control Systems*, CRC Press, Boca Raton, 2000.
95. Saltelli, A. et al., Sensitivity analysis of model output: An investigation of new techniques, *Comput. Statist. Data Anal.*, 15, 211, 1993.
96. Saltelli, A. and Sobol', I.M., About the use of rank transformation in sensitivity analysis of model output, *Reliab. Eng. Syst. Safety*, 50, 225, 1995.
97. Saltelli, A. et al., A quantitative, model independent method for global sensitivity analysis of model output, *Technometrics*, 41, 39, 1999.
98. Sanchez, M.A. and Blower, S.M., Uncertainty and sensitivity analysis of the basic reproductive rate. Tuberculosis as an example, *Am. J. Epidemiol.*, 145, 1127, 1997.
99. Schlesinger, M. E. and Gates, W. L., The January and July performance of the OSU two-level atmospheric general circulation model, *J. Atmos. Sci.*, 37, 1914, 1980.
100. Schwarzkopf, M.D. and Fels, S.B., Improvements to the algorithm for computing CO_2 transmissivities and cooling rates, *J. Geophys. Res.*, 90, 10541, 1985.
101. Schwarzkopf, M.D. and Fels, S.B., The simplified exchange method revisited: An accurate, rapid method for computation of infrared cooling rate and fluxes. *J. Geophys. Res.*, 96, 9075, 1991.
102. Sepold, L. et al., Investigation of an overheated PWR-Type fuel rod simulator bundle cooled down by steam; Part I: Experimental and

calculational results of the QUENCH-04 Test, Forschungszentrum Karlsruhe, FZKA 6412, 2002.
103. Shapiro, S.S. and Gross, A.J., *Statistical Modeling Techniques*, Marcel Dekker, New York,, 1981.
104. Slingo, J.M., The development and verification of a cloud prediction scheme for the ECMWF model, *Quart. J. Roy. Meteorol. Soc.*, 113, 899, 1987.
105. Smith, D.L., *Probability, Statistics, and Data Uncertainties in Nuclear Science and Technology*, American Nuclear Society, LaGrange Park, IL, 1991.
106. Sobol', I.M., Sensitivity analysis for non-linear mathematical models, *Math. Model. Comput. Exp*., 1, 407, 1993.
107. Stephens, G.L., The parameterization of radiation for numerical weather prediction and climate models, *Mon. Wea. Rev*, 112, 827, 1984.
108. Stone, C.J., Optimal global rate of convergence for nonparametric regression, *Ann. Statist*., 10, 1040, 1982.
109. Stone, C.J., Additive regression and other nonparametric models, *Ann. Statist.*, 13, 689, 1985.
110. Takacs, L.L., Molod, A., and Wang, T., Documentation of the Goddard Earth Observing System (GEOS) general circulation model - Version 1. NASA Tech. Memo. 104606, Vol. 1., 1994.
111. Tomovic, R. and Vucobratovic, M., *General Sensitivity Theory*, Elsevier, New York, 1972.
112. Tracton, M. S. et al., Dynamical extended range forecasting (DERF) at the National Meteorological Center, *Mon. Wea. Rev.*, 117, 1606, 1989.
113. Turanyi, T., Sensitivity analysis of complex kinetic systems. Tools and applications, *J. Math. Chem.*, 5, 203, 1990.
114. US NRC (Nuclear Regulatory Commission), Severe accident risks: An assessment for five U.S. nuclear power plants, NUREG-1150, US Nuclear Regulatory Commission, Washington, DC, 1990-1991.
115. US DOE (US Department of Energy), Title 40CFR Part 191 Compliance Certification Application for the Waste Isolation Pilot Plant, DOE/CAO-1996-2184, US Department of Energy, Carlsbad Area Office, Carlsbad, NM, 1996.
116. Xiang, Y. and Mishra, S., Probabilistic multiphase flow modelling using the limit-state method, *Groundwater*, 35(5), 820, 1997.
117. Yamanouchi, T. and Charlock, T.P., Comparison of radiation budget at the TOA and surface in the Antarctic from ERBE and ground surface measurements, *J. Climate*, 8, 3109, 1995.
118. Yang, W. and I.M. Navon, Documentation of the tangent linear model and its adjoint of the adiabatic version of the NASA GEOS-1 C-grid GCM - version 5.2. NASA Tech. Memo. 104606, Vol.8. 61pp, 1996.
119. Yang, W., I.M. Navon, and R. Todling, Documentation of the tangent linear and adjoint models of the Relaxed Arakawa-Schubert moisture

parameterization packages of the NASA GEOS-1 GCM (version 5.2). NASA Tech. Memo. 104606, 11. 37, 1997.
120. Yang, Y. et al., Sensitivity to large-scale environmental fields of the relaxed Arakawa-Schubert parameterization in the NASA GEOS-1 GCM, *Monthly Weather Review*, 127, 2359, 1999.
121. Zhang, M.H., et al., Approach of comparison for clear-sky radiative fluxes from general circulation models with Earth Radiation Budget Experiment data, *J. Geophys. Res.*, 99, 5515, 1994.
122. Zhang, M.H. et al., Diagnostic study of climate feedback processes in atmospheric general circulation models, *J. Geophys. Res.*, 99, 5525, 1994.
123. Zhu, Y., and Navon, I. M., Documentation of the Tangent-Linear and Adjoint Models of the radiation and boundary layer parameterization packages of the FSU Global Spectral Model T42L12. *Tech. Report*, FSU-SCRI-97-98, 1997.
124. Zhu, Y., and Navon, I.M., FSU-GSM forecast error sensitivity to initial conditions: Application to Indian Summer Monsoon, *Meteorology and Atmospheric Physics*, 68, 35, 1998.
125. Zou, X., Tangent linear and adjoint of "on-off" processes and their feasibility for use in 4-dimensional variational assimilation, *Tellus*, 49A, 3, 1997.
126. Zou, X. et al., An adjoint sensitivity study of blocking in a two-layer isentropic model, *Mon. Wea. Rev.*, 121, 2833, 1993.